The Incorporation of Atmospheric Variability into DIRSIG

by

Brian M. Dobbs

B.A. State University of New York College at Geneseo

(2000)

A thesis submitted in partial fulfillment of the
requirements for the degree of Master of Science
in the Chester F. Carlson Center for Imaging Science
of The College of Science
Rochester Institute of Technology

October 4, 2006

Signature of the Author _____

Accepted by _____
Coordinator, M.S. Degree Program Date

Chester F. Carlson
Center for Imaging Science
College of Science
Rochester Institute of Technology
Rochester, NY

Certificate of Approval

M.S. Degree Thesis

The MS Degree Thesis of Brian M. Dobbs
has been examined and approved by the
thesis committee as satisfactory for the
thesis requirement for the
Master of Science degree

Dr. John Schott, Thesis Advisor

Dr. Carl Salvaggio

Dr. Rolando Raqueño

Date

Thesis Release Permission
Rochester Institute of Technology
College of Science
Chester F. Carlson
Center for Imaging Science

Title of Thesis: The Incorporation of Atmospheric Variability into DIRSIG

I, Brian M. Dobbs, hereby grant permission to Wallace Memorial Library of R.I.T. to reproduce in whole or in part. Any reproduction will not be for commercial use or profit.

Signature: _____

Date: _____

The Incorporation of Atmospheric Variability into DIRSIG

by

Brian M. Dobbs

Submitted to the
Chester F. Carlson
Center for Imaging Science
College of Science
in partial fulfillment of the requirements
for the Master of Science Degree
at the Rochester Institute of Technology

ABSTRACT

The goal of this research can be divided into two main areas. The first is to improve the existing manner in which DIRSIG samples and references the atmosphere. The second is to give DIRSIG the ability to incorporate atmospheric inhomogeneities, as well as the ability to accurately model them.

DIRSIG has limitations in how it currently samples the atmosphere. From a geometric standpoint, it does not fully sample the energy which is scattered by the atmosphere towards the sensor (upwelled radiance). There are also other geometric issues which lead to inaccurate modeling results. One significant inaccuracy is the fact that DIRSIG can mis-calculate the atmospheric effects resulting from modeling objects with non-zero altitudes. The plan is to correct this by completely reworking the procedure and geometry used by DIRSIG to sample the atmosphere.

This research will also study the effects of an inhomogeneous atmosphere and the methods involved in modeling its effects. DIRSIG currently utilizes a single atmospheric look up table (LUT) that it references when creating an image. This LUT contains the information DIRSIG will need to predict the various radiance and transmission values for a homogeneous sky. There is no ability for DIRSIG to make one part of the sky optically thick, and the other clear. This will be remedied by having DIRSIG create a series of LUTs with different atmospheric properties that it can reference. With this ability DIRSIG can reference an optically different atmosphere depending on its viewing geometry, allowing a horizontally varying atmosphere.

ACKNOWLEDGEMENTS

I would like to dedicate this work to my family, friends, and all of the people at the Center of Imaging Science.

Specifically, I'd like to thank my Mom, Dad, and my brother Bill for providing me with all of the love, support and advice through the years. They've truly shaped what I am today and inspired me to pursue my academic career.

I'd like to thank Cindy Scigaj for all of her patience and support through this entire process. She's been there with me through all of the ups and downs of graduate school, and I value all of those moments.

As well, thank you to all of the wonderful people I've met at the Center. It is truly an incredible, unique place, where I always felt accepted and appreciated. I'd like to thank Scott Brown, Niek Sanders, and Paul Lee for showing me the ropes of programming in the DIRSIG universe. I'd like to thank Cindy Schultz and Sue Chan for their patience and for helping me through many hurdles. And many thanks to everyone that I've left off this list.

And none of this would be possible without the opportunities given to me by my advisor, Dr. John Schott, and my thesis committee members Dr. Carl Salvaggio, and Dr. Rolando Raqueño. Their patience and guidance are greatly appreciated.

Contents

1 Background **25**

1.1 Image Modeling . . . 25
1.2 Motivation . . . 26
1.3 The Remote Sensing Equation . . . 26
1.3.1 The Effect of Inhomogeneities on the Remote Sensing Equation . . . 30
1.4 Overview of DIRSIG . . . 31
1.4.1 Image Rendering . . . 31
1.4.2 Function of the Atmospheric Database (ADB) . . . 32
1.4.3 Structure of the ADB . . . 33
1.4.4 ADB Construction . . . 35

2 Atmospheric Modeling: Issues and Solutions **39**

2.1 Geometric Issues . . . 39
2.1.1 The High-Altitude Object Issue . . . 39
2.1.2 The Solution to the High-Altitude Object Issue . . . 44
2.1.3 Current Atmospheric Sampling . . . 47
2.1.4 New Method of Atmospheric Sampling . . . 49
2.1.5 Horizon Issues . . . 51
2.1.6 Resolution of Horizon Issues . . . 55
2.2 Atmospheric Inhomogeneities . . . 59
2.2.1 Atmospheric Inhomogeneities Issues . . . 59
2.2.2 Implementation of Atmospheric Inhomogeneities . . . 59

3 Algorithm Description **63**

3.1 Atmospheric Database Generation . . . 63
3.1.1 Creating MODTRAN Input Files . . . 64
3.1.2 Setting Input Parameters . . . 64
3.1.3 Nested Loops . . . 70
3.2 Atmospheric Interpolator . . . 73
3.2.1 computeSolarIrradiance . . . 73

3.2.2 computeLunarIrradiance . . . 74
3.2.3 computePathRadiance . . . 75
3.2.4 computePathTransmission . . . 76
3.2.5 computeSkyRadiance . . . 76
3.2.6 Atmospheric Interpolation Tools . . . 76
3.3 Test Cases for Verification . . . 82
3.3.1 Atmospheric Database Generation Verification . . . 82
3.3.2 Atmospheric Interpolator Verification . . . 83

4 Test Scenes **85**
4.1 Geometry Test Scenes . . . 86
4.1.1 Highlighting Angular Features . . . 86
4.1.2 Highlighting Altitude Changes . . . 112
4.2 Atmospheric Variability Test Scenes . . . 127
4.2.1 Highlighting Water Vapor Changes . . . 127
4.2.2 Highlighting Visibility Changes . . . 144
4.3 Test Image Error Summary . . . 173
4.4 Demonstration Images . . . 177
4.4.1 Megascene . . . 177

5 Conclusions, Recommendations, and Future Directions **185**
5.1 Conclusions . . . 185
5.2 Recommendations and Future Directions . . . 185

A Experiments **191**
A.1 Non-Zero Altitude Object Test . . . 191
A.1.1 Background . . . 191
A.1.2 Setup and Procedure . . . 192
A.1.3 Results and Conclusions . . . 192
A.2 Upwelled Sampling: Geometry . . . 194
A.2.1 Background . . . 194
A.2.2 Setup and Procedure . . . 194
A.2.3 Results and Conclusions . . . 194
A.3 Upwelled Sampling: Atmospheric Inhomogeneities . . . 200
A.3.1 Background . . . 200
A.3.2 Setup and Procedure . . . 200
A.3.3 Results and Conclusions . . . 200

B Test Scene Results **203**
B.1 Test Image 1a . . . 204

B.1.1 Test Image 1a Zenith Variation. . . . 204
B.1.2 Test Image 1a Azimuth Variations. . . . 215
B.1.3 Test Image 1a Grid Results 223
B.2 Test Image 1b 225
B.2.1 Test Image 1b Zenith Variation. . . . 225
B.2.2 Test Image 1b Azimuth Variation. . . . 230
B.2.3 Test Image 1b Grid Results. . . . 235
B.3 Test Image 1c 236
B.3.1 Test Image 1c Zenith Variation. . . . 236
B.3.2 Test Image 1c Azimuth Variation. . . . 241
B.3.3 Test Image 1c Grid Results. . . . 245
B.4 Test Image 1a_urban. . . . 246
B.4.1 Test Image 1a_urban Grid Results. . . . 256
B.5 Test Image 2a. . . . 258
B.5.1 Test Image 2a Altitude Variation. . . . 258
B.5.2 Test Image 2a Grid Results 269
B.6 Test Image 2b 271
B.6.1 Test Image 2b Altitude Variation. . . . 271
B.6.2 Test Image 2b Grid Results. . . . 276
B.7 Test Image 2c 277
B.7.1 Test Image 2c Altitude Variation. . . . 277
B.7.2 Test Image 2c Grid Results. . . . 282
B.8 Test Image 3 283
B.8.1 Test Image 3 Water Variation 284
B.8.2 Test Image 3 Grid Results 297
B.9 Test Image 4a 299
B.9.1 Test Image 4a Visibility Variation 300
B.9.2 Test Image 4a Grid Results 312
B.10 Test Image 5 314
B.10.1 Test Image 5 Grid Results 314

C Horizon Calculator **317**
C.1 Determine the MODTRAN horizon 317
C.2 The Function getModtran 318

D Sample DIRSIG configuration (CFG) file **321**

E Sample Atmospheric Database (ADB) file **325**

F Sample MODTRAN input file (tape5) **329**

G Interpolator Inputs **331**

List of Figures

1.1 This shows the possible paths a photon could take to significantly affect the radiance reaching a given sensor. It is important to account for all of these paths in rendering an image in order to accurately model the real world. [8] . . . 26

1.2 The solar photon paths of the Big Equation.[8] . . . 27

1.3 The thermal photon paths of the Big Equation. [8] . . . 28

1.4 The effect of inhomogeneities in the atmosphere on different photon paths. . . . 29

1.5 The transmission of a mid-latitude, winter atmosphere. . . . 30

1.6 The transmission of a mid-latitude, winter atmosphere. . . . 31

1.7 A simple framing array imaging system. [8] . . . 32

1.8 A flow chart showing the construction of the Atmospheric Database. . . . 33

1.9 The general structure of the current Atmospheric Database. . . . 34

1.10 The general structure of the current Atmospheric Database. This shows the radiometric terms associated with each section. . . . 34

1.11 This is a representation of the geometry associated with creating the source path section of the ADB. MODTRAN is run from the target towards the source. . . . 35

1.12 This is a representation of the current generation of the upwelled (sensor path) section of the ADB, where each of the dots represents a MODTRAN run, from the sensor to that point. . . . 36

1.13 This shows the layout of method used to sample the sky dome in the downwelled section of the ADB. The blue dots represent a sampled point in the sky, where DIRSIG will execute a MODTRAN run and store the results in the ADB. Interpolation is used to get the values in between the sampled points. . . . 37

2.1 This is what is expected to happen in a real scene when a ray encounters an object of non-zero altitude. . . . 40

2.2 This is what actually happens in DIRSIG. Each layer of the atmosphere is scaled down to compensate for the change in range between the sensor and the object. Passing the ray through the lower layers adds more atmospheric effects than would be in the real scene. . . . 40

2.3 A diagram of the altitude experiment. The upwelling radiance and transmission from a non-reflective object were measured by DIRSIG and MODTRAN, and their results compared. . . . 41

2.4 These are typical results for the altitude interpolation experiment. This graph shows the change in path transmission as a function of target altitude. Notice the artificial linearity produced by DIRSIG. The sensor for this experiment was at 100 km. . . . 42

2.5 These are typical results for the altitude interpolation experiment. This graph shows the path radiance as a function of target altitude. Notice the artificial linearity produced by DIRSIG. The sensor, again, was at 100 km. 42

2.6 This shows the results of the same experiment when only the region below 1 km is examined. 43

2.7 This shows that the path radiance also behaves in a linear fashion when examined at altitudes below 1 km. 43

2.8 This graph shows the transmission as a function of target altitude (with the sensor at 100km) if DIRSIG scaled the atmosphere from approximately 1 km, not at the sensor altitude. . . . 44

2.9 This graph shows the path radiance as a function of target altitude (with the sensor at 100km) if DIRSIG scaled the atmosphere from approximately 1 km, not at the sensor altitude. 44

2.10 A graphic of the proposed method of upwelled sampling. 45

2.11 A graphic showing the multiple altitude region sampling scheme. 46

2.12 The upper diagrams show the upwelled radiance sampling scheme, and the lower show the resulting upwelling radiance map. The diagrams on the left (A. and C.) represent the current method of sampling the upwelling radiance and transmission of the atmosphere. The set on the right (B. and D.) show the proposed scheme, with azimuth angles to detect any azimuthal variation in the atmosphere. 47

2.13 A flow chart demonstrating the current method of referencing the sensor section of the Atmospheric Database. 48

2.14 A flow chart demonstrating the current method of referencing the downwelled section of the Atmospheric Database. 48

2.15 This is a diagram of the proposed structure of the new upwelled section of the ADB. Note that this structure samples in the azimuth and altitude dimensions as well as the zenith dimension. 49

2.16 This figure depicts a flow chart of the new multi-dimensional interpolation scheme of DIRSIG. 50

2.17 The structure for the proposed ADB. This shows the new geometric structure, including the addition of multiple altitudes and angles. 53

2.18 This artificial horizon is the result of the inability of DIRSIG to sample the downwelling radiance from the sky below 90 above. It substitutes those sky radiance values *above* 90 degrees with those *below* 90 degrees. This means that the values at +10 degrees are identical to those at -10 degrees, which creates this false "mirroring" effect in the sky. [10] 54

2.19 This represents the problem when synthesizing an image which contains the horizon. In addition to the "mirroring" effect (figure 2.18), there is a problem related to the height scaling problem. 55

2.20 The geometry associated with calculating the default range used in the horizon spectral blocks. 57

2.21 This shows the proposed solution to the intervening object problem. In sampling at multiple ranges, the scaling problem will be lessened. 58

2.22 A set of ADBs will be produced for each of the atmospheric species. Each one of these ADBs will have a complete set of geometries, enabling DIRSIG to reference any concentration at any look angle. Water vapor is shown here, with each ADB having a difference water vapor concentration. 59

2.23 The structure for the proposed ADB. A unique set of spectral blocks will be created for each combination of aerosol visibility, type, and water vapor density. 60

2.24 An illustration of downwelled sampling of atmospheric inhomogeneities. 62

3.1 The structure of the Atmospheric Database Generation code. 64

3.2 The structure of the source section interpolator. 73

3.3 The structure of the upwelled and downwelled section interpolators. 75

3.4 This is a graphic representing the reduction of the dimensionality carried out by the source section interpolator. 79

3.5 This is a graphic representing the reduction of the dimensionality carried out by the source section interpolator. 79

3.6 This figure shows a representative set of values which are read into the tool linear_interp. . . . 80

4.1 This scene highlights the changes in the angular structure of the upwelling radiance in the image, due to the new method of sampling the atmosphere. 86

4.2 The blue path radiance obtained during sunset from the DIRSIG 3 and DIRSIG 4 interpolator over the "truncated pyramid" test scene. In order to highlight the changes in radiance in the image, the dynamic range of the image was increased by using the Histogram Equalization enhancement tool in ENVI. 87

4.3 The visible path radiance obtained during sunset from the DIRSIG 3 interpolator over the "truncated pyramid" test scene. (displayed in RGB.) 88

4.4 The visible path radiance obtained during sunset from the DIRSIG 4 interpolator over the "truncated pyramid" test scene. (displayed in RGB.) Notice the relative red color of the Western sky (positive y) 88

4.5 The linearly and circularly organized dots represent points analyzed in the zenith and azimuth studies, respectively. 89

4.6 Test Scene 1a (varying zenith angle): The upper graph shows the blue path radiance obtained by MODTRAN, DIRSIG 4 and DIRSIG 3. The lower graph shows the percent error of DIRSIG 4 and DIRSIG 3 relative to MODTRAN. The RMS error for the points shown on the graph are listed below the graphs. 90

4.7 Test Scene 1a (zenith variation): The upper graph shows the green path radiance obtained by MODTRAN, DIRSIG 4 and DIRSIG 3. The lower graph shows the percent error of DIRSIG 4 and DIRSIG 3 relative to MODTRAN. The RMS errors for the points shown on the graph are listed below the graphs. 91

4.8 Test Scene 1a (zenith variation): The upper graph shows the red path radiance obtained by MODTRAN, DIRSIG 4 and DIRSIG 3. The lower graph shows the percent error of DIRSIG 4 and DIRSIG 3 relative to MODTRAN. The RMS errors for the points shown on the graph are listed below the graphs. 92

4.9 Test Scene 1a (zenith variation): The upper graph shows the NIR path radiance obtained by MODTRAN, DIRSIG 4 and DIRSIG 3. The lower graph shows the percent error of DIRSIG 4 and DIRSIG 3 relative to MODTRAN. The RMS errors for the points shown on the graph are listed below the graphs. 93

4.10 Test Scene 1a (zenith variation): The upper graph shows the thermal path radiance obtained by MODTRAN, DIRSIG 4 and DIRSIG 3. The lower graph shows the percent error of DIRSIG 4 and DIRSIG 3 relative to MODTRAN. The RMS errors for the points shown on the graph are listed below the graphs. 94

4.11 Test Scene 1a (zenith variation): The upper graph shows the blue path transmission obtained by MODTRAN, DIRSIG 4 and DIRSIG 3. The lower graph shows the percent error of DIRSIG 4 and DIRSIG 3 relative to MODTRAN. The RMS error for the points shown on the graph are listed below the graphs. 95

4.12 Test Scene 1a (zenith variation): The upper graph shows the green path transmission obtained by MODTRAN, DIRSIG 4 and DIRSIG 3. The lower graph shows the percent error of DIRSIG 4 and DIRSIG 3 relative to MODTRAN. The RMS errors for the points shown on the graph are listed below the graphs. 96

4.13 Test Scene 1a (zenith variation): The upper graph shows the red path transmission obtained by MODTRAN, DIRSIG 4 and DIRSIG 3. The lower graph shows the percent error of DIRSIG 4 and DIRSIG 3 relative to MODTRAN. The RMS errors for the points shown on the graph are listed below the graphs. 97

4.14 Test Scene 1a (zenith variation): The upper graph shows the NIR path transmission obtained by MODTRAN, DIRSIG 4 and DIRSIG 3. The lower graph shows the percent error of DIRSIG 4 and DIRSIG 3 relative to MODTRAN. The RMS errors for the points shown on the graph are listed below the graphs. 98

4.15 Test Scene 1a (zenith variation): The upper graph shows the thermal path transmission obtained by MODTRAN, DIRSIG 4 and DIRSIG 3. The lower graph shows the percent error of DIRSIG 4 and DIRSIG 3 relative to MODTRAN. The RMS errors for the points shown on the graph are listed below the graphs. 99

4.16 Test Scene 1a: The upper graph shows the blue path radiance obtained by MODTRAN, DIRSIG 4 and DIRSIG 3. The lower graph shows the percent error of DIRSIG 4 and DIRSIG 3 relative to MODTRAN. The RMS error for the points shown on the graph are listed below the graphs. 101

4.17 Test Scene 1a (azimuth variation): The upper graph shows the green path radiance obtained by MODTRAN, DIRSIG 4 and DIRSIG 3. The lower graph shows the percent error of DIRSIG 4 and DIRSIG 3 relative to MODTRAN. The RMS errors for the points shown on the graph are listed below the graphs. 102

4.18 Test Scene 1a (azimuth variation): The upper graph shows the red path radiance obtained by MODTRAN, DIRSIG 4 and DIRSIG 3. The lower graph shows the percent error of DIRSIG 4 and DIRSIG 3 relative to MODTRAN. The RMS errors for the points shown on the graph are listed below the graphs. 103

4.19 Test Scene 1a (azimuth variation): The upper graph shows the NIR path radiance obtained by MODTRAN, DIRSIG 4 and DIRSIG 3. The lower graph shows the percent error of DIRSIG 4 and DIRSIG 3 relative to MODTRAN. The RMS errors for the points shown on the graph are listed below the graphs. 104

4.20 Test Scene 1a: The upper graph shows the blue path transmission obtained by MODTRAN, DIRSIG 4 and DIRSIG 3. The lower graph shows the percent error of DIRSIG 4 and DIRSIG 3 relative to MODTRAN. The RMS error for the points shown on the graph are listed below the graphs. 105

4.21 Test Scene 1a (azimuth variation): The upper graph shows the green path transmission obtained by MODTRAN, DIRSIG 4 and DIRSIG 3. The lower graph shows the percent error of DIRSIG 4 and DIRSIG 3 relative to MODTRAN. The RMS errors for the points shown on the graph are listed below the graphs. 106

4.22 Test Scene 1a (azimuth variation): The upper graph shows the red path transmission obtained by MODTRAN, DIRSIG 4 and DIRSIG 3. The lower graph shows the percent error of DIRSIG 4 and DIRSIG 3 relative to MODTRAN. The RMS errors for the points shown on the graph are listed below the graphs. 107

4.23 Test Scene 1a (azimuth variation): The upper graph shows the NIR path transmission obtained by MODTRAN, DIRSIG 4 and DIRSIG 3. The lower graph shows the percent error of DIRSIG 4 and DIRSIG 3 relative to MODTRAN. The RMS errors for the points shown on the graph are listed below the graphs. 108

4.24 The dots represent points analyzed in the image. 109

4.25 This shows the RMS error in path radiance (by band) over the image 1a. 110

4.26 This shows the RMS error in path transmission (by band) over the image 1a. 111

4.27 This scene highlights the changes in upwelled radiance and transmission as a function of altitude.112

4.28 The visible path radiance obtained during sunset from the DIRSIG 3 and DIRSIG 4 interpolator over the "pyramid" test scene (RGB display). In order to highlight the changes in radiance in the image, the dynamic range of the image was increased by using the Histogram Equalization enhancement tool in ENVI. 113

4.29 The red dots represent points analyzed in the altitude studies. 113

4.30 Test Scene 2a (varying altitude): The upper graph shows the blue path radiance obtained by MODTRAN, DIRSIG 4 and DIRSIG 3. The lower graph shows the percent error of DIRSIG 4 and DIRSIG 3 relative to MODTRAN. The RMS error for the points shown on the graph are listed below the graphs. 114

4.31 Test Scene 2a (altitude variation): The upper graph shows the green path radiance obtained by MODTRAN, DIRSIG 4 and DIRSIG 3. The lower graph shows the percent error of DIRSIG 4 and DIRSIG 3 relative to MODTRAN. The RMS errors for the points shown on the graph are listed below the graphs. 115

4.32 Test Scene 2a (altitude variation): The upper graph shows the red path radiance obtained by MODTRAN, DIRSIG 4 and DIRSIG 3. The lower graph shows the percent error of DIRSIG 4 and DIRSIG 3 relative to MODTRAN. The RMS errors for the points shown on the graph are listed below the graphs. 116

4.33 Test Scene 2a (altitude variation): The upper graph shows the NIR path radiance obtained by MODTRAN, DIRSIG 4 and DIRSIG 3. The lower graph shows the percent error of DIRSIG 4 and DIRSIG 3 relative to MODTRAN. The RMS errors for the points shown on the graph are listed below the graphs. 117

4.34 Test Scene 2a (altitude variation): The upper graph shows the thermal path radiance obtained by MODTRAN, DIRSIG 4 and DIRSIG 3. The lower graph shows the percent error of DIRSIG 4 and DIRSIG 3 relative to MODTRAN. The RMS errors for the points shown on the graph are listed below the graphs. 118

4.35 Test Scene 2a (altitude variation): The upper graph shows the blue path transmission obtained by MODTRAN, DIRSIG 4 and DIRSIG 3. The lower graph shows the percent error of DIRSIG 4 and DIRSIG 3 relative to MODTRAN. The RMS errors for the points shown on the graph are listed below the graphs. 119

4.36 Test Scene 2a (altitude variation): The upper graph shows the green path transmission obtained by MODTRAN, DIRSIG 4 and DIRSIG 3. The lower graph shows the percent error of DIRSIG 4 and DIRSIG 3 relative to MODTRAN. The RMS errors for the points shown on the graph are listed below the graphs. 120

4.37 Test Scene 2a (altitude variation): The upper graph shows the red path transmission obtained by MODTRAN, DIRSIG 4 and DIRSIG 3. The lower graph shows the percent error of DIRSIG 4 and DIRSIG 3 relative to MODTRAN. The RMS errors for the points shown on the graph are listed below the graphs. 121

4.38 Test Scene 2a (altitude variation): The upper graph shows the NIR path transmission obtained by MODTRAN, DIRSIG 4 and DIRSIG 3. The lower graph shows the percent error of DIRSIG 4 and DIRSIG 3 relative to MODTRAN. The RMS errors for the points shown on the graph are listed below the graphs. 122

4.39 Test Scene 2a (altitude variation): The upper graph shows the thermal path transmission obtained by MODTRAN, DIRSIG 4 and DIRSIG 3. The lower graph shows the percent error of DIRSIG 4 and DIRSIG 3 relative to MODTRAN. The RMS errors for the points shown on the graph are listed below the graphs. 123

4.40 This shows the RMS error in path radiance (by band) over image 2a. 125

4.41 This shows the RMS error in path transmission (by band) over image 2a. 126

4.42 This scene highlights the effect that water vapor has on upwelled radiance and transmission in a very simple scene. 127

4.43 Test image 3, the path radiance in the 'water2' band (940 nm), rendered by DIRSIG 4. . . . 128

4.44 Test image 3, the path radiance in the 'water2' band (940 nm), rendered by DIRSIG 4. . . . 128

4.45 Test Scene 3 (water variation): The upper graph shows the blue path radiance obtained by MODTRAN, DIRSIG 4 and DIRSIG 3. The lower graph shows the percent error of DIRSIG 4 and DIRSIG 3 relative to MODTRAN. The RMS errors for the points shown on the graph are listed below the graphs. 130

4.46 Test Scene 3 (water variation): The upper graph shows the green path radiance obtained by MODTRAN, DIRSIG 4 and DIRSIG 3. The lower graph shows the percent error of DIRSIG 4 and DIRSIG 3 relative to MODTRAN. The RMS errors for the points shown on the graph are listed below the graphs. 131

4.47 Test Scene 3 (water variation): The upper graph shows the red path radiance obtained by MODTRAN, DIRSIG 4 and DIRSIG 3. The lower graph shows the percent error of DIRSIG 4 and DIRSIG 3 relative to MODTRAN. The RMS errors for the points shown on the graph are listed below the graphs. 132

4.48 Test Scene 3 (water variation): The upper graph shows the NIR path radiance obtained by MODTRAN, DIRSIG 4 and DIRSIG 3. The lower graph shows the percent error of DIRSIG 4 and DIRSIG 3 relative to MODTRAN. The RMS errors for the points shown on the graph are listed below the graphs. 133

4.49 Test Scene 3 (water variation): The upper graph shows the water2 path radiance obtained by MODTRAN, DIRSIG 4 and DIRSIG 3. The lower graph shows the percent error of DIRSIG 4 and DIRSIG 3 relative to MODTRAN. The RMS errors for the points shown on the graph are listed below the graphs. 134

4.50 Test Scene 3 (water variation): The upper graph shows the Thermal path radiance obtained by MODTRAN, DIRSIG 4 and DIRSIG 3. The lower graph shows the percent error of DIRSIG 4 and DIRSIG 3 relative to MODTRAN. The RMS errors for the points shown on the graph are listed below the graphs. 135

4.51 Test Scene 3 (water variation): The upper graph shows the blue path transmission obtained by MODTRAN, DIRSIG 4 and DIRSIG 3. The lower graph shows the percent error of DIRSIG 4 and DIRSIG 3 relative to MODTRAN. The RMS errors for the points shown on the graph are listed below the graphs. 136

4.52 Test Scene 3 (water variation): The upper graph shows the green path transmission obtained by MODTRAN, DIRSIG 4 and DIRSIG 3. The lower graph shows the percent error of DIRSIG 4 and DIRSIG 3 relative to MODTRAN. The RMS errors for the points shown on the graph are listed below the graphs. 137

4.53 Test Scene 3 (water variation): The upper graph shows the red path transmission obtained by MODTRAN, DIRSIG 4 and DIRSIG 3. The lower graph shows the percent error of DIRSIG 4 and DIRSIG 3 relative to MODTRAN. The RMS errors for the points shown on the graph are listed below the graphs. 138

4.54 Test Scene 3 (water variation): The upper graph shows the NIR path transmission obtained by MODTRAN, DIRSIG 4 and DIRSIG 3. The lower graph shows the percent error of DIRSIG 4 and DIRSIG 3 relative to MODTRAN. The RMS errors for the points shown on the graph are listed below the graphs. 139

4.55 Test Scene 3 (water variation): The upper graph shows the water2 path transmission obtained by MODTRAN, DIRSIG 4 and DIRSIG 3. The lower graph shows the percent error of DIRSIG 4 and DIRSIG 3 relative to MODTRAN. The RMS errors for the points shown on the graph are listed below the graphs. 140

4.56 Test Scene 3 (water variation): The upper graph shows the Thermal path transmission obtained by MODTRAN, DIRSIG 4 and DIRSIG 3. The lower graph shows the percent error of DIRSIG 4 and DIRSIG 3 relative to MODTRAN. The RMS errors for the points shown on the graph are listed below the graphs. 141

4.57 This shows the RMS error in path radiance (by band) over image 3a. 142

4.58 This shows the RMS error in path transmission (by band) over image 3a. 143

4.59 The RGB path radiance of test image 4, rendered by DIRSIG 4. 144

4.60 Test Scene 4a (visibility variation): The upper graph shows the blue path radiance obtained by MODTRAN, DIRSIG 4 and DIRSIG 3. The lower graph shows the percent error of DIRSIG 4 and DIRSIG 3 relative to MODTRAN. The RMS errors for the points shown on the graph are listed below the graphs. 145

4.61 Test Scene 4a (visibility variation): The upper graph shows the green path radiance obtained by MODTRAN, DIRSIG 4 and DIRSIG 3. The lower graph shows the percent error of DIRSIG 4 and DIRSIG 3 relative to MODTRAN. The RMS errors for the points shown on the graph are listed below the graphs. 146

4.62 Test Scene 4a (visibility variation): The upper graph shows the red path radiance obtained by MODTRAN, DIRSIG 4 and DIRSIG 3. The lower graph shows the percent error of DIRSIG 4 and DIRSIG 3 relative to MODTRAN. The RMS errors for the points shown on the graph are listed below the graphs. 147

4.63 Test Scene 4a (visibility variation): The upper graph shows the NIR path radiance obtained by MODTRAN, DIRSIG 4 and DIRSIG 3. The lower graph shows the percent error of DIRSIG 4 and DIRSIG 3 relative to MODTRAN. The RMS errors for the points shown on the graph are listed below the graphs. 148

4.64 Test Scene 4a (visibility variation): The upper graph shows the water2 path radiance obtained by MODTRAN, DIRSIG 4 and DIRSIG 3. The lower graph shows the percent error of DIRSIG 4 and DIRSIG 3 relative to MODTRAN. The RMS errors for the points shown on the graph are listed below the graphs. 149

4.65 Test Scene 4a (visibility variation): The upper graph shows the Thermal path radiance obtained by MODTRAN, DIRSIG 4 and DIRSIG 3. The lower graph shows the percent error of DIRSIG 4 and DIRSIG 3 relative to MODTRAN. The RMS errors for the points shown on the graph are listed below the graphs. 150

4.66 Test Scene 4a (visibility variation): The upper graph shows the blue path transmission obtained by MODTRAN, DIRSIG 4 and DIRSIG 3. The lower graph shows the percent error of DIRSIG 4 and DIRSIG 3 relative to MODTRAN. The RMS errors for the points shown on the graph are listed below the graphs. 151

4.67 Test Scene 4a (visibility variation): The upper graph shows the green path transmission obtained by MODTRAN, DIRSIG 4 and DIRSIG 3. The lower graph shows the percent error of DIRSIG 4 and DIRSIG 3 relative to MODTRAN. The RMS errors for the points shown on the graph are listed below the graphs. 152

4.68 Test Scene 4a (visibility variation): The upper graph shows the red path transmission obtained by MODTRAN, DIRSIG 4 and DIRSIG 3. The lower graph shows the percent error of DIRSIG 4 and DIRSIG 3 relative to MODTRAN. The RMS errors for the points shown on the graph are listed below the graphs. 153

4.69 Test Scene 4a (visibility variation): The upper graph shows the NIR path transmission obtained by MODTRAN, DIRSIG 4 and DIRSIG 3. The lower graph shows the percent error of DIRSIG 4 and DIRSIG 3 relative to MODTRAN. The RMS errors for the points shown on the graph are listed below the graphs. 154

4.70 Test Scene 4a (visibility variation): The upper graph shows the water2 path transmission obtained by MODTRAN, DIRSIG 4 and DIRSIG 3. The lower graph shows the percent error of DIRSIG 4 and DIRSIG 3 relative to MODTRAN. The RMS errors for the points shown on the graph are listed below the graphs. 155

4.71 Test Scene 4a (visibility variation): The upper graph shows the Thermal path transmission obtained by MODTRAN, DIRSIG 4 and DIRSIG 3. The lower graph shows the percent error of DIRSIG 4 and DIRSIG 3 relative to MODTRAN. The RMS errors for the points shown on the graph are listed below the graphs. 156

4.72 This shows the RMS error in path radiance (by band) over image 4a. 157

4.73 This shows the RMS error in path transmission (by band) over image 4a. 158

4.74 Test Scene 4aa (visibility variation): The upper graph shows the blue path radiance obtained by MODTRAN, DIRSIG 4 and DIRSIG 3. The lower graph shows the percent error of DIRSIG 4 and DIRSIG 3 relative to MODTRAN. The RMS errors for the points shown on the graph are listed below the graphs. 159

4.75 Test Scene 4aa (visibility variation): The upper graph shows the green path radiance obtained by MODTRAN, DIRSIG 4 and DIRSIG 3. The lower graph shows the percent error of DIRSIG 4 and DIRSIG 3 relative to MODTRAN. The RMS errors for the points shown on the graph are listed below the graphs. 160

4.76 Test Scene 4aa (visibility variation): The upper graph shows the red path radiance obtained by MODTRAN, DIRSIG 4 and DIRSIG 3. The lower graph shows the percent error of DIRSIG 4 and DIRSIG 3 relative to MODTRAN. The RMS errors for the points shown on the graph are listed below the graphs. 161

4.77 Test Scene 4aa (visibility variation): The upper graph shows the NIR path radiance obtained by MODTRAN, DIRSIG 4 and DIRSIG 3. The lower graph shows the percent error of DIRSIG 4 and DIRSIG 3 relative to MODTRAN. The RMS errors for the points shown on the graph are listed below the graphs. 162

4.78 Test Scene 4aa (visibility variation): The upper graph shows the water2 path radiance obtained by MODTRAN, DIRSIG 4 and DIRSIG 3. The lower graph shows the percent error of DIRSIG 4 and DIRSIG 3 relative to MODTRAN. The RMS errors for the points shown on the graph are listed below the graphs. 163

4.79 Test Scene 4aa (visibility variation): The upper graph shows the Thermal path radiance obtained by MODTRAN, DIRSIG 4 and DIRSIG 3. The lower graph shows the percent error of DIRSIG 4 and DIRSIG 3 relative to MODTRAN. The RMS errors for the points shown on the graph are listed below the graphs. 164

4.80 Test Scene 4aa (visibility variation): The upper graph shows the blue path transmission obtained by MODTRAN, DIRSIG 4 and DIRSIG 3. The lower graph shows the percent error of DIRSIG 4 and DIRSIG 3 relative to MODTRAN. The RMS errors for the points shown on the graph are listed below the graphs. 165

4.81 Test Scene 4aa (visibility variation): The upper graph shows the green path transmission obtained by MODTRAN, DIRSIG 4 and DIRSIG 3. The lower graph shows the percent error of DIRSIG 4 and DIRSIG 3 relative to MODTRAN. The RMS errors for the points shown on the graph are listed below the graphs. 166

4.82 Test Scene 4aa (visibility variation): The upper graph shows the red path transmission obtained by MODTRAN, DIRSIG 4 and DIRSIG 3. The lower graph shows the percent error of DIRSIG 4 and DIRSIG 3 relative to MODTRAN. The RMS errors for the points shown on the graph are listed below the graphs. 167

4.83 Test Scene 4aa (visibility variation): The upper graph shows the NIR path transmission obtained by MODTRAN, DIRSIG 4 and DIRSIG 3. The lower graph shows the percent error of DIRSIG 4 and DIRSIG 3 relative to MODTRAN. The RMS errors for the points shown on the graph are listed below the graphs. 168

4.84 Test Scene 4aa (visibility variation): The upper graph shows the water2 path transmission obtained by MODTRAN, DIRSIG 4 and DIRSIG 3. The lower graph shows the percent error of DIRSIG 4 and DIRSIG 3 relative to MODTRAN. The RMS errors for the points shown on the graph are listed below the graphs. 169

4.85 Test Scene 4aa (visibility variation): The upper graph shows the thermal path transmission obtained by MODTRAN, DIRSIG 4 and DIRSIG 3. The lower graph shows the percent error of DIRSIG 4 and DIRSIG 3 relative to MODTRAN. The RMS errors for the points shown on the graph are listed below the graphs. 170

4.86 This shows the RMS error in path radiance (by band) over image 4aa. 171

4.87 This shows the RMS error in path transmission (by band) over image 4aa. 172

4.88 This shows the RMS errors associated with radiance for each band, for each test image. . . . 173

4.89 This shows the RMS errors associated with transmission for each band, for each test image. . 174

4.90 This shows the RMS errors associated with radiance for each band, for each test image. The y-axis has been scaled to better show the trend in the lower test cases. 174

4.91 This shows the RMS errors associated with transmission for each band, for each test image. The y-axis has been scaled to better show the trend in the lower test cases. 175

4.92 This shows the ratio of the radiance RMS errors in DIRSIG 3 to the RMS errors in DIRSIG 4.175

4.93 This shows the ratio of the transmission RMS errors in DIRSIG 3 to the RMS errors in DIRSIG 4. 176

4.94 This shows the resulting RGB radiance of the Megascene. (ENVI Gaussian equalization was applied to the image.) 177

4.95 This shows the water vapor map used in the rendering of the Megascene. 178

4.96 This shows the RGB bands when DIRSIG 4 renders the Megascene with a 'realistic' water vapor map. 178

4.97 This shows the red band when DIRSIG 4 renders the Megascene with a 'realistic' water vapor map. 179

4.98 This shows the water2 (940 nm) band when DIRSIG 4 renders the Megascene with a 'realistic' water vapor map. 179

4.99 This shows the results of the water vapor retrieval method shown in equation 4.3. 180

4.100This shows the 'realistic' visibility map. 181

4.101This shows the RGB bands when DIRSIG 4 renders the Megascene with a 'realistic' visibility map. 182

4.102This shows the RGB path radiance bands when DIRSIG 4 renders the Megascene with a 'realistic' visibility map. 182

4.103This shows the RGB bands when DIRSIG 4 renders the Megascene with a 'realistic' visibility map ranging from 20 to 25 km. 183

4.104This shows the path radiance associated with the RGB bands when DIRSIG 4 renders the Megascene with a 'realistic' visibility map ranging from 20 to 25 km. 183

5.1 The "z-hit" map for the horizon test scene. 187

5.2 This figure shows the z-hit value for each line in the image. 187

A.1 In the new ADB, upper-atmospheric regions can be added where clouds (or any objects, for that matter) can be placed, and the transmission and path radiance can be predicted with similar accuracy as in the region below 1 kilometer. 193

A.2 An illustration of how the midpoint between interpolation points may not always be the maximum error. 195

A.3 Each point on this graph represents the maximum of the difference matrix. 196

A.4 Each point on this graph represents the maximum of the difference matrix. 196

A.5 Each point on this graph represents the maximum of the difference matrix. 197

A.6 Each point on this graph represents the maximum of the difference matrix. 197

A.7 Each point on this graph represents the average error in interpolation associated the number of LUT points used. 198

A.8 Each point on this graph represents the average error in interpolation associated the number of LUT points used. 198

A.9 Each point on this graph represents the average error in interpolation associated the number of LUT points used. 199

A.10 Each point on this graph represents the average error in interpolation associated the number of LUT points used. 199

A.11 Each point on this graph represents the maximum of the difference matrix. 201

A.12 Each point on this graph represents the average error in interpolation associated the number of LUT points used. 201

A.13 Each point on this graph represents the maximum of the difference matrix. 202

A.14 Each point on this graph represents the average error in interpolation associated the number of LUT points used. 202

B.1 Test Scene 1a (zenith variation): The upper graph shows the blue path radiance obtained by MODTRAN, DIRSIG 4 and DIRSIG 3. The lower graph shows the percent error of DIRSIG 4 and DIRSIG 3 relative to MODTRAN. The RMS errors for the points shown on the graph are listed below the graphs. 205

B.2 Test Scene 1a (zenith variation): The upper graph shows the green path radiance obtained by MODTRAN, DIRSIG 4 and DIRSIG 3. The lower graph shows the percent error of DIRSIG 4 and DIRSIG 3 relative to MODTRAN. The RMS errors for the points shown on the graph are listed below the graphs. 206

B.3 Test Scene 1a (zenith variation): The upper graph shows the red path radiance obtained by MODTRAN, DIRSIG 4 and DIRSIG 3. The lower graph shows the percent error of DIRSIG 4 and DIRSIG 3 relative to MODTRAN. The RMS errors for the points shown on the graph are listed below the graphs. 207

B.4 Test Scene 1a (zenith variation): The upper graph shows the NIR path radiance obtained by MODTRAN, DIRSIG 4 and DIRSIG 3. The lower graph shows the percent error of DIRSIG 4 and DIRSIG 3 relative to MODTRAN. The RMS errors for the points shown on the graph are listed below the graphs. 208

B.5 Test Scene 1a (zenith variation): The upper graph shows the thermal path radiance obtained by MODTRAN, DIRSIG 4 and DIRSIG 3. The lower graph shows the percent error of DIRSIG 4 and DIRSIG 3 relative to MODTRAN. The RMS errors for the points shown on the graph are listed below the graphs. 209

B.6 Test Scene 1a (zenith variation): The upper graph shows the blue path transmission obtained by MODTRAN, DIRSIG 4 and DIRSIG 3. The lower graph shows the percent error of DIRSIG 4 and DIRSIG 3 relative to MODTRAN. The RMS errors for the points shown on the graph are listed below the graphs. 210

B.7 Test Scene 1a (zenith variation): The upper graph shows the green path transmission obtained by MODTRAN, DIRSIG 4 and DIRSIG 3. The lower graph shows the percent error of DIRSIG 4 and DIRSIG 3 relative to MODTRAN. The RMS errors for the points shown on the graph are listed below the graphs. 211

B.8 Test Scene 1a (zenith variation): The upper graph shows the red path transmission obtained by MODTRAN, DIRSIG 4 and DIRSIG 3. The lower graph shows the percent error of DIRSIG 4 and DIRSIG 3 relative to MODTRAN. The RMS errors for the points shown on the graph are listed below the graphs. 212

B.9 Test Scene 1a (zenith variation): The upper graph shows the NIR path transmission obtained by MODTRAN, DIRSIG 4 and DIRSIG 3. The lower graph shows the percent error of DIRSIG 4 and DIRSIG 3 relative to MODTRAN. The RMS errors for the points shown on the graph are listed below the graphs. 213

B.10 Test Scene 1a (zenith variation): The upper graph shows the thermal path transmission obtained by MODTRAN, DIRSIG 4 and DIRSIG 3. The lower graph shows the percent error of DIRSIG 4 and DIRSIG 3 relative to MODTRAN. The RMS errors for the points shown on the graph are listed below the graphs. 214

B.11 Test Scene 1a (azimuth variation): The upper graph shows the blue path radiance obtained by MODTRAN, DIRSIG 4 and DIRSIG 3. The lower graph shows the percent error of DIRSIG 4 and DIRSIG 3 relative to MODTRAN. The RMS errors for the points shown on the graph are listed below the graphs. 215

B.12 Test Scene 1a (azimuth variation): The upper graph shows the green path radiance obtained by MODTRAN, DIRSIG 4 and DIRSIG 3. The lower graph shows the percent error of DIRSIG 4 and DIRSIG 3 relative to MODTRAN. The RMS errors for the points shown on the graph are listed below the graphs. 216

B.13 Test Scene 1a (azimuth variation): The upper graph shows the red path radiance obtained by MODTRAN, DIRSIG 4 and DIRSIG 3. The lower graph shows the percent error of DIRSIG 4 and DIRSIG 3 relative to MODTRAN. The RMS errors for the points shown on the graph are listed below the graphs. 217

B.14 Test Scene 1a (azimuth variation): The upper graph shows the NIR path radiance obtained by MODTRAN, DIRSIG 4 and DIRSIG 3. The lower graph shows the percent error of DIRSIG 4 and DIRSIG 3 relative to MODTRAN. The RMS errors for the points shown on the graph are listed below the graphs. 218

B.15 Test Scene 1a (azimuth variation): The upper graph shows the blue path transmission obtained by MODTRAN, DIRSIG 4 and DIRSIG 3. The lower graph shows the percent error of DIRSIG 4 and DIRSIG 3 relative to MODTRAN. The RMS errors for the points shown on the graph are listed below the graphs. 219

B.16 Test Scene 1a (azimuth variation): The upper graph shows the green path transmission obtained by MODTRAN, DIRSIG 4 and DIRSIG 3. The lower graph shows the percent error of DIRSIG 4 and DIRSIG 3 relative to MODTRAN. The RMS errors for the points shown on the graph are listed below the graphs. 220

B.17 Test Scene 1a (azimuth variation): The upper graph shows the red path transmission obtained by MODTRAN, DIRSIG 4 and DIRSIG 3. The lower graph shows the percent error of DIRSIG 4 and DIRSIG 3 relative to MODTRAN. The RMS errors for the points shown on the graph are listed below the graphs. 221

B.18 Test Scene 1a (azimuth variation): The upper graph shows the NIR path transmission obtained by MODTRAN, DIRSIG 4 and DIRSIG 3. The lower graph shows the percent error of DIRSIG 4 and DIRSIG 3 relative to MODTRAN. The RMS errors for the points shown on the graph are listed below the graphs. 222

B.19 The dots represent points analyzed in the image. 223

B.20 The RMS error in radiance for each band in image 1a. 223

B.21 The RMS error in transmission for each band in image 1a. 224

B.22 Test Scene 1b (zenith variation): The upper graph shows the blue path radiance obtained by MODTRAN, DIRSIG 4 and DIRSIG 3. The lower graph shows the percent error of DIRSIG 4 and DIRSIG 3 relative to MODTRAN. The RMS errors for the points shown on the graph are listed below the graphs. 225

B.23 Test Scene 1b (zenith variation): The upper graph shows the green path radiance obtained by MODTRAN, DIRSIG 4 and DIRSIG 3. The lower graph shows the percent error of DIRSIG 4 and DIRSIG 3 relative to MODTRAN. The RMS errors for the points shown on the graph are listed below the graphs. 226

B.24 Test Scene 1b (zenith variation): The upper graph shows the red path radiance obtained by MODTRAN, DIRSIG 4 and DIRSIG 3. The lower graph shows the percent error of DIRSIG 4 and DIRSIG 3 relative to MODTRAN. The RMS errors for the points shown on the graph are listed below the graphs. 227

B.25 Test Scene 1b (zenith variation): The upper graph shows the NIR path radiance obtained by MODTRAN, DIRSIG 4 and DIRSIG 3. The lower graph shows the percent error of DIRSIG 4 and DIRSIG 3 relative to MODTRAN. The RMS errors for the points shown on the graph are listed below the graphs. 228

B.26 Test Scene 1b (zenith variation): The upper graph shows the thermal path radiance obtained by MODTRAN, DIRSIG 4 and DIRSIG 3. The lower graph shows the percent error of DIRSIG 4 and DIRSIG 3 relative to MODTRAN. The RMS errors for the points shown on the graph are listed below the graphs. 229

B.27 Test Scene 1b (azimuth variation): The upper graph shows the blue path radiance obtained by MODTRAN, DIRSIG 4 and DIRSIG 3. The lower graph shows the percent error of DIRSIG 4 and DIRSIG 3 relative to MODTRAN. The RMS errors for the points shown on the graph are listed below the graphs. 230

B.28 Test Scene 1b (azimuth variation): The upper graph shows the green path radiance obtained by MODTRAN, DIRSIG 4 and DIRSIG 3. The lower graph shows the percent error of DIRSIG 4 and DIRSIG 3 relative to MODTRAN. The RMS errors for the points shown on the graph are listed below the graphs. 231

B.29 Test Scene 1b (azimuth variation): The upper graph shows the red path radiance obtained by MODTRAN, DIRSIG 4 and DIRSIG 3. The lower graph shows the percent error of DIRSIG 4 and DIRSIG 3 relative to MODTRAN. The RMS errors for the points shown on the graph are listed below the graphs. 232

B.30 Test Scene 1b (azimuth variation): The upper graph shows the NIR path radiance obtained by MODTRAN, DIRSIG 4 and DIRSIG 3. The lower graph shows the percent error of DIRSIG 4 and DIRSIG 3 relative to MODTRAN. The RMS errors for the points shown on the graph are listed below the graphs. 233

B.31 A graphic representing the path radiance as seen from overhead. 234

B.32 A graphic representing the source of the asymmetry error in the DIRSIG 4 results. 234

B.33 The RMS error in radiance for each band in image 1b. 235

B.34 Test Scene 1c (zenith variation): The upper graph shows the blue path radiance obtained by MODTRAN, DIRSIG 4 and DIRSIG 3. The lower graph shows the percent error of DIRSIG 4 and DIRSIG 3 relative to MODTRAN. The RMS errors for the points shown on the graph are listed below the graphs. 236

B.35 Test Scene 1c (zenith variation): The upper graph shows the green path radiance obtained by MODTRAN, DIRSIG 4 and DIRSIG 3. The lower graph shows the percent error of DIRSIG 4 and DIRSIG 3 relative to MODTRAN. The RMS errors for the points shown on the graph are listed below the graphs. 237

B.36 Test Scene 1c (zenith variation): The upper graph shows the red path radiance obtained by MODTRAN, DIRSIG 4 and DIRSIG 3. The lower graph shows the percent error of DIRSIG 4 and DIRSIG 3 relative to MODTRAN. The RMS errors for the points shown on the graph are listed below the graphs. 238

B.37 Test Scene 1c (zenith variation): The upper graph shows the NIR path radiance obtained by MODTRAN, DIRSIG 4 and DIRSIG 3. The lower graph shows the percent error of DIRSIG 4 and DIRSIG 3 relative to MODTRAN. The RMS errors for the points shown on the graph are listed below the graphs. 239

B.38 Test Scene 1c (zenith variation): The upper graph shows the thermal path radiance obtained by MODTRAN, DIRSIG 4 and DIRSIG 3. The lower graph shows the percent error of DIRSIG 4 and DIRSIG 3 relative to MODTRAN. The RMS errors for the points shown on the graph are listed below the graphs. 240

B.39 Test Scene 1c (azimuth variation): The upper graph shows the blue path radiance obtained by MODTRAN, DIRSIG 4 and DIRSIG 3. The lower graph shows the percent error of DIRSIG 4 and DIRSIG 3 relative to MODTRAN. The RMS errors for the points shown on the graph are listed below the graphs. 241

B.40 Test Scene 1c (azimuth variation): The upper graph shows the green path radiance obtained by MODTRAN, DIRSIG 4 and DIRSIG 3. The lower graph shows the percent error of DIRSIG 4 and DIRSIG 3 relative to MODTRAN. The RMS errors for the points shown on the graph are listed below the graphs. 242

B.41 Test Scene 1c (azimuth variation): The upper graph shows the red path radiance obtained by MODTRAN, DIRSIG 4 and DIRSIG 3. The lower graph shows the percent error of DIRSIG 4 and DIRSIG 3 relative to MODTRAN. The RMS errors for the points shown on the graph are listed below the graphs. 243

B.42 Test Scene 1c (azimuth variation): The upper graph shows the NIR path radiance obtained by MODTRAN, DIRSIG 4 and DIRSIG 3. The lower graph shows the percent error of DIRSIG 4 and DIRSIG 3 relative to MODTRAN. The RMS errors for the points shown on the graph are listed below the graphs. 244

B.43 The RMS error in radiance for each band in image 1c. 245

B.44 Test Scene 1a_urban (azimuth variation): The upper graph shows the blue path radiance obtained by MODTRAN, DIRSIG 4 and DIRSIG 3. The lower graph shows the percent error of DIRSIG 4 and DIRSIG 3 relative to MODTRAN. The RMS errors for the points shown on the graph are listed below the graphs. 246

B.45 Test Scene 1a_urban (azimuth variation): The upper graph shows the green path radiance obtained by MODTRAN, DIRSIG 4 and DIRSIG 3. The lower graph shows the percent error of DIRSIG 4 and DIRSIG 3 relative to MODTRAN. The RMS errors for the points shown on the graph are listed below the graphs. 247

B.46 Test Scene 1a_urban (azimuth variation): The upper graph shows the red path radiance obtained by MODTRAN, DIRSIG 4 and DIRSIG 3. The lower graph shows the percent error of DIRSIG 4 and DIRSIG 3 relative to MODTRAN. The RMS errors for the points shown on the graph are listed below the graphs. 248

B.47 Test Scene 1a_urban (azimuth variation): The upper graph shows the NIR path radiance obtained by MODTRAN, DIRSIG 4 and DIRSIG 3. The lower graph shows the percent error of DIRSIG 4 and DIRSIG 3 relative to MODTRAN. The RMS errors for the points shown on the graph are listed below the graphs. 249

B.48 Test Scene 1a_urban (azimuth variation): The upper graph shows the thermal path radiance obtained by MODTRAN, DIRSIG 4 and DIRSIG 3. The lower graph shows the percent error of DIRSIG 4 and DIRSIG 3 relative to MODTRAN. The RMS errors for the points shown on the graph are listed below the graphs. 250

B.49 Test Scene 1a_urban (azimuth variation): The upper graph shows the blue path transmission obtained by MODTRAN, DIRSIG 4 and DIRSIG 3. The lower graph shows the percent error of DIRSIG 4 and DIRSIG 3 relative to MODTRAN. The RMS errors for the points shown on the graph are listed below the graphs. 251

B.50 Test Scene 1a_urban (azimuth variation): The upper graph shows the green path transmission obtained by MODTRAN, DIRSIG 4 and DIRSIG 3. The lower graph shows the percent error of DIRSIG 4 and DIRSIG 3 relative to MODTRAN. The RMS errors for the points shown on the graph are listed below the graphs. 252

B.51 Test Scene 1a_urban (azimuth variation): The upper graph shows the red path transmission obtained by MODTRAN, DIRSIG 4 and DIRSIG 3. The lower graph shows the percent error of DIRSIG 4 and DIRSIG 3 relative to MODTRAN. The RMS errors for the points shown on the graph are listed below the graphs. 253

B.52 Test Scene 1a_urban (azimuth variation): The upper graph shows the NIR path transmission obtained by MODTRAN, DIRSIG 4 and DIRSIG 3. The lower graph shows the percent error of DIRSIG 4 and DIRSIG 3 relative to MODTRAN. The RMS errors for the points shown on the graph are listed below the graphs. 254

B.53 Test Scene 1a_urban (azimuth variation): The upper graph shows the thermal path transmission obtained by MODTRAN, DIRSIG 4 and DIRSIG 3. The lower graph shows the percent error of DIRSIG 4 and DIRSIG 3 relative to MODTRAN. The RMS errors for the points shown on the graph are listed below the graphs. 255

B.54 The RMS error in radiance for each band in image 1a_urban. 256

B.55 The RMS error in transmission for each band in image 1a_urban. 257

B.56 The dots represent points analyzed in the image. 258

B.57 Test Scene 2a (altitude variation): The upper graph shows the blue path radiance obtained by MODTRAN, DIRSIG 4 and DIRSIG 3. The lower graph shows the percent error of DIRSIG 4 and DIRSIG 3 relative to MODTRAN. The RMS errors for the points shown on the graph are listed below the graphs. 259

B.58 Test Scene 2a (altitude variation): The upper graph shows the green path radiance obtained by MODTRAN, DIRSIG 4 and DIRSIG 3. The lower graph shows the percent error of DIRSIG 4 and DIRSIG 3 relative to MODTRAN. The RMS errors for the points shown on the graph are listed below the graphs. 260

B.59 Test Scene 2a (altitude variation): The upper graph shows the red path radiance obtained by MODTRAN, DIRSIG 4 and DIRSIG 3. The lower graph shows the percent error of DIRSIG 4 and DIRSIG 3 relative to MODTRAN. The RMS errors for the points shown on the graph are listed below the graphs. 261

B.60 Test Scene 2a (altitude variation): The upper graph shows the NIR path radiance obtained by MODTRAN, DIRSIG 4 and DIRSIG 3. The lower graph shows the percent error of DIRSIG 4 and DIRSIG 3 relative to MODTRAN. The RMS errors for the points shown on the graph are listed below the graphs. 262

B.61 Test Scene 2a (altitude variation): The upper graph shows the thermal path radiance obtained by MODTRAN, DIRSIG 4 and DIRSIG 3. The lower graph shows the percent error of DIRSIG 4 and DIRSIG 3 relative to MODTRAN. The RMS errors for the points shown on the graph are listed below the graphs. 263

B.62 Test Scene 2a (altitude variation): The upper graph shows the blue path transmission obtained by MODTRAN, DIRSIG 4 and DIRSIG 3. The lower graph shows the percent error of DIRSIG 4 and DIRSIG 3 relative to MODTRAN. The RMS errors for the points shown on the graph are listed below the graphs. 264

B.63 Test Scene 2a (altitude variation): The upper graph shows the green path transmission obtained by MODTRAN, DIRSIG 4 and DIRSIG 3. The lower graph shows the percent error of DIRSIG 4 and DIRSIG 3 relative to MODTRAN. The RMS errors for the points shown on the graph are listed below the graphs. 265

B.64 Test Scene 2a (altitude variation): The upper graph shows the red path transmission obtained by MODTRAN, DIRSIG 4 and DIRSIG 3. The lower graph shows the percent error of DIRSIG 4 and DIRSIG 3 relative to MODTRAN. The RMS errors for the points shown on the graph are listed below the graphs. 266

B.65 Test Scene 2a (altitude variation): The upper graph shows the NIR path transmission obtained by MODTRAN, DIRSIG 4 and DIRSIG 3. The lower graph shows the percent error of DIRSIG 4 and DIRSIG 3 relative to MODTRAN. The RMS errors for the points shown on the graph are listed below the graphs. 267

B.66 Test Scene 2a (altitude variation): The upper graph shows the thermal path transmission obtained by MODTRAN, DIRSIG 4 and DIRSIG 3. The lower graph shows the percent error of DIRSIG 4 and DIRSIG 3 relative to MODTRAN. The RMS errors for the points shown on the graph are listed below the graphs. 268

B.67 The RMS error in radiance for each band in image 2a. 269

B.68 The RMS error in transmission for each band in image 2a. 270

B.69 Test Scene 2b (altitude variation): The upper graph shows the blue path radiance obtained by MODTRAN, DIRSIG 4 and DIRSIG 3. The lower graph shows the percent error of DIRSIG 4 and DIRSIG 3 relative to MODTRAN. The RMS errors for the points shown on the graph are listed below the graphs. 271

B.70 Test Scene 2b (altitude variation): The upper graph shows the green path radiance obtained by MODTRAN, DIRSIG 4 and DIRSIG 3. The lower graph shows the percent error of DIRSIG 4 and DIRSIG 3 relative to MODTRAN. The RMS errors for the points shown on the graph are listed below the graphs. 272

B.71 Test Scene 2b (altitude variation): The upper graph shows the red path radiance obtained by MODTRAN, DIRSIG 4 and DIRSIG 3. The lower graph shows the percent error of DIRSIG 4 and DIRSIG 3 relative to MODTRAN. The RMS errors for the points shown on the graph are listed below the graphs. 273

B.72 Test Scene 2b (altitude variation): The upper graph shows the NIR path radiance obtained by MODTRAN, DIRSIG 4 and DIRSIG 3. The lower graph shows the percent error of DIRSIG 4 and DIRSIG 3 relative to MODTRAN. The RMS errors for the points shown on the graph are listed below the graphs. 274

B.73 Test Scene 2b (altitude variation): The upper graph shows the thermal path radiance obtained by MODTRAN, DIRSIG 4 and DIRSIG 3. The lower graph shows the percent error of DIRSIG 4 and DIRSIG 3 relative to MODTRAN. The RMS errors for the points shown on the graph are listed below the graphs. 275

B.74 The RMS error in radiance for each band in image 2b. 276

B.75 Test Scene 2c (altitude variation): The upper graph shows the blue path radiance obtained by MODTRAN, DIRSIG 4 and DIRSIG 3. The lower graph shows the percent error of DIRSIG 4 and DIRSIG 3 relative to MODTRAN. The RMS errors for the points shown on the graph are listed below the graphs. 277

B.76 Test Scene 2c (altitude variation): The upper graph shows the green path radiance obtained by MODTRAN, DIRSIG 4 and DIRSIG 3. The lower graph shows the percent error of DIRSIG 4 and DIRSIG 3 relative to MODTRAN. The RMS errors for the points shown on the graph are listed below the graphs. 278

B.77 Test Scene 2c (altitude variation): The upper graph shows the red path radiance obtained by MODTRAN, DIRSIG 4 and DIRSIG 3. The lower graph shows the percent error of DIRSIG 4 and DIRSIG 3 relative to MODTRAN. The RMS errors for the points shown on the graph are listed below the graphs. 279

B.78 Test Scene 2c (altitude variation): The upper graph shows the NIR path radiance obtained by MODTRAN, DIRSIG 4 and DIRSIG 3. The lower graph shows the percent error of DIRSIG 4 and DIRSIG 3 relative to MODTRAN. The RMS errors for the points shown on the graph are listed below the graphs. 280

B.79 Test Scene 2c (altitude variation): The upper graph shows the thermal path radiance obtained by MODTRAN, DIRSIG 4 and DIRSIG 3. The lower graph shows the percent error of DIRSIG 4 and DIRSIG 3 relative to MODTRAN. The RMS errors for the points shown on the graph are listed below the graphs. 281

B.80 The RMS error in radiance for each band in image 2c. 282

B.81 The path radiance of image 3 in the 'water2' band (940 nm), rendered by DIRSIG 4. 283

B.82 The path radiance of image 3 in the 'water2' band (940 nm), rendered by DIRSIG 4. 284

B.83 Test Scene 3 (water variation): The upper graph shows the blue path radiance obtained by MODTRAN, DIRSIG 4 and DIRSIG 3. The lower graph shows the percent error of DIRSIG 4 and DIRSIG 3 relative to MODTRAN. The RMS errors for the points shown on the graph are listed below the graphs. 285

B.84 Test Scene 3 (water variation): The upper graph shows the green path radiance obtained by MODTRAN, DIRSIG 4 and DIRSIG 3. The lower graph shows the percent error of DIRSIG 4 and DIRSIG 3 relative to MODTRAN. The RMS errors for the points shown on the graph are listed below the graphs. 286

B.85 Test Scene 3 (water variation): The upper graph shows the red path radiance obtained by MODTRAN, DIRSIG 4 and DIRSIG 3. The lower graph shows the percent error of DIRSIG 4 and DIRSIG 3 relative to MODTRAN. The RMS errors for the points shown on the graph are listed below the graphs. 287

B.86 Test Scene 3 (water variation): The upper graph shows the NIR path radiance obtained by MODTRAN, DIRSIG 4 and DIRSIG 3. The lower graph shows the percent error of DIRSIG 4 and DIRSIG 3 relative to MODTRAN. The RMS errors for the points shown on the graph are listed below the graphs. 288

B.87 Test Scene 3 (water variation): The upper graph shows the water2 path radiance obtained by MODTRAN, DIRSIG 4 and DIRSIG 3. The lower graph shows the percent error of DIRSIG 4 and DIRSIG 3 relative to MODTRAN. The RMS errors for the points shown on the graph are listed below the graphs. 289

B.88 Test Scene 3 (water variation): The upper graph shows the Thermal path radiance obtained by MODTRAN, DIRSIG 4 and DIRSIG 3. The lower graph shows the percent error of DIRSIG 4 and DIRSIG 3 relative to MODTRAN. The RMS errors for the points shown on the graph are listed below the graphs. 290

B.89 Test Scene 3 (water variation): The upper graph shows the blue path transmission obtained by MODTRAN, DIRSIG 4 and DIRSIG 3. The lower graph shows the percent error of DIRSIG 4 and DIRSIG 3 relative to MODTRAN. The RMS errors for the points shown on the graph are listed below the graphs. 291

B.90 Test Scene 3 (water variation): The upper graph shows the green path transmission obtained by MODTRAN, DIRSIG 4 and DIRSIG 3. The lower graph shows the percent error of DIRSIG 4 and DIRSIG 3 relative to MODTRAN. The RMS errors for the points shown on the graph are listed below the graphs. 292

B.91 Test Scene 3 (water variation): The upper graph shows the red path transmission obtained by MODTRAN, DIRSIG 4 and DIRSIG 3. The lower graph shows the percent error of DIRSIG 4 and DIRSIG 3 relative to MODTRAN. The RMS errors for the points shown on the graph are listed below the graphs. 293

B.92 Test Scene 3 (water variation): The upper graph shows the NIR path transmission obtained by MODTRAN, DIRSIG 4 and DIRSIG 3. The lower graph shows the percent error of DIRSIG 4 and DIRSIG 3 relative to MODTRAN. The RMS errors for the points shown on the graph are listed below the graphs. 294

B.93 Test Scene 3 (water variation): The upper graph shows the water2 path transmission obtained by MODTRAN, DIRSIG 4 and DIRSIG 3. The lower graph shows the percent error of DIRSIG 4 and DIRSIG 3 relative to MODTRAN. The RMS errors for the points shown on the graph are listed below the graphs. 295

B.94 Test Scene 3 (water variation): The upper graph shows the Thermal path transmission obtained by MODTRAN, DIRSIG 4 and DIRSIG 3. The lower graph shows the percent error of DIRSIG 4 and DIRSIG 3 relative to MODTRAN. The RMS errors for the points shown on the graph are listed below the graphs. 296

B.95 The RMS error in radiance for each band in image 3. 297

B.96 The RMS error in transmission for each band in image 3. 298

B.97 The RGB path radiance of test image 4a rendered by DIRSIG 4. 299

B.98 Test Scene 4a (visibility variation): The upper graph shows the blue path radiance obtained by MODTRAN, DIRSIG 4 and DIRSIG 3. The lower graph shows the percent error of DIRSIG 4 and DIRSIG 3 relative to MODTRAN. The RMS errors for the points shown on the graph are listed below the graphs. 300

B.99 Test Scene 4a (visibility variation): The upper graph shows the green path radiance obtained by MODTRAN, DIRSIG 4 and DIRSIG 3. The lower graph shows the percent error of DIRSIG 4 and DIRSIG 3 relative to MODTRAN. The RMS errors for the points shown on the graph are listed below the graphs. 301

B.100Test Scene 4a (visibility variation): The upper graph shows the red path radiance obtained by MODTRAN, DIRSIG 4 and DIRSIG 3. The lower graph shows the percent error of DIRSIG 4 and DIRSIG 3 relative to MODTRAN. The RMS errors for the points shown on the graph are listed below the graphs. 302

B.101Test Scene 4a (visibility variation): The upper graph shows the NIR path radiance obtained by MODTRAN, DIRSIG 4 and DIRSIG 3. The lower graph shows the percent error of DIRSIG 4 and DIRSIG 3 relative to MODTRAN. The RMS errors for the points shown on the graph are listed below the graphs. 303

B.102 Test Scene 4a (visibility variation): The upper graph shows the water2 path radiance obtained by MODTRAN, DIRSIG 4 and DIRSIG 3. The lower graph shows the percent error of DIRSIG 4 and DIRSIG 3 relative to MODTRAN. The RMS errors for the points shown on the graph are listed below the graphs. 304

B.103 Test Scene 4a (visibility variation): The upper graph shows the Thermal path radiance obtained by MODTRAN, DIRSIG 4 and DIRSIG 3. The lower graph shows the percent error of DIRSIG 4 and DIRSIG 3 relative to MODTRAN. The RMS errors for the points shown on the graph are listed below the graphs. 305

B.104 Test Scene 4a (visibility variation): The upper graph shows the blue path transmission obtained by MODTRAN, DIRSIG 4 and DIRSIG 3. The lower graph shows the percent error of DIRSIG 4 and DIRSIG 3 relative to MODTRAN. The RMS errors for the points shown on the graph are listed below the graphs. 306

B.105 Test Scene 4a (visibility variation): The upper graph shows the green path transmission obtained by MODTRAN, DIRSIG 4 and DIRSIG 3. The lower graph shows the percent error of DIRSIG 4 and DIRSIG 3 relative to MODTRAN. The RMS errors for the points shown on the graph are listed below the graphs. 307

B.106 Test Scene 4a (visibility variation): The upper graph shows the red path transmission obtained by MODTRAN, DIRSIG 4 and DIRSIG 3. The lower graph shows the percent error of DIRSIG 4 and DIRSIG 3 relative to MODTRAN. The RMS errors for the points shown on the graph are listed below the graphs. 308

B.107 Test Scene 4a (visibility variation): The upper graph shows the NIR path transmission obtained by MODTRAN, DIRSIG 4 and DIRSIG 3. The lower graph shows the percent error of DIRSIG 4 and DIRSIG 3 relative to MODTRAN. The RMS errors for the points shown on the graph are listed below the graphs. 309

B.108 Test Scene 4a (visibility variation): The upper graph shows the water2 path transmission obtained by MODTRAN, DIRSIG 4 and DIRSIG 3. The lower graph shows the percent error of DIRSIG 4 and DIRSIG 3 relative to MODTRAN. The RMS errors for the points shown on the graph are listed below the graphs. 310

B.109 Test Scene 4a (visibility variation): The upper graph shows the Thermal path transmission obtained by MODTRAN, DIRSIG 4 and DIRSIG 3. The lower graph shows the percent error of DIRSIG 4 and DIRSIG 3 relative to MODTRAN. The RMS errors for the points shown on the graph are listed below the graphs. 311

B.110 The RMS error in radiance for each band in image 4a. 312

B.111 The RMS error in transmission for each band in image 4a. 313

B.112 The RMS error in radiance for each band in image 5a. 314

B.113 The RMS error in transmission for each band in image 5a. 315

Chapter 1

Background

Contents

1.1 Image Modeling 25
1.2 Motivation 26
1.3 The Remote Sensing Equation 26
1.3.1 The Effect of Inhomogeneities on the Remote Sensing Equation 30
1.4 Overview of DIRSIG 31
1.4.1 Image Rendering 31
1.4.2 Function of the Atmospheric Database (ADB) 32
1.4.3 Structure of the ADB 33
1.4.4 ADB Construction 35

1.1 Image Modeling

In the field of remote sensing, image modeling has become an important area of study. A properly rendered image can provide the user with valuable information, such as the ground truth of a scene, the behavior of the atmosphere, and the performance of a given sensor. Image modeling has many uses, including photo-interpretation training and the evaluation of atmospheric algorithms and proposed new imaging systems.

Image modeling has many advantages, such as the complete control over the factors which influence the resulting image. This allows the user to precisely know, for example, the ground truth in the case of evaluating an atmospheric algorithm. Having the ability to customize the atmosphere allows the user to test multiple trials of the algorithm on the same scene with different atmospheres. In the case of evaluating a theoretical imaging system, image modeling provides a very valuable diagnostic of specific components of the system. Considerable resources can be saved in assuring that a system can perform as expected before any physical components are built.

DIRSIG (Digital Imaging and Remote Sensing Image Generation) is image modeling software developed by the remote sensing laboratory (DIRS - Digital Imaging and Remote Sensing) of RIT's Center for Imaging Science. It is an attempt to synthesize an image using a physics based model. It accounts for everything involved with the image chain, from the material in the scene, including textures and transmissivity, to atmospheric properties, to focal plane response and noise.

1.2 Motivation

The use of modeling mentioned above which will benefit the most from this work is the testing of atmospheric algorithms. Giving DIRSIG the ability to model atmospheres with horizontally varying atmospheric properties will make the DIRSIG atmosphere more realistic. The results of testing hyperspectral atmospheric algorithms will, therefore, be more accurate.

The overall goal of these atmospheric algorithms is, generally, to derive the reflectance of the pixels in the scene. Once the reflectance of a pixel is known, the ability to decipher what material it consists of is increased. The performance of these algorithms can be greatly dependent on the constituents of the atmosphere.

Two such constituents are water vapor and aerosols (fine particles in the atmosphere). Water vapor is practically omnipresent in the atmosphere. Ignoring it can lead to significant errors in the performance of algorithms [5]. As well, the presence of aerosols can affect the ability of an algorithm to derive reflectances [4]. Even image classification, the attempt to automatically or semi-automatically assign pixels to a material class based on their reflectivity, can be hindered by the presence of these atmospheric species [3]. Some of these atmospheric algorithms use the water vapor and/or aerosols in the atmosphere to aid in the derivation of the reflectance image [2]. Therefore, it is essential that these species, and their radiometric effect on an image are modeled accurately. Allowing for horizontally varying spatial structures with these species is essential to mimic their natural behavior. As a result of this work, DIRSIG will have this ability to incorporate horizontally varying aerosol and water vapor properties.

1.3 The Remote Sensing Equation

In modeling what a sensor detects from the real world, it is important to account for as many interactions as possible in order to achieve high fidelity. Quantifying this detected energy (sensor-reaching radiance) directly from fundamental physics equations is one way of accomplishing this. The various photon paths which are accounted for in DIRSIG are shown in figure 1.1.

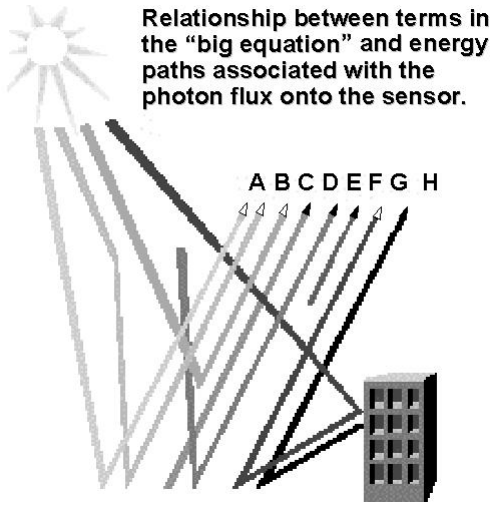

Figure 1.1: This shows the possible paths a photon could take to significantly affect the radiance reaching a given sensor. It is important to account for all of these paths in rendering an image in order to accurately model the real world. [8]

Eq. 1.1 gives the total radiance arriving at a sensor, L, which is a sum of all these photon paths.

$$L = L_A + L_B + L_D + L_E + L_G + L_H + L_C + L_F \tag{1.1}$$

Here, L represents the total radiance reaching the sensor for a given scene. Each term represents the contribution of the photons from the various paths, as seen in figure 1.1. [8]

The terms in equation 1.1 can be separated into two groups; the solar terms and the thermal terms. The solar terms deal with the photons from the sun (mainly from the visible spectrum, out to about 2.5 microns), and the thermal terms deal with photons which originate from the Earth, atmosphere, or the surrounding objects. These two regions of the EM spectrum can be separated when observing the Earth because of the nature of the sources. (It should be noted that all of these terms are spectral in nature.)

The paths for the solar and thermal photons are shown in figures 1.2 and 1.3, respectively. For the solar photons, those photons with a wavelength between approximately 0.4 and 2.5 microns, the sun is the major contributor of these photons. Although it is true that the sun emits photons in what is considered to be the thermal window of the spectrum (8 - 14 microns), the number reaching the Earth is insignificant when compared to what objects at ambient temperature radiate at these wavelengths. For example, for a 10% reflector at 300 K, only one photon in four or five thousand will be from the sun. In the solar, or reflective region, a similar, but opposite, effect occurs. The number of photons in the reflective region emitted by the Earth is negligible when compared to that of the sun. [8]

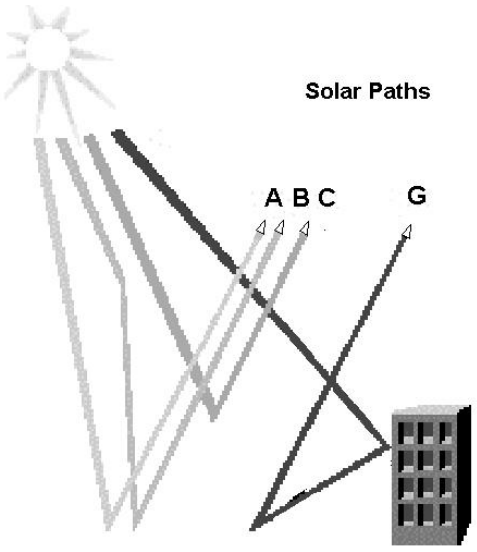

Figure 1.2: The solar photon paths of the Big Equation.[8]

If Eq. 1.1 is broken down, photon paths A and D can be considered the "direct" paths. Path 'A' comes from the sun, reflects off of the target, and then reaches sensor. Path 'D' represents the energy radiated directly from the target to the sensor (self emitted).

The radiance due to 'A' photons can be represented by equation 1.2 [8]

$$L_A = E_s \tau_1 \cos\sigma (r/\pi) \tau_2 \tag{1.2}$$

Here,

- E_s is the exoatmospheric solar irradiance
- τ_1 is the transmission of the atmosphere, from space to the target
- σ is the solar declination angle, with respect to nadir.
- r is the reflectivity of the target
- τ_2 is the transmission from the ground up to the sensor

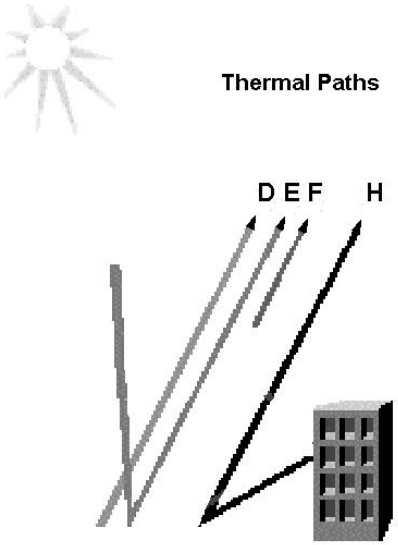

Figure 1.3: The thermal photon paths of the Big Equation. [8]

In the above equation (Equation 1.2), π can be thought of as a "conversion" factor so the term is in the correct units of radiance. For more on this topic, the reader is referred to the "Magic Pi" derivation by Schott [8].

The radiance from the next photon path, 'D' can be expressed as shown in equation 1.3.

$$L_D = \varepsilon L_T \tau_2 \tag{1.3}$$

Here, ε is the emissivity of the target in the thermal, and L_T is the thermal upwelled radiance self emitted from the target. The transmission from the target to the sensor is τ_2.

Photon paths 'B' and 'E' can be considered downwelled paths. 'B' photons originate at the sun, pass though the atmosphere, scatter in the atmosphere on the way down, reflect off of the target, and then reach the sensor. 'E' photons are similar, but they originate in the atmosphere. The atmosphere emits photons in the thermal region which reflect off of the target and reach the sensor.

Mathematically, the radiance can be defined for the 'B' photons as:

$$L_B = F L_{ds} r_d \tau_2 \tag{1.4}$$

A new term is introduced here, F. This is the shape factor. This can be thought of as the fraction of sky that a given pixel "sees". For example, if a pixel was in a scene with no objects, and could "see" the entire sky dome, it would have a shape factor of 1. If it happened to be next to a very tall building or other object, then the shape factor would be close to 0.5, for it could only "see" about half of the sky dome. L_{ds} is the solar downwelled radiance striking the target. r_d is the diffuse reflectance of the target. This can be thought of as the total reflectivity of a material, with the specular component removed. (See [8] for a full description.) Again, the τ_2 factor is seen, representing the transmission from target to sensor.

The equation for the radiance of the 'E' photons (Eq. 1.5) is almost identical. The only difference is that the downwelling radiance term is a result of self emission from the atmosphere, instead of solar scattering.

$$L_E = F L_{d\varepsilon} r_d \tau_2 \tag{1.5}$$

'G' and 'H' photons are photons which interact with the surrounding non-target objects. The 'G' photon

originates at the sun, reflects off of a nearby object, reflects off of the target, and then reaches the sensor. Again, the 'H' photon is similar, but it is emitted from the nearby object, and follows the same general path.

Equation 1.6 defines 'G' photons.

$$L_G = (1 - F)L_{bs}r_d\tau_2 \tag{1.6}$$

Here, again, is the shape factor. However, the term is multiplied by the factor $(1 - F)$. This factor can be thought of as how much of the sky dome the surrounding objects occupy. Logic follows that if F is the fraction of *clear* sky the pixel sees, then the term $(1 - F)$ is the fraction of obscured sky. L_{bs} is the reflected background radiance, which is the solar radiance reflected off the background object. This is all multiplied by the transmission term, τ_2.

Similarly, equation 1.7 defines 'H' photons.

$$L_H = (1 - F)L_{b\varepsilon}r_d\tau_2 \tag{1.7}$$

The only difference is that the background radiance term is emitted, not reflected. The argument for the presence of the $(1 - F)$ is the same.

Finally, the 'C' and 'F' photon paths are known as the upwelling paths. These only interact with the atmosphere, not reflecting off of any target or object. 'C' photons are the solar photons, starting at the sun and scattering in the atmosphere. 'F' photons are emitted directly from the atmosphere to the sensor. [8] The equations for these last two photon paths are the simplest. They are shown in equations 1.8 and 1.9, respectively.

$$L_C = L_{us} \tag{1.8}$$

$$L_F = L_{u\varepsilon} \tag{1.9}$$

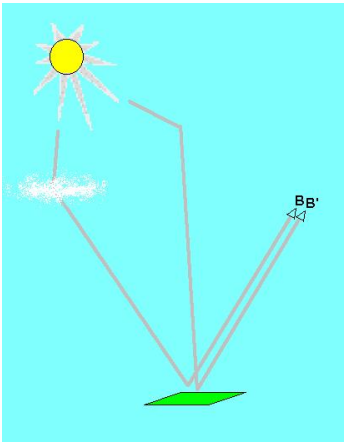

Figure 1.4: The effect of inhomogeneities in the atmosphere on different photon paths.

1.3.1 The Effect of Inhomogeneities on the Remote Sensing Equation

The addition of inhomogeneities in the atmosphere can significantly alter the values from these paths. For example, consider two different 'B' path photon rays that have different trajectories, but that both reach the detector, and both travel through an optically identical atmosphere. In rendering an image, the two most important values are the path transmission, and the path radiance. Therefore, understanding these paths is essential for accurate modeling. Transmission can be thought of as the fraction of photons at a given wavelength which travel the entire path and are not scattered or absorbed. Path radiance is the amount of energy which is scattered either towards the sensor (upwelled or upwelling radiance) or towards the target (downwelled or downwelling radiance).

DIRSIG uses ray tracers to simulate these photon paths. The atmospheric transmission and radiance values associated with various angles and geometries are stored in look up tables (LUTs). This structure and use of these LUTs and how they relate to ray tracing will be discussed in more detail later.

Under the current ray tracing scheme, these two rays would be treated very similarly, their values being taken from the same look up table. This look up table consists of a set of spectral data for each look angle. Within the spectral data, atmospheric properties such as path radiance and transmission are listed as a function of wavelength. The current method involves interpolating between the angles within this LUT to calculate various values needed for the sensor-reaching radiance calculation.

Now, if inhomogeneities are present, then each of these rays would travel through a unique atmosphere, with its own optical properties. This is displayed in figure 1.4. The current method of sampling only allows for one type of atmosphere. This would not allow for DIRSIG to compensate for the increased water vapor amount in path 'B'. Figure 1.5 shows the results of a MODTRAN run using a standard, mid-latitude winter atmosphere. The blue line represents the transmission of the atmosphere when no water is present, and the pink line shows the transmission with 1.37 grams of water per square centimeter. This shows that the effect of water vapor, although localized to absorption features, can have a significant effect on the atmospheric transmission.

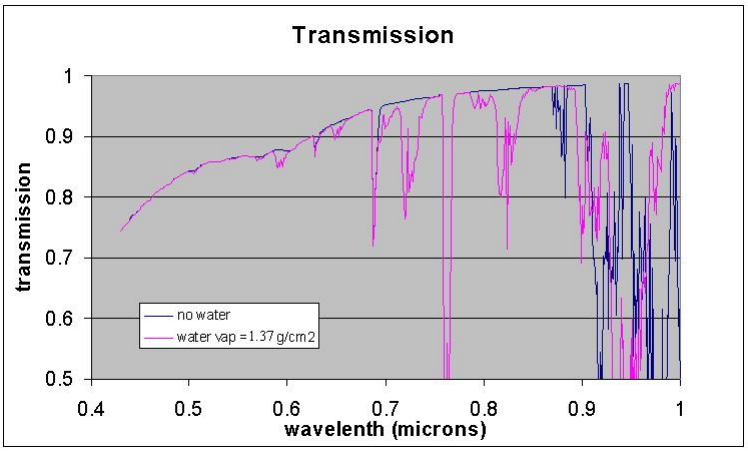

Figure 1.5: The transmission of a mid-latitude, winter atmosphere.

Aerosols, as well, can can have a dramatic effect on the transmission and path radiance. Figure 1.6 shows the atmospheric transmission of a MODTRAN mid-latitude winter atmosphere. The figure shows that the presence of aerosols can have a dramatic effect on the atmosphere.

So, from a radiometry point of view, these atmospheric species can significantly affect the values which are required for accurate image modeling. It is important to give DIRSIG the ability to model variabilities in these species.

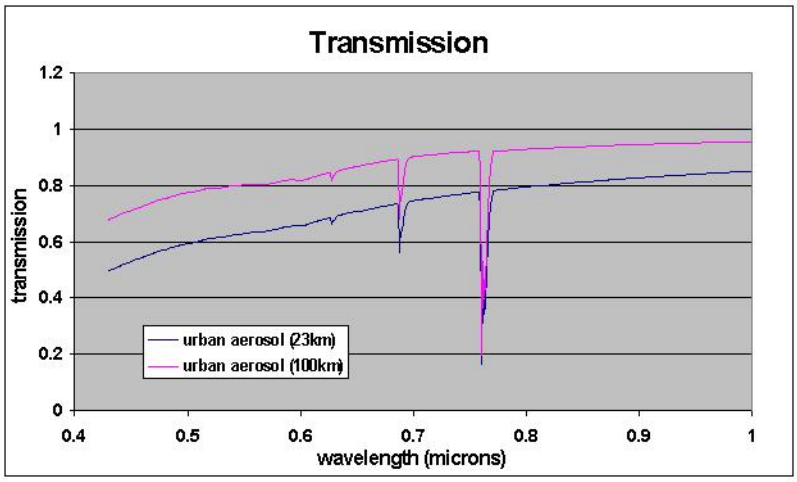

Figure 1.6: The transmission of a mid-latitude, winter atmosphere.

1.4 Overview of DIRSIG

Before going into how DIRSIG is to be modified, it is important to understand how DIRSIG works, the motivation behind it, and how it renders a synthetic image.

DIRSIG is the synthetic image generation tool created by the Digital Imaging and Remote Sensing (DIRS) group at RIT's Center for Imaging Science. It is used for a variety of applications from sensor design to photo-interpretation training [8]. In remote sensing there is a considerable amount of work done in the field of hyperspectral algorithms. Modeling, in general, provides a means to analyze and evaluate these algorithms. For example, if the atmospheric conditions are able to be controlled, along with other aspects of a synthetic scene, then there can be exact knowledge of the ground truth in the scene. Precisely knowing ground truth helps gauge the performance of these hyperspectral algorithms as a function of various environmental and imagery parameters.

The main drive behind the modeling of atmospheric inhomogeneities is that they can greatly affect the performance of these algorithms by adding considerable error. These "confusion factors" are essential if there is to be any analysis of these algorithms or how they work in realistic situations.

1.4.1 Image Rendering

This section will step through a very basic description of how DIRSIG renders an image. A simple framing array imaging system will be analyzed (see figure 1.7). DIRSIG uses ray tracing. A ray originates at the focus, and passes through the image plane, striking a spot on the virtual ground.

For each of these spots, DIRSIG first calculates the amount of energy (radiance) reaching the ground from the various sources. These sources can be celestial objects like the sun, moon, or even starlight. Or in the case of the thermal region, the Earth or nearby objects can be the source. DIRSIG also calculates the solar scattered and thermally emitted radiance which originates from the sky (downwelled radiance) or nearby objects and strikes the target.

In figure 1.1, this corresponds to photon paths A, B, G in the solar spectral region, and photon paths D, E and H in the thermal region.

DIRSIG then uses the material properties to determine the amount of energy that is reflected and/or emitted from the target in the direction of the sensor.

The amount of radiance heading towards the sensor from the target can then be established. DIRSIG then combines this energy with that of the upwelled photons. These are the photons that are either scattered off

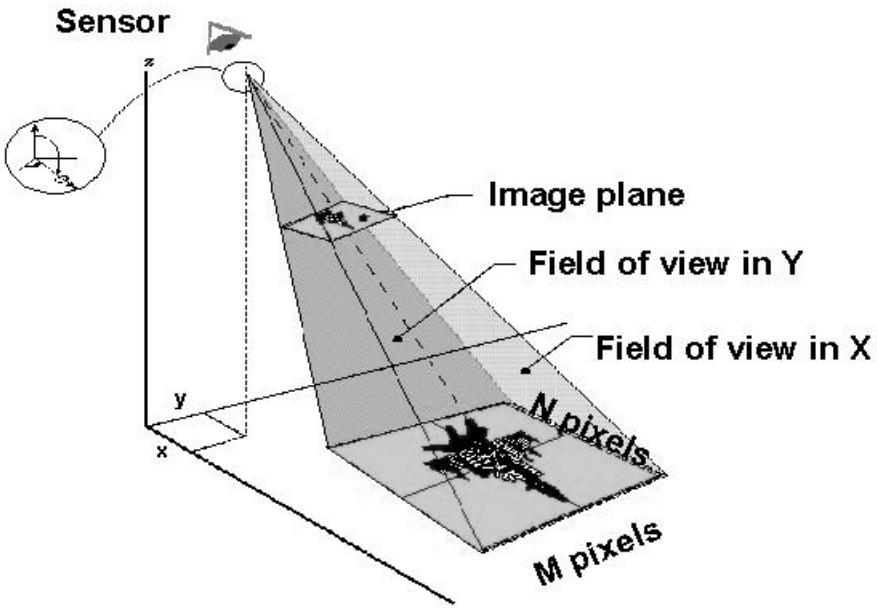

Figure 1.7: A simple framing array imaging system. [8]

of or emitted from the atmosphere towards the sensor. This set of photons is shown in figure 1.1 as photon paths C and F (solar and thermal, respectively).

Using the values for all of these paths, DIRSIG calculates the sensor-reaching radiance for the scene. (It should be noted that transmission losses for each of these paths is included.)

1.4.2 Function of the Atmospheric Database (ADB)

The procedure described in the previous section is the method by which DIRSIG renders a given pixel in a scene. For each one of these photon paths outlined above, DIRSIG needs to know properties of the atmosphere from a variety of angles and locations. In order to do this, DIRSIG references a look up table (LUT), which consists of outputs from MODTRAN. (This LUT is created before the image rendering process to eliminate the need for running MODTRAN as needed, which is very time-consuming.)

MODTRAN is an atmospheric propagation model developed by the Air Force Research Laboratory and Spectral Sciences, Inc., which yields transmission and path radiances between points in the atmosphere for a wide variety of atmospheric conditions.[1] MODTRAN is a well established atmospheric propagation tool in the remote sensing community.

The input file for MODTRAN is known as a tape5 file. (See Appendix F for a complete tape5 file.) This is a text file that contains values for a wide variety of atmospheric conditions, including geometric information such as look-angles, and radiation source positions. These atmospheric conditions simulate everything from temperature, humidity and precipitation to clouds, aerosols and even volcanic activity. [1].

The LUT that DIRSIG creates is known as the ADB, (the Atmospheric DataBase).

The DIRSIG ".cfg" (configuration) file contains all the information about the sensor and scene geometry. The ADB construction program will read in the ".cfg" file and calculate which specific look angles need to be run in MODTRAN. See figure 1.8 for a flow chart of the LUT construction procedure. A sample .cfg file is shown in Appendix D.

The program which creates the ADB then uses MODTRAN to generate a spectral block (a list of radiometric values for a number of wavelengths) for that specific look angle. This spectral block is then taken by the

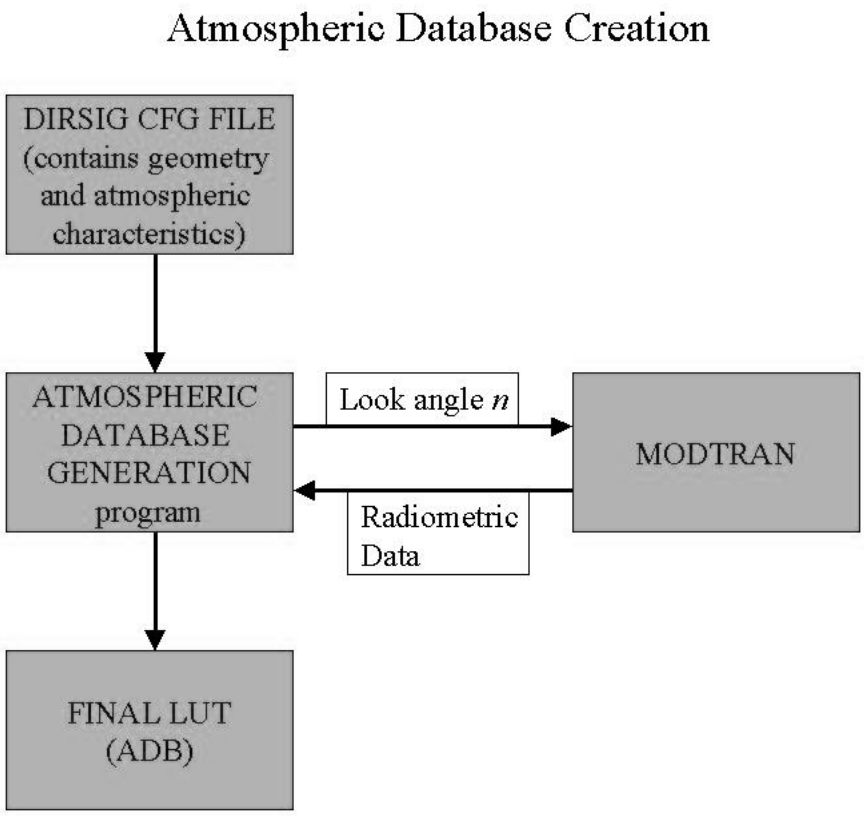

Figure 1.8: A flow chart showing the construction of the Atmospheric Database.

ADB construction file and placed in its output file, the ADB look up table.

1.4.3 Structure of the ADB

There are three main components of the ADB. The first part is a spectral block that MODTRAN calculates directly from the source (the sun or the moon). The next is a list of spectral blocks containing the upwelling (solar and thermal) radiance and transmission (from the ground to the sensor) at each wavelength, for a number of look angles. This will aid DIRSIG in the calculation of the contributions of the "C" and "F" photons in figure 1.1. The third part of the ADB contains a similar list of blocks containing downwelling radiance values, which account for the "B" and "E" photons. (The contributions from the remaining photon paths will be calculated during image rendering.) The downwelled section also contains a spectral block of the total integrated downwelling radiance from the sky dome. These radiometric component sections will be described in more detail in the following sub-sections.

Figure 1.9 shows the sections of the ADB. Figure 1.10 shows how these sections relate to the radiometric terms. For an example ADB file, see Appendix E.

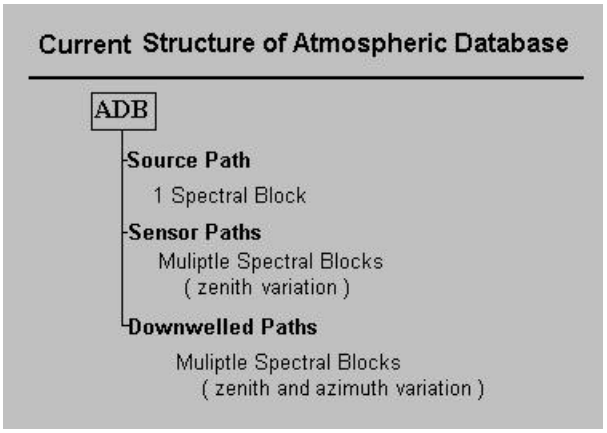

Figure 1.9: The general structure of the current Atmospheric Database.

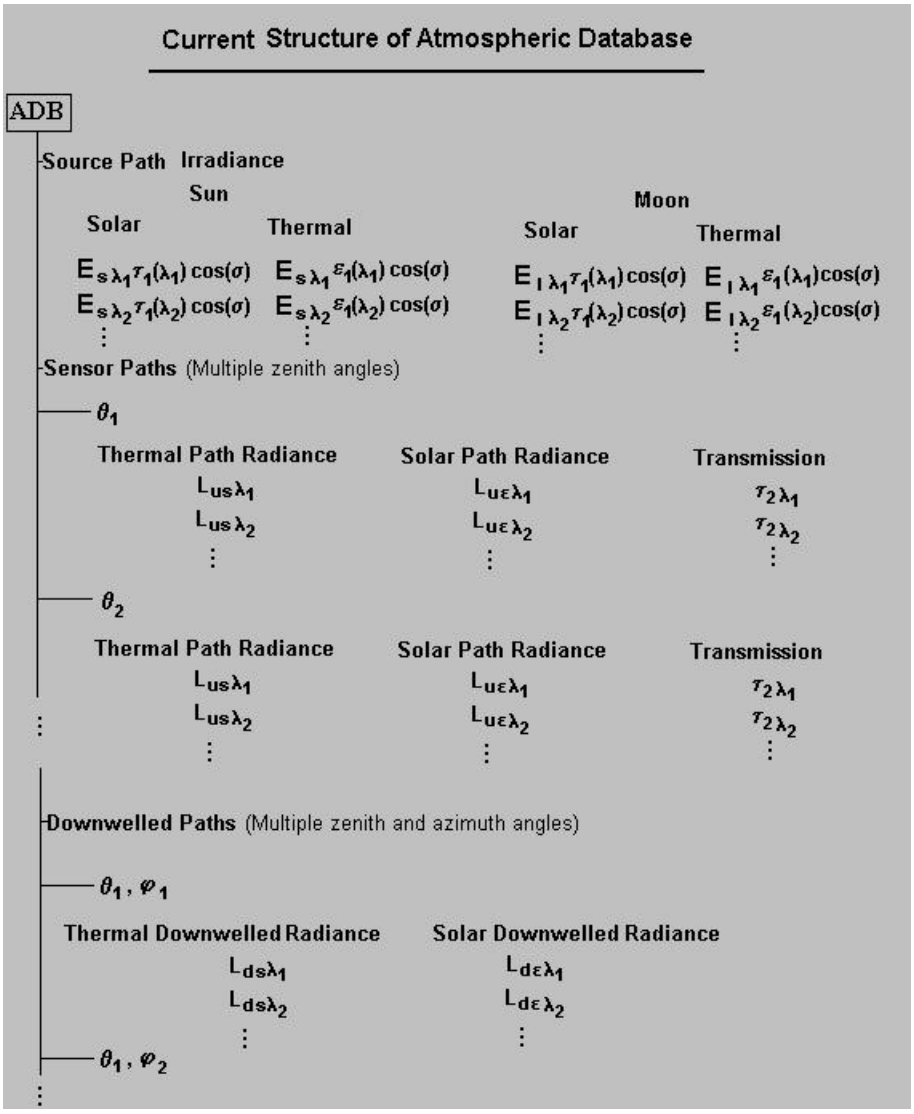

Figure 1.10: The general structure of the current Atmospheric Database. This shows the radiometric terms associated with each section.

1.4.4 ADB Construction

Source Paths

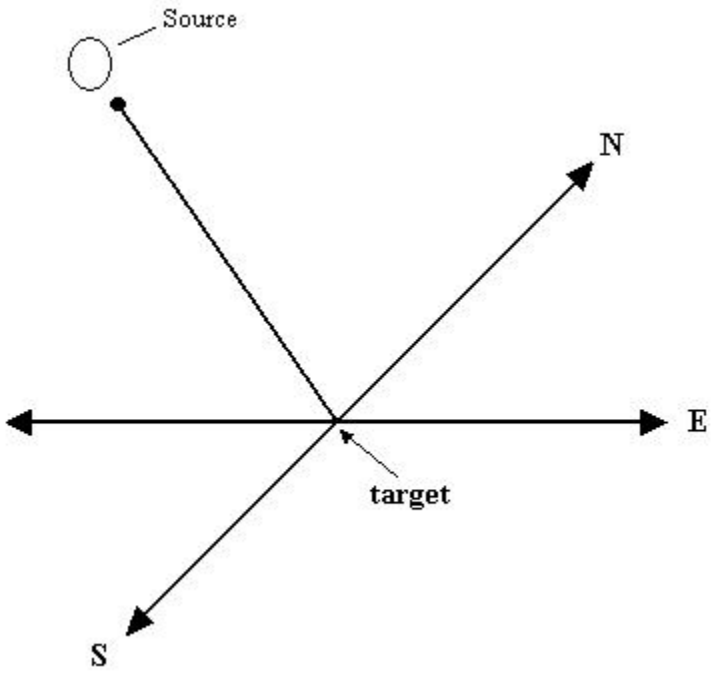

Figure 1.11: This is a representation of the geometry associated with creating the source path section of the ADB. MODTRAN is run from the target towards the source.

The construction of the ADB is carried out by a program called make_adb. The first section of the ADB contains the spectral blocks directly from the source(s), and for this case, either the sun or the moon (Figure 1.11). The geometry used as an input to MODTRAN is taken from the ".cfg" file by make_adb. (See Appendix D for a complete ".cfg" file.) This file has the three dimensional coordinates of the target and the sensor, as well as the time of day, day of year, latitude and longitude to calculate exactly where the sun (or the moon) is when the synthetic image is made. It takes this information and passes it to MODTRAN.

Using this geometric information and the tape5 file, MODTRAN creates a spectral block, which contains the irradiances and transmissions of the sun and the moon, over the spectral range and resolution specified by the ".cfg" file. Once this spectral block is complete, make_adb places it in its output file (known as the ADB).

This section is used in the first step of image rendering, calculating the amount of energy reaching the ground at a specific spot.

Sensor Paths

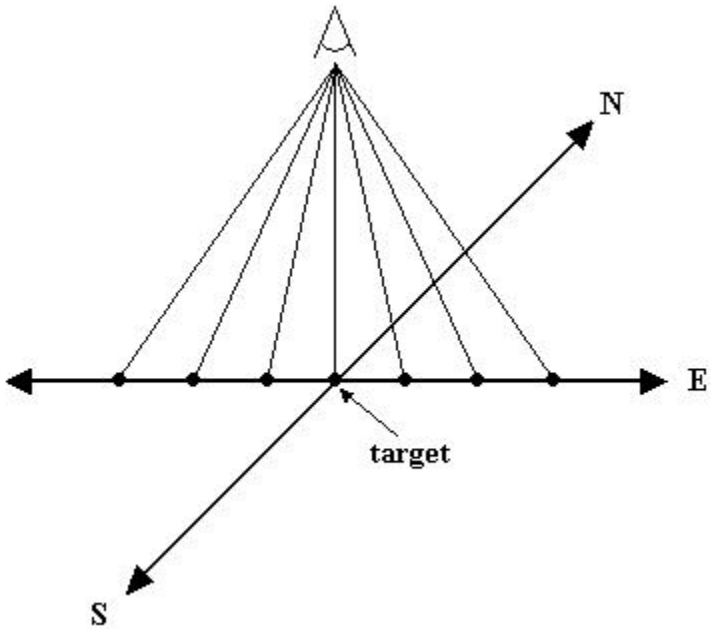

Figure 1.12: This is a representation of the current generation of the upwelled (sensor path) section of the ADB, where each of the dots represents a MODTRAN run, from the sensor to that point.

To create the second part of the ADB, the sensor paths section, make_adb again uses the geometry in the ".cfg" file to calculate the look angle of the sensor with respect to the target. It then creates a list of zenith angles at which to sample. This list is dependent on the field of view of the sensor and generally includes angles greater than and less than the look angle for a nadir view. The range and spacing of these angles is generally centered around this look angle.

For each zenith angle specified, make_adb will call MODTRAN, which will generate a spectral block (see Fig 1.12), which are then placed in the ADB (the output file).

This section is used in the last step in image rendering mentioned: calculating the amount of radiance from the source that is scattered off of the atmosphere towards the sensor.

Downwelled Paths

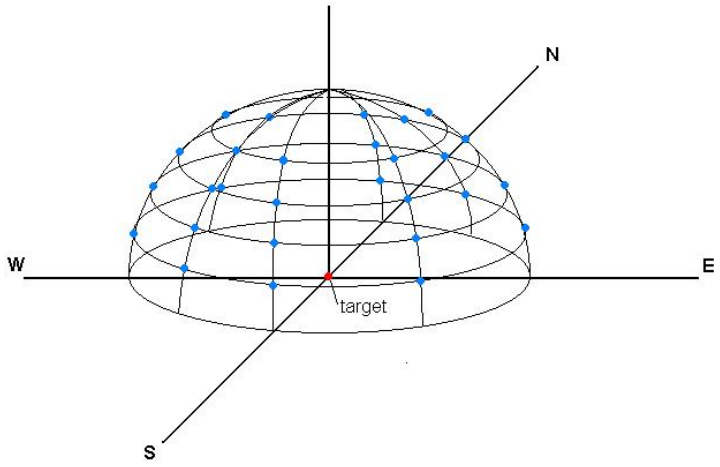

Figure 1.13: This shows the layout of method used to sample the sky dome in the downwelled section of the ADB. The blue dots represent a sampled point in the sky, where DIRSIG will execute a MODTRAN run and store the results in the ADB. Interpolation is used to get the values in between the sampled points.

The third and last section contains the downwelled radiance. For this section, no geometric information is needed from the ".cfg" file, however, the solar position will be determined from the time of year, local time of day, latitude and longitude. The goal of this section is to have a sampling of the entire hemisphere of the sky. This will allow DIRSIG to derive how much radiation is reaching the target as a result of the sky radiance *not* directly from the sun (or moon). A diagram of the sampling scheme is show in figure 1.13. Here, MODTRAN places the sensor at the center point on the ground, and looks up towards the sky. This section is also used in the first step of image rendering: calculating the radiance reaching the ground.

The last part of the downwelling section contains the total, spatially integrated downwelled sky radiance over the whole hemisphere. There is a time-saving option available in DIRSIG which allows the user to bypass specific downwelled radiance calculations and use the total integrated radiance. This will ignore any shape factor effects brought upon by objects between the target and the sky.

This chapter's intent was to introduce the basic operation and function of DIRSIG, and identify the specific aspects of DIRSIG which will be looked at in future chapters.

The next chapter will address the specific features within DIRSIG which will be augmented. It will assess the current limitations of the implementation of those features, as well as provide solutions which will expand DIRSIG's capabilities.

Chapter 2

Atmospheric Modeling: Issues and Solutions

Contents

2.1 Geometric Issues 39
2.1.1 The High-Altitude Object Issue 39
2.1.2 The Solution to the High-Altitude Object Issue 44
2.1.3 Current Atmospheric Sampling 47
2.1.4 New Method of Atmospheric Sampling 49
2.1.5 Horizon Issues 51
2.1.6 Resolution of Horizon Issues 55
2.2 Atmospheric Inhomogeneities 59
2.2.1 Atmospheric Inhomogeneities Issues 59
2.2.2 Implementation of Atmospheric Inhomogeneities 59

The overall goal of this work is to allow DIRSIG to model horizontally varying atmospheric characteristics. To accomplish this, certain aspects of the method by which DIRSIG samples the atmosphere must first be addressed. These limitations of DIRSIG are geometrical in nature, and will be improved upon with the use of a more robust sampling scheme.

This chapter will address these specific geometric limitations and propose solutions to them. As well, it will discuss the proposed method of incorporating atmospheric variability into DIRSIG.

2.1 Geometric Issues

2.1.1 The High-Altitude Object Issue

The first of these geometric issues that will be discussed is the altitude scaling issue. This occurs when DIRSIG is rendering an image and encounters an object with a non-zero height. What is expected to happen during ray tracing, is that the ray will only pass through layers of the atmosphere that the object is actually in. (See figure 2.1). However, what DIRSIG does is scale the path length of the atmosphere to compensate for the difference in range (see figure 2.2), thus making each layer of the atmosphere a bit thinner.

The problem is that the ray continues to pass through *all* the layers of the atmosphere, including the layers the object is not in. Passing the ray through these extra layers of the atmosphere, in particular the lower ones, can introduce significant change in the upwelling and transmission terms.

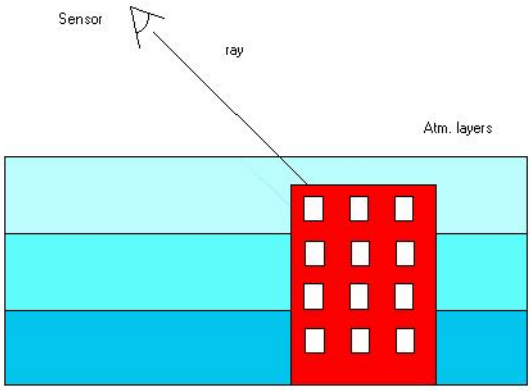

Figure 2.1: This is what is expected to happen in a real scene when a ray encounters an object of non-zero altitude.

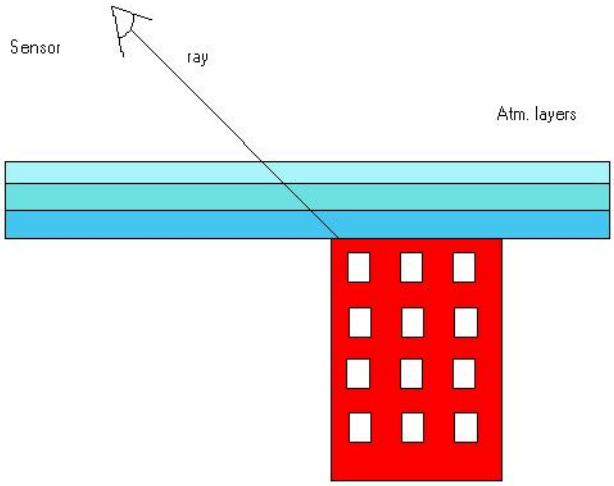

Figure 2.2: This is what actually happens in DIRSIG. Each layer of the atmosphere is scaled down to compensate for the change in range between the sensor and the object. Passing the ray through the lower layers adds more atmospheric effects than would be in the real scene.

This property of DIRSIG had been overlooked mainly because the majority of DIRSIG objects are well below the level at which this change becomes significant. However, if higher objects like mountains, or even clouds, are introduced these differences can be significant. As well, when earlier versions of DIRSIG were developed, there was a tighter restriction on the number of MODTRAN runs that were feasible due to the limitations of computational speed at the time. This limit on the number of MODTRAN runs will be elaborated on later.

To determine where and how severe these problems were, an experiment was performed which consisted of creating a non-reflective object and measuring the transmission and path radiance from it. A DIRSIG as well as a MODTRAN sensor were set up looking straight down at it through the atmosphere (see figure 2.3) This would determine the changes in these terms as the target's altitude increased.

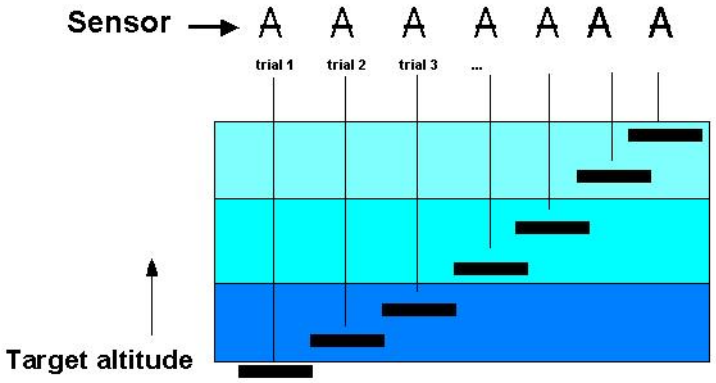

Figure 2.3: A diagram of the altitude experiment. The upwelling radiance and transmission from a non-reflective object were measured by DIRSIG and MODTRAN, and their results compared.

Looking at some sample results in figures 2.4 and 2.5, the outputs of both DIRSIG and MODTRAN are compared. These graphs show a spectral average (300 nm to 800 nm) of the path transmission and radiance. As the target approaches the altitude of the sensor, there will be less and less atmosphere between the two. With nothing to get in the way of the photons, its expected that the transmission will approach unity as the amount of atmosphere between the two approaches zero. This can be seen in figure 2.4. As well, with less and less atmosphere to scatter light off of, it is expected that the path radiance will drop to 0, as is seen in figure 2.5. In both of these figures, if is important to note the artificial linear change of both terms in the DIRSIG results. This is because, as the target is moved up an increment, DIRSIG thins each layer of the atmosphere by a uniform "sub-interval". It makes each layer just a bit thinner, to compensate for the overall shortening of the range from target to sensor. MODTRAN, however, knows that it is not looking through these lower layers. MODTRAN shows a more expected, exponential change and will be considered "truth" in all experiments. (Note: As far as DIRSIG is concerned, a direct MODTRAN run is the best approximation of the atmosphere. This is why the DIRSIG results are compared to the MODTRAN results, and MODTRAN is considered truth.)

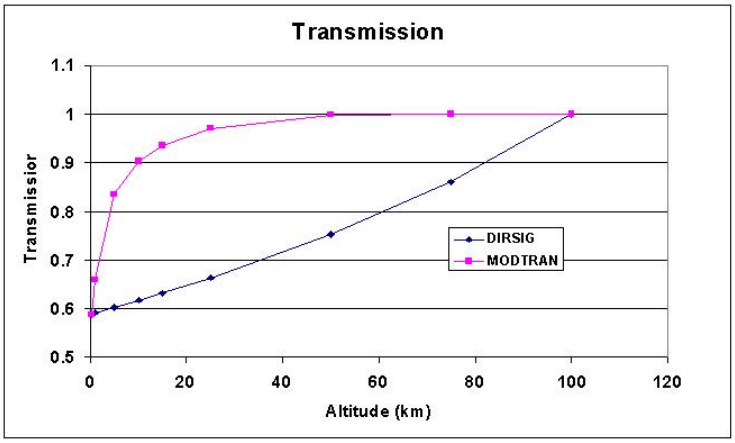

Figure 2.4: These are typical results for the altitude interpolation experiment. This graph shows the change in path transmission as a function of target altitude. Notice the artificial linearity produced by DIRSIG. The sensor for this experiment was at 100 km.

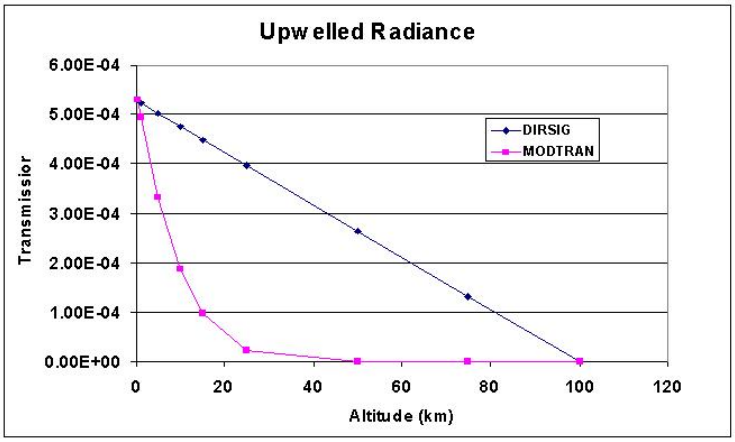

Figure 2.5: These are typical results for the altitude interpolation experiment. This graph shows the path radiance as a function of target altitude. Notice the artificial linearity produced by DIRSIG. The sensor, again, was at 100 km.

Now, the results of the altitude interpolation experiment (figures 2.4 and 2.5), as displayed, do not help much; not many objects in DIRSIG are present at 50 km. The same experiment was redone and only the region of the atmosphere below 1 km was looked at. The sensor was kept at 100 km. These results are shown in figures 2.6 and 2.7. Here, it can be seen that, even according to MODTRAN, the changes in these values at these altitudes are very linear. Exploiting the linearity of this behavior will greatly help in improving the accuracy of DIRSIG, as will be explained in the next section.

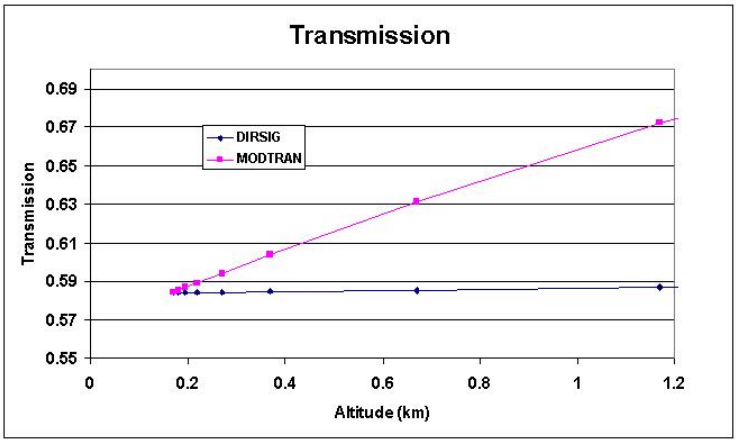

Figure 2.6: This shows the results of the same experiment when only the region below 1 km is examined.

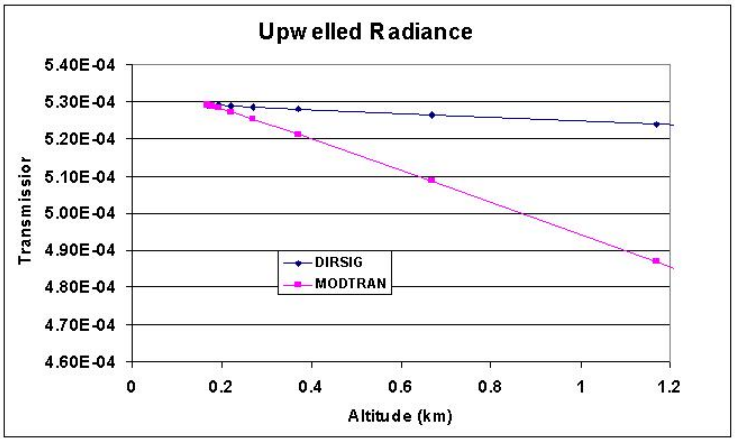

Figure 2.7: This shows that the path radiance also behaves in a linear fashion when examined at altitudes below 1 km.

2.1.2 The Solution to the High-Altitude Object Issue

The linear change in the atmospheric transmission and path radiance values with an increase in altitude is good from a modeling point of view. Predicting this linear process can be accomplished by using a simple linear interpolation. The goal here is to get DIRSIG's results to "look like" MODTRAN's. Looking at results like those in figures 2.6 and 2.7, it can be seen that if just one of DIRSIG's "endpoints" is changed, the graph would resemble MODTRAN's quite well. The way that it can be done is by sampling the atmosphere at another altitude. This will force DIRSIG's values to match MODTRAN's at that altitude.

For example, if the atmosphere is now sampled at 1 km, as well as the ground, and interpolation is used to get the values that lay between them, a prediction can be made that is much closer to the MODTRAN values. Figures 2.8 and 2.9 shows how this extra sampling point will help us.

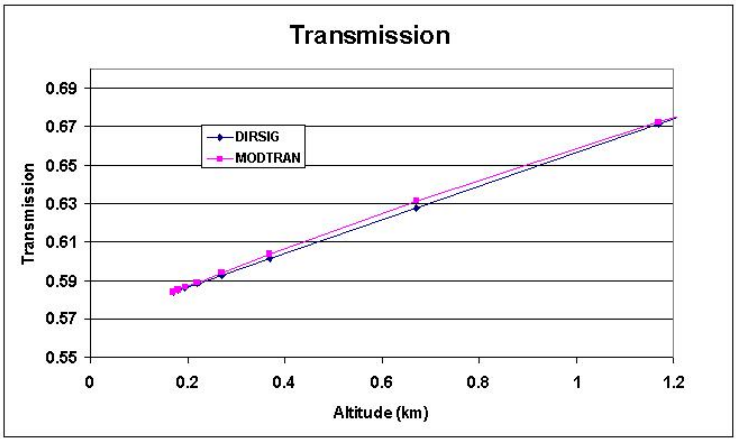

Figure 2.8: This graph shows the transmission as a function of target altitude (with the sensor at 100km) if DIRSIG scaled the atmosphere from approximately 1 km, not at the sensor altitude.

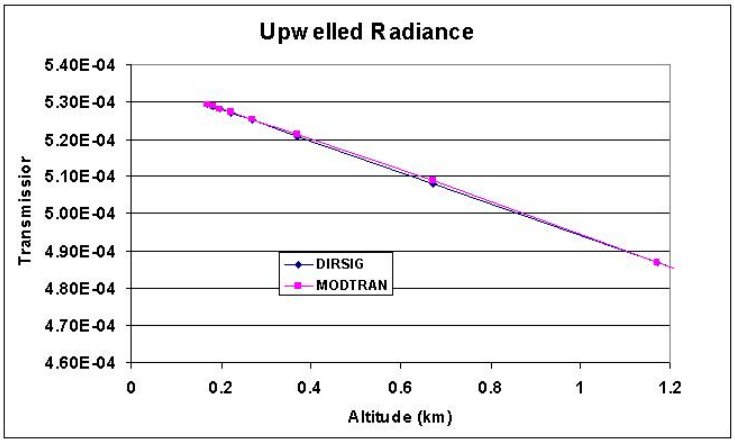

Figure 2.9: This graph shows the path radiance as a function of target altitude (with the sensor at 100km) if DIRSIG scaled the atmosphere from approximately 1 km, not at the sensor altitude.

Here, DIRSIG is still doing its linear scaling, but if sampling occurs at 1 km, the endpoints of this line can be made the same as MODTRAN. [1] By taking advantage of the natural linearity of the changes in the terms in this region, DIRSIG's line can be made to look more like the MODTRAN line. (See appendix 4 for a related study.)

[1] The graphs 2.8 and 2.9 do not represent actual data, and are representations of what the new values will resemble.

If the old upwelled sampling scheme is represented by figure 1.12, then the new sampling scheme is represented by 2.10.

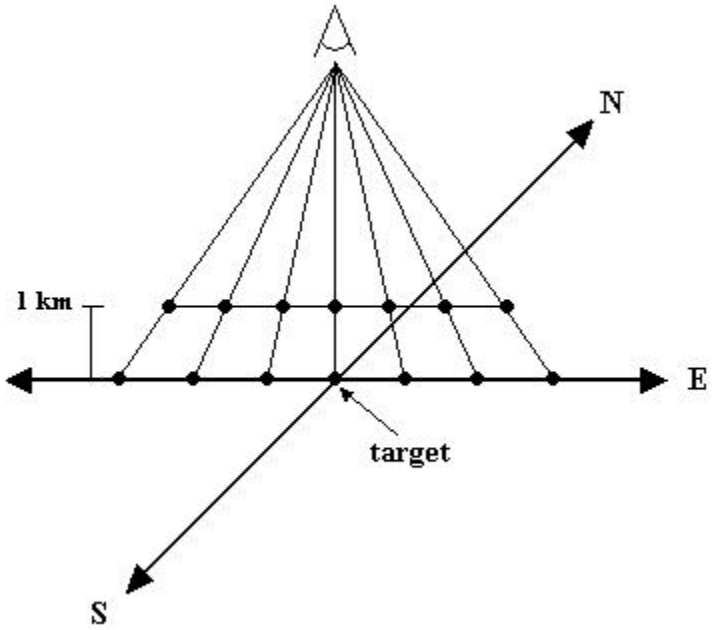

Figure 2.10: A graphic of the proposed method of upwelled sampling.

This method of sampling will sufficiently handle objects which are found at or below 1 km. If clouds are introduced, or other objects that would be found at much higher altitudes, the sampling scheme of "ground and ground + 1 km" could not be used. Using this specific sampling scheme to predict values above 1 km would not work much better than the original method.

Assuming that the lowest 1 kilometer of the atmosphere is the most optically dynamic, then accurate interpolation can be done on any 1 kilometer segment of the atmosphere.

For example, if a cloud or airplane was included as a DIRSIG object, sampling at 2 km and again at 3 km would allow the prediction of all the transmissions and upwelled radiance in that region. A graphic showing this multiple altitude region sampling scheme is shown in figure 2.11.

(The complete experiment is described in Appendix A.)

Now, the upwelled radiance is not the only value affected by this scaling. An object at high altitudes also receives less downwelled radiance from the sky than an object at ground level. For this reason, the atmospheric database will now have multiple altitudes in the downwelled section. So, the downwelled radiance from the sky (at each angle) will be sampled for the same number of altitudes as the upwelled section. From a geometry point of view, this sampling scheme would be analogous to executing the sampling scheme seen in figure 1.13, but at multiple ground levels. During rendering, interpolation between altitudes will take place for a given ray. This process will be similar to the upwelled case, which will be discussed in future sections.

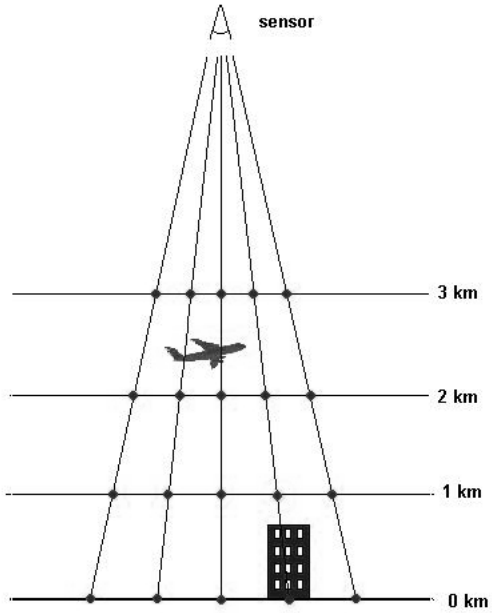

Figure 2.11: A graphic showing the multiple altitude region sampling scheme.

2.1.3 Current Atmospheric Sampling

Another main geometric issue that will be addressed is that of the current upwelled sampling scheme. Currently, the program which creates the ADB, make_adb, does not sample the upwelling radiance as thoroughly as is needed. In order to be able to actually measure these atmospheric inhomogeneities that are going to be added to DIRSIG, a more robust sampling scheme is needed for the upwelled radiance. As shown in (figure 2.12), the current scheme only samples in the zenith dimension, and ignores any azimuthal variation. The result is a circularly symmetric upwelled radiance map. This method of sampling will fail to model azimuthal features of the atmosphere. This must be fixed if horizontally varying atmospheric characteristics are to be included.

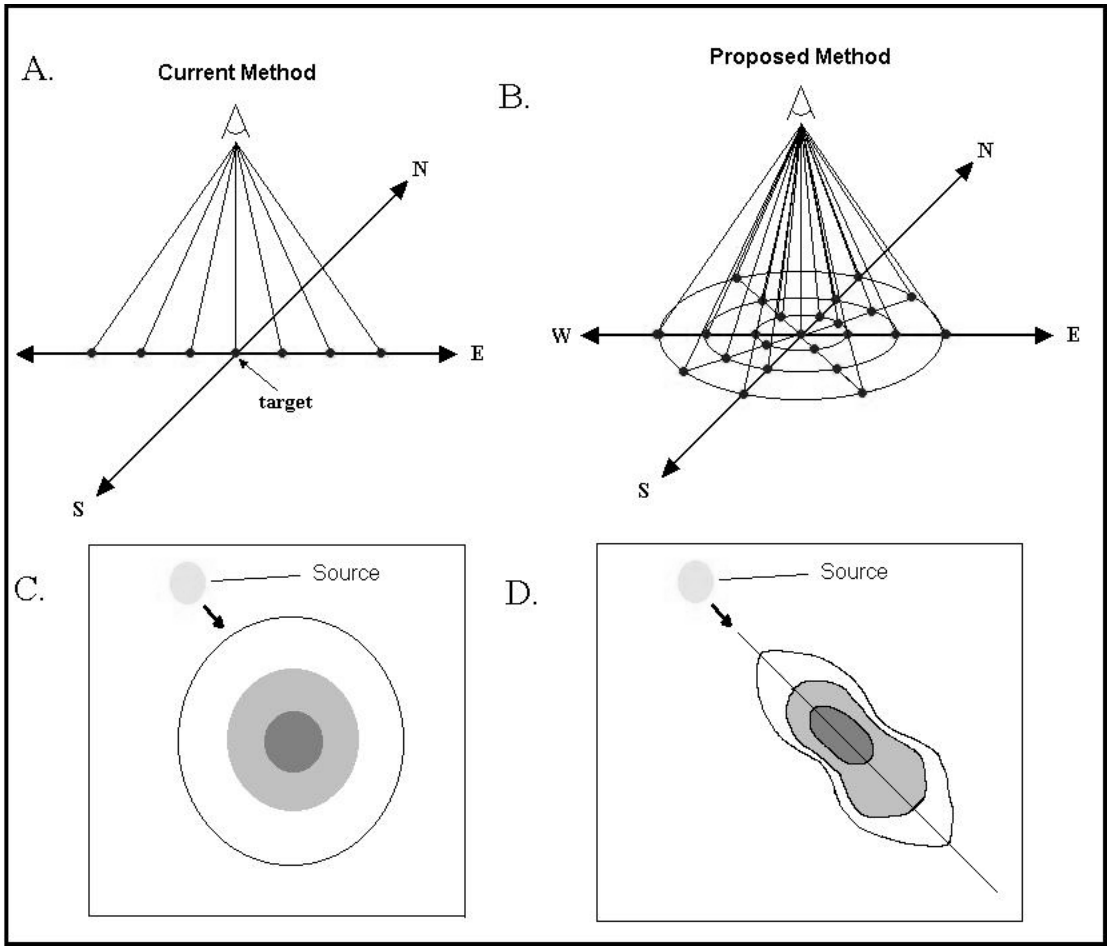

Figure 2.12: The upper diagrams show the upwelled radiance sampling scheme, and the lower show the resulting upwelling radiance map. The diagrams on the left (A. and C.) represent the current method of sampling the upwelling radiance and transmission of the atmosphere. The set on the right (B. and D.) show the proposed scheme, with azimuth angles to detect any azimuthal variation in the atmosphere.

Figure 2.13 shows a flow chart of the current method of how DIRSIG references the sensor paths section of the ADB. For each pixel in the synthetic image being rendered, DIRSIG's ray tracer will provide it with a zenith angle associated with that particular pixel. DIRSIG will then reference the ADB, finding the two adjacent zenith angles. Each of these zenith angles in the ADB will have associated with it, a spectral block. It will then perform a simple linear interpolation between the two adjacent zenith angles, and estimate the values of this intermediate spectral block.

For each pixel in the synthetic image, the downwelling radiance will also have to be calculated. The process

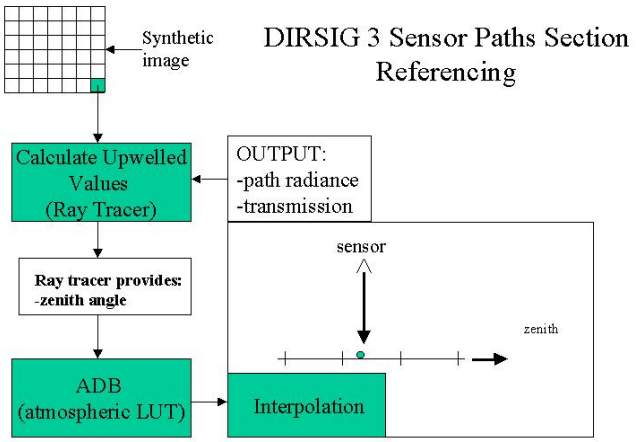

Figure 2.13: A flow chart demonstrating the current method of referencing the sensor section of the Atmospheric Database.

of referencing the downwelled section of the ADB is nearly identical to that of referencing the sensor section. The only difference here is that there are 2 dimensions to interpolate over. Figure 2.14 is a flow chart showing the method of referencing the downwelled section of the ADB.

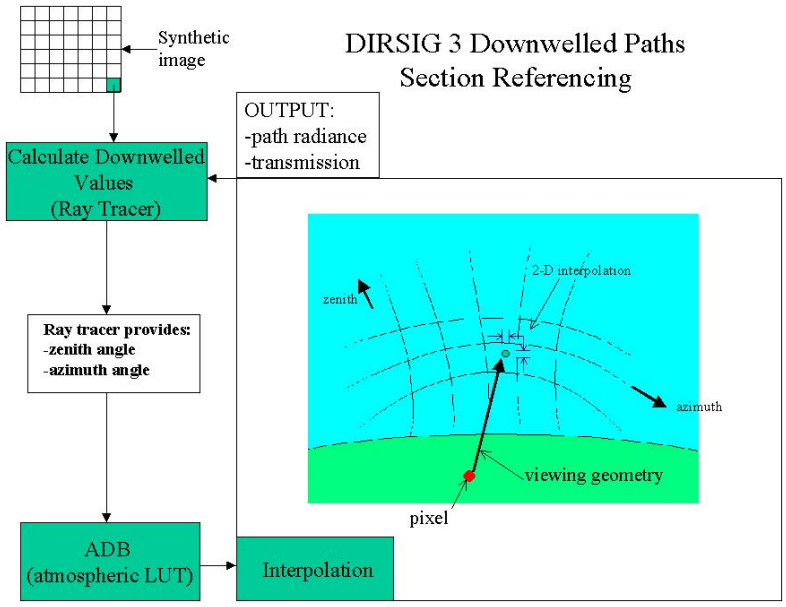

Figure 2.14: A flow chart demonstrating the current method of referencing the downwelled section of the Atmospheric Database.

The proposed scheme of upwelled sampling involves including azimuth angles as well as zenith angles. This will allow a more comprehensive sampling of the atmosphere and would be able to capture any azimuthal variability. (See figure 2.12.)

2.1.4 New Method of Atmospheric Sampling

The simplest correction to this problem is to compute the atmospheric parameters using MODTRAN at each of the pixels in a given scene. This brute force method, conceptually, would give the most accurate atmospheric values. However, it would result in an extremely large number of MODTRAN runs. Also, it is wasteful when one considers that the difference in transmission and path radiance from pixel to pixel in a typical image generally does not change drastically enough to merit a complete atmospheric prediction for each pixel.

The solution is found in interpolation. The goal is to find the delicate balance between accuracy and time expenditure. A large portion of this work is an exploration of the appropriate interpolation scheme that will allow this compromise.

In order to more properly represent the dynamic nature of the atmosphere, a new ADB will need more than just a series of zenith angles at which to sample the upwelling radiance and transmission. This new ADB will have multiple zenith and azimuth angles for a given scene. This will allow a more robust sampling of the atmosphere.

During rendering, as DIRSIG calculates the upwelled radiance and transmission, it utilizes ray tracing. Each ray will have a unique geometry associated with it. Specifically, this consists of a zenith angle, an azimuth angle, and an altitude. All three of these dimensions will exist in the new ADB. Figure 2.15 shows a representation of the new sampling structure. Accessing all of these dimensions is an issue of three dimensional interpolation.

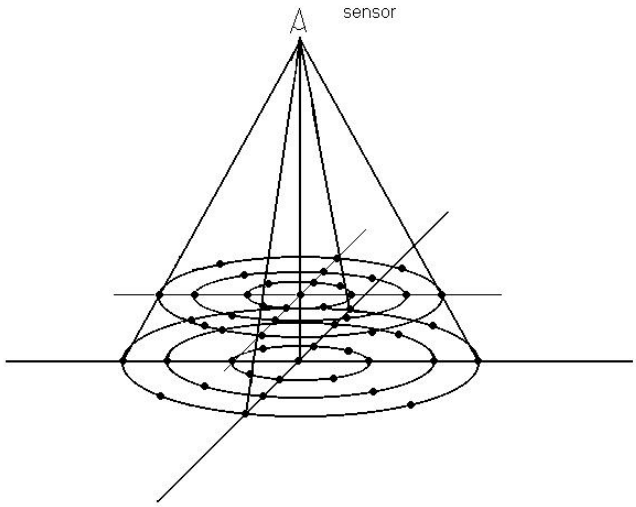

Figure 2.15: This is a diagram of the proposed structure of the new upwelled section of the ADB. Note that this structure samples in the azimuth and altitude dimensions as well as the zenith dimension.

The first step is to find between which two zenith angles the run falls. The ADB will have regularly spaced zenith angles. The difference between the zenith value of the ray and that of the closest zenith in the ADB (referred to here as delta zenith) is then calculated.

Using this delta zenith, the path radiance and transmission values (referred to here as simply the values) are calculated for both of the adjacent azimuth angles as well. These are needed as the endpoints for interpolation in the azimuthal dimension. Similarly, this process must be repeated at the two adjacent altitudes, for the same reason. (See A. in figure 2.16)

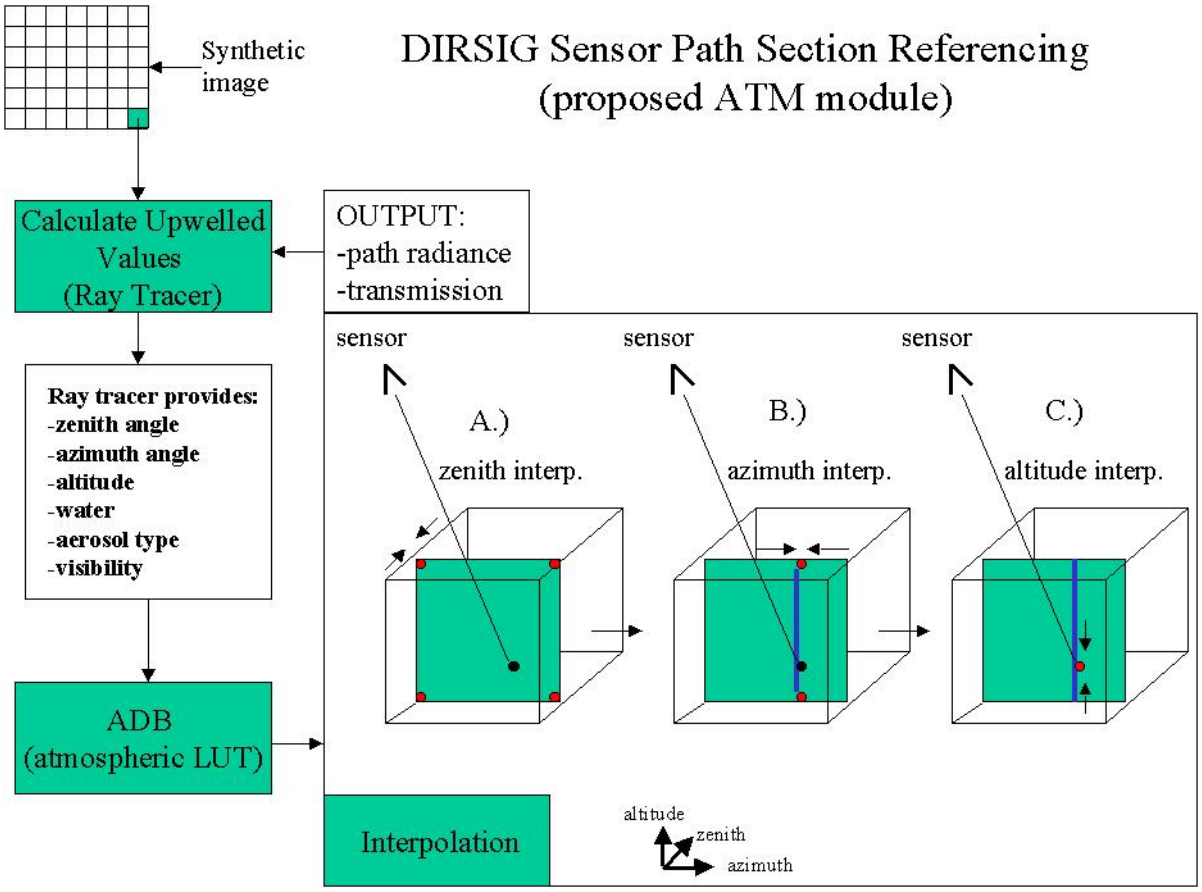

Figure 2.16: This figure depicts a flow chart of the new multi-dimensional interpolation scheme of DIRSIG.

Next, the difference between the azimuth associated with the ray and the closest azimuth in the ADB is calculated. The values previously calculated (a result of the zenith dimension interpolations) are now used as endpoints for the azimuthal interpolation. (See B. in figure 2.16) Again, this must be done at both adjacent altitudes to provide the endpoints for interpolation in the altitude dimension.

Finally, the difference between the ray's altitude and the closest altitude in the ADB is calculated. Again, the two results from the previous azimuthal interpolations are used as the endpoints for this interpolation.

This process provides the ray tracer with a set of upwelled radiance and transmission values by linearly interpolating over three geometric dimensions. In section 2.2.2, I will describe a similar process which is done for atmospheric inhomogeneities.

Exactly where to sample the atmosphere was the subject of a series of sensitivity experiments, (See appendix A, section A.2.2 for the complete experiment.) the results of which lead to a recommended number of sample points for each dimension. These suggested numbers will be used as a default setting in the new atmospheric module. The experiments also estimate the error associated with running the module at at different resolutions (number of sample points) than the default, for different atmospheric conditions. [2] This is provided in case the user wishes to use different resolutions to customize the total run time or the overall accuracy of the atmospheric module.

Downwelled Sampling

Angular interpolation of the downwelled radiance will not change in the new atmospheric model. However, there is an inaccuracy inherent in the current implementation of the referencing of the downwelled data. In calculating the downwelled radiance reaching a given synthetic pixel, DIRSIG assumes that the downwelled radiance reaching the center (target) pixel is the same for all other pixels. In creating the ADB, DIRSIG runs a full sampling of the sky only at the center pixel, and uses these values for all downwelled transmission and radiance values in the scene. This method ignores the fact that the source-target-sensor geometry changes depending on where the pixel is located in the image. The pixel at the far corner of an image, can, potentially, have a vastly different source-target-sensor geometry than the center. However, this is only relevant when the image is large enough that the latitude or longitude varies significantly from image edge to image edge.

Correcting this issue would require a method of sampling the downwelled radiance at multiple pixels locations on the ground. This would add a very large number of MODTRAN runs used in the creation of the ADB, and would, therefore, lead to a substantial increase in run time. As well, a further study would have to be done to determine which pixels to choose to sample the downwelled data. Considering the time that these tasks would take, in both experimentation and ADB generation time, it was deemed not worth the time to pursue improving the downwelled sampling in this atmospheric module.

That being the case, improvements will still be made to the downwelling section of the ADB. This was mentioned earlier in the chapter and involves simply repeating the downwelled sampling that exists now, but at multiple altitudes. The new downwelled sampling scheme will not be analyzed as thoroughly as the upwelled sampling because, in many cases, the contribution of the downwelled radiance to the overall sensor-reaching radiance is much less than that of the upwelling component.

An outline of the proposed structure of the new ADB is shown in figure 2.17.

2.1.5 Horizon Issues

Artificial Horizon

In creating the sensor and downwelled paths in the Atmospheric Database, MODTRAN is run in two modes, depending on whether it is calculating values for the sensor section or the downwelled section. MODTRAN uses the "point to point" mode to calculate values in the sensor paths section, and the "slant path to space" mode to calculate values in the downwelled section. Generally, DIRSIG was designed to have all of the sensor

[2] It should be noted that these experiments were done spectrally.

paths in the Atmospheric Database start at the sensor and look down onto the ground. Conversely, all of the paths in the downwelled section were assumed to be originating at the target, and extend into space, thus sampling the sky dome. The artificial horizon issue comes to the surface when, through the geometry of the scene, these MODTRAN modes and the expected geometry get mixed up.

Generally, the upwelled section deals with the atmosphere between the zenith angles of 90 degrees to 180 degrees zenith (straight down in MODTRAN notation). The downwelled section deals with the zenith angles values between 90 degrees and 0 degrees (straight up).

So, if the DIRSIG sensor is looking down (zenith above 90 degrees), it expects to see the ground. However, if the sensor-target geometry is such that the horizon or sky is included in the scene, there is an ambiguity as to how to appropriately model the situation. DIRSIG does not have any way to reference an angle greater than 90 degrees which sees the sky. The current method substitutes the sky radiance from the downwelled case in place of the upwelled. To illustrate this, if DIRSIG was used to render a pixel that was ten degrees below the the horizon. This pixel, from the sensor's point of view will be sky. DIRSIG does not have a path in the ADB to reference which is both above 90 degrees *and* sky. Instead, DIRSIG uses the radiance value at ten degrees *below* the horizon, taking data from the downwelled section of the LUT. The result of this transplantation of radiance values is that an artificial horizon appears in the rendered image at 90 degrees. (see Fig 2.18).

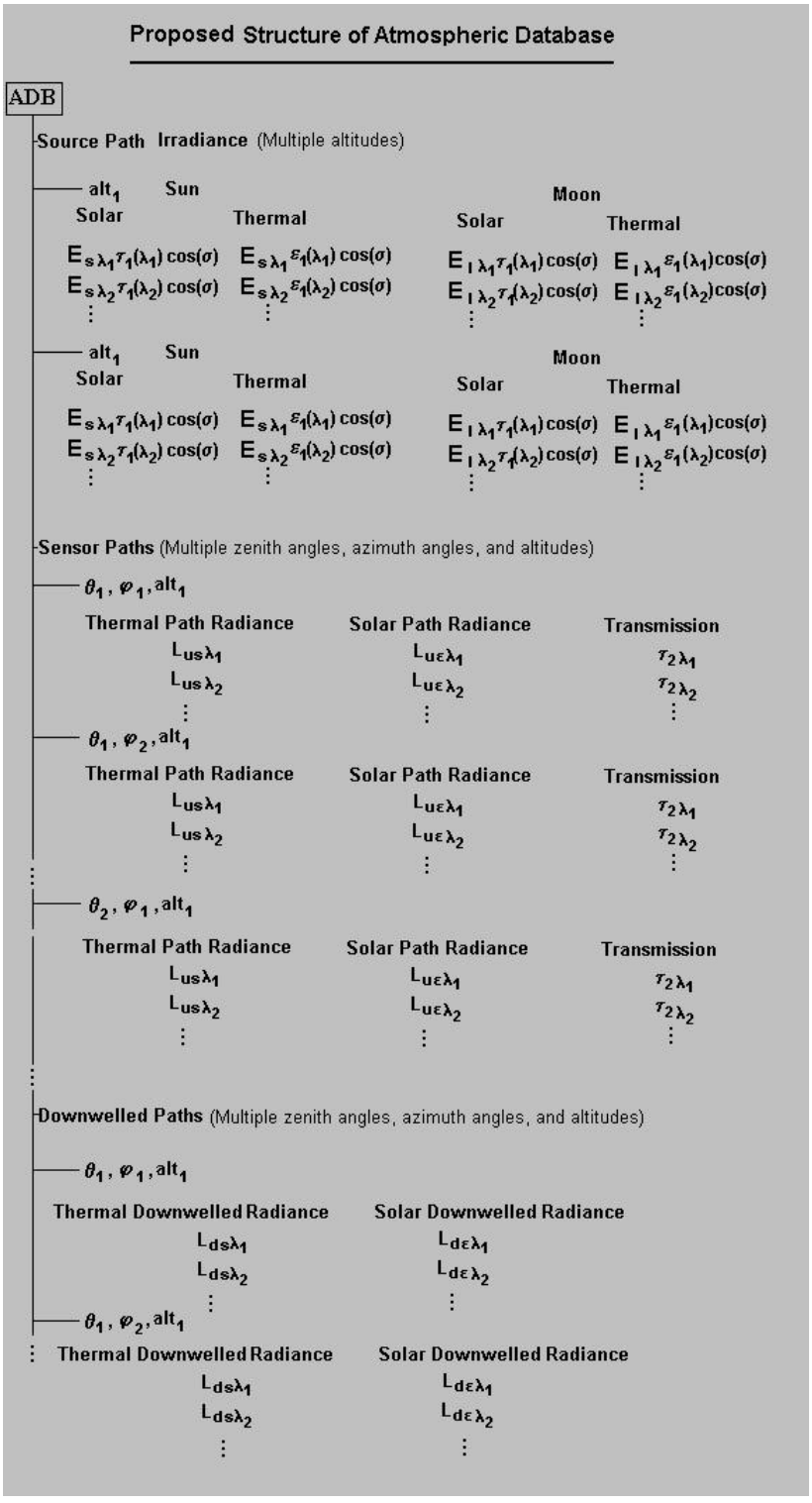

Figure 2.17: The structure for the proposed ADB. This shows the new geometric structure, including the addition of multiple altitudes and angles.

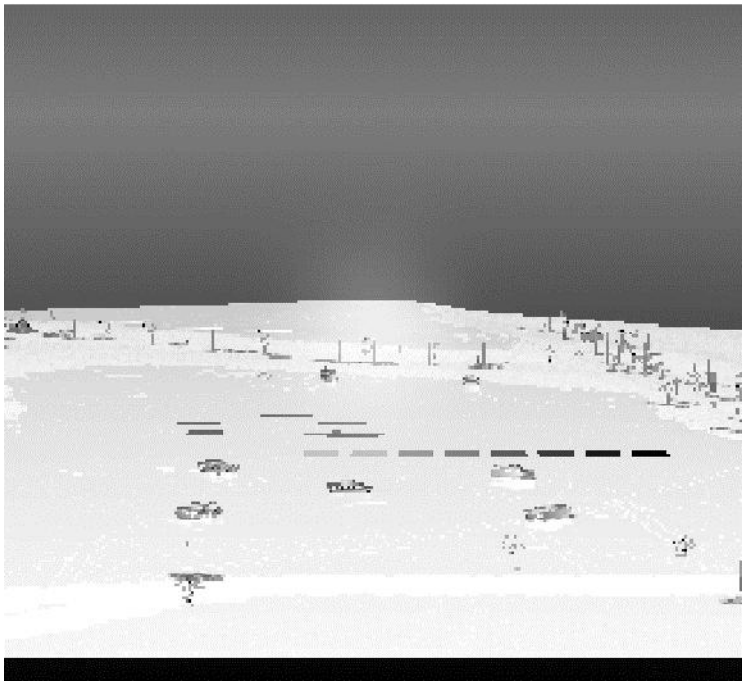

Figure 2.18: This artificial horizon is the result of the inability of DIRSIG to sample the downwelling radiance from the sky below 90 above. It substitutes those sky radiance values *above* 90 degrees with those *below* 90 degrees. This means that the values at +10 degrees are identical to those at -10 degrees, which creates this false "mirroring" effect in the sky. [10]

Intervening Object

Another problem related to the artificial horizon effect occurs when there is an intervening object in this view of the horizon. Imagine a sensor looking at the horizon, and there is a tall building or mountain off in the distance. (see Fig 2.19). If the ray tracer hits this object, DIRSIG will then scale the atmosphere to fit in the space between the sensor and the object. This is almost identical to the high altitude object problem addressed earlier. The solution, as well, will be similar.

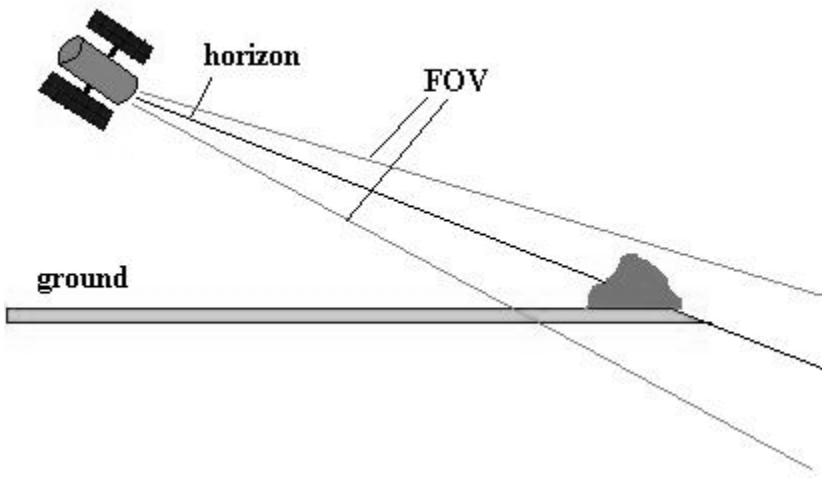

Figure 2.19: This represents the problem when synthesizing an image which contains the horizon. In addition to the "mirroring" effect (figure 2.18), there is a problem related to the height scaling problem.

2.1.6 Resolution of Horizon Issues

To deal with the horizon issues, there must be an increase in the abilities of this new ADB construction scheme.

Artificial Horizon

In the new atmospheric module, if a synthetic scene includes parts of the sky, a new method of sampling the sensor section of the atmospheric database must be used. To get path radiance and transmission values for pixels in the image that contain the sky, MODTRAN will be run in a different mode than when retrieving data for "ground" pixels. This change will take place in the creation of the Atmospheric Database.

The first step is to determine where the horizon exists in the MODTRAN geometry. This was done experimentally. An IDL (Interactive Data Language) program was written to determine the precise zenith angle of the horizon at a specific sensor altitude within 6 decimal places. The program exploited the fact that MODTRAN will crash if the "slant path to space" mode is used and its line of sight intersects with the ground.

This method of finding the horizon was done because even if an empirical formula could be found, the spectral nature of this horizon value would have to be taken into account. Due to the spectral nature of the index of refraction of the atmosphere, it is possible for different wavelengths to have different horizons. This experimental method will allow a more direct agreement with MODTRAN at where the horizon truly lay.

After determining the horizon, a simple modification to the Atmospheric Database generation code is made. In the section of the code where MODTRAN is called, the zenith angle being passed to MODTRAN is checked to see if it is above or below the horizon. If is above the horizon then the "point to point" mode in

MODTRAN is activated. If the zenith angle is below this horizon, then the "slant path to space" mode is triggered. The elegance of this method is that the rest of DIRSIG will remain ignorant of the horizon. The sensor paths and downwelled sections of the ADB will be of the same format, but if there exists spectral blocks in the sensor section which have zenith angles which point to the sky, these will have the correct sky radiance associated with them. In the actual rendering process, if DIRSIG encounters a pixel in the image which is sky, it will be ignorant of that fact. It will simply call the transmission and radiance from whatever angle is called. Any question of whether a pixel is sky or ground is settled in the ADB.

Intervening Object

Related to this problem is the case where there is an object in this horizon view. If DIRSIG encounters this object, it will perform its scaling, and put the entire path (from the sensor to space) between the sensor and the building. This is very similar to the normal scaling problem mentioned in section 2.1.1, but, potentially not solved as easily. In that problem, the solution was to sample at two points, and interpolate. However, those points were relatively close together when compared to the distance between the sensor and the upper point, and the sensor and the lower point. Here, if you compare the distance from the sensor to a nearby building, and the distance to the "ground" (which is actually the path to space), it can be much bigger. This is strictly due to geometry (see figure 2.19).

In the new scheme of dealing with the horizon, the problem becomes even worse. To correctly image the sky, DIRSIG will reference MODTRAN runs that have been run as a "slant path to space", meaning that it incorporates all of the atmosphere between the sensor and space, and scales that to fit between the sensor and the building. So, depending on where the building is located, there could be a very large difference in the radiance and transmission values at the building and that of the entire atmosphere along the path to space. There is no evidence that this change is as linear as the change was in the vertical scaling problem.

The solution to this problem will involve a sampling scheme similar to that of the proposed upwelled path sampling. As the upwelled section of the ADB is being created, if the zenith angle is less than the horizon, thus ending its path in space, the two altitudes which would normally be sampled will instead be replaced with two ranges. The first range will be infinity, thus utilizing MODTRAN's "slant path to space" mode. The second will be a set range, which is calculated using simple trigonometry (see equation 2.1).

$$R_{tan} = h/cos(180 - zenith) \tag{2.1}$$

Here, the tangent range R_{tan} is equal to the sensor altitude, h, divided by the cosine of 180 degrees minus the zenith angle, $zenith$. (See figure 2.20).

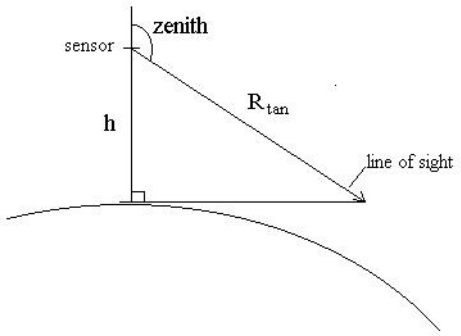

Figure 2.20: The geometry associated with calculating the default range used in the horizon spectral blocks.

This set up is shown in 2.21. (These spectral blocks will still have altitudes associated with them. This is just for ease of interpolation. Specifically, to avoid complications arising from attempting to interpolate using infinity as an endpoint.)

During image rendering, a ray striking the object which would normally go off into space will have a range associated with it. (This can be seen in figure 2.21 as the ray striking the mountain.) This range will be translated to a different coordinate system for interpolation (or extrapolation). This coordinate system is based on the "altitude" used in the initial sampling. Again, this is to avoid interpolating or extrapolating with infinity as an endpoint. For example, if we have a scene where we are sampling the atmosphere at 0 and 1 km, and the zenith angle sees space, the "altitudes" at that look angle would be listed in the ADB as 0 and 1 km. But in reality, the spectral block sampled at 1 km would be sampled at the point calculated

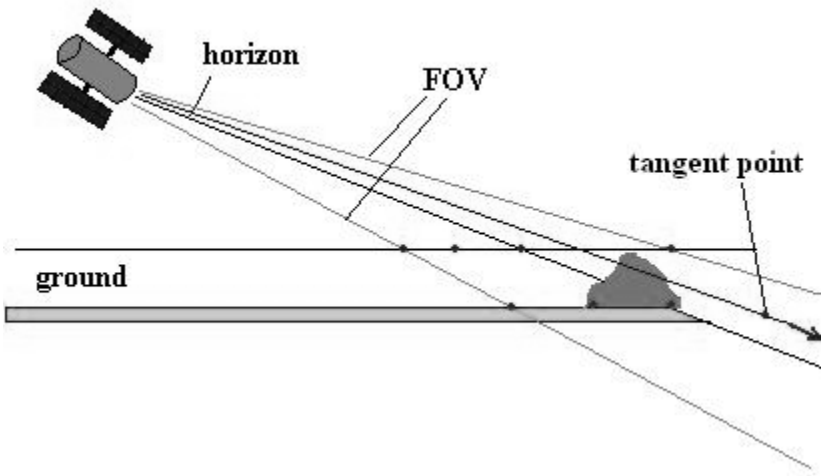

Figure 2.21: This shows the proposed solution to the intervening object problem. In sampling at multiple ranges, the scaling problem will be lessened.

by equation 2.1, and the 0km spectral block will be calculated at infinity, using the "slant path to space" mode. When DIRSIG traces the ray that hits the mountain, it will get an altitude associated with that mountain. It will then interpolate between what it thinks is 0 and 1 km, but in reality it uses this calculated midpoint, and infinity. This method is not guaranteed to produce accuracy similar to the scaling solution stated in section 2.1.1, because the atmospheric values from this midpoint to infinity change in a very drastic, non-linear manner. A better solution would be an increase in the number of ranges which are sampled in the ADB, but this would require much more processing time, and a logical method for choosing the ranges at which to sample. This issue is not trivial, and is not addressed in this work. The solution to this problem will require an ADB with multiple ranges, zenith and azimuth angles.

2.2 Atmospheric Inhomogeneities

2.2.1 Atmospheric Inhomogeneities Issues

As stated before, the ability to model atmospheric inhomogeneities will allow a better test of the validity of hyperspectral algorithms, as well as allow the better modeling of the real world in general. It will allow DIRSIG to include such features as horizontally varying water vapor and aerosol concentrations in the synthetic atmosphere.

Currently, DIRSIG is unable to model an atmosphere which varies horizontally. It can model, for example, an atmosphere with a given water vapor profile. However, this profile will be the same at every point in the scene.

This treatment of the atmosphere as homogeneous slabs is actually a limitation of MODTRAN. Within MODTRAN, there can be vertical variations within the profile, but there can be no change in the horizontal struction of the atmosphere.

2.2.2 Implementation of Atmospheric Inhomogeneities

In order to accomplish this, DIRSIG must be able to use different MODTRAN atmospheres for different look angles. Under the current scheme, no matter where DIRSIG looks in the sky, it sees the exact same atmosphere. DIRSIG must be able to look at any angle and see a unique atmosphere. Not only that, it must also have accurate measurements of the transmission and path radiance for each of those angles.

The solution to this which will be pursued is to create a set of ADBs for each of the inhomogeneities. For example, for water vapor, there will be a set of ADBs, each with a varying amount of water vapor.

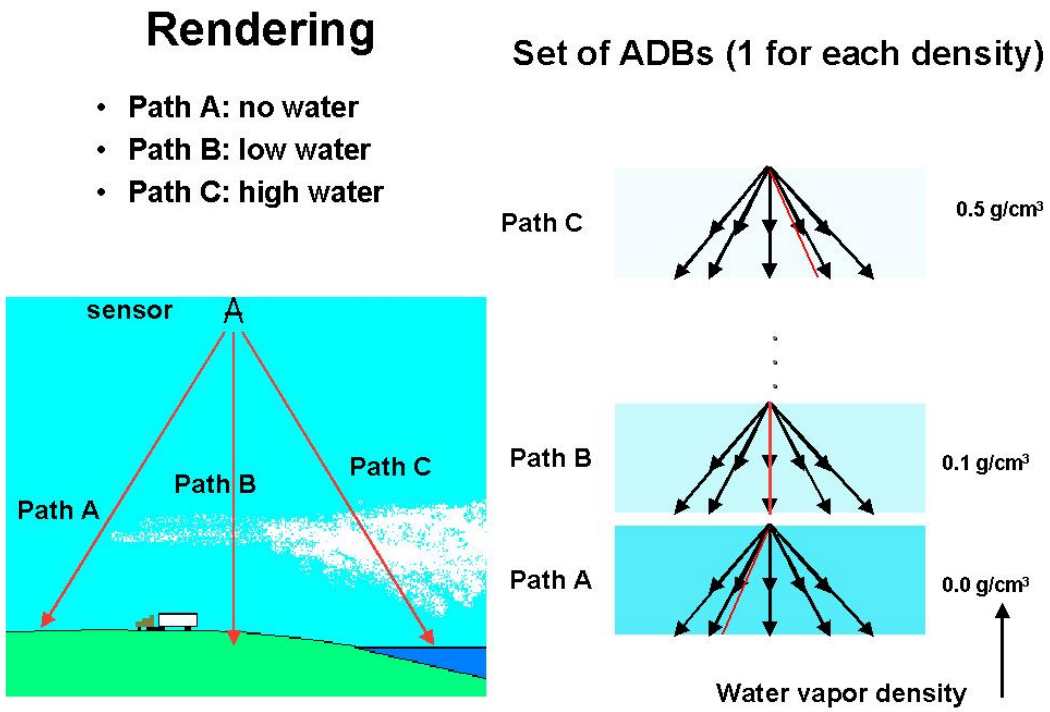

Figure 2.22: A set of ADBs will be produced for each of the atmospheric species. Each one of these ADBs will have a complete set of geometries, enabling DIRSIG to reference any concentration at any look angle. Water vapor is shown here, with each ADB having a difference water vapor concentration.

Each one of these ADBs will be made by creating a fully geometric sampling of the scene. The new ADB structure can be thought of as simpling adding on dimensions to the existing structure. Water vapor, for example, is one of these dimensions. Figure 2.22 shows a scene with horizontally varying water vapor densities. During rendering, if the ray from DIRSIG passes through path A, it will encounter the water vapor map. The map will "tell" the ray that the water vapor density there is 0. Knowing this, DIRSIG will then reference the ADB rendered with a water vapor of zero. It will get the transmission and path radiance, as it normally does. Now, if the ray takes path B, the water vapor map will say that there is a small about of water vapor at that spot. DIRSIG will then reference a different ADB, this one with a small amount of water vapor. This new ADB will have the same geometries of the original, but will have a layer of water vapor of a specific density.

All thermal effects resulting from the presence of water vapor in the atmosphere should be accounted for. Values for path radiance and transmission will be interpolated from values generated by a MODTRAN run. The handling of thermal effects will be limited only by MODTRAN's ability.

An outline of the structure of the new ADB, including inhomogeneities, can be seen in figure 2.23.

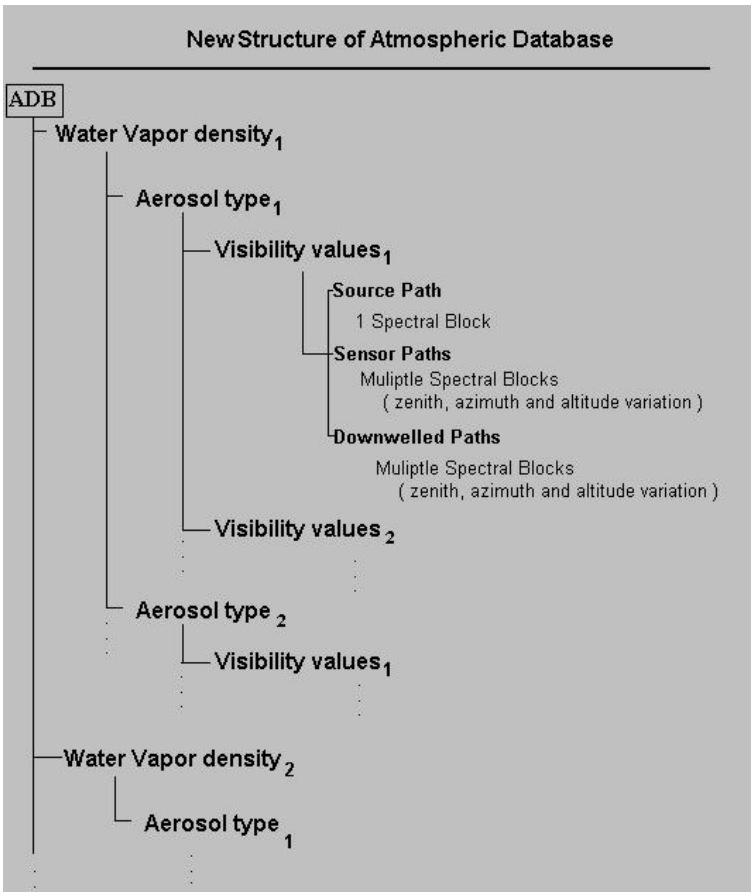

Figure 2.23: The structure for the proposed ADB. A unique set of spectral blocks will be created for each combination of aerosol visibility, type, and water vapor density.

The interpolation between these atmospheric species will be handled in a nearly identical method as the geometric interpolation described in section 2.1.4. Instead of interpolating between three spatial dimensions, the new module will interpolate between two "species" dimensions. In this case, as well, the number of interpolation points will determine the relative error associated with interpolation.

Where to sample the atmosphere was the subject of another series of sensitivity experiments. (See appendix A, section A.3 for the complete experiment.) These differ from those discussed in section 2.1.4 only in that

"species" dimensions were used, instead of geometric dimensions. In this case, these dimensions were water vapor and aerosol visibility. Interpolation *between* aerosol types was not attempted.

This study was used to provide an appropriate number of points to be used in the LUT for each dimension. These will be used as a default setting in the new atmospheric module. The experiments also estimate the error associated with running the module at different resolutions (number of sample points) than the default. [3] This is provided in case the user wishes to use different resolutions to customize the total run time or the overall accuracy of the atmospheric module.

In addition to these new ADBs, another key element is needed to successfully render horizontally varying atmospheric inhomogeneities. This element is maps. In DIRSIG, maps are used to assign properties to objects or locations. For example, if spatial texture were to be given to an object or surface, maps would be used. These are becoming very useful and even invaluable in DIRSIG. One of the reasons is that, upon encountering a map surface a ray can return the map's location, and even some properties, such as temperature. The new atmospheric module will use these maps to insert inhomogeneities. This is a very powerful technique, because maps can be inserted wherever the user desires. However, for this study, atmospheric maps will be exclusively flat, two dimensional, infinite planes. The user will provide an envi-format "*.img" floating point image file, with values corresponding to the specific inhomogeneity. For example, a water vapor map image would be an image of arbitrary size, with values ranging from 0 to 2.5 grams per square centimeter. Once in DIRSIG, the image map will be infinitely tiled. As well, multiple images can be used. For example, if there were two discrete altitudes which had water vapor, both could be entered. The ray tracer, when passing through these levels, can report all encounters with any maps, their location, and the specific water vapor amount. This map data, along with the standard geometric information will allow the interpolator to provide an interpolated spectral block of data for that specific look angle and water vapor concentration.

Downwelled Inhomogeneities

Although the geometric structure of the downwelled radiance sampling is not changing (aside from the addition of multiple altitude sampling), the process itself is. The sky will be sampled at the sample combinations of look angles (6 zenith angles, and 12 azimuth angles), but will be done for a number of atmospheric conditions. Like the upwelled case, there will be interpolation between two "species" dimensions. This will allow for the downwelled section of the ADB to account for horizontally varying atmospheric conditions. As well, a pixel on the ground will see these inhomogeneities at the correct angle. Figure 2.24 illustrates this. Here, an area of high water vapor is located directly above the center of the synthetic image. In sampling the sky for the pixel located at the corner along the red line (situation "A".), the ray tracer will return values which will be nearly identical to the values associated with situation B. In the figure, side A shows what would happen during rendering; a ray is sampling the sky, and encounters a specific water vapor value. Side B shows a path which has been pre-calculated in the ADB. The ray tracer's would return values identical to the results from side B. This method will capture the *relative* angle relationship between the pixel and the cloud, and that is the more important relationship

This will allow the ray tracer to handle any concentration of inhomogeneities at any viewing geometry. In short, the ADB will tell it what a cloud looks like from any angle. This is a very important feature, because the amount of sky radiance reaching a pixel is crucial in correctly rendering an image. An obvious case is that in which the pixel is in direct sunlight versus when it is in a shadow.

The improvements to DIRSIG detailed in this chapter will eliminate the geometric issues which would prevent the accurate modeling of atmospheric inhomogeneities, and allow DIRSIG to successfully incorporate various atmospheric species, including any horizontal spatial structure they might have.

The next chapter will provide a description of the specific algorithms which make the changes described in this chapter.

[3] It should be noted that these experiments were done spectrally.

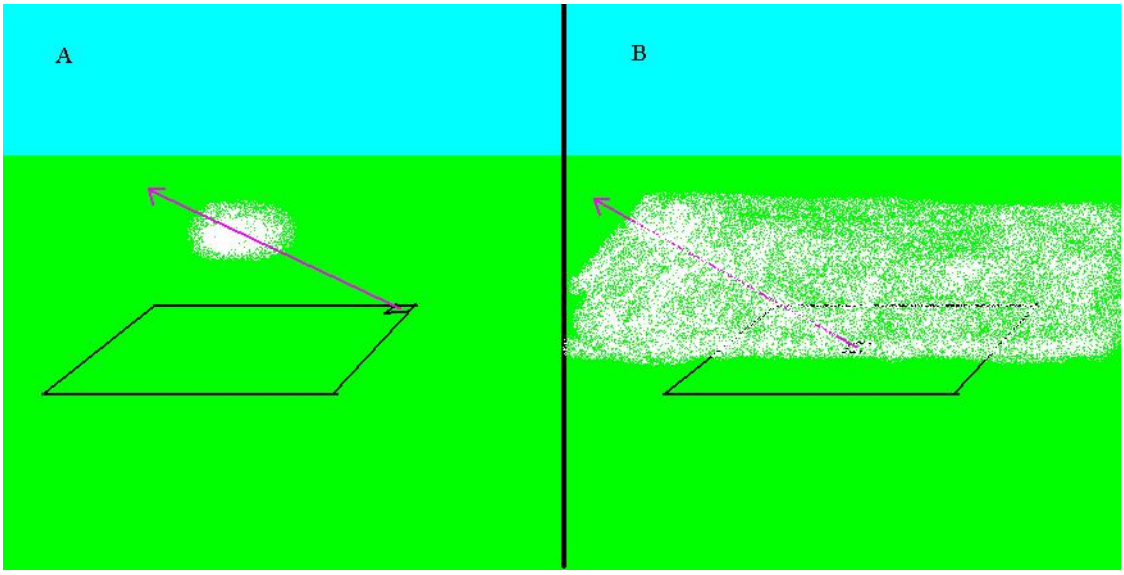

Figure 2.24: An illustration of downwelled sampling of atmospheric inhomogeneities.

Chapter 3

Algorithm Description

Contents

3.1 Atmospheric Database Generation 63
3.1.1 Creating MODTRAN Input Files 64
3.1.2 Setting Input Parameters 64
3.1.3 Nested Loops 70
3.2 Atmospheric Interpolator 73
3.2.1 computeSolarIrradiance 73
3.2.2 computeLunarIrradiance 74
3.2.3 computePathRadiance 75
3.2.4 computePathTransmission 76
3.2.5 computeSkyRadiance 76
3.2.6 Atmospheric Interpolation Tools 76
3.3 Test Cases for Verification 82
3.3.1 Atmospheric Database Generation Verification 82
3.3.2 Atmospheric Interpolator Verification 83

The intent of this chapter is to allow for the smooth transition from the process described in this thesis to proper code which can be integrated into DIRSIG 4.0. There are two main sets of programs which need to be described. The first, is the code which generates the new atmospheric database. The second is the atmospheric interpolator.

It should be noted that the algorithms described here are simply prototypes, and are not intended to be efficient nor elegant from a computer science perspective. The purpose is to explain the intent of the algorithms and so that a computer programer can seamlessly integrate them into DIRSIG.

3.1 Atmospheric Database Generation

In short, the code which generates the new atmospheric database creates a look up table consisting of MODTRAN values. A set of MODTRAN input files are created using pre-set input parameters. These MODTRAN files are run, their results harvested, and placed into an output file.

All of these programs are written in the Interactive Data Language (IDL).

A flow chart showing the overall structure of the code is seen in figure 3.1.

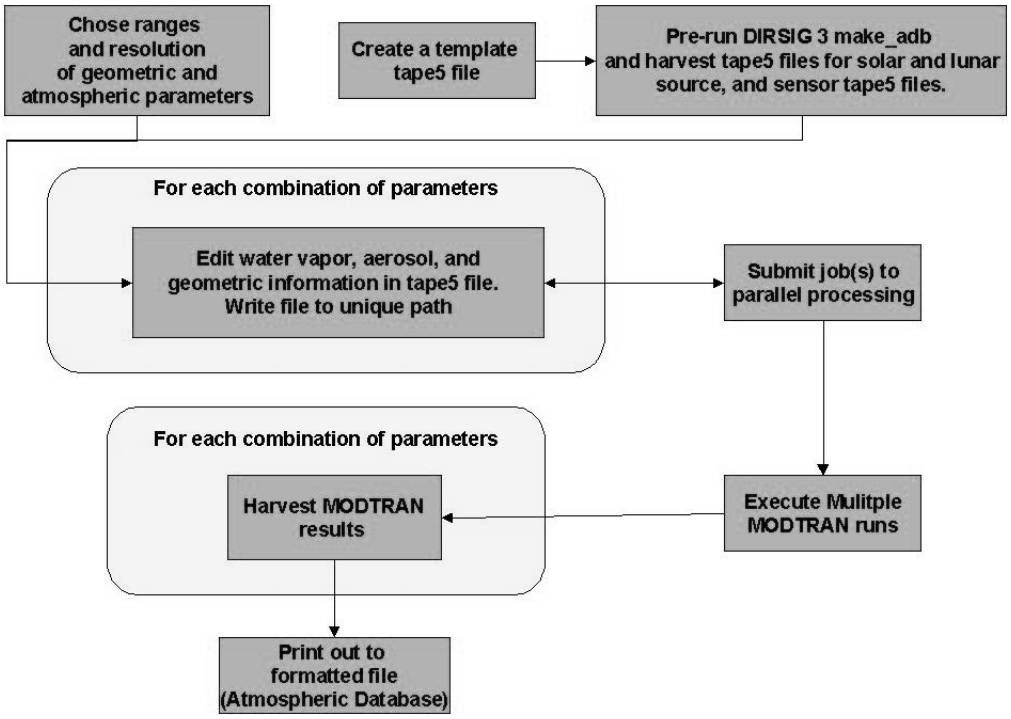

Figure 3.1: The structure of the Atmospheric Database Generation code.

3.1.1 Creating MODTRAN Input Files

The first step is to create a MODTRAN input file (tape5) with the desired atmospheric properties. (See reference [1] for a complete description of what is required of a MODTRAN input file.) This will be used as an input to DIRSIG 3's make_adb program. This is only to take advantage of the existing ephemeris and geometric tools already present in DIRSIG 3. If the proper time, latitude and longitude are set, DIRSIG will produce tape5 files with the correct surface temperature and source and sensor latitude and longitude. As well, all of the other MODTRAN parameters (those which will not be overwritten) will be translated from the original. This process of running DIRSIG 3 can and should be eliminated once this code is streamlined and incorporated into the DIRSIG 4 code.

Three separate tape5 "prototypes" are needed as inputs to the ADB construction code. These include a solar source and a lunar source tape5 file. These can be acquired by copying the "tape5" from the working directory while the make_adb code is calculating the source section of the ADB. While running make_adb, DIRSIG will output "Computing solar and lunar paths ... ". This is when the solar and lunar source tape5 files can be copied.

The other tape5 "prototype" needed is the sensor section tape5. This can be copied while DIRSIG is in the sensor section calculation phase of make_adb. This is evident when DIRSIG displays "Computing sensor paths .....". This method is crude, but effective.

3.1.2 Setting Input Parameters

Calculating the Solar Azimuth Angle

The first parameter which needs to be set is found by taking values from the sensor section "prototype" tape5 file. These are the sensor's (or observer's) and source's (sun's) location in latitude and longitude. These values are used to calculation the solar azimuth angle, with respect to North. The variables are known as *s_lat* for source's latitude, *s_long* for source's longitude, *o_long* for observer's latitude, and *o_long*, for

observer's longitude. These terms are used below.

The process is described below, and the angle is used in the algorithm to exploit the symmetric nature of the solar path radiance about the solar azimuth angle. To save time processing redundant MODTRAN runs, only azimuth angles between the solar azimuth angle, and 180 plus the solar azimuth angle will be sampled.

Process A. *(Calculation of the solar azimuth angle).* This algorithm uses the location of the sensor and the source (generally the sun) to determine the solar azimuth angle relative to North.

Required variables

- *s_long* The location (in longitude) of the source. [degrees]
- *s_lat* The location (in latitude) of the source. [degrees]
- *o_long* The location (in longitude) of the observer. [degrees]
- *o_lat* The location (in latitude) of the observer. [degrees]

A1. [Define the variable *num* as the difference between the source and observer's longitude.] Declare variable *num* as a float equal to *s_long* - *o_long*.

A2. [Define the variable *denom* as the difference between the source and observer's latitude.] Declare variable *denom* as a float equal to *s_lat* - *o_lat*.

A3. [Determine if variable *denom* is equal to 0] If it is, then set new variable $offset$ to 90; otherwise set *denom* equal to $(180.0/3.14159) * atan((s_long - o_long)/(demon))$.

A4. [Determine if variable *num* is equal to 0] If it is, then set variable $offset$ to 0.

Upwelled Section Geometry Values

The next step involves creating a set of input parameters which are needed to construct the atmospheric database (ADB). These, and their units (if any) are shown below.

Geometry Parameters

- number of sensor section zenith angles [NA]
- maximum sensor section zenith angle [degrees]
- minimum sensor section zenith angle [degrees]
- number of sensor section azimuth angles [NA]
- number of sensor section altitude [NA]
- maximum sensor section altitude [km]
- minimum sensor section altitude [km]
- number of downwelled section altitude [NA]
- maximum downwelled section altitude [km]
- minimum downwelled section altitude [km]
- sensor altitude [km]

Atmospheric Parameters

- number of water vapor amounts [NA]

- maximum column water vapor amount [g/cm^2]
- minimum column water vapor amount [g/cm^2]
- number of aerosol types [NA]
- number of visibilities [NA]
- maximum visibility value [km]
- minimum visibility value [km]

Using these parameters, the ADB generation code will create a multi-dimensional look up table, using the number, minimum and maximum of each above parameter to determine the range and resolution of parameter. For example, if the parameter "number of sensor altitudes" is equal to 3, and the maximum and minimum altitude values are 0.0 km and 1.0 km, respectively, the algorithm will sample the altitude at 0.0 km, 0.5 km, and 1.0 km when building the sensor section of the ADB.

Sampling, in this description, means setting up and running MODTRAN for a given geometry, and then harvesting the output data.

The process by which the ranges and resolutions are used to generate a set of values at which to sample is shown below.

Process B. *(Calculating upwelled zenith angle sampling values [interpolation endpoints])*

Required variables

- *zenithcount* The number of zenith angles at which to sample [NA]
- *maxzenith* The maximum zenith angle value [degrees]
- *minzenith* The minimum zenith angle value [degrees]

B1.[Declare a zenith array] Declare a 1-D array *zenith* of size *zenithcount*.

B2.[Define a step size for the zenith array] Set variable *dzenith* equal to $(maxzenith - minzenith)/(zenithcount - 1)$

B3.[Declare a minimum zenith value in the array] Set element $zenith[0]$ equal to *minzenith*.

B4.[Loop on i] Perform step B5, for $i = 1, 2, ...zenithcount - 1$

B5.[Populate *zenith* array] Set $zenith[i]$ equal to $zenith[i-1] + dzenith$.

B6.[Convert *zenith* array to MODTRAN convention for zenith angles [1]] Set *zenith* equal to $180.0 - zenith$.

The process for defining the other sets of parameters is very similar, but some have differences. The next parameter is the azimuth angle. As stated before, the fact that the values derived form MODTRAN are symmetric about the solar azimuth angle, the angle values used will not cover a full range of 360 degrees. To increase the resolution at which the atmosphere is sampled, the algorithm samples the atmosphere at azimuths between the calculated offset, and the offset plus 180. During rendering, if an azimuth value falling outside this range is passed to the tool, the values from the angle reflected in this offset angle will be returned. For example, if the offset is 10 degrees, the ranges over which the atmosphere will be sampled is 10 degrees and 10 + 180 degrees (190). Suppose, during rendering, an angle of 5 is passed to the interpolator tool. This is out of the range of the sampled points. The solution is to pass back the atmospheric values as if the angled passed in was 15. Because of the symmetry along the solar azimuth axis, these atmospheric values should be indistinguishable.

The process for assigning the azimuth angle values at which the atmosphere will be sampled is described below.

[1] It should be noted that the original convention for zenith angles (a zenith angle of 0 is looking straight down) is only kept because DIRSIG 3 uses this convention in its atmospheric database.

Process C. *(Calculating upwelled azimuth angle sampling values [interpolation endpoints])*

Required variables

- *azimuthcount* The number of azimuth angles at which to sample [NA]
- *maxazimuth* The maximum azimuth angle value [degrees]
- *minazimuth* The minimum azimuth angle value [degrees]
- $offset$ The solar azimuth angle [degrees]

C1.[Declare an azimuth array] Declare a 1-D array *azimuth* of size *azimuthcount*.

C2.[Define a step size for the azimuth array] Set variable *dazimuth* equal to $180/(azimuthcount - 1)$

C3.[Declare a minimum azimuth value in the array] Set element $azimuth[0]$ equal to $offset$.

C4.[Loop on i] Perform step C5, for $i = 1, 2, ...azimuthcount - 1$

C5.[Populate *azimuth* array] Set $azimuth[i]$ equal to $azimuth[i - 1] + dazimuth$.

The next set of values which must be calculated is the altitudes at which the atmosphere is to be sampled. The process for this is described below.

Process D. *(Calculating altitude sampling values [interpolation endpoints])*

Required variables

- *altcount* The number of altitudes at which to sample [NA]
- *maxalt* The maximum altitude value [km]
- *ground_alt* The altitude of the ground value [km]

D1.[Declare an altitude array] Declare a 1-D array *alt* of size *altcount*.

D2.[Define a step size for the altitude array] Set variable *dalt* equal to $(maxalt - ground_alt)/(altcount - 1)$

D3.[Declare a minimum altitude value in the array] Set element $alt[0]$ equal to *ground_alt*.

D4.[Loop on i] Perform step D5, for $i = 1, 2, ...altcount - 1$

D5.[Populate *alt* array] Set $alt[i]$ equal to $alt[i - 1] + dalt$. [2]

Downwelled Section Geometry Values

The previous processes described the methods of selecting sampling points for the upwelled section of the atmospheric database. The next three descriptions explain the similar processes used to generate the sets of geometric data used in the downwelled section of the ADB. The purpose of these data sets are the same as those in the upwelled section: to tell the algorithm where to sample the atmosphere. It should be noted that, with the exception of the altitude component (and the ending zenith angle), this process should produce roughly the same structure as the downwelled section in DIRSIG 3.

Process E. *(Calculating downwelled zenith angle sampling values [interpolation endpoints])*

Required variables

- *down_zenith_count* The number of zenith angles at which to sample [NA]
- *down_horizon* The zenith angle of the horizon [3] [degrees]

[2] The source section will use this exact same set of altitudes when sampling the atmosphere.

[3] This value is calculated from a separate program and is discussed in appendix C

- *down_zenith_start* The minimum zenith angle value [degrees]

E1.[Declare a zenith array] Declare a 1-D array *down_zenith* of size *down_zenith_count*.

E2.[Define a step size for the zenith array] Set variable *down_dzenith* equal to $(down_zenith_end - down_zenith_start)/(down_zenith_count - 1)$

E3.[Declare a minimum zenith value in the array] Set element *down_zenith*[0] equal to *down_zenith_start*.

E4.[Loop on i] Perform step E5, for $i = 1, 2, ...down_zenithcount - 1$

E5.[Populate *down_zenith* array] Set *down_zenith*[i] equal to $down_zenith[i-1] + down_dzenith$.

The following described the process for selecting the azimuth angles to sample for the downwelled section of the ADB.

Process F. *(Calculating downwelled azimuth angle sampling values [interpolation endpoints])*

Required variables

- *down_az_count* The number of azimuth angles at which to sample [NA]
- *down_daz* The number of azimuth angles at which to sample [NA]

F1.[Declare an azimuth array] Declare a 1-D array *down_az* of size *azimuthcount*.

F2.[Declare a minimum azimuth value in the array] Set element *down_az*[0] equal to 0.

F3.[Loop on i] Perform step F4, for $i = 1, 2, ...down_az_count - 1$

F5.[Populate *down_az* array] Set *down_az*[i] equal to $down_az[i-1] + down_daz$.

The following described the process for selecting the altitudes to sample for the downwelled section of the ADB.

Process G. *(Calculating downwelled section altitude sampling values [interpolation endpoints])*

Required variables

- *down_altcount* The number of altitudes at which to sample [NA]
- *maxdown_alt* The maximum altitudes value [km]
- *ground_alt* The altitude of the ground [km]

G1.[Declare an altitude array] Declare a 1-D array *down_alt* of size *down_altcount*.

G2.[Define a step size for the altitude array] Set variable *down_dalt* equal to $(maxdown_alt - ground_alt)/(down_altcount - 1)$

G3.[Declare a minimum altitude value in the array] Set element *down_alt*[0] equal to *ground_alt*.

G4.[Loop on i] Perform step G5, for $i = 1, 2, ...down_altcount - 1$

G5.[Populate *down_alt* array] Set *down_alt*[i] equal to $down_alt[i-1] + down_dalt$.

Atmospheric Constituent Values

The final set of values which must be defined are the atmospheric constituents. Namely, the water vapor content and visibilities. The aerosol types need not be calculated; MODTRAN ihaze parameters are simply assigned to an integer array.

Assigning the water vapor values is very similar to those mentioned above, and is described below.

Process H. *(Calculating the water vapor sampling values [interpolation endpoints])*

Required variables

- *number_of_water_amounts* The number of water vapor values at which to sample [NA]
- *min_water* The minimum water vapor amount at which to be sampled [g/cm^2]
- *maxwater* The maximum water vapor amount at which to be sampled [g/cm^2]
- *default_water* The water vapor used if only one value is chosen [g/cm^2]

H1.[Declare a water array] Declare a 1-D array *water* of size *numer_of_water_amounts*.

H2.[Define a step size for the water array] Set variable *dwater* equal to $(maxwater - minwater)/(number_of_water_amounts - 1)$

H3.[Declare a minimum water value in the array] Set element $water[0]$ equal to *min_water*.

H4.[Loop on i] Perform step H5, for $i = 1, 2, ...number_of_water_amounts - 1$

H5.[Populate *water* array] Set $water[i]$ equal to $water[i-1] + dwater$.

The visibility values are found in a slightly different manner than the other sets of values. The spacing is actually in even intervals in inverse visibility space (referred to "extinction" space here). The process is described below.

Process I. *(Calculating the visibility sampling values [interpolation endpoints])*

Required variables

- *number_of_visibilities* The number of visibility values at which to sample [NA]
- *minvis* The minimum visibility amount at which to be sampled
- *maxvis* The maximum visibility amount at which to be sampled

I1.[Declare an extinction array] Declare a 1-D array *ext* of size *number_of_visibilities*.

I2.[Define a step size for the extinction array] Set variable *dext* equal to $((1/minvis) - (1/maxvis))/(number_of_visibilities - 1)$

I3.[Declare a minimum extinction value in the array] Set element $ext[0]$ equal to $1/maxvis$.

I4.[Loop on i] Perform step I5, for $i = 1, 2, ...number_of_visibilities - 1$

I5.[Populate *ext* array] Set $ext[i]$ equal to $ext[i-1] + dext$.

I6.[Create *vis* array] Set *vis* equal to $1/ext$ (in the reverse order).

Spectral Information

For each spectral band desired, a complete MODTRAN card 4 must be created. Refer to [1] for the exact structure. The card 4 holds the band's range, resolution, and the full-width at half-max value, as well as other required MODTRAN tags, such as the spectral units. This information is hard-coded in lines 336 to 371 of "build_lut_i_repeat.pro" [4] of the ADB generation code. The values as of the writing of this document are as follows:

```
green  = '  0.507000  0.511000  0.001000  0.001000TMtesting mtaa'
red    = '  0.647000  0.651000  0.001000  0.001000TMtesting mtaa'
NIR    = '  0.849000  0.851000  0.001000  0.001000TMtesting mtaa'
water band 1 = '  0.879000  0.882000  0.001000  0.001000TMtesting mtaa'
water band 2 = '  0.936000  0.939000  0.001000  0.001000TMtesting mtaa'
water band 3 = '  0.999000  1.001000  0.001000  0.001000TMtesting mtaa'
thermal = '  9.900000 10.100000  0.100000  0.100000TMtesting mtaa'
```

[4]This file is only one of a set of IDL programs which are required to create the new ADB file.

3.1.3 Nested Loops

The next step in ADB construction is to loop over the values defined for each variable and set up a MODTRAN run with that specific combination of values. The outermost loop loops over the water vapor values, followed by the aerosol types, and then the visibilities. For each combination of the above parameters, a complete geometric sampling of the atmosphere is performed. So, for example, if you used 2 aerosol types, 2 visibilities, and 2 water vapor values, there would be 8 total combinations for which geometric sampling will take place. A complete geometric sampling consists of the following combinations in order:

Source Section

- altitudes

Sensor Section

- zenith angles
- azimuth angles
- altitudes

Downwelled Section

- zenith angles
- azimuth angles
- altitudes

For each combination of atmospheric geometric parameters (and bands, if more than one), a unique MODTRAN input file is created, and run. [5] The specific modifications to the MODTRAN tape5 file are shown below for the source section. For a complete description of the individual parameters, see [1].

MODTRAN Parameters Changed : Source Section [6]

Card 1A:

- H2OSTR (This customizes the column water vapor amount [g/cm^2] when used as "gX.X")

Card 2:

- IHAZE (This sets the aerosol type.)
- VIS (This sets the meteorological visibility. [km])

Card 4:

- ALL (The entire card 4 is manually set as a string in the ADB generation code.)

MODTRAN Parameters Changed : Sensor Section

Card 1A:

[5] If this is run in series, meaning when one run completes, the next one starts, then the total run time can be quite large. It is recommended that a parallel processing be used if possible.

[6] The source section is done this way for both the solar and lunar primary sources. This is to preserve the lunar source option available in DIRSIG 3. However, at the time the interpolation code was written, lunar ephemeris functions were not available in DIRSIG 4. Thus the robust atmospheric interpolator in DIRSIG 4 described in this work does not allow for modeling with the moon as the primary source. However, those lunar ephemeris tools have been created and can be incorporated into this work.

- H2OSTR (This customizes the column water vapor amount [g/cm^2] when used as "gX.X".)

Card 2:

- IHAZE (This sets the aerosol type.)
- VIS (This sets the meteorological visibility. [km])

Card 3:

- H1 (This sets the altitude of the sensor. [km])
- H2 (This sets the altitude of the target. [km])
- ANGLE (This sets the target's zenith angle, as seen from the sensor. [degree])

Card 3:

- PSIPO (This sets the target's azimuth angle, East of North, as seen from the sensor. [degree])

Card 4:

- ALL (The entire card 4 is manually set as a string in the ADB generation code.)

MODTRAN Parameters Changed : Downwelled Section

Card 1:

- ITYPE (This changes MODTRAN's run mode from "point to point" to "Slant path to space".)

Card 1A:

- H2OSTR (This customizes the column water vapor amount [g/cm^2] when used as "gX.X".)

Card 2:

- IHAZE (This sets the aerosol type.)
- VIS (This sets the meteorological visibility. [km])

Card 3:

- H1 (This sets the altitude of the sensor. [km])
- H2 (This sets the tangent path of the viewing geometry, and is set to 0.0 indicating a ray of infinite length. [km])
- ANGLE (This sets the sensor's zenith viewing angle, measured from nadir. [degree])

Card 3:

- PSIPO (This sets the sensor's azimuth viewing angle, East of North. [degree])

Card 4:

- ALL (The entire card 4 is manually set as a string in the ADB generation code.)

Once all of the MODTRAN runs have completed, all of the tape7.scn files are read in and the relevant data recorded in the output file. Specifically, columns 0, 3, and 1 for the source sections (representing, respectively, the spectral center, the solar or lunar irradiance reaching the target, and the transmission from the source to the target). For the sensor and downwelled sections, the columns are 0, 2, 4, 1. These represent the spectral center, thermal path radiance from target to sensor, solar path radiance from target to sensor, and the transmission from target to sensor. These values, in this order, are printed out into the output file. [7]

In pseudo-code, the above process can be described as such:

```
for each [water vapor value] do {
  for each [aerosol type] do {
    for each [visibility] do {
      for each [source altitude] do {
        (create unique input file and run MODTRAN)
        (harvest and print out MODTRAN results)
      }
      for each [sensor zenith angle] do {
        for each [sensor azimuth angle] do {
          for each [sensor altitude ] do {
            (create unique input file and run MODTRAN)
            (harvest and print out MODTRAN results)
          }
        }
      }
      for each [downwelled zenith angle] do {
        for each [downwelled azimuth angle] do {
          for each [downwelled altitude] do {
            (create unique input file and run MODTRAN)
            (harvest and print out MODTRAN results)
          }
        }
      }
    }
  }
}
```

This process will create an ADB which has a structure similar to a combination of the outlines shown in figures 2.17 and 2.23.

[7] If a parallel processing tool is implemented, then the this loop will have to be done twice; once to create and submit the MODTRAN runs, and a second time to harvest the results when the runs are complete.

3.2 Atmospheric Interpolator

In upgrading the atmospheric model for DIRSIG 4, There were certain functions that needed to be modified. These included any function in which DIRSIG's ray tracer needed to reference the atmospheric database. As stated previously, the current ability of these functions is not sufficient to allow for the addition of horizontally varying atmospheric inhomogeneities. The next few sections will give an overview of these functions, describe how I changed them, and what new tools were needed to complete these changes.

All of these functions are written in C++.

3.2.1 computeSolarIrradiance

A flow chart showing the overall structure of the function is seen in figure 3.2.

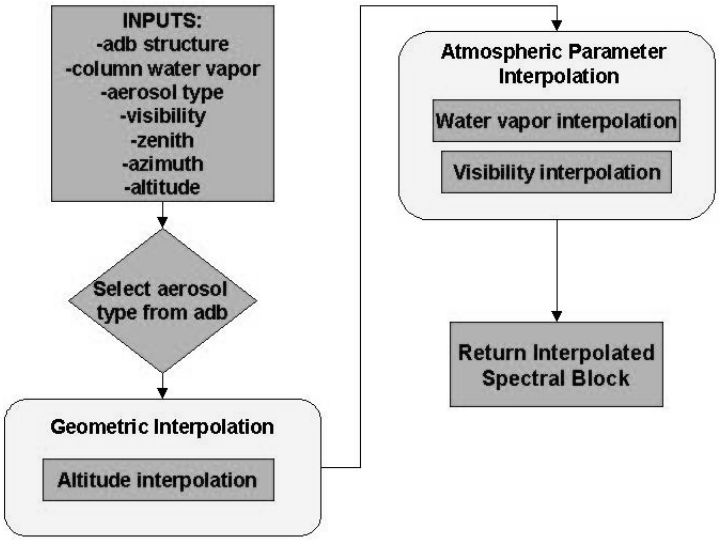

Figure 3.2: The structure of the source section interpolator.

The function computeSolarIrradiance has, as an input, a point in the image. This "location" variable is a CDPoint object [8], and therefore, has three coordinates associated with it: X, Y, and Z. These represent, respectively, East, North, and altitude. All are in meters, with 0,0,0 being the center of the image. This function returns the solar irradiance value for each of the spectral points. (The actual object returned is a CDSpectralVector object), which has more information associated with it.

In DIRSIG 3, This function would just read the source section of the atmospheric database. There was only one "source section" in the DIRSIG 3 atmospheric database. In DIRSIG 4, there will be multiple source sections in the DIRSIG 4 ADB. One for each combination of water vapor, aerosol type, visibility, and altitude. This means that interpolation may be required to get an intermediate spectral vector.

In order to pass these values to this source section interpolator, this function will need to have the ability to cast a ray in a specific direction. This ability is needed in order for the ray to interact with the inhomogeneity maps which will return required information about the atmosphere at that particular look angle. To do this, an accurate sun position is needed. Specifically the solar zenith and azimuth are needed. This is found by using the DIRSIG tool called solarPosition. This will take in a set of geometric and time parameters, and return the solar zenith and azimuth angles. These values will be read in from the ADB when the function executes the tool readadbtent, which is the first step of computeSolarIrradiance. In short, this tool will read in all of the data in the ADB file, and store it in a structure, which will then be passed back to computeSolarIrradiance. The complete description of computeSolarIrradiance can be found in section 3.2.6.

[8] See current DIRSIG documentation for the definition and usage of specific DIRSIG C++ objects.

Once these geometric and time parameters have been read in, computeSolarIrradiance can then create the necessary ray. This ray has its origin at position of the "location" variable, and extends through the solar zenith and azimuth angle. This is because the values in the source section spectral block(s) of the ADB represent data taken when the MODTRAN sensor is pointed directly at the sun. It is crucial, then, to re-created the exact same angle when ray tracing.

Using a CDRay object, and the set of coordinates stored in the "location" input variable, an atmospheric ray is created. The required inputs to solarPosition are listed below, and are read in from the atmospheric database file.

Inputs to solarPosition

- local time
- Greenwich mean time offset
- day of year
- month
- year
- latitude
- longitude

It should be noted that this calculation is not exactly perfect. The exact solar zenith and azimuth will change for each pixel in the scene. However, this issue is only significant if the change in latitude and longitude over the scene is large. This problem is very similar to that described in section 2.1.4. And this problem , as well, would take significant rendering time to correct.

Once the atmospheric ray is defined, it is cast throughout the atmosphere, and reports back information about the atmosphere at that particular look angle. This information includes the water vapor value, aerosol type, and visibility for each atmospheric map it encounters.

In the case that multiple maps of the same type (water vapor or aerosol) are encountered, one of two things will happen. If there are multiple water vapor maps hit, then the average of all return water vapor values are used. If the maps are aerosol maps, then the map with the lowest altitude is used, and the others are ignored.

The next step taken by computeSourceIrradiance is calling the atmospheric tool known as sourceSectionInt. See section 3.2.6 for a description. This tool takes, as an input, the column water vapor, aerosol type, and visibility (all taken from the atmospheric maps), the altitude of the "location" variable, and the atmospheric database (stored in a structure, taken from readadbtent). Its output is the solar irradiance reaching the position described by the "location" variable for each spectral point (interpolated).

This spectral data (referred to as a block) returned from sourceSectionInt is then packaged up as a spectral vector (a CDSpectralVecor object). This is what is returned from the function computeSolarIrradiance

3.2.2 computeLunarIrradiance

This function is nearly identical to computeSolarIrradiance, except that it uses lunar zenith and azimuth values, and returns the lunar irradiance at a given location. However, there is no function which exists in DIRSIG which will return a lunar zenith and azimuth at the writing of this document. Because these angles are crucial for a correct ray to be traced, this function is not yet used in this algorithm.

3.2.3 computePathRadiance

A flow chart showing the overall structure of this function is seen in figure 3.3.

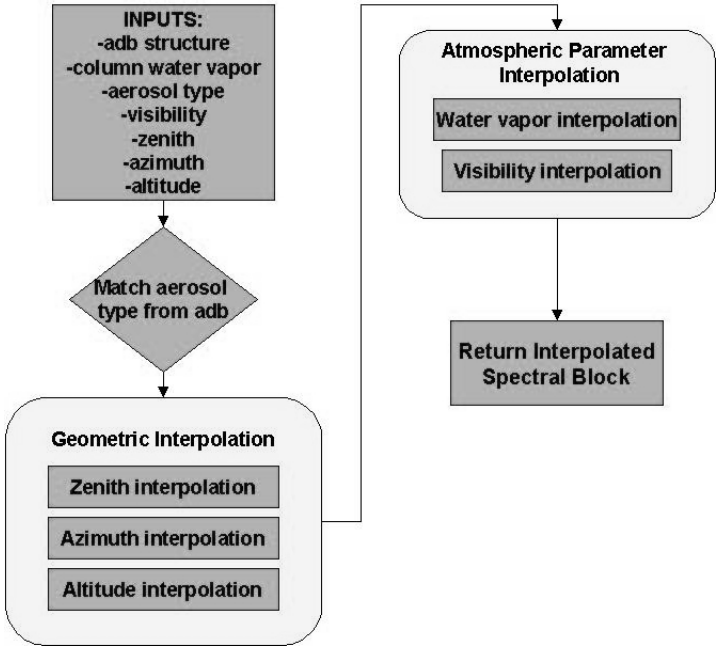

Figure 3.3: The structure of the upwelled and downwelled section interpolators.

The function computePathRadiance is similar to computeSolarIrradiance in that it accepts location information, and outputs spectral data. However, it has *two* CDPoint objects as its input: a target location and a sensor location. The function uses these points to determine the upwelling path radiance reaching the sensor for a given look angle. These points are CDPoint objects and each have three coordinates associated with them: X, Y, and Z. These represent, respectively, East, North, and altitude. All are in meters, with 0,0,0 being the center of the image. This function returns the solar path radiance value for each of the spectral points. This is the energy scattered from the atmosphere, which goes directly to the sensor without reflecting off the target or ground. Again, the actual object returned is a CDSpectralVector object, which has more information associated with it. Consult the latest DIRSIG documentation for a description.

Similar to computeSolarIrradiance, this function will have to provide the interpolator with a number of atmospheric parameters. As well, several geometric parameters will be needed. To get these, this function, will cast a ray from the target to the sensor. Again, this ray (a CDRay object) will return the atmospheric information about any atmospheric map it intersects with. The parameters, again, are column water vapor, aerosol type, and visibility.

Like computeSolarIrradiance, the first step of this function is to read in the entire ADB using the atmospheric tool readadbtent, the complete description of which can be found in section 3.2.6.

In the case that multiple maps of the same type (water vapor or aerosol) are encountered, one of two things will happen. If there are multiple water vapor maps hit, then the average of all return water vapor values are used. This is done because the parameter this algorithm is using in MODTRAN represents a cumulative water vapor amount for the whole atmosphere, *not* a single layer of water vapor. So, summing these values would not be an accurate representation of the meaning of the maps. If the maps are aerosol maps, then the map with the lowest altitude is used, and the others are ignored.

The next step taken by computePathRadiance is calling the atmospheric tool known as upwelledandtransmissiontent. See section 3.2.6 for a description. This tool takes, as an input, the column water vapor, aerosol type, and visibility (all taken from the atmospheric maps), the target point, the sensor point, and the the

atmospheric database (stored in a structure, taken from readadbtent). Its output is the solar path radiance reaching the sensor for each spectral point (interpolated).

This spectral data (referred to as a block) returned from upwelledandtransmissiontent is then packaged up as a spectral vector (a CDSpectralVecor object). This is what is returned from the function computePathRadiance

3.2.4 computePathTransmission

This function is identical to computePathRadiance, except that the value returned from upwelledandtransmissiontent and computePathTransmission is the transmission between the target and the senor.

3.2.5 computeSkyRadiance

This function is very similar to computePathTransmission and computePathTransmission. It, too, takes in the target and sensor CDPoint objects. It uses these to trace a ray from the target not to the sensor, but to a specific point in the sky. It obtains the usual set of atmospheric parameters, and inputs these, along with the target location, sensor location, and ADB structure variable into an interpolator. The interpolator for computeSkyRadiance is known as downtent. This interpolator returns the sky radiance reaching the point known as target. Again, this data is packaged up as a spectral vector, and is what is returned from the function computeSkyRadiance.

3.2.6 Atmospheric Interpolation Tools

This section will detail the specific interpolation tools used by the functions described earlier. Most involve linear interpolation, and have similar inputs and outputs. These require a full set of single-valued atmospheric parameters (column water vapor, aerosol type, and visibility), as well as some form of geometric data. These interpolation tools output a spectral block containing either irradiance, radiance, or transmission.

All are located in the same file, knows as "CDModtranTent.nw", which is in "noweb" format. Each tool will be described in detail in the following sections. "CDModtranTent.nw" has in it a C++ header file which sets up numerous input parameters as well as the structure which will hold all of the spectral data for the entire ADB. An example of this header can be seen in appendix G.

readadbtent

This tool fills the important role of reading in the atmospheric database and storing the information into a structure, such that all of the data can easily pass between functions and tools.

The first step in the tool is to open the file "tent.adb". This file name is hard-coded as of the writing of this document. After which, the tool starts reading in each line of the ADB file. The positions of the relevant data and the irrelevant lines follow a very specific pattern governed by the ADB construction code.

The first section contains scene information needed for geometry and time-related calculations. These parameters, in order, are listed below.

Scene Parameters Read in from the ADB.

- - Sensor altitude
- - Ground altitude
- - day
- - month
- - year

- - local time
- - Greenwich Mean time
- - Greenwich Mean time offset
- - Latitude
- - Longitude

These parameters are placed in the data structure after being read in. They will be used by other functions or tools to calculate necessary geometric values, such as the solar zenith and azimuth angles.

It then reads in the number of column water vapor values, aerosol types, visibilities, zeniths, azimuths, and altitudes over which the atmosphere is sampled. It then compares these values to those set in the header. It is important that these numbers match. It then uses these values to set up nested for loops over each parameter in turn. For every combination of atmospheric parameters, there will be a source section, and sensor section and a downwelled section. Each source section spectral block will have an altitude associated with it. Each sensor and downwelled block will have an altitude, zenith, and azimuth associated with it.

Starting with the water vapor loop, each individual water vapor value is read in for each step of the loop. This value will be assigned to all spectral blocks in that loop. This process repeats all the way down to the altitude. So for each spectral block, every parameter that was used to create it can be stored in the structure. For example, the below line represents the thermal radiance value in the sensor section spectral block.

```
a.water[ i ].aerosol_type[ j ].visibility[ k ].section_2[ m ].
                spectral_data.thermal[ point ] = thermal[ point ];
```

Here, a is the name of the atmospheric structure, i is the index of the water vapor amount, as is j and k for the aerosol type and visibility, respectively. The presence of *section_2* indicates that this is a sensor section spectral block, and we are referencing spectral block m, which will have the zenith angle, azimuth angle, and altitude attached to it. To reference these parameters, use the form shown below, where the zenith angle is referenced:

```
a.water[ i ].aerosol_type[ j ].visibility[ k ].section_2[ m ].zenith;
```

The full behavior of this structure is found in appendix G

Using this process, all spectral blocks are read in and stored in the structure. [9]

[9]The last thing the readadbtent tool does is calculate the total integrated downwelled radiance. This is not needed for this implementation of DIRSIG 4, but is left in for backwards compatibility with DIRSIG 3. There is an option in DIRSIG 3 which decreases run time by bypassing any downwelled interpolation and reporting the total integrated downwelled radiance.

sourceSectionInt (The Source Section Interpolator)

This is the first of the interpolators which will be described. The general function of these tools is to take in a number of parameters, interpolate between the spectral blocks, and return an interpolated spectral block.

Inputs to sourceSectionInt

- - Atmospheric database structure
- - Column water vapor amount
- - Aerosol type
- - Visibility
- - Altitude

The first step this tool takes is to assert that the aerosol type that it is given is found in the ADB. Assuming that this is the case, it then finds the water vapor values in the ADB which the input water vapor value is in between. [10] It does the same for the visibility. Any water vapor or visibility value which falls outside the ranges in the ADB are clipped to the highest or lowest value that exists in the ADB.

Once these surrounding values are found, variables called "diff_water" and "diff_vis" are created by subtracting the input value from the next lower value in the ADB. For example, if the input water is 0.5 g/cm^2, and the two values it lays between in the ADB are 1.0 g/cm^2 and 2.5 g/cm^2, then the value of "diff_water" would be 0.5 g/cm^2. This variable will be used when another tool, linear_interp, is called.

This same process of determining the surrounding values in the ADB for a given input and the difference between it and the next lowest value is repeated for the altitude as well. This sets up three dimensions over which we must interpolate. (The algorithm does not interpolate over aerosol types, but, once one is read in, interpolates exclusively within that aerosol type.)

Once all of the endpoints and "diff" values are calculated, the first interpolation takes place. Now, because there are three dimensions to interpolate, each with two endpoints each, there will be a total of eight endpoints to consider. The interpolation process is one of systematically decreasing the dimensionality of the problem. The first dimension to be reduced is altitude. Four altitude interpolations are performed. One for each combination of water vapor and visibility endpoint. This reduces the problem by one dimension. So, for each combination of water vapor and visibility endpoint, the spectral data at the input altitude is known.

In the graphic seen in figure 3.4, a structure is shown which represents the three dimensions visibility, water vapor, and altitude. The blue dots represent the original eight endpoints, and the red show the remaining four endpoints after altitude dimension has been reduced.

It should be noted that there is inherent spectral nature of these points. No interpolation occurs in these dimensions so they are not extensively covered. The red dots in figure 3.4 represent all of the spectral data at that point. So, for the source section, this represents the solar and lunar irradiance and transmission for each spectral point. For each altitude interpolation, for example, interpolation must be done for each parameter in the spectral block, and for each spectral point.

The next step is to again reduce the dimensionality of the problem. The algorithm next interpolates over the water vapor values. This process is very similar to the one used to eliminate the altitude dimension. Using the (now) four total endpoints, the algorithm finds the value of the spectral data at the two visibility endpoints. Likewise, once this is accomplished, the algorithm reduces the dimensionality one more time, and interpolates those two visibility values into one interpolated spectral block. Figure 3.5 shows these two final dimensionality reductions.

[10] If there is no aerosol type match, the current version of the code crashes. This is left in the code for testing purposes. There are a few of these points in the code which could be modified to prevent crashing (for example, having a default aerosol type in the case where one is not matched. But, for testing it was more important to have all the unexpected code failures terminate the program so the user could address the specific problem.

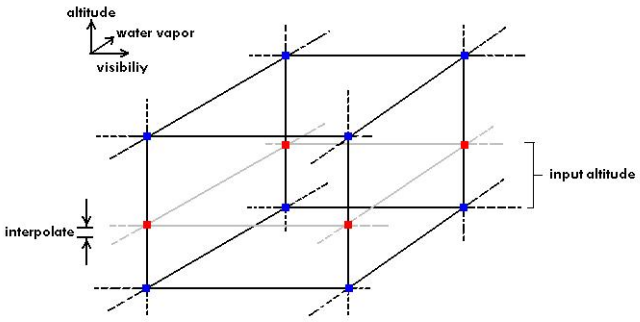

Figure 3.4: This is a graphic representing the reduction of the dimensionality carried out by the source section interpolator.

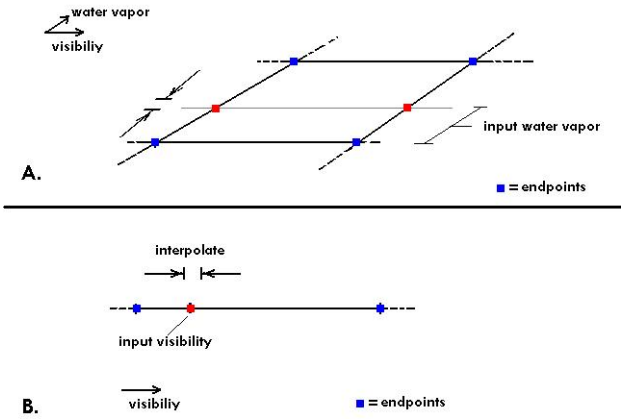

Figure 3.5: This is a graphic representing the reduction of the dimensionality carried out by the source section interpolator.

Finally, the algorithm returns this interpolated spectral block. This, again will have solar and lunar irradiances and transmissions for each spectral point.

upwelledandtransmissiontent

(The Sensor Section Interpolator)

This atmospheric tool is very similar to the source section interpolator. The only difference is that there are two additional dimensions to consider. The same process of dimensional reduction is applied in this tool. The two additional dimensions are the zenith and azimuth dimensions. Because these are geometric, it is useful to separate out the geometric dimensions (zenith, azimuth and altitude) from what will be refer to as the "constituent" dimensions (water vapor, aerosol type, and visibility.) In short, the algorithm interpolates to get the atmospheric values at a give look angle (and altitude) in the sky for each combination of water vapor and visibility endpoint (4 total). This is similar to the source section interpolation, in that there was only one geometric dimension (altitude) to be collapsed. In the sensor section the algorithm collapses the zenith dimension, the azimuth dimension, and *then* the altitude dimension to return to a similar problem as the one described in section 3.2.6.

The general function of this tools is to take in a number of parameters, interpolate between the spectral

blocks, and return an interpolated spectral block. For the sensor section interpolator, the specific input parameters are listed below.

Inputs to upwelledandtransmissiontent

- - Atmospheric database structure
- - Column water vapor amount
- - Aerosol type
- - Visibility
- - Zenith
- - Azimuth
- - Altitude

Like the source section interpolator, this function returns an interpolated spectral block.

downtent (The Downwelled Section Interpolator)

From a functional point of view, this tool behaves exactly the same as the upwelledandtransmissiontent tool. The only real difference in the tools is that this tool references a different section of the atmospheric database (the Downwelled Section).

linear_interp

This tool is a custom linear interpolator. For simplicity, it was designed to accept 5 values, which are shown in figure 3.6 for a simple function. In the figure, the red dots represent the endpoints (in one dimension), with x_0, x_1, y_0, and y_1, as their abscissa and ordinate values, respectively. The green dot represents the value of the function at the value x_factor, which is a measure of the difference between the given input parameter and the previous endpoint. The value $result$ shown in the diagram is the ordinate value associated with $x_0 + x_factor$, and is the desired result which the tool returns.

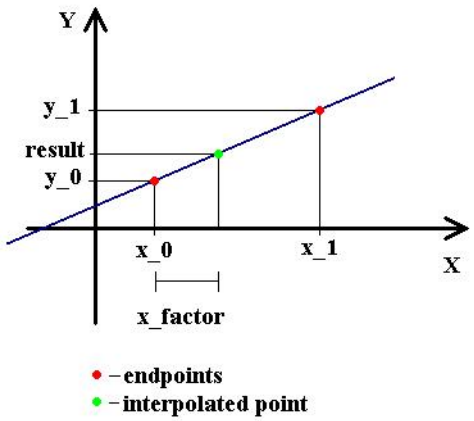

Figure 3.6: This figure shows a representative set of values which are read into the tool linear_interp.

The algorithm is outlined in more detail here:

Algorithm H: *(Linear Interpolation)* The algorithm takes in five values: abscissa values (x_0, x_1) and ordinate values (y_0, and y_1) of two endpoints. The fifth entry is the distance from the first abscissa value (x_0) and the abscissa value to be interpolated.

H1. [Define all of the variables used in the algorithm.] Declare variables b (with a value equal to y_0), m, and y as floating numbers.

H2. [Determine if x_0 equals x_1.] If it is, then set y equal to b; otherwise continue to H3.

H2a. [Calculate a denominator.] Declare the variable *denom* as a float with value equal to the absolute value of (x_1 - x_0).

H2b. [Determine if x_0 equals 330.0 and x_1 equals 0.0] If so, set $denom = 30.0$

H2c. [Set slope of linear interpolator] Set m equal to ((y_1 - y_0)/*denom*).

H2d. [Calculate result of interpolation] Set y equal to $m*x_factor = b$.

H3. [Return interpolation result (y).]

3.3 Test Cases for Verification

The purpose of this section is to provide simple inputs and outputs to various portions of the algorithm so that anyone reproducing this algorithm may have a method of checking that the processes were repeated correctly.

3.3.1 Atmospheric Database Generation Verification

The first test will test the atmospheric database generation code. Provided below is a set of input parameters. When these parameters are used as the input to the atmospheric database generation code, the resulting ADB should be identical to the file "tent_sunrise_2water_2aero_2vis_8zen_8az.adb"

Located in "/dirs/home/bmd1603/prop/verification_folder/make_adb/" is the finished atmospheric database, as well as the input MODTRAN "prototype" files for the solar and lunar source files, and the source section file ("band0.tp5"). The specific input parameters are listed below.

Geometry Parameters

- number of sensor section zenith angles [NA] 8
- maximum sensor section zenith angle [degrees] 0
- minimum sensor section zenith angle [degrees] 23
- number of sensor section azimuth angles [NA] 8
- number of sensor section altitude [NA] 2
- maximum sensor section altitude [km] 1
- minimum sensor section altitude [km] 0
- number of downwelled section altitude [NA] 2
- maximum downwelled section altitude [km] 1
- minimum downwelled section altitude [km] 0
- sensor altitude [km] 50

Atmospheric Parameters

- number of water vapor amounts [NA] 2
- maximum column water vapor amount [g/cm^2] 2.5
- minimum column water vapor amount [g/cm^2] 0.0
- number of aerosol types [NA] 2
- number of visibilities [NA] 2
- maximum visibility value [km] 1.0
- minimum visibility value [km] 23.0

3.3.2 Atmospheric Interpolator Verification

This section will provide inputs and outputs for the atmospheric interpolator verification. Using the same atmospheric database as mentioned above ("tent_sunrise_2water_2aero_2vis_8zen_8az.adb"), as well as an aerosol value of 1 (rural aerosols), a visibility of 23 km, and a water vapor value of zero, a set of points and angles will be fed into each interpolator. (These atmospheric values can be gotten by using the maps "zero.img" and "nuclear_waste.img", which can be found in "/dirs/home/bmd1603/prop/verification_folder/interpolator/"

The output of the interpolators, as well as the input geometry values are found in the the file "interpolator_output.txt" in that same directory.

The next chapter will provide a description of test scenes which will help demonstrate and quantify these improvements to DIRSIG.

Chapter 4

Test Scenes

Contents

4.1 Geometry Test Scenes 86
4.1.1 Highlighting Angular Features 86
4.1.2 Highlighting Altitude Changes 112
4.2 Atmospheric Variability Test Scenes 127
4.2.1 Highlighting Water Vapor Changes 127
4.2.2 Highlighting Visibility Changes 144
4.3 Test Image Error Summary 173
4.4 Demonstration Images 177
4.4.1 Megascene 177

Test scenes are an important method of demonstrating concepts and evaluating results. This chapter describes test scenes which were constructed in order to highlight the improvements made to DIRSIG. The results will be demonstrated both by displaying images, as well as providing quantitative evaluations of the images.

This section describes how the performance of this atmospheric model was analyzed. Visually confirming that the model is performing as expected is an important part of demonstrating its functionality, however it is also very valuable to determine, quantitatively, how well DIRSIG is modeling the atmosphere and predicting atmospheric values.

For most of the images described in this chapter, a simple root-mean-squared error metric was applied. For several key points in each the rendered test scenes, the atmospheric values were recorded. These scenes were also rendered using the existing DIRSIG model, and the same key points analyzed. Both of these values were then compared to the results of a MODTRAN run, executed under identical atmospheric and geometric conditions. The error metric is a root-mean-squared error, assuming that the MODTRAN results are truth.

It is expected that the new method of sampling will be considerably closer to the MODTRAN results than the current sampling method, primarily because the current method does not have the ability to sample in the azimuth or altitude dimensions. Geometric issues aside, the new method of sampling (DIRSIG 4) is not expected to produce any improvements in the prediction of atmospheric values when only water vapor and/or aerosols are investigated. This is simply because the ability did not exist in the previous version (DIRSIG 3). The purpose of this work, with regard to these atmospheric characteristics, is to allow them to vary horizontally within the DIRSIG atmosphere.

In general, RMS error calculation was done on a band by band basis, for a set of points in the image.

As previously stated, the DIRSIG 3 model only interpolates over one dimension: zenith angle. This chapter will show, progressively, how more complicated images (ones with more dimensions), cause the results from the DIRSIG 3 model to increasing diverge from those of MODTRAN (truth). For example, if we examine a

scene with constant atmospheric properties, with all objects at zero altitude, and look only at atmospheric values at 0 degrees azimuth (where DIRSIG 3 samples the atmosphere), there should be no noticeable improvement due to the DIRSIG 4 atmospheric model. This is because we are limiting the interpolation to the dimensions that DIRSIG 3 normally interpolates over.

Now, if a point in the image is examined which has a different azimuth angle, this moves the analysis to a dimension that DIRSIG 3 does not interpolate over. At this point, the DIRSIG 4 model has the clear advantage, as it has multiple azimuth angles at which it has sampled.

This process of increasing the dimensionality of the test image was repeated for not only azimuth, but altitude, then water vapor and visibility. With each dimension, the performance of DIRSIG 4's atmospheric model should increase with respect to DIRSIG 3's.

4.1 Geometry Test Scenes

4.1.1 Highlighting Angular Features

The first scene is a very simple one. This scene consists of one large panel horizontally oriented, at ground level. On top of this panel are two objects which can be described as pyramids with the tops cut off. All objects in the scene have zero reflectivity. A model of this scene can be seen in figure 4.1

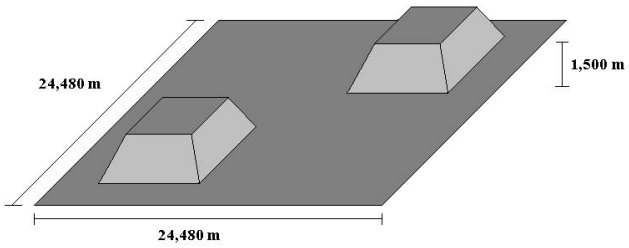

Figure 4.1: This scene highlights the changes in the angular structure of the upwelling radiance in the image, due to the new method of sampling the atmosphere.

The scene is observed from directly overhead, at an altitude of 50 km. The purpose of this particular image is to study the relative performances of the DIRSIG 4 and DIRSIG 3 atmospheric models when looking at a simple scene (all points at zero altitude, and constant atmospheric parameters), and varying the azimuth angle. The objects in the image are not needed for this first set of experiments, but will be used in later ones.

This image was analyzed under three conditions: sunset, noon, and sunrise.

The analysis was done by first rendering this scene using both DIRSIG 3 and DIRSIG 4. Then, a set of points were selected which would highlight a specific area of the image. For each of these points, the path radiance and transmission (for each band) were recorded for each of the images. As well, the geometry of that particular point (zenith, azimuth, and altitude) was obtained from the truth image, using these geometry values, and a MODTRAN input file similar to that used to construct the ADBs, a MODTRAN run was executed and the path radiance and transmission for each band was harvested. Using the three sets of data (DIRSIG 3, DIRSIG 4, and MODTRAN results), the values in DIRSIG 3 and 4 were compared to that retrieved from MODTRAN. The error for each was calculated using the formula 4.1.

$$E_i = \sqrt{(X_i - Y_i)^2/n} \tag{4.1}$$

In this equation, i is the band, E_i is the RMS (root-mean-squared) error (for either DIRSIG 3 or 4), X_i

is either the path radiance or transmission for band i taken from DIRSIG 3 or 4, Y_i is the corresponding MODTRAN value for the path radiance or transmission for band i, and n is the number of points analyzed.

Sunset Case (Image 1a)

The first set of data includes results obtained by analyzing the images which were rendered at sunset.

As stated earlier, for each set of conditions, a series of points was be looked at in each image. The first set will contain points which lay entirely on the 0-180 degree azimuth line. The goal here is to show the worst case scenario for the DIRSIG 4 interpolator.

First of all, figure 4.2, shows the path radiance (blue band) obtained from DIRSIG 3 and 4. This will be used as an aid in showing exactly where the image was analyzed. Note the relatively lower amount of path radiance over the pyramid objects. This is due to the fact that these objects are at a higher altitude than the surrounding areas. Because of this, there is significantly less atmosphere for the light to scatter off of This effect will be looked at in test case 2a.

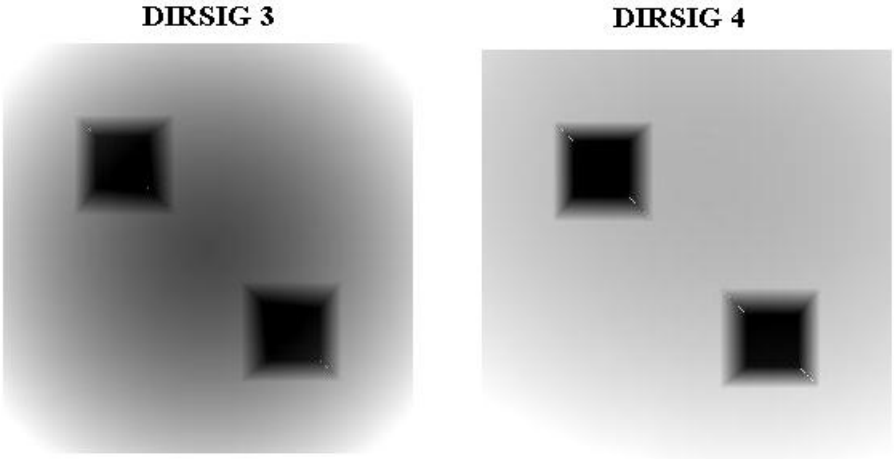

Figure 4.2: The blue path radiance obtained during sunset from the DIRSIG 3 and DIRSIG 4 interpolator over the "truncated pyramid" test scene. In order to highlight the changes in radiance in the image, the dynamic range of the image was increased by using the Histogram Equalization enhancement tool in ENVI.

The following figures (4.3 and 4.4) show, qualitatively, the different outputs when running DIRSIG 3 or DIRSIG 4 respectively. Notice the lack of azimuthal variation in figure 4.3, and its presence in the DIRSIG 4 rendering in figure 4.4, which even shows the expected reddening of the sky during sunset in the Western portion of the image (positive y in this image).

The bright spots on the upper left and lower right corners of the objects in figure 4.3 are artifacts caused by DIRSIG's handling of the facets. These are in no way caused by the atmosphere, and therefore will be ignored in this study.

The zenith angle in figure 4.3 ranges from 180 degrees (straight down, using the MODTRAN convention) at the very center of the image, to about 161 degrees, at the corner of the image. Because this image is one where the sensor is looking directly down, all azimuth angles are present.

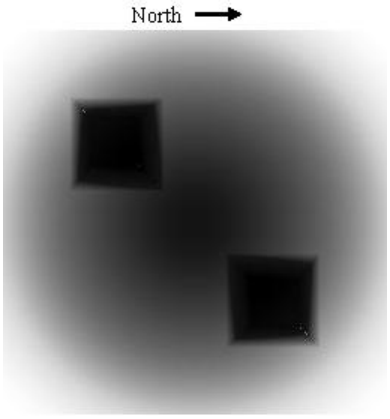

Figure 4.3: The visible path radiance obtained during sunset from the DIRSIG 3 interpolator over the "truncated pyramid" test scene. (displayed in RGB.)

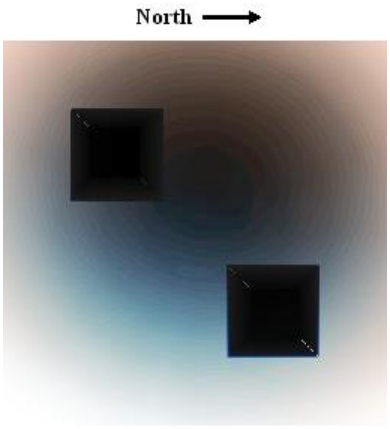

Figure 4.4: The visible path radiance obtained during sunset from the DIRSIG 4 interpolator over the "truncated pyramid" test scene. (displayed in RGB.) Notice the relative red color of the Western sky (positive y)

In order to better quantify the improved accuracy of the new atmospheric model, as stated before, the images were analyzed at specific points. These points are shown in figure 4.5. The dots in a horizontal line represent the points analyzed for the study which highlights the variations in the zenith dimension. The dots organize in a circle are those used in the azimuthal variation study.

Results of Varying Zenith Angle

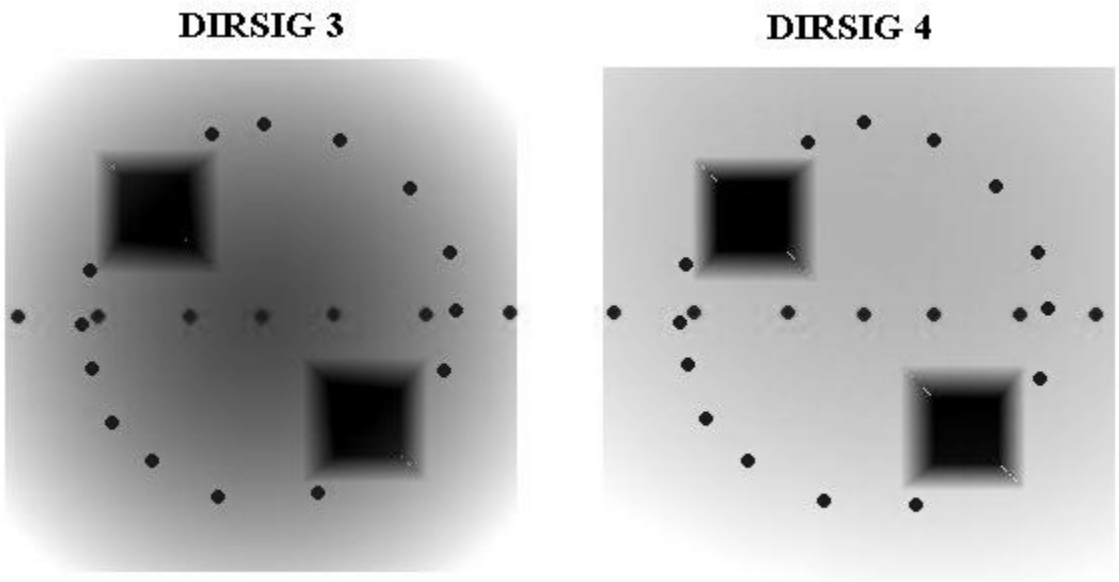

Figure 4.5: The linearly and circularly organized dots represent points analyzed in the zenith and azimuth studies, respectively.

For each of the "horizontal line" dots seen in figure 4.5, the relative percent error was calculated for both the DIRSIG 4 and DIRSIG 3 interpolators. The results for all of the bands, as well as the calculated RMS for all of the points, can be seen in figures 4.6 through 4.10 (radiance) and 4.11 through 4.15 (transmission). (The full results for most of the test images can be seen in appendix. B.)

These results show that DIRSIG 4's interpolator exhibits poorer performance than DIRSIG 3's regarding the path transmission. This is expected, because the DIRSIG 3 ADB samples the atmosphere at azimuth values of 0 degrees. Because the DIRSIG 4's ADB contains azimuth values which are based on the solar azimuth angle, it does not necessarily sample at 0 degrees azimuth. This means that any values at 0 degrees in the DIRSIG 4 interpolator will be a result of interpolation in at least one (probably two) dimensions. The nature of the structure of the DIRSIG 3 ADB allows the interpolator to more accurately reproduce MODTRAN values at 0 degrees azimuth. As the next study will show, this is *not* the case for all azimuth angles.

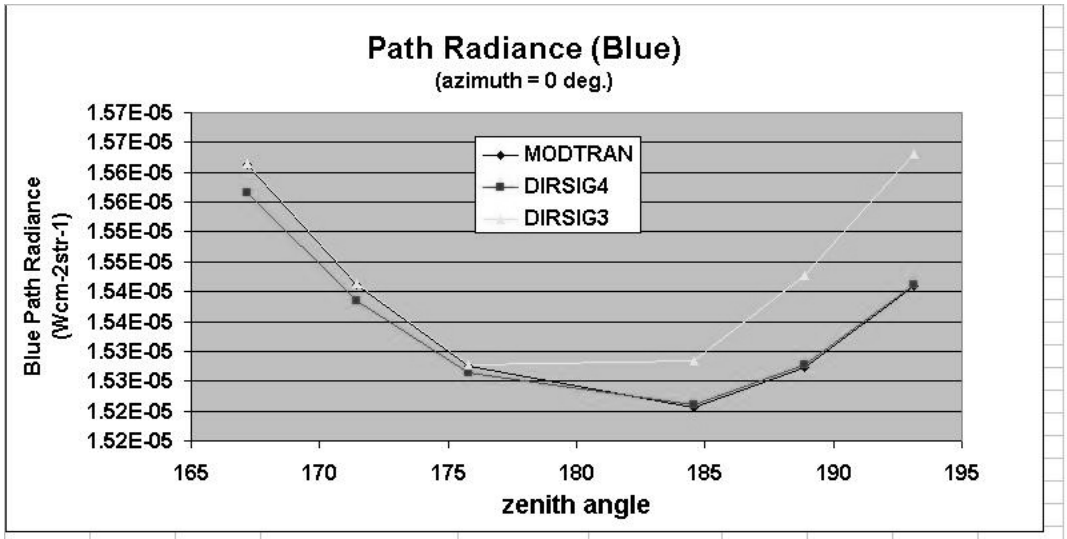

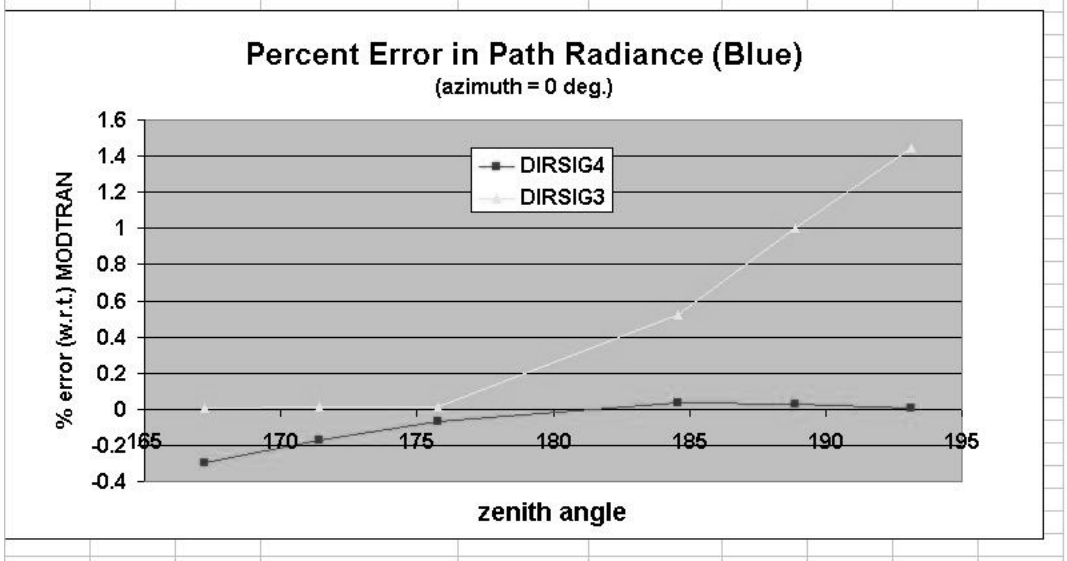

	DIRSIG 4	DIRSIG 3
RMS Error (Blue band)	2.21743E-08	1.1484E-07

Figure 4.6: Test Scene 1a (varying zenith angle): The upper graph shows the blue path radiance obtained by MODTRAN, DIRSIG 4 and DIRSIG 3. The lower graph shows the percent error of DIRSIG 4 and DIRSIG 3 relative to MODTRAN. The RMS error for the points shown on the graph are listed below the graphs.

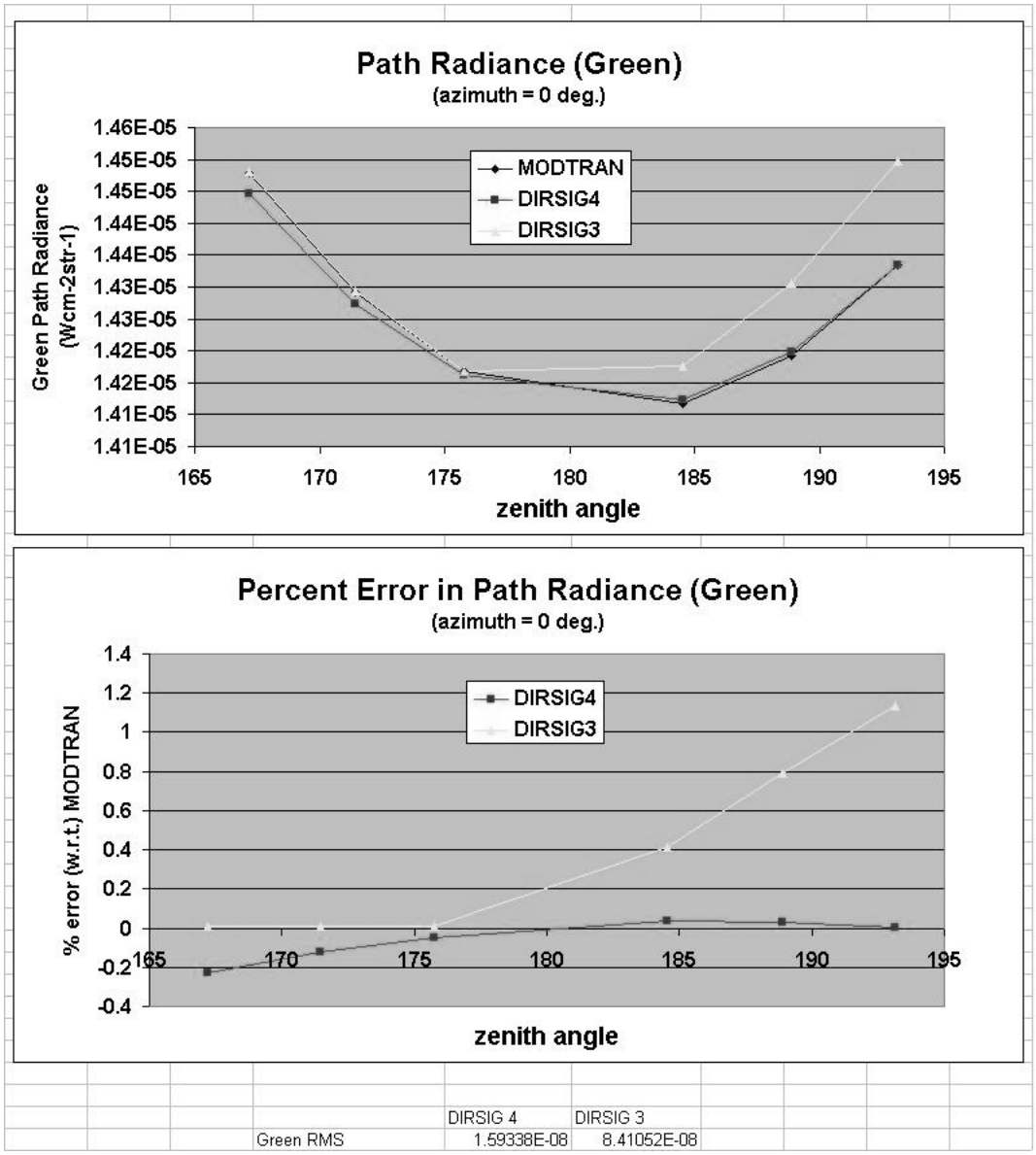

Figure 4.7: Test Scene 1a (zenith variation): The upper graph shows the green path radiance obtained by MODTRAN, DIRSIG 4 and DIRSIG 3. The lower graph shows the percent error of DIRSIG 4 and DIRSIG 3 relative to MODTRAN. The RMS errors for the points shown on the graph are listed below the graphs.

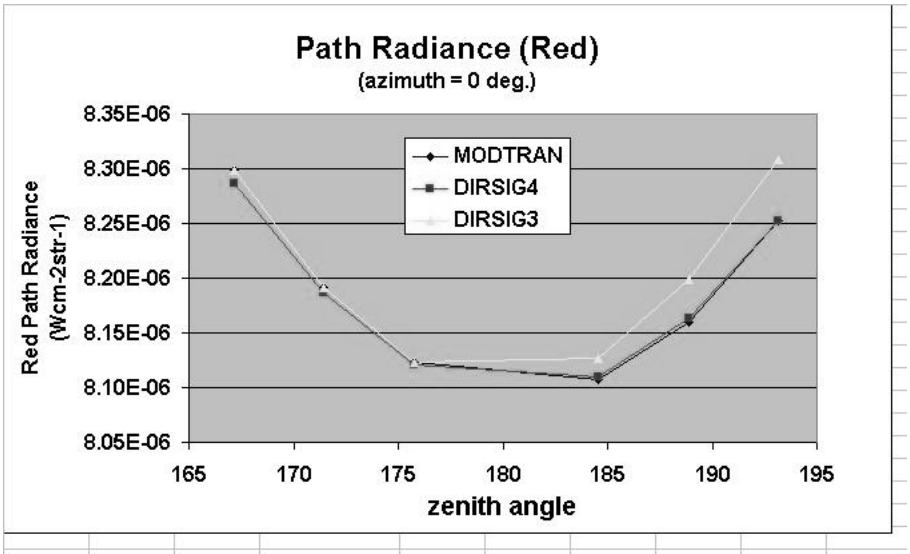

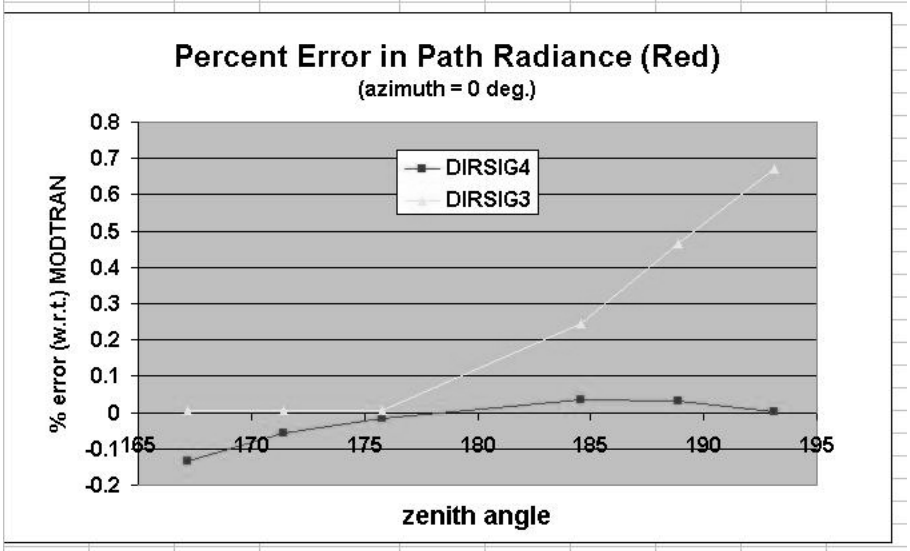

	DIRSIG 4	DIRSIG 3
RMS Error (red)	5.18E-09	2.86E-08

Figure 4.8: Test Scene 1a (zenith variation): The upper graph shows the red path radiance obtained by MODTRAN, DIRSIG 4 and DIRSIG 3. The lower graph shows the percent error of DIRSIG 4 and DIRSIG 3 relative to MODTRAN. The RMS errors for the points shown on the graph are listed below the graphs.

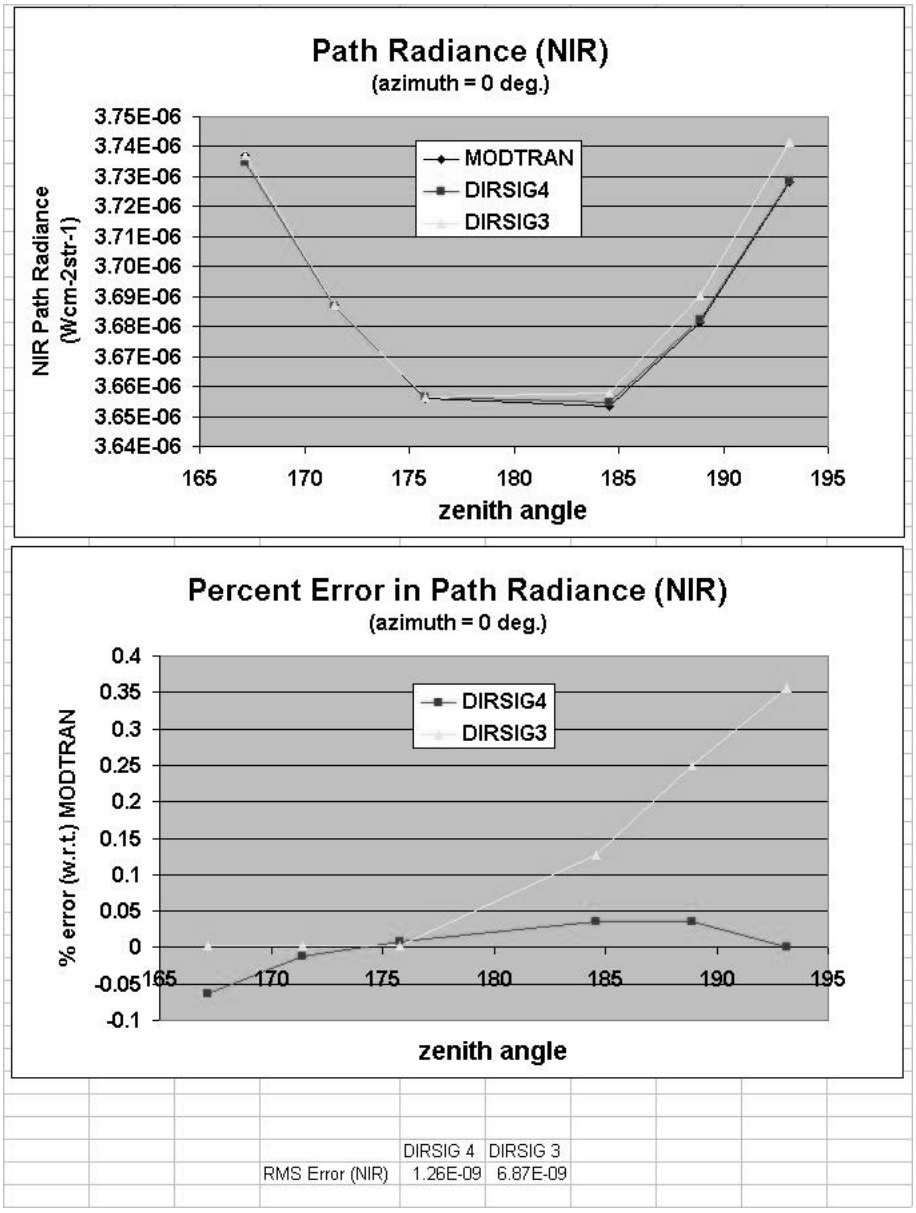

Figure 4.9: Test Scene 1a (zenith variation): The upper graph shows the NIR path radiance obtained by MODTRAN, DIRSIG 4 and DIRSIG 3. The lower graph shows the percent error of DIRSIG 4 and DIRSIG 3 relative to MODTRAN. The RMS errors for the points shown on the graph are listed below the graphs.

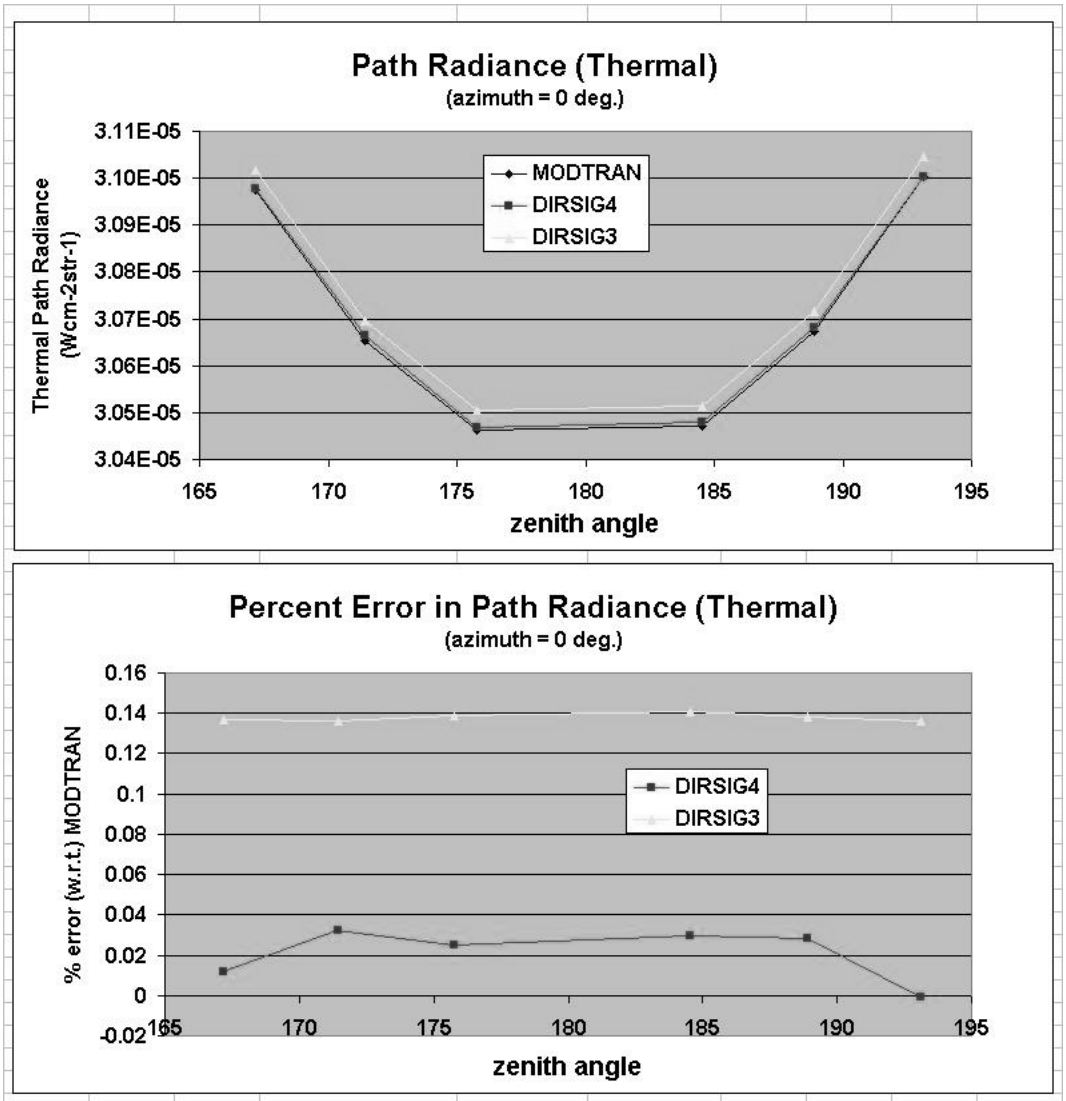

Figure 4.10: Test Scene 1a (zenith variation): The upper graph shows the thermal path radiance obtained by MODTRAN, DIRSIG 4 and DIRSIG 3. The lower graph shows the percent error of DIRSIG 4 and DIRSIG 3 relative to MODTRAN. The RMS errors for the points shown on the graph are listed below the graphs.

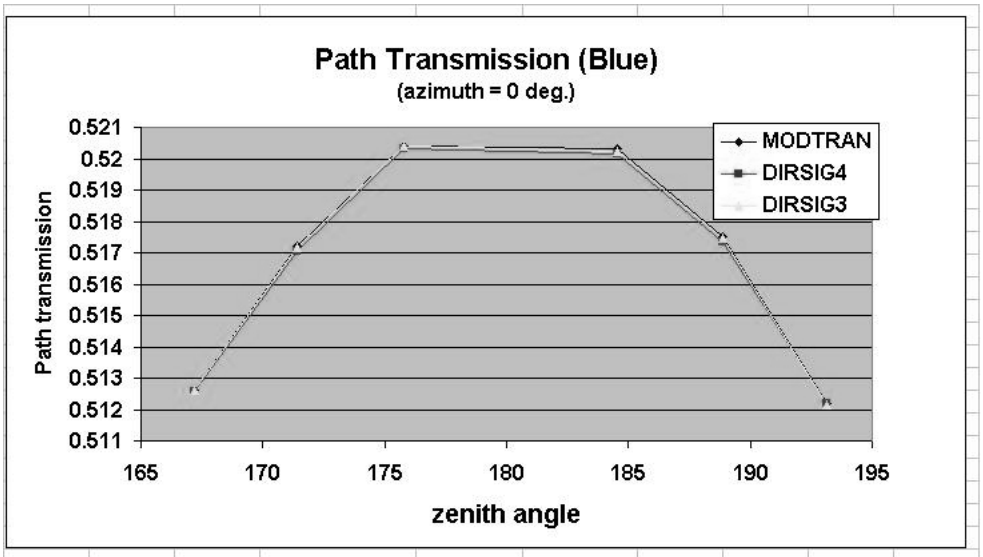

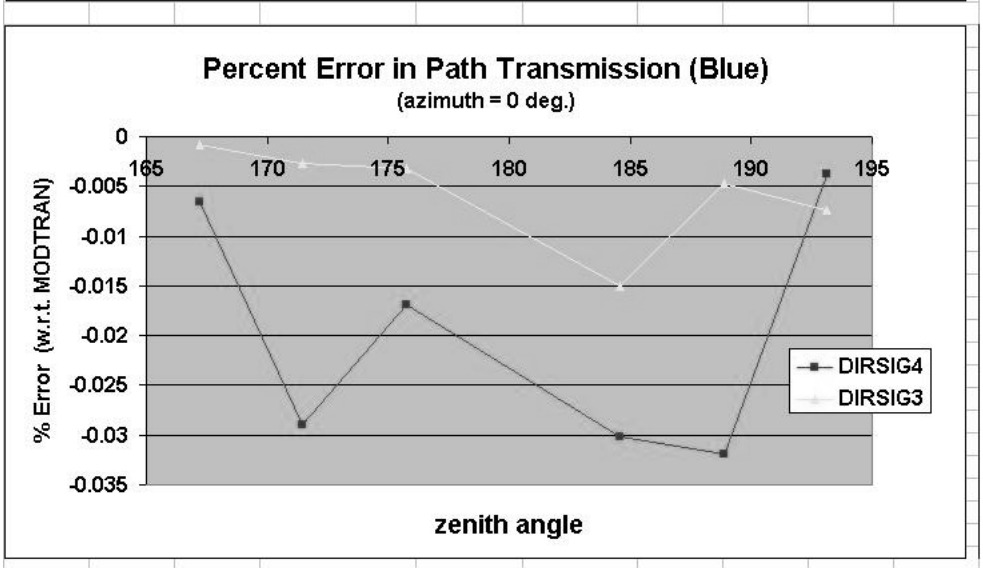

	DIRSIG 4	DIRSIG 3
RMS Error (Blue)	0.00011806	3.78704E-05

Figure 4.11: Test Scene 1a (zenith variation): The upper graph shows the blue path transmission obtained by MODTRAN, DIRSIG 4 and DIRSIG 3. The lower graph shows the percent error of DIRSIG 4 and DIRSIG 3 relative to MODTRAN. The RMS error for the points shown on the graph are listed below the graphs.

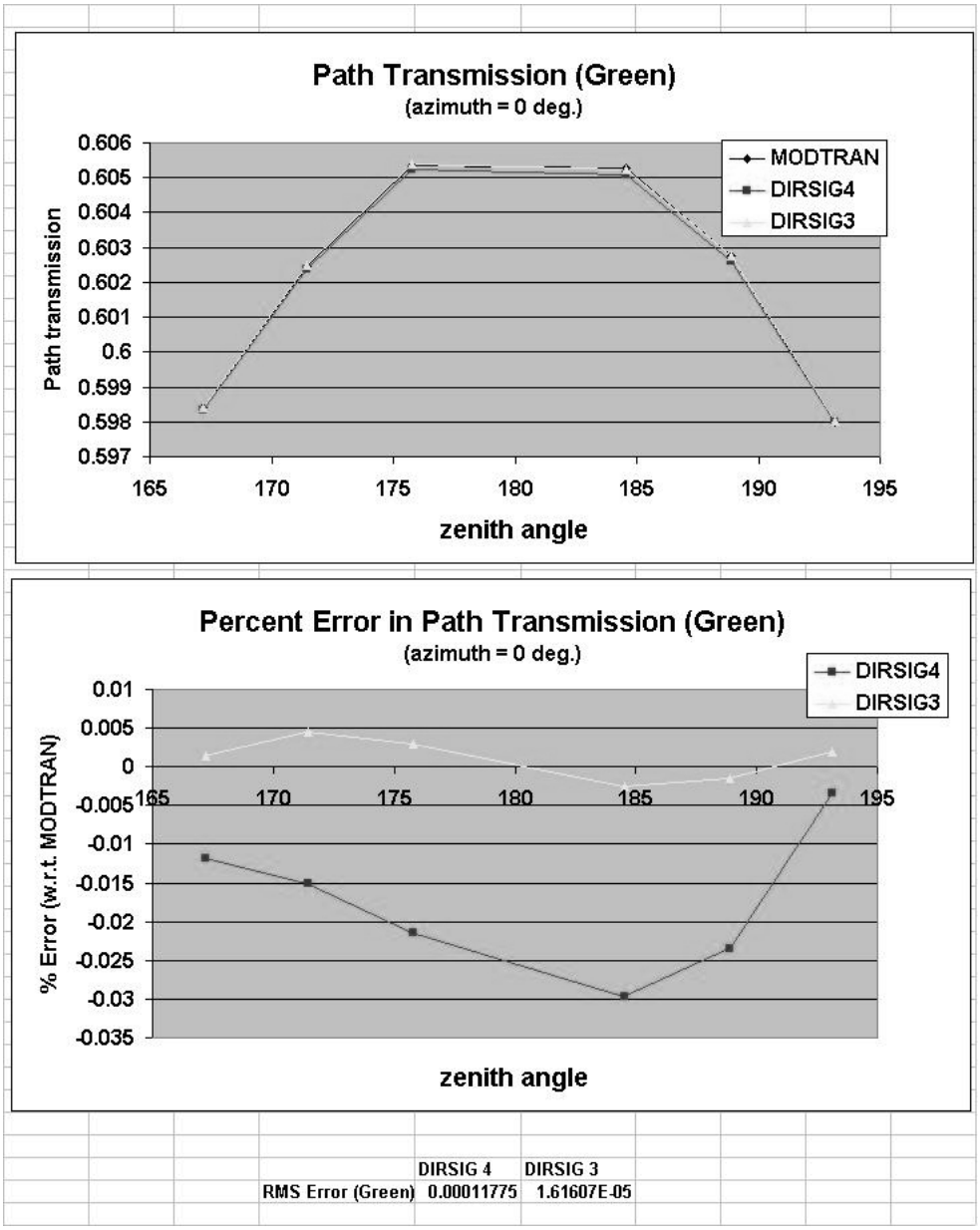

Figure 4.12: Test Scene 1a (zenith variation): The upper graph shows the green path transmission obtained by MODTRAN, DIRSIG 4 and DIRSIG 3. The lower graph shows the percent error of DIRSIG 4 and DIRSIG 3 relative to MODTRAN. The RMS errors for the points shown on the graph are listed below the graphs.

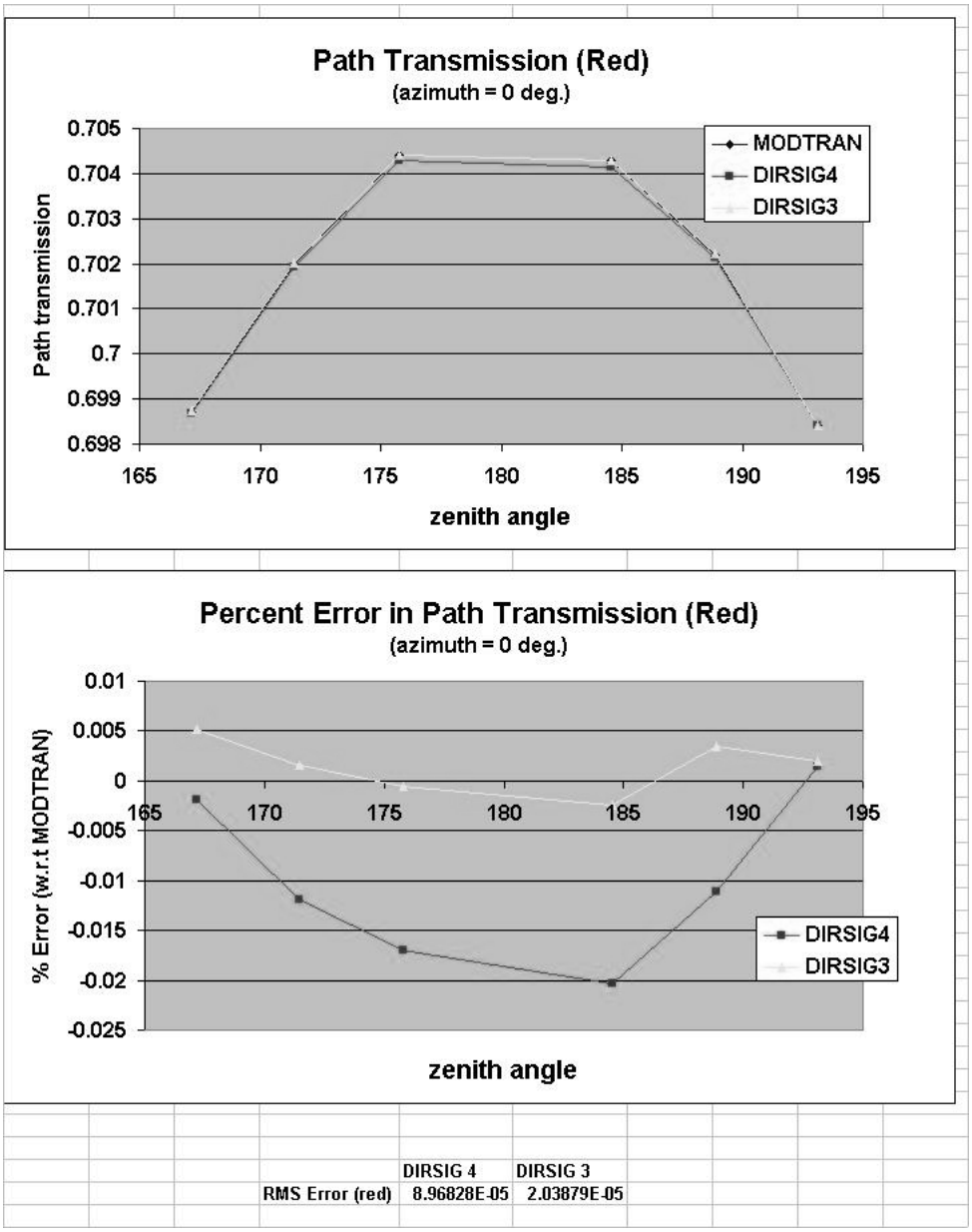

Figure 4.13: Test Scene 1a (zenith variation): The upper graph shows the red path transmission obtained by MODTRAN, DIRSIG 4 and DIRSIG 3. The lower graph shows the percent error of DIRSIG 4 and DIRSIG 3 relative to MODTRAN. The RMS errors for the points shown on the graph are listed below the graphs.

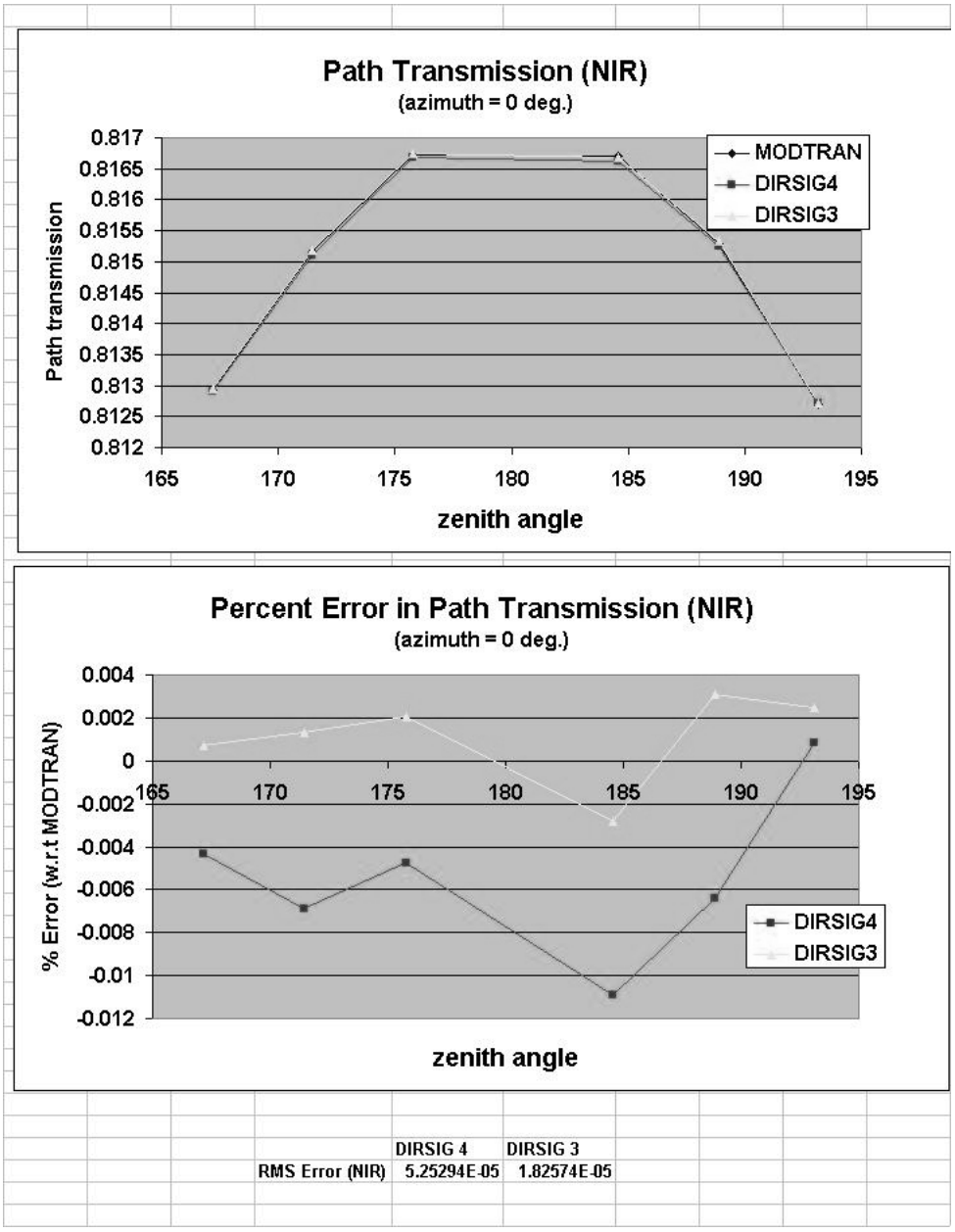

Figure 4.14: Test Scene 1a (zenith variation): The upper graph shows the NIR path transmission obtained by MODTRAN, DIRSIG 4 and DIRSIG 3. The lower graph shows the percent error of DIRSIG 4 and DIRSIG 3 relative to MODTRAN. The RMS errors for the points shown on the graph are listed below the graphs.

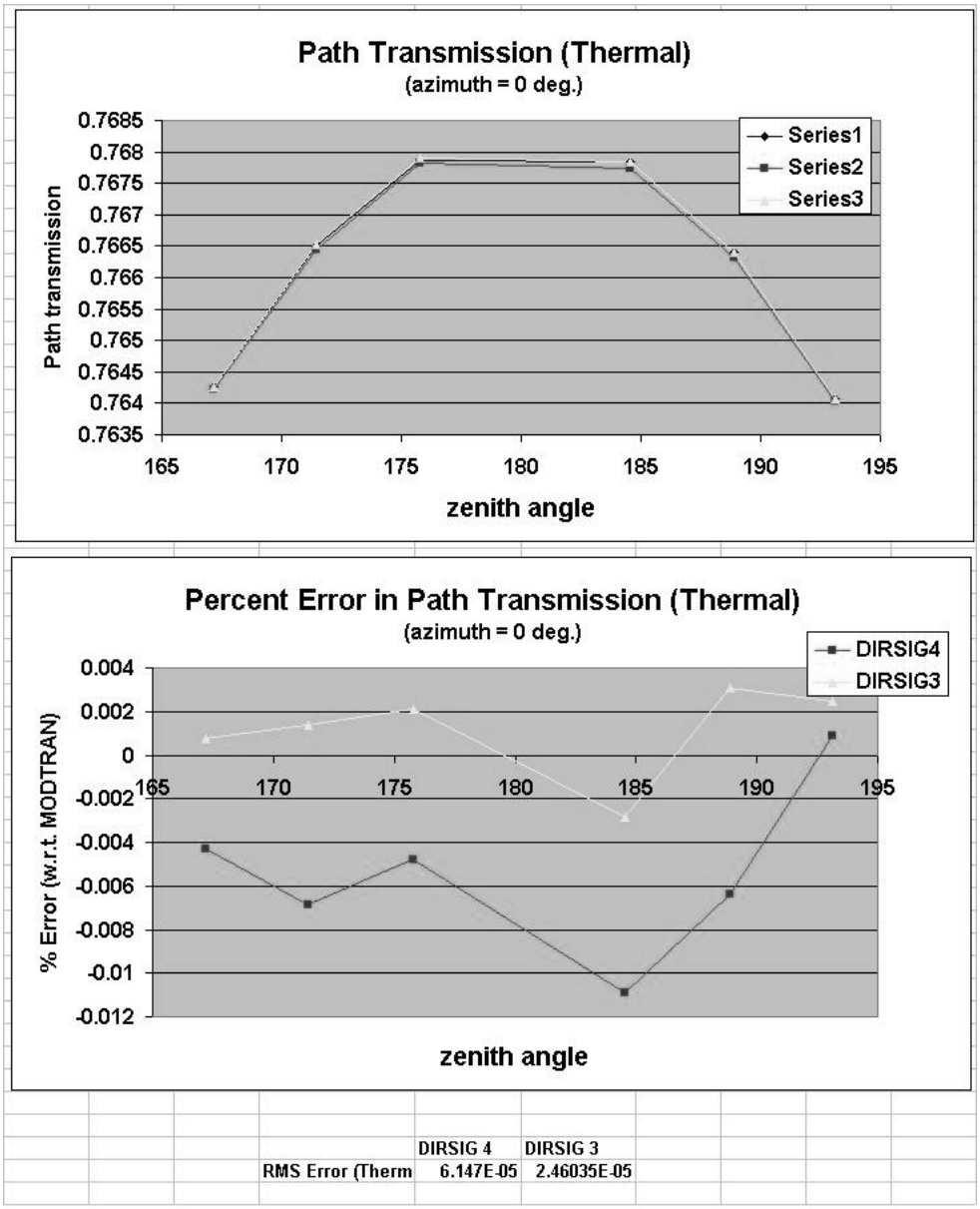

Figure 4.15: Test Scene 1a (zenith variation): The upper graph shows the thermal path transmission obtained by MODTRAN, DIRSIG 4 and DIRSIG 3. The lower graph shows the percent error of DIRSIG 4 and DIRSIG 3 relative to MODTRAN. The RMS errors for the points shown on the graph are listed below the graphs.

Results of Varying Azimuth Angle

This test shows the results of running the above experiment, but varying the azimuth angle (at a constant zenith angle). For each of the circularly arranged dots seen in figure 4.5, the relative percent error was calculated for both the DIRSIG 4 and DIRSIG 3 interpolators. The results for the blue band can be seen in figures 4.16 through 4.19 (radiance) and 4.20 through 4.23 (transmission).

(The full results can be seen in appendix B.)

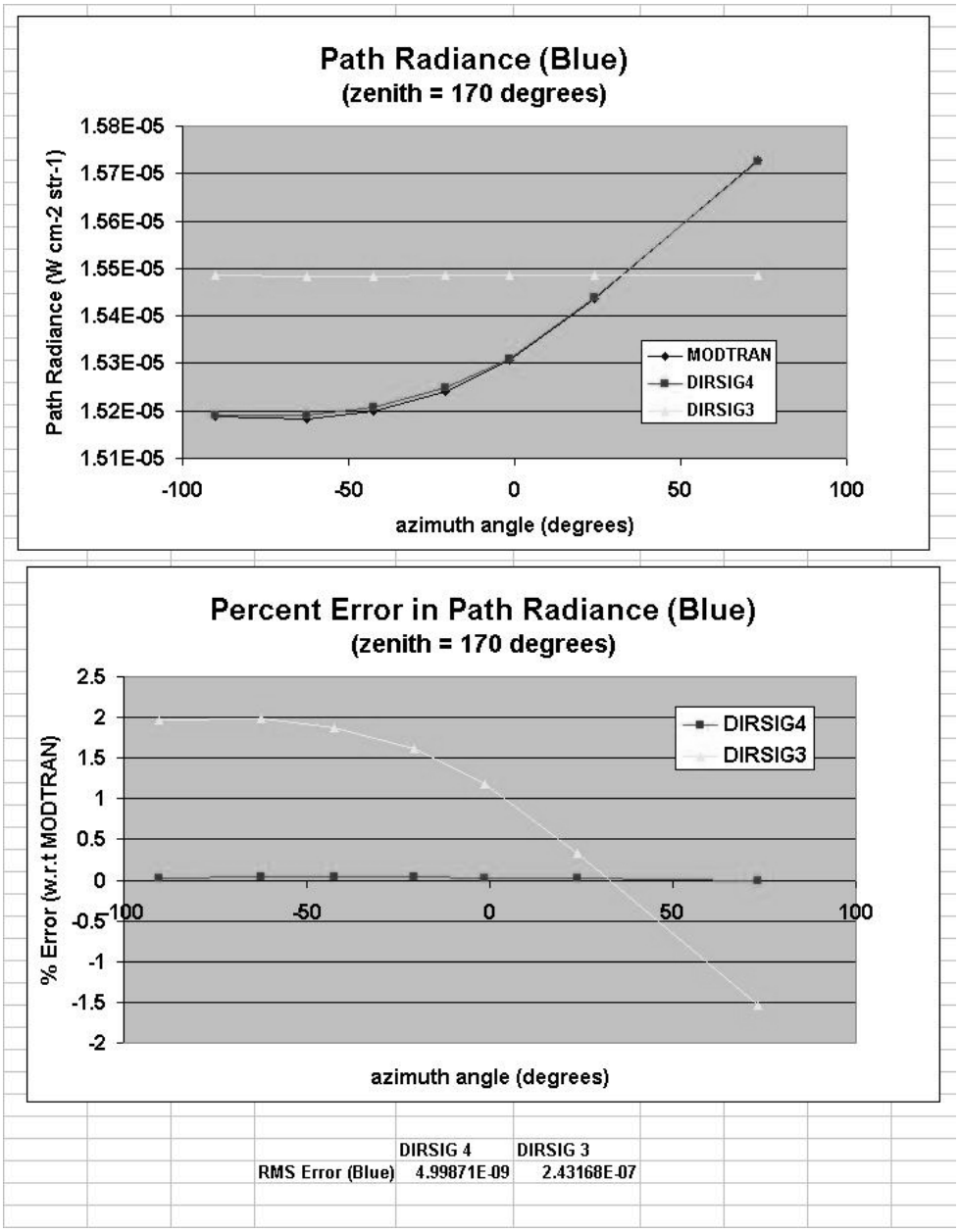

Figure 4.16: Test Scene 1a: The upper graph shows the blue path radiance obtained by MODTRAN, DIRSIG 4 and DIRSIG 3. The lower graph shows the percent error of DIRSIG 4 and DIRSIG 3 relative to MODTRAN. The RMS error for the points shown on the graph are listed below the graphs.

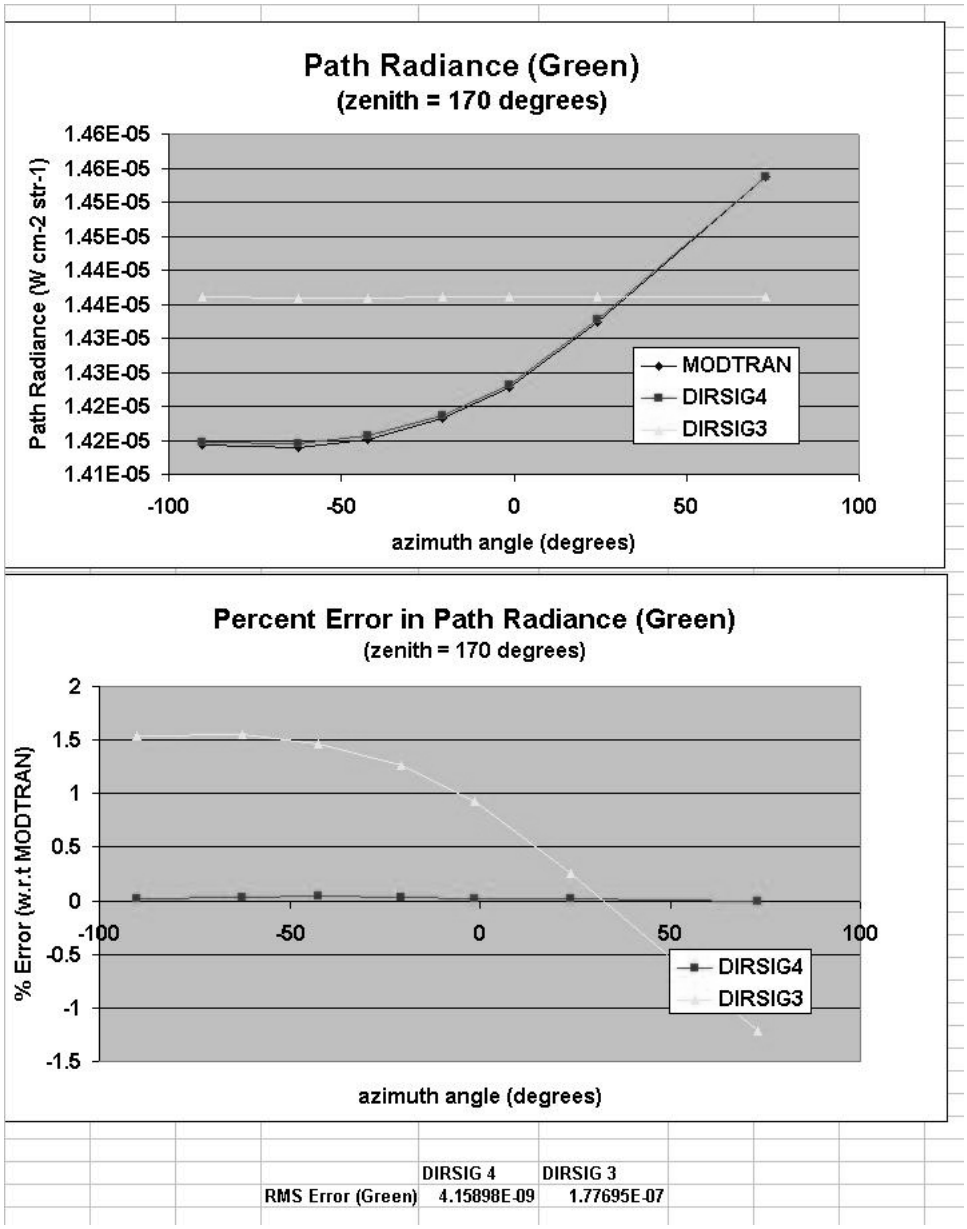

Figure 4.17: Test Scene 1a (azimuth variation): The upper graph shows the green path radiance obtained by MODTRAN, DIRSIG 4 and DIRSIG 3. The lower graph shows the percent error of DIRSIG 4 and DIRSIG 3 relative to MODTRAN. The RMS errors for the points shown on the graph are listed below the graphs.

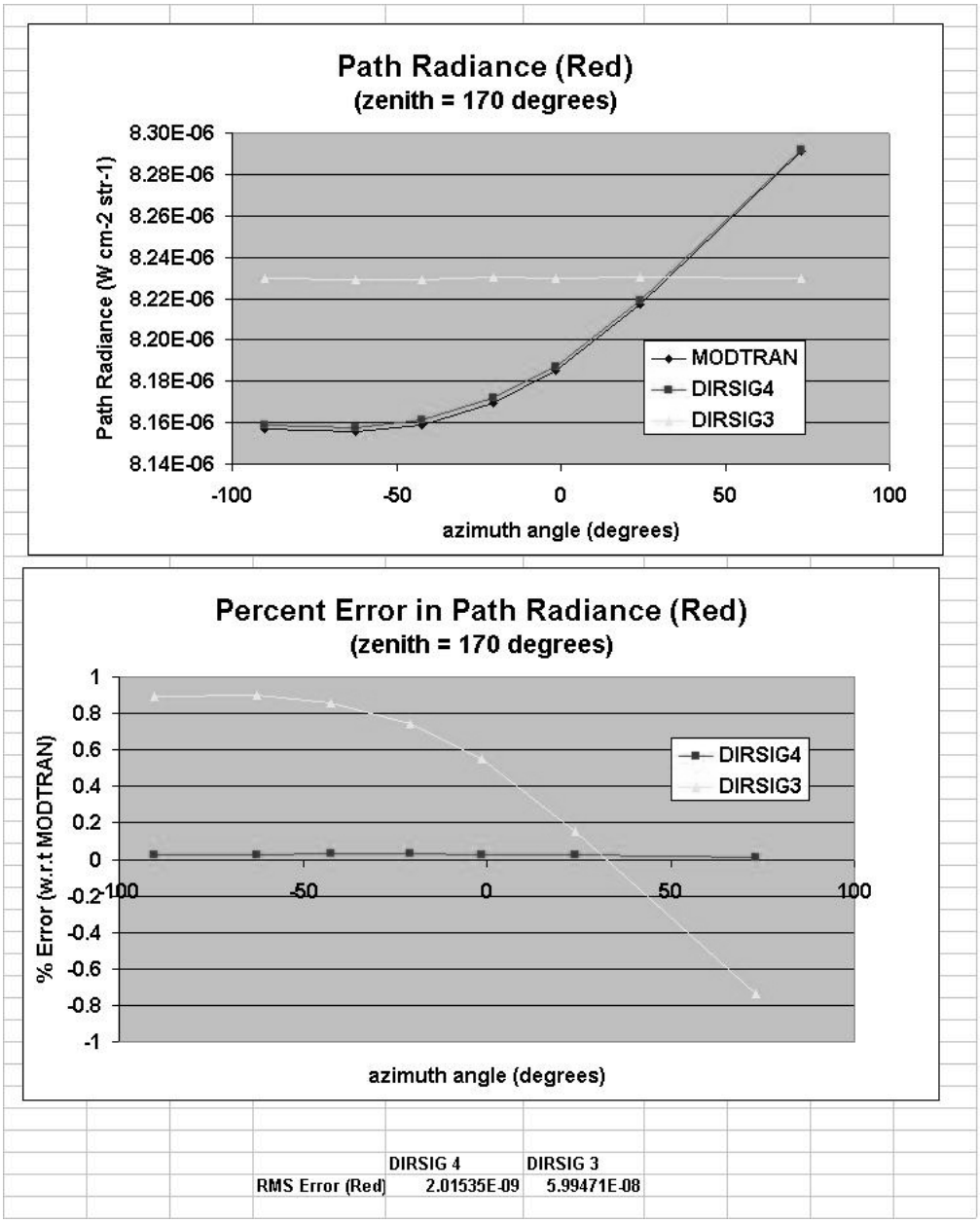

Figure 4.18: Test Scene 1a (azimuth variation): The upper graph shows the red path radiance obtained by MODTRAN, DIRSIG 4 and DIRSIG 3. The lower graph shows the percent error of DIRSIG 4 and DIRSIG 3 relative to MODTRAN. The RMS errors for the points shown on the graph are listed below the graphs.

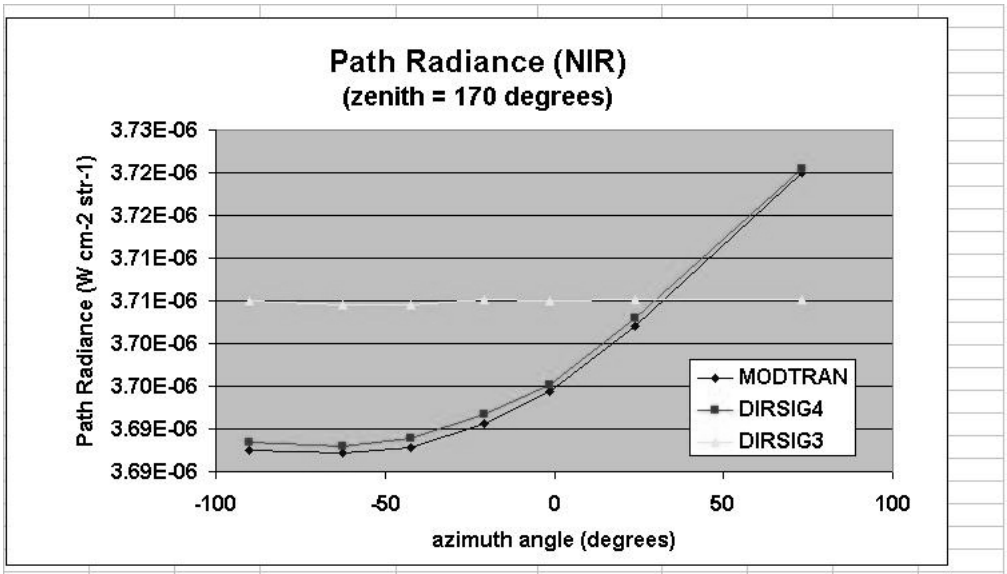

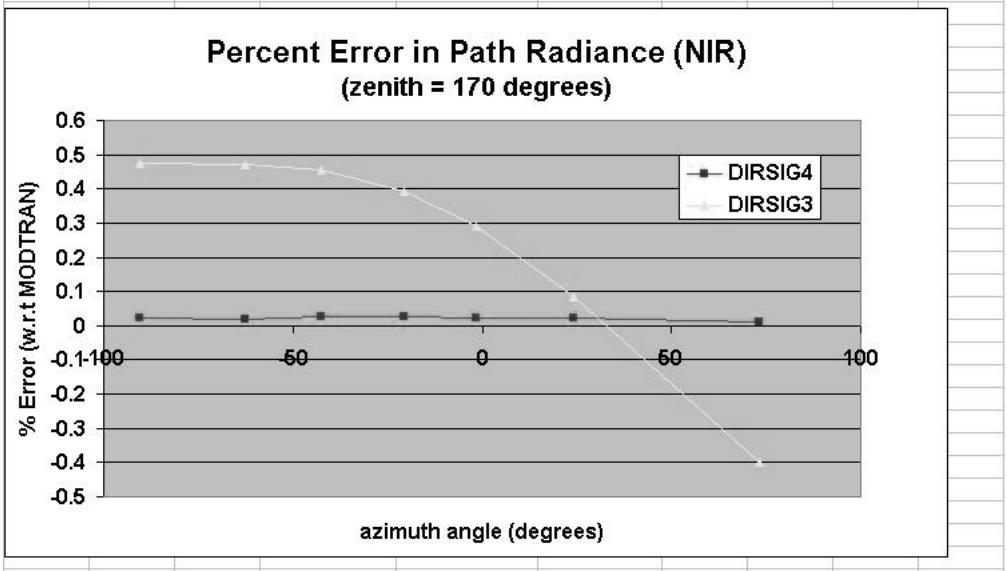

	DIRSIG 4	DIRSIG 3
RMS Error (NIR)	8.48806E-10	1.43907E-08

Figure 4.19: Test Scene 1a (azimuth variation): The upper graph shows the NIR path radiance obtained by MODTRAN, DIRSIG 4 and DIRSIG 3. The lower graph shows the percent error of DIRSIG 4 and DIRSIG 3 relative to MODTRAN. The RMS errors for the points shown on the graph are listed below the graphs.

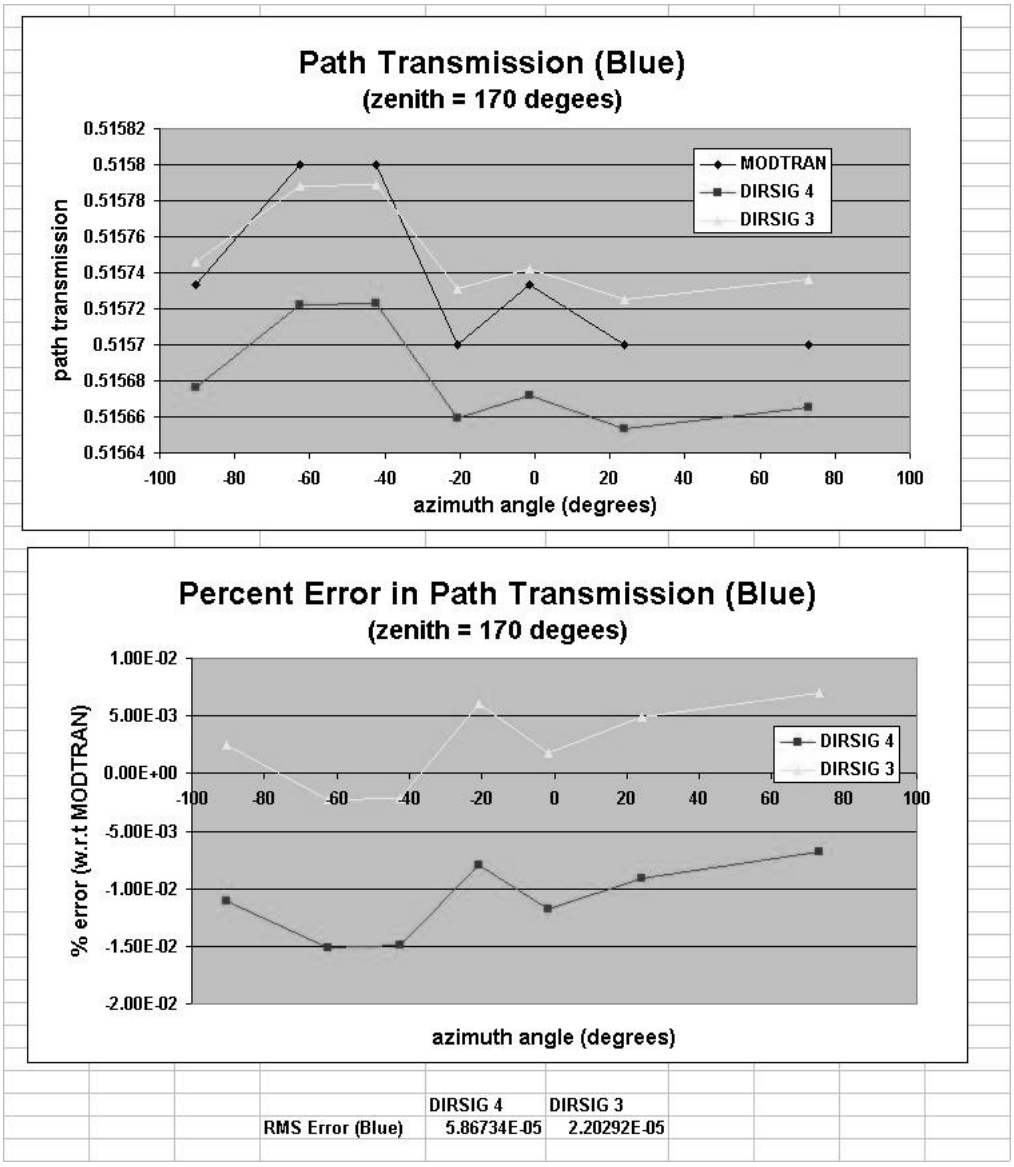

Figure 4.20: Test Scene 1a: The upper graph shows the blue path transmission obtained by MODTRAN, DIRSIG 4 and DIRSIG 3. The lower graph shows the percent error of DIRSIG 4 and DIRSIG 3 relative to MODTRAN. The RMS error for the points shown on the graph are listed below the graphs.

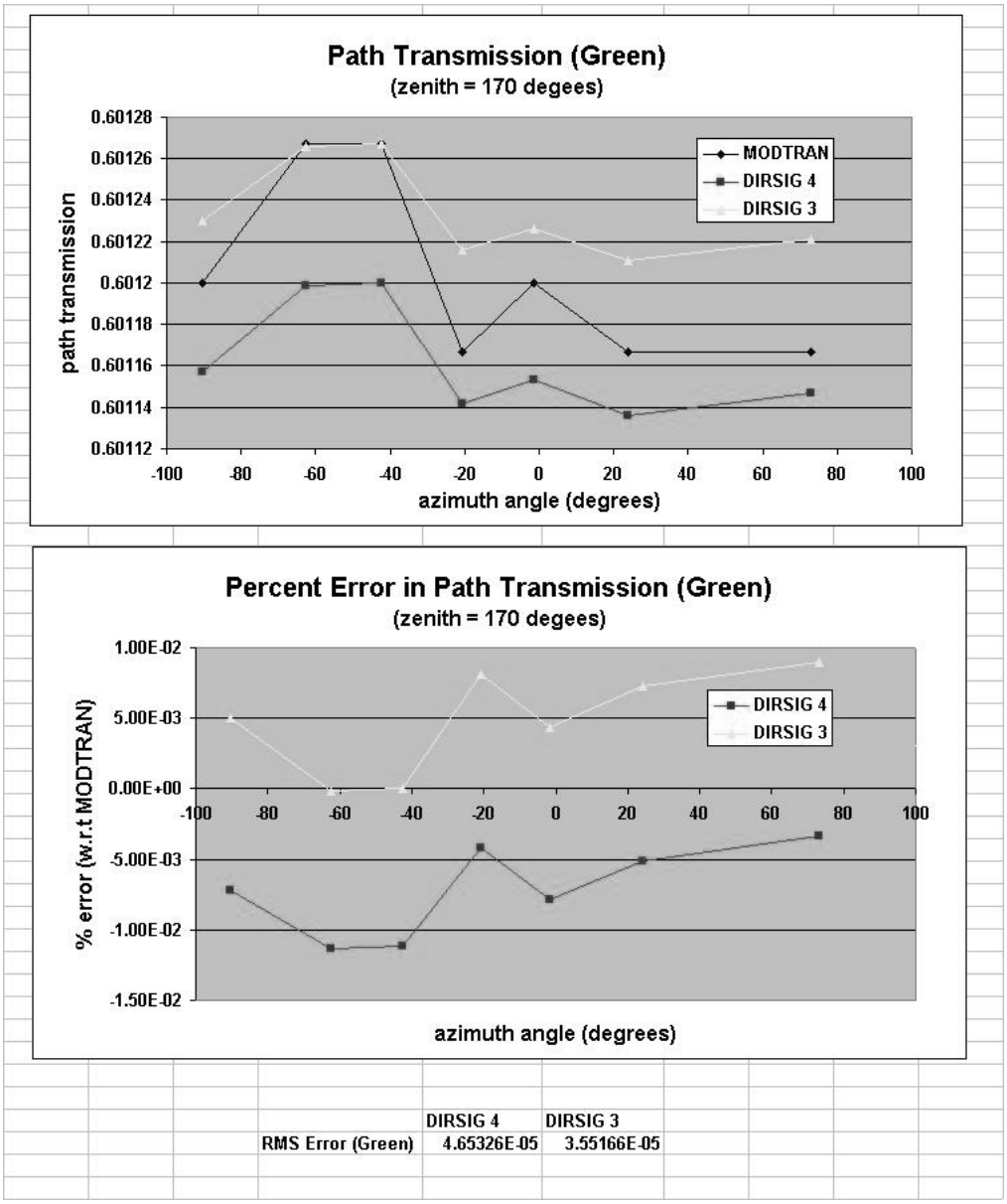

	DIRSIG 4	DIRSIG 3
RMS Error (Green)	4.65326E-05	3.55166E-05

Figure 4.21: Test Scene 1a (azimuth variation): The upper graph shows the green path transmission obtained by MODTRAN, DIRSIG 4 and DIRSIG 3. The lower graph shows the percent error of DIRSIG 4 and DIRSIG 3 relative to MODTRAN. The RMS errors for the points shown on the graph are listed below the graphs.

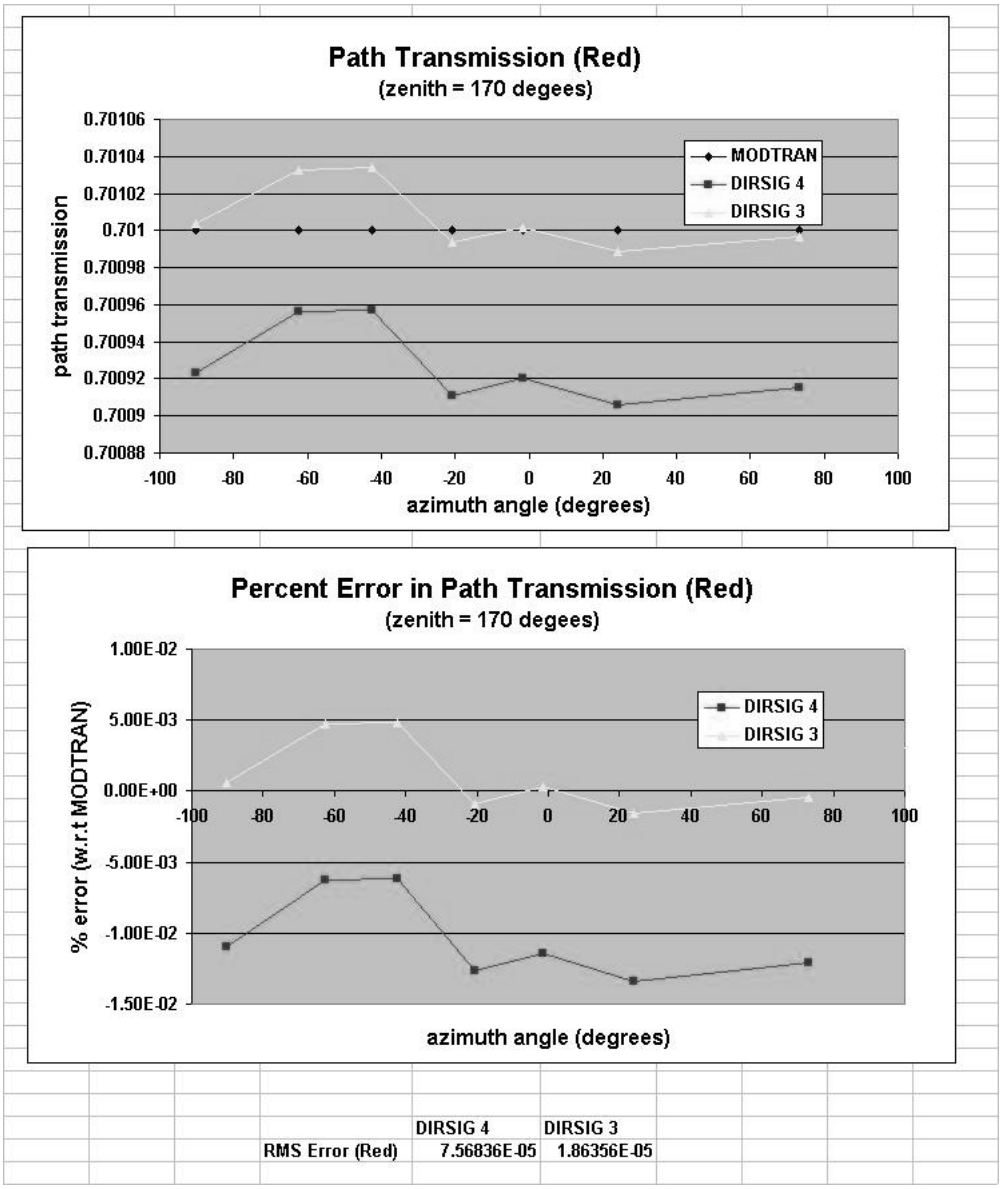

Figure 4.22: Test Scene 1a (azimuth variation): The upper graph shows the red path transmission obtained by MODTRAN, DIRSIG 4 and DIRSIG 3. The lower graph shows the percent error of DIRSIG 4 and DIRSIG 3 relative to MODTRAN. The RMS errors for the points shown on the graph are listed below the graphs.

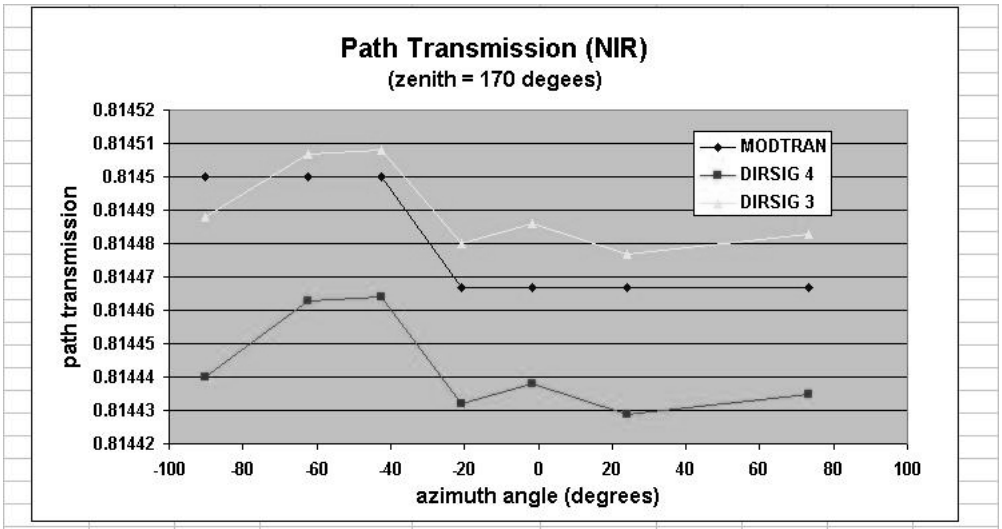

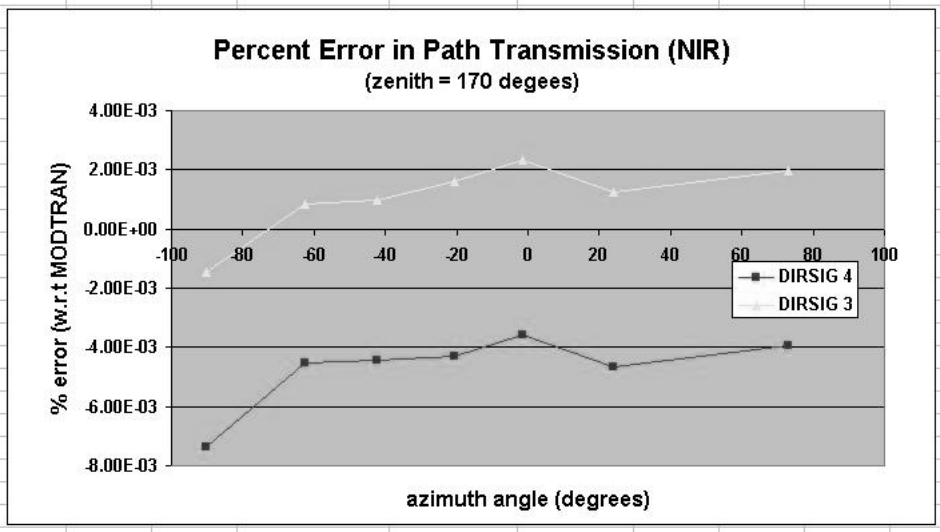

	DIRSIG 4	DIRSIG 3
RMS Error (NIR)	3.92774E-05	1.27783E-05

Figure 4.23: Test Scene 1a (azimuth variation): The upper graph shows the NIR path transmission obtained by MODTRAN, DIRSIG 4 and DIRSIG 3. The lower graph shows the percent error of DIRSIG 4 and DIRSIG 3 relative to MODTRAN. The RMS errors for the points shown on the graph are listed below the graphs.

The thermal band was not analyzed in this test image because the thermal radiance did not vary in any significant amount. Generally, these results show how DIRSIG 4's interpolator more closely matches the MODTRAN results. However, there is a noticeable lack of performance by the DIRSIG 4 interpolator in predicting the transmission. As seen in any of the above transmission result graphs, (4.20 through 4.23), the DIRSIG 4 interpolator actually results in more error. This, however, is not a significant problem for two reasons. First, the actual error is not very high, (on the order of 10e5 reflectance units). Second, the error in DIRSIG 3 seems to trend along with DIRSIG 4's error. This implies that this is an internal DIRSIG inconsistency, and thus common to any atmospheric interpolator applied.

DIRSIG 4's error is slightly higher that DIRSIG 3's. This error is very small, and possibly due to the fact that DIRSIG 4 is interpolating over more dimensions. If any error is contributed by this interpolation, it will be increased in the DIRSIG 4 calculation.

Grid Results

These test have focused on specific azimuth or zenith values. To get a better assessment of how the different interpolators work on a more general basis, the images were sampled at a nearly regular grid of points. A visual representation of the points sampled is seen in figure 4.24

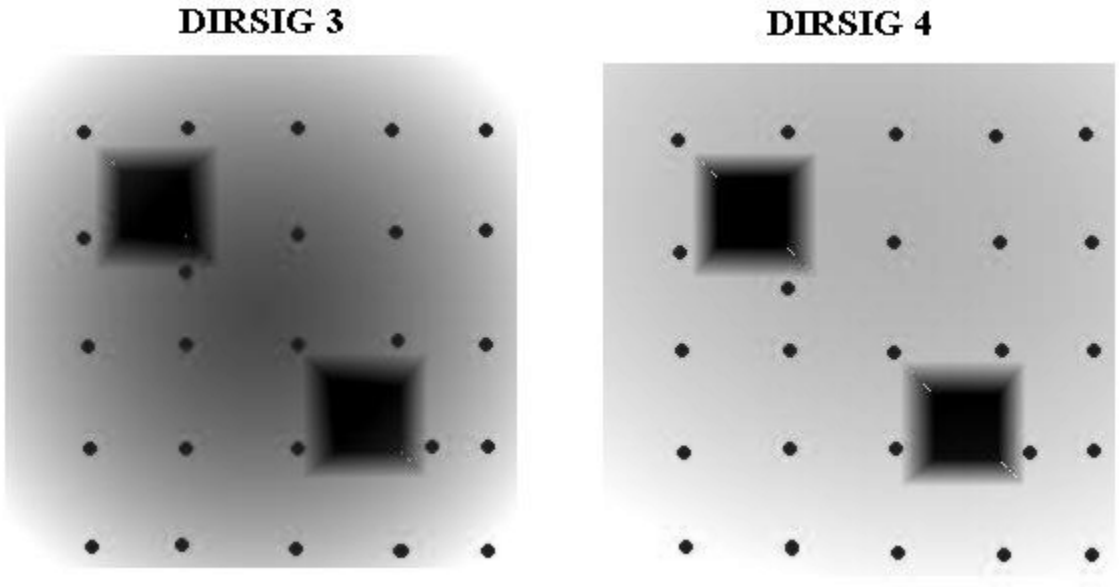

Figure 4.24: The dots represent points analyzed in the image.

The RMS error (by band) is shown in figure 4.25 for the path radiance and in figure 4.26 for the transmission.

So, when not confined to a single azimuth angle, the DIRSIG 4 interpolator has more ability to match the results of MODTRAN than DIRSIG 3's.

Noon and Sunrise Cases (Images 1b and 1c)

The same experiment and analysis was performed on the exact same image rendered at noon and at sunrise. The results follow the same trends, with no significant new information. The results of these studies can be found in appendix B.

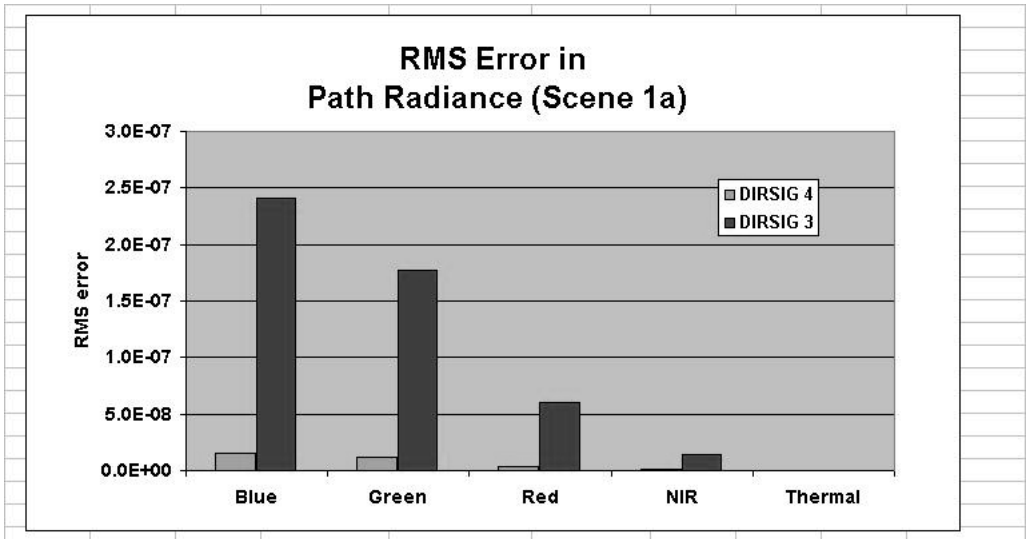

band	DIRSIG 4	DIRSIG 3
Blue	1.558756E-08	2.413167E-07
Green	1.126833E-08	1.769902E-07
Red	3.798459E-09	6.039392E-08
NIR	1.130964E-09	1.458304E-08
Thermal	4.221559E-14	3.120861E-12

Figure 4.25: This shows the RMS error in path radiance (by band) over the image 1a.

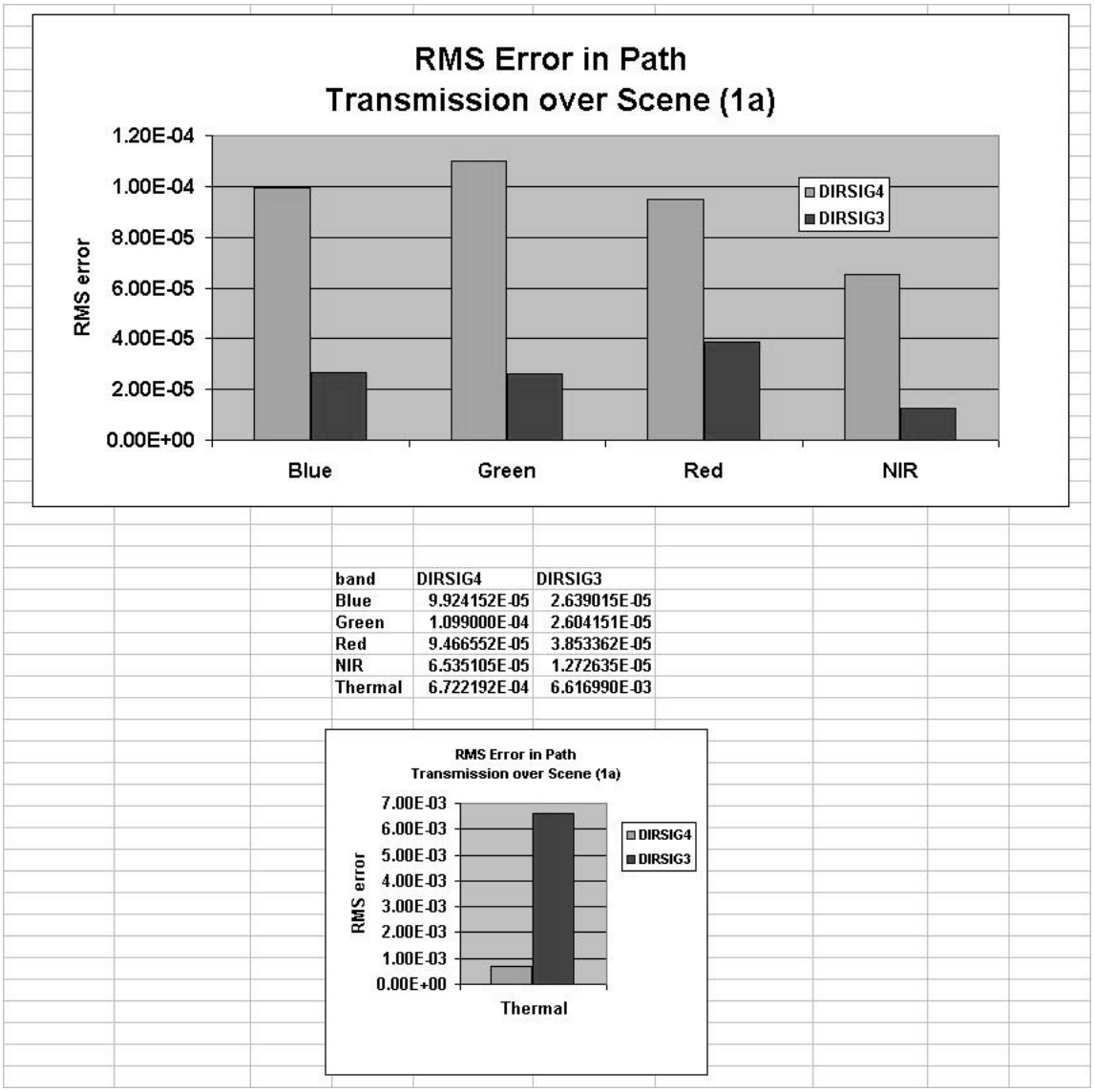

band	DIRSIG4	DIRSIG3
Blue	9.924152E-05	2.639015E-05
Green	1.099000E-04	2.604151E-05
Red	9.466552E-05	3.853362E-05
NIR	6.535105E-05	1.272635E-05
Thermal	6.722192E-04	6.616990E-03

Figure 4.26: This shows the RMS error in path transmission (by band) over the image 1a.

4.1.2 Highlighting Altitude Changes

Another image was rendered to better highlight how the new sampling method handles the changes in the altitude of the objects in the scene. It is presented to address the sampling issues mentioned in section 2.1.1. Like the previous test scene (1), this scene was rendered at sunset, noon, and sunrise. The scene consists of a single pyramid comprised of a non-reflective material. (See figure 4.27). As in the other scenes to be studied, a comparison will be made between the two methods' ability to replicate MODTRAN values.

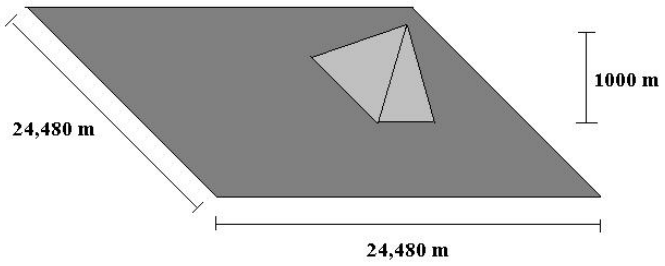

Figure 4.27: This scene highlights the changes in upwelled radiance and transmission as a function of altitude.

Sunset case (Image 2a)

The first set of data includes results obtained by analyzing the images which were rendered at sunset.

As stated earlier, for each set of conditions, a series of points was looked at in each image. The next set contains points which steadily increase in altitude. The goal is to highlight the deficiency of DIRSIG 3's interpolator to handle non-zero altitudes.

Figure 4.28, shows an RGB path radiance image obtained from DIRSIG 3 and 4. This will be used as an aid in showing exactly where the image was analyzed. This figure shows, qualitatively, the different outputs when running DIRSIG 3 or DIRSIG 4 respectively. Notice the lack of azimuthal variation in the DIRSIG 3 result , and its presence in the DIRSIG 4 rendering. This image, again, shows the expected reddening of the sky during sunset in the Western portion of the image (positive y in this image).

In order to better quantify the improved accuracy of the new atmospheric model, as stated before, the images were analyzed at specific points. These points are shown in figure 4.29. The red dots represent the points analyzed for the study which highlights the variations in the altitude dimension.

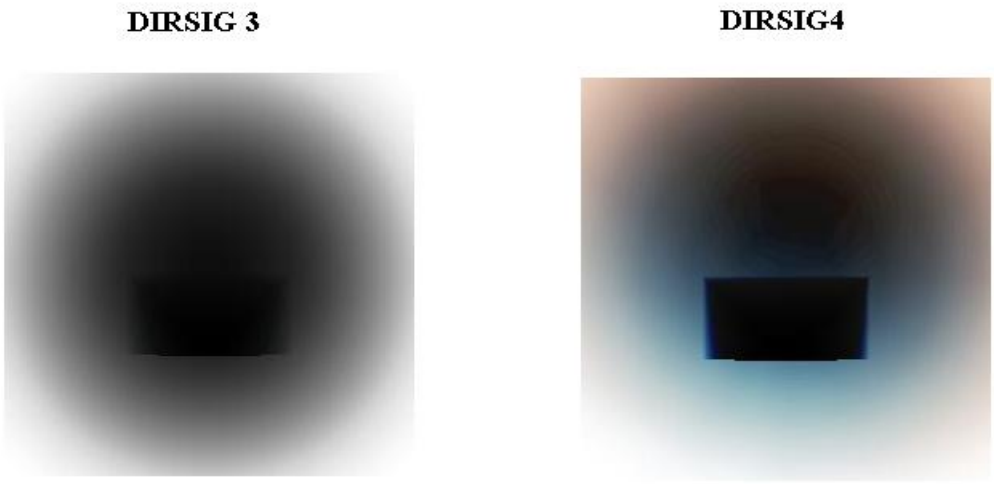

Figure 4.28: The visible path radiance obtained during sunset from the DIRSIG 3 and DIRSIG 4 interpolator over the "pyramid" test scene (RGB display). In order to highlight the changes in radiance in the image, the dynamic range of the image was increased by using the Histogram Equalization enhancement tool in ENVI.

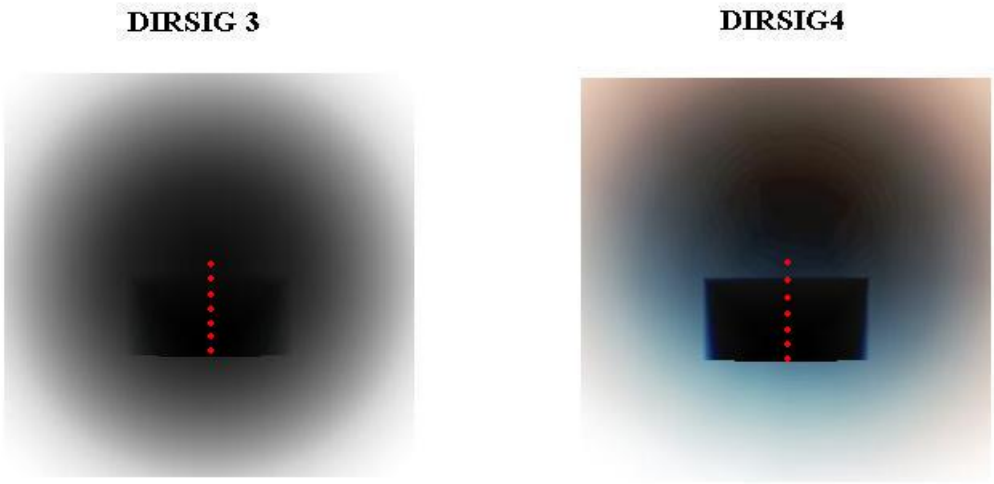

Figure 4.29: The red dots represent points analyzed in the altitude studies.

Results of Varying Altitude

The results for all of the bands, as well as the calculated RMS for all of the points, can be seen in figures 4.30 through 4.34 (radiance) and 4.35 through 4.39 (transmission). (The full results can be seen in appendix B.)

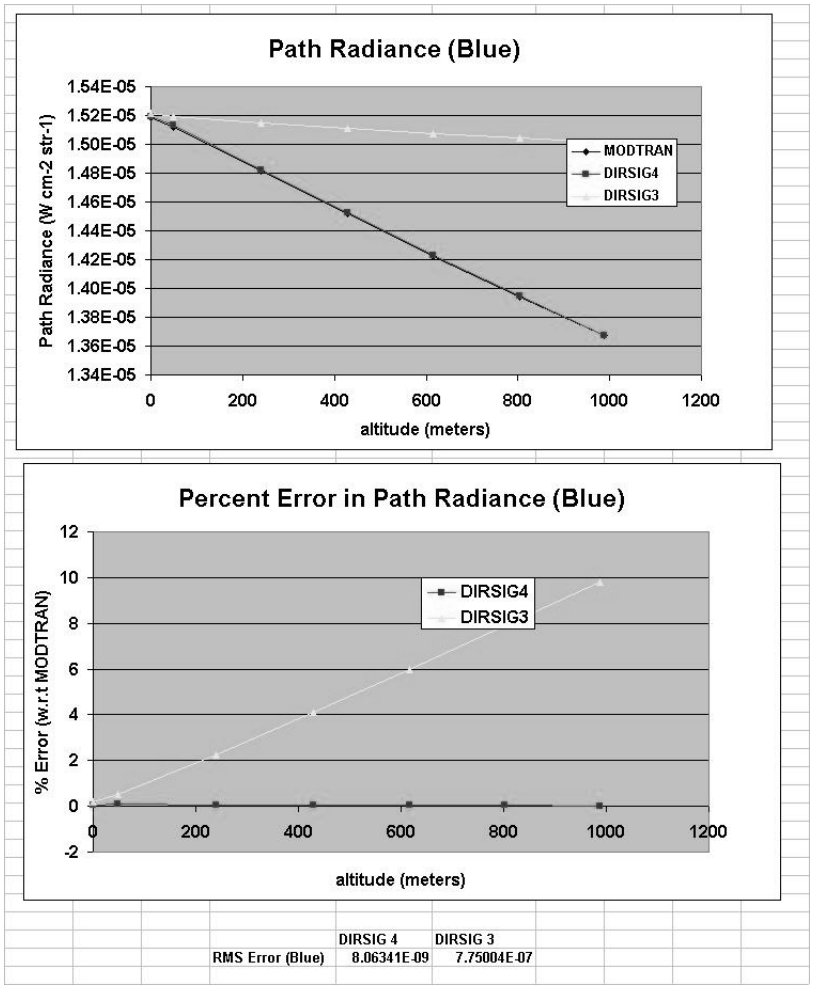

Figure 4.30: Test Scene 2a (varying altitude): The upper graph shows the blue path radiance obtained by MODTRAN, DIRSIG 4 and DIRSIG 3. The lower graph shows the percent error of DIRSIG 4 and DIRSIG 3 relative to MODTRAN. The RMS error for the points shown on the graph are listed below the graphs.

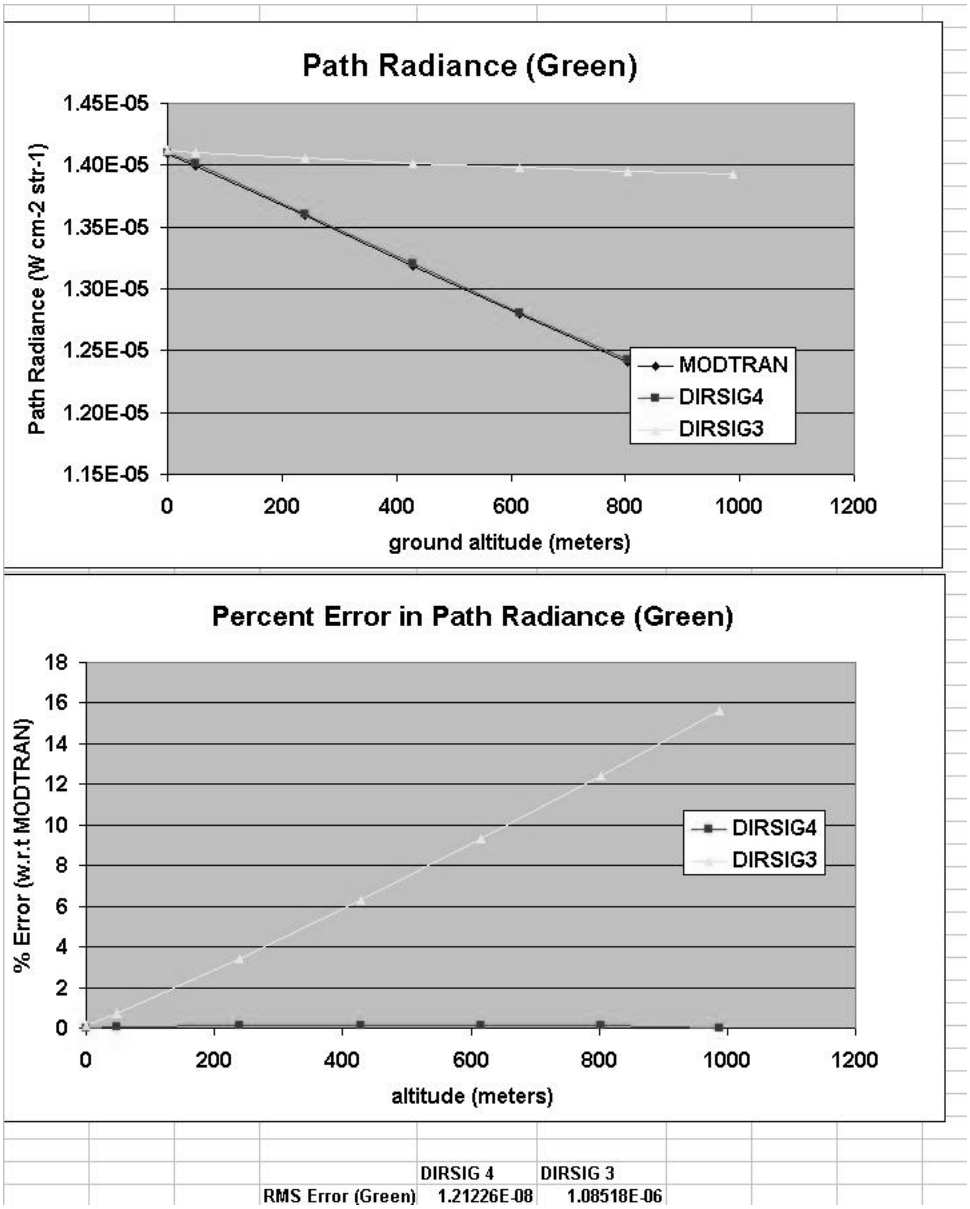

Figure 4.31: Test Scene 2a (altitude variation): The upper graph shows the green path radiance obtained by MODTRAN, DIRSIG 4 and DIRSIG 3. The lower graph shows the percent error of DIRSIG 4 and DIRSIG 3 relative to MODTRAN. The RMS errors for the points shown on the graph are listed below the graphs.

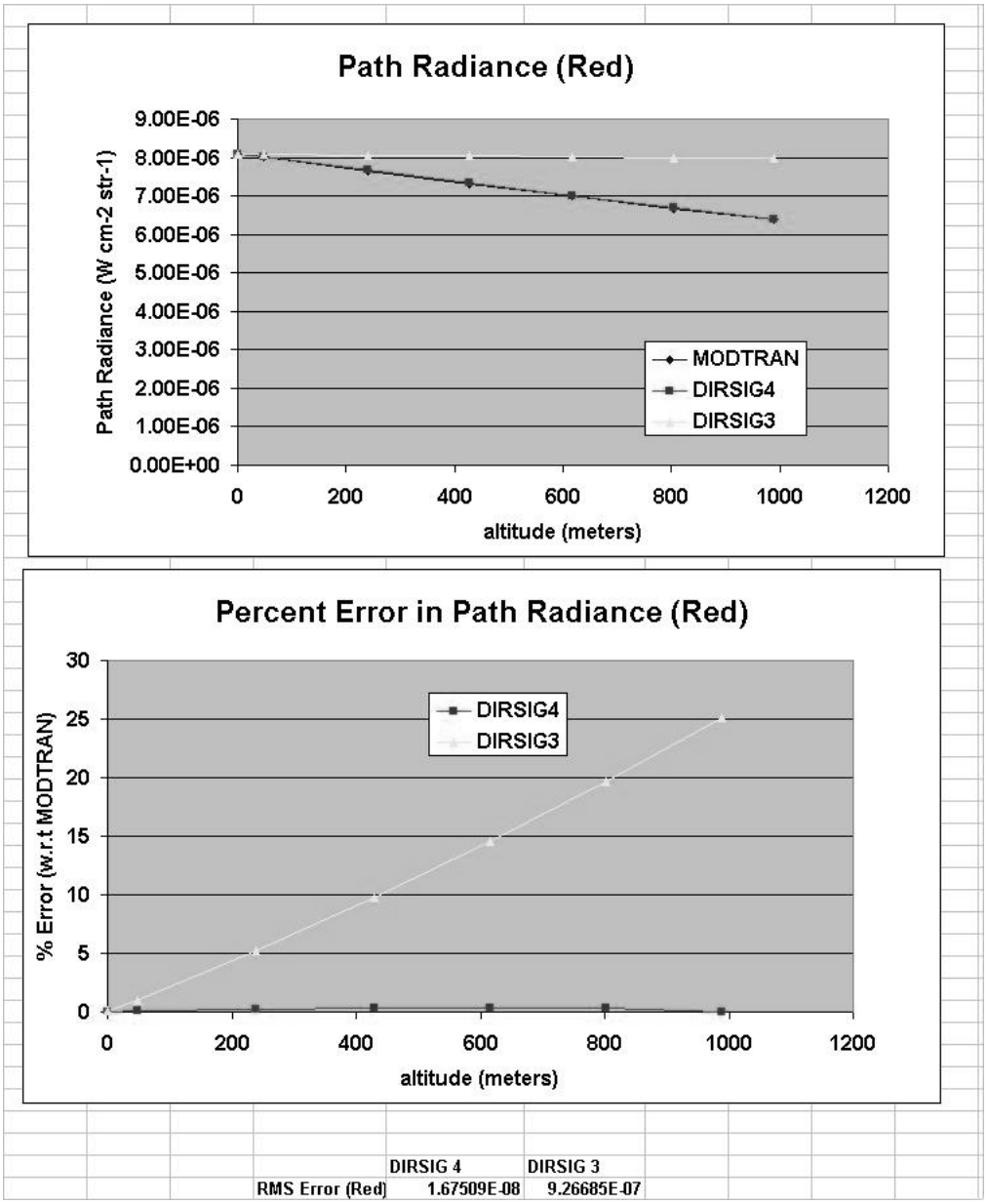

Figure 4.32: Test Scene 2a (altitude variation): The upper graph shows the red path radiance obtained by MODTRAN, DIRSIG 4 and DIRSIG 3. The lower graph shows the percent error of DIRSIG 4 and DIRSIG 3 relative to MODTRAN. The RMS errors for the points shown on the graph are listed below the graphs.

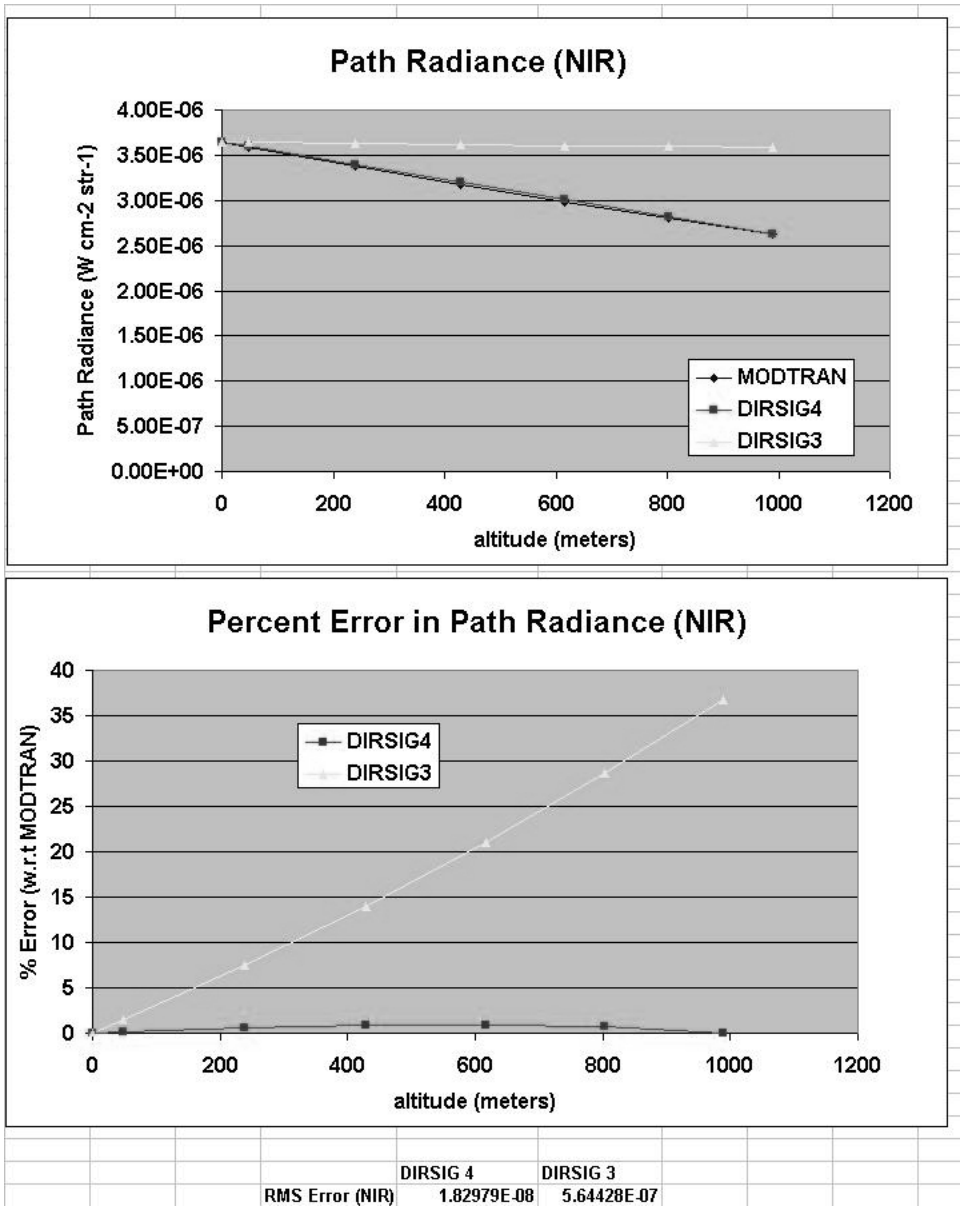

Figure 4.33: Test Scene 2a (altitude variation): The upper graph shows the NIR path radiance obtained by MODTRAN, DIRSIG 4 and DIRSIG 3. The lower graph shows the percent error of DIRSIG 4 and DIRSIG 3 relative to MODTRAN. The RMS errors for the points shown on the graph are listed below the graphs.

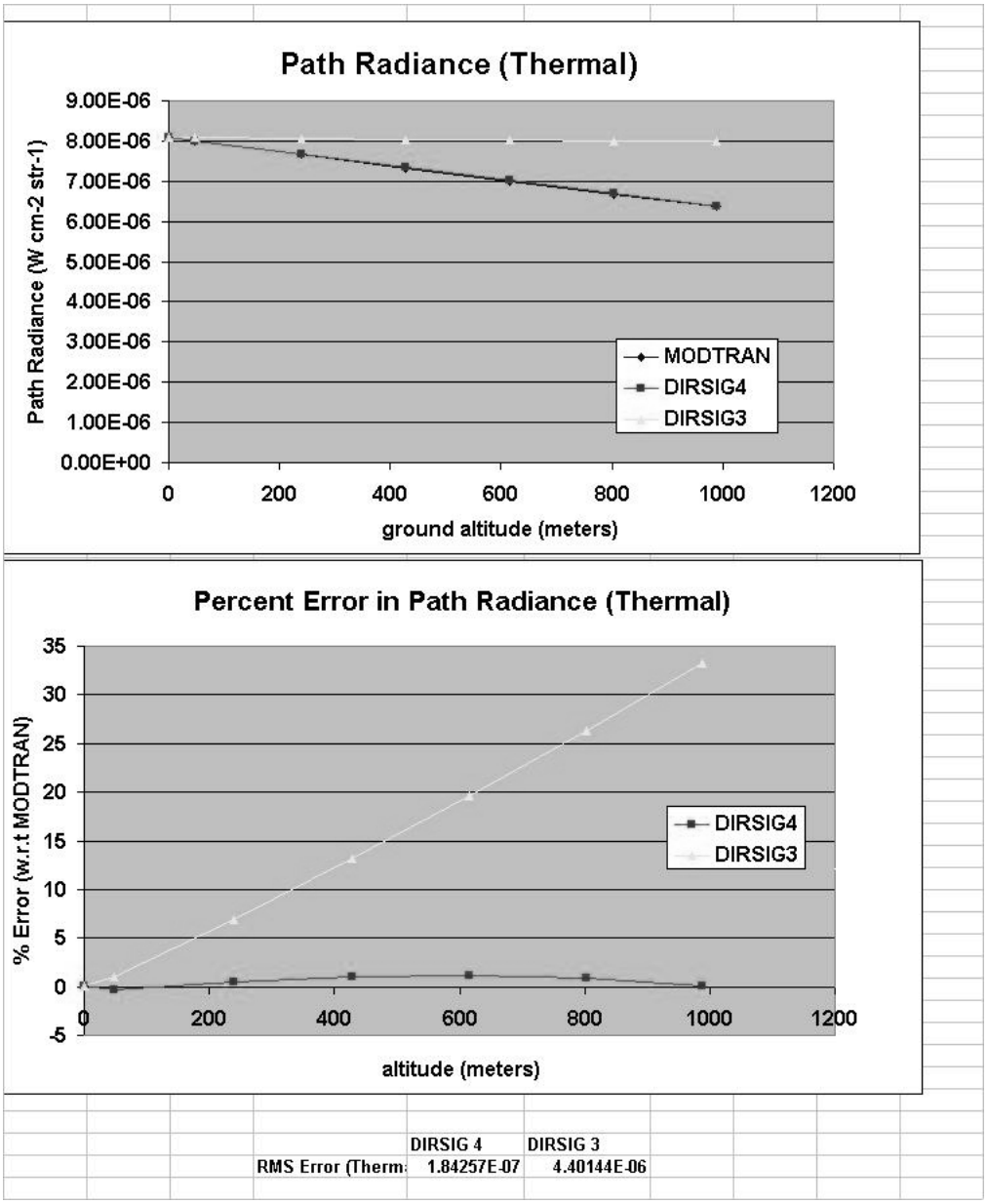

Figure 4.34: Test Scene 2a (altitude variation): The upper graph shows the thermal path radiance obtained by MODTRAN, DIRSIG 4 and DIRSIG 3. The lower graph shows the percent error of DIRSIG 4 and DIRSIG 3 relative to MODTRAN. The RMS errors for the points shown on the graph are listed below the graphs.

The next set of figures (4.35 through 4.39) shows the path transmission results of the same study.

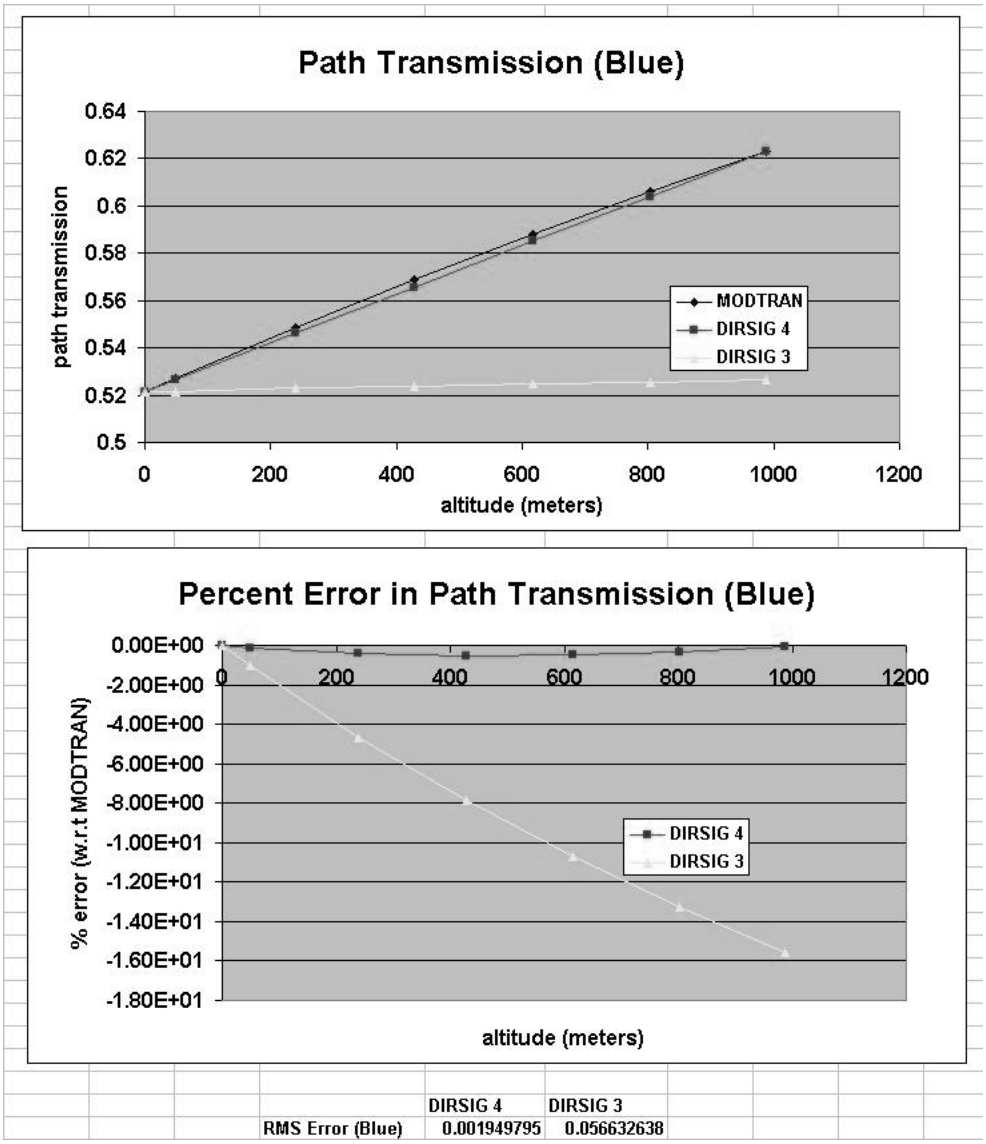

Figure 4.35: Test Scene 2a (altitude variation): The upper graph shows the blue path transmission obtained by MODTRAN, DIRSIG 4 and DIRSIG 3. The lower graph shows the percent error of DIRSIG 4 and DIRSIG 3 relative to MODTRAN. The RMS errors for the points shown on the graph are listed below the graphs.

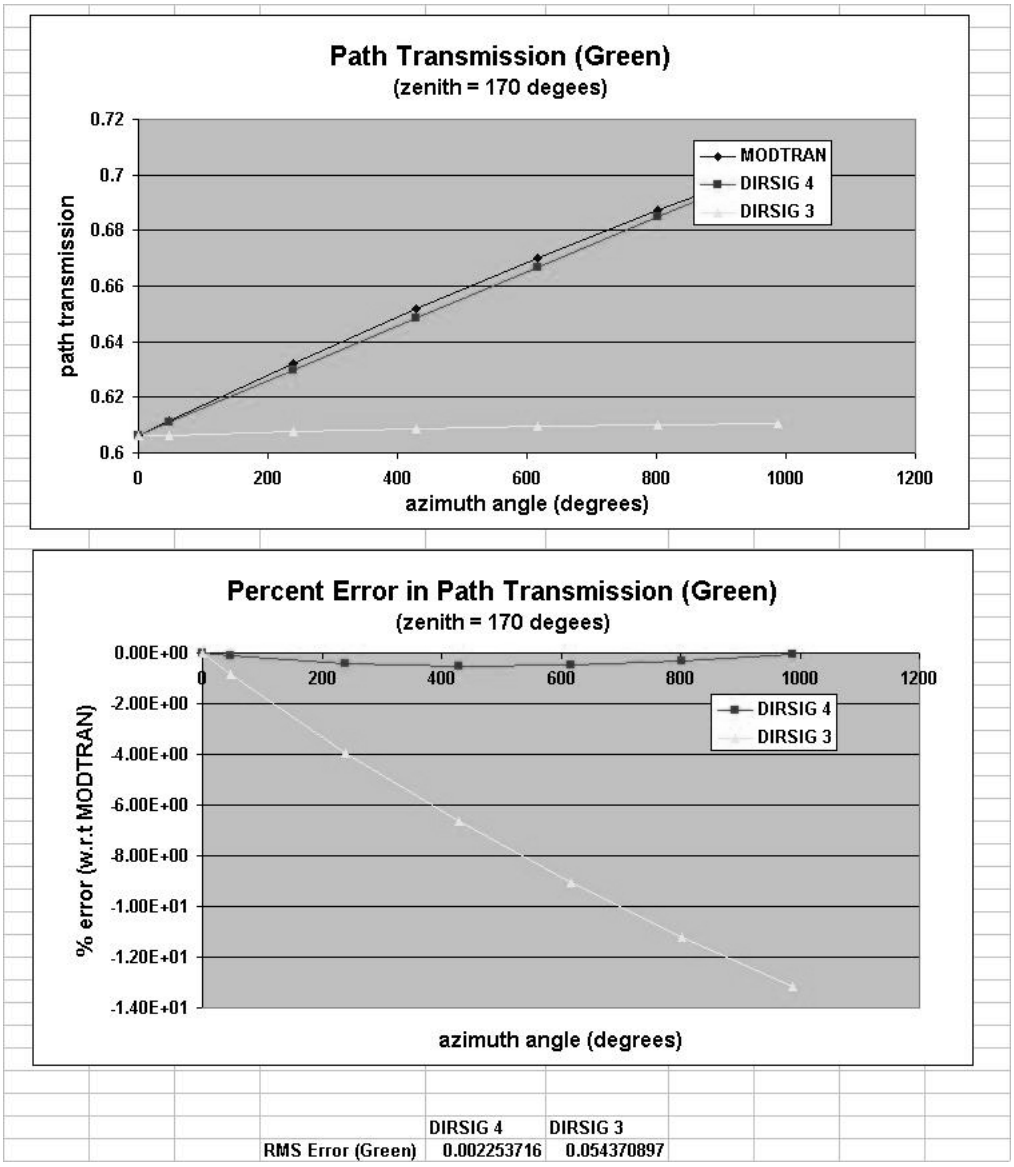

Figure 4.36: Test Scene 2a (altitude variation): The upper graph shows the green path transmission obtained by MODTRAN, DIRSIG 4 and DIRSIG 3. The lower graph shows the percent error of DIRSIG 4 and DIRSIG 3 relative to MODTRAN. The RMS errors for the points shown on the graph are listed below the graphs.

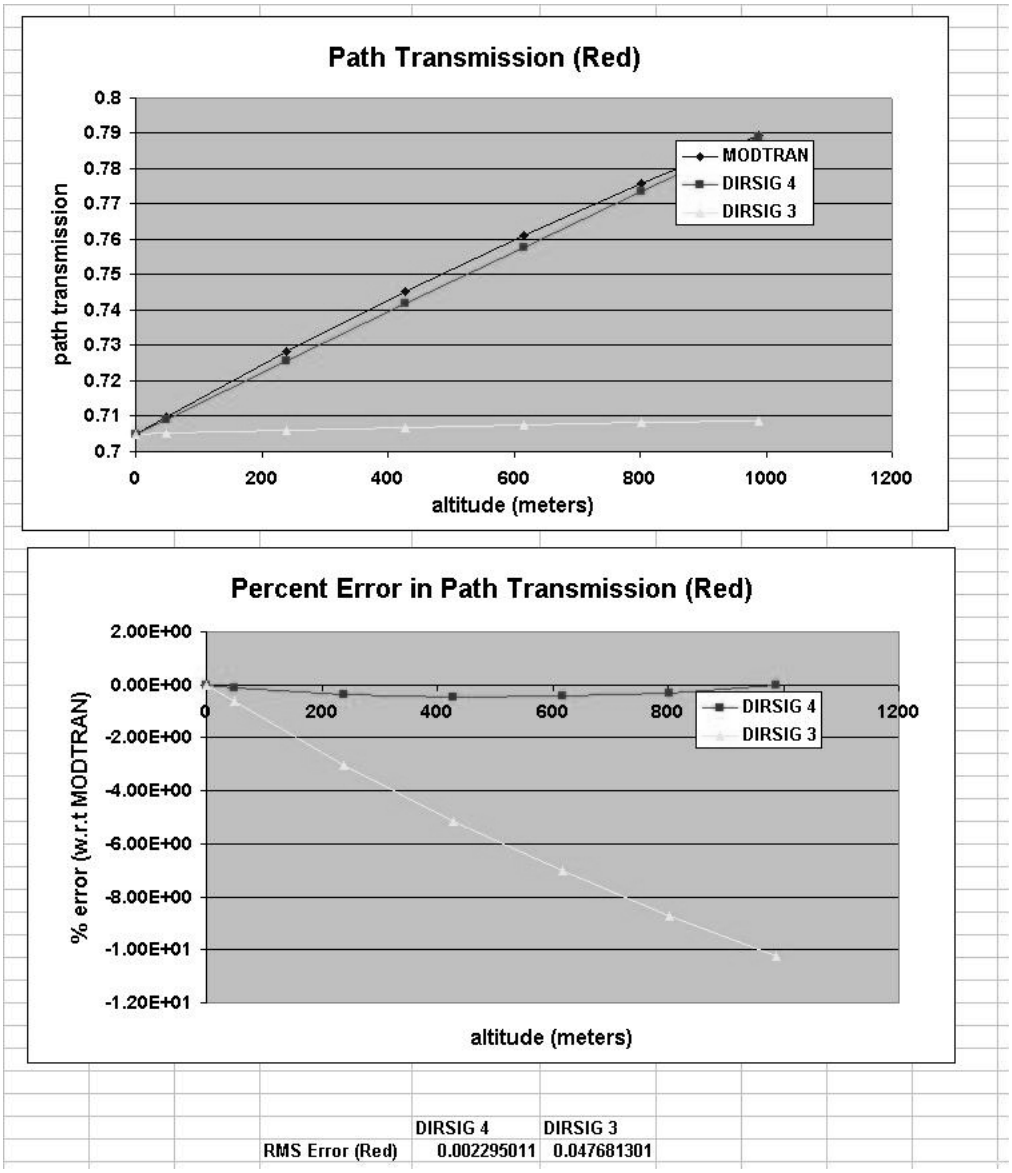

Figure 4.37: Test Scene 2a (altitude variation): The upper graph shows the red path transmission obtained by MODTRAN, DIRSIG 4 and DIRSIG 3. The lower graph shows the percent error of DIRSIG 4 and DIRSIG 3 relative to MODTRAN. The RMS errors for the points shown on the graph are listed below the graphs.

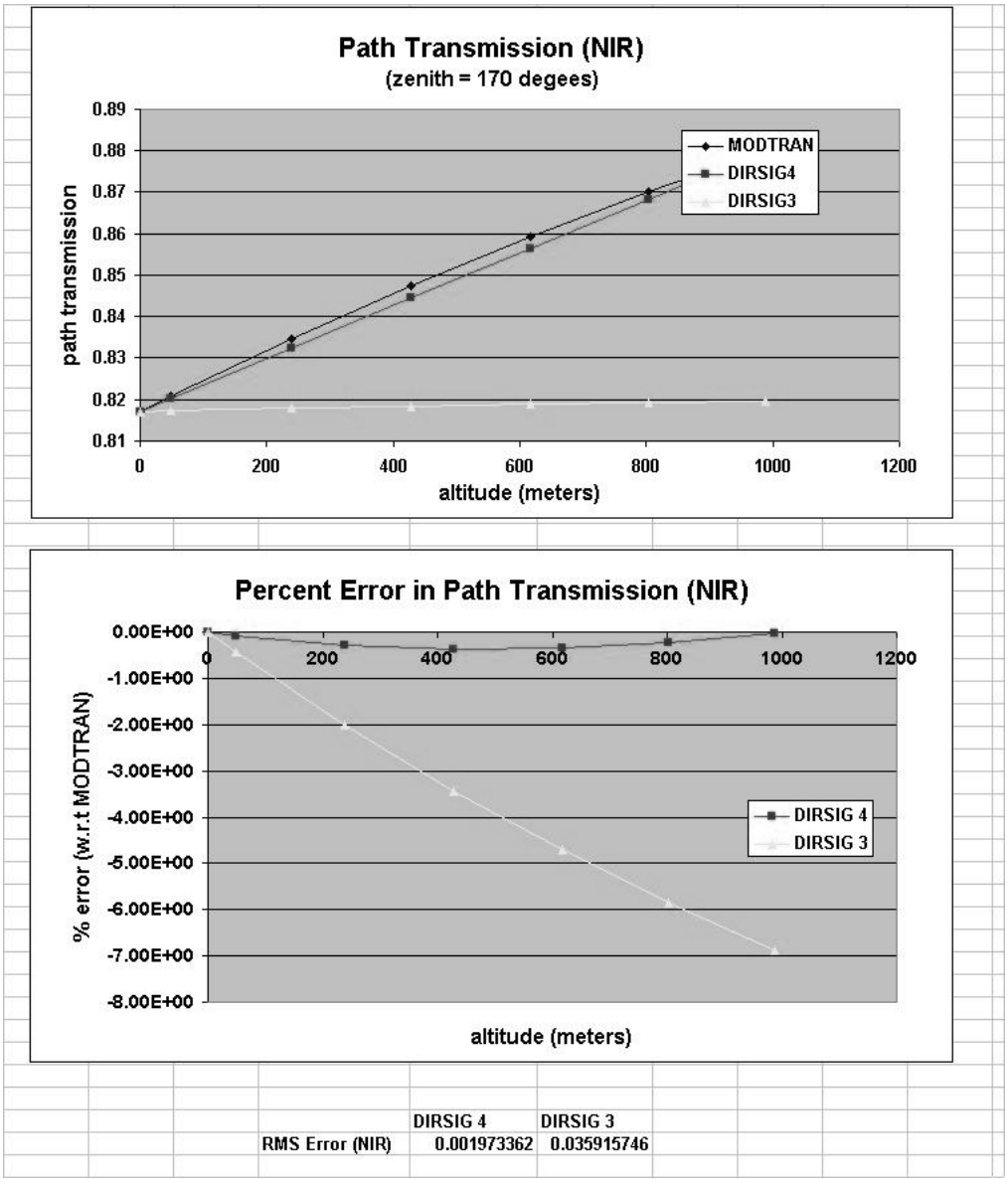

Figure 4.38: Test Scene 2a (altitude variation): The upper graph shows the NIR path transmission obtained by MODTRAN, DIRSIG 4 and DIRSIG 3. The lower graph shows the percent error of DIRSIG 4 and DIRSIG 3 relative to MODTRAN. The RMS errors for the points shown on the graph are listed below the graphs.

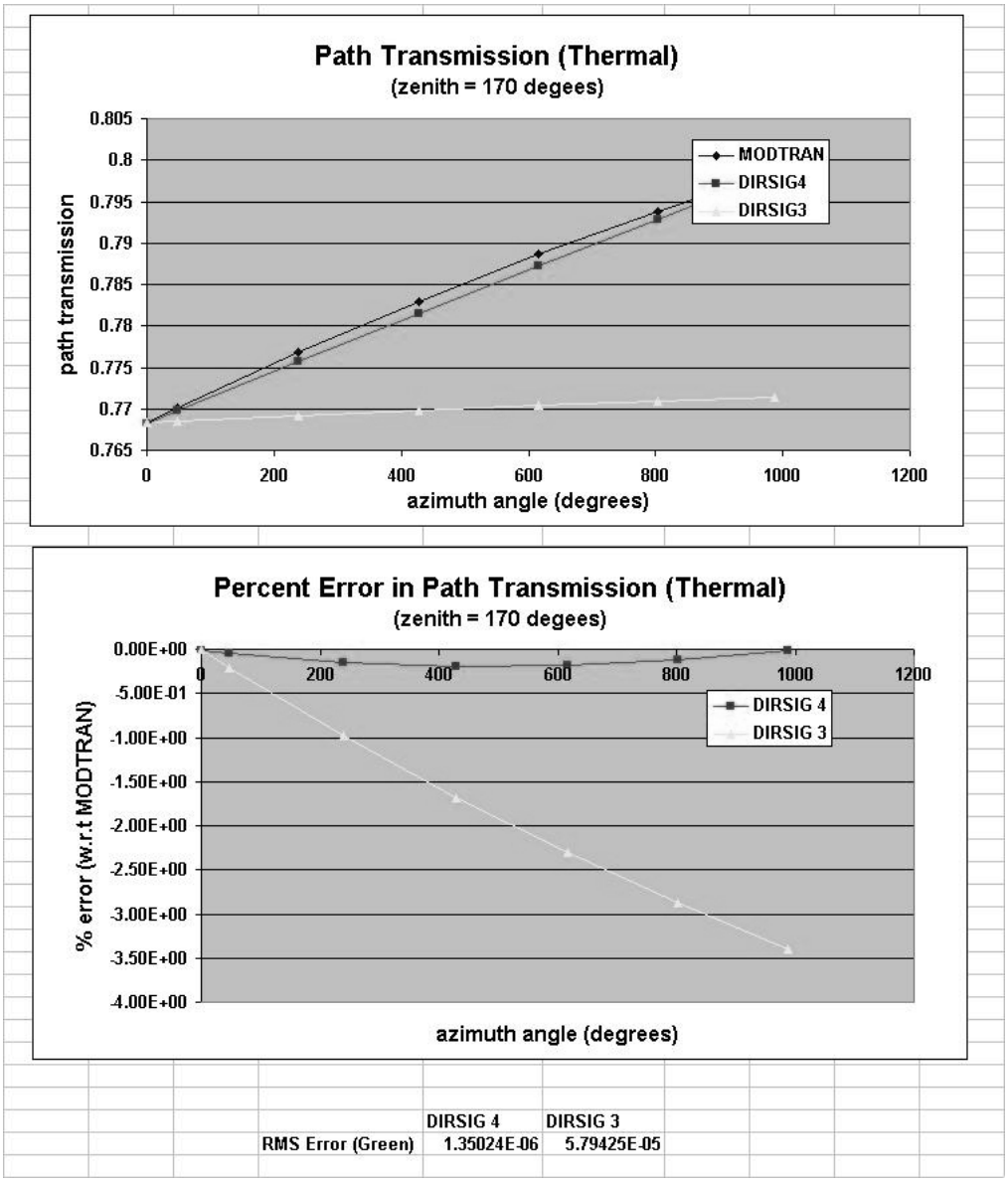

Figure 4.39: Test Scene 2a (altitude variation): The upper graph shows the thermal path transmission obtained by MODTRAN, DIRSIG 4 and DIRSIG 3. The lower graph shows the percent error of DIRSIG 4 and DIRSIG 3 relative to MODTRAN. The RMS errors for the points shown on the graph are listed below the graphs.

It is apparent that the DIRSIG 4 interpolator performs much better that DIRSIG 3. This test case, however, is showing a very extreme case of altitude variation within a scene (0 to 1 km), which is not typically witnessed in practical remote sensing. A benefit of the versatility of the DIRSIG 4 atmospheric interpolator is that the user can specify the altitudes at which the atmosphere is sampled.

The results of the DIRSIG 4 interpolator, for example in figure 4.35, show the maximum error occurs at around 500 meters. This is because at this point, in the altitude dimension, the sample point is farthest from any altitude interpolation point. Assuming that the user requires a sample point at 1 km, the accuracy can be increased by adding another altitude at which to sample. However, this is not free. It would require, potentially, many more MODTRAN runs to populate the ADB.

A formula for calculating the number of MODTRAN runs (excluding source section runs and running over separate bands) can be found in equation 4.2.

$$N = ((n_zenith * n_azimuth * n_alt) + (6 * 12 * n_alt)) * (n_water * n_aerosoltypes * n_visibilities) \quad (4.2)$$

Here, N is the total number of MODTRAN runs required in the ADB and n_X is the number of values for each parameter 'X'. So, if there are 8 zenith and azimuth angles, 2 altitudes, 2 water vapor amounts, 2 aerosol types, and two visibilities, there are 2176 MODTRAN runs required. Adding one altitude to the ADB results in 3264 total runs, an increase of over one thousand runs. Again, the balance between accuracy and run time must be struck.

Grid Results

To get a better assessment of how the different interpolators work on a more general basis, the images were sampled at a nearly regular grid of points. A visual representation of the points sampled is similar to those seem in figure 4.24

The RMS error (by band) is shown in figure 4.40 for the path radiance and in figure 4.41 for the transmission.

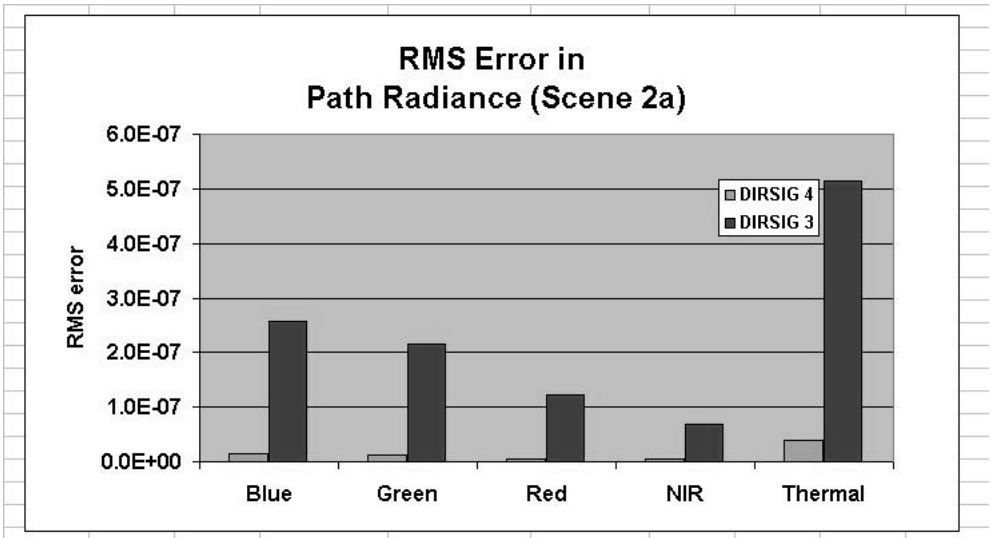

band	DIRSIG 4	DIRSIG 3
Blue	1.554921E-08	2.566496E-07
Green	1.148758E-08	2.150688E-07
Red	5.953634E-09	1.214150E-07
NIR	5.660207E-09	6.756662E-08
Thermal	3.842272E-08	5.142521E-07

Figure 4.40: This shows the RMS error in path radiance (by band) over image 2a.

Noon and Sunrise Cases (Images 2b and 2c)

The same experiment and analysis was performed on the exact same image rendered at noon and at sunrise. The results follow the same trends, with no significant new information. The results of these studies can be found in appendix B.

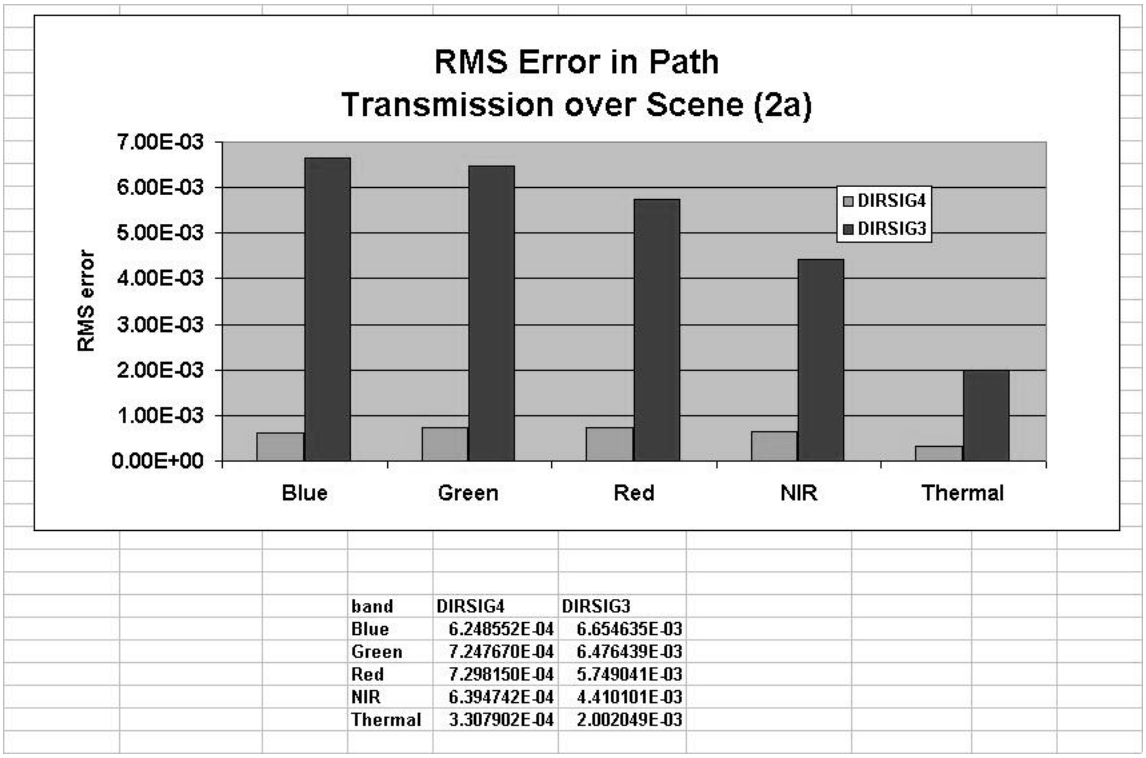

band	DIRSIG4	DIRSIG3
Blue	6.248552E-04	6.654635E-03
Green	7.247670E-04	6.476439E-03
Red	7.298150E-04	5.749041E-03
NIR	6.394742E-04	4.410101E-03
Thermal	3.307902E-04	2.002049E-03

Figure 4.41: This shows the RMS error in path transmission (by band) over image 2a.

4.2 Atmospheric Variability Test Scenes

In order to demonstrate the implementation of the atmospheric inhomogeneities, an existing scene was used. A layer of horizontally varying water vapor and, later, aerosols were added to the scene shown in figure 4.1. The new atmospheric model was then tested at a specific set of points in the image by comparing the resulting transmission and path radiances to that of a direct MODTRAN result. Because the existing method of atmospheric sampling does not allow for the input of atmospheric species with horizontal variability, there is no existing method within DIRSIG to test this against.

(Note: The focus of this work is on the radiometric effects of the inhomogeneities, not necessarily the accuracy of the spatial structure of them.)

4.2.1 Highlighting Water Vapor Changes

The first test scene analyzes the effect of changing water vapor over an image. This analysis was done on the "truncated pyramid" image (figure 4.1), with a "wedge" of water vapor above it. This wedge is an atmospheric map which has a column water vapor value of 1 g/cm2 at the upper (Western) edge of the image. The water vapor value increases linearly to the East until it reaches a maximum of 2.5 g/cm2 at the lower (Eastern) edge.

A graphic of the scene is shown in figure 4.42

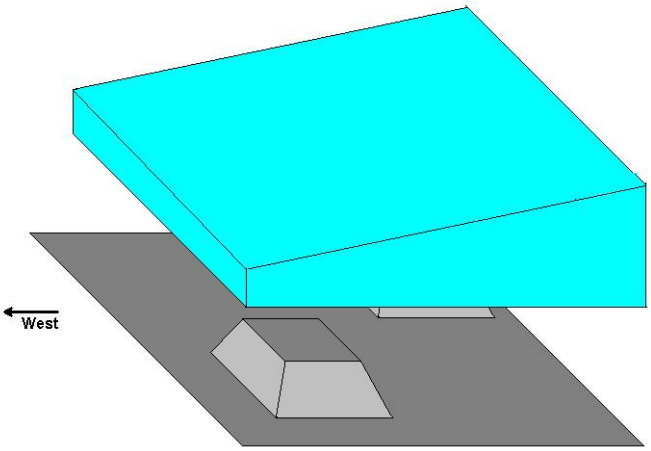

Figure 4.42: This scene highlights the effect that water vapor has on upwelled radiance and transmission in a very simple scene.

Figure 4.44 shows the radiance of test image 3. The band used in this figure was the water2 band (the 940 nm water feature). This band was selected as it is the most sensitive of the bands for this image, and therefore the image has considerable dynamic range.

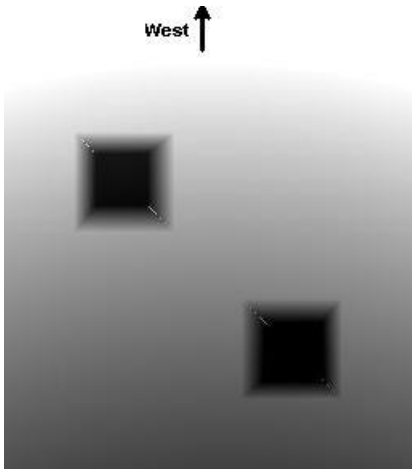

Figure 4.43: Test image 3, the path radiance in the 'water2' band (940 nm), rendered by DIRSIG 4.

To observe the effect of the water vapor wedge, a line of points were analyzed. These points are shown in figure 4.44, and mark roughly a linear increase in the amount of water vapor present in the atmosphere. It should be noted that all of the other dimensions (zenith, azimuth, and altitude) except for visibility vary as well.

The DIRSIG 3 images were rendered with a single water vapor value (1.75 g/cm2), which is the average of the two extremes used in the water vapor map. This explains why the DIRSIG 3 results are relatively flat.

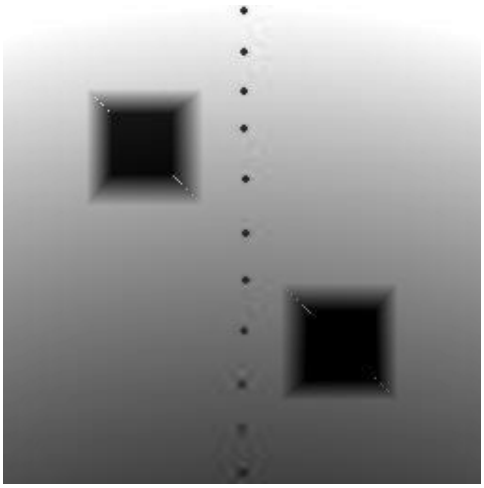

Figure 4.44: Test image 3, the path radiance in the 'water2' band (940 nm), rendered by DIRSIG 4.

The radiance results for all of the bands are shown in the following figures (4.45 through 4.50.)

bw/

The dip in error seen in the radiance graphs, most noticeably in the NIR radiance graph in figure 4.48 can be explained by the fact that the zenith angle is also varying along this x axis of the graph. In figure 4.9, the error at the edges of the image due to interpolation in the zenith dimension in the NIR band is approximately 0.05 percent. But at the center of the graph, the error is almost zero. If you look at the trend in figure 4.48 adding 0.05 percent to the center of the graph (at about 1.6) puts the error at a point that seems to fit the trend shown in the graph. The dip is a result of competing error contributions.

The transmission results for all of the bands are shown in the following figures (Figures 4.51 through 4.56.) The data in figure 4.51 looks considerably different than the other transmission results in test case 3 because

water vapor has less of an effect in the blue region of the spectrum.

Looking at these graphs, again, it is clear that the DIRSIG 4 interpolator has a clear advantage over DIRSIG 3's. As well, the trend shows that the error associated with DIRSIG 4 approaches zero at the endpoints of the water vapor dimension (1.0 and 2.5g/cm2). It should be noted that the other dimensions are changing in the image as well.

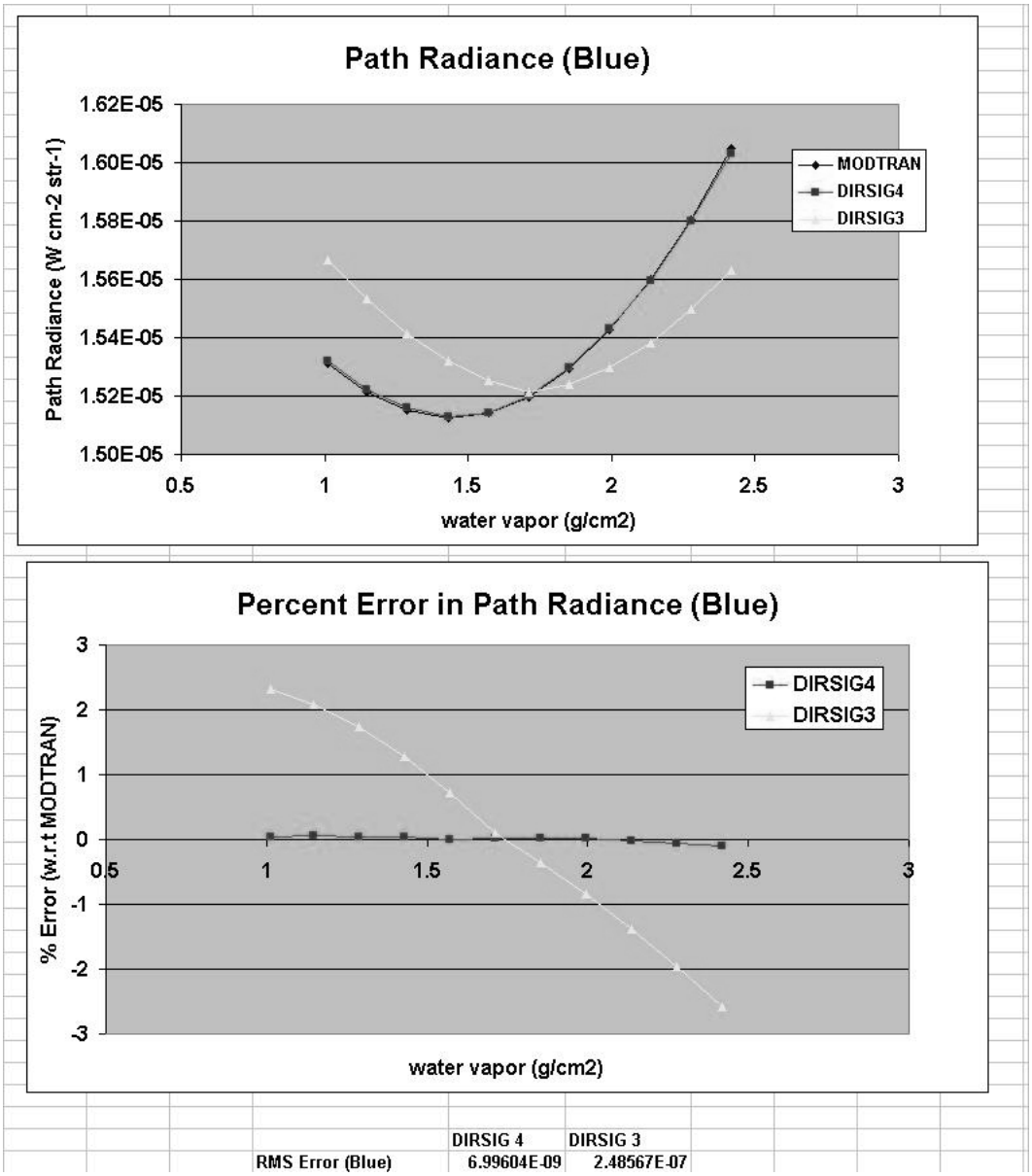

Figure 4.45: Test Scene 3 (water variation): The upper graph shows the blue path radiance obtained by MODTRAN, DIRSIG 4 and DIRSIG 3. The lower graph shows the percent error of DIRSIG 4 and DIRSIG 3 relative to MODTRAN. The RMS errors for the points shown on the graph are listed below the graphs.

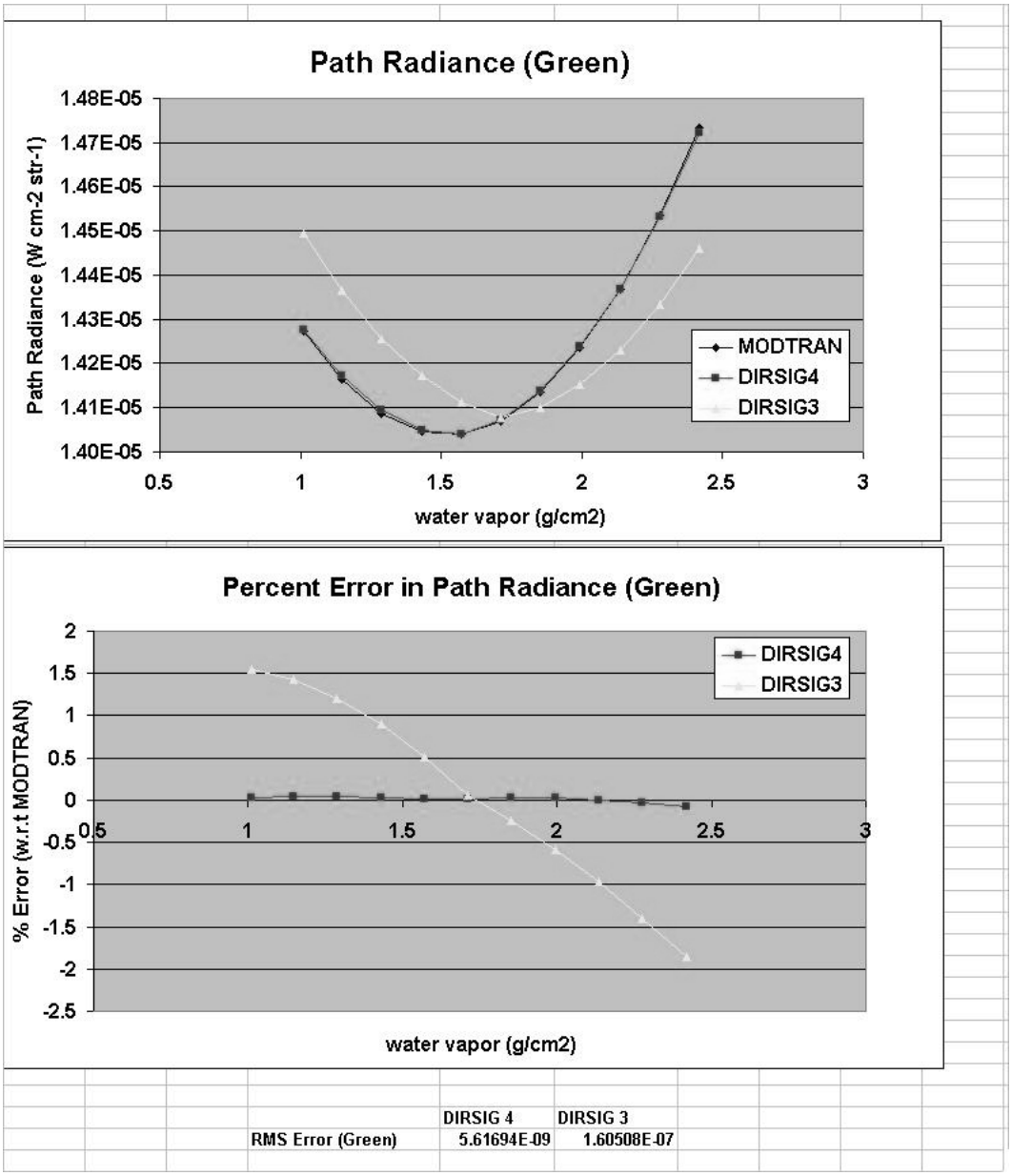

Figure 4.46: Test Scene 3 (water variation): The upper graph shows the green path radiance obtained by MODTRAN, DIRSIG 4 and DIRSIG 3. The lower graph shows the percent error of DIRSIG 4 and DIRSIG 3 relative to MODTRAN. The RMS errors for the points shown on the graph are listed below the graphs.

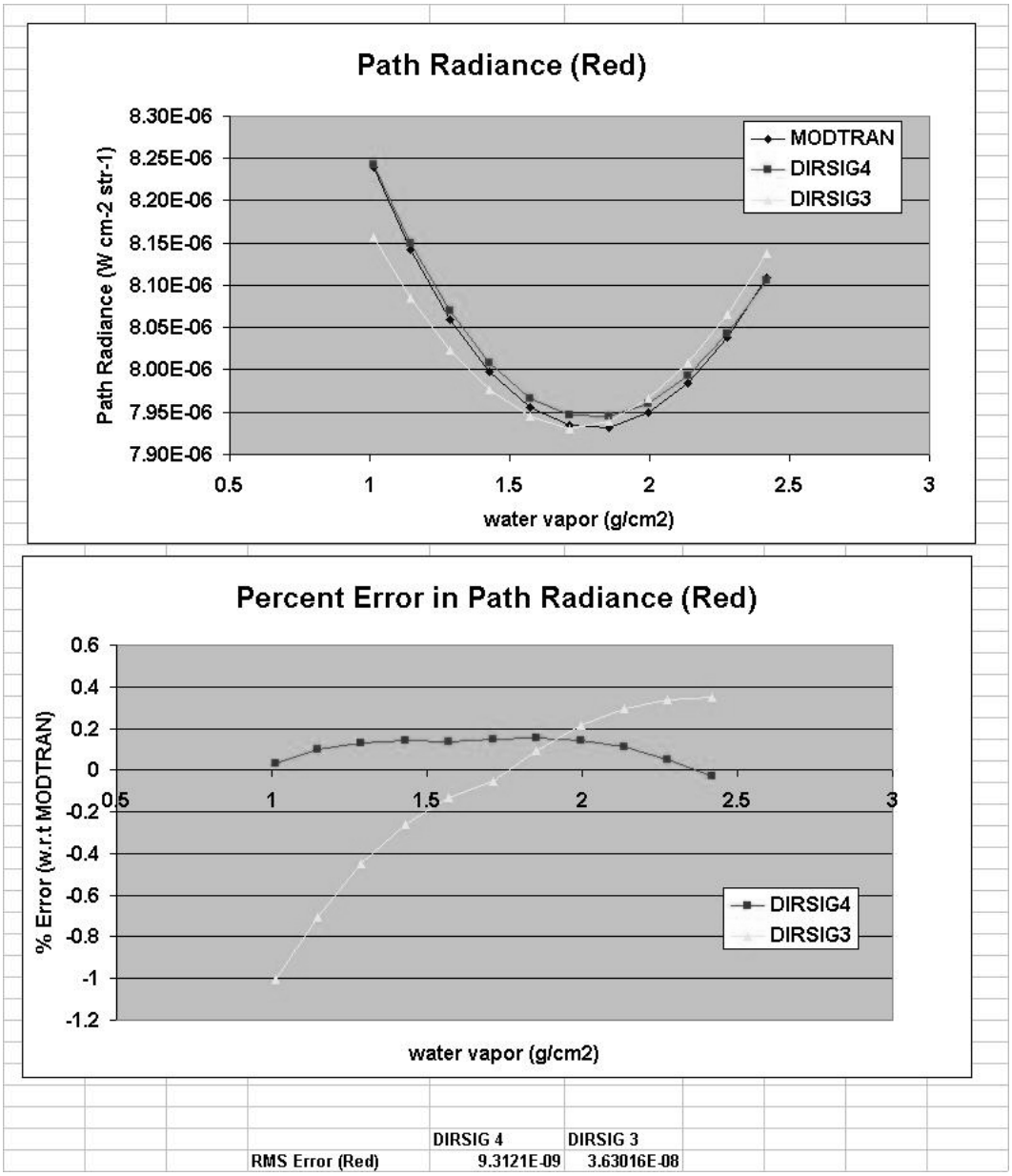

Figure 4.47: Test Scene 3 (water variation): The upper graph shows the red path radiance obtained by MODTRAN, DIRSIG 4 and DIRSIG 3. The lower graph shows the percent error of DIRSIG 4 and DIRSIG 3 relative to MODTRAN. The RMS errors for the points shown on the graph are listed below the graphs.

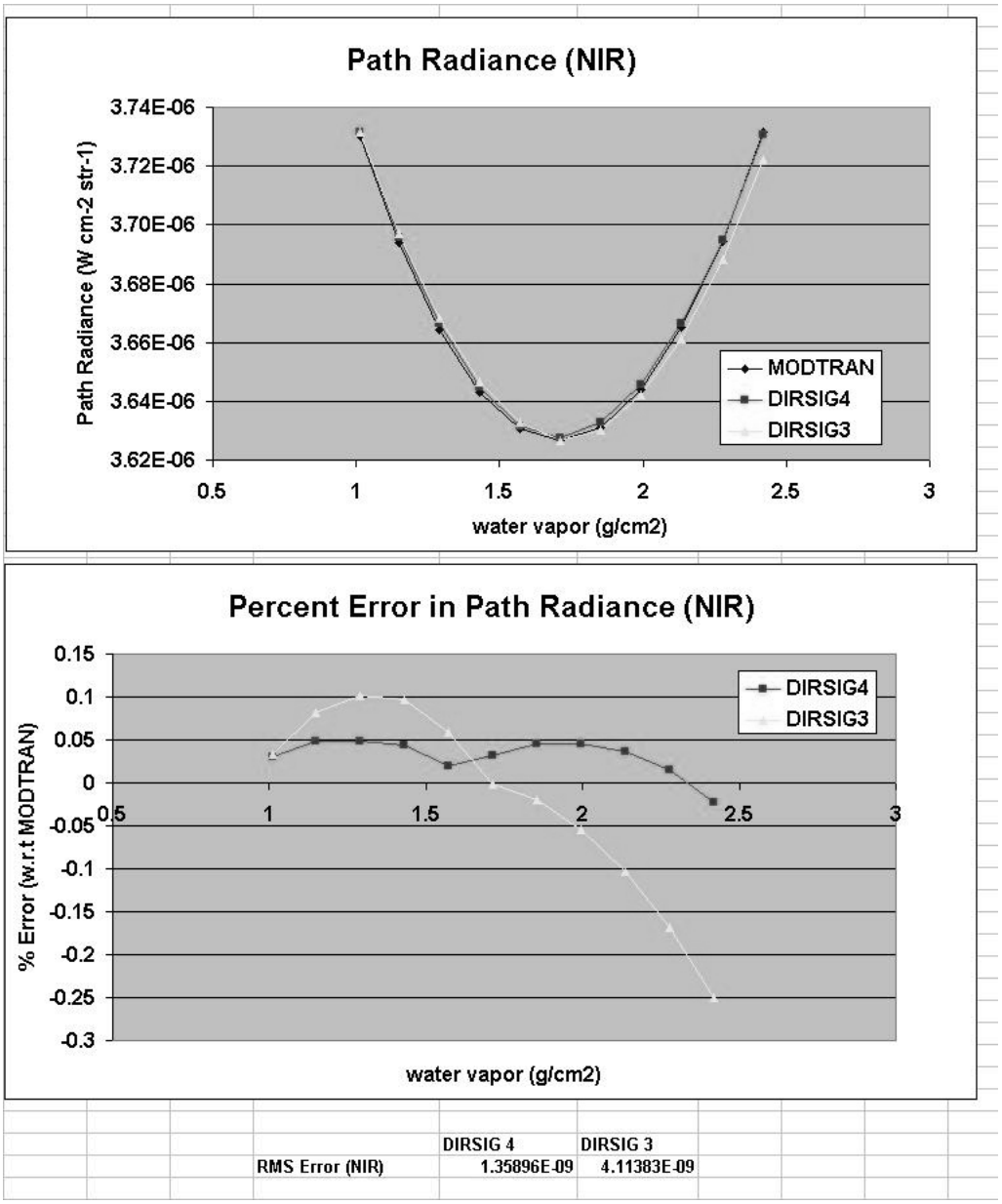

Figure 4.48: Test Scene 3 (water variation): The upper graph shows the NIR path radiance obtained by MODTRAN, DIRSIG 4 and DIRSIG 3. The lower graph shows the percent error of DIRSIG 4 and DIRSIG 3 relative to MODTRAN. The RMS errors for the points shown on the graph are listed below the graphs.

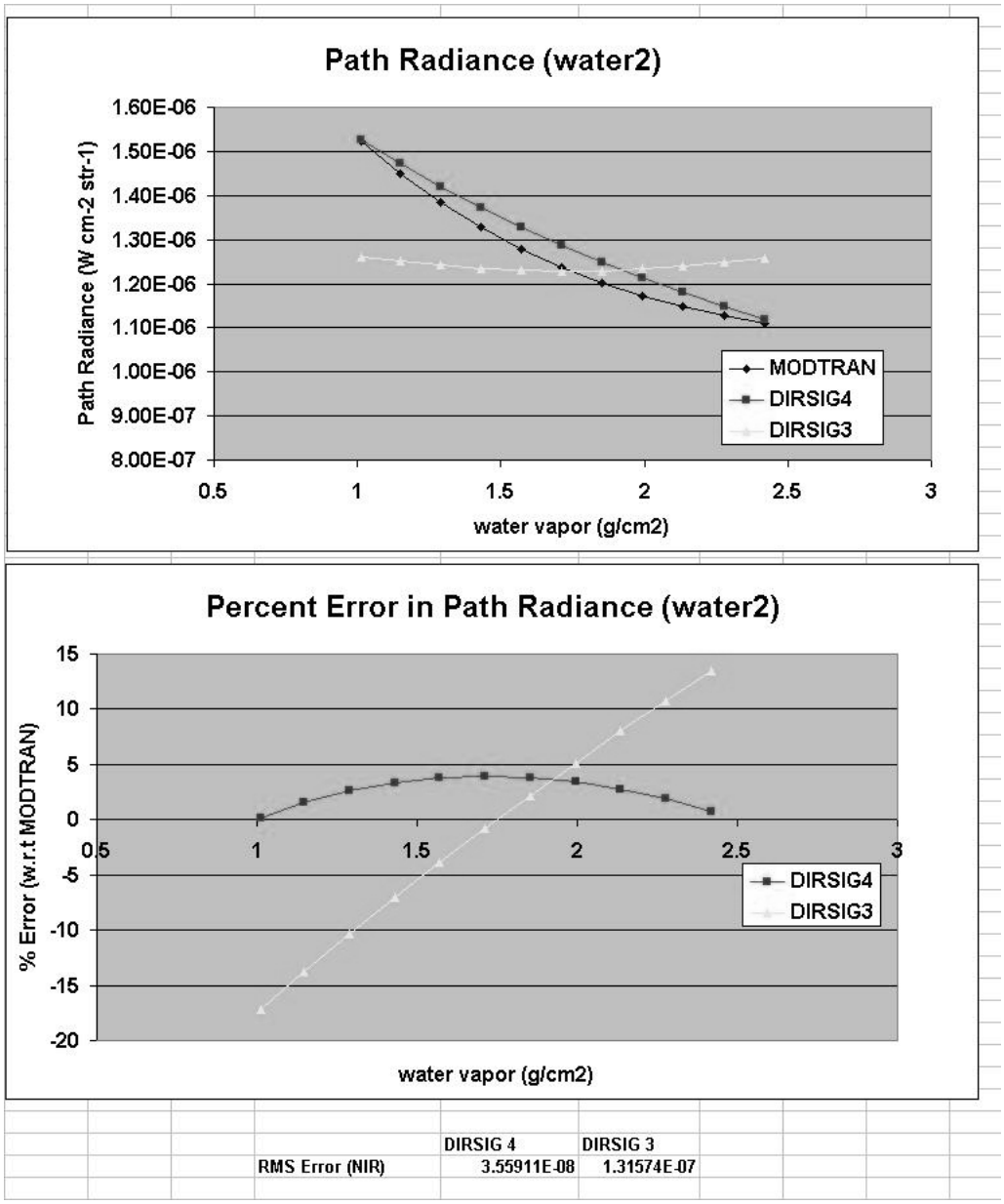

Figure 4.49: Test Scene 3 (water variation): The upper graph shows the water2 path radiance obtained by MODTRAN, DIRSIG 4 and DIRSIG 3. The lower graph shows the percent error of DIRSIG 4 and DIRSIG 3 relative to MODTRAN. The RMS errors for the points shown on the graph are listed below the graphs.

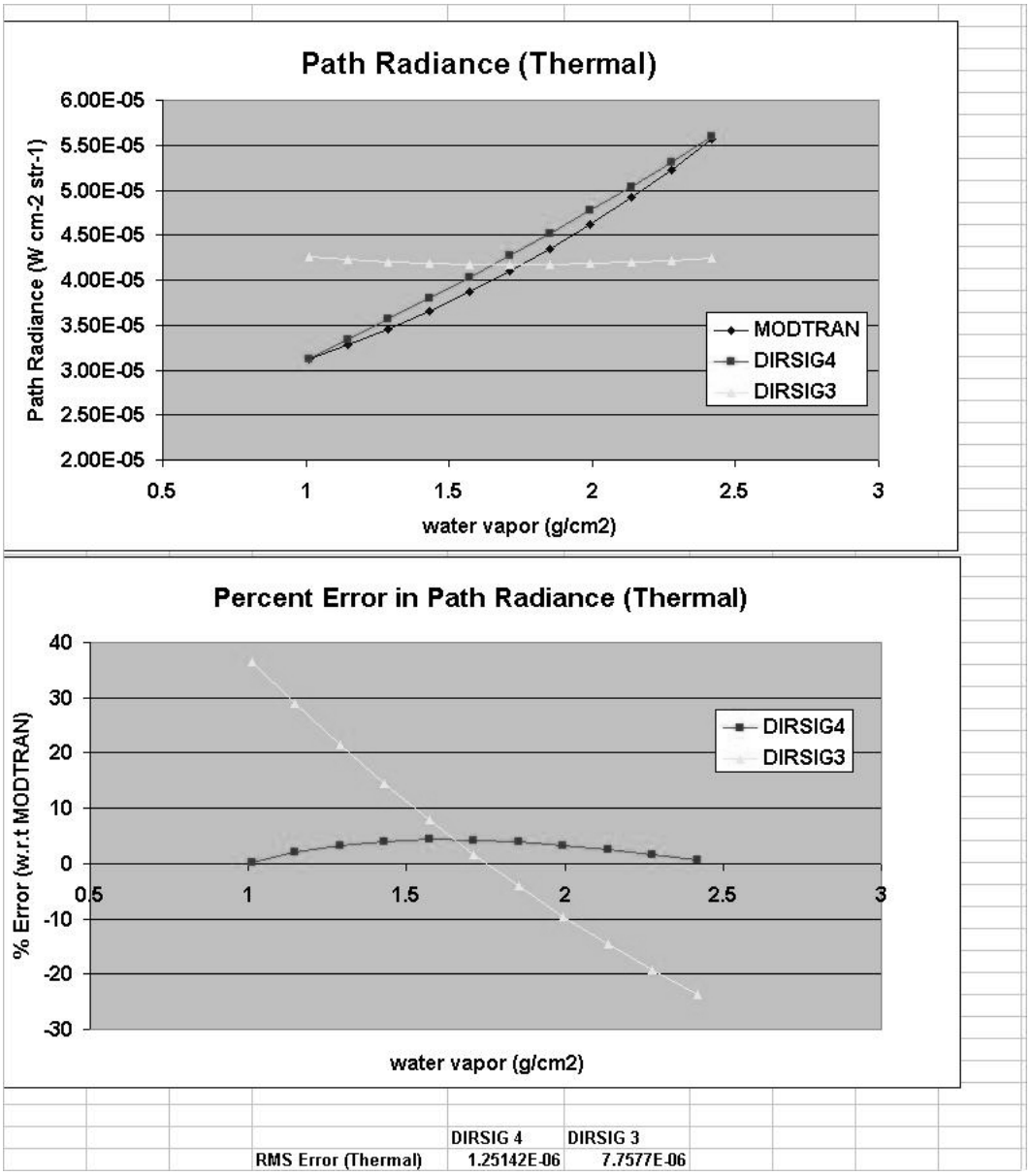

Figure 4.50: Test Scene 3 (water variation): The upper graph shows the Thermal path radiance obtained by MODTRAN, DIRSIG 4 and DIRSIG 3. The lower graph shows the percent error of DIRSIG 4 and DIRSIG 3 relative to MODTRAN. The RMS errors for the points shown on the graph are listed below the graphs.

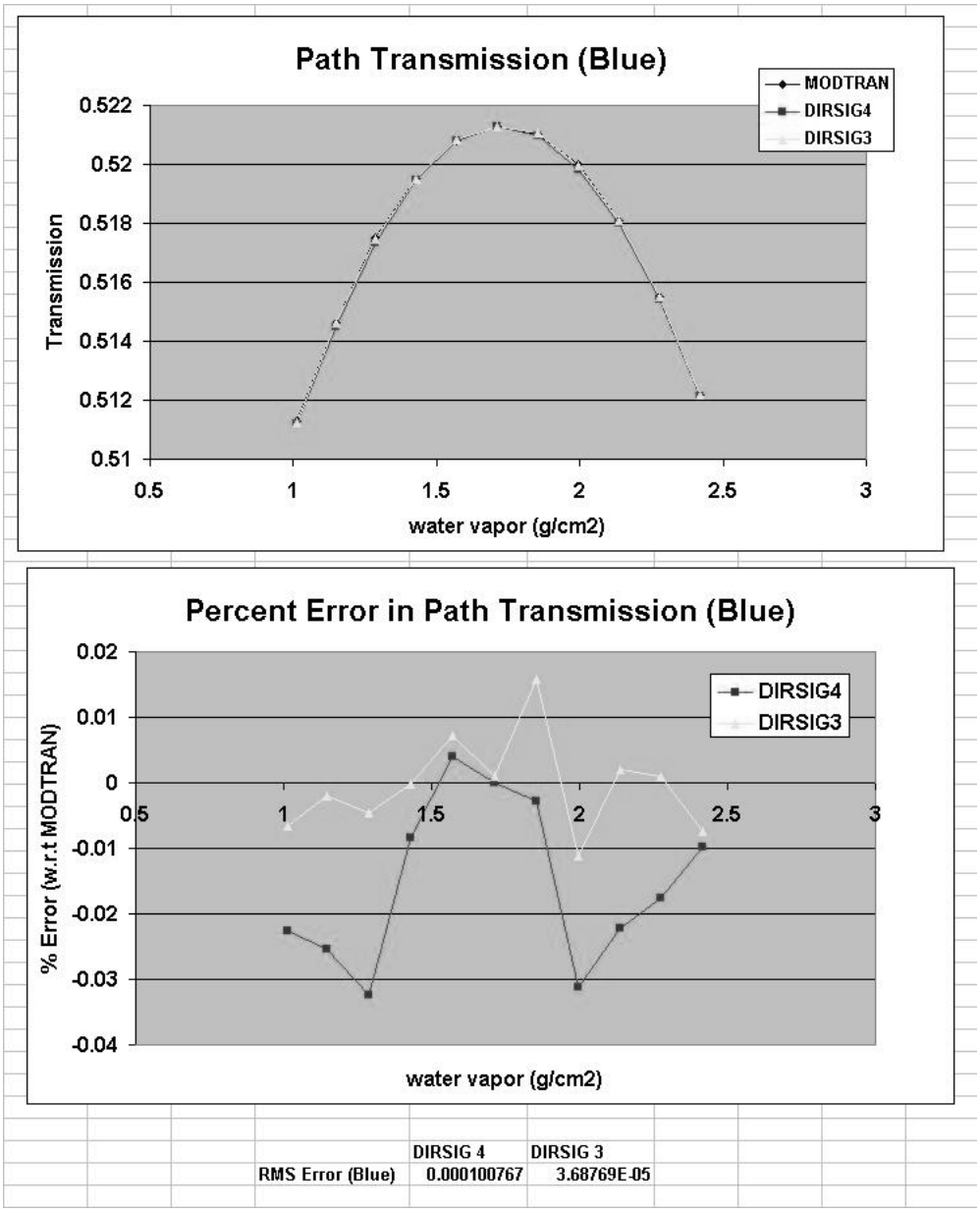

Figure 4.51: Test Scene 3 (water variation): The upper graph shows the blue path transmission obtained by MODTRAN, DIRSIG 4 and DIRSIG 3. The lower graph shows the percent error of DIRSIG 4 and DIRSIG 3 relative to MODTRAN. The RMS errors for the points shown on the graph are listed below the graphs.

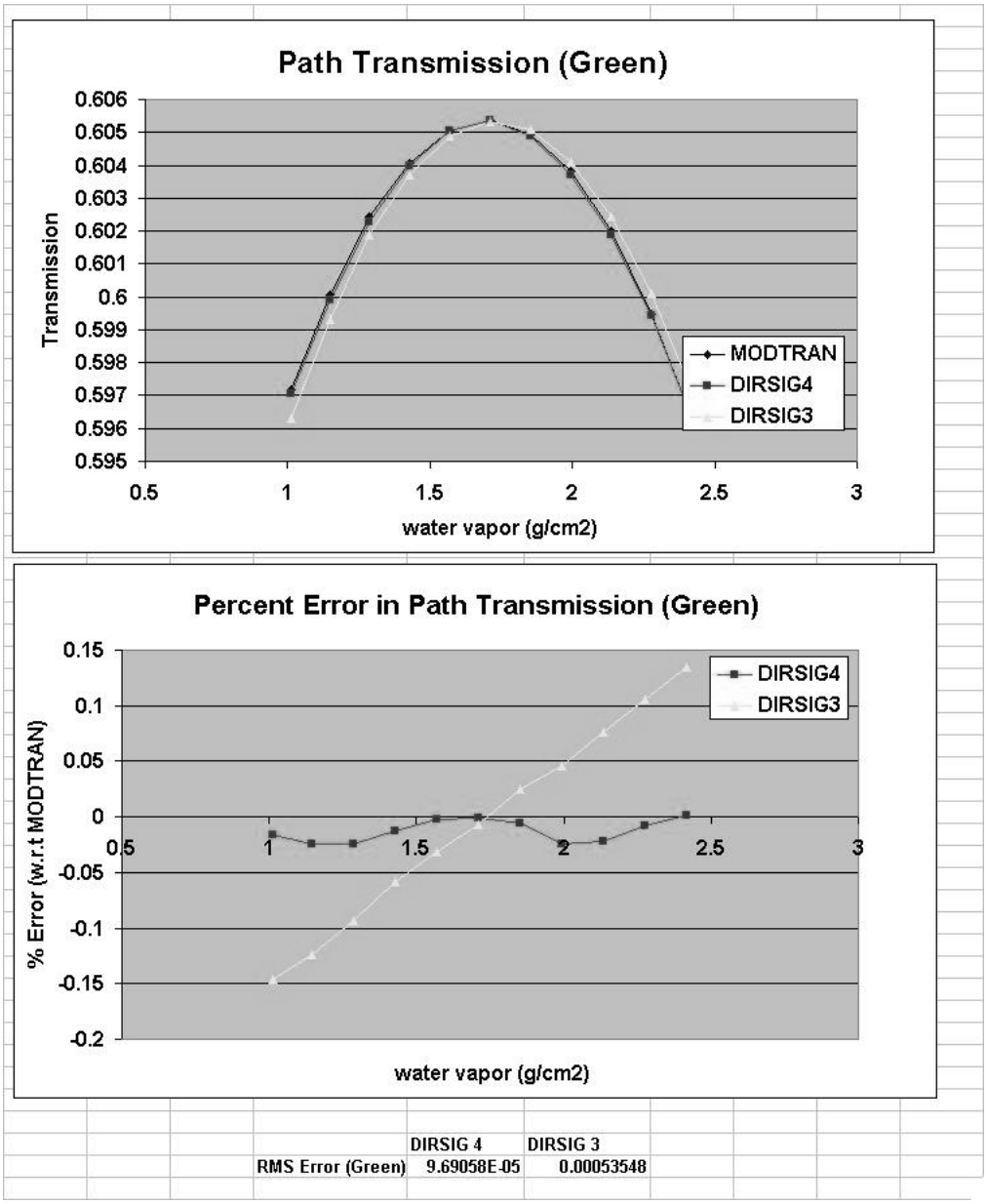

Figure 4.52: Test Scene 3 (water variation): The upper graph shows the green path transmission obtained by MODTRAN, DIRSIG 4 and DIRSIG 3. The lower graph shows the percent error of DIRSIG 4 and DIRSIG 3 relative to MODTRAN. The RMS errors for the points shown on the graph are listed below the graphs.

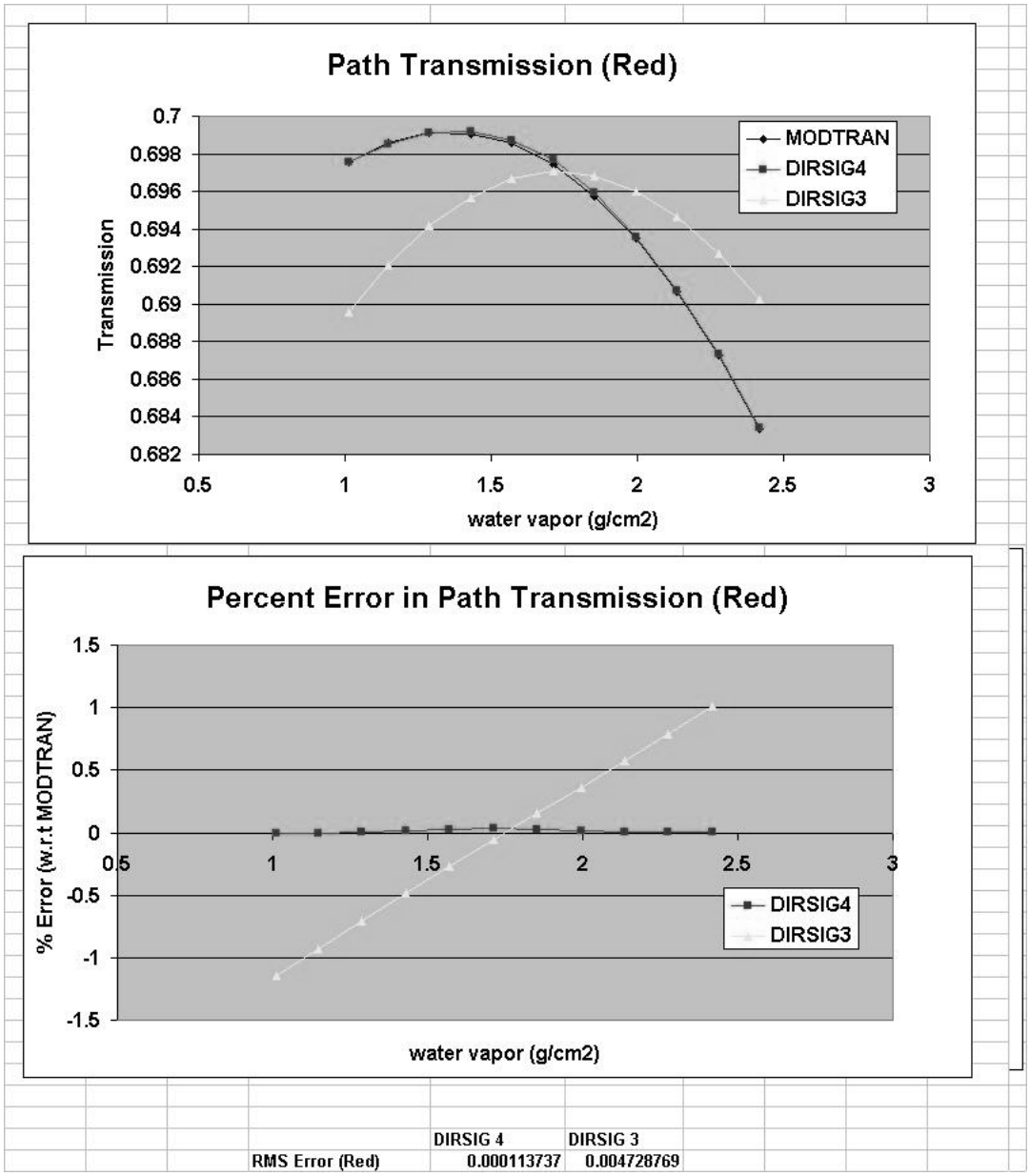

Figure 4.53: Test Scene 3 (water variation): The upper graph shows the red path transmission obtained by MODTRAN, DIRSIG 4 and DIRSIG 3. The lower graph shows the percent error of DIRSIG 4 and DIRSIG 3 relative to MODTRAN. The RMS errors for the points shown on the graph are listed below the graphs.

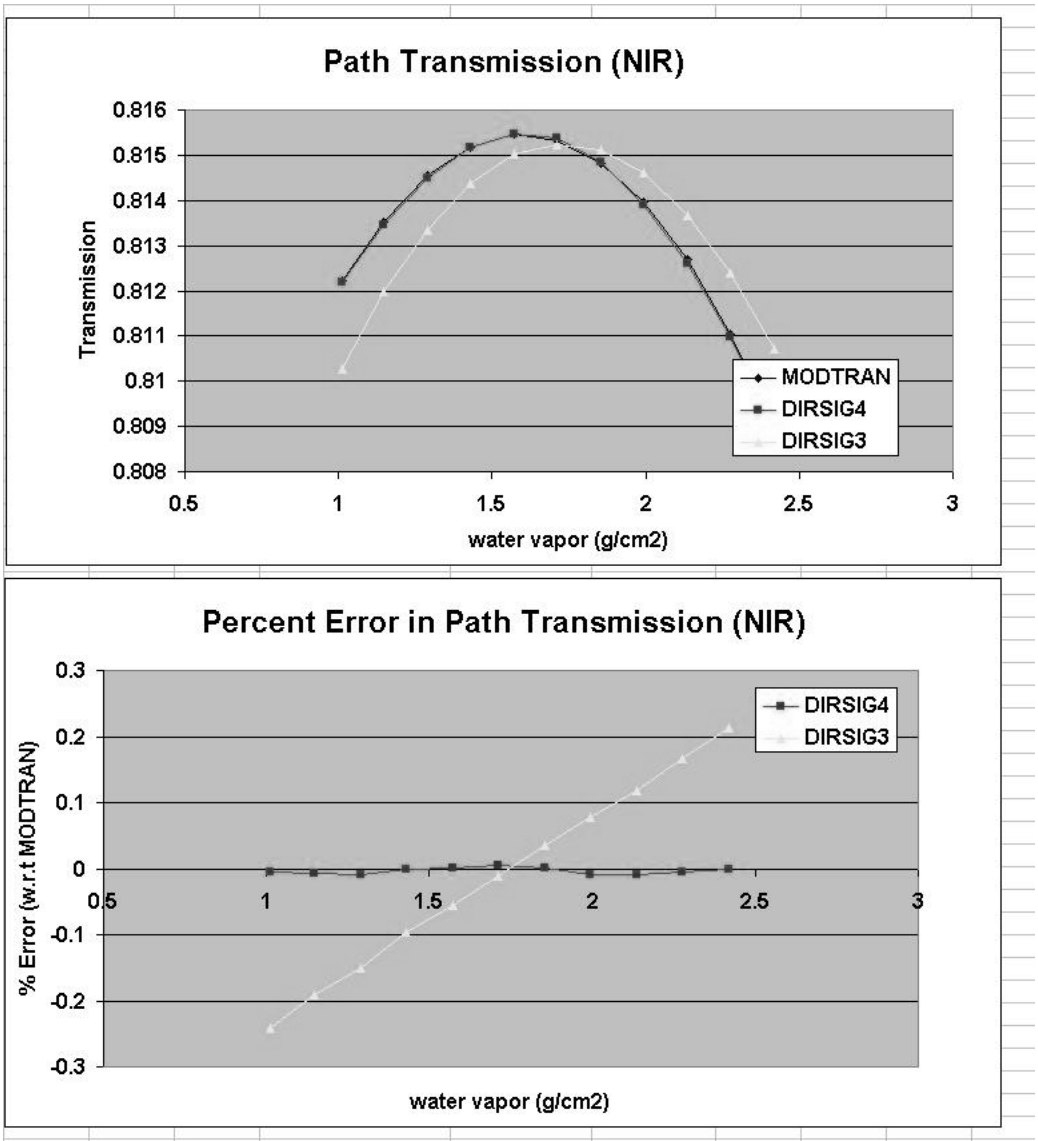

Figure 4.54: Test Scene 3 (water variation): The upper graph shows the NIR path transmission obtained by MODTRAN, DIRSIG 4 and DIRSIG 3. The lower graph shows the percent error of DIRSIG 4 and DIRSIG 3 relative to MODTRAN. The RMS errors for the points shown on the graph are listed below the graphs.

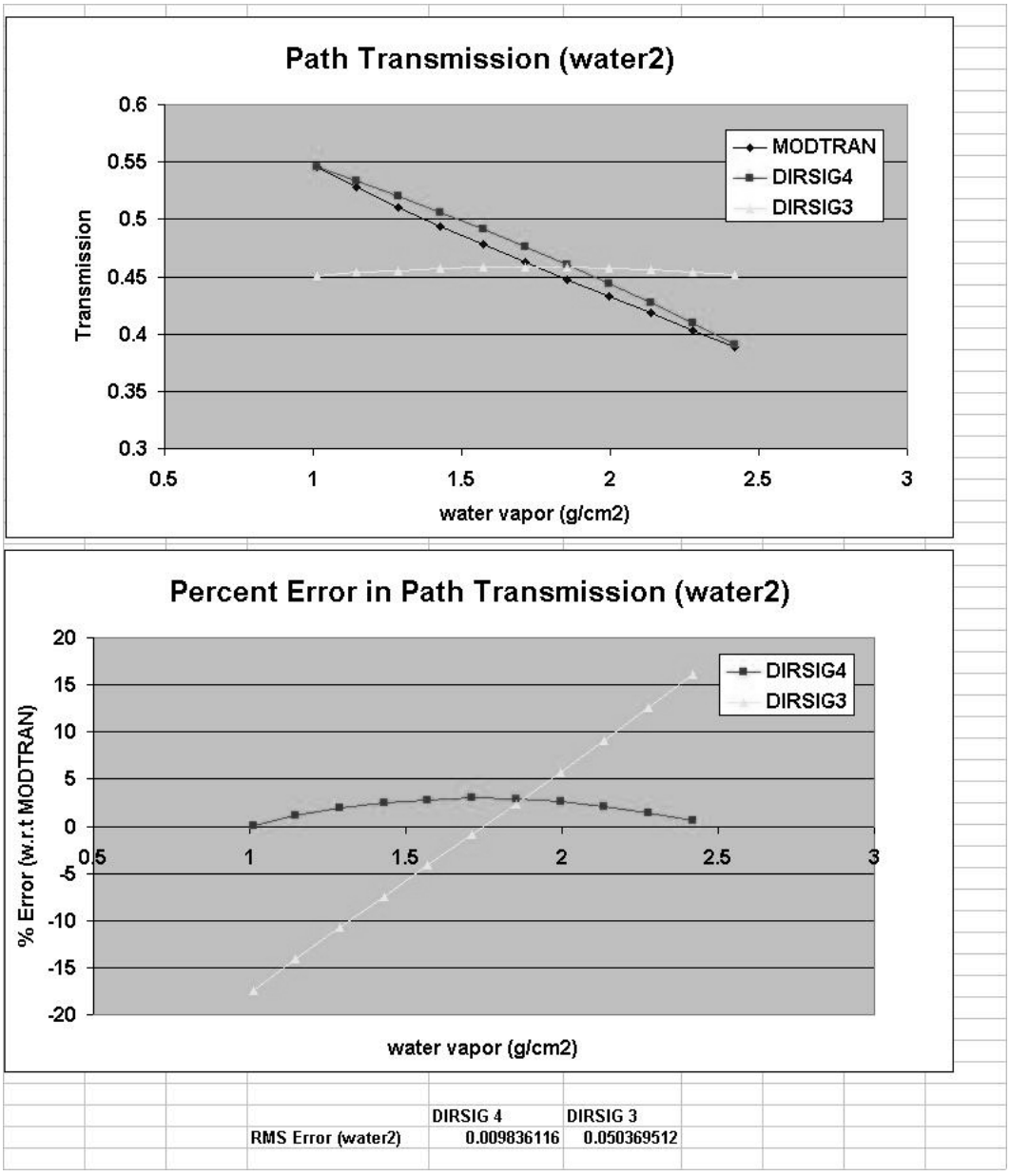

	DIRSIG 4	DIRSIG 3
RMS Error (water2)	0.009836116	0.050369512

Figure 4.55: Test Scene 3 (water variation): The upper graph shows the water2 path transmission obtained by MODTRAN, DIRSIG 4 and DIRSIG 3. The lower graph shows the percent error of DIRSIG 4 and DIRSIG 3 relative to MODTRAN. The RMS errors for the points shown on the graph are listed below the graphs.

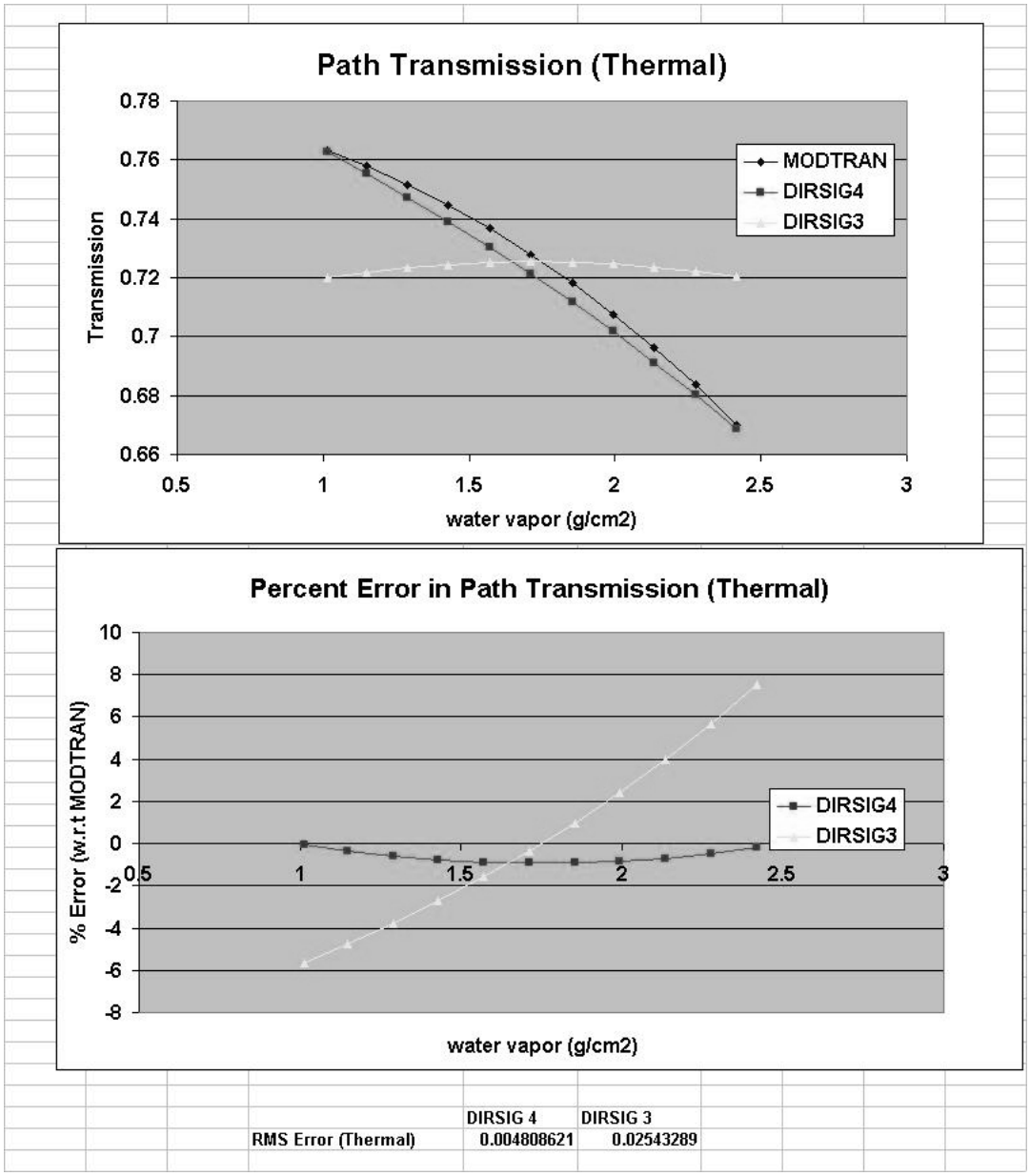

Figure 4.56: Test Scene 3 (water variation): The upper graph shows the Thermal path transmission obtained by MODTRAN, DIRSIG 4 and DIRSIG 3. The lower graph shows the percent error of DIRSIG 4 and DIRSIG 3 relative to MODTRAN. The RMS errors for the points shown on the graph are listed below the graphs.

Grid Results

Like the other test images, this image was sampled at a nearly regular grid of points. A visual representation of the points sampled is similar to those seem in figure 4.24

The RMS error (by band) is shown in figure 4.57 for the path radiance and in figure 4.58 for the transmission.

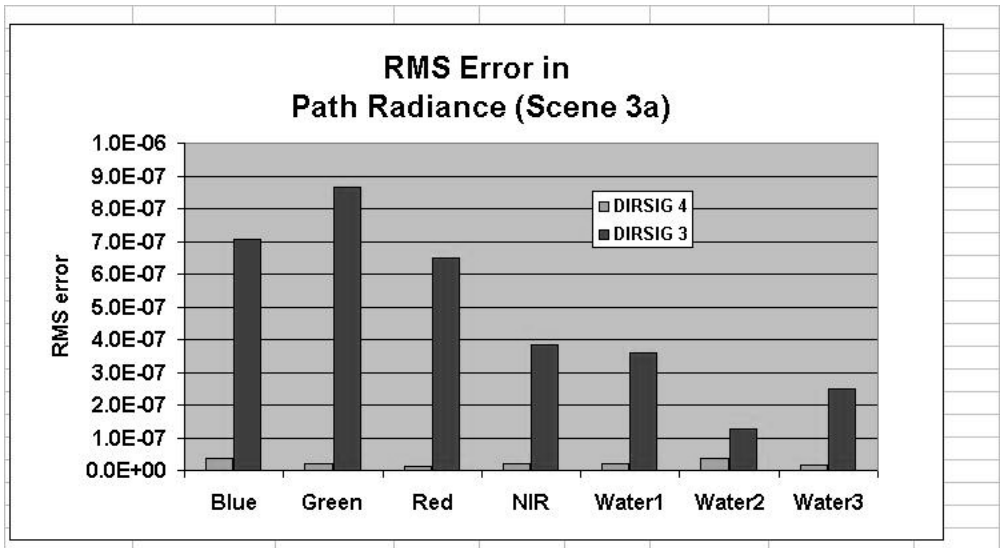

band	DIRSIG 4	DIRSIG 3
Blue	3.541827E-08	7.061488E-07
Green	2.139628E-08	8.639773E-07
Red	1.038756E-08	6.504945E-07
NIR	1.867803E-08	3.829265E-07
Water1	1.931853E-08	3.611747E-07
Water2	3.730402E-08	1.269342E-07
Water3	1.576366E-08	2.473453E-07
Thermal	1.384556E-06	8.433062E-06

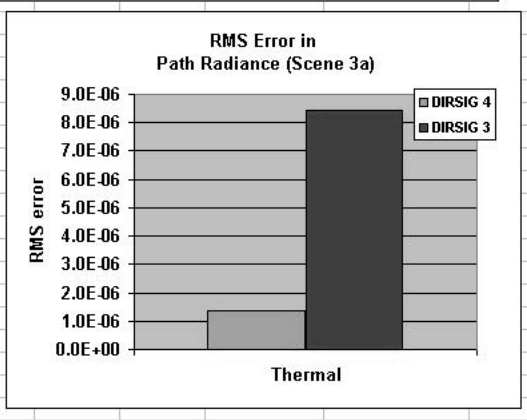

Figure 4.57: This shows the RMS error in path radiance (by band) over image 3a.

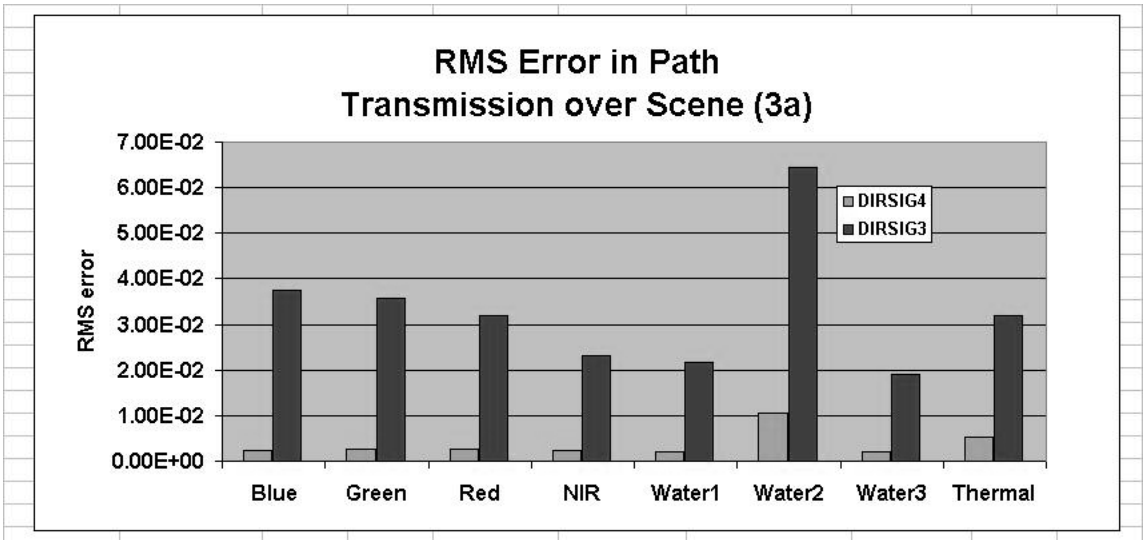

band	DIRSIG4	DIRSIG3
Blue	2.377344E-03	3.759451E-02
Green	2.674025E-03	3.567550E-02
Red	2.691113E-03	3.191789E-02
NIR	2.271498E-03	2.307631E-02
Water1	2.182873E-03	2.175919E-02
Water2	1.046241E-02	6.430360E-02
Water3	1.965138E-03	1.912360E-02
Thermal	5.131777E-03	3.183733E-02

Figure 4.58: This shows the RMS error in path transmission (by band) over image 3a.

4.2.2 Highlighting Visibility Changes

The next test scene analyzes the effect of changing visibility over an image. This analysis was done on the "truncated pyramid" image (figure 4.1), with a "wedge" of visibility above it. This wedge is an atmospheric map which has a visibility value of 1 km at the upper (Western) edge of the image. The visibility value increases linearly to the East until it reaches a maximum of 23 km at the lower (Eastern) edge.

The graphic shown in figure 4.42 represents the scene, but with visibility values replacing the water vapor values.

Figure 4.59 shows the RGB radiance of test image 4.

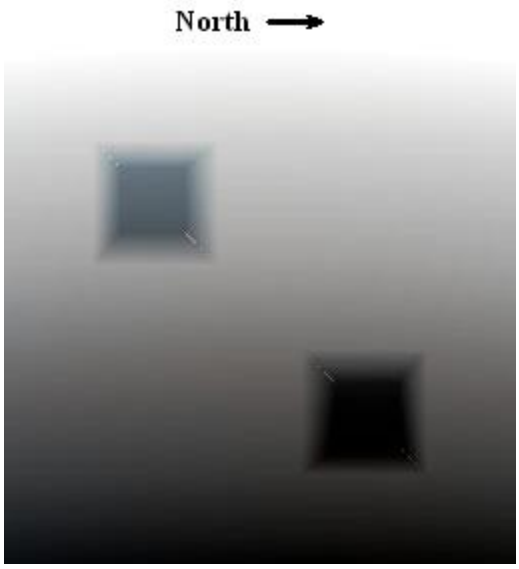

Figure 4.59: The RGB path radiance of test image 4, rendered by DIRSIG 4.

Like image 3, for image 4 a line of points were analyzed. These points are the same as those shown in figure 4.44, and mark roughly a linear increase in the visibility of the aerosols present in the atmosphere. It should be noted that all of the other dimensions (zenith, azimuth, and altitude) except for water vapor vary as well.

The DIRSIG 3 images were rendered with a single visibility value (1.84615 km), which is the reciprocal of the average of the reciprocals of the two extremes used in the visibility map. This explains why the DIRSIG 3 results are relatively flat. The reciprocal of the average of the reciprocals was used to find the "midpoint" of the visibility map because the inverse of the visibility is more linear that the visibility, as it pertains to atmospheric radiance and transmission values.

The radiance results for all of the bands are shown in the following figures (Figures 4.60 through 4.65.)

The transmission results for all of the bands are shown in the following figures (Figures 4.66 through 4.71.)

DIRSIG 4's interpolator shows better accuracy over DIRSIG 3's. Although the error is significantly high, the trend shows that the error associated with DIRSIG 4 approaches zero at the endpoints of the visibility dimension (1.0 and 23 km). It should be noted that the other dimensions are changing in the image as well. These high errors are address later in this chapter.

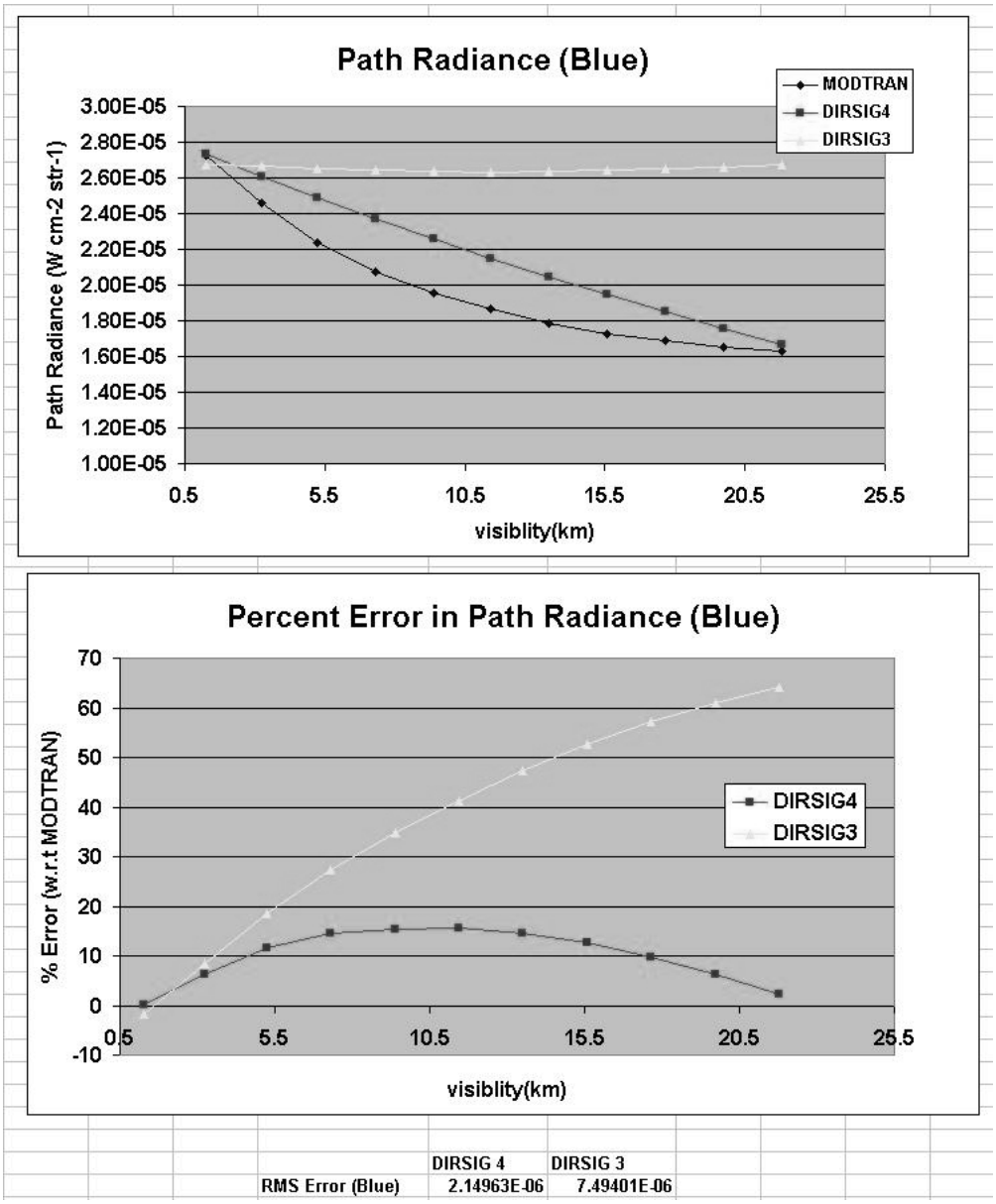

Figure 4.60: Test Scene 4a (visibility variation): The upper graph shows the blue path radiance obtained by MODTRAN, DIRSIG 4 and DIRSIG 3. The lower graph shows the percent error of DIRSIG 4 and DIRSIG 3 relative to MODTRAN. The RMS errors for the points shown on the graph are listed below the graphs.

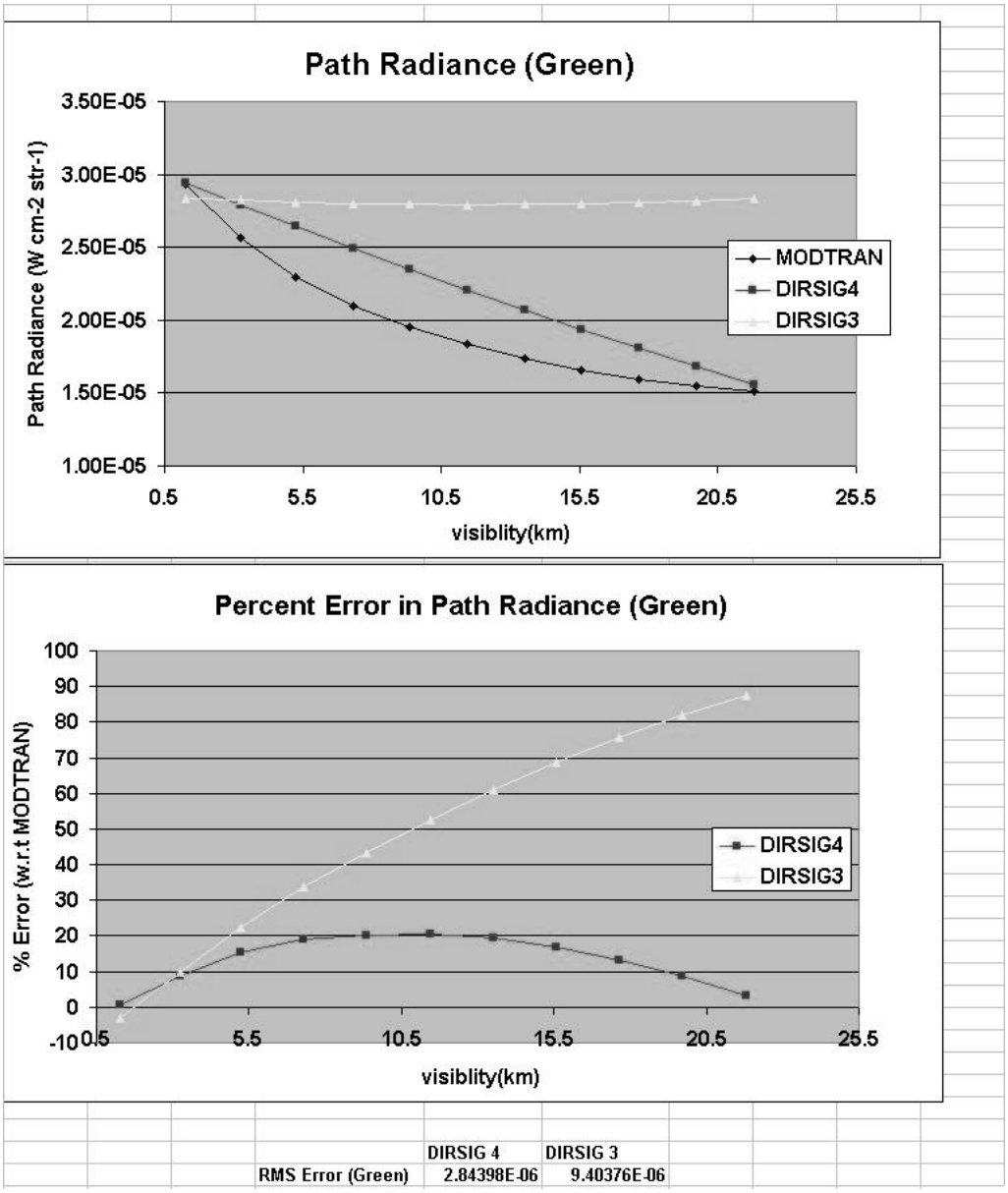

Figure 4.61: Test Scene 4a (visibility variation): The upper graph shows the green path radiance obtained by MODTRAN, DIRSIG 4 and DIRSIG 3. The lower graph shows the percent error of DIRSIG 4 and DIRSIG 3 relative to MODTRAN. The RMS errors for the points shown on the graph are listed below the graphs.

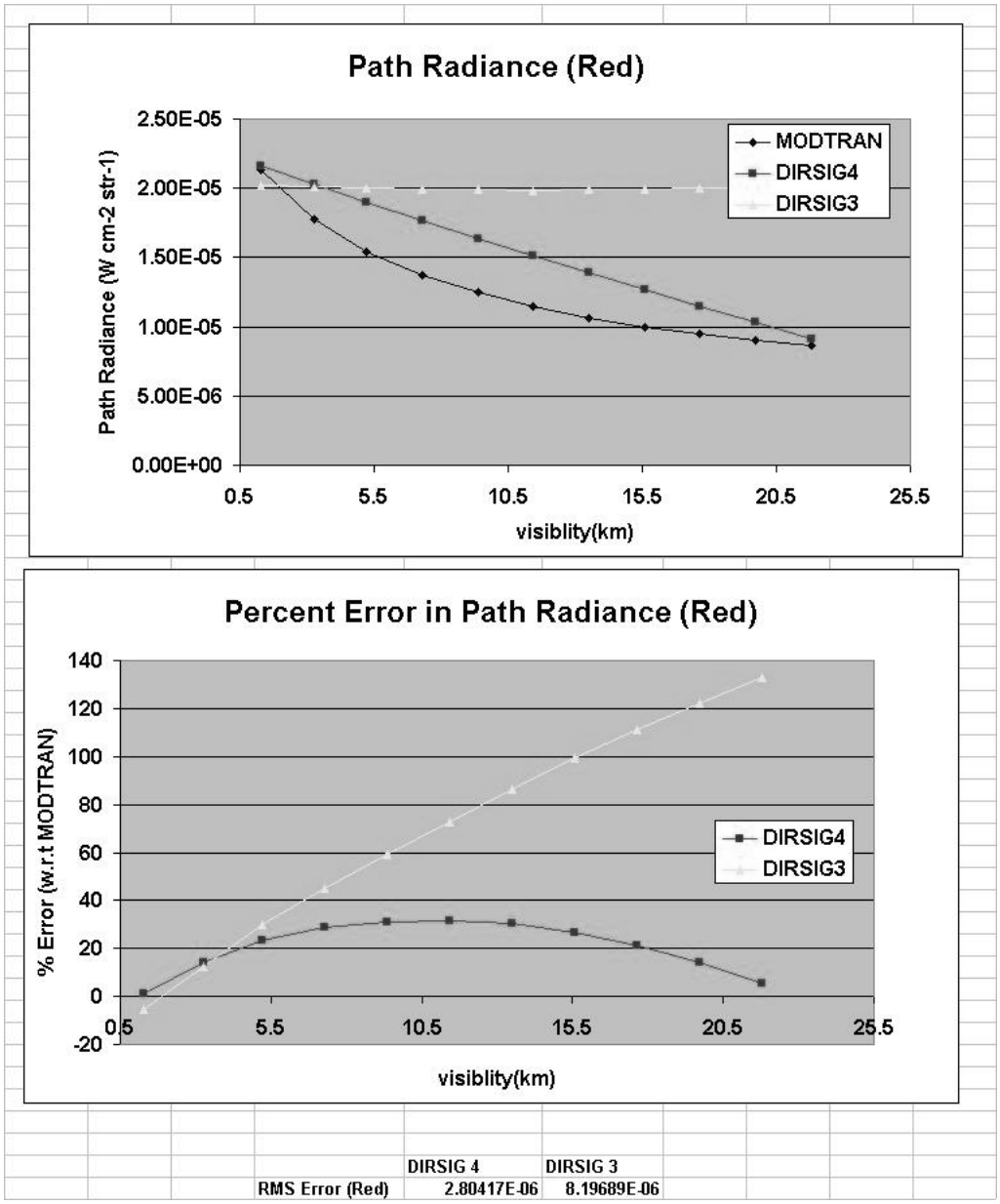

Figure 4.62: Test Scene 4a (visibility variation): The upper graph shows the red path radiance obtained by MODTRAN, DIRSIG 4 and DIRSIG 3. The lower graph shows the percent error of DIRSIG 4 and DIRSIG 3 relative to MODTRAN. The RMS errors for the points shown on the graph are listed below the graphs.

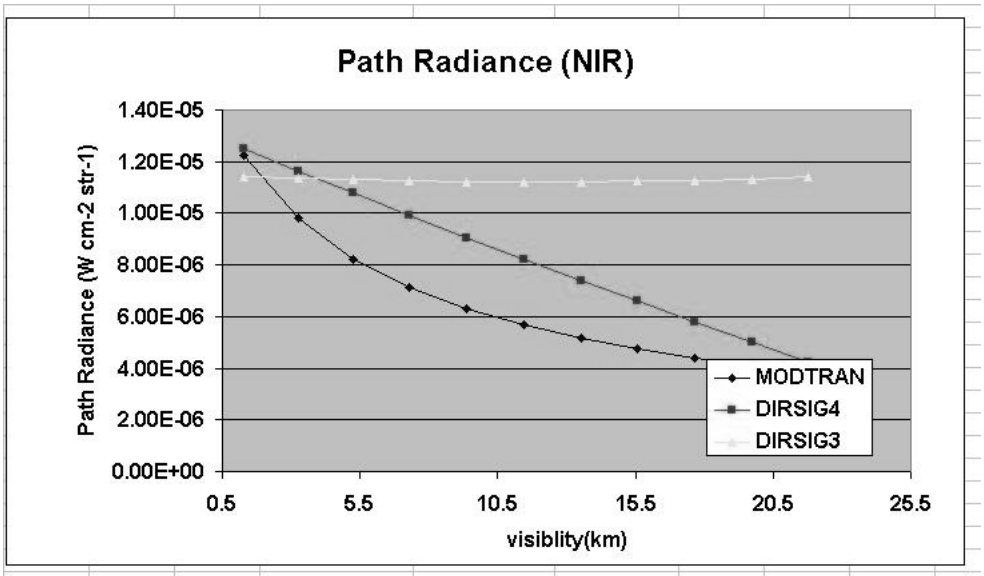

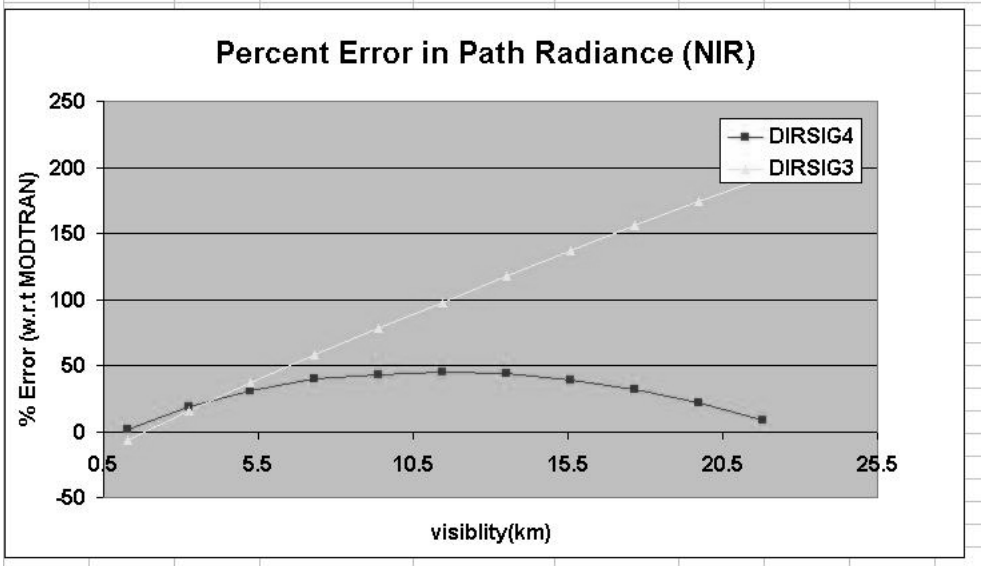

	DIRSIG 4	DIRSIG 3
RMS Error (NIR)	1.97994E-06	5.3874E-06

Figure 4.63: Test Scene 4a (visibility variation): The upper graph shows the NIR path radiance obtained by MODTRAN, DIRSIG 4 and DIRSIG 3. The lower graph shows the percent error of DIRSIG 4 and DIRSIG 3 relative to MODTRAN. The RMS errors for the points shown on the graph are listed below the graphs.

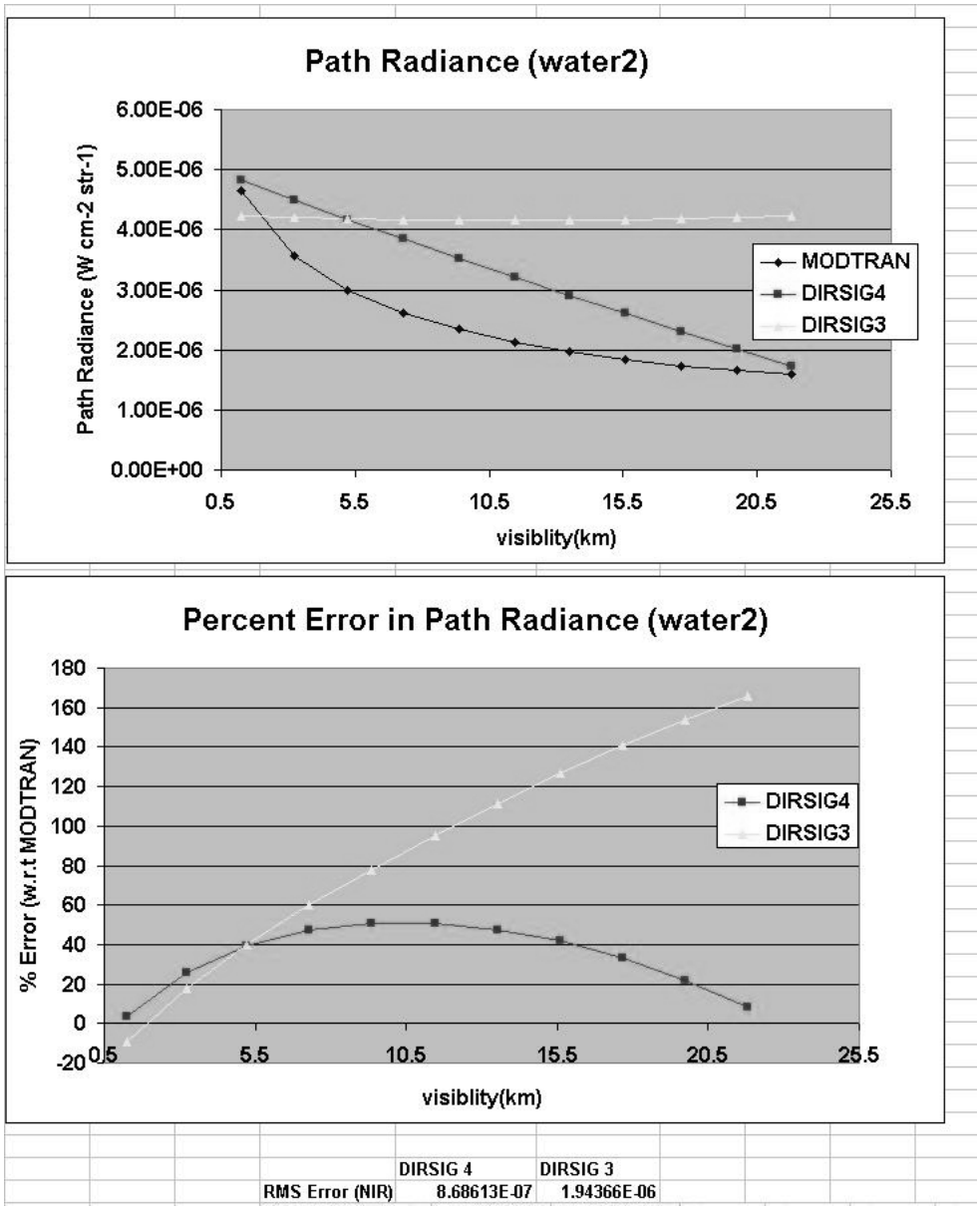

Figure 4.64: Test Scene 4a (visibility variation): The upper graph shows the water2 path radiance obtained by MODTRAN, DIRSIG 4 and DIRSIG 3. The lower graph shows the percent error of DIRSIG 4 and DIRSIG 3 relative to MODTRAN. The RMS errors for the points shown on the graph are listed below the graphs.

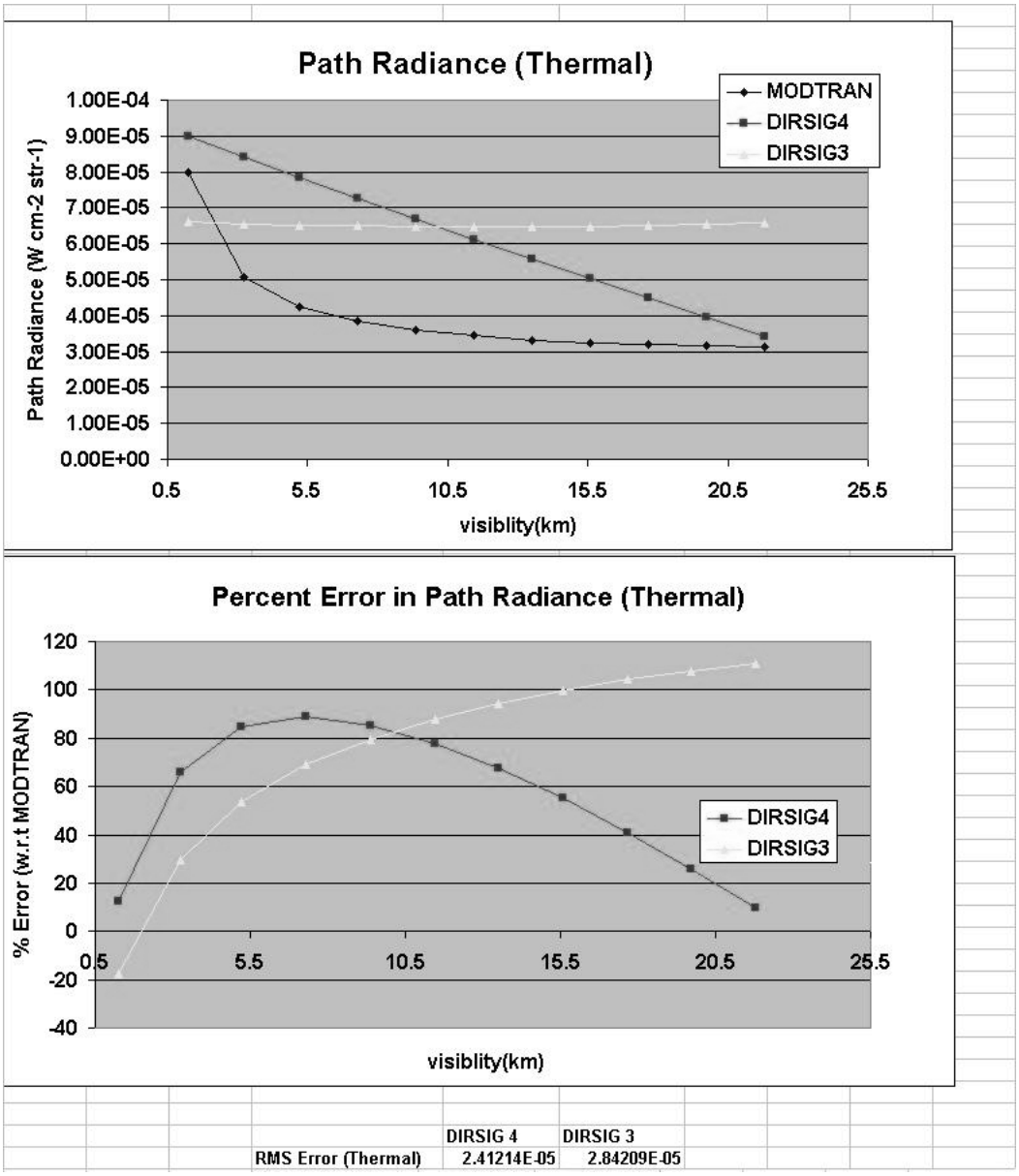

Figure 4.65: Test Scene 4a (visibility variation): The upper graph shows the Thermal path radiance obtained by MODTRAN, DIRSIG 4 and DIRSIG 3. The lower graph shows the percent error of DIRSIG 4 and DIRSIG 3 relative to MODTRAN. The RMS errors for the points shown on the graph are listed below the graphs.

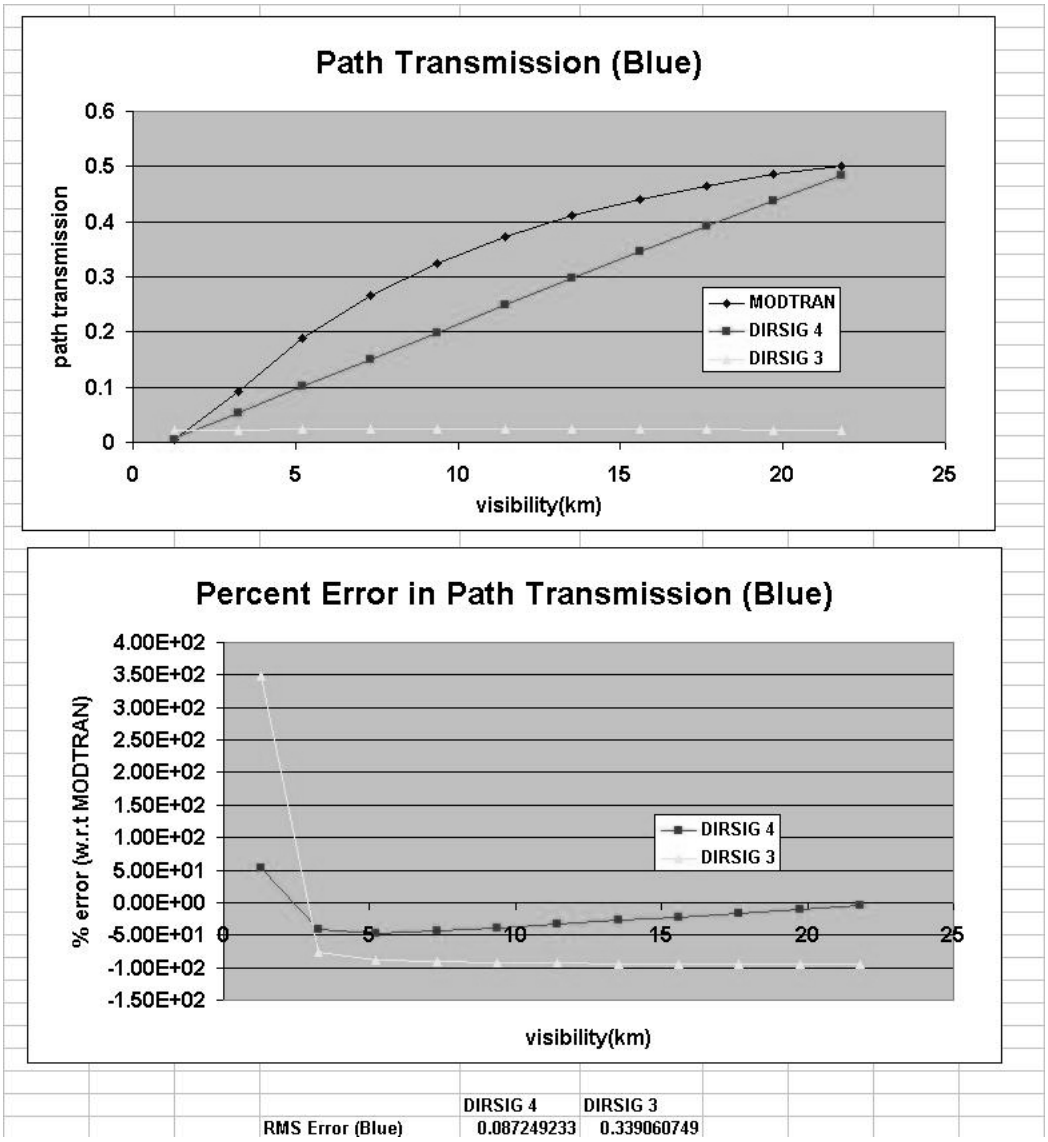

Figure 4.66: Test Scene 4a (visibility variation): The upper graph shows the blue path transmission obtained by MODTRAN, DIRSIG 4 and DIRSIG 3. The lower graph shows the percent error of DIRSIG 4 and DIRSIG 3 relative to MODTRAN. The RMS errors for the points shown on the graph are listed below the graphs.

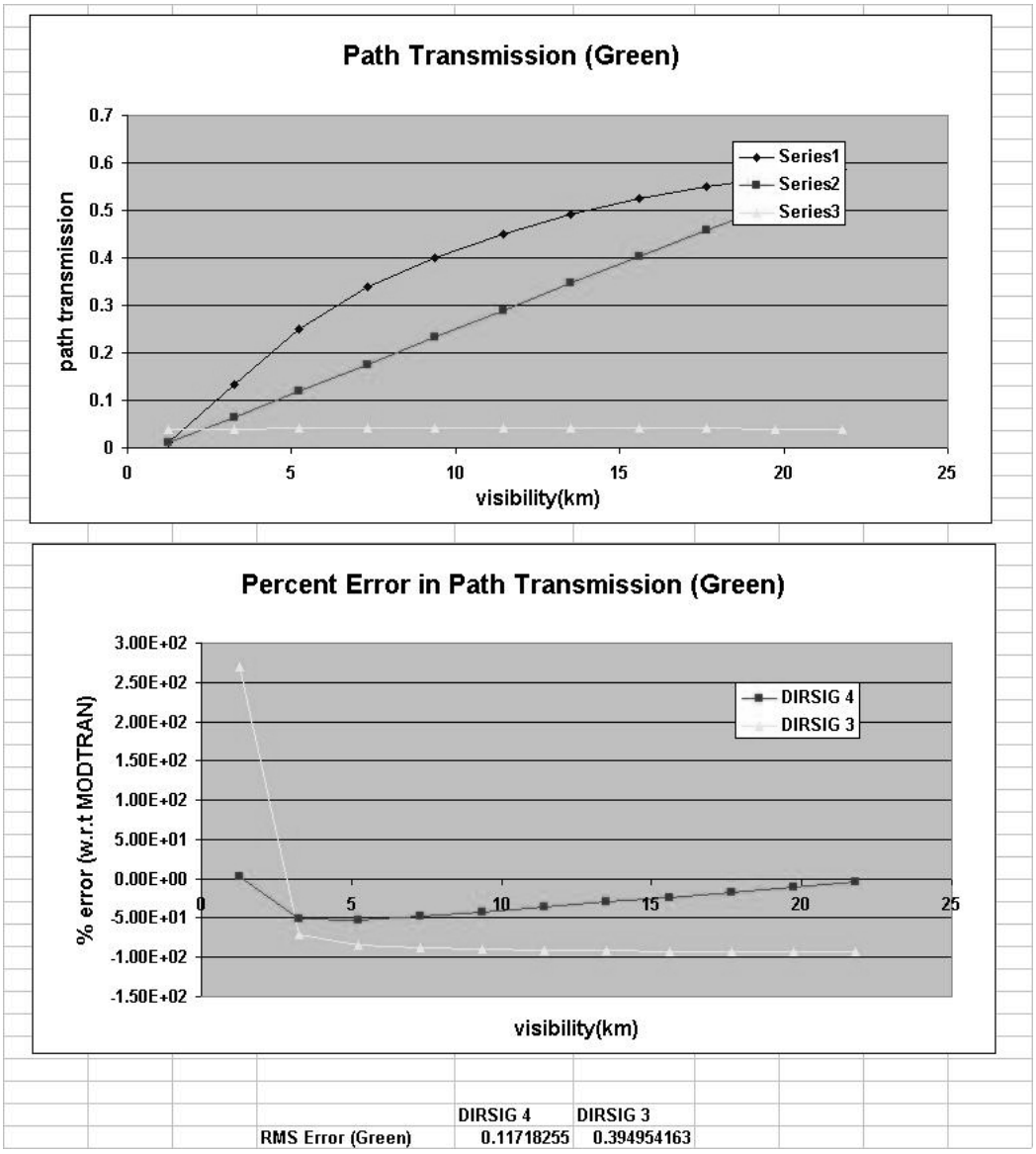

Figure 4.67: Test Scene 4a (visibility variation): The upper graph shows the green path transmission obtained by MODTRAN, DIRSIG 4 and DIRSIG 3. The lower graph shows the percent error of DIRSIG 4 and DIRSIG 3 relative to MODTRAN. The RMS errors for the points shown on the graph are listed below the graphs.

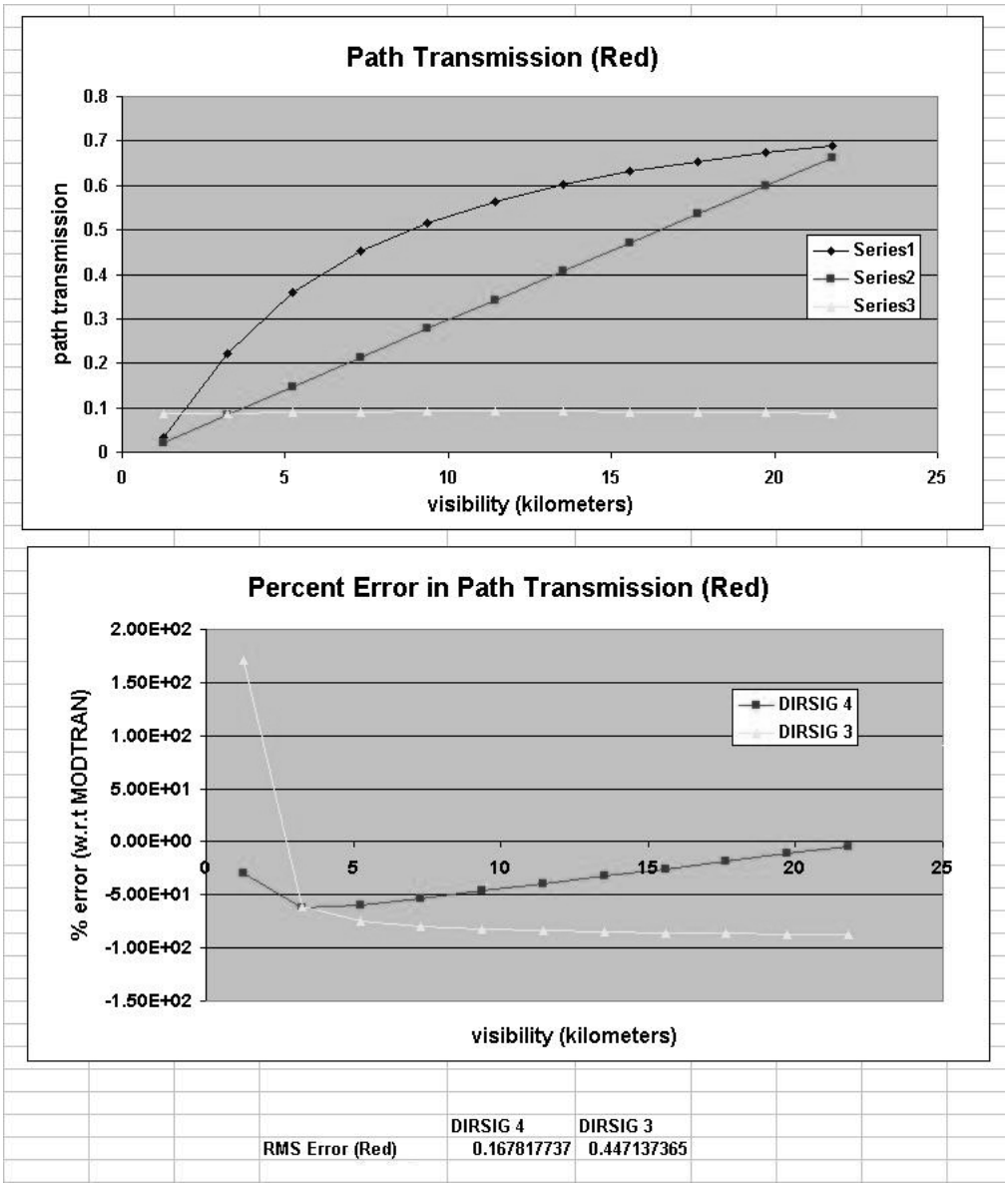

Figure 4.68: Test Scene 4a (visibility variation): The upper graph shows the red path transmission obtained by MODTRAN, DIRSIG 4 and DIRSIG 3. The lower graph shows the percent error of DIRSIG 4 and DIRSIG 3 relative to MODTRAN. The RMS errors for the points shown on the graph are listed below the graphs.

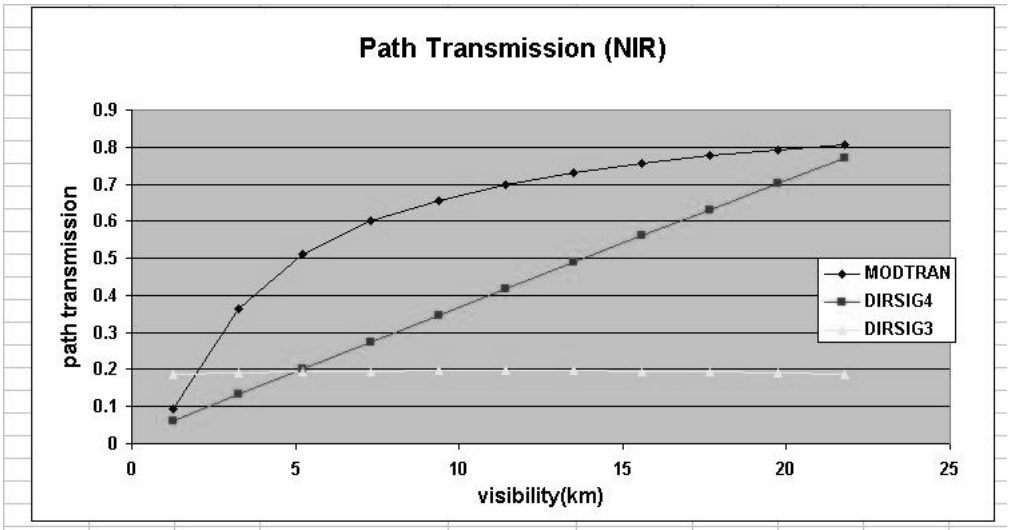

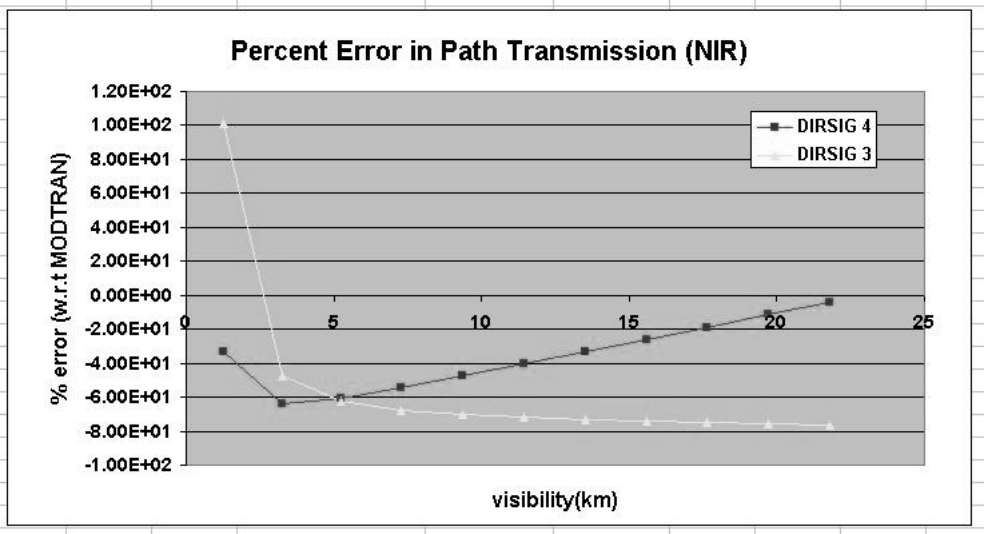

	DIRSIG 4	DIRSIG 3
RMS Error (NIR)	0.225215308	0.471375154

Figure 4.69: Test Scene 4a (visibility variation): The upper graph shows the NIR path transmission obtained by MODTRAN, DIRSIG 4 and DIRSIG 3. The lower graph shows the percent error of DIRSIG 4 and DIRSIG 3 relative to MODTRAN. The RMS errors for the points shown on the graph are listed below the graphs.

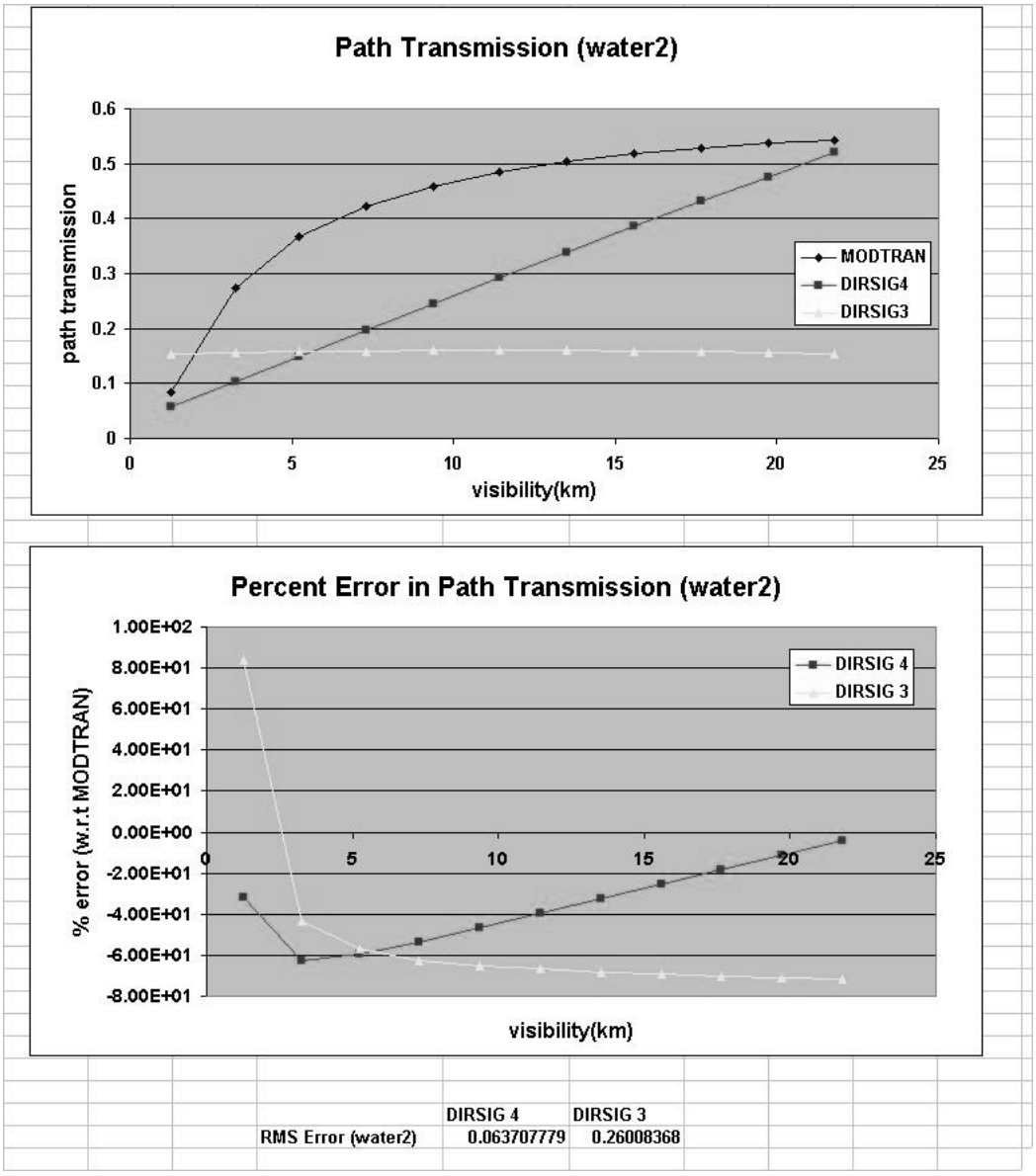

	DIRSIG 4	DIRSIG 3
RMS Error (water2)	0.063707779	0.26008368

Figure 4.70: Test Scene 4a (visibility variation): The upper graph shows the water2 path transmission obtained by MODTRAN, DIRSIG 4 and DIRSIG 3. The lower graph shows the percent error of DIRSIG 4 and DIRSIG 3 relative to MODTRAN. The RMS errors for the points shown on the graph are listed below the graphs.

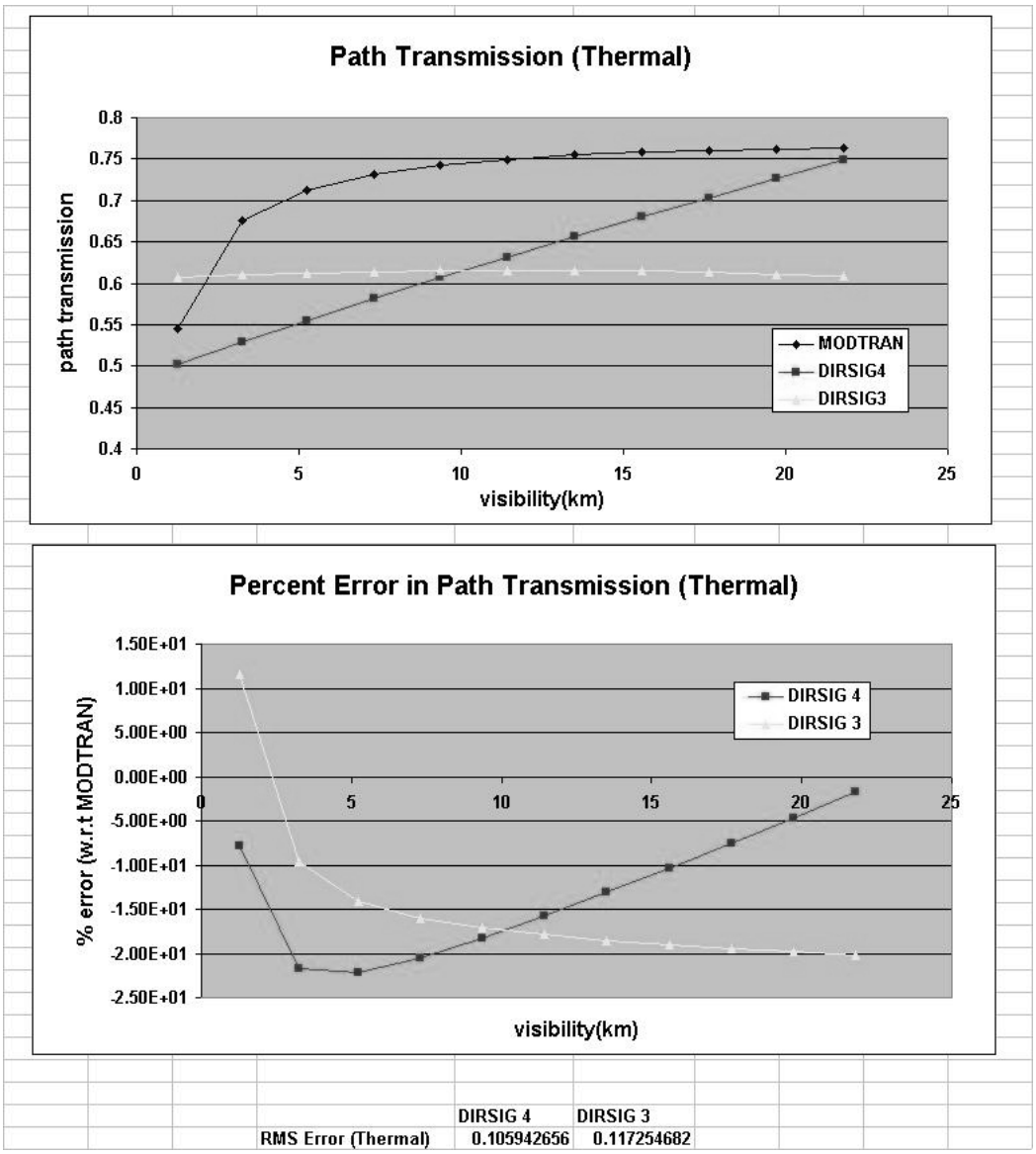

	DIRSIG 4	DIRSIG 3
RMS Error (Thermal)	0.105942656	0.117254682

Figure 4.71: Test Scene 4a (visibility variation): The upper graph shows the Thermal path transmission obtained by MODTRAN, DIRSIG 4 and DIRSIG 3. The lower graph shows the percent error of DIRSIG 4 and DIRSIG 3 relative to MODTRAN. The RMS errors for the points shown on the graph are listed below the graphs.

Grid Results

Like the other test images, this image was sampled at a nearly regular grid of points. A visual representation of the points sampled is similar to those seem in figure 4.24

The RMS error (by band) is shown in figure 4.72 for the path radiance and in figure 4.73 for the transmission.

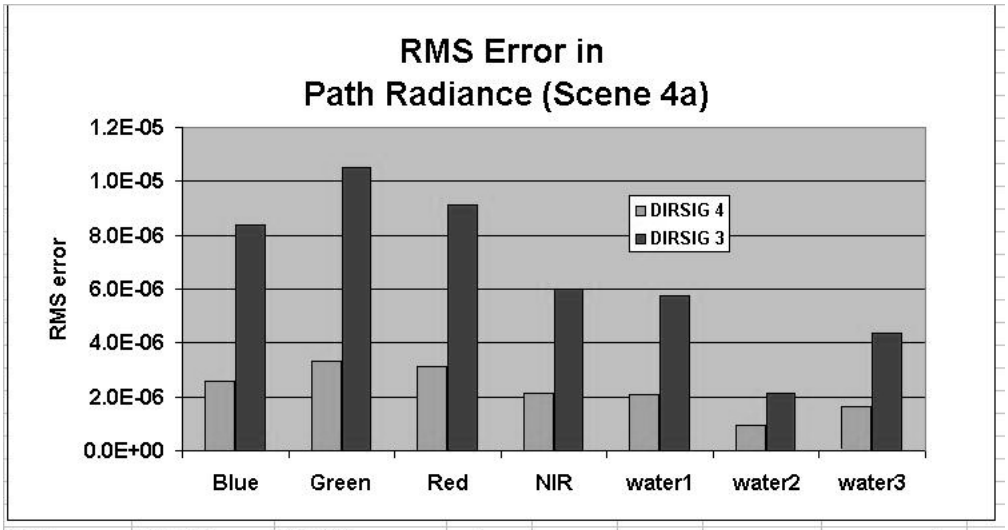

band	DIRSIG 4	DIRSIG 3
Blue	2.573181E-06	8.367654E-06
Green	3.333684E-06	1.050941E-05
Red	3.129291E-06	9.131512E-06
NIR	2.129757E-06	5.984098E-06
water1	2.058766E-06	5.737088E-06
water2	9.241937E-07	2.140534E-06
water3	1.649444E-06	4.374523E-06
Thermal	2.421366E-05	3.121015E-05

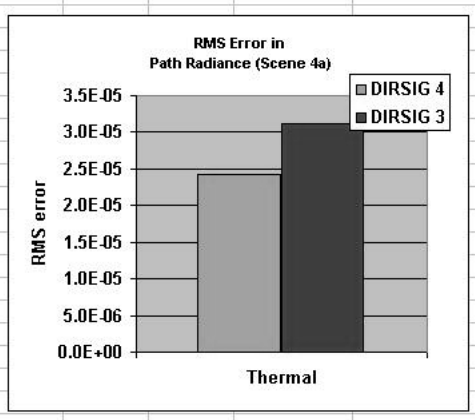

Figure 4.72: This shows the RMS error in path radiance (by band) over image 4a.

The errors associated with DIRSIG 4 in this test image (4a) are significant. This is due to the fact that the interpolation is being done over a very large visibility range. The path radiance and transmission of the atmosphere is vastly different at 1 km and 23 km visibility. More importantly, it varies in a very non-linear fashion. This contributes to a very large error, especially in the middle part of the image, where the sample point is farthest from the visibility interpolation points. This large error can be seen in any of the graphs in figures 4.60 through 4.71, with errors ranging up to approximately 90% in radiance and 62% in transmission. These errors are not of major concern for two reasons. The first is that these visibility ranges are not normally encountered in remote sensing. Secondly, even if they are, the user can reduce this error by either decreasing the overall range of the atmospheric database, or by increasing the number of point sampled in the visibility dimension.

To show this, a visibility value of 10 km was added to the database used to generate this test image. To show an example of how this error can be reduced, the same analysis was performed on this test case with an augmented atmospheric database. Figures 4.74 through 4.79 show the radiance results of this test.

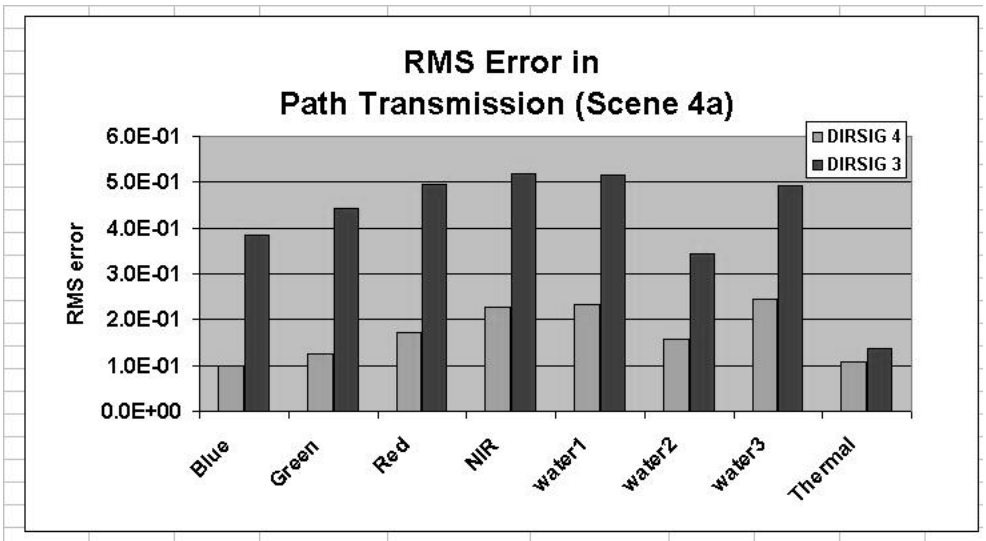

band	DIRSIG 4	DIRSIG 3
Blue	9.882552E-02	3.844451E-01
Green	1.253754E-01	4.431449E-01
Red	1.718385E-01	4.958410E-01
NIR	2.274717E-01	5.171230E-01
water1	2.328728E-01	5.148695E-01
water2	1.575418E-01	3.428576E-01
water3	2.452037E-01	4.932932E-01
Thermal	1.064599E-01	1.379924E-01

Figure 4.73: This shows the RMS error in path transmission (by band) over image 4a.

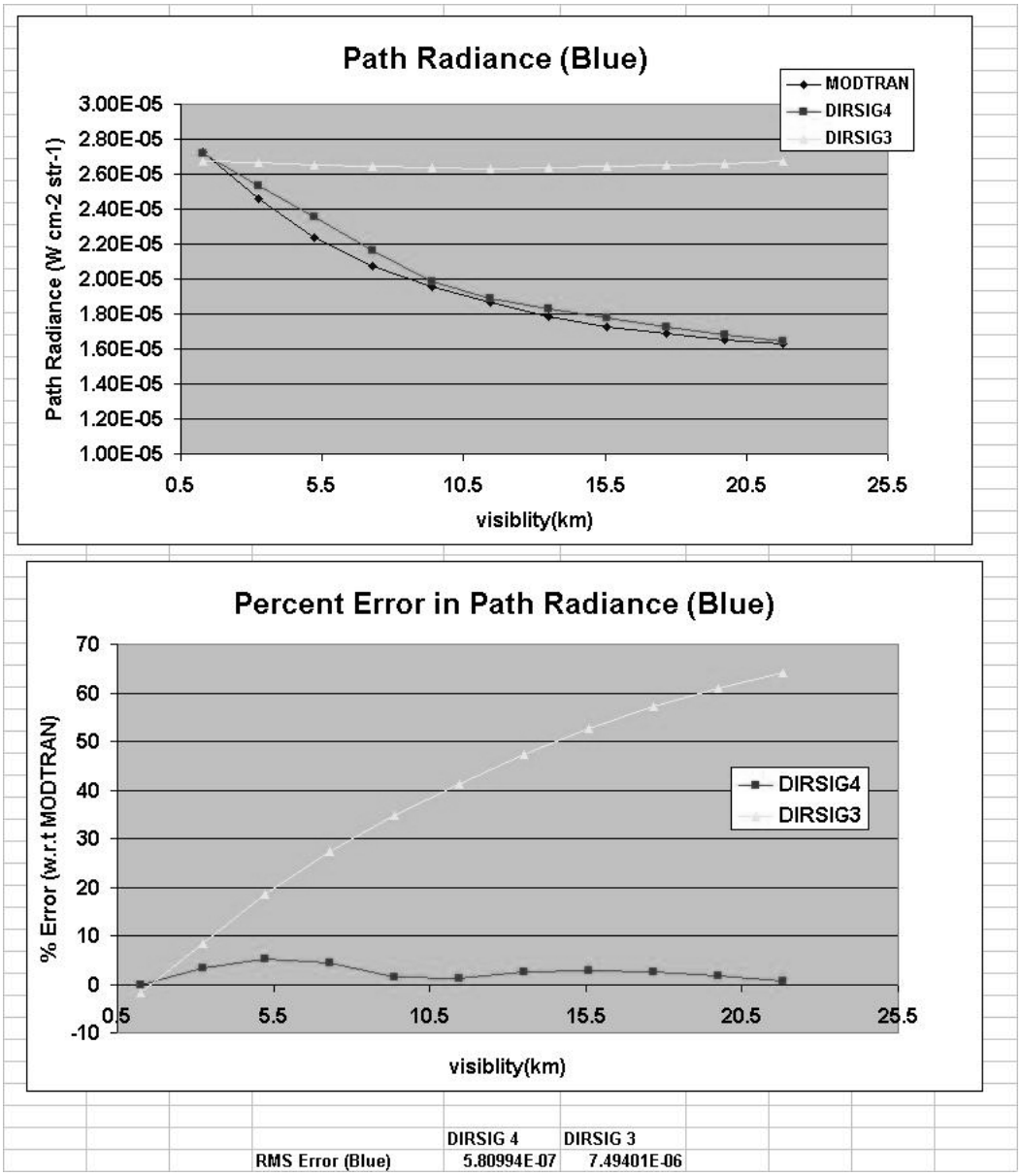

Figure 4.74: Test Scene 4aa (visibility variation): The upper graph shows the blue path radiance obtained by MODTRAN, DIRSIG 4 and DIRSIG 3. The lower graph shows the percent error of DIRSIG 4 and DIRSIG 3 relative to MODTRAN. The RMS errors for the points shown on the graph are listed below the graphs.

It should be noted that in figure 4.78 that graph does not show a trend consistent with the other graphs. This is because test scene 4aa was accidentally run with a different definition of the water2 band. That is why the endpoint errors do not match up with those seen in figure B.102. The other bands should be unaffected by this.

Figures 4.80 through 4.85 show the transmission results.

Notice how adding this interpolation point forces the interpolated value to equal MODTRAN at that point. This demonstrates that with a reasonable visibility range, and wise selection of interpolation endpoints, large errors can be avoided.

Also, the results in figure 4.84 are invalid because of the same reasons given for the radiance results; test scene 4aa was run with a different definition of the water2 band.

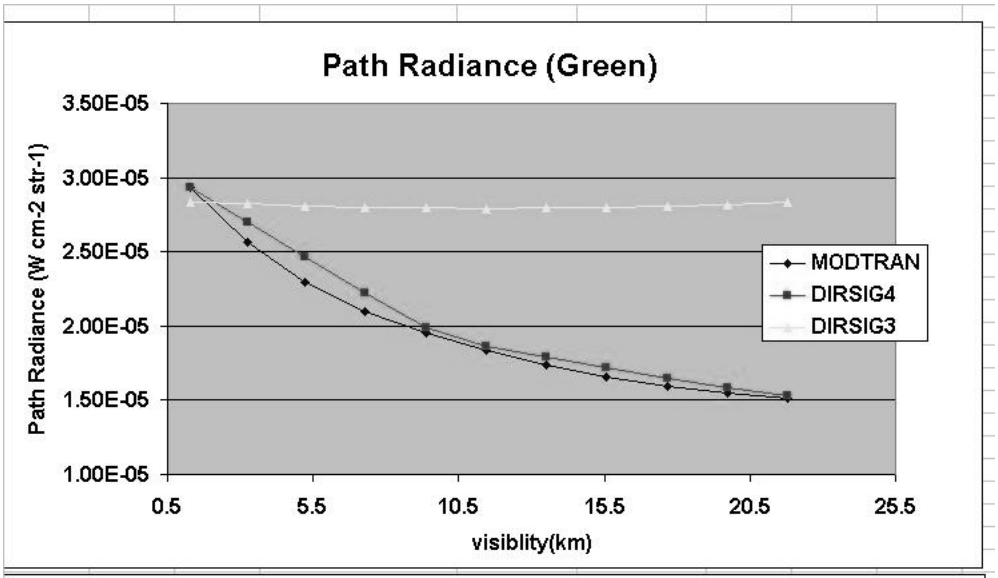

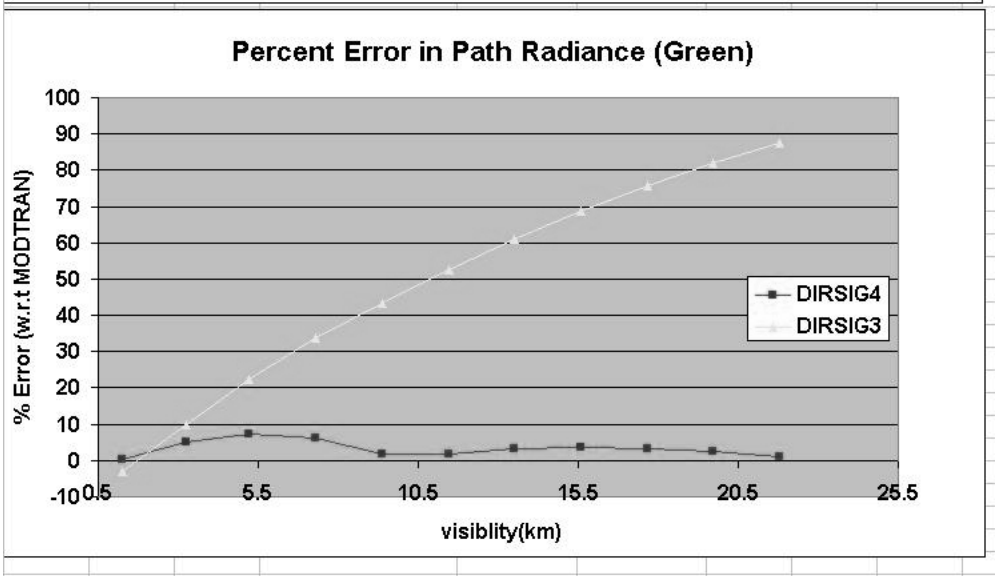

	DIRSIG 4	DIRSIG 3
RMS Error (Green)	8.18917E-07	9.40376E-06

Figure 4.75: Test Scene 4aa (visibility variation): The upper graph shows the green path radiance obtained by MODTRAN, DIRSIG 4 and DIRSIG 3. The lower graph shows the percent error of DIRSIG 4 and DIRSIG 3 relative to MODTRAN. The RMS errors for the points shown on the graph are listed below the graphs.

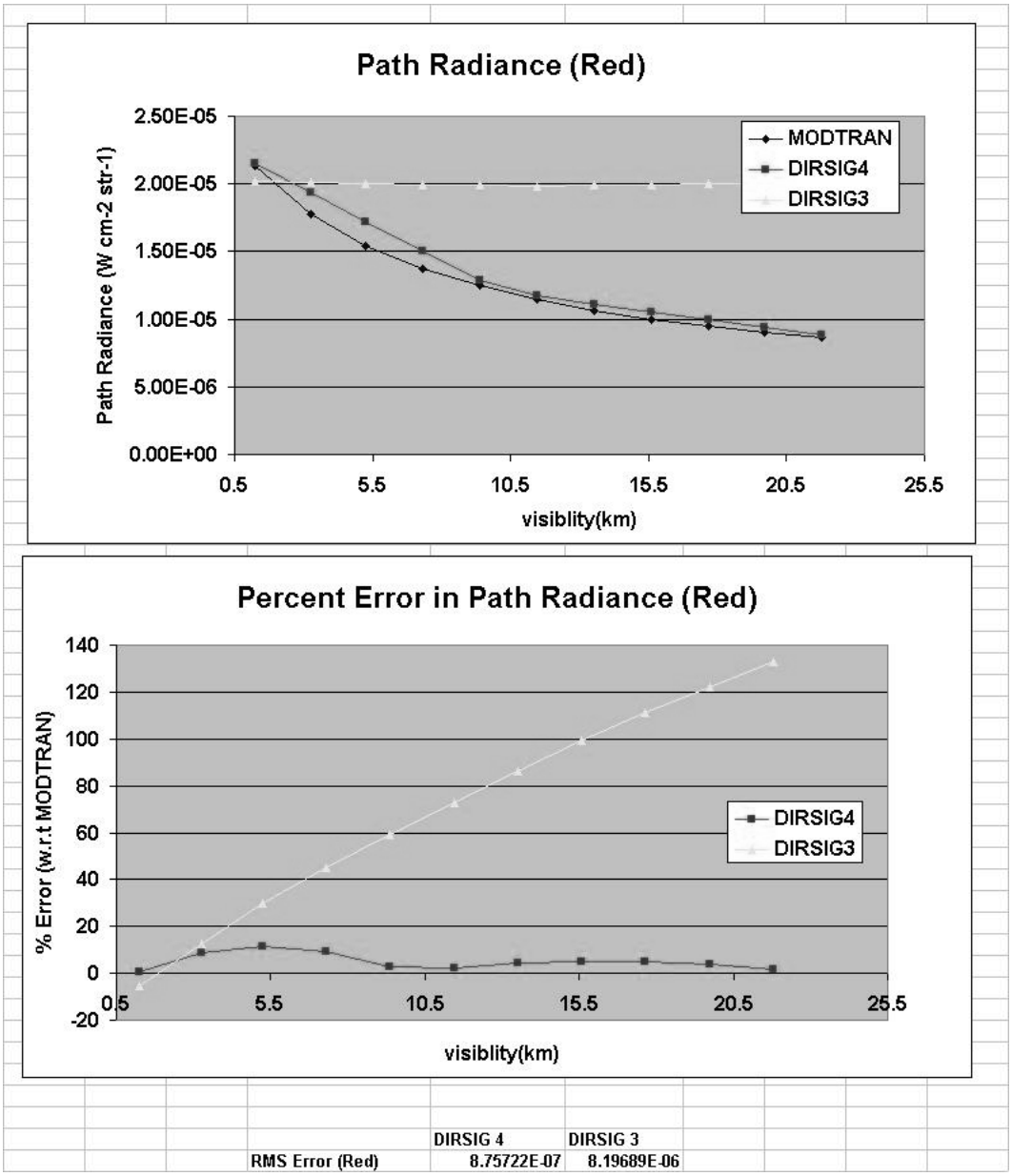

Figure 4.76: Test Scene 4aa (visibility variation): The upper graph shows the red path radiance obtained by MODTRAN, DIRSIG 4 and DIRSIG 3. The lower graph shows the percent error of DIRSIG 4 and DIRSIG 3 relative to MODTRAN. The RMS errors for the points shown on the graph are listed below the graphs.

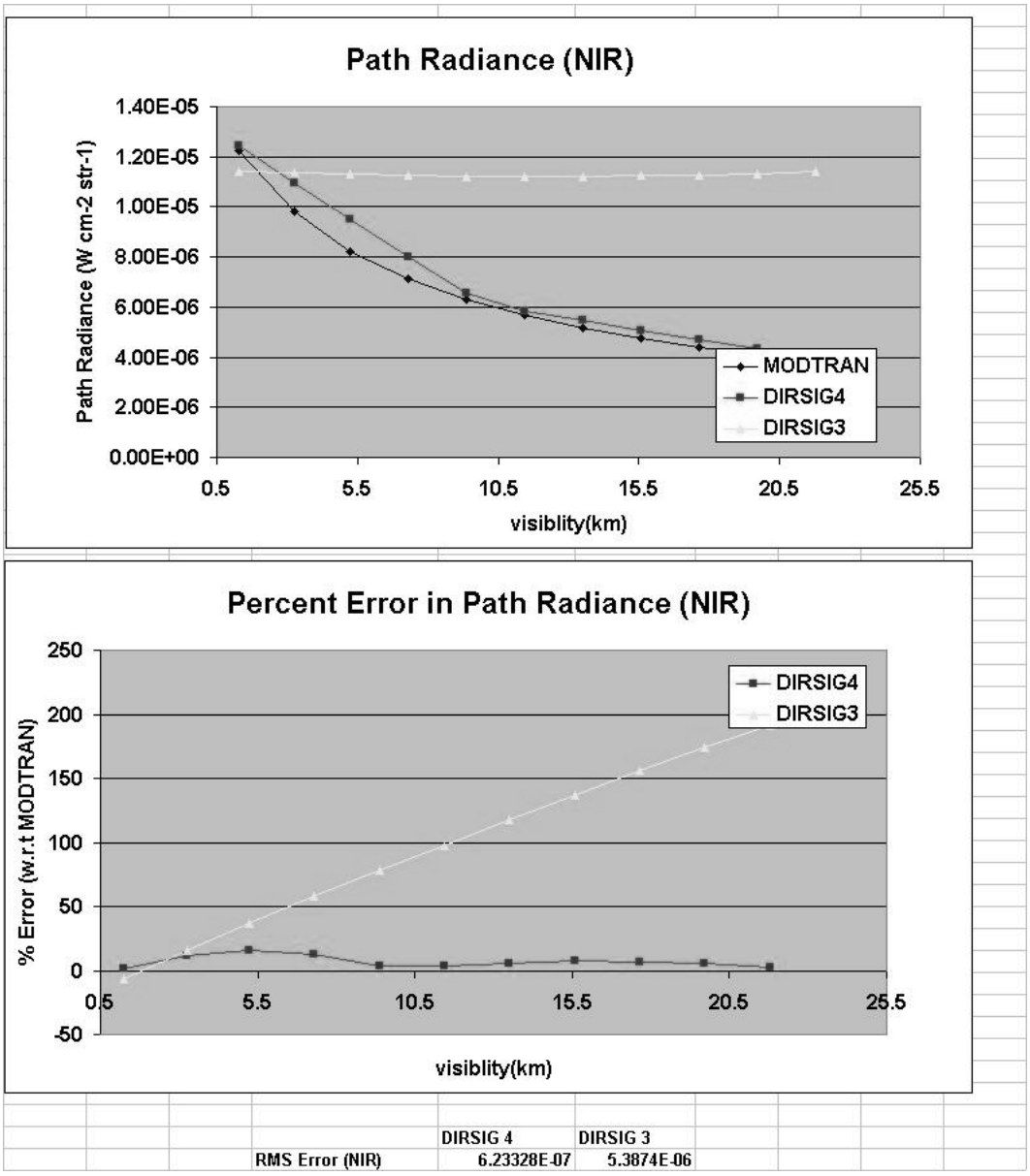

Figure 4.77: Test Scene 4aa (visibility variation): The upper graph shows the NIR path radiance obtained by MODTRAN, DIRSIG 4 and DIRSIG 3. The lower graph shows the percent error of DIRSIG 4 and DIRSIG 3 relative to MODTRAN. The RMS errors for the points shown on the graph are listed below the graphs.

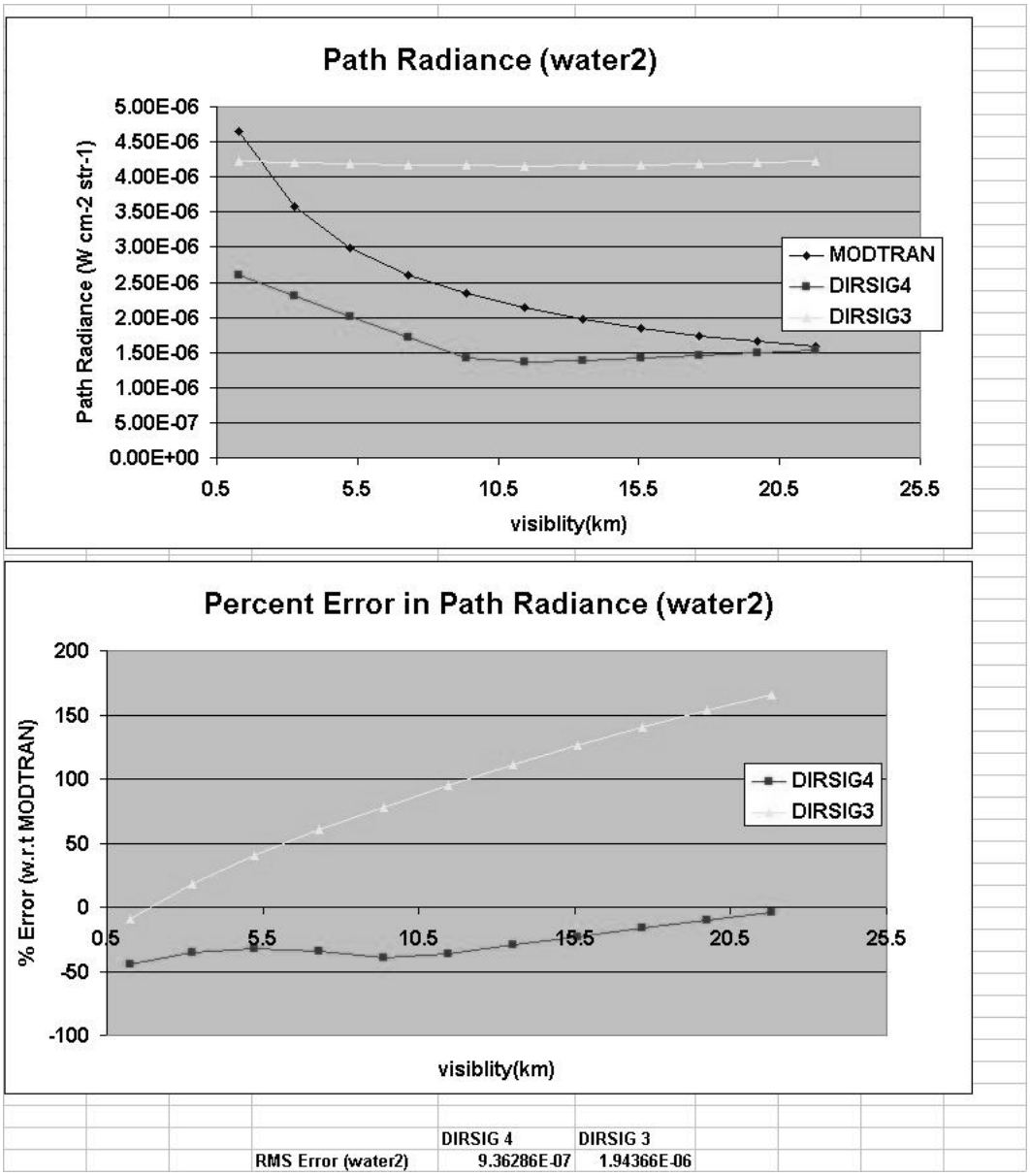

Figure 4.78: Test Scene 4aa (visibility variation): The upper graph shows the water2 path radiance obtained by MODTRAN, DIRSIG 4 and DIRSIG 3. The lower graph shows the percent error of DIRSIG 4 and DIRSIG 3 relative to MODTRAN. The RMS errors for the points shown on the graph are listed below the graphs.

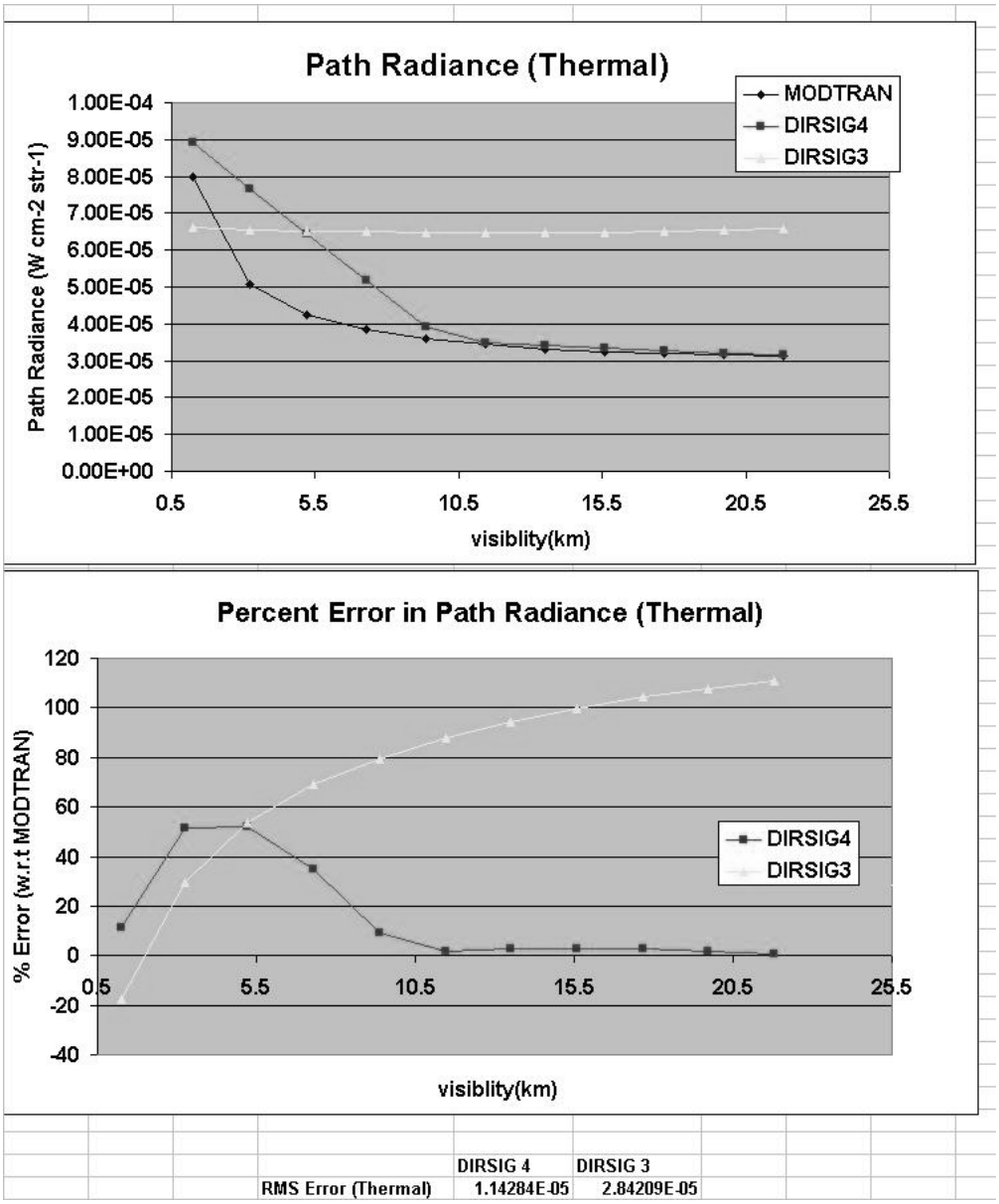

Figure 4.79: Test Scene 4aa (visibility variation): The upper graph shows the Thermal path radiance obtained by MODTRAN, DIRSIG 4 and DIRSIG 3. The lower graph shows the percent error of DIRSIG 4 and DIRSIG 3 relative to MODTRAN. The RMS errors for the points shown on the graph are listed below the graphs.

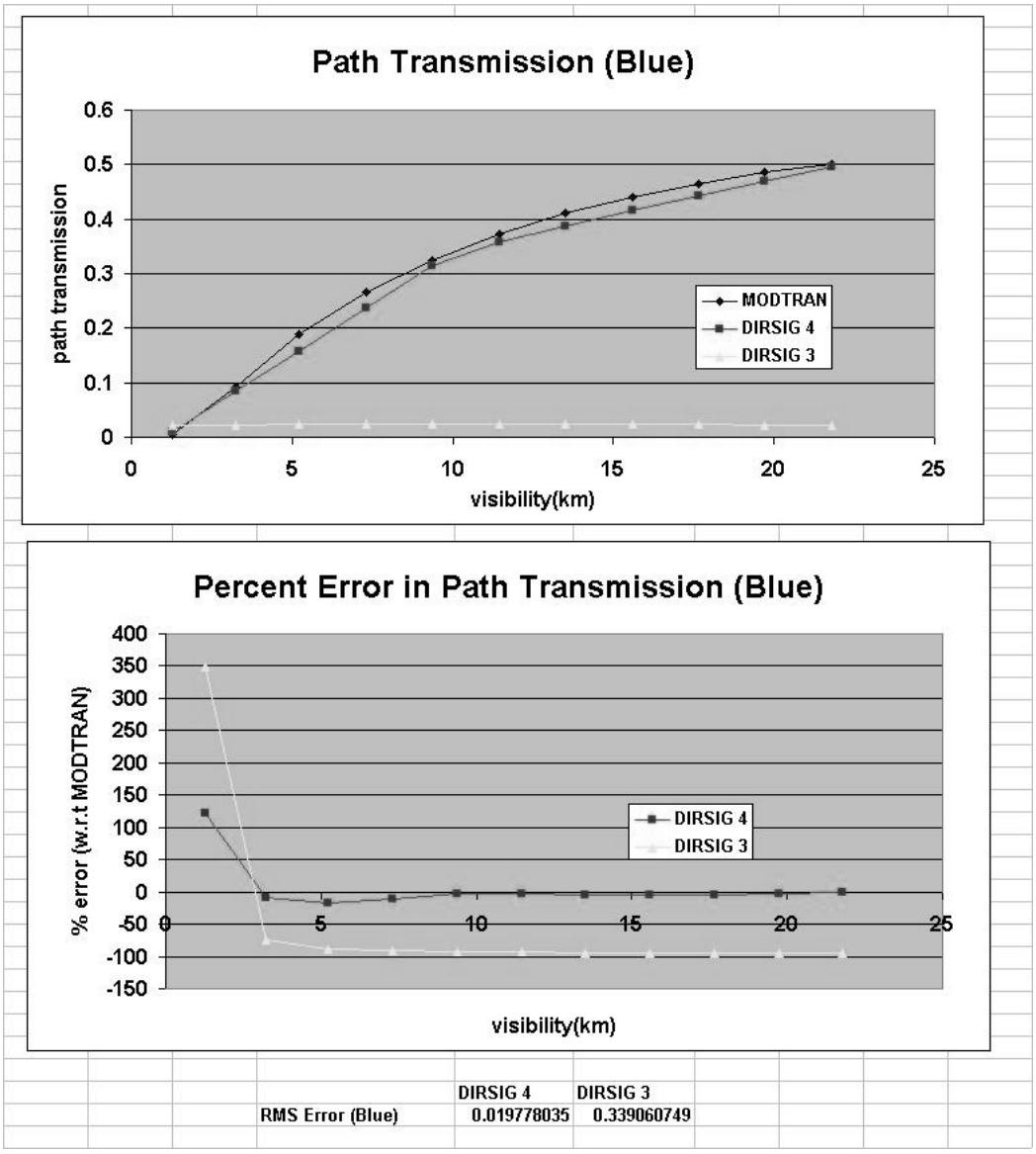

Figure 4.80: Test Scene 4aa (visibility variation): The upper graph shows the blue path transmission obtained by MODTRAN, DIRSIG 4 and DIRSIG 3. The lower graph shows the percent error of DIRSIG 4 and DIRSIG 3 relative to MODTRAN. The RMS errors for the points shown on the graph are listed below the graphs.

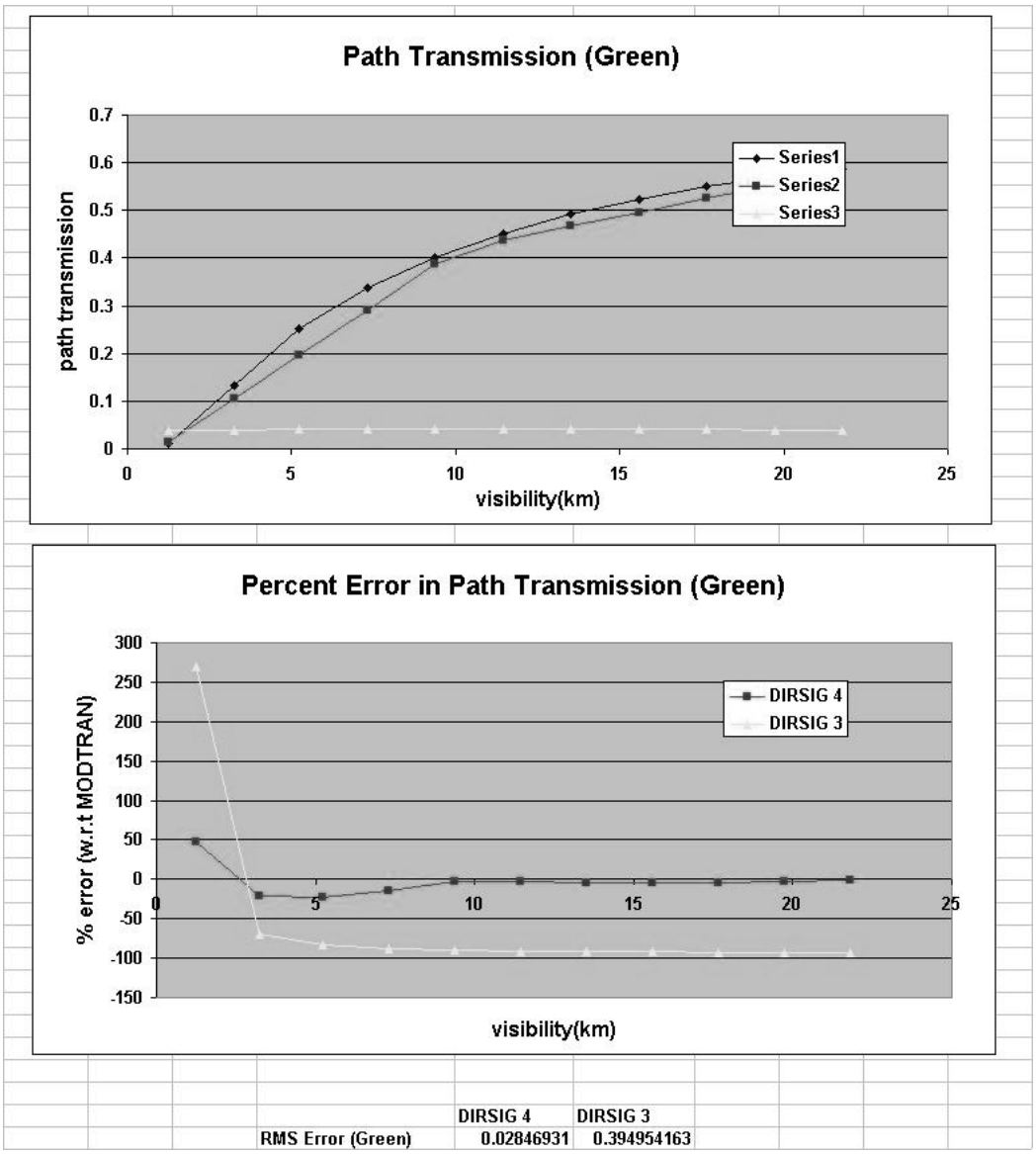

Figure 4.81: Test Scene 4aa (visibility variation): The upper graph shows the green path transmission obtained by MODTRAN, DIRSIG 4 and DIRSIG 3. The lower graph shows the percent error of DIRSIG 4 and DIRSIG 3 relative to MODTRAN. The RMS errors for the points shown on the graph are listed below the graphs.

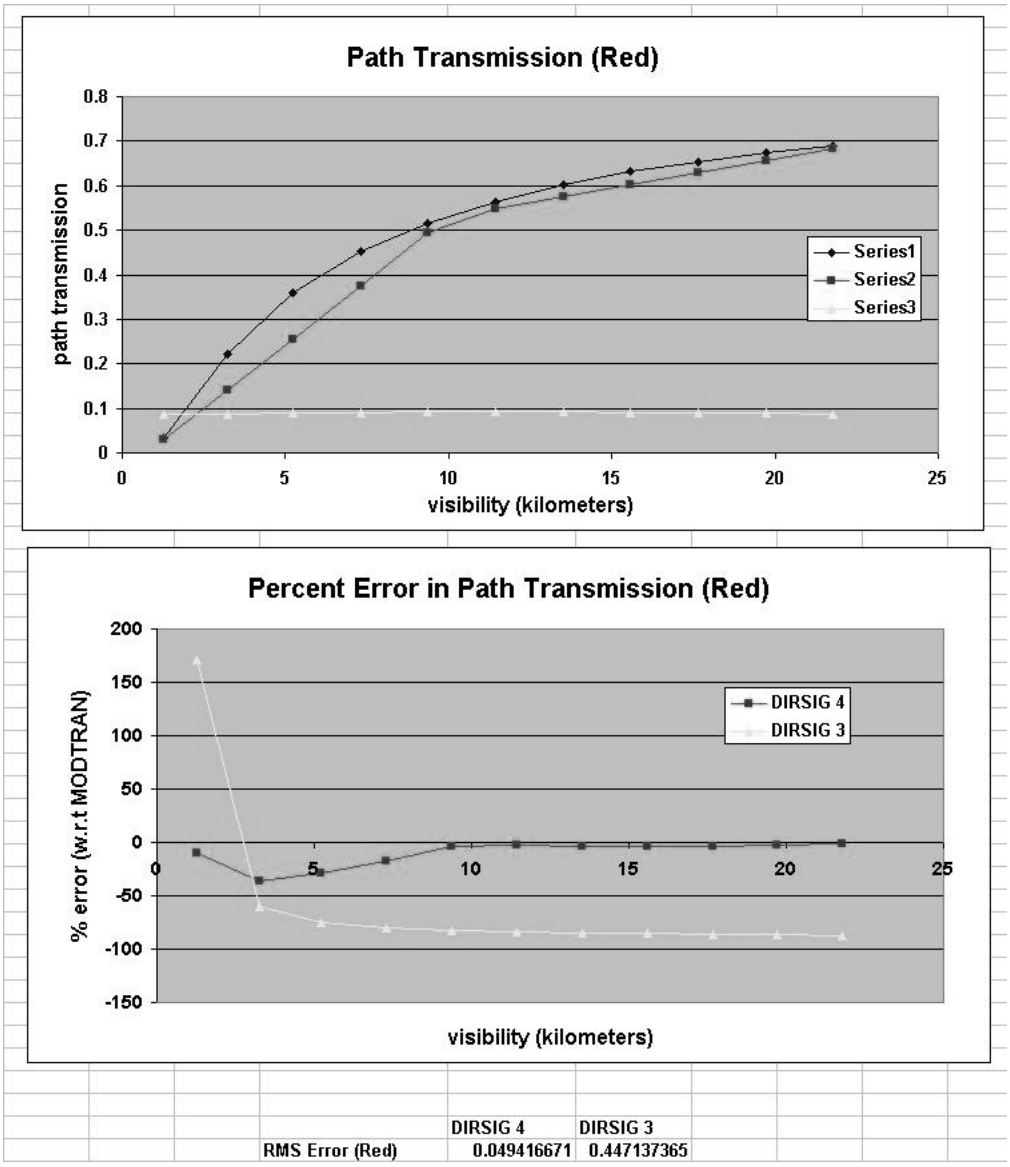

	DIRSIG 4	DIRSIG 3
RMS Error (Red)	0.049416671	0.447137365

Figure 4.82: Test Scene 4aa (visibility variation): The upper graph shows the red path transmission obtained by MODTRAN, DIRSIG 4 and DIRSIG 3. The lower graph shows the percent error of DIRSIG 4 and DIRSIG 3 relative to MODTRAN. The RMS errors for the points shown on the graph are listed below the graphs.

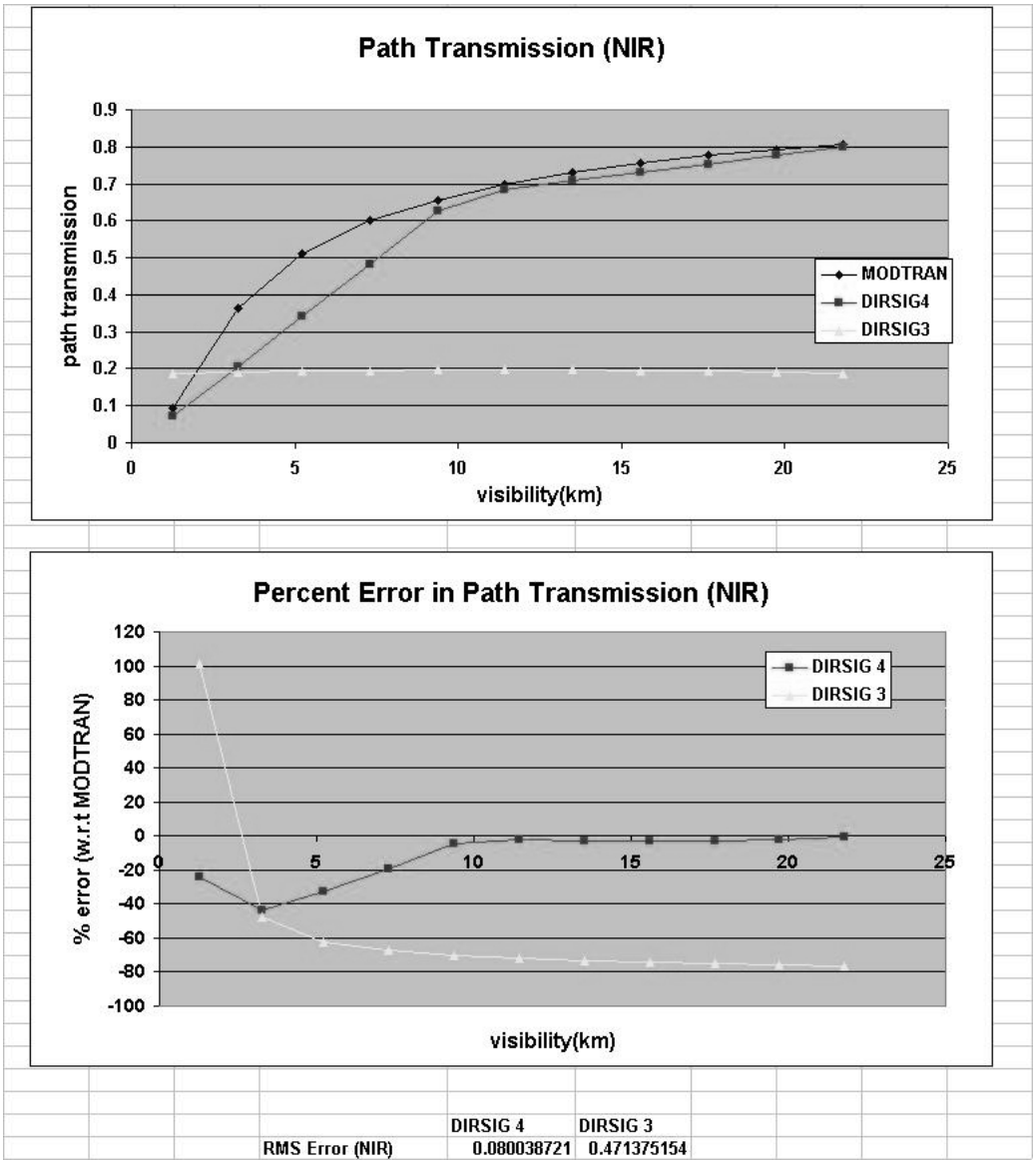

	DIRSIG 4	DIRSIG 3
RMS Error (NIR)	0.080038721	0.471375154

Figure 4.83: Test Scene 4aa (visibility variation): The upper graph shows the NIR path transmission obtained by MODTRAN, DIRSIG 4 and DIRSIG 3. The lower graph shows the percent error of DIRSIG 4 and DIRSIG 3 relative to MODTRAN. The RMS errors for the points shown on the graph are listed below the graphs.

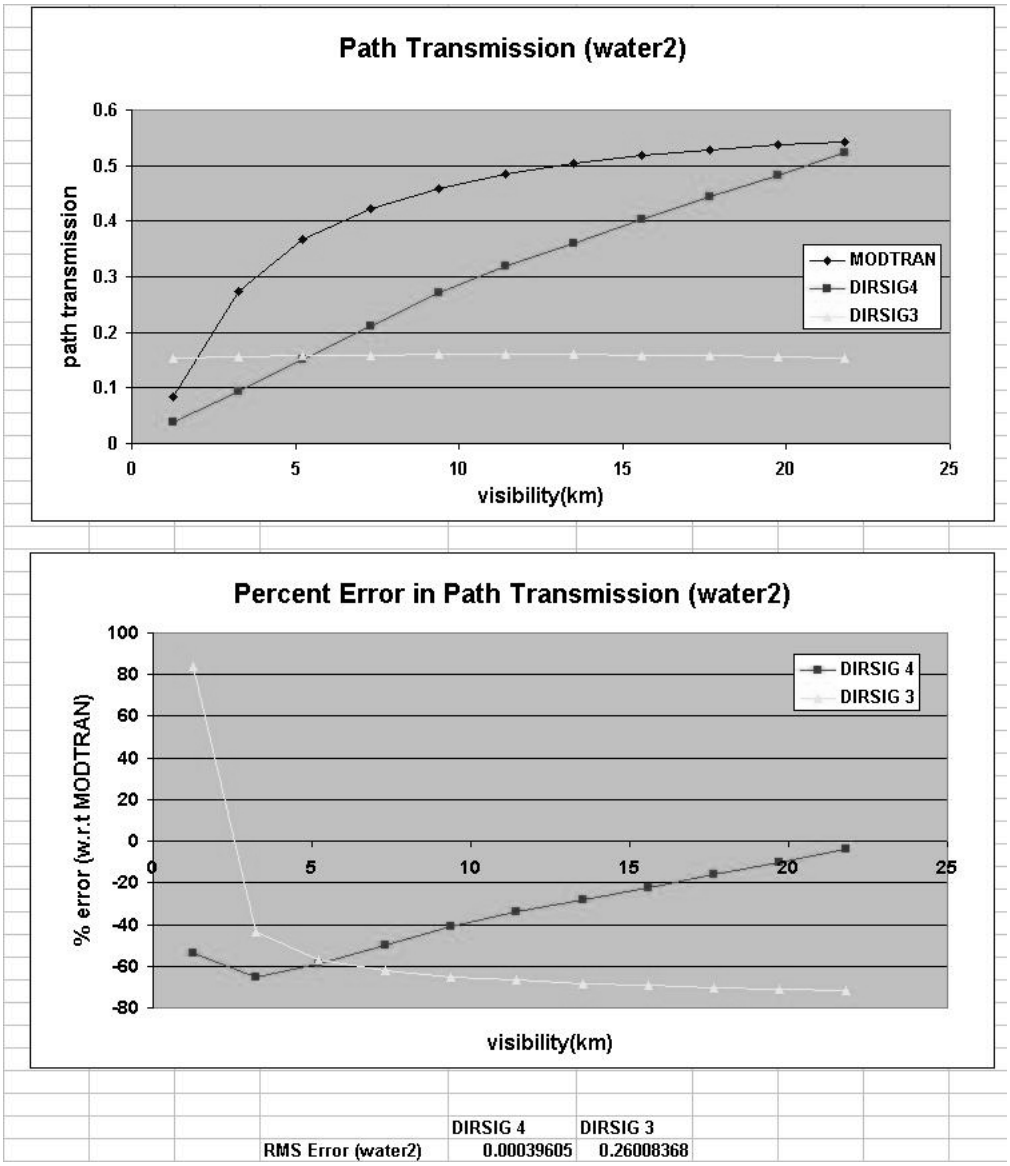

	DIRSIG 4	DIRSIG 3
RMS Error (water2)	0.00039605	0.26008368

Figure 4.84: Test Scene 4aa (visibility variation): The upper graph shows the water2 path transmission obtained by MODTRAN, DIRSIG 4 and DIRSIG 3. The lower graph shows the percent error of DIRSIG 4 and DIRSIG 3 relative to MODTRAN. The RMS errors for the points shown on the graph are listed below the graphs.

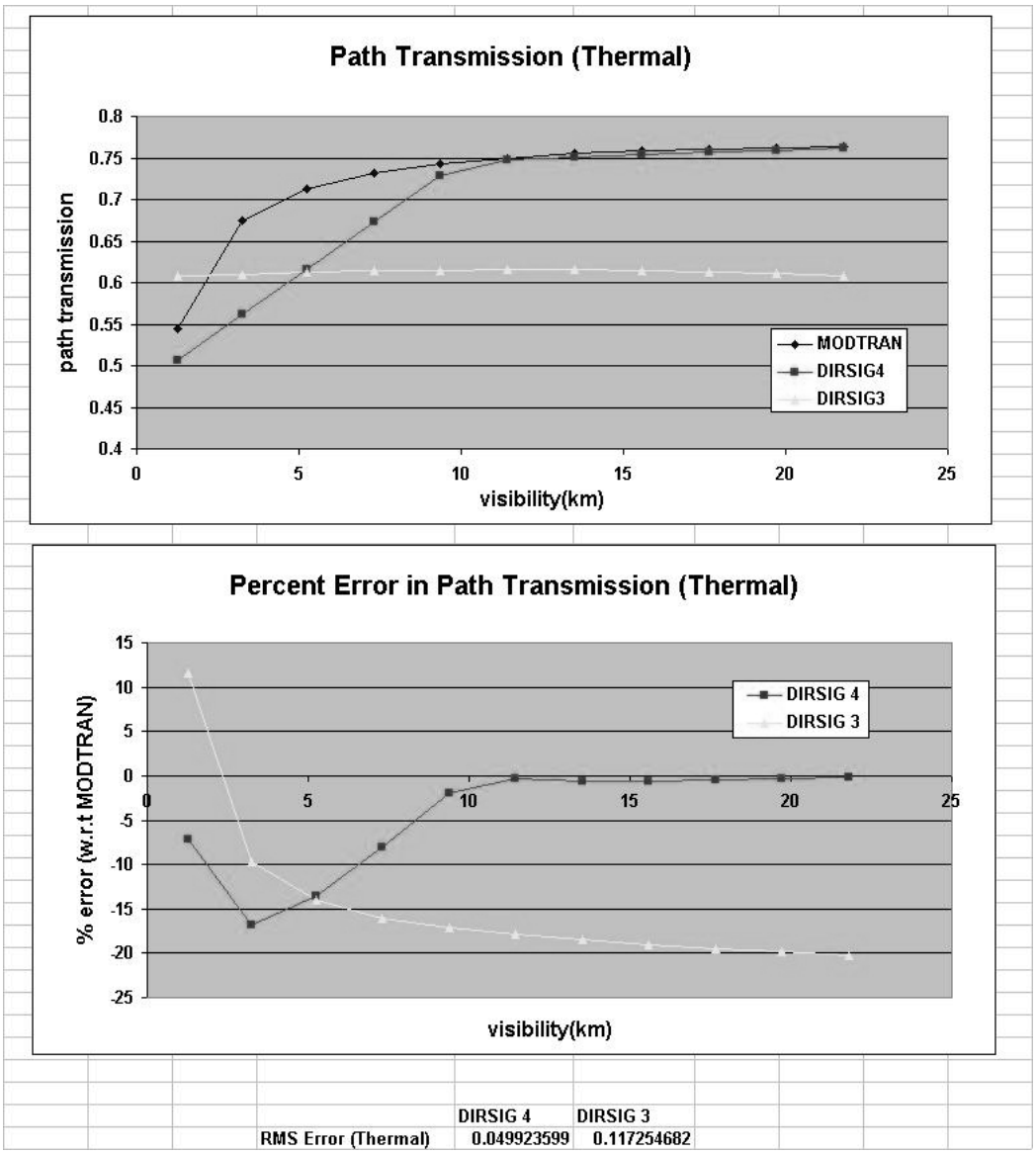

	DIRSIG 4	DIRSIG 3
RMS Error (Thermal)	0.049923599	0.117254682

Figure 4.85: Test Scene 4aa (visibility variation): The upper graph shows the thermal path transmission obtained by MODTRAN, DIRSIG 4 and DIRSIG 3. The lower graph shows the percent error of DIRSIG 4 and DIRSIG 3 relative to MODTRAN. The RMS errors for the points shown on the graph are listed below the graphs.

Grid Results

The graphs 4.86 and 4.87 show the results of the different DIRSIG interpolation methods sampled at nearly regularly spaced intervals.

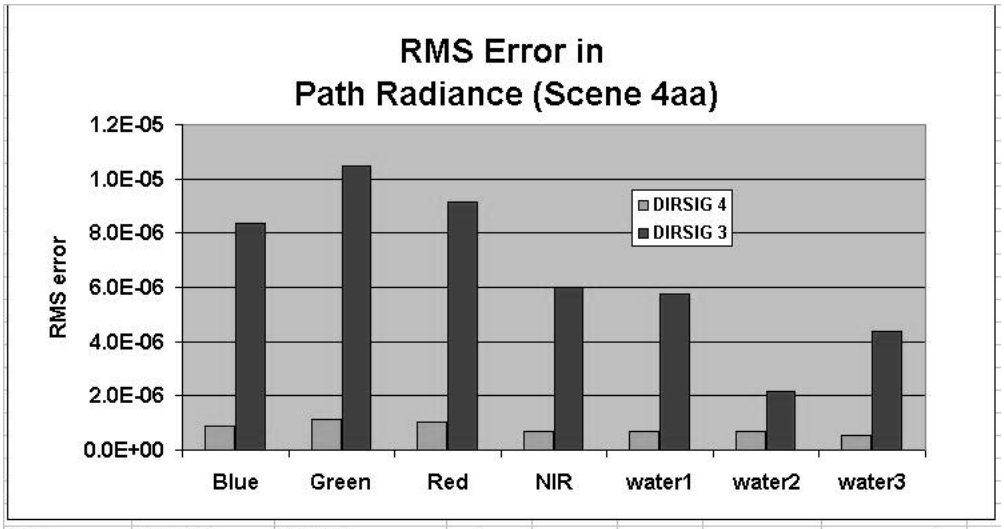

band	DIRSIG 4	DIRSIG 3
Blue	8.829934E-07	8.359439E-06
Green	1.145212E-06	1.049786E-05
Red	1.056921E-06	9.123456E-06
NIR	6.911319E-07	5.980925E-06
water1	6.663041E-07	5.734402E-06
water2	6.851573E-07	2.140436E-06
water3	5.368392E-07	4.373651E-06
Thermal	1.074712E-05	3.121319E-05

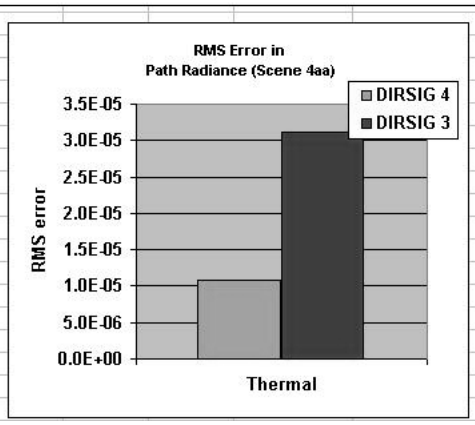

Figure 4.86: This shows the RMS error in path radiance (by band) over image 4aa.

Note that the error associated with this test image is significantly lower than that of test image 4a. This shows that the user can increase the accuracy of the interpolator by increasing the number and/or locations of the points sampled in the ADB where needed.

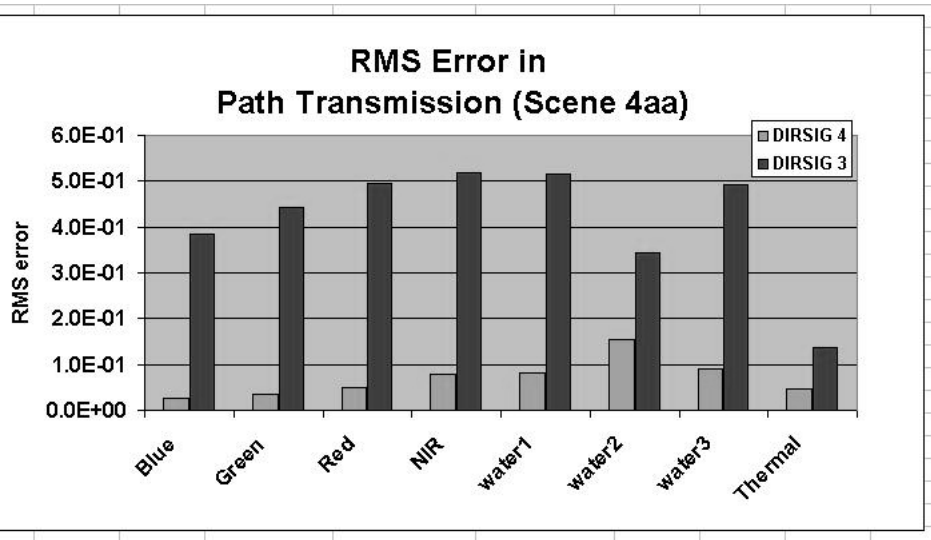

band	DIRSIG 4	DIRSIG 3
Blue	2.746619E-02	3.838289E-01
Green	3.351818E-02	4.427153E-01
Red	5.090722E-02	4.957398E-01
NIR	7.916105E-02	5.173229E-01
water1	8.240336E-02	5.150969E-01
water2	1.544682E-01	3.425919E-01
water3	9.138730E-02	4.935759E-01
Thermal	4.701382E-02	1.380275E-01

Figure 4.87: This shows the RMS error in path transmission (by band) over image 4aa.

4.3 Test Image Error Summary

The graphs seen in figures 4.88 and 4.89 show the average RMS error for each band, for each of the test cases. In the cases where images were run under different solar conditions (sunrise, noon, and sunset), the values were averaged together.

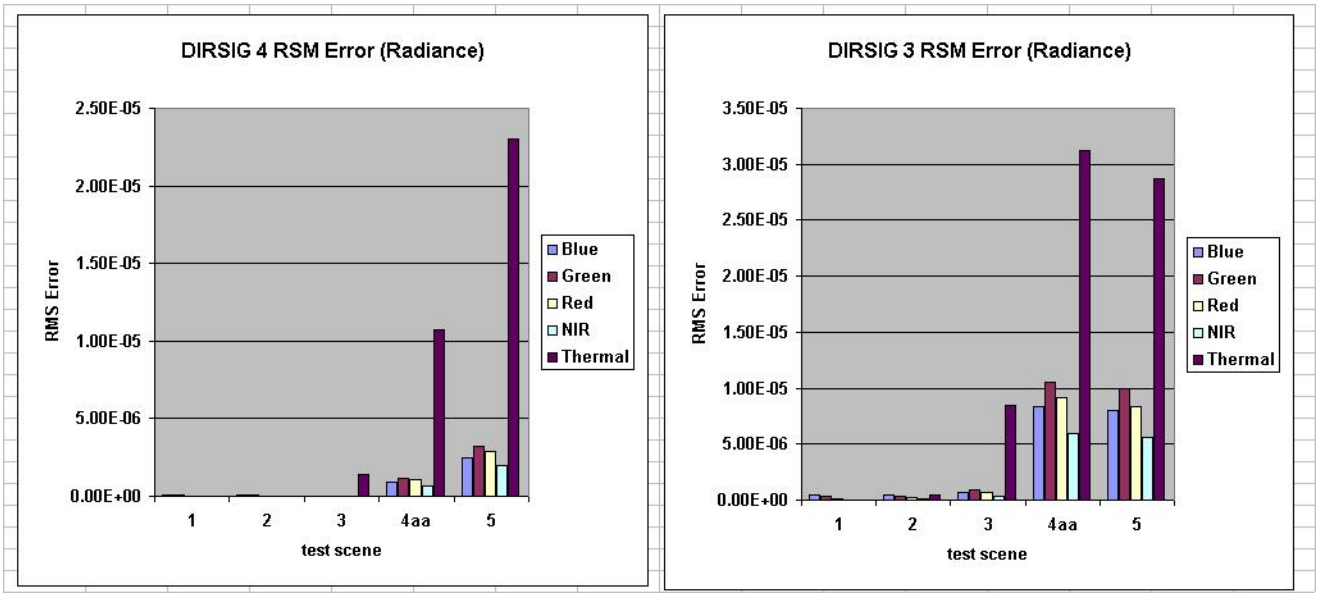

Figure 4.88: This shows the RMS errors associated with radiance for each band, for each test image.

To get a better idea of the trend, the information was graphed so that the values associated with test cases 1 and 2 are easier to see. These graphs (in figures 4.90 and 4.91) show the exact same data as those in figures 4.88 and 4.89.

As well, to show the relative increase in accuracy of DIRSIG 4 with respect to DIRSIG 3, a simple ratio of these values (DIRSIG 3's RMS error divided by DIRSIG 4's RMS error) was taken, and are graphed in figures 4.92 and 4.93. These graphs can be thought of as a relative performance metric. The higher the value, the worse DIRSIG 3 is performing with respect to DIRSIG 4.

As expected, we see a general trend of DIRSIG 3's error increasing at a greater rate than DIRSIG 4's as the number of dimensions interpolated over increases. Recall that test case 1 there was only interpolation in the zenith and azimuth dimension, while in test case 2, interpolation over altitudes was added. Continuing this trend, water vapor interpolation was added in test case 3, visibility interpolation in test case 4, and both water vapor and visibility in test case 5[1]

However, there is a drop off in this ratio after test case 3. This is most likely due to the visibility interpolation issue described in section 4.2.2. As well, it should be noted that the enhancement made to test case 4 (adding a visibility interpolation point) was not done for test case 5. With the addition of more visibility interpolation points, or if the total visibility range of the scene was smaller, the DIRSIG 4 results would greatly improve.

[1]Test case 5 is designed as a hybrid of test cases 3 and 4, and has one of the atmospheric maps rotated 90 degrees. A more complete description can be found in appendix B.

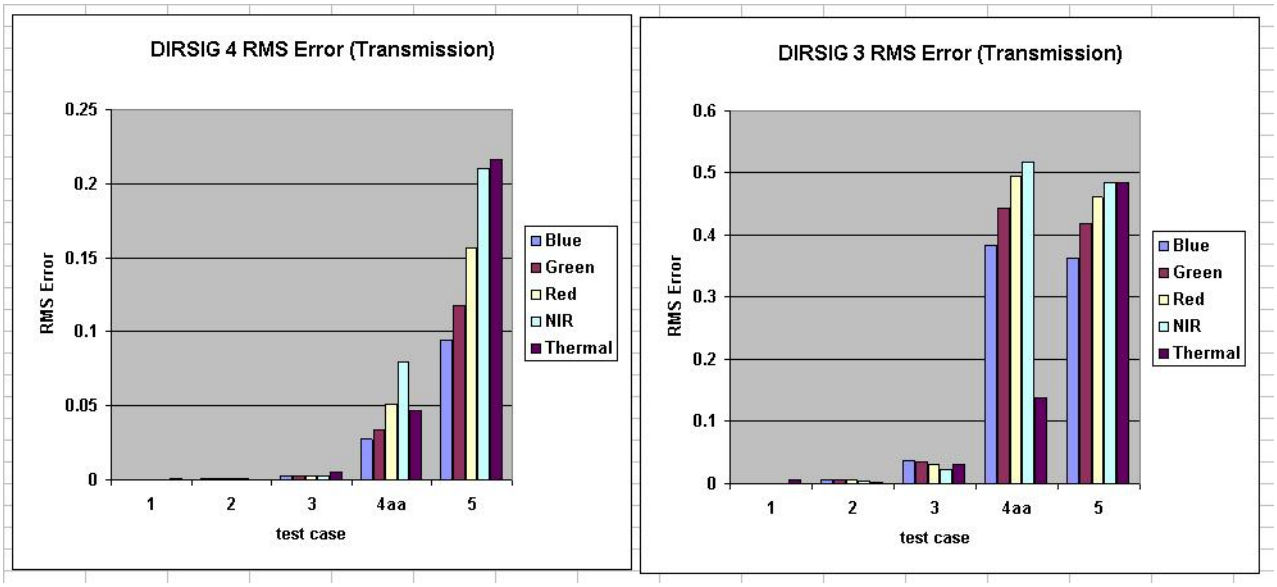

Figure 4.89: This shows the RMS errors associated with transmission for each band, for each test image.

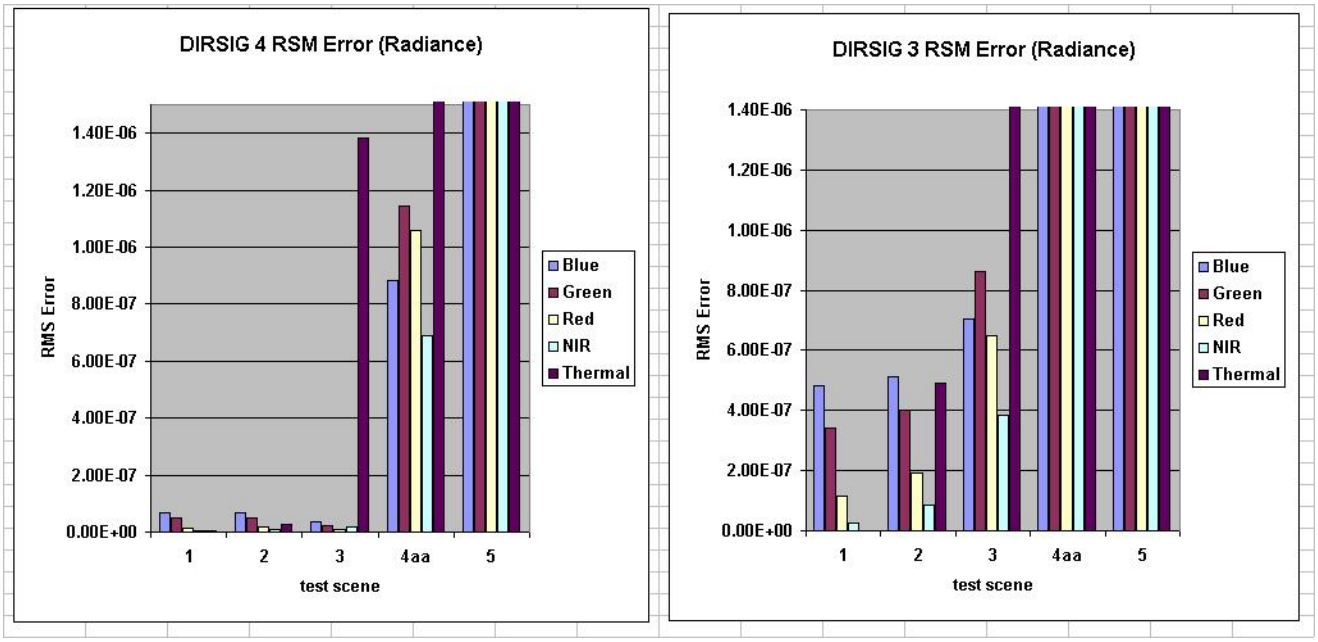

Figure 4.90: This shows the RMS errors associated with radiance for each band, for each test image. The y-axis has been scaled to better show the trend in the lower test cases.

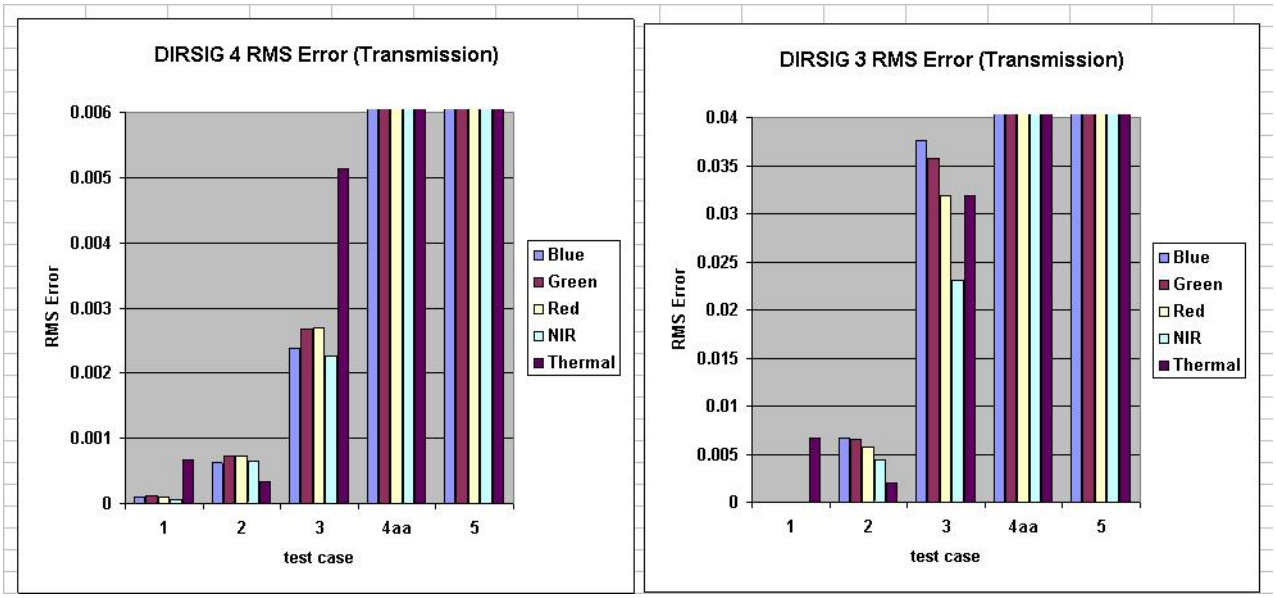

Figure 4.91: This shows the RMS errors associated with transmission for each band, for each test image. The y-axis has been scaled to better show the trend in the lower test cases.

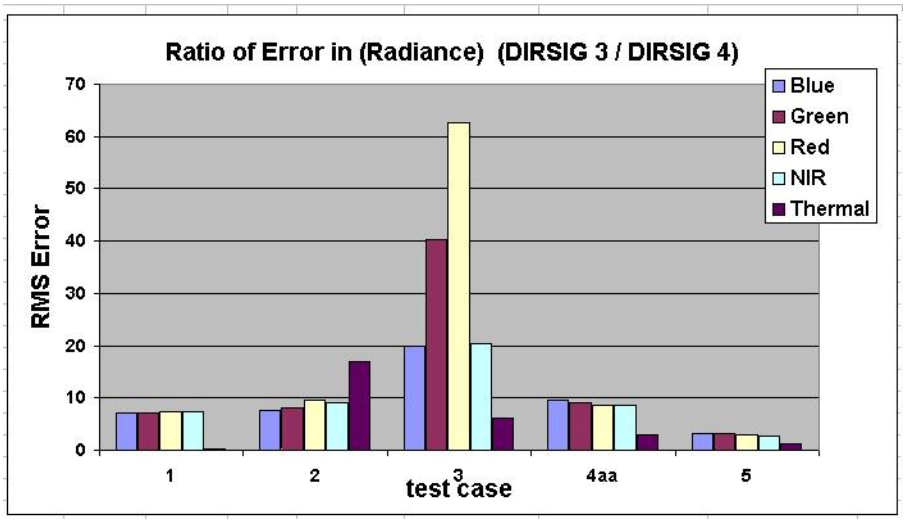

Figure 4.92: This shows the ratio of the radiance RMS errors in DIRSIG 3 to the RMS errors in DIRSIG 4.

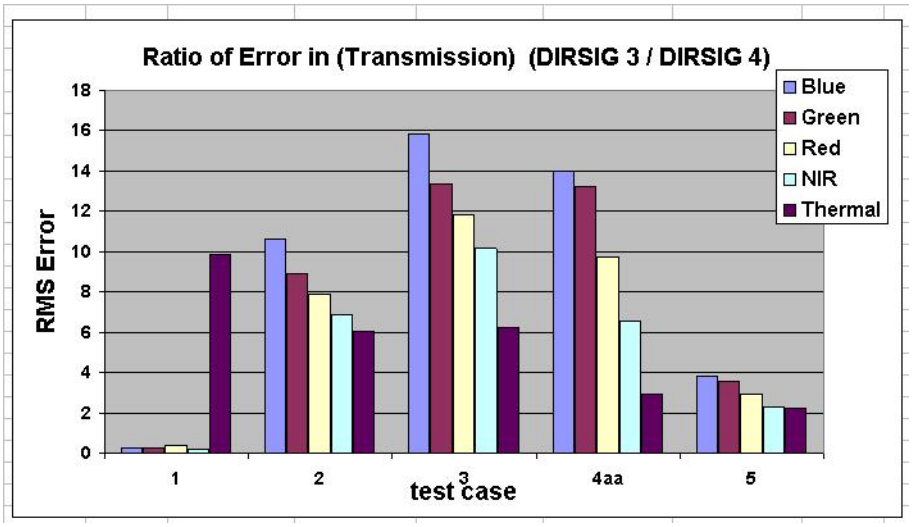

Figure 4.93: This shows the ratio of the transmission RMS errors in DIRSIG 3 to the RMS errors in DIRSIG 4.

4.4 Demonstration Images

This section is comprised of images which are intended for informal visual inspection. Therefore, these images will not be analyzed from a radiometric standpoint.

4.4.1 Megascene

The Megascene is an endeavor by RIT's remote sensing lab to accurately model a section of Rochester, NY within DIRSIG. An RGB radiance image of this scene run with no atmospheric changes can be seen in figure 4.94.

Figure 4.94: This shows the resulting RGB radiance of the Megascene. (ENVI Gaussian equalization was applied to the image.)

Water Vapor Over The Megascene

The Megascene facets were used along with a 'realistic' water vapor map to demonstrate how atmospheric inhomogeneities might look over a real scene. This water vapor map can be seen in figure 4.95, and was derived from a separate water vapor retrieval process.

The resulting radiance image, in RGB bands, is seen in figure 4.96.

In the visible spectrum, there does not seem to be any noticeable difference between the scene rendered with or without the water vapor. To compare the effect of water vapor, figure 4.97 and figure 4.98 show, respectively, the red band and the water2 (940 nm) band of the same image.

Notice that the water2 band is affected significantly by the presence of water vapor, even if this effect is not observed in the visible bands.

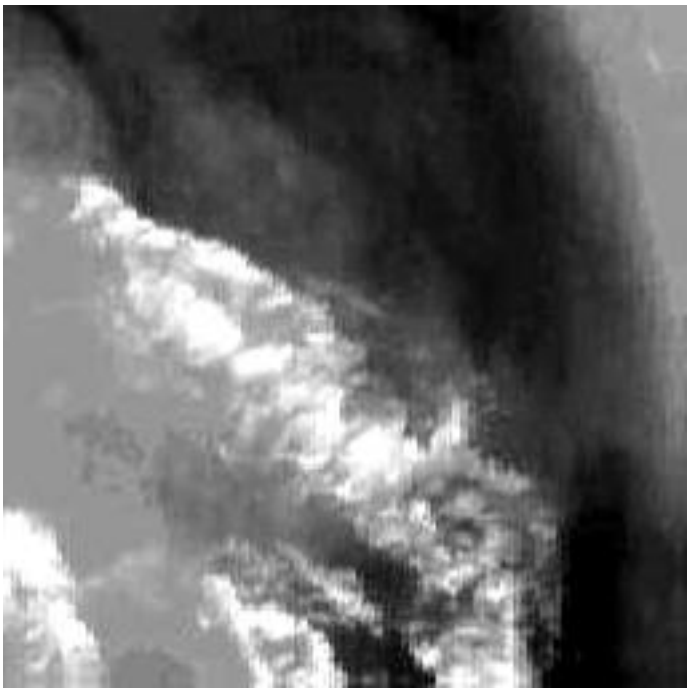

Figure 4.95: This shows the water vapor map used in the rendering of the Megascene.

Figure 4.96: This shows the RGB bands when DIRSIG 4 renders the Megascene with a 'realistic' water vapor map.

Figure 4.97: This shows the red band when DIRSIG 4 renders the Megascene with a 'realistic' water vapor map.

Figure 4.98: This shows the water2 (940 nm) band when DIRSIG 4 renders the Megascene with a 'realistic' water vapor map.

Figure 4.99 shows the result of an attempt to retrieve the water vapor from the Megascene using a band ratio method. The method involves taking the ratio of the average of bands water_line1 and water_line3 to water_line2. (See equation 4.3

$$relativeWaterVapor = \frac{average(water_line1, water_line3)}{water_line2} \tag{4.3}$$

This method yields the relative water vapor values and the resulting image's structure should resemble the structure seen in figure 4.95.

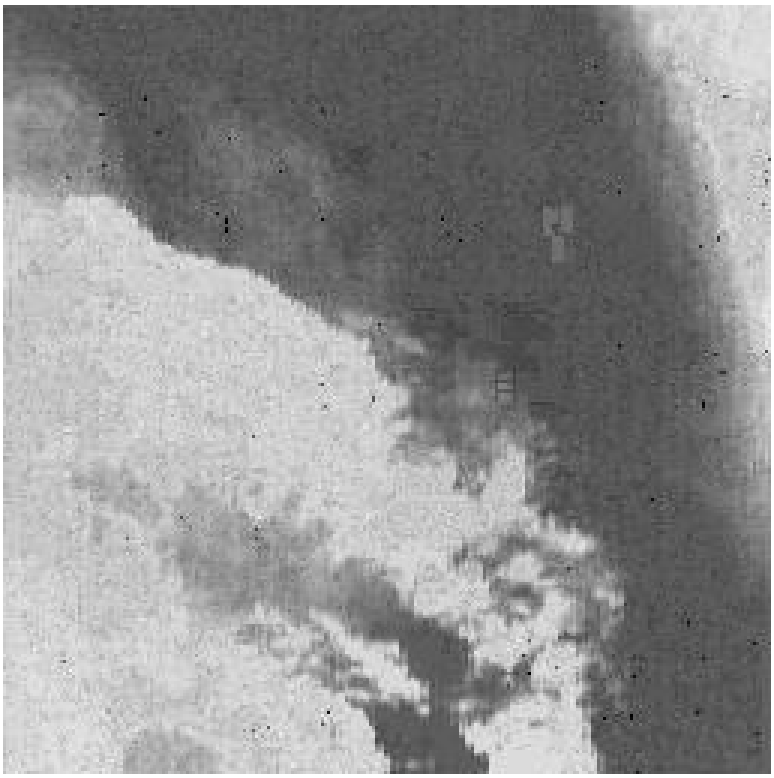

Figure 4.99: This shows the results of the water vapor retrieval method shown in equation 4.3.

Aerosols Over The Megascene

To show the effect of aerosols over the Megascene, a map (shown in figure 4.100) was inserted into the scene, with visibility values instead of water vapor. The visibility ranged between 0 and 23 km. The resulting RGB image as rendered by DIRSIG 4 is seen in figure 4.101.

%clearpage

The image seen in figure 4.101 may seem counterintuitive, as its expected that the regions of low visibility, there will be more haze. This is not the case in this image. What is happening is that the transmission losses are more dominant than the increases in path radiance.

Figure 4.102 shows only the path radiance in the RBG bands. Comparing this image to the aerosol visibility map seen in figure 4.100, it is clear that the regions of low visibility correspond to the regions of high path radiance, as expected.

This behavior was also seen when the same scene was run with rural aerosols.

To determine if the aerosols exhibit a more scattering-dominated behavior at higher visibilities, the scene was

Figure 4.100: This shows the 'realistic' visibility map.

run with a range of visibilities between 20 and 25 km. (A new ADB was constructed, with visibility endpoints of 20 and 25 kilometers.) The rendered result is displayed in rgb bands in figure 4.103. Unfortunately, any dynamic range added to the image is masked by the variability between the objects in the scene, and therefore is not visible. The path radiance associated with this scene is shown in figure 4.104.

Figure 4.101: This shows the RGB bands when DIRSIG 4 renders the Megascene with a 'realistic' visibility map.

Figure 4.102: This shows the RGB path radiance bands when DIRSIG 4 renders the Megascene with a 'realistic' visibility map.

Figure 4.103: This shows the RGB bands when DIRSIG 4 renders the Megascene with a 'realistic' visibility map ranging from 20 to 25 km.

Figure 4.104: This shows the path radiance associated with the RGB bands when DIRSIG 4 renders the Megascene with a 'realistic' visibility map ranging from 20 to 25 km.

Chapter 5

Conclusions, Recommendations, and Future Directions

5.1 Conclusions

This work shows that horizontally varying atmospheric inhomogeneities can be included into the current DIRSIG software. This ability is a very desirable one for many reasons, the primary one being the testing and analysis of hyperspectral atmospheric algorithms which attempt to retrieve the ground reflectance of a scene or target.

Adding this ability to DIRSIG required a major reworking of the current methods of sampling the atmospheric data. In short, it meant giving DIRSIG the ability to sample the atmosphere in more dimensions. The new dimensions sampled include values of concentrations of atmospheric constituents (water vapor and visibility), as well as new geometric dimensions (azimuth and altitude).

These abilities, once incorporated into DIRSIG, show a significant improvement in the ability of DIRSIG to predict the atmospheric values of path radiance and path transmission. The error associated with predicting these values were shown to be reasonable when constrained to normally observed atmospheric conditions.

5.2 Recommendations and Future Directions

As stated before, the actual code used in this work was not written in a very efficient manner, and should (and will) be re-written by a computer scientist familiar with the DIRSIG code, as well as with the language it is written in.

Several improvements should be made to the ADB generation code. The first of which would be to add intelligence to the selection of the interpolation endpoints in the ADB. For example, if the overall range of the visibilities in a scene were known ahead of time, then the interpolation endpoints for visibility could be used in the beginning of the ADB generation to define where (in the visibility dimension) the atmosphere should be sampled. This would increase the efficiency of the ADB, in that it would not hold values which were not going to be referenced.

The same argument can be made for all of the dimensions. Using only the information in the cfg file, the code should be able to determine the zenith range needed (as DIRSIG 3 currently does), along with the azimuth range ("does the sensor only face West?"), which would eliminate the need for the ADB to hold values for an azimuth that can not be seen in the scene. In addition to these, the altitude range, the water vapor range, and the visibility range can all be derived from either the gdb (geometric database) files used in the scene, in the case of the altitude, or from the atmospheric maps included in the cfg file. This would aid in the goal of striking a balance between accuracy and time expenditure, for it would greatly cut down

on the time used by eliminating MODTRAN processing values which will not be used. All of this will be possible once the ADB generation code is fully integrated into DIRSIG 4 as it is in DIRSIG 3.

In building the atmospheric interpolator, the values of input parameters (altitude, water vapor and visibility) which fell outside of values in the ADB, generally, were set to the closest outer range. For example, if the ADB had values for the zenith angle between 0 and 23 degrees, and a value of 24 degrees was passed to the interpolator, that value was reduced to 23 degrees. The algorithm should be changed so that there is extrapolation outside the bounds of the ADB, where applicable and logical. This will prevent any unnatural hard "edges" in the scene rendering. Although not radiometrically perfect, extrapolation should provide a better answer than a clipped value.

Additionally, it would be valuable for DIRSIG to display to the user error estimates based on the endpoint values chosen for the interpolator. For example, if the user is rendering a specific scene, the code will read in the range for all of the interpolation dimensions, as taken from the cfg file, the gdb file, and/or the atmospheric maps, and use pre-computed error calculations (similar to, but more robust than those found in this work) to display to the user the error contributions due to each of the interpolation dimensions. This way, for example, if the user is rendering a specific scene with a high visibility range, the software will display how much error is expected from the visibility range. The user can then alter the number of visibility points sampled to get the desired accuracy. As well, next to these errors, should be the estimated time cost involved in obtaining that accuracy.

A possible alternative to this approach to the implementation of horizontally varying atmospheric species, or a potential improvement on this method, is the incorporation of MOD3D into DIRSIG. MOD3D is a three-dimensional, voxelized version of MODTRAN. (A voxel is defined as a 'volume element'.) MOD3D has the ability to specify, in three dimensions, different atmospheric species. This program shows great potential because it used many of the tools within MODTRAN itself. The reason why MOD3D was not used in this work was because it was not released in a workable form at the time this work began.

The solution to the horizon issue outlined in chapter 2 encounters challenges in its implementation. This is because there are some characterists inherent to DIRSIG which must be addressed. First of all, there is a "default" object in DIRSIG. This is a sphere in which all objects and sensors exist. Because of this, there seems to be an issue with passing the altitude variable. A test image was created, in which the sensor looks almost directly at the horizon, with no object in the scene other than this default DIRSIG sphere. Figure 5.1 shows the "z-hit" truth image. This shows the altitude for each pixel in the image. The vertical profile down the center of the image is seen in figure 5.2. The zenith range in this image is approximately from 110 degrees at the bottom, to 85 degrees, as measured from straight up.

This will cause a problem in the new horizon handling section algorithm because it expects to have a negative z-hit value when below the horizon. Either way, there must be a system in place with works with this DIRSIG sphere and all of is interactions. As of this point, any images of the horizon should not be assumed to be radiometrically accurate.

As well, there seems to be an object which is in addition to this sphere, at a zenith angle between 90 and 95. The resolution of these issues is beyond the scope of this work.

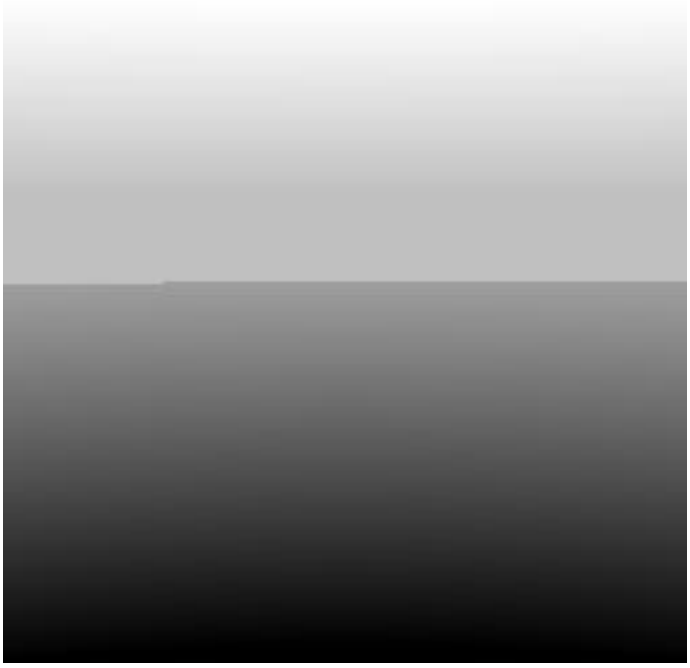

Figure 5.1: The "z-hit" map for the horizon test scene.

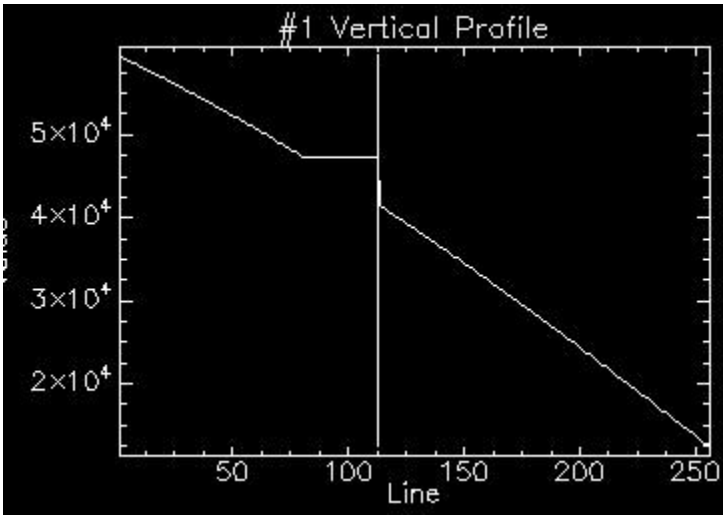

Figure 5.2: This figure shows the z-hit value for each line in the image.

Bibliography

[1] Berk, A., et al, *MODTRAN4 User's Manual*, Air Force Research Laboratory, June 1, 1999.

[2] Kaufman, Y.J. "Operational Remote Sensing of tropospheric aerosol over land from EOS moderate resolution image spectroradiometer", *Journal of Geophysical Research* Vol. 102, no.D14, pages 17.051 - 17,067, July 27, 1997.

[3] Kerekes, John, P. "Modeling, Simulation and Analysis of Optical Remote Sensing Systems", (PhD Thesis) Technical Report TR-EE 89-49 Purdue School of Electrical Engineering , August 1989

[4] Liang, Shunlin, "Atmospheric Correction of Landsat ETM+ Land Surface Imagery – Part I: Methods", *IEEE Transactions on Geosciences and Remote Sensing*, 39:2490-2498, 2001.

[5] Poutier, Laurent, et al, *"COMANCHE and COCHISE: two reciprocal atmospheric codes for hyperspectral remote sensing"* ; Proceedings of AVIRIS 2002 Workshop, Pasadena (USA), March 2002.

[6] Raqueño, R.V., Brown, S.D., and Schott, J.R., "Incorporation of Transmissive Scene Element Modeling in Multispectral Image Simulation Tools," SPIE Optical Science, Engineering, and Instrumentation Annual Meeting, Denver, CO August 1996.

[7] Raqueño, Rolando, and Salvaggio, Carl, Personal interview, August 12, 2003.

[8] Schott, John *Remote Sensing: The Image Chain Approach.*, Oxford University Press, New York, 1997.

[9] Schott, John, et al, *DIRSIG - Digital Imaging and Remote Sensing Image Generation Model: Description, Enhancements and Validation.*, RIT/DIRS Report 92/93-51-146, July, 1993.

[10] Tantalo, Frank *Modeling the MTF and noise characteristics of an image chain for a synthetic image generation system*, Thesis (M.S) - Rochester Institute of Technology, 1996.

Appendix A

Experiments

Contents

A.1 Non-Zero Altitude Object Test 191
A.1.1 Background 191
A.1.2 Setup and Procedure 192
A.1.3 Results and Conclusions 192
A.2 Upwelled Sampling: Geometry 194
A.2.1 Background 194
A.2.2 Setup and Procedure 194
A.2.3 Results and Conclusions 194
A.3 Upwelled Sampling: Atmospheric Inhomogeneities 200
A.3.1 Background 200
A.3.2 Setup and Procedure 200
A.3.3 Results and Conclusions 200

This chapter introduces and discusses various experiments performed. These experiments had one of two purposes. The first, was to define and characterize the limitations in the current version of DIRSIG. The second was to test out the validity of a new feature which will be added to DIRSIG.

A.1 Non-Zero Altitude Object Test

A.1.1 Background

One of the first issues addressed was that of the non-zero altitude object. This is caused by DIRSIG's current treatment of an object with a non-zero altitude. The issue arises when DIRSIG calculates the upwelling radiance and path transmission from an object. If the object is at ground level, DIRSIG simply interpolates between the values that are pre-calculated in the ADB. Now, if DIRSIG encounters an object *not* at ground-level, then it scales the existing calculated values to reflect the change in range from target to sensor.

Graphically, this can be seen in figure 2.2, which shows DIRSIG's treatment of the atmosphere when dealing with an object not at ground level. The more accurate treatment of the atmosphere is MODTRAN's method, which is illustrated in figure 2.1.

The problem with DIRSIG's method, is that these pre-calculated values in the ADB include results from rays which were passed through all of the layers of the atmosphere. This included the lower layers which account for considerably more transmission loss and path radiance increase than the others. The properties

of the actual atmosphere (more accurately reflected in MODTRAN) do not change linearly, as will be seen in the results of this experiment.

The goal of this experiment is to better understand how the path radiance and transmission change from an overhead perspective as the target's altitude increases. Specifically, how well DIRSIG estimates these values, and to determine if and how to better model them.

A.1.2 Setup and Procedure

To determine the location and severity of this problem, an experiment was conducted in which a very simple DIRSIG scene was analyzed by both DIRSIG and MODTRAN. The scene that was constructed consisted of a plane of a theoretical, non-reflective. A series of runs were then made in both DIRSIG and MODTRAN for different altitudes of this plane.

To accomplish this, the one-object scene was rendered by DIRSIG, its altitude increasing for each run. In MODTRAN, the albedo of the Earth was set to 0 (non-reflective), and the height of the "object" was simply the target height (h2) in the tape5 file. In both cases, MODTRAN and DIRSIG with sampling only the transmission and path radiance resulting from the atmosphere *only*, with absolutely no influence form other objects or surface characteristics.

As stated before, to calculate the atmospheric properties, DIRSIG makes use of the ADB file. Now, the ADB file is made up of the results of MODTRAN runs. At first glance, one might ask how the results could possibly differ. Keep in mind that it is the results at different altitudes that is being investigated. It will be shown that DIRSIG and MODTRAN handle different target altitudes in very different ways, with very different results.

The results in the visible spectrum were examined, because any change in path radiance and transmission will be more obvious here than in the thermal.

The upwelled radiance and transmission was recorded at each target altitude and compared (Figures 2.4 and 2.5). The output from both DIRSIG and MODTRAN was a complete spectral block, which was then spectrally integrated for ease of display. This graph shows the trend of these two characteristics of the atmosphere, but is of little practical use. The reason is that very few, if any, DIRSIG objects exist at such high altitudes. In fact, few ever even approach 1 km. So, the exact same experiment was done, but this time, only target altitudes at and below 1 km were examined.

A.1.3 Results and Conclusions

The results of this experiment showed that the change in upwelled radiance and transmission as altitude increases is roughly linear in the region below 1 km. (Figures 2.6 and 2.7) This is where the vast majority of synthetic imaging is done in DIRSIG.

Because of this linearity, if the upwelled radiance can be sampled and transmission of the atmosphere at 1 km as well as ground (0 km), then these values (upwelled radiance and transmission) can be calculated at any altitude in between through basic linear interpolation with good confidence. The goal of this research can be over-simplified by saying that it is to make DIRSIG's atmospheric values closer to MODTRAN's. With that in mind, figures 2.8 and 2.9 show that sampling the atmosphere at another altitude (in this case, about 1 km.) can make the resulting DIRSIG values much closer to the MODTRAN values.

The linear behavior of the lowest section of the atmosphere allows for the successful interpolation between two ranges. This lower section of the atmosphere also appeared to be the most dynamic, in terms of path radiance and transmission as a function of altitude. Therefore, if it is assumed that any 1 km vertical segment of the atmosphere also behaves as linearly as the lowest 1 km segment, then this sampling scheme can be repeated at any altitude. This means that if the atmosphere is sampled at a pair of altitude levels for a "cloud region," the values of path radiance and transmission in that region can be successfully interpolated, as long as it is not substantially thicker than 1 km. As well, more altitude regions could be created to include any set of objects that are grouped by similar altitudes (i.e. different types of clouds). (See figure

A.1.) However, this increase in the number of altitudes at which the atmosphere is sample comes at a cost of increased processing time.

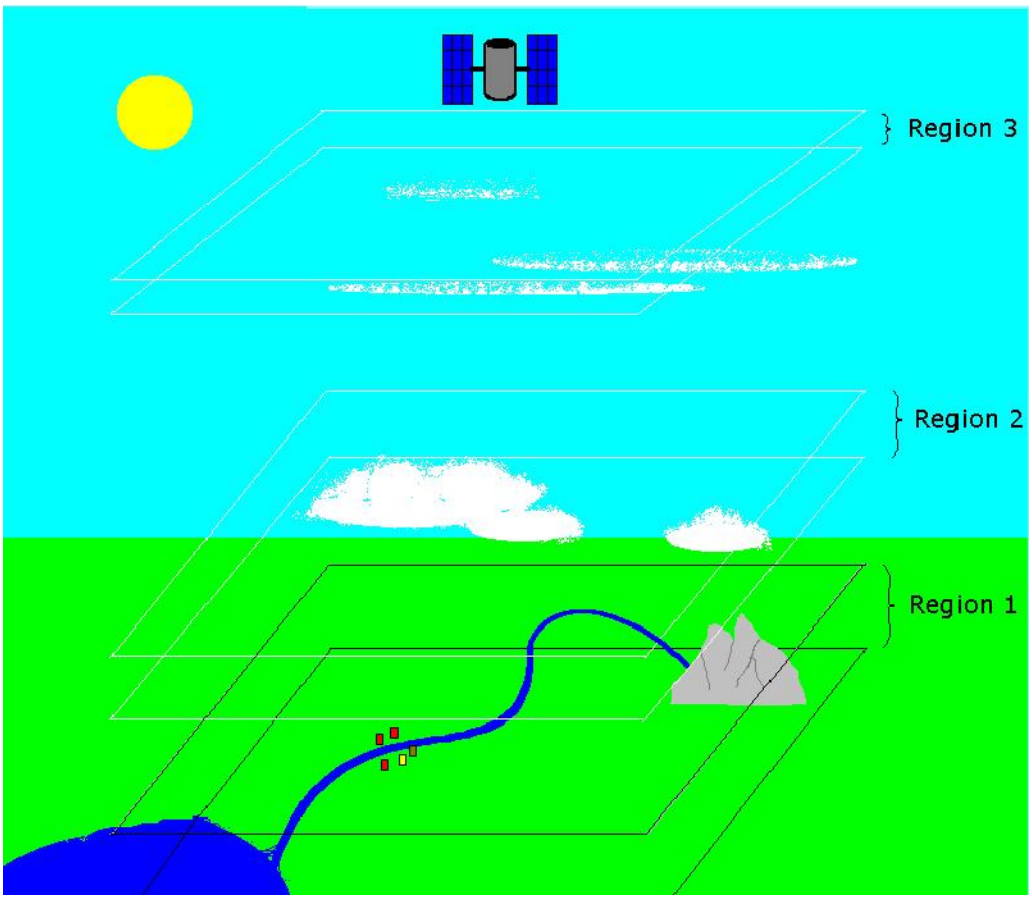

Figure A.1: In the new ADB, upper-atmospheric regions can be added where clouds (or any objects, for that matter) can be placed, and the transmission and path radiance can be predicted with similar accuracy as in the region below 1 kilometer.

A.2 Upwelled Sampling: Geometry

A.2.1 Background

One of the vital steps to achieving the overall goal of the research of incorporating atmospheric variability in DIRSIG is making the sampling of the atmosphere more robust. For example, consider the current method of sampling the upwelling radiance and transmission of the atmosphere discussed in section 1.4.4. Only sampling the atmosphere in a straight line, varying only in the zenith direction, can not provide accurate path radiance and transmission data of the atmosphere. First of all, it ignores any azimuthal structure of the upwelled radiance and transmission. Secondly, any effect horizontally varying inhomogeneities would have on the path radiance and transmission would also be ignored. Basically, the atmosphere is undersampled.

From a functional standpoint, when using the atmospheric module described in this work, DIRSIG will reference a five-dimensional look up table for its calculation of any atmospheric values. These dimensions are zenith, azimuth, altitude, water vapor, and visibility. The goal of this experiment is to determine the specific points in each dimension of that look up table.

Assuming that the altitude dimension has already been analyzed (see section A.1), there are four dimensions of interpolation that need to be analyzed. These are, namely, zenith, azimuth, water vapor, and visibility. Each of these dimensions will be handled independently. The first two are purely geometric, and the last two deal with atmospheric constituents. However, the process of determining the frequency of sampling will be nearly identical for all four. This section deals with the geometric dimensions. The atmospheric inhomogeneities will be dealt with in section A.3.

To figure out where, specifically, sampling of the upwelling radiance and transmission should be done, the results of a linear interpolator were compared with the results of MODTRAN runs. The goal was to determine how well a linear interpolator not unlike the one used in DIRSIG compares to a direct MODTRAN run.

A.2.2 Setup and Procedure

For each of the dimensions, a similar setup and procedure was used. In the case of the zenith dimension, a range of values was established. In a real DIRSIG scene, the zenith angle may change depending on the viewing geometry and size of the synthetic image. For this study, the zenith ranged from 180 to 100 degrees. [1]

For azimuth, the range is 180 degrees, starting from the solar azimuth angle. This assumes that the atmospheric values calculated by MODTRAN are symmetric about the solar azimuth angle.

At each one of these increments, in this case, zenith angles, MODTRAN is run, and the results stored in a LUT. When this is complete, a second set of zenith angles is run. These new angles are at the midpoints of the LUT angles. It is assumed that the maximum amount of interpolation error will be seen at these intermediate points. This may not be entirely accurate, as there is a chance that the radiance or transmission of the atmosphere may change in a manner such that this sampling scheme is to coarse. (See figure A.2.) However, to run the experiment at a finer angular resolution would mean a considerable increase in the time duration of the experiment. It is assumed that this effect will not affect the results of the experiment to a significant degree.

A.2.3 Results and Conclusions

For each look angle described above, the data will be in the form of a two dimensional matrix. One axis will be the value (either transmission or path radiance), and the other a set of spectral points. There is a band

[1] Zenith angles are kept in the MODTRAN convention for this section. Therefore, 180 degrees indicates a MODTRAN run where the sensor is directly above the target, looking down. A zenith angle of 0 would indicate that the sensor is looking straight up.

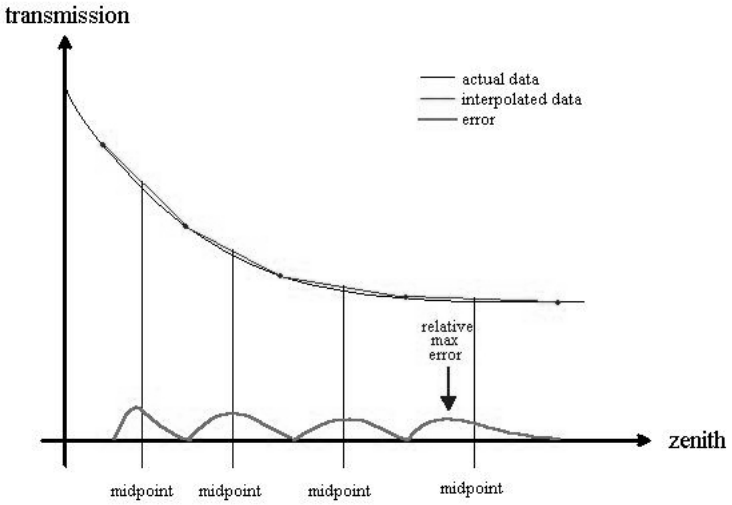

Figure A.2: An illustration of how the midpoint between interpolation points may not always be the maximum error.

for each of the following: blue centered at 440 nm, green at 510 nm, red at 650 nm, a near infrared band at 850 nm, three water bands at 880 nm, 940 nm, and 1000 nm, and a thermal band at 10.0 microns.

At each look angle, there will be a complete matrix of these values. For each angle that will be examined (the angles directly in between the angles in the LUT), there will be two matrices, one directly calculated from MODTRAN, and the other interpolated from the surrounding LUT points (matrices). So, the matrix to be examined is actually a matrix composed of the absolute value of the differences between the direct and the interpolated matrices (normalized with respect to the directly measured matrix.) Taking the maximum value of this matrix assures finding the "worst case" of calculation error. So, the result is that for each of these intermediate points, there is a metric which yields an error. An example of this data is show in figure A.3. Note how the error generally decreases as more LUT points are used.

In this chapter, the term 'relative error' is found using equation A.1.

$$REL_ERR = abs((V - T)/T) \tag{A.1}$$

In equation A.1, REL_ERR is the absolute relative error, V is the experimental value, and T is the truth value.

Two atmospheric conditions were used. A relatively clear atmosphere (no aerosols, or water vapor) and an optically thick atmosphere (urban aerosols, visibility of 1 km, and 2.5 grams of water vapor per square centimeter). The clear atmosphere was predicted with less error than that of the thicker atmosphere. The rest of the results can be seen in figures A.4, A.5, and A.6.

Reducing this data further, the average error for each run was taken. This yields the average error associated with the number of LUT points selected. Figures A.7 through A.10 shows how as the number of LUT points selected increases, the average error decrease.

Returning to the goal of this experiment, to determine where and how to sample the atmosphere in this new module, the desired result should be a set number of LUT points to use for each dimension. Analyzing these graphs, it appears that 8 zenith angles and 8 azimuth angles appear to provide the best accuracy for the time expenditure required. Sampling more frequently than this would not increase the accuracy enought to justify the exponential increase in time that would arise from adding more sampling points.

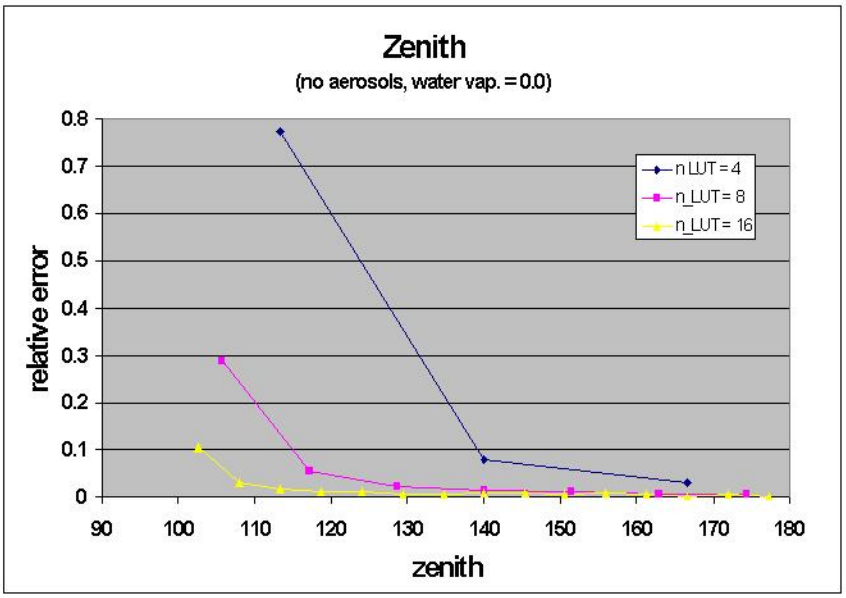

Figure A.3: Each point on this graph represents the maximum of the difference matrix.

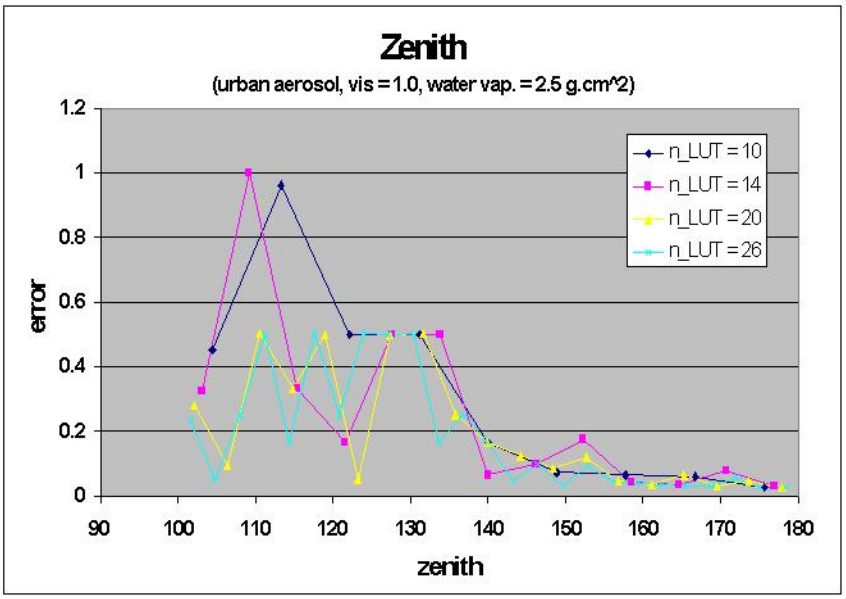

Figure A.4: Each point on this graph represents the maximum of the difference matrix.

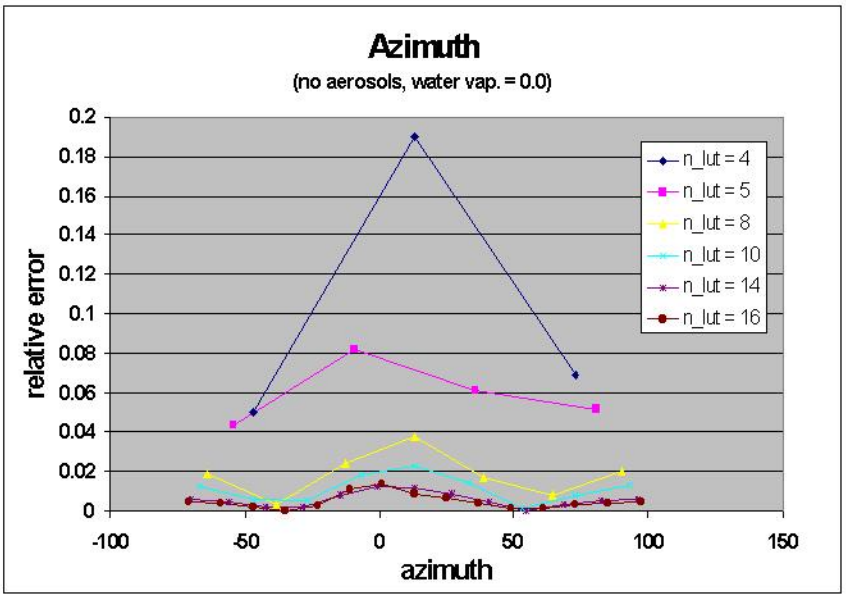

Figure A.5: Each point on this graph represents the maximum of the difference matrix.

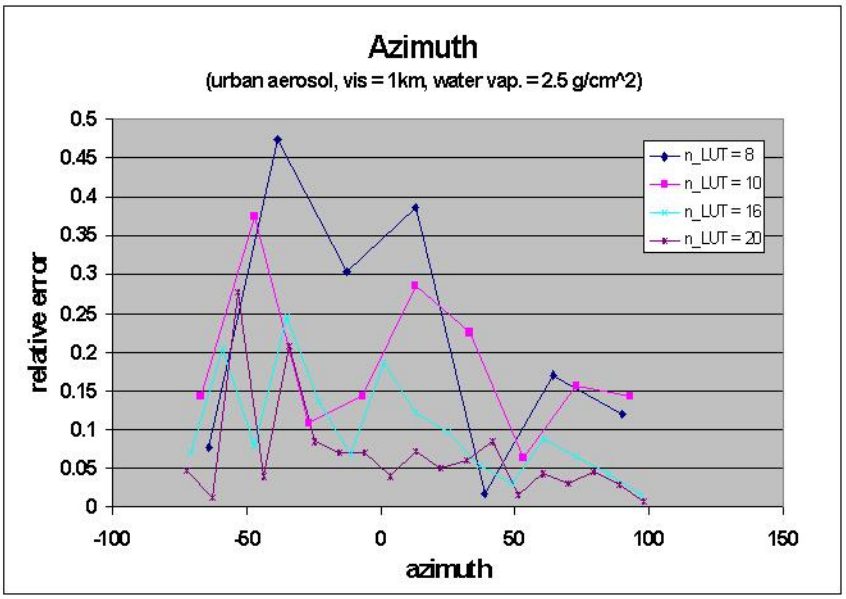

Figure A.6: Each point on this graph represents the maximum of the difference matrix.

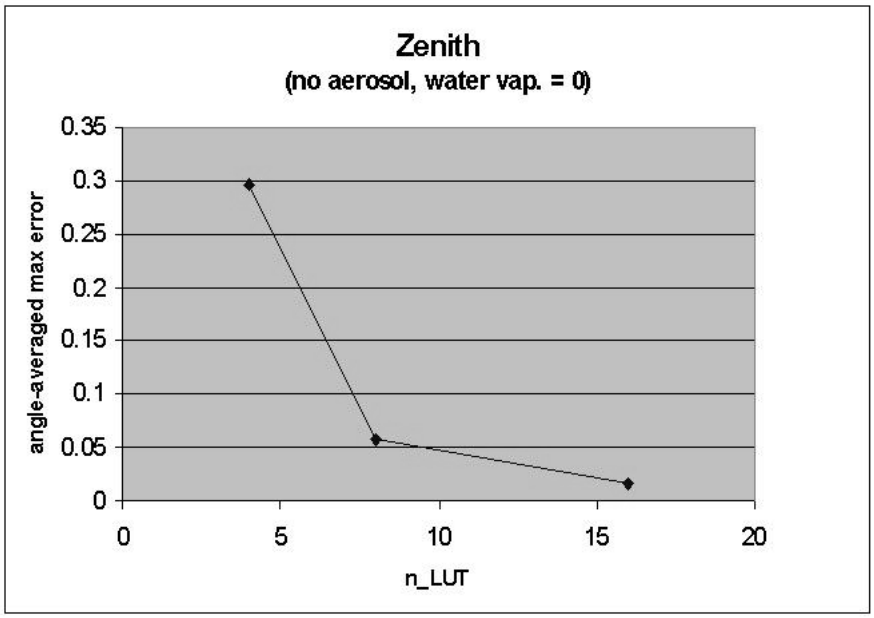

Figure A.7: Each point on this graph represents the average error in interpolation associated the number of LUT points used.

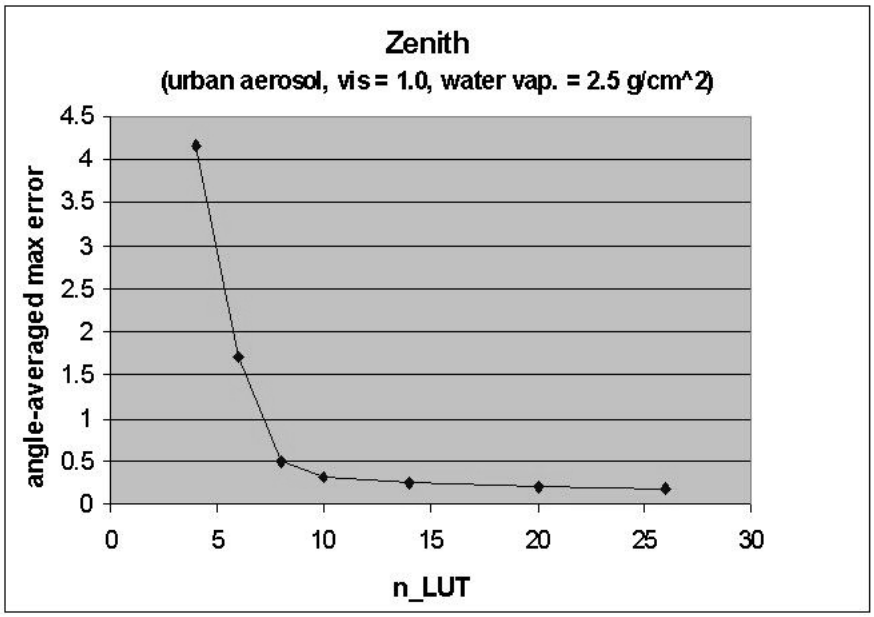

Figure A.8: Each point on this graph represents the average error in interpolation associated the number of LUT points used.

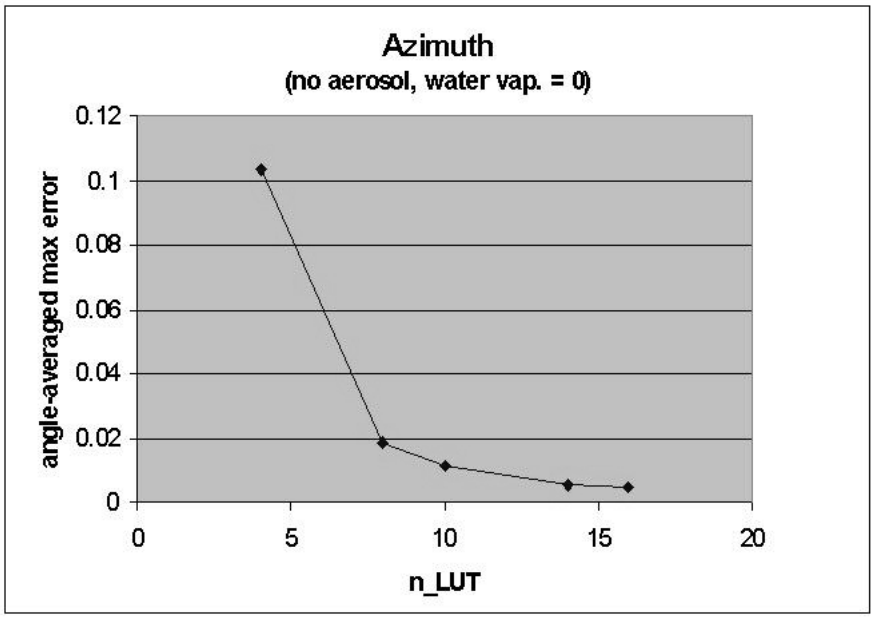

Figure A.9: Each point on this graph represents the average error in interpolation associated the number of LUT points used.

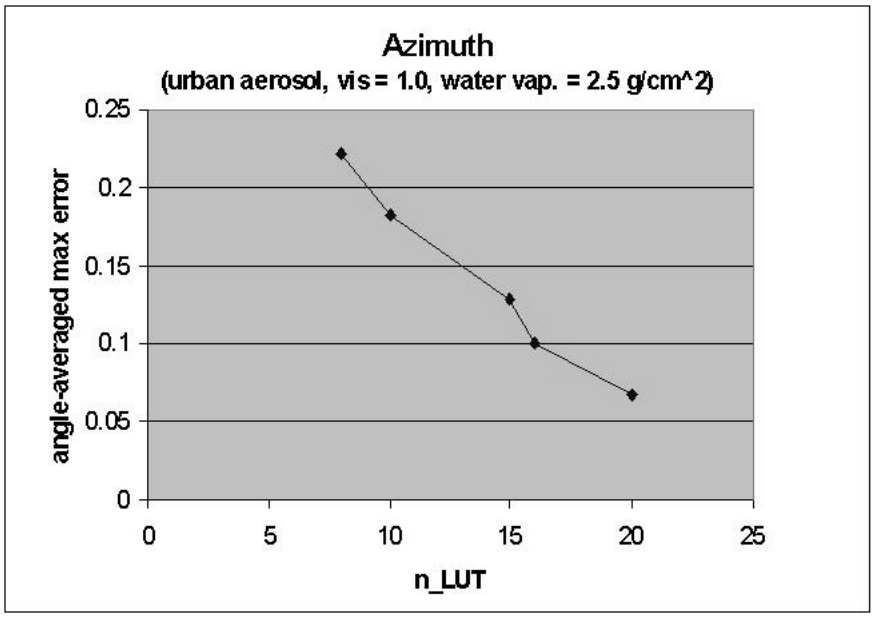

Figure A.10: Each point on this graph represents the average error in interpolation associated the number of LUT points used.

A.3 Upwelled Sampling: Atmospheric Inhomogeneities

A.3.1 Background

This experiment is, structurally, very similar to the one described in the "Upwelled Sampling: Geometry" section (section A.2). The same format of selecting an appropriate range of values and creating a look up table at a given number of points was used.

Again, the goal was to find where sampling of the upwelling radiance and transmission should be done. In this case, the sampling is done is either water vapor space or visibility space. This is done because it is intended that this experiment study the changes in path transmission and radiance as atmospheric content varies, *not* look angle. These dimensions, as well, are studied separately, because it is assumed that these variables are not separable, and dependently contribute to the path radiance and transmission.

A.3.2 Setup and Procedure

The number of sample points is then chosen, and the range is divided up into equally spaced increments. However, in the case of the visibility dimension, the intervals were not uniform. They were found by inverting the endpoints of the visibility and creating equally spaced increments in extinction space. Extinction is defined here as the inverse of visibility. This was done because the path radiance and transmission of the atmosphere change in a more linear fashion in extinction space than in visibility space. Therefore, It is more accurate to linearly interpolate between visibility values which are spaced in regular intervals in extinction space.

Again, the look up tables are generated, as are the intermediate values (directly in between the LUT values). The maximum normalized errors between these intermediate values and direct MODTRAN runs are calculated. The error associated with each number of LUT points selected for that particular run is then calculated.

The ranges used in these experiments are, for water vapor, 0 to 2.5 g/cm, and for visibility (for a given aerosol) from 1 to 23 km [7]. These are chosen as they represent common values for water vapor amounts and visibility.

A.3.3 Results and Conclusions

The explanation of the results of the experiment are nearly identical to that described in section A.2.3. These results, produce by similar means, are shown in figures A.11 and A.12, for water vapor, and figures A.13 and A.14, for visibility (urban aerosol). (Note: The two graphs in figure A.13 show the same data. The lower one simply has fewer series for ease of display.)

Analyzing these graphs, the most effective number of points for the water vapor section is 4, and 8 for the number of visibilities per aerosol. These numbers will be used as the defaults.

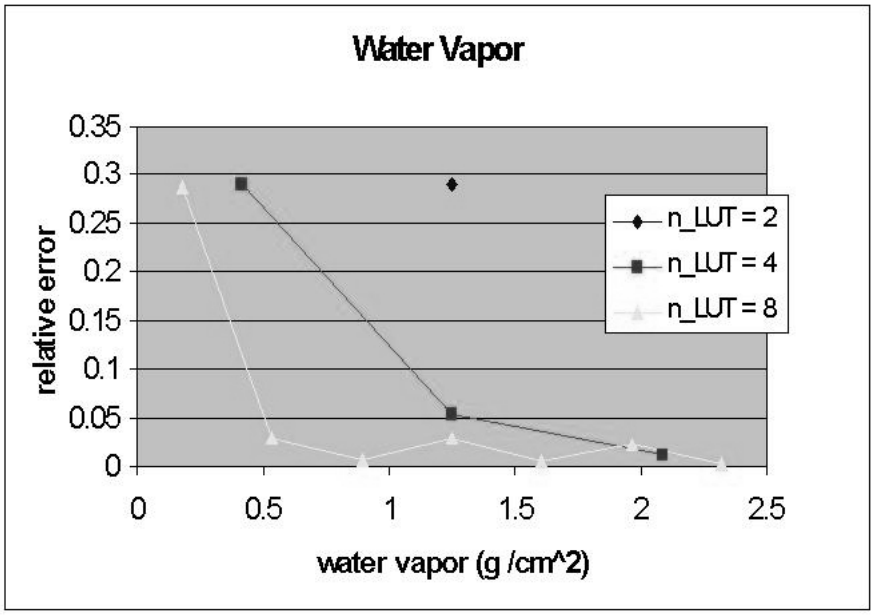

Figure A.11: Each point on this graph represents the maximum of the difference matrix.

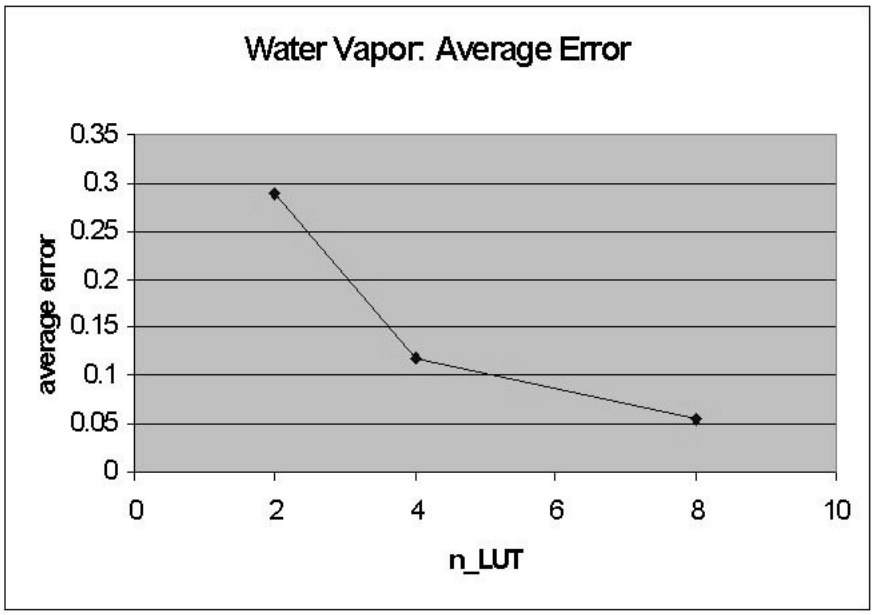

Figure A.12: Each point on this graph represents the average error in interpolation associated the number of LUT points used.

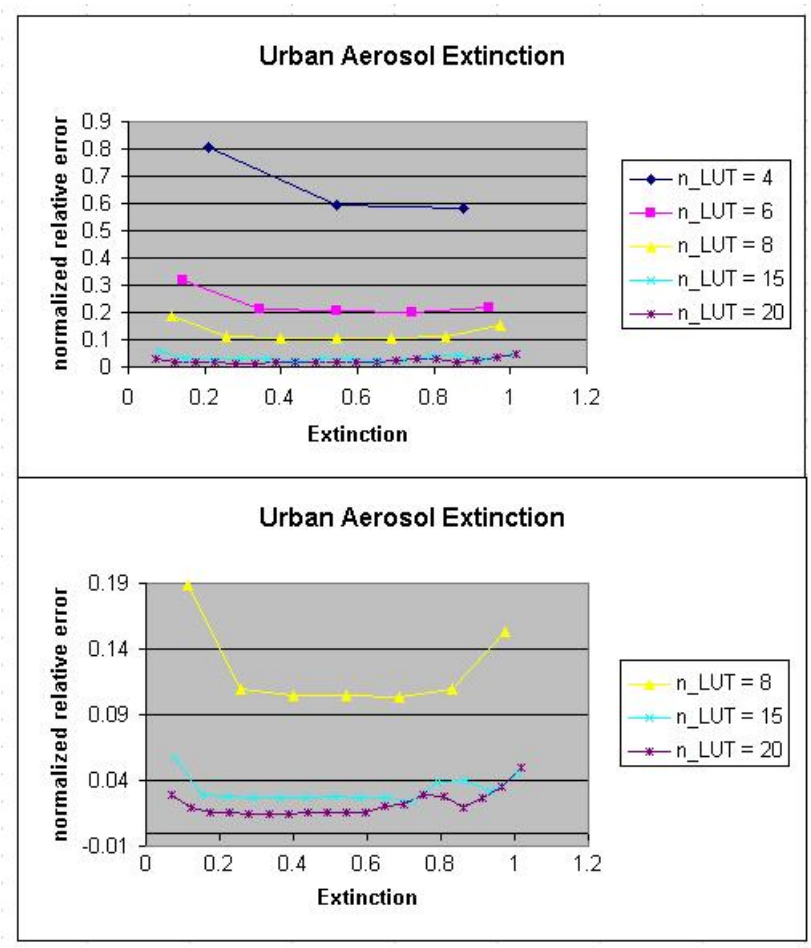

Figure A.13: Each point on this graph represents the maximum of the difference matrix.

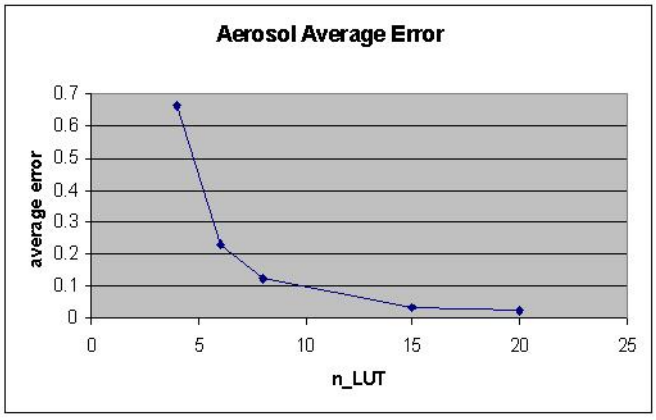

Figure A.14: Each point on this graph represents the average error in interpolation associated the number of LUT points used.

Appendix B

Test Scene Results

Contents

B.1 Test Image 1a . . . 204
B.1.1 Test Image 1a Zenith Variation. . . . 204
B.1.2 Test Image 1a Azimuth Variations. . . . 215
B.1.3 Test Image 1a Grid Results . . . 223
B.2 Test Image 1b . . . 225
B.2.1 Test Image 1b Zenith Variation. . . . 225
B.2.2 Test Image 1b Azimuth Variation. . . . 230
B.2.3 Test Image 1b Grid Results. . . . 235
B.3 Test Image 1c . . . 236
B.3.1 Test Image 1c Zenith Variation. . . . 236
B.3.2 Test Image 1c Azimuth Variation. . . . 241
B.3.3 Test Image 1c Grid Results. . . . 245
B.4 Test Image 1a_urban. . . . 246
B.4.1 Test Image 1a_urban Grid Results. . . . 256
B.5 Test Image 2a. . . . 258
B.5.1 Test Image 2a Altitude Variation. . . . 258
B.5.2 Test Image 2a Grid Results . . . 269
B.6 Test Image 2b . . . 271
B.6.1 Test Image 2b Altitude Variation. . . . 271
B.6.2 Test Image 2b Grid Results. . . . 276
B.7 Test Image 2c . . . 277
B.7.1 Test Image 2c Altitude Variation. . . . 277
B.7.2 Test Image 2c Grid Results. . . . 282
B.8 Test Image 3 . . . 283
B.8.1 Test Image 3 Water Variation . . . 284
B.8.2 Test Image 3 Grid Results . . . 297
B.9 Test Image 4a . . . 299
B.9.1 Test Image 4a Visibility Variation . . . 300
B.9.2 Test Image 4a Grid Results . . . 312
B.10 Test Image 5 . . . 314
B.10.1 Test Image 5 Grid Results . . . 314

This chapter contains the results of the analysis of the test scenes. A further discussion of the test cases can be found in chapter 4.

B.1 Test Image 1a

Test image 1a consists of very simple structures. There are three main objects. The first is a single, large, flat facet of a material with a reflectance of zero. This is located at the ground (0 km). In addition, in the Southwest and Northeast of the image are objects which resemble pyramids with the tops cut off to produce a flat surface. These objects, as well, are created with a reflectance of zero. (A graphical representation of the scene, as well as the points at which they were sampled can be seen in chapter 4.)

The atmosphere for test scene 1a was rendered under sunset conditions. This, in theory, will allow for more dynamic atmospheric values.

B.1.1 Test Image 1a Zenith Variation.

The first set of data represents the results of a run where only the zenith of the points was varied across the image.

The first set of graphs show the path radiance and relative error for each band, and the RMS (root-mean-squared) error for all of the points. These are found in figures B.1 through B.10.

All of the relative errors were found using the equation B.1.

$$E_i = 100.0 * (X_i - Y_i)/Y_i \tag{B.1}$$

Where i is the band, E_i is the percent error (for either DIRSIG 3 or 4), X_i is either the path radiance or transmission for band i taken from DIRSIG 3 or 4, and Y_i is the corresponding MODTRAN value for the path radiance or transmission for band i.

Figures B.2 through B.5 show the results for the green band, the red band and the Near Infra-red band (NIR).

The next set of figures (B.6 through B.10) shows the path transmission results of the same study.

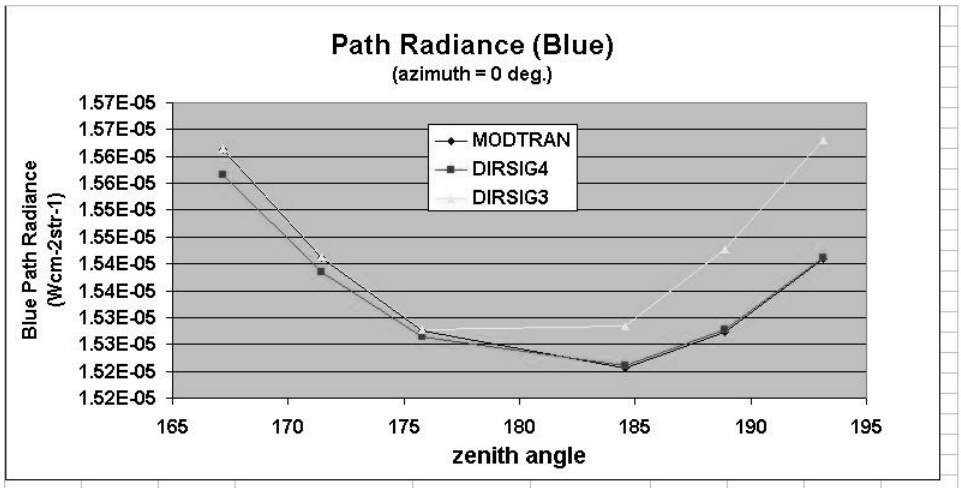

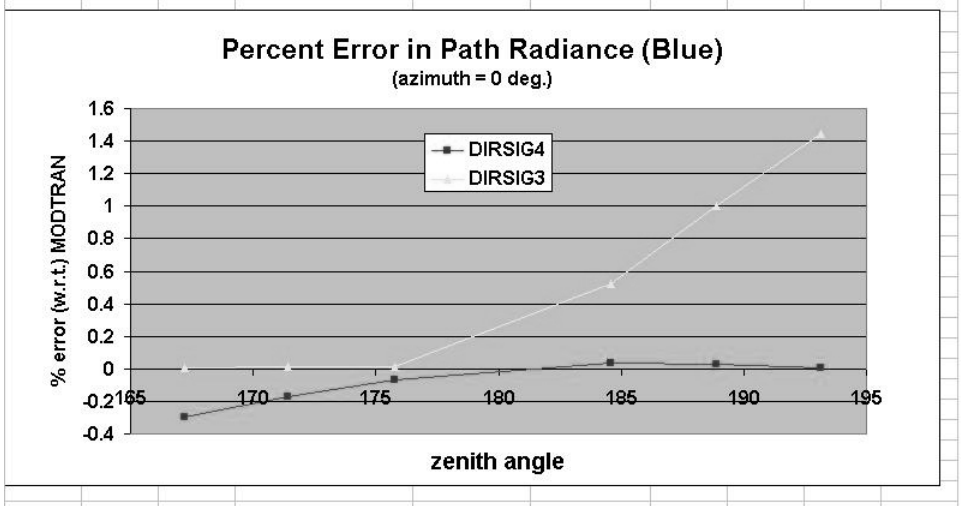

	DIRSIG 4	DIRSIG 3
RMS Error (Blue band)	2.21743E-08	1.1484E-07

Figure B.1: Test Scene 1a (zenith variation): The upper graph shows the blue path radiance obtained by MODTRAN, DIRSIG 4 and DIRSIG 3. The lower graph shows the percent error of DIRSIG 4 and DIRSIG 3 relative to MODTRAN. The RMS errors for the points shown on the graph are listed below the graphs.

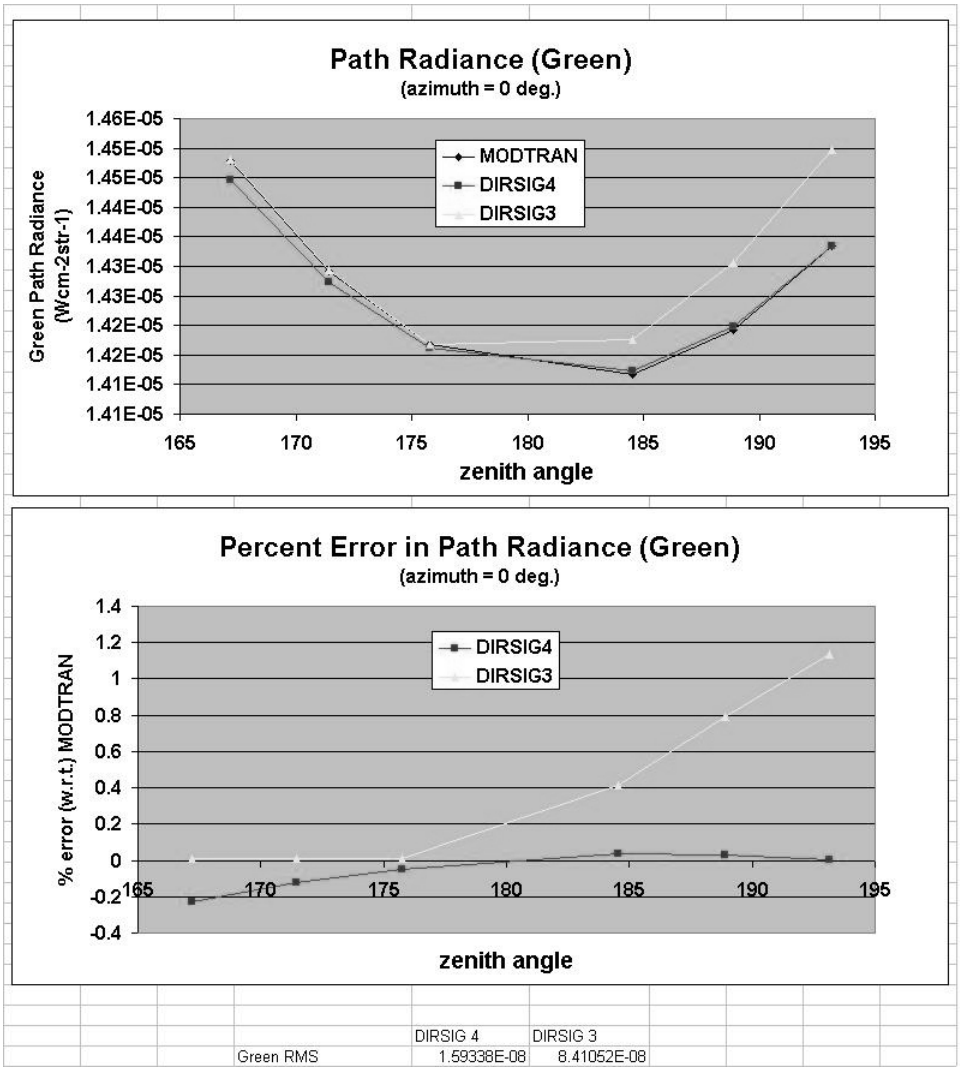

Figure B.2: Test Scene 1a (zenith variation): The upper graph shows the green path radiance obtained by MODTRAN, DIRSIG 4 and DIRSIG 3. The lower graph shows the percent error of DIRSIG 4 and DIRSIG 3 relative to MODTRAN. The RMS errors for the points shown on the graph are listed below the graphs.

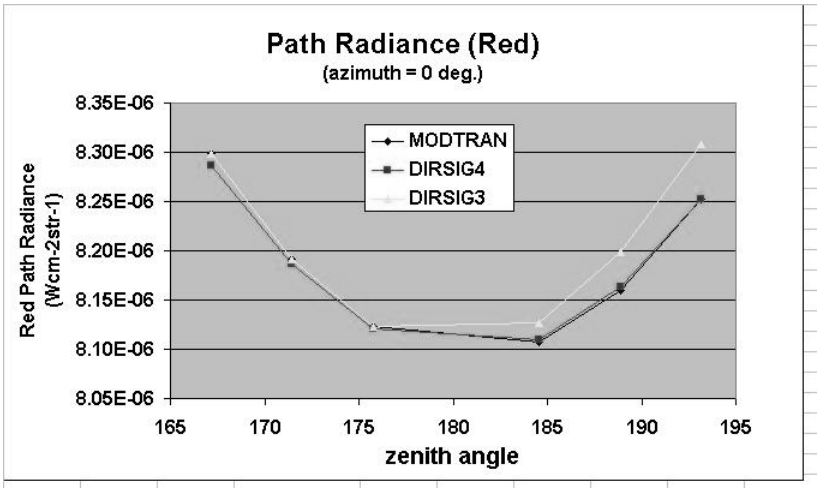

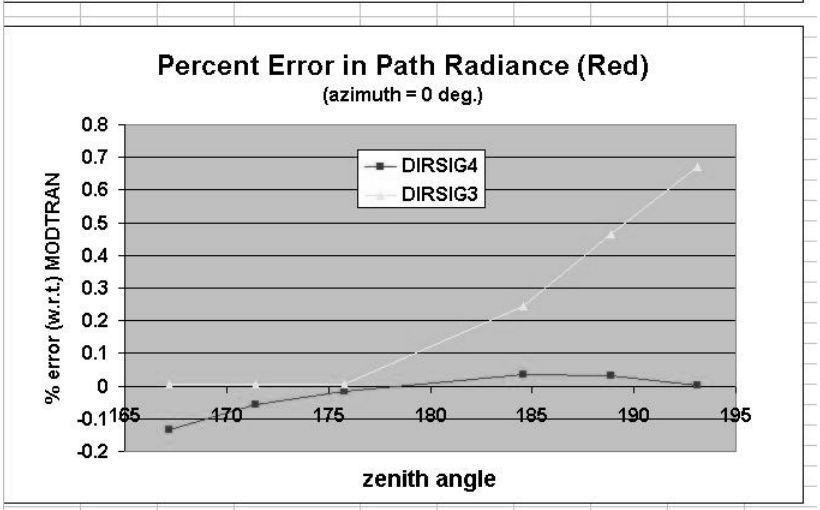

	DIRSIG 4	DIRSIG 3
RMS Error (red)	5.18E-09	2.86E-08

Figure B.3: Test Scene 1a (zenith variation): The upper graph shows the red path radiance obtained by MODTRAN, DIRSIG 4 and DIRSIG 3. The lower graph shows the percent error of DIRSIG 4 and DIRSIG 3 relative to MODTRAN. The RMS errors for the points shown on the graph are listed below the graphs.

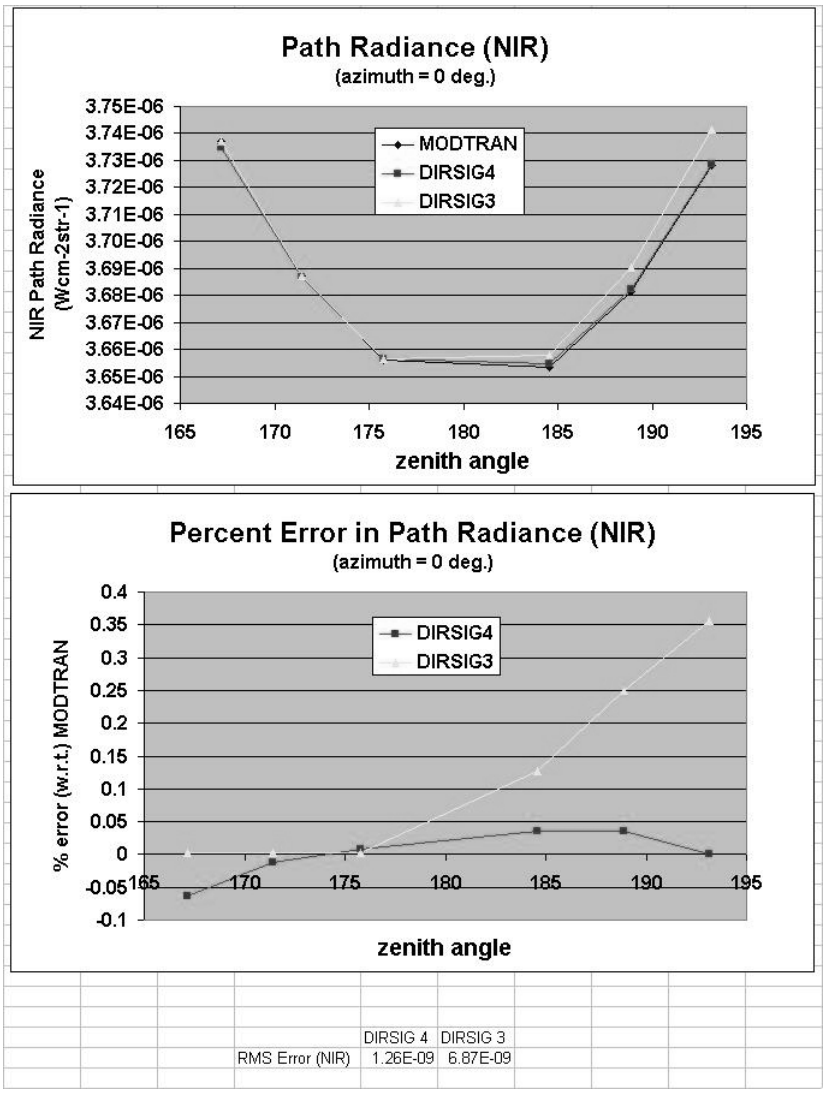

	DIRSIG 4	DIRSIG 3
RMS Error (NIR)	1.26E-09	6.87E-09

Figure B.4: Test Scene 1a (zenith variation): The upper graph shows the NIR path radiance obtained by MODTRAN, DIRSIG 4 and DIRSIG 3. The lower graph shows the percent error of DIRSIG 4 and DIRSIG 3 relative to MODTRAN. The RMS errors for the points shown on the graph are listed below the graphs.

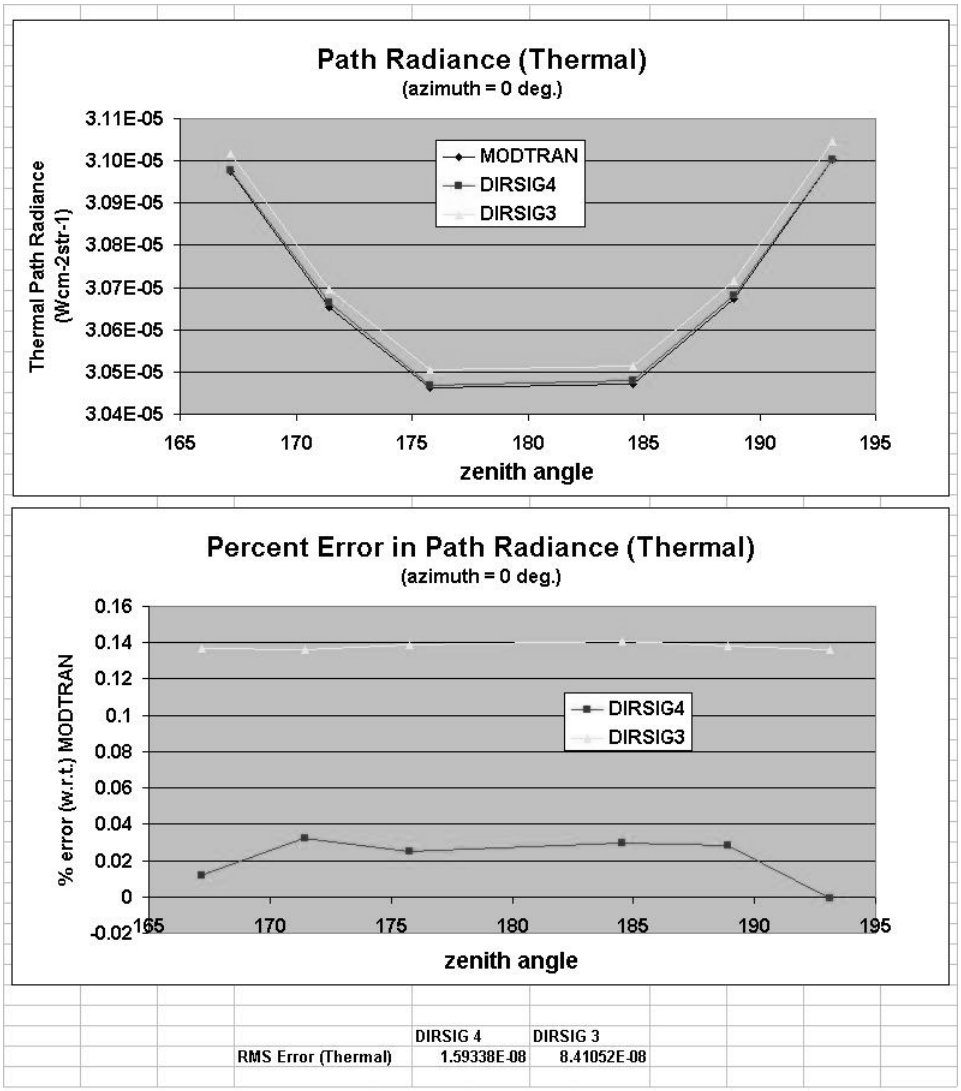

	DIRSIG 4	DIRSIG 3
RMS Error (Thermal)	1.59338E-08	8.41052E-08

Figure B.5: Test Scene 1a (zenith variation): The upper graph shows the thermal path radiance obtained by MODTRAN, DIRSIG 4 and DIRSIG 3. The lower graph shows the percent error of DIRSIG 4 and DIRSIG 3 relative to MODTRAN. The RMS errors for the points shown on the graph are listed below the graphs.

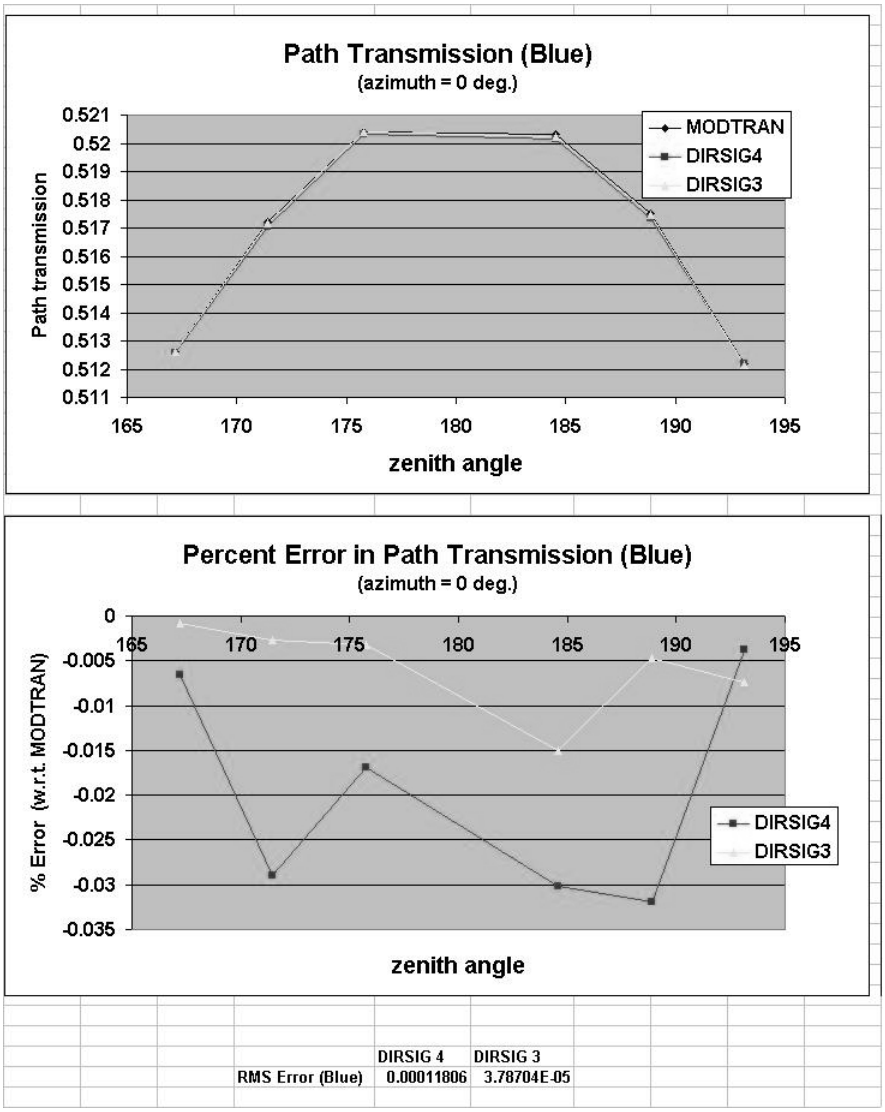

Figure B.6: Test Scene 1a (zenith variation): The upper graph shows the blue path transmission obtained by MODTRAN, DIRSIG 4 and DIRSIG 3. The lower graph shows the percent error of DIRSIG 4 and DIRSIG 3 relative to MODTRAN. The RMS errors for the points shown on the graph are listed below the graphs.

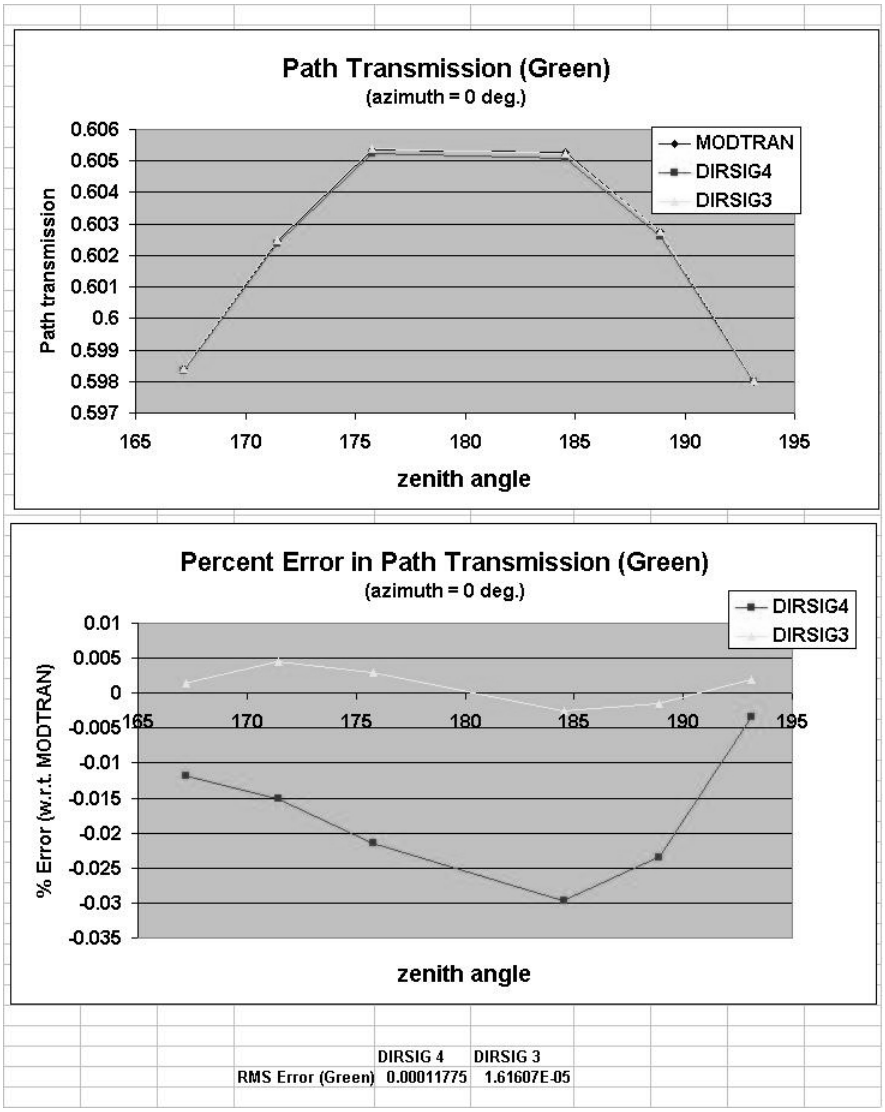

Figure B.7: Test Scene 1a (zenith variation): The upper graph shows the green path transmission obtained by MODTRAN, DIRSIG 4 and DIRSIG 3. The lower graph shows the percent error of DIRSIG 4 and DIRSIG 3 relative to MODTRAN. The RMS errors for the points shown on the graph are listed below the graphs.

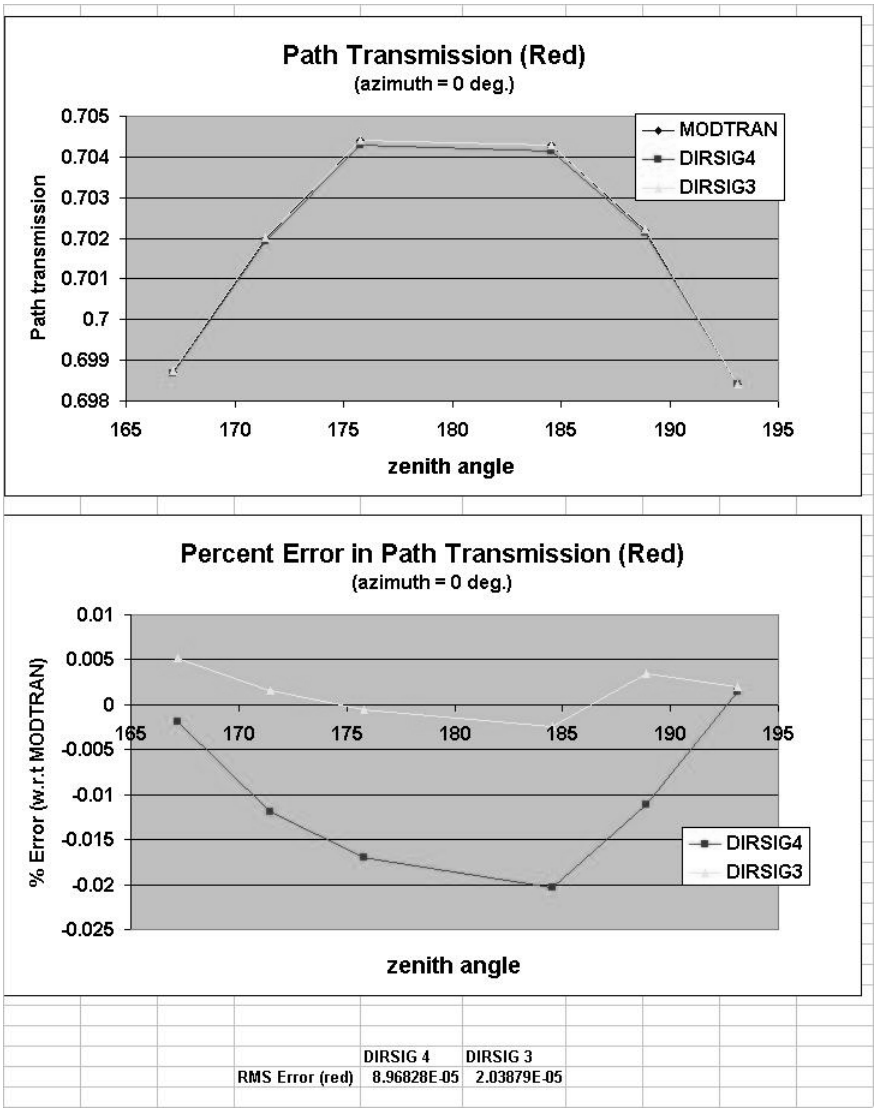

Figure B.8: Test Scene 1a (zenith variation): The upper graph shows the red path transmission obtained by MODTRAN, DIRSIG 4 and DIRSIG 3. The lower graph shows the percent error of DIRSIG 4 and DIRSIG 3 relative to MODTRAN. The RMS errors for the points shown on the graph are listed below the graphs.

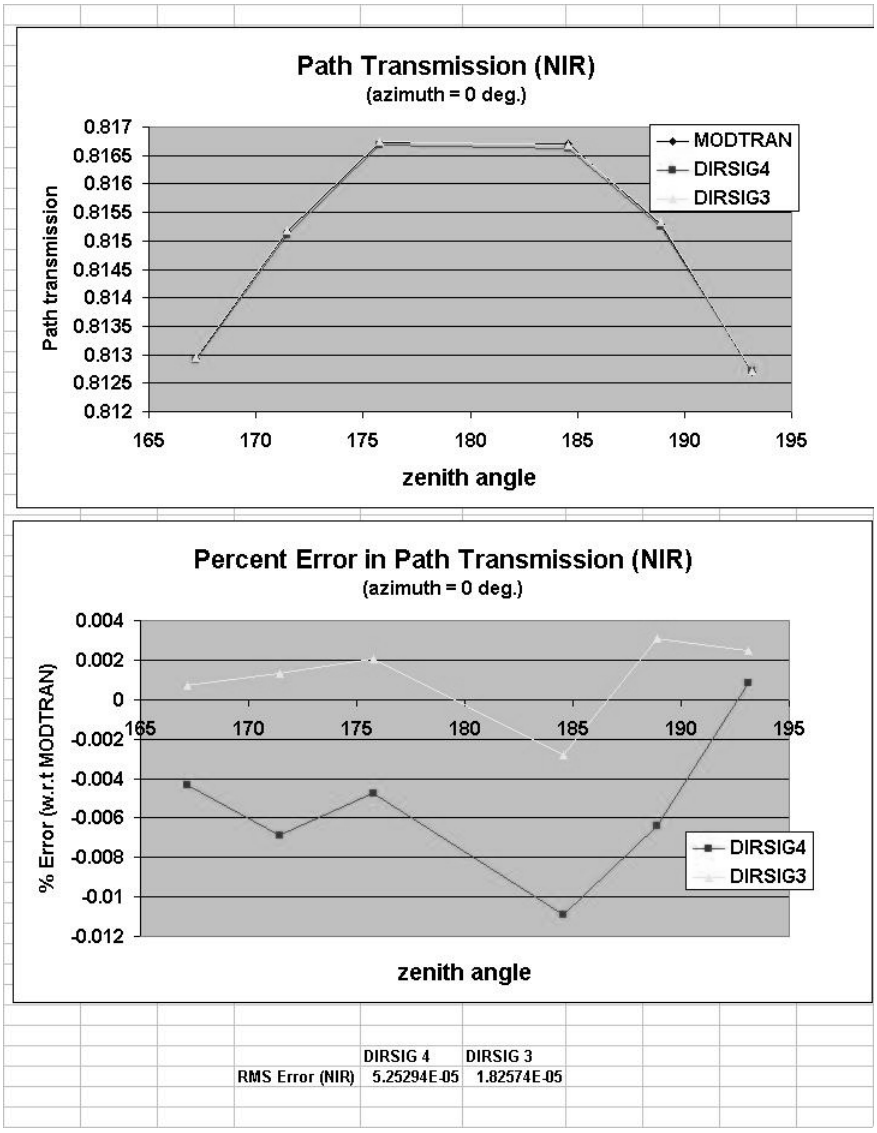

Figure B.9: Test Scene 1a (zenith variation): The upper graph shows the NIR path transmission obtained by MODTRAN, DIRSIG 4 and DIRSIG 3. The lower graph shows the percent error of DIRSIG 4 and DIRSIG 3 relative to MODTRAN. The RMS errors for the points shown on the graph are listed below the graphs.

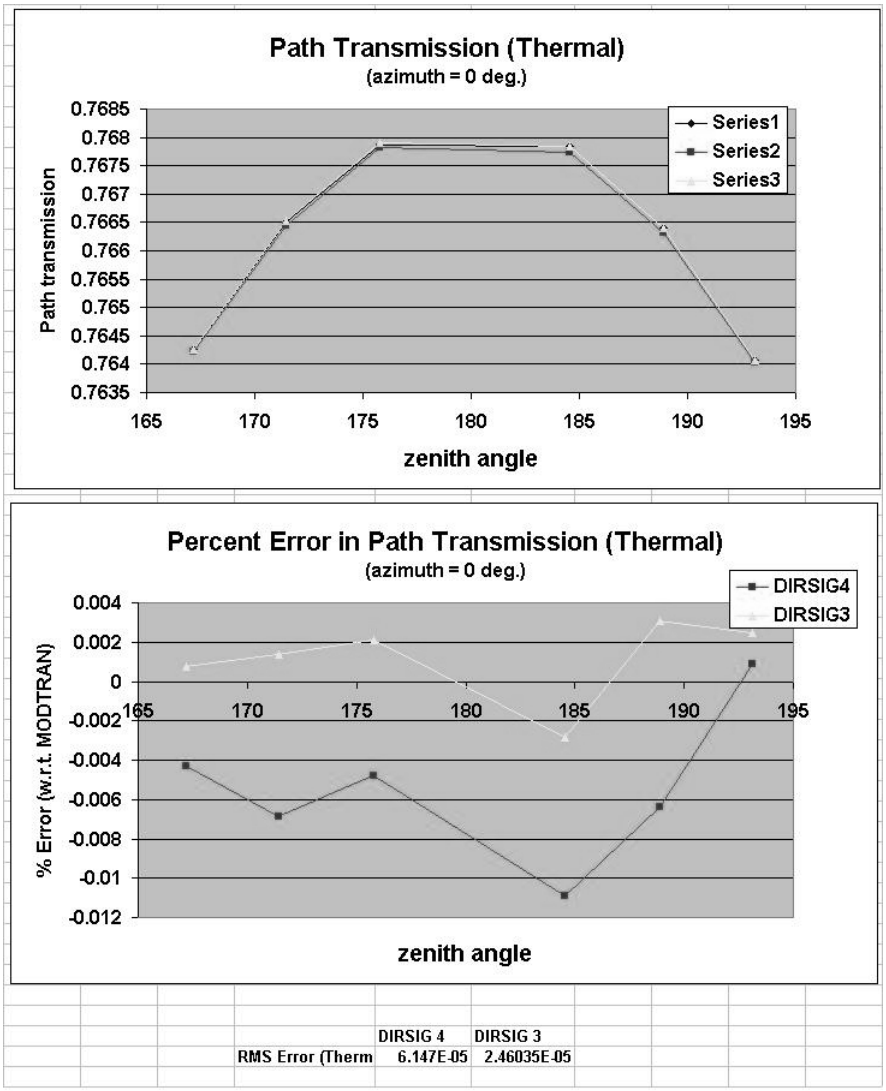

Figure B.10: Test Scene 1a (zenith variation): The upper graph shows the thermal path transmission obtained by MODTRAN, DIRSIG 4 and DIRSIG 3. The lower graph shows the percent error of DIRSIG 4 and DIRSIG 3 relative to MODTRAN. The RMS errors for the points shown on the graph are listed below the graphs.

B.1.2 Test Image 1a Azimuth Variations.

This set of data represents the results of a run where only the azimuth angle of the points was varied across the image.

All of the relative errors were found using equation B.1.

Figures B.11 through B.14 show the radiance results. (The thermal results were omitted because the thermal radiance did not vary significantly.)

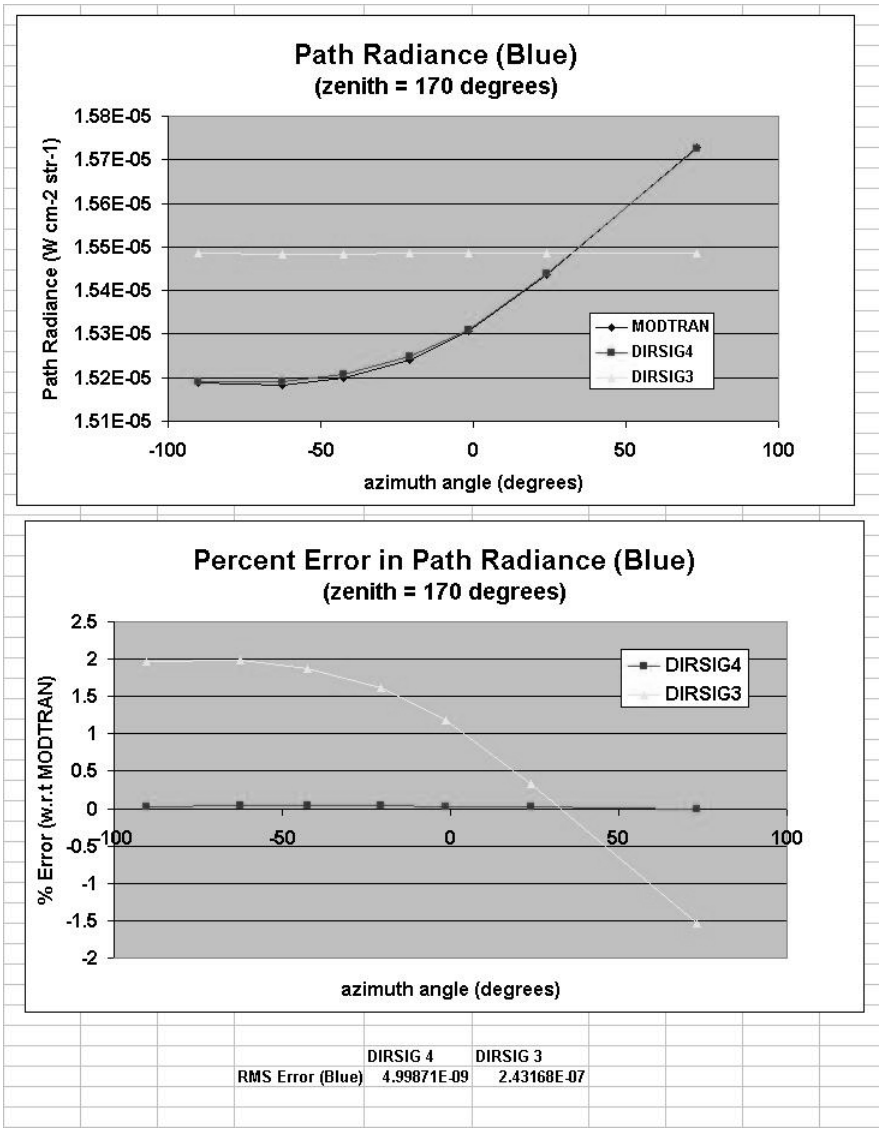

Figure B.11: Test Scene 1a (azimuth variation): The upper graph shows the blue path radiance obtained by MODTRAN, DIRSIG 4 and DIRSIG 3. The lower graph shows the percent error of DIRSIG 4 and DIRSIG 3 relative to MODTRAN. The RMS errors for the points shown on the graph are listed below the graphs.

The next set of figures (B.15 through B.18) shows the path transmission results of the same study.

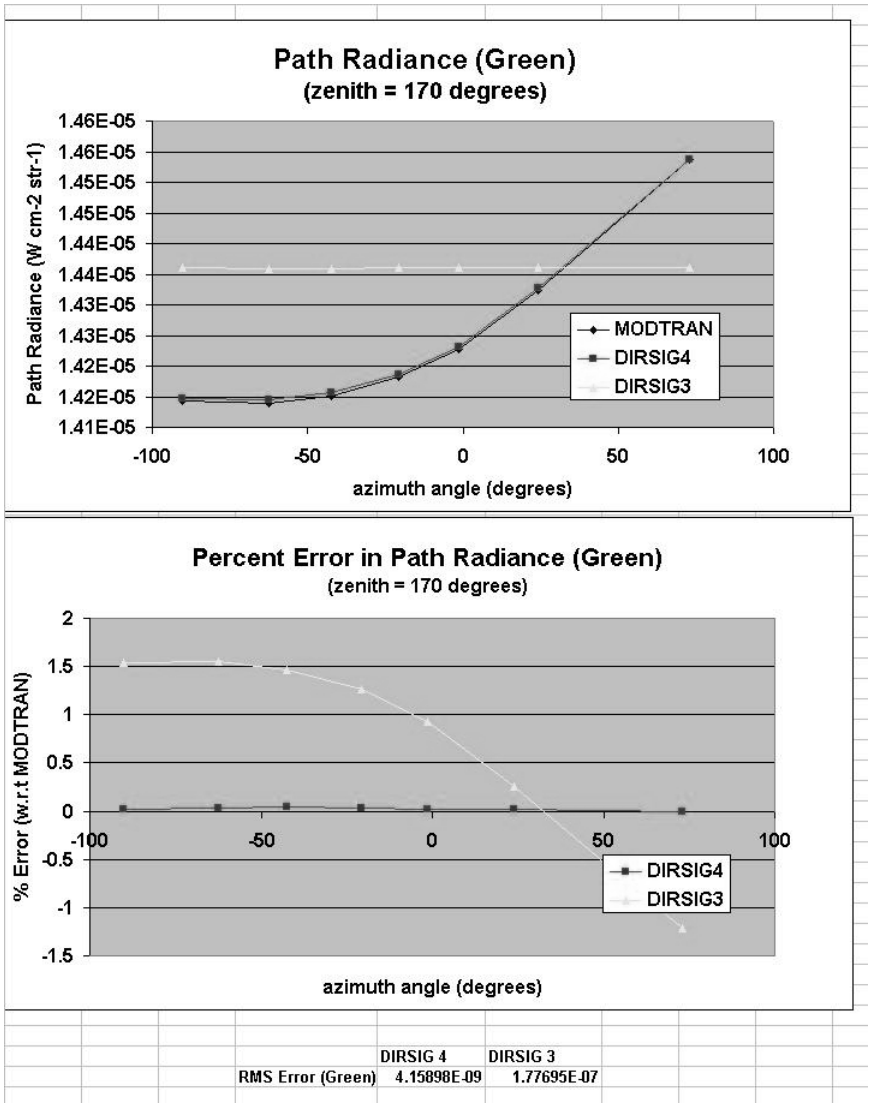

Figure B.12: Test Scene 1a (azimuth variation): The upper graph shows the green path radiance obtained by MODTRAN, DIRSIG 4 and DIRSIG 3. The lower graph shows the percent error of DIRSIG 4 and DIRSIG 3 relative to MODTRAN. The RMS errors for the points shown on the graph are listed below the graphs.

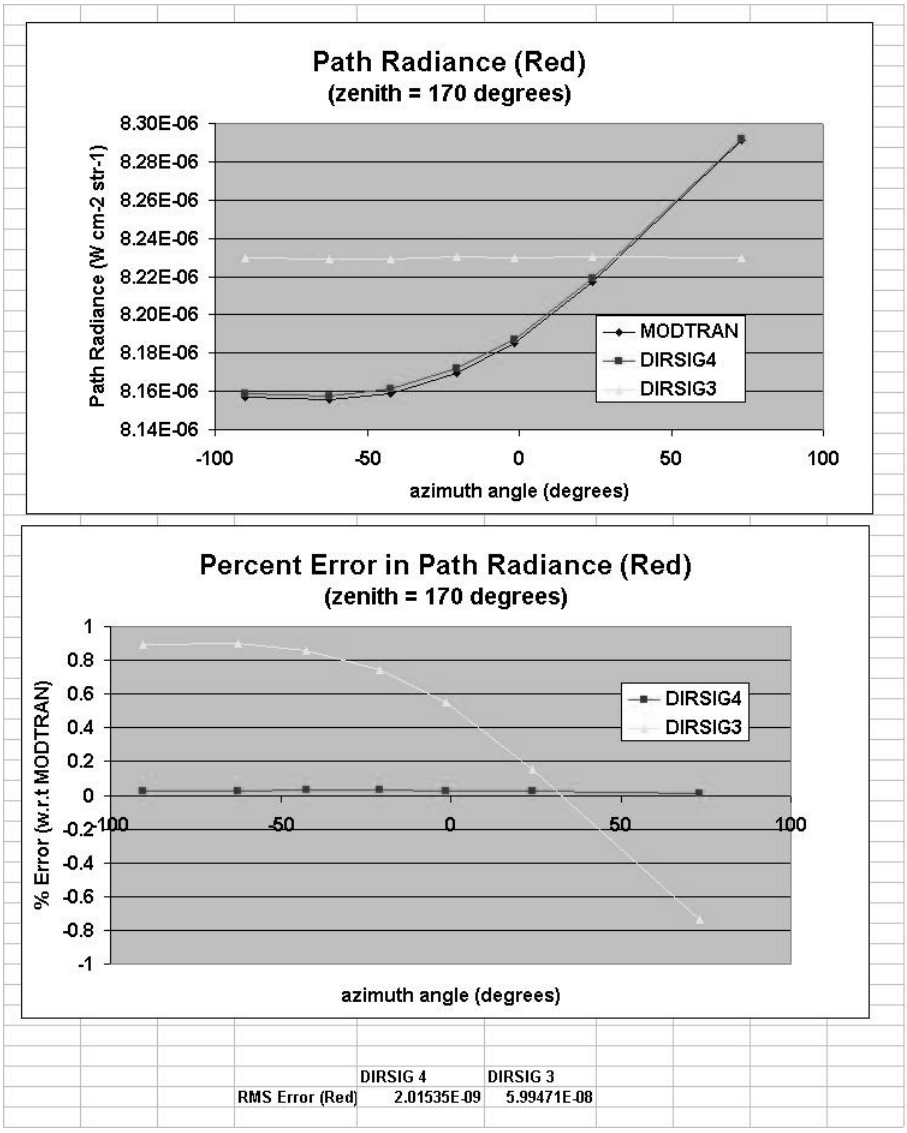

Figure B.13: Test Scene 1a (azimuth variation): The upper graph shows the red path radiance obtained by MODTRAN, DIRSIG 4 and DIRSIG 3. The lower graph shows the percent error of DIRSIG 4 and DIRSIG 3 relative to MODTRAN. The RMS errors for the points shown on the graph are listed below the graphs.

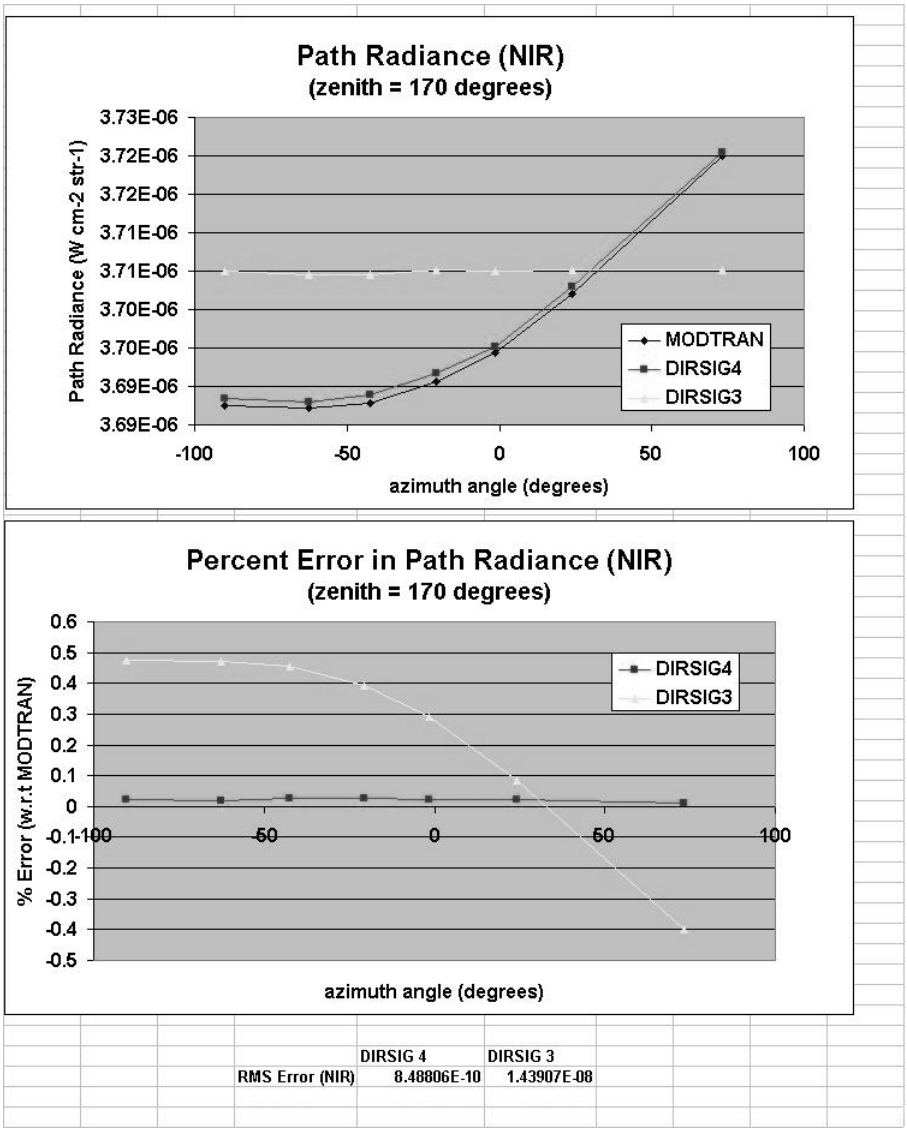

Figure B.14: Test Scene 1a (azimuth variation): The upper graph shows the NIR path radiance obtained by MODTRAN, DIRSIG 4 and DIRSIG 3. The lower graph shows the percent error of DIRSIG 4 and DIRSIG 3 relative to MODTRAN. The RMS errors for the points shown on the graph are listed below the graphs.

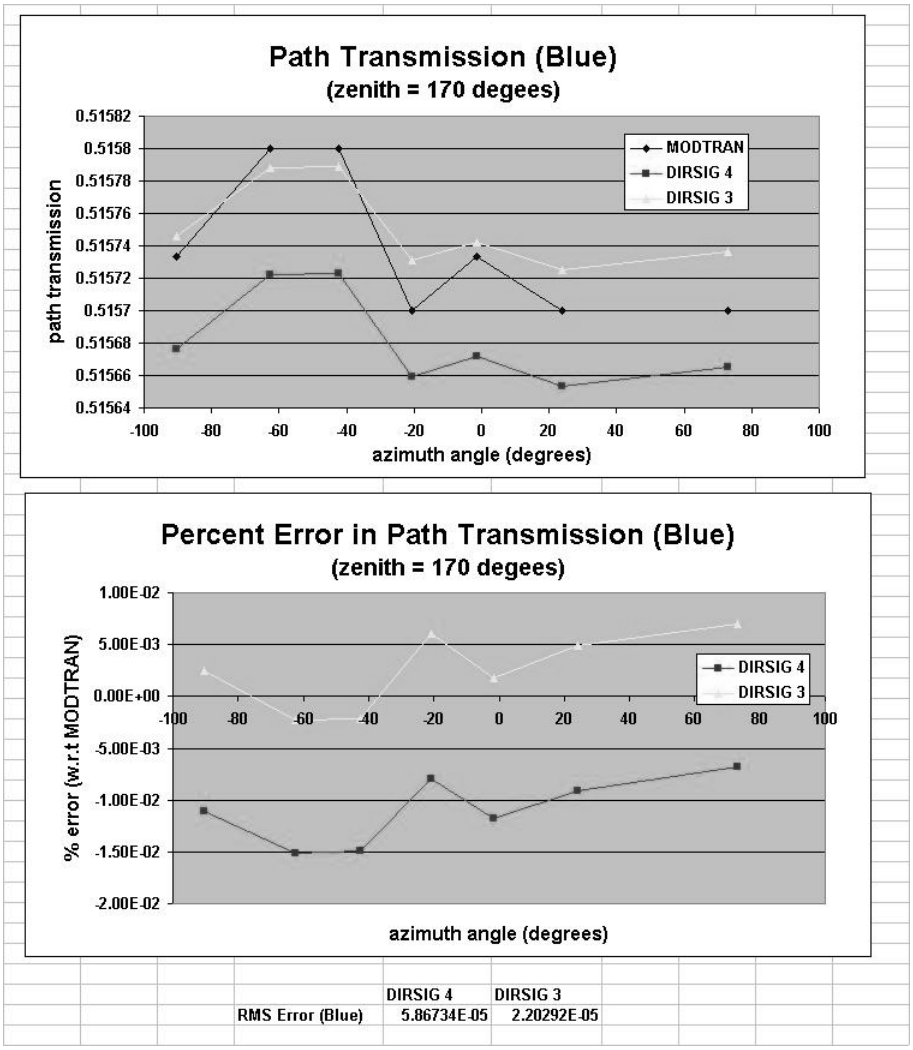

Figure B.15: Test Scene 1a (azimuth variation): The upper graph shows the blue path transmission obtained by MODTRAN, DIRSIG 4 and DIRSIG 3. The lower graph shows the percent error of DIRSIG 4 and DIRSIG 3 relative to MODTRAN. The RMS errors for the points shown on the graph are listed below the graphs.

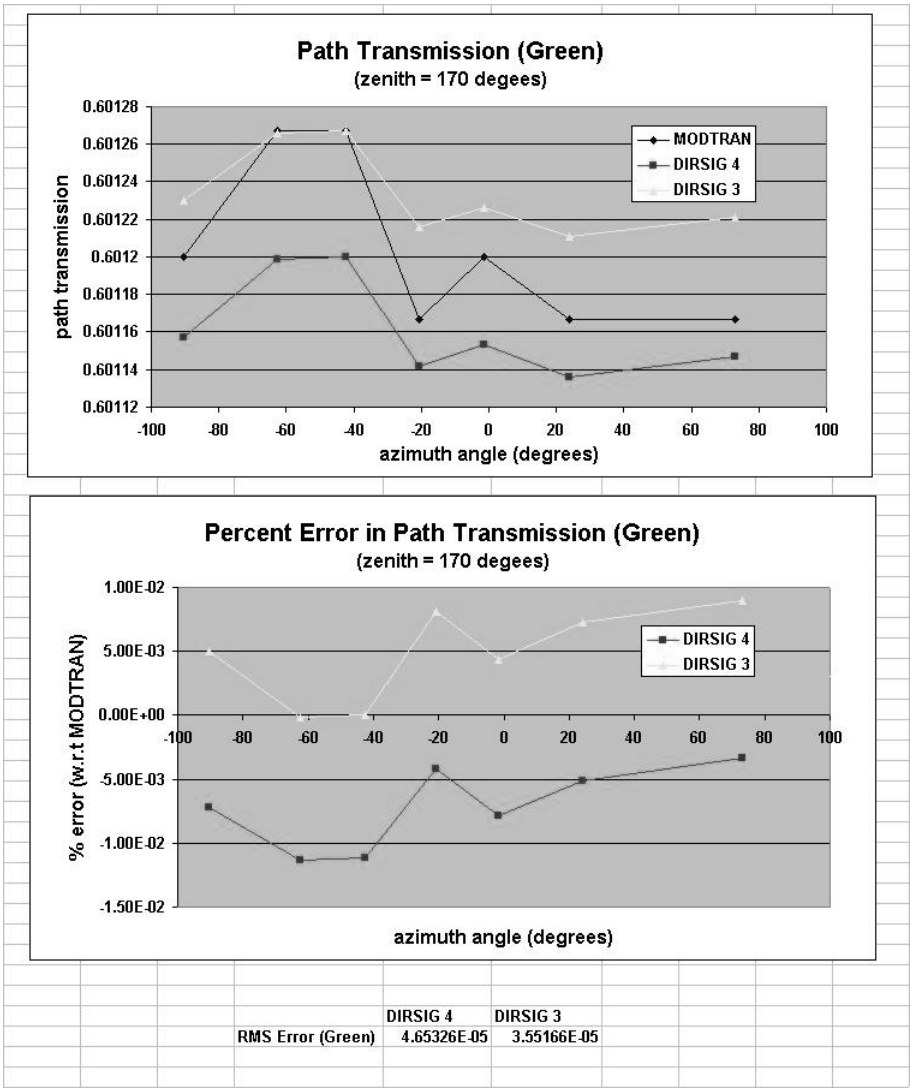

Figure B.16: Test Scene 1a (azimuth variation): The upper graph shows the green path transmission obtained by MODTRAN, DIRSIG 4 and DIRSIG 3. The lower graph shows the percent error of DIRSIG 4 and DIRSIG 3 relative to MODTRAN. The RMS errors for the points shown on the graph are listed below the graphs.

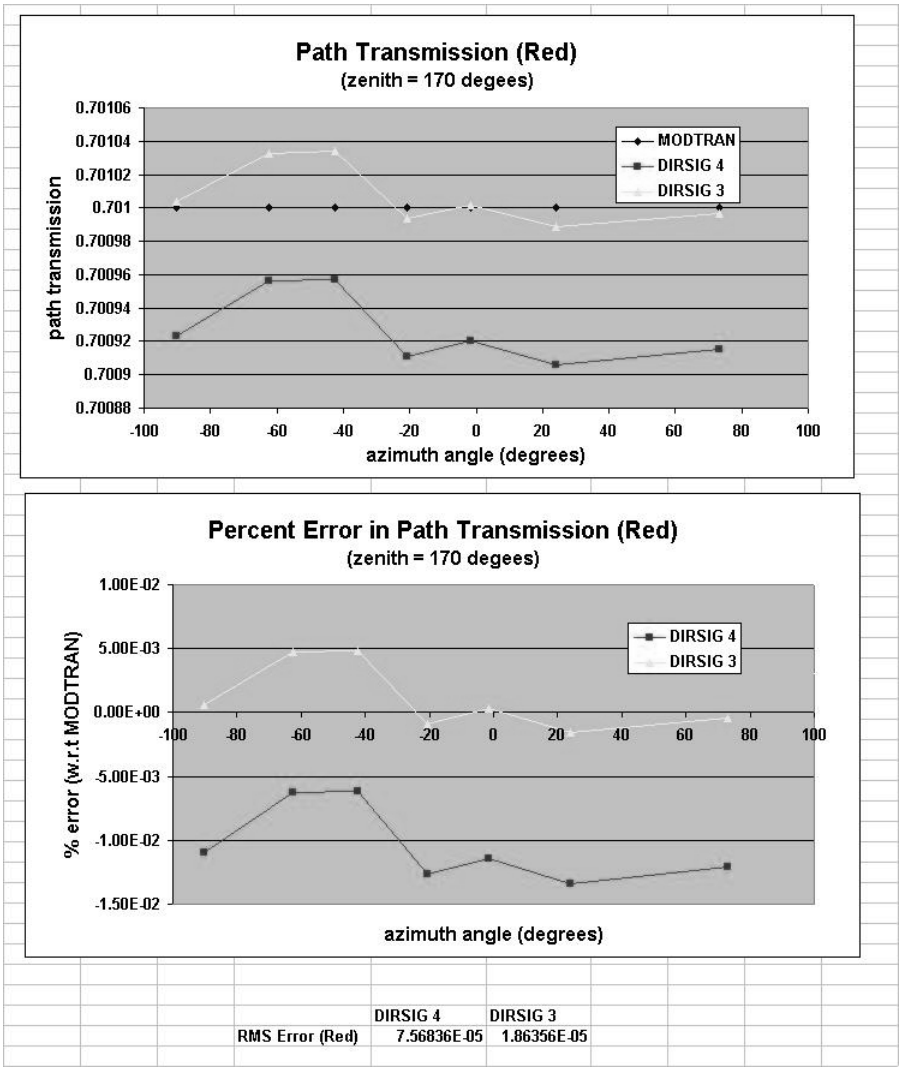

Figure B.17: Test Scene 1a (azimuth variation): The upper graph shows the red path transmission obtained by MODTRAN, DIRSIG 4 and DIRSIG 3. The lower graph shows the percent error of DIRSIG 4 and DIRSIG 3 relative to MODTRAN. The RMS errors for the points shown on the graph are listed below the graphs.

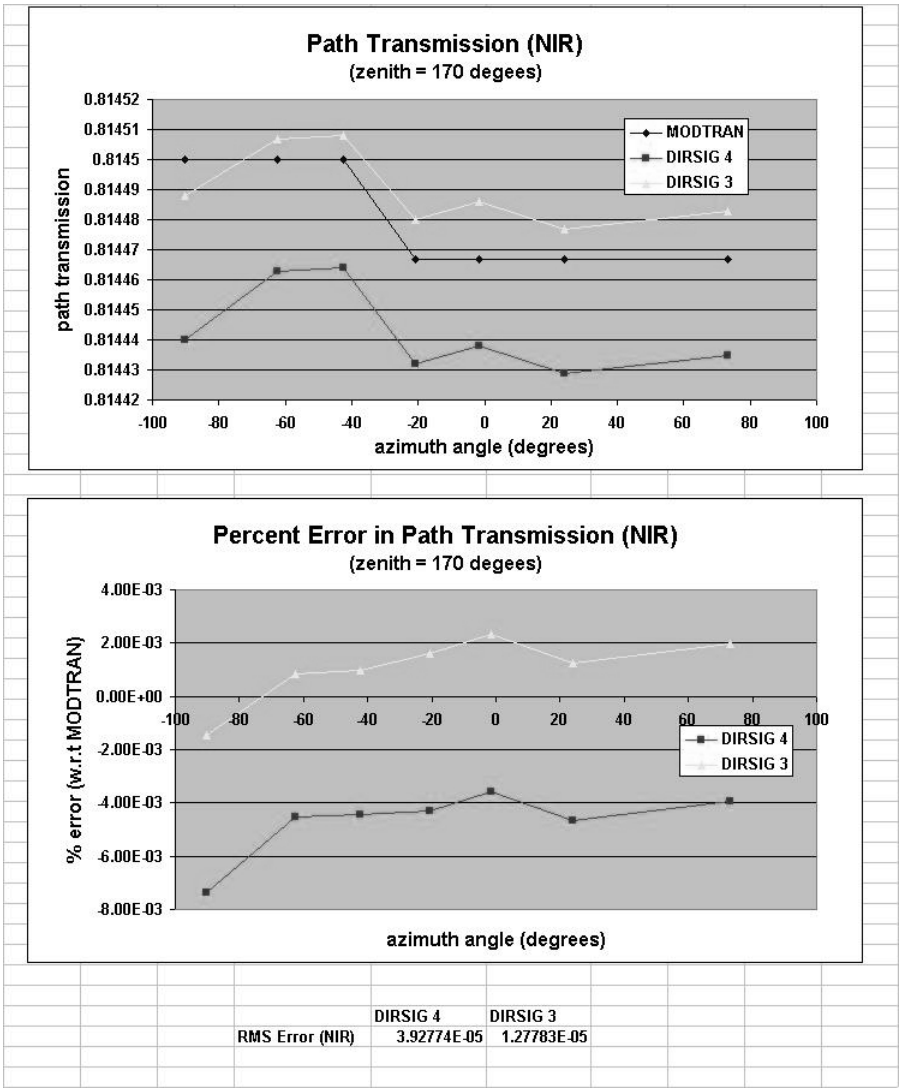

Figure B.18: Test Scene 1a (azimuth variation): The upper graph shows the NIR path transmission obtained by MODTRAN, DIRSIG 4 and DIRSIG 3. The lower graph shows the percent error of DIRSIG 4 and DIRSIG 3 relative to MODTRAN. The RMS errors for the points shown on the graph are listed below the graphs.

B.1.3 Test Image 1a Grid Results

To assess the performance of both interpolators independent of angle, the images were analyzed at nearly regular spatial intervals (see figure B.19). The RMS error for each band was calculated for all of the points. The RMS error (by band) is shown in figure B.20 for the path radiance and in figure B.21 for the transmission.

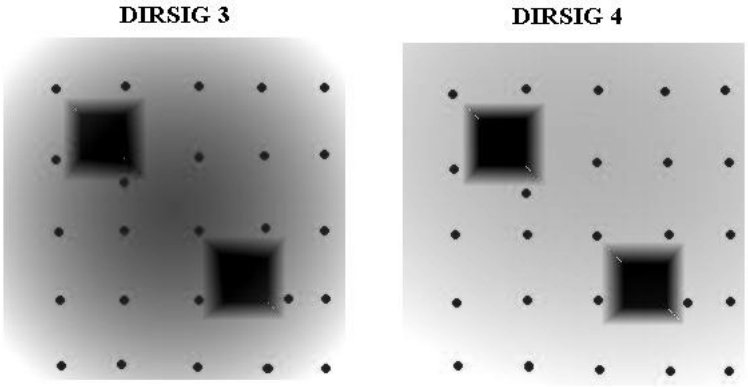

Figure B.19: The dots represent points analyzed in the image.

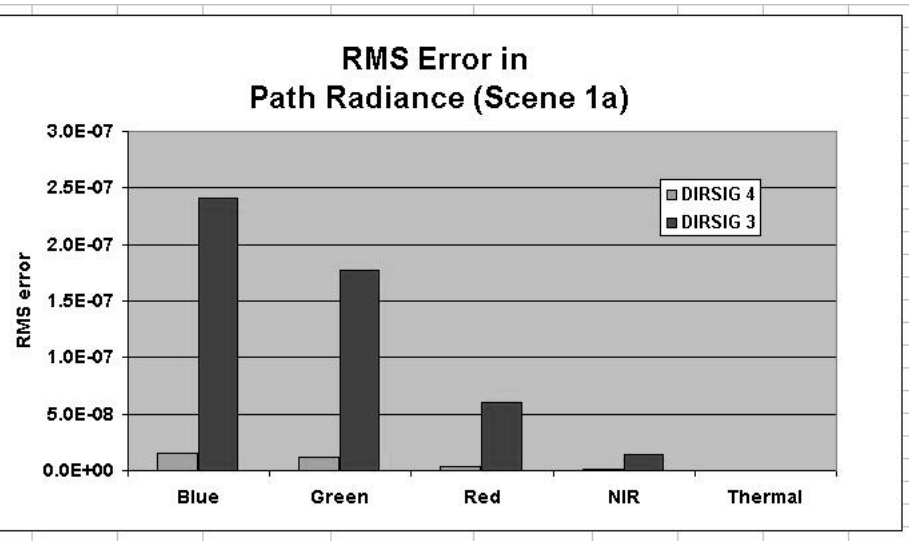

band	DIRSIG 4	DIRSIG 3
Blue	1.558756E-08	2.413167E-07
Green	1.126833E-08	1.769902E-07
Red	3.798459E-09	6.039392E-08
NIR	1.130964E-09	1.458304E-08
Thermal	4.221559E-14	3.120861E-12

Figure B.20: The RMS error in radiance for each band in image 1a.

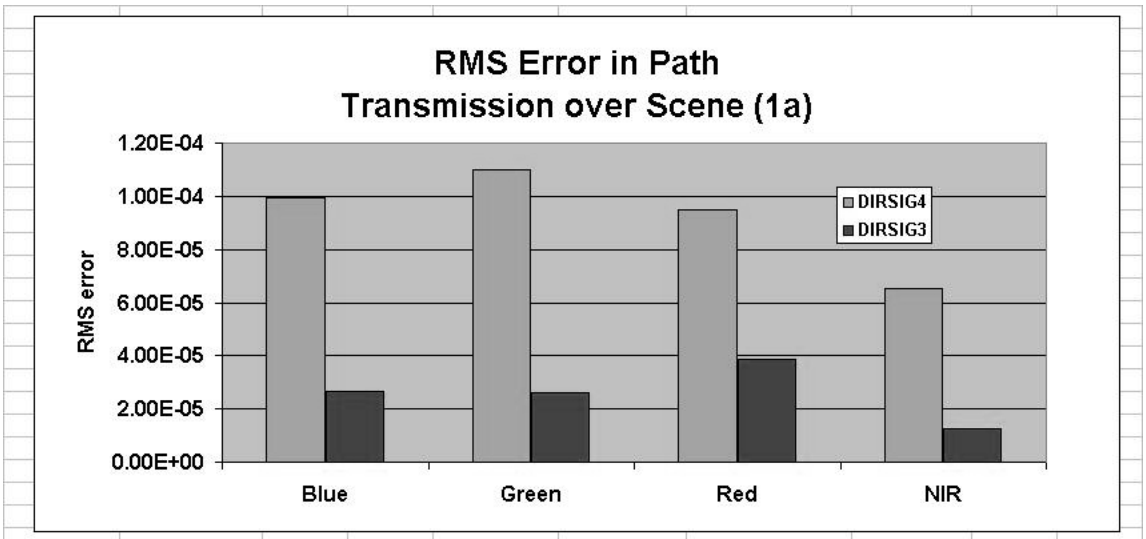

band	DIRSIG4	DIRSIG3
Blue	9.924152E-05	2.639015E-05
Green	1.099000E-04	2.604151E-05
Red	9.466552E-05	3.853362E-05
NIR	6.535105E-05	1.272635E-05
Thermal	6.722192E-04	6.616990E-03

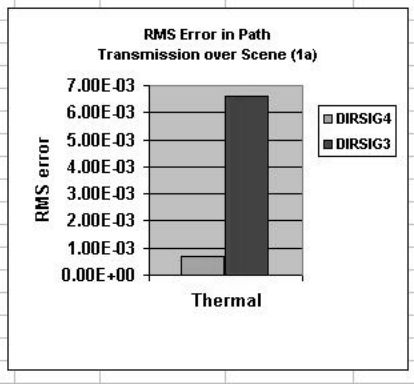

Figure B.21: The RMS error in transmission for each band in image 1a.

B.2 Test Image 1b

This test image is identical to image 1a, the only difference is that it was rendered at noon. The same analysis was done on this image as well. However, because the transmission values will not change with the sun's position, the transmission results for image 1b will be identical to those in 1a, and are therefore omitted.

B.2.1 Test Image 1b Zenith Variation.

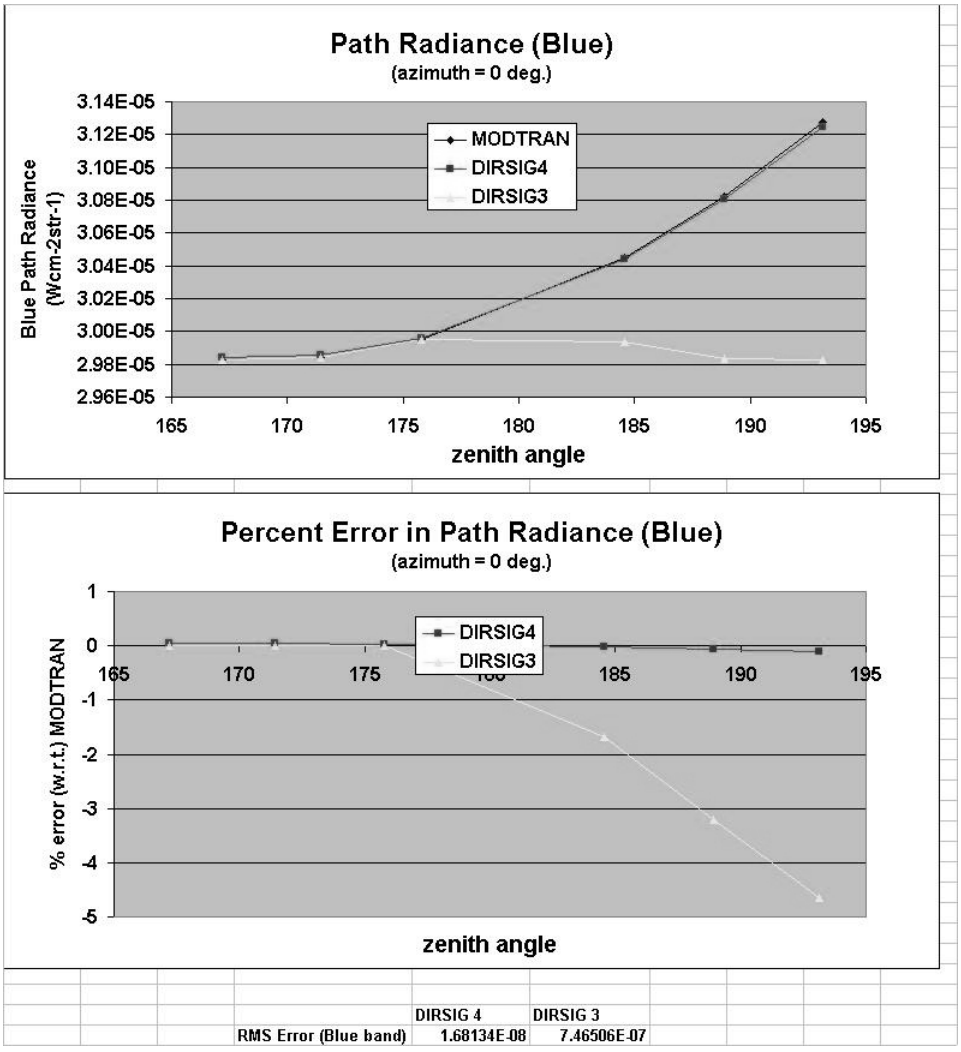

Figure B.22: Test Scene 1b (zenith variation): The upper graph shows the blue path radiance obtained by MODTRAN, DIRSIG 4 and DIRSIG 3. The lower graph shows the percent error of DIRSIG 4 and DIRSIG 3 relative to MODTRAN. The RMS errors for the points shown on the graph are listed below the graphs.

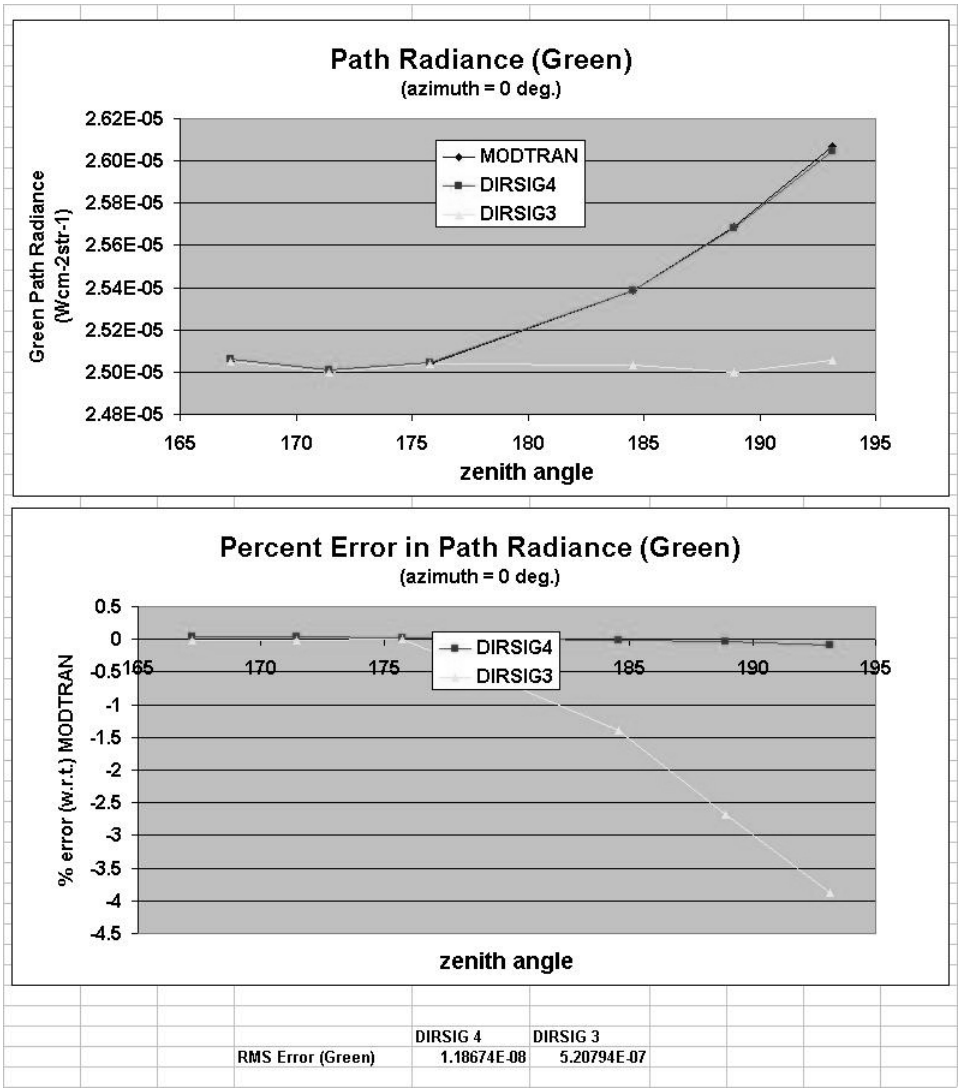

Figure B.23: Test Scene 1b (zenith variation): The upper graph shows the green path radiance obtained by MODTRAN, DIRSIG 4 and DIRSIG 3. The lower graph shows the percent error of DIRSIG 4 and DIRSIG 3 relative to MODTRAN. The RMS errors for the points shown on the graph are listed below the graphs.

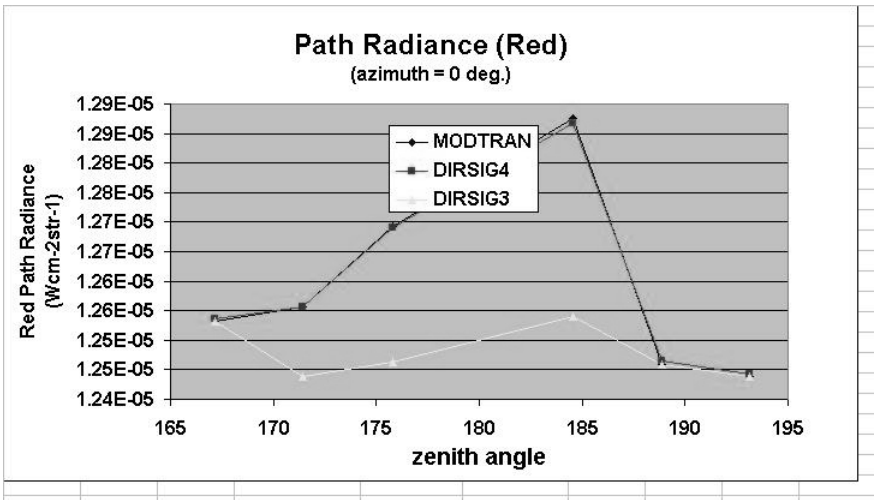

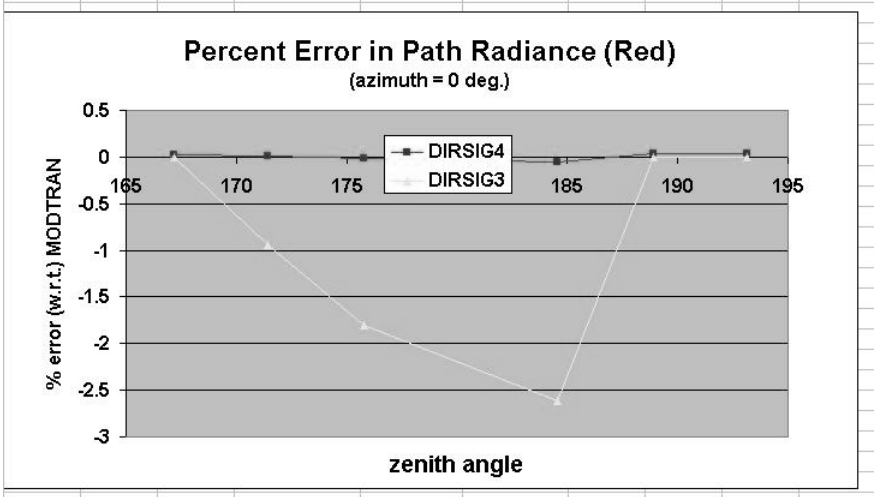

	DIRSIG 4	DIRSIG 3
RMS Error (red)	4.2901E-09	1.72968E-07

Figure B.24: Test Scene 1b (zenith variation): The upper graph shows the red path radiance obtained by MODTRAN, DIRSIG 4 and DIRSIG 3. The lower graph shows the percent error of DIRSIG 4 and DIRSIG 3 relative to MODTRAN. The RMS errors for the points shown on the graph are listed below the graphs.

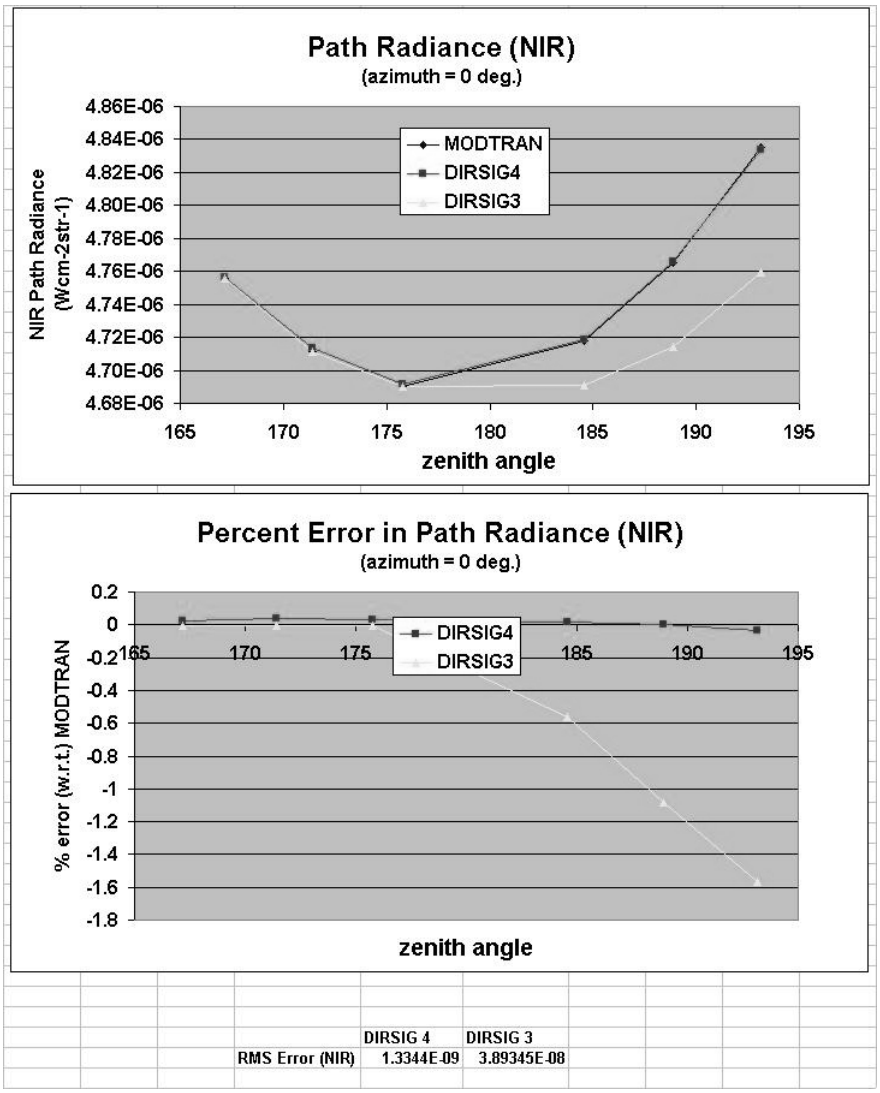

Figure B.25: Test Scene 1b (zenith variation): The upper graph shows the NIR path radiance obtained by MODTRAN, DIRSIG 4 and DIRSIG 3. The lower graph shows the percent error of DIRSIG 4 and DIRSIG 3 relative to MODTRAN. The RMS errors for the points shown on the graph are listed below the graphs.

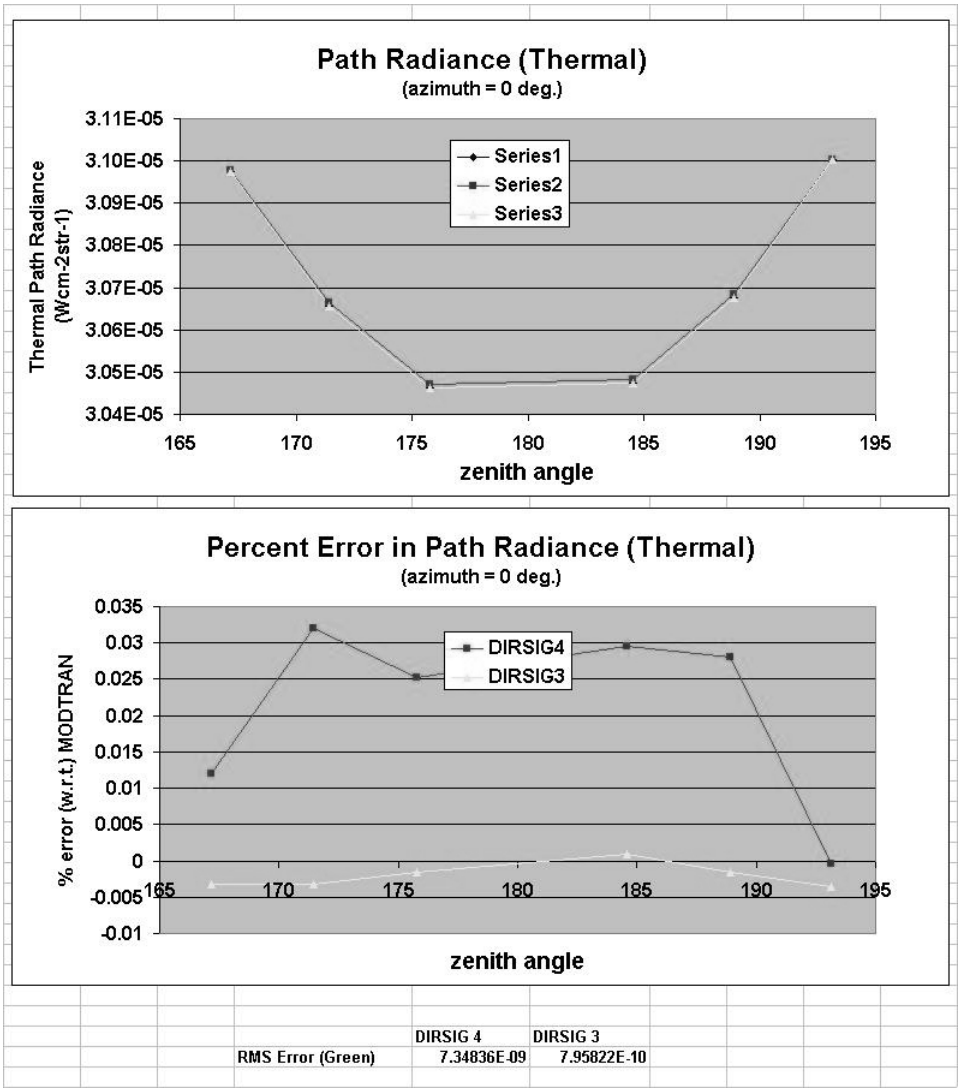

Figure B.26: Test Scene 1b (zenith variation): The upper graph shows the thermal path radiance obtained by MODTRAN, DIRSIG 4 and DIRSIG 3. The lower graph shows the percent error of DIRSIG 4 and DIRSIG 3 relative to MODTRAN. The RMS errors for the points shown on the graph are listed below the graphs.

B.2.2 Test Image 1b Azimuth Variation.

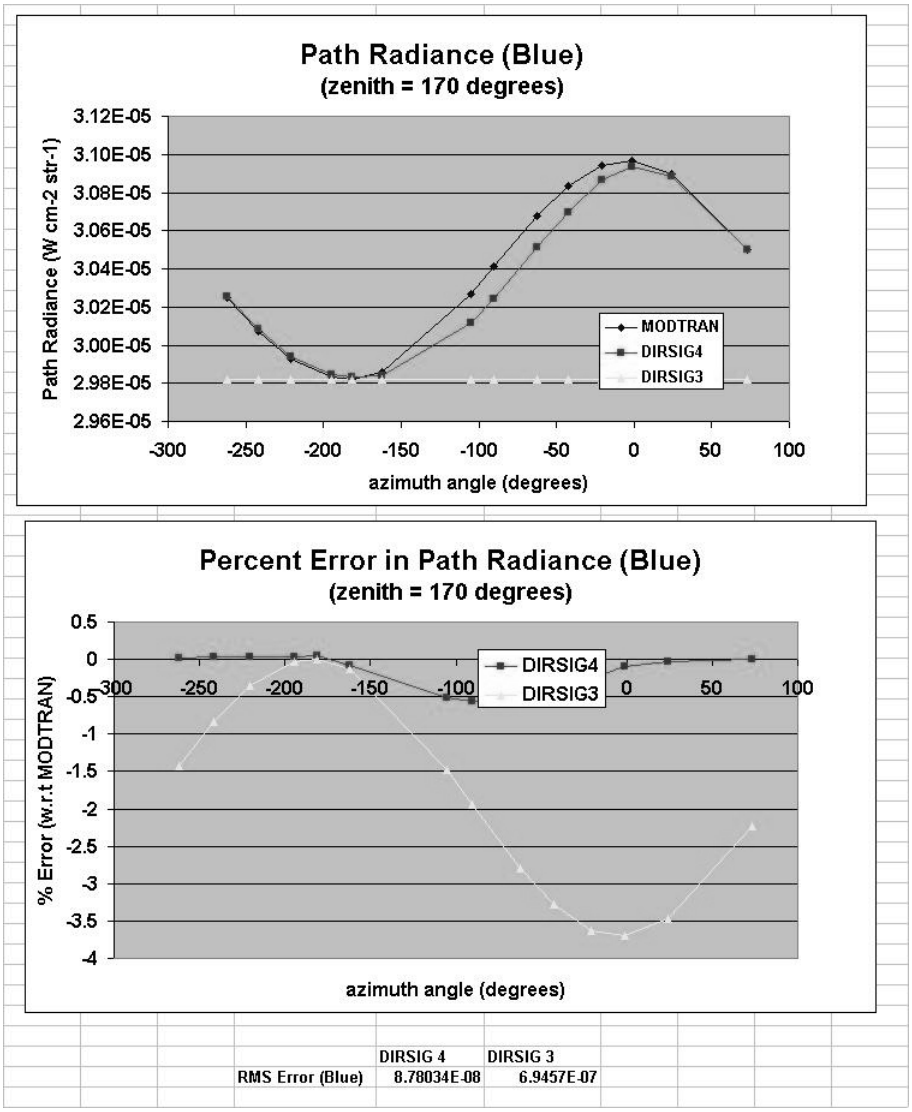

Figure B.27: Test Scene 1b (azimuth variation): The upper graph shows the blue path radiance obtained by MODTRAN, DIRSIG 4 and DIRSIG 3. The lower graph shows the percent error of DIRSIG 4 and DIRSIG 3 relative to MODTRAN. The RMS errors for the points shown on the graph are listed below the graphs.

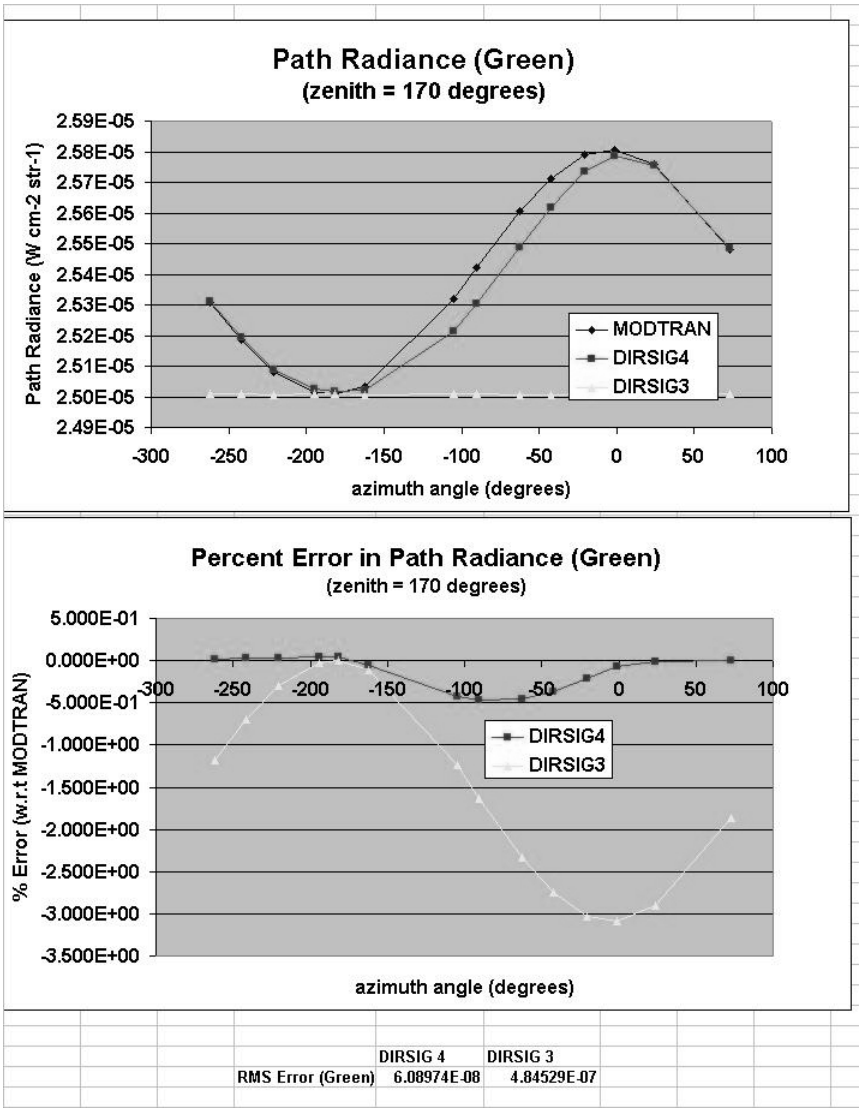

Figure B.28: Test Scene 1b (azimuth variation): The upper graph shows the green path radiance obtained by MODTRAN, DIRSIG 4 and DIRSIG 3. The lower graph shows the percent error of DIRSIG 4 and DIRSIG 3 relative to MODTRAN. The RMS errors for the points shown on the graph are listed below the graphs.

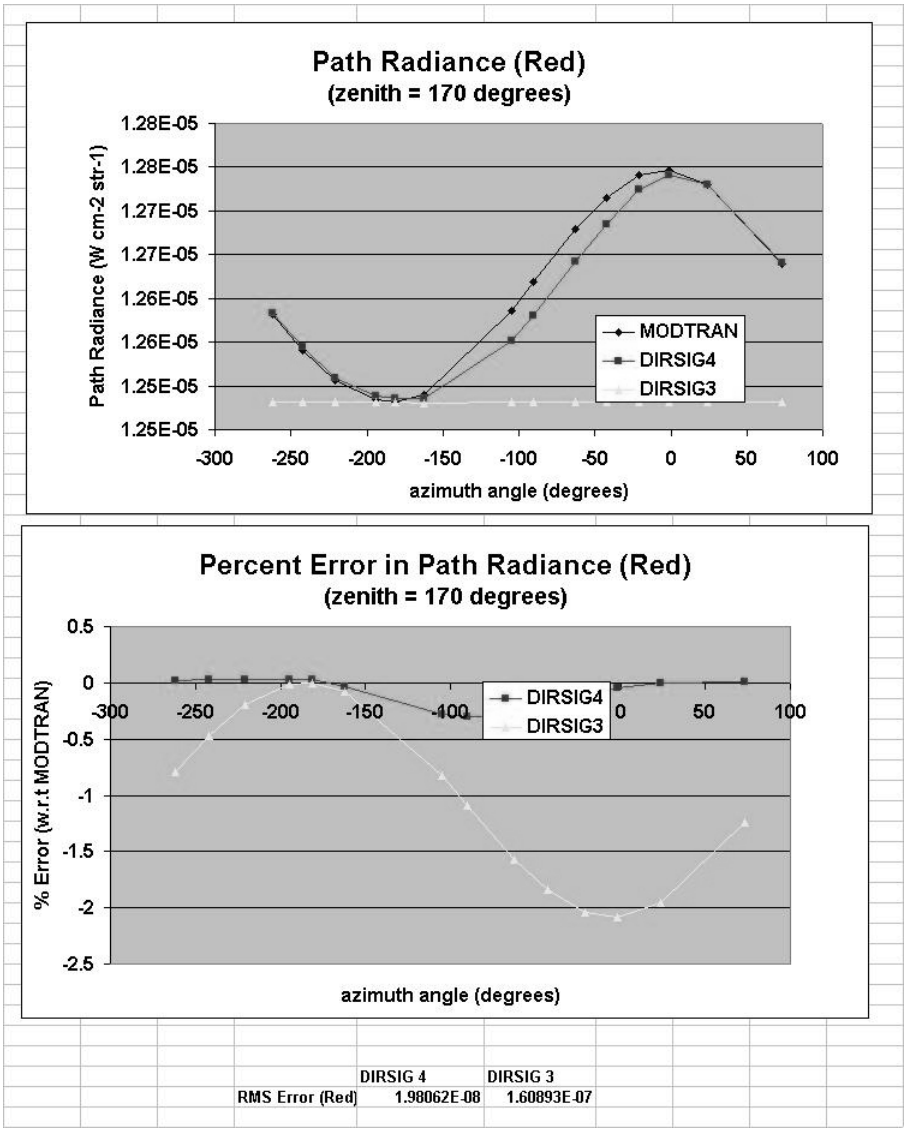

Figure B.29: Test Scene 1b (azimuth variation): The upper graph shows the red path radiance obtained by MODTRAN, DIRSIG 4 and DIRSIG 3. The lower graph shows the percent error of DIRSIG 4 and DIRSIG 3 relative to MODTRAN. The RMS errors for the points shown on the graph are listed below the graphs.

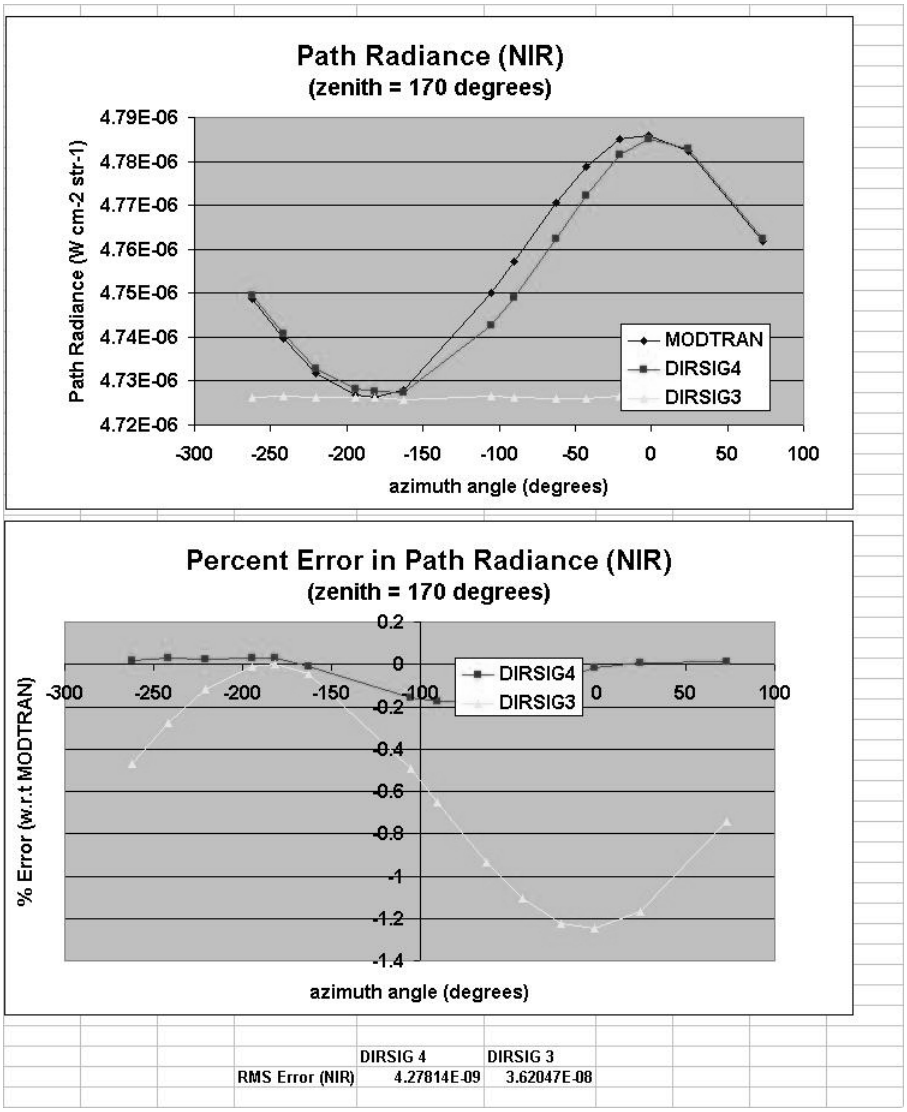

Figure B.30: Test Scene 1b (azimuth variation): The upper graph shows the NIR path radiance obtained by MODTRAN, DIRSIG 4 and DIRSIG 3. The lower graph shows the percent error of DIRSIG 4 and DIRSIG 3 relative to MODTRAN. The RMS errors for the points shown on the graph are listed below the graphs.

In many of the graphs analyzing the azimuth dimension, an asymmetry is seen in the DIRSIG 4 results. This is most likely due to two aspects of the ADB generation code. The first is that the interpolator only samples half of the atmosphere. It calculates the solar azimuth angle, and samples between this angle and 180 degrees of this angle. When DIRSIG encounters values which are greater than 180 plus the solar azimuth angle, it substitutes values reflected through the solar azimuth line. The second aspect which actually causes this error is in the method by which the solar azimuth angle is sampled. If this angle is not calculated exactly, then the symmetry can not be exploited fully. Figure B.31 shows a graphic, where the elliptical shape represents path radiance. The radius that the line is from the center of the image represents the radiance. The line from the sun represents the true solar azimuth line.

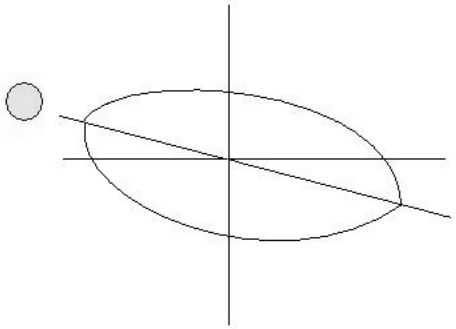

Figure B.31: A graphic representing the path radiance as seen from overhead.

Now, figure B.32 shows an overlay of a grey line, representing the calculated solar azimuth angle. The dots represent the sampling of upwelled radiance. Above the solar azimuth line shows real samples, and those below show the values found throughout the exploitation of the symmetry. As you can see, if the solar azimuth angle is mis-calculated, the values below (in the graphic) will not be properly represented by those above the line. It is this discrepancy which is most likely behind the apparent asymmetry of the DIRSIG 4 results seen in figures B.27 and B.39, to name a few. This explains why on about half of the azimuth angles, DIRSIG 4 matches MODTRAN nicely, but on the other half (*not* directly sampled), the values do not match up. DIRSIG 4 itself is self-symmetric, but is off from the true MODTRAN values because of a poor solar azimuth angle estimation.

This problem can easily be fixed in implementation by using a more robust calculation of the solar azimuth angle. These tools may already exist in other modules of DIRSIG.

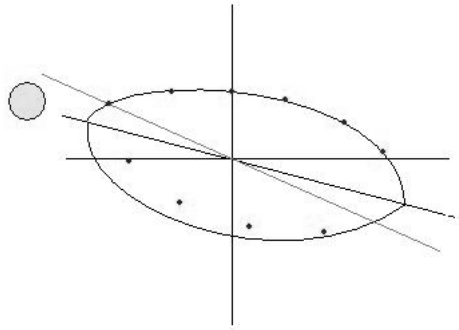

Figure B.32: A graphic representing the source of the asymmetry error in the DIRSIG 4 results.

B.2.3 Test Image 1b Grid Results.

To assess the performance of both interpolators independent of angle, the images were analyzed at nearly regular spatial intervals (see figure B.19). The RMS error for each band was calculated for all of the points, as in image 1a. The RMS error (by band) in path radiance is shown in figure B.33.

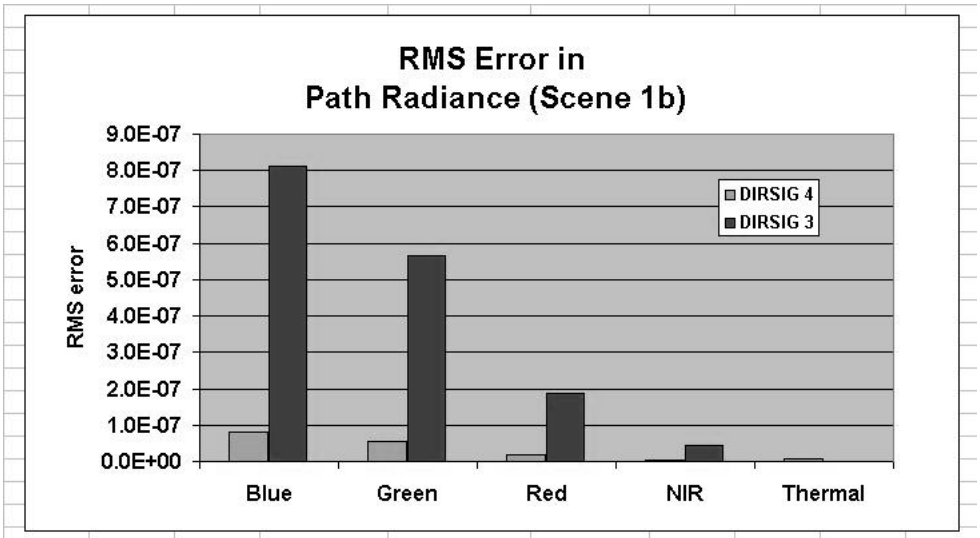

band	DIRSIG 4	DIRSIG 3
Blue	7.974398E-08	8.101502E-07
Green	5.502845E-08	5.653977E-07
Red	1.772793E-08	1.878260E-07
NIR	3.818577E-09	4.228025E-08
Thermal	7.452302E-09	1.197330E-09

Figure B.33: The RMS error in radiance for each band in image 1b.

B.3 Test Image 1c

This test image is identical to image 1a, the only difference is that it was rendered at sunrise. The same analysis was done on this image as well. However, because the transmission values will not change with the sun's position, the results for image 1c will be identical to those in 1a. Those transmission analysis results are omitted.

B.3.1 Test Image 1c Zenith Variation.

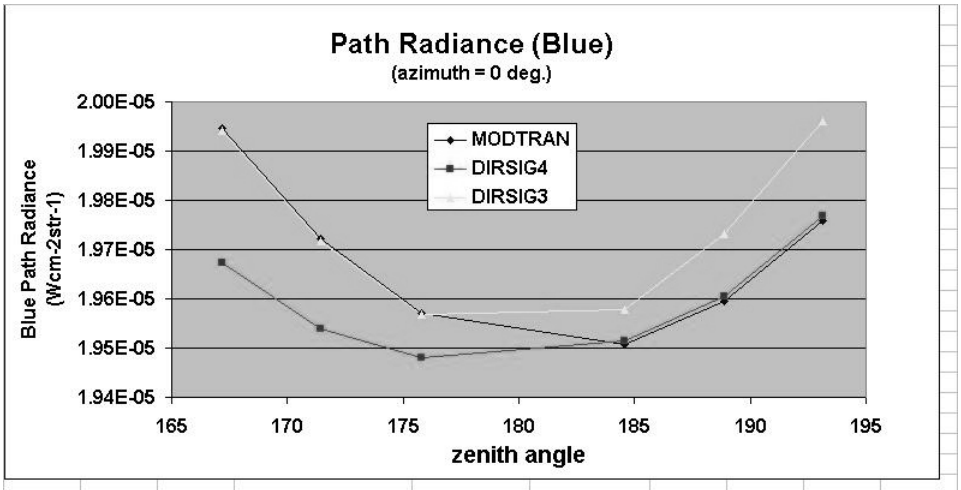

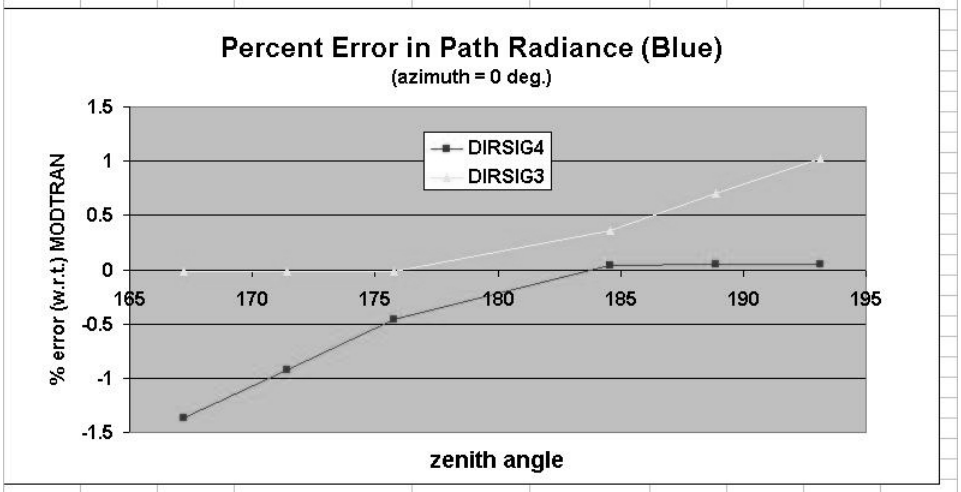

	DIRSIG 4	DIRSIG 3
RMS Error (Blue band)	1.39194E-07	1.04088E-07

Figure B.34: Test Scene 1c (zenith variation): The upper graph shows the blue path radiance obtained by MODTRAN, DIRSIG 4 and DIRSIG 3. The lower graph shows the percent error of DIRSIG 4 and DIRSIG 3 relative to MODTRAN. The RMS errors for the points shown on the graph are listed below the graphs.

The error in DIRSIG 4's results are a bit higher in test scene 1c than in scenes 1b and 1a. This discrepancy in values is existent in the adb and is not a result of the interpolator. This error is just an example of the fact that the DIRSIG 3 ADB samples at the azimuth value of 0, and the DIRSIG 4 ABD samples about the solar azimuth angle. Due to the low sun angle in this test scene, the azimuthal variation of the solar path radiance is high, and therefore the error is amplified.

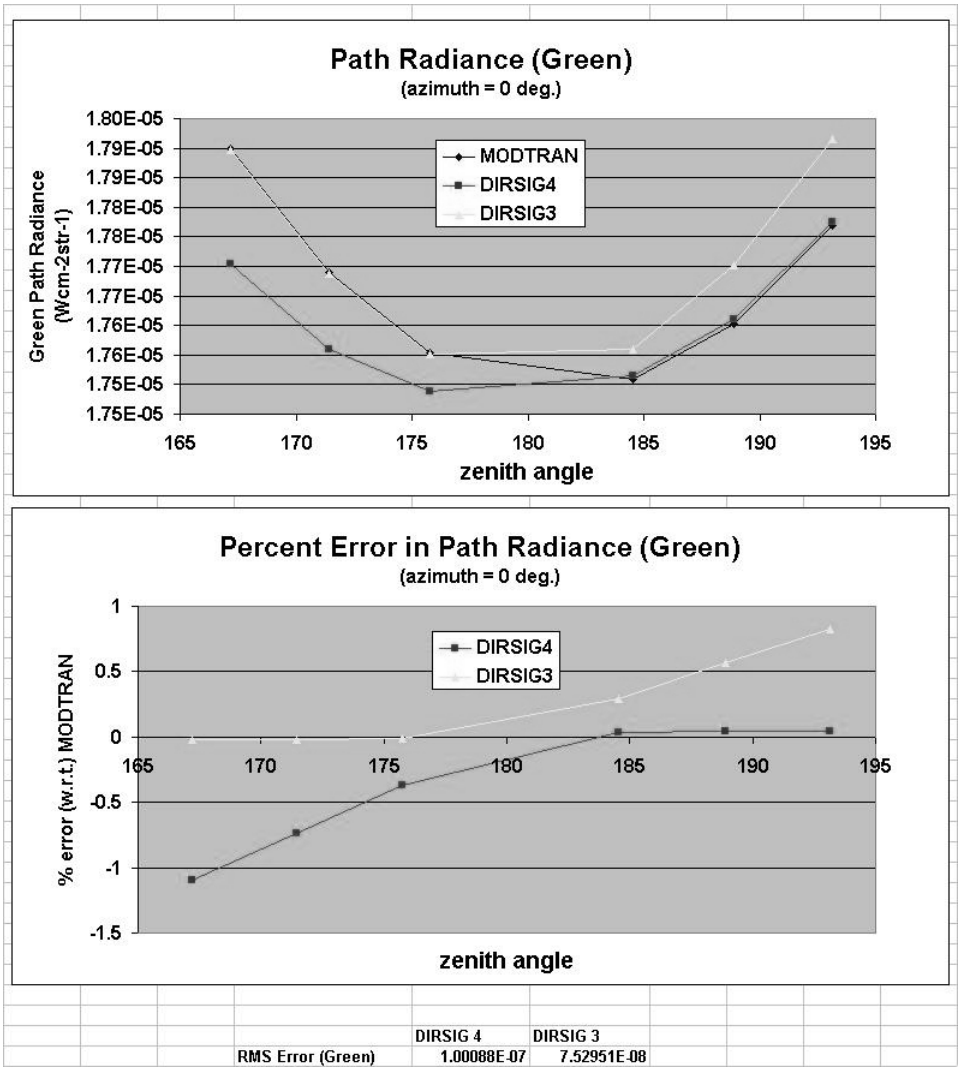

Figure B.35: Test Scene 1c (zenith variation): The upper graph shows the green path radiance obtained by MODTRAN, DIRSIG 4 and DIRSIG 3. The lower graph shows the percent error of DIRSIG 4 and DIRSIG 3 relative to MODTRAN. The RMS errors for the points shown on the graph are listed below the graphs.

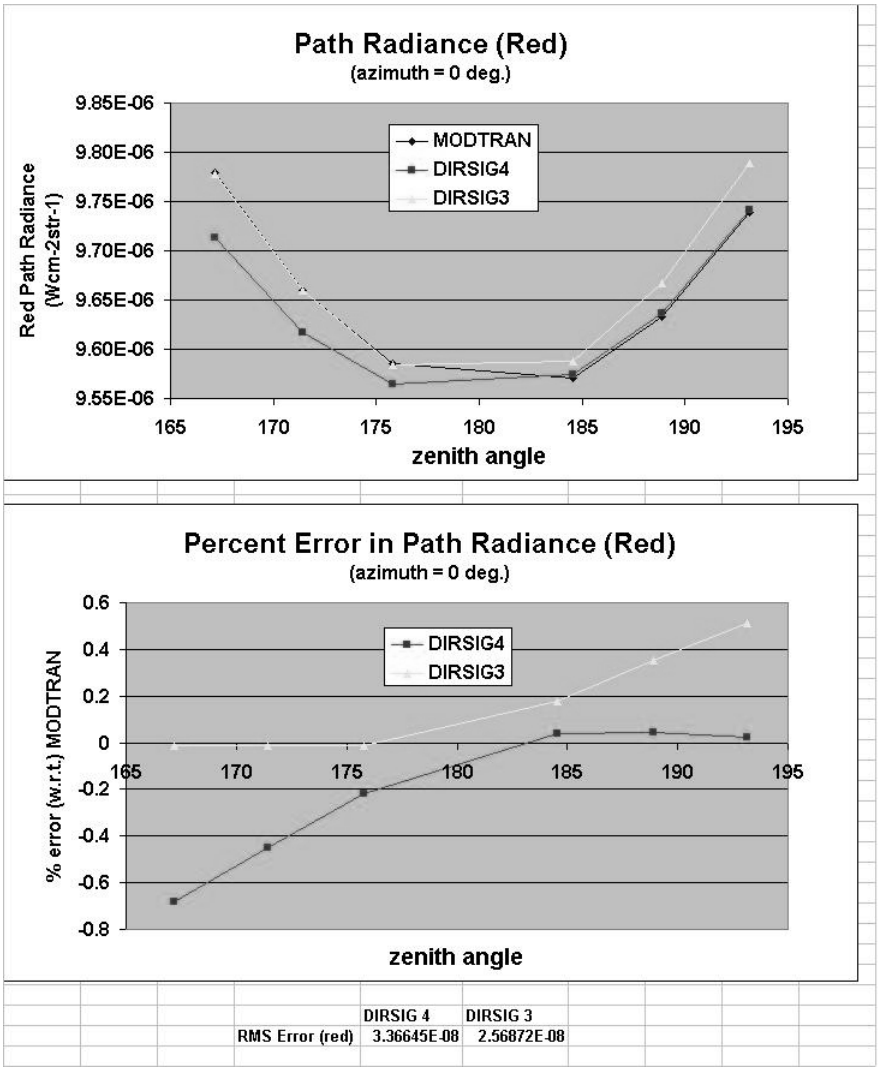

	DIRSIG 4	DIRSIG 3
RMS Error (red)	3.36645E-08	2.56872E-08

Figure B.36: Test Scene 1c (zenith variation): The upper graph shows the red path radiance obtained by MODTRAN, DIRSIG 4 and DIRSIG 3. The lower graph shows the percent error of DIRSIG 4 and DIRSIG 3 relative to MODTRAN. The RMS errors for the points shown on the graph are listed below the graphs.

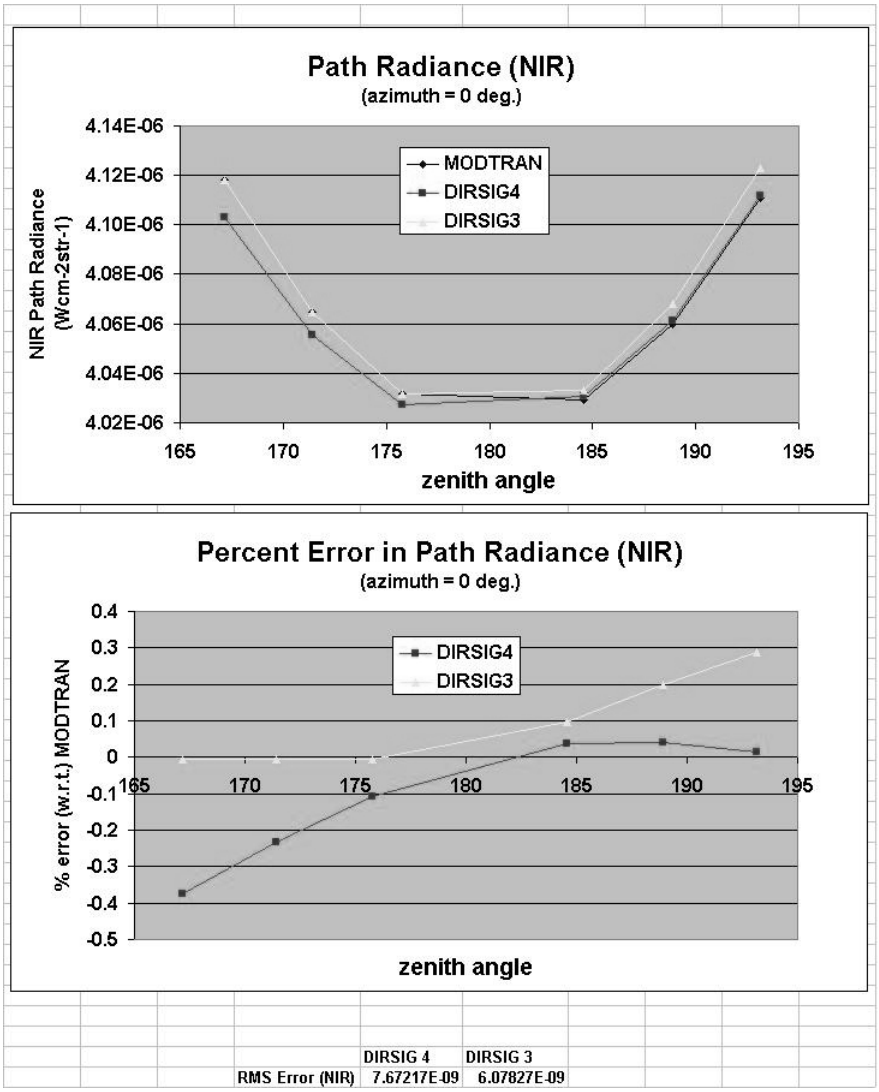

Figure B.37: Test Scene 1c (zenith variation): The upper graph shows the NIR path radiance obtained by MODTRAN, DIRSIG 4 and DIRSIG 3. The lower graph shows the percent error of DIRSIG 4 and DIRSIG 3 relative to MODTRAN. The RMS errors for the points shown on the graph are listed below the graphs.

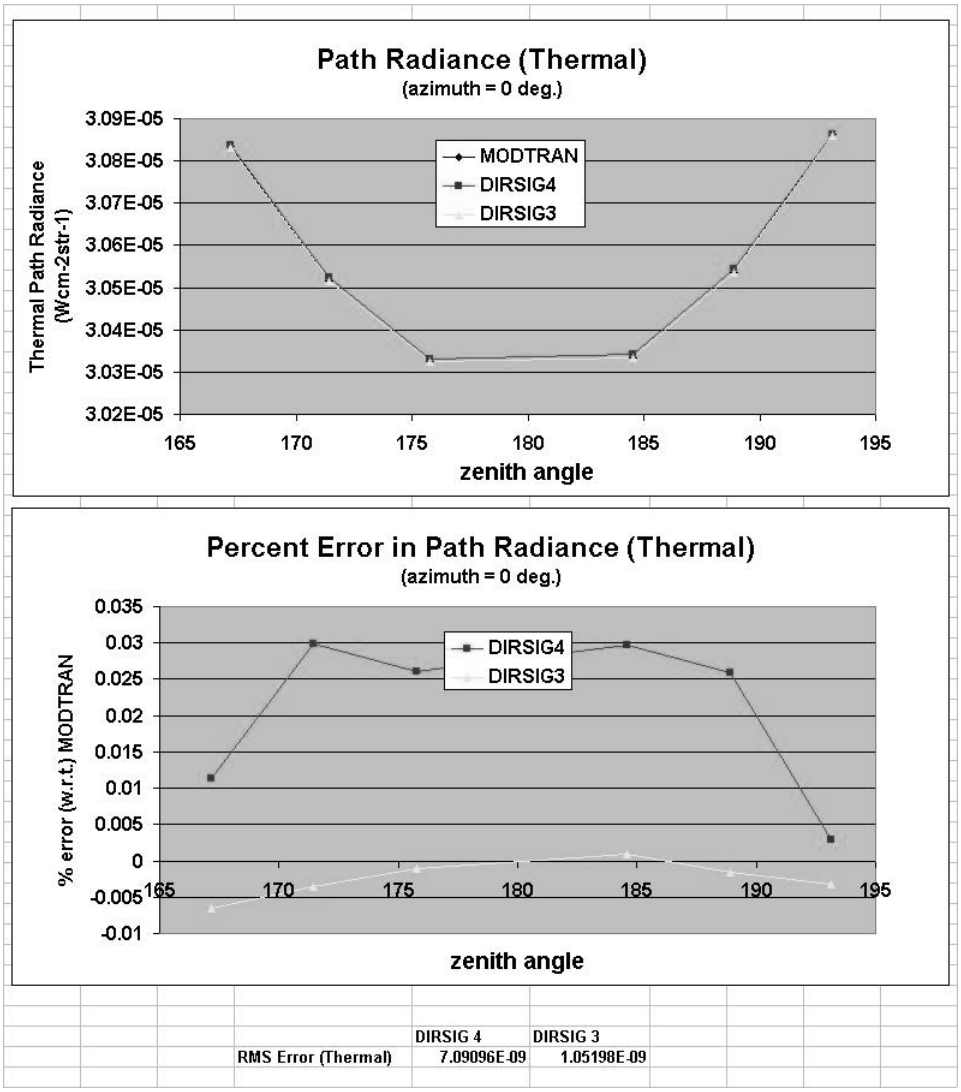

Figure B.38: Test Scene 1c (zenith variation): The upper graph shows the thermal path radiance obtained by MODTRAN, DIRSIG 4 and DIRSIG 3. The lower graph shows the percent error of DIRSIG 4 and DIRSIG 3 relative to MODTRAN. The RMS errors for the points shown on the graph are listed below the graphs.

B.3.2 Test Image 1c Azimuth Variation.

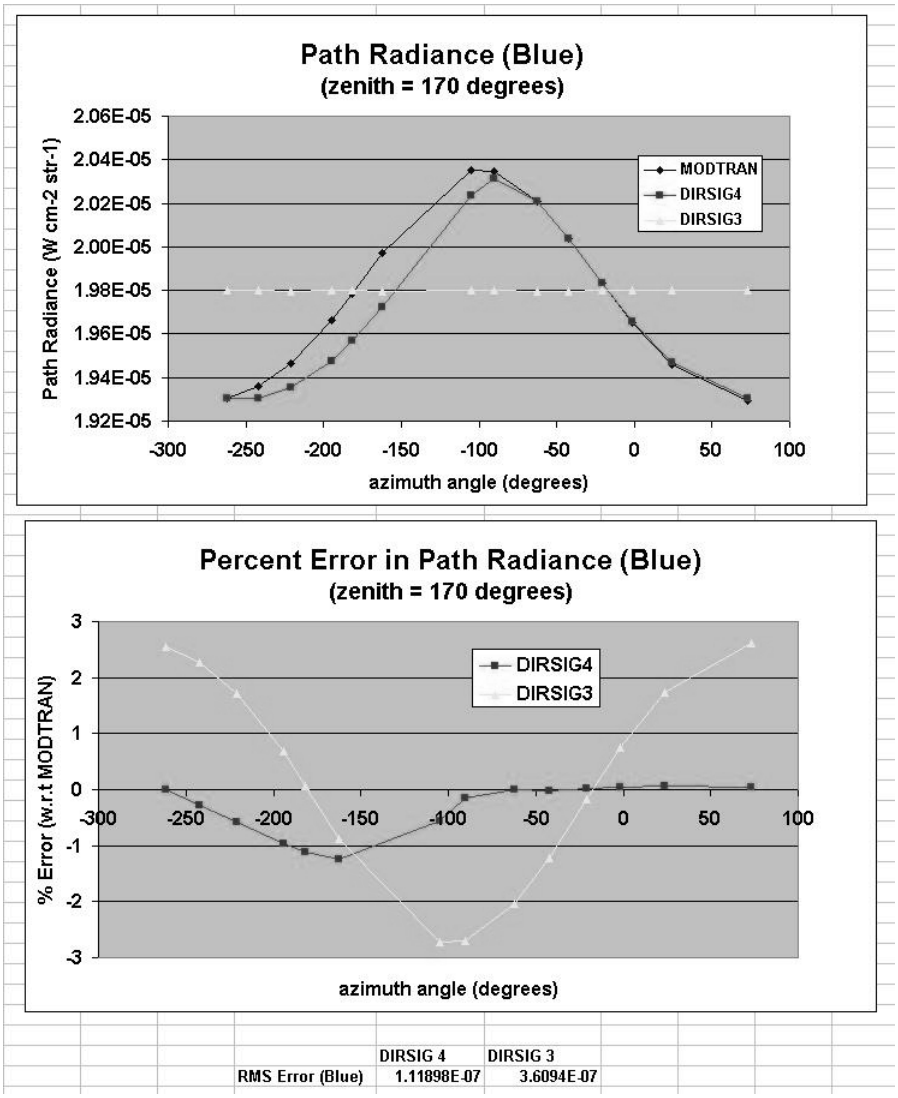

Figure B.39: Test Scene 1c (azimuth variation): The upper graph shows the blue path radiance obtained by MODTRAN, DIRSIG 4 and DIRSIG 3. The lower graph shows the percent error of DIRSIG 4 and DIRSIG 3 relative to MODTRAN. The RMS errors for the points shown on the graph are listed below the graphs.

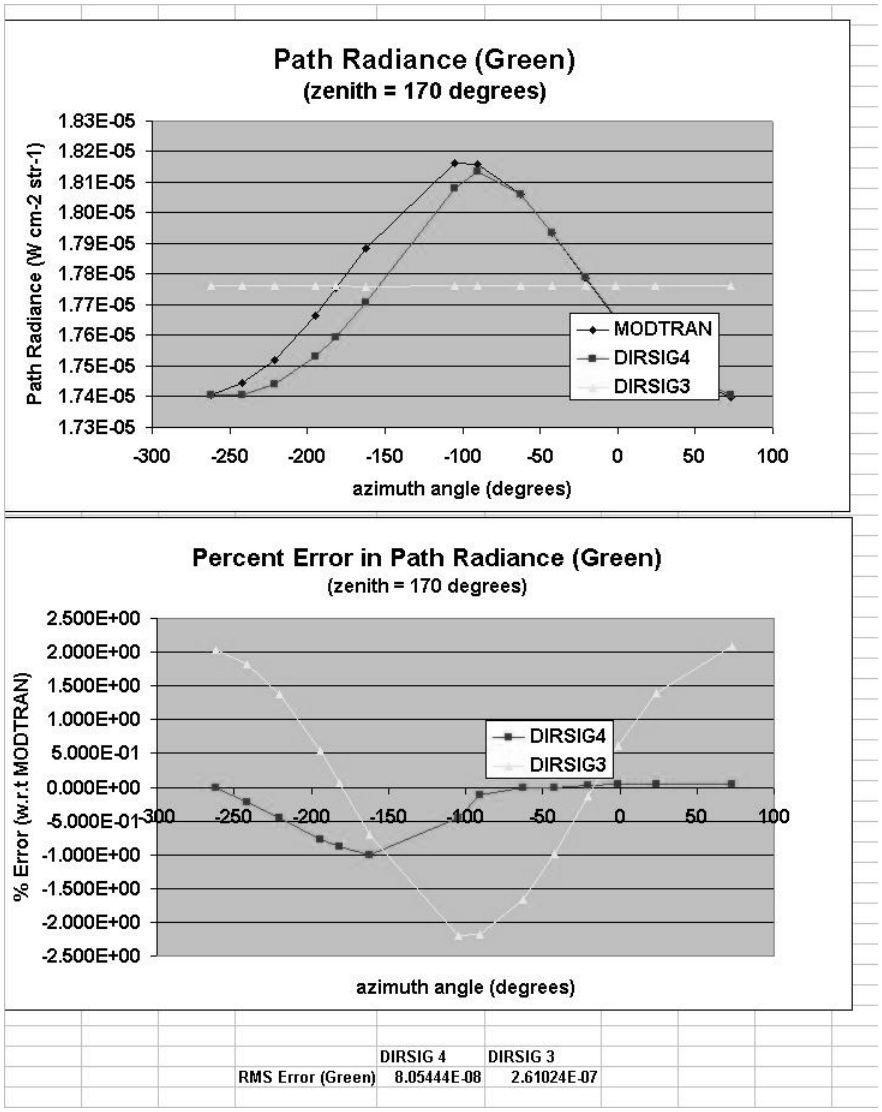

Figure B.40: Test Scene 1c (azimuth variation): The upper graph shows the green path radiance obtained by MODTRAN, DIRSIG 4 and DIRSIG 3. The lower graph shows the percent error of DIRSIG 4 and DIRSIG 3 relative to MODTRAN. The RMS errors for the points shown on the graph are listed below the graphs.

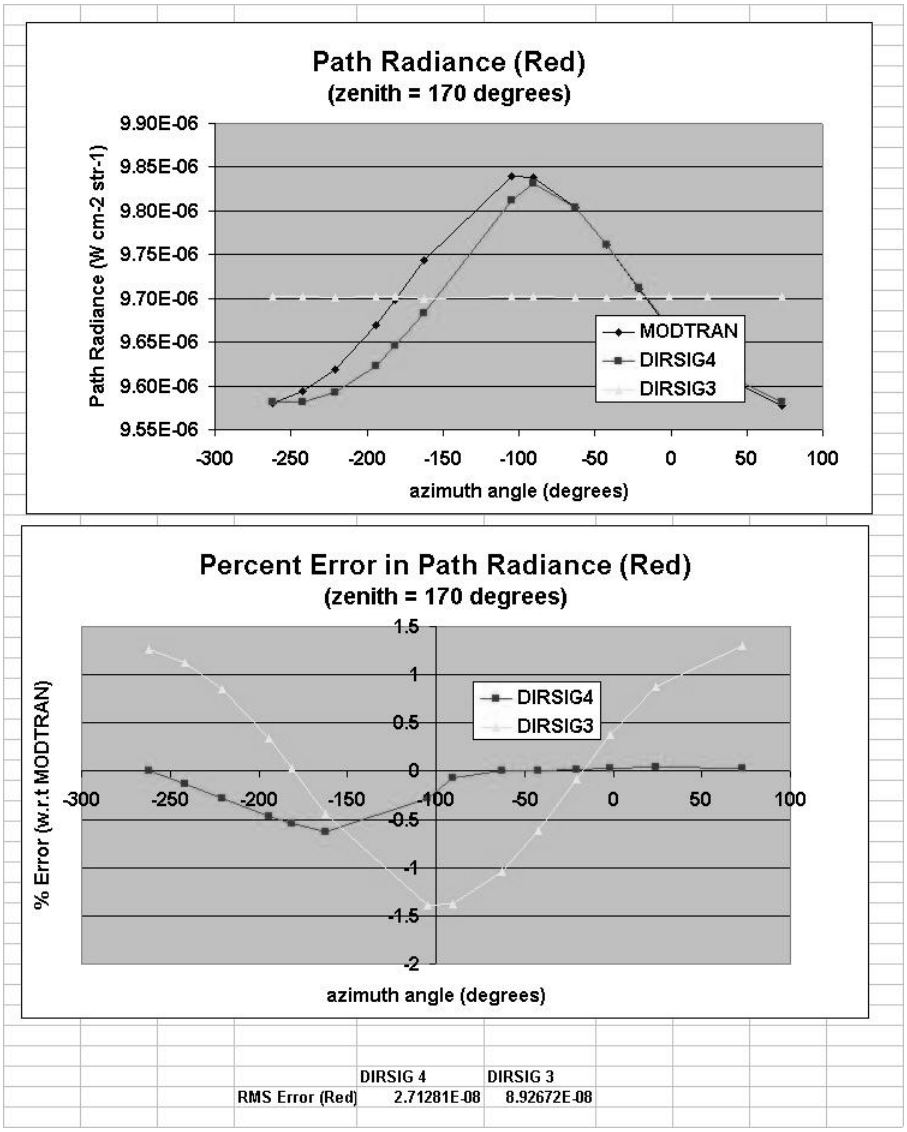

Figure B.41: Test Scene 1c (azimuth variation): The upper graph shows the red path radiance obtained by MODTRAN, DIRSIG 4 and DIRSIG 3. The lower graph shows the percent error of DIRSIG 4 and DIRSIG 3 relative to MODTRAN. The RMS errors for the points shown on the graph are listed below the graphs.

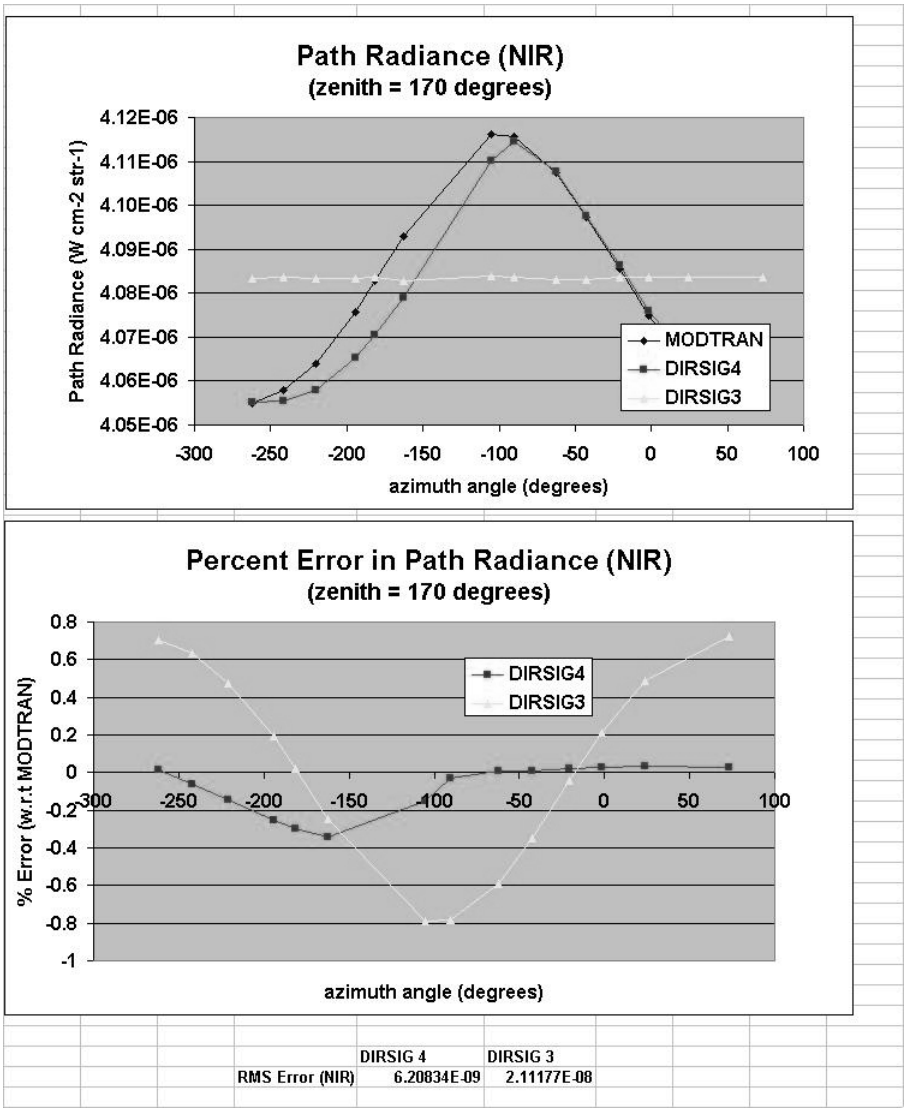

Figure B.42: Test Scene 1c (azimuth variation): The upper graph shows the NIR path radiance obtained by MODTRAN, DIRSIG 4 and DIRSIG 3. The lower graph shows the percent error of DIRSIG 4 and DIRSIG 3 relative to MODTRAN. The RMS errors for the points shown on the graph are listed below the graphs.

B.3.3 Test Image 1c Grid Results.

To assess the performance of both interpolators independent of angle, the images were analyzed at nearly regular spatial intervals (see figure B.19). The RMS error for each band was calculated for all of the points, as in image 1a. The RMS error (by band) in path radiance is shown in figure B.43.

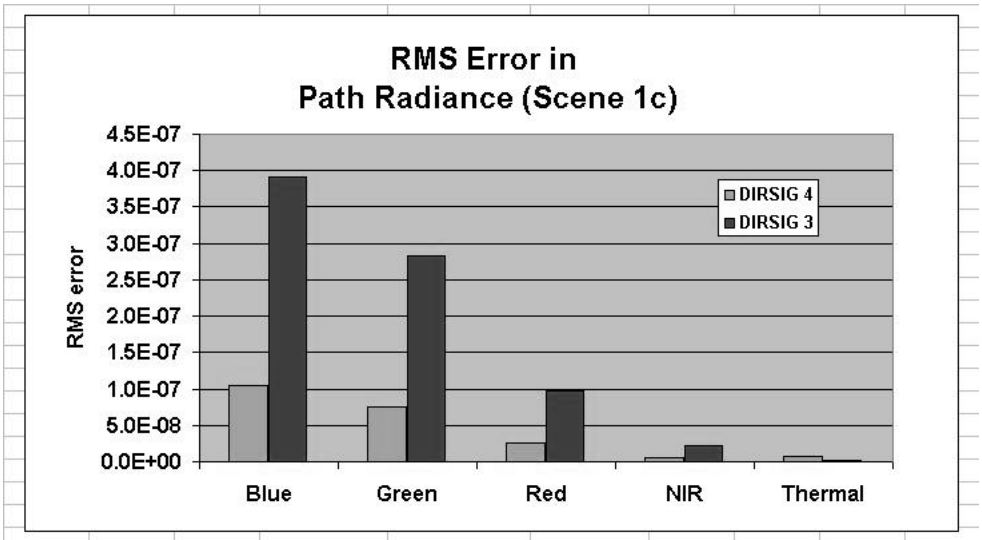

band	DIRSIG 4	DIRSIG 3
Blue	1.052584E-07	3.919653E-07
Green	7.571844E-08	2.833797E-07
Red	2.553335E-08	9.680649E-08
NIR	5.851304E-09	2.287507E-08
Thermal	7.511937E-09	1.235799E-09

Figure B.43: The RMS error in radiance for each band in image 1c.

B.4 Test Image 1a_urban.

The purpose of this test case was to investigate whether the aerosol type would have a significant effect on the ability of the interpolators to predict the atmospheric values.

The image is identical to that in 1a, except that the aerosol used in the atmosphere synthesis was urban (IHAZE = 5), not rural (IHAZE = 1).

As well, the performance of the algorithms in the thermal band were analyzed over the azimuthal dimension. There was not expected to be any significant variation in the thermal band in the azimuth dimension, so this was the only instance this was studied.

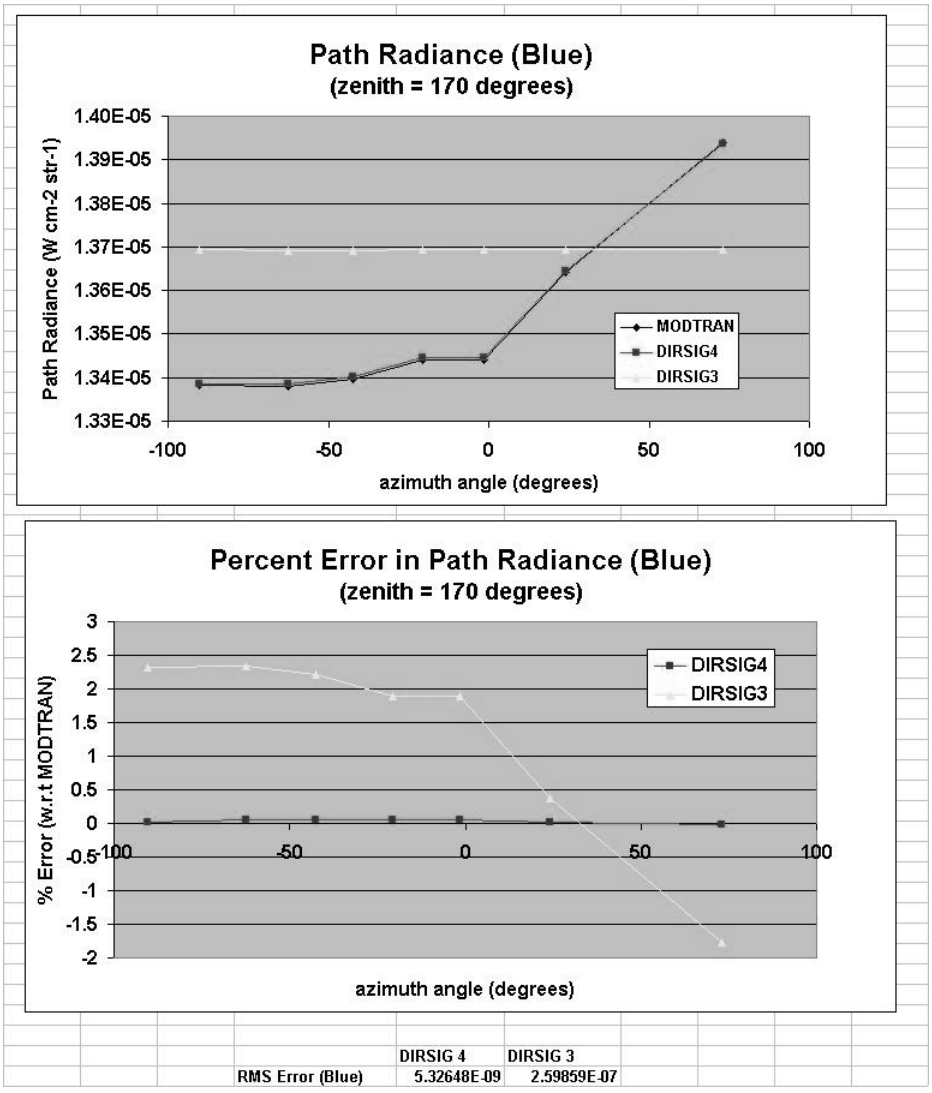

Figure B.44: Test Scene 1a_urban (azimuth variation): The upper graph shows the blue path radiance obtained by MODTRAN, DIRSIG 4 and DIRSIG 3. The lower graph shows the percent error of DIRSIG 4 and DIRSIG 3 relative to MODTRAN. The RMS errors for the points shown on the graph are listed below the graphs.

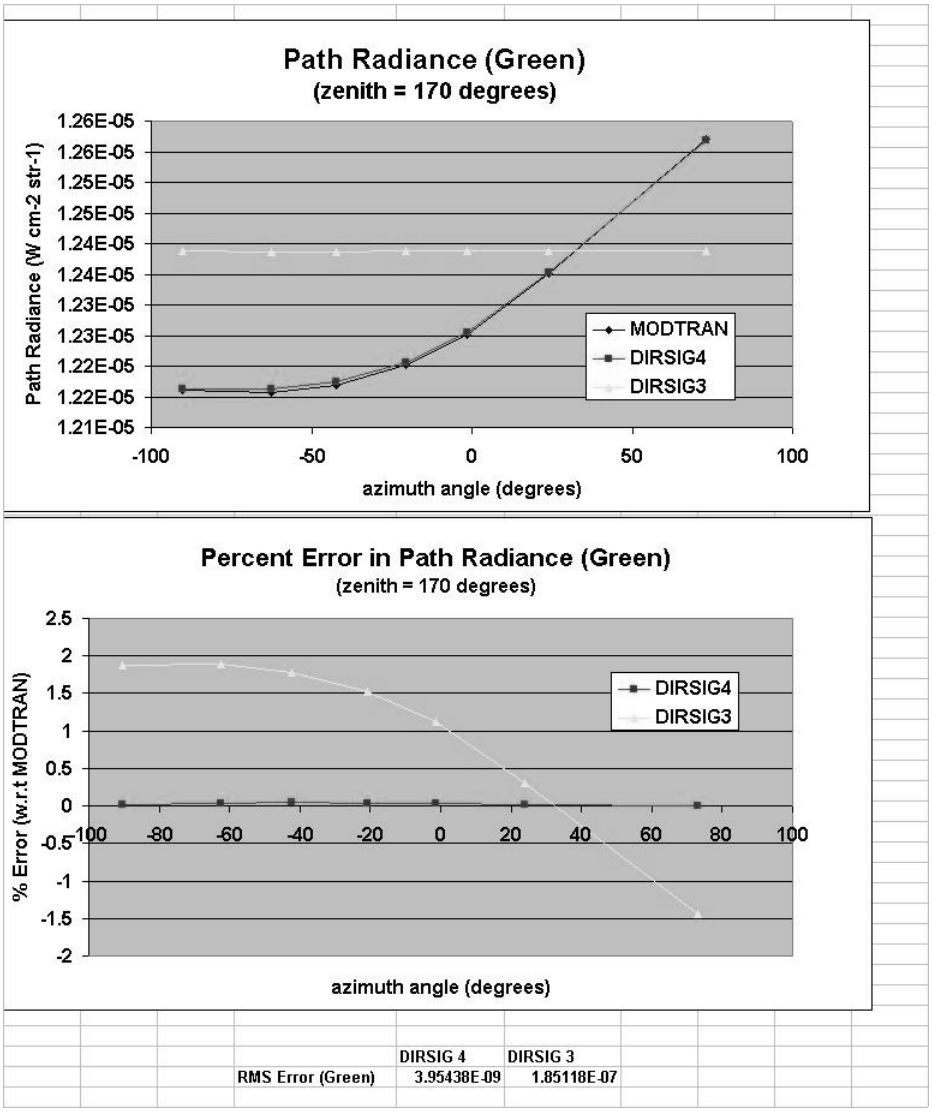

Figure B.45: Test Scene 1a_urban (azimuth variation): The upper graph shows the green path radiance obtained by MODTRAN, DIRSIG 4 and DIRSIG 3. The lower graph shows the percent error of DIRSIG 4 and DIRSIG 3 relative to MODTRAN. The RMS errors for the points shown on the graph are listed below the graphs.

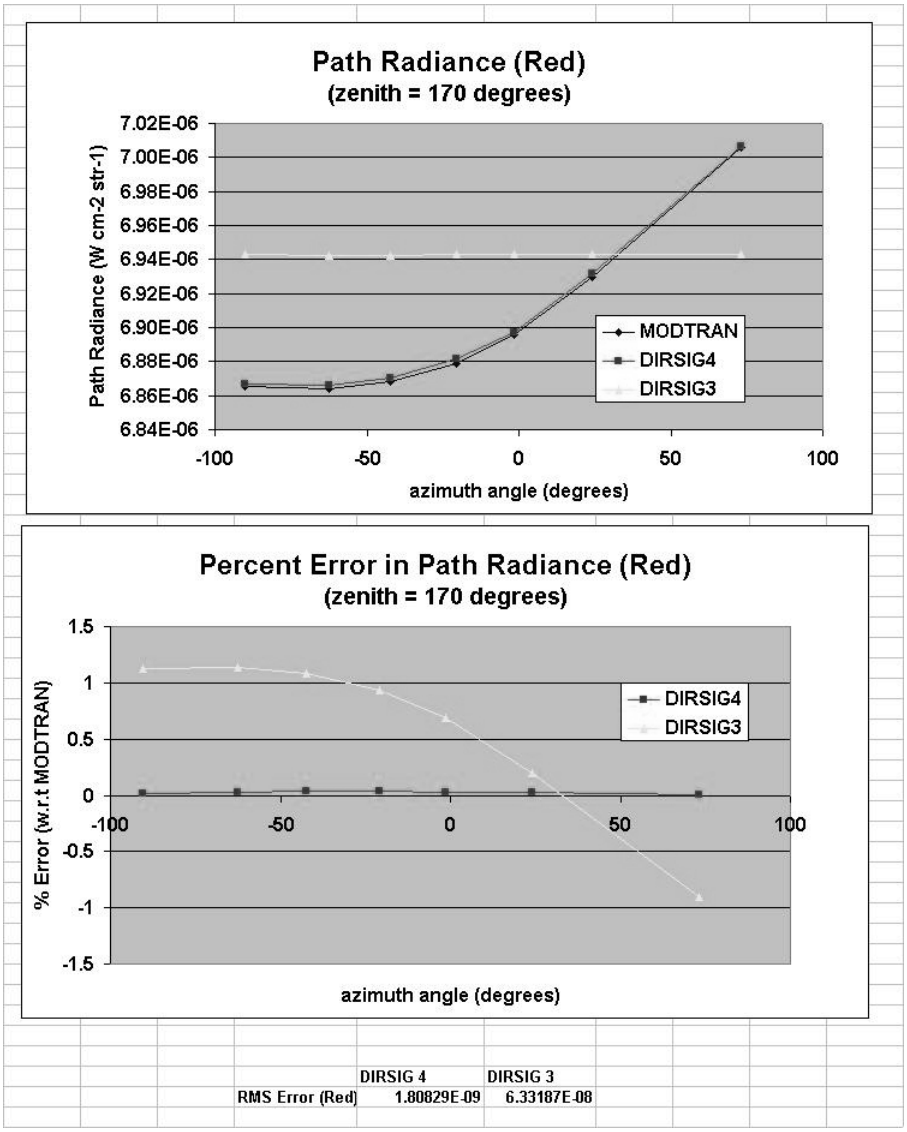

Figure B.46: Test Scene 1a_urban (azimuth variation): The upper graph shows the red path radiance obtained by MODTRAN, DIRSIG 4 and DIRSIG 3. The lower graph shows the percent error of DIRSIG 4 and DIRSIG 3 relative to MODTRAN. The RMS errors for the points shown on the graph are listed below the graphs.

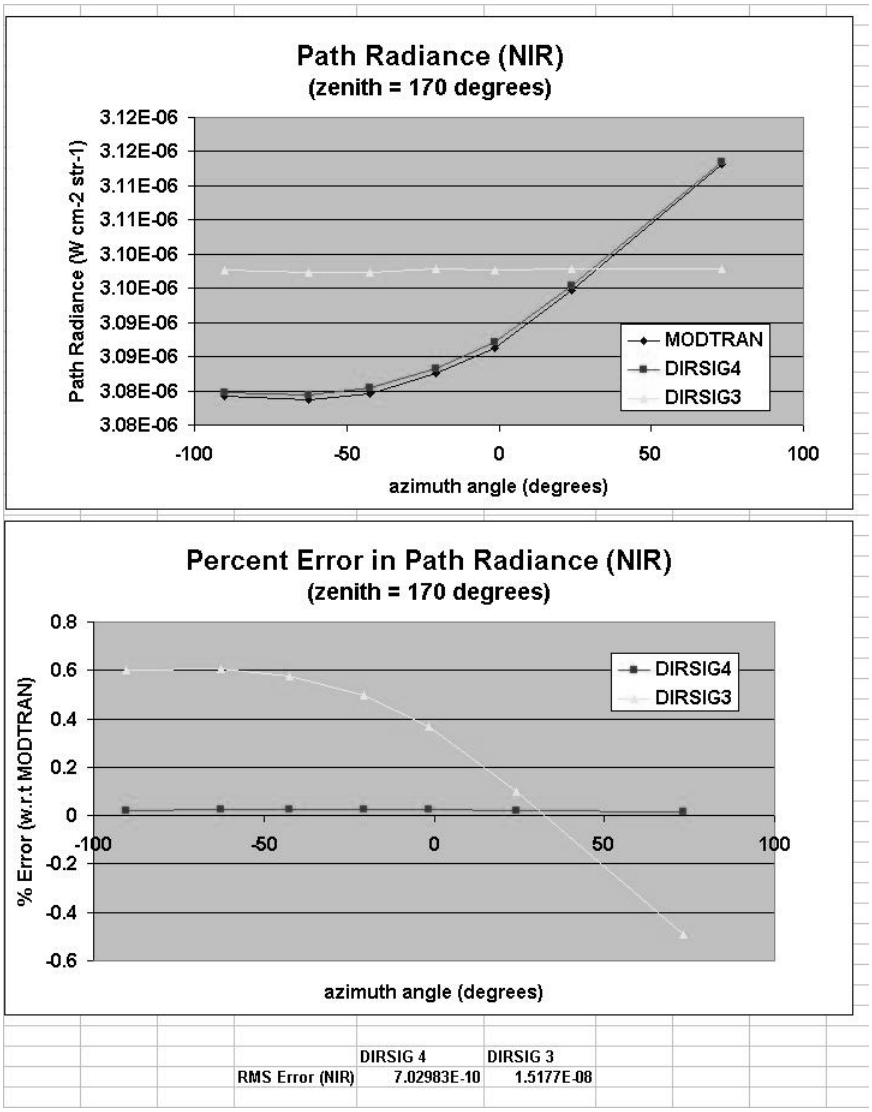

Figure B.47: Test Scene 1a_urban (azimuth variation): The upper graph shows the NIR path radiance obtained by MODTRAN, DIRSIG 4 and DIRSIG 3. The lower graph shows the percent error of DIRSIG 4 and DIRSIG 3 relative to MODTRAN. The RMS errors for the points shown on the graph are listed below the graphs.

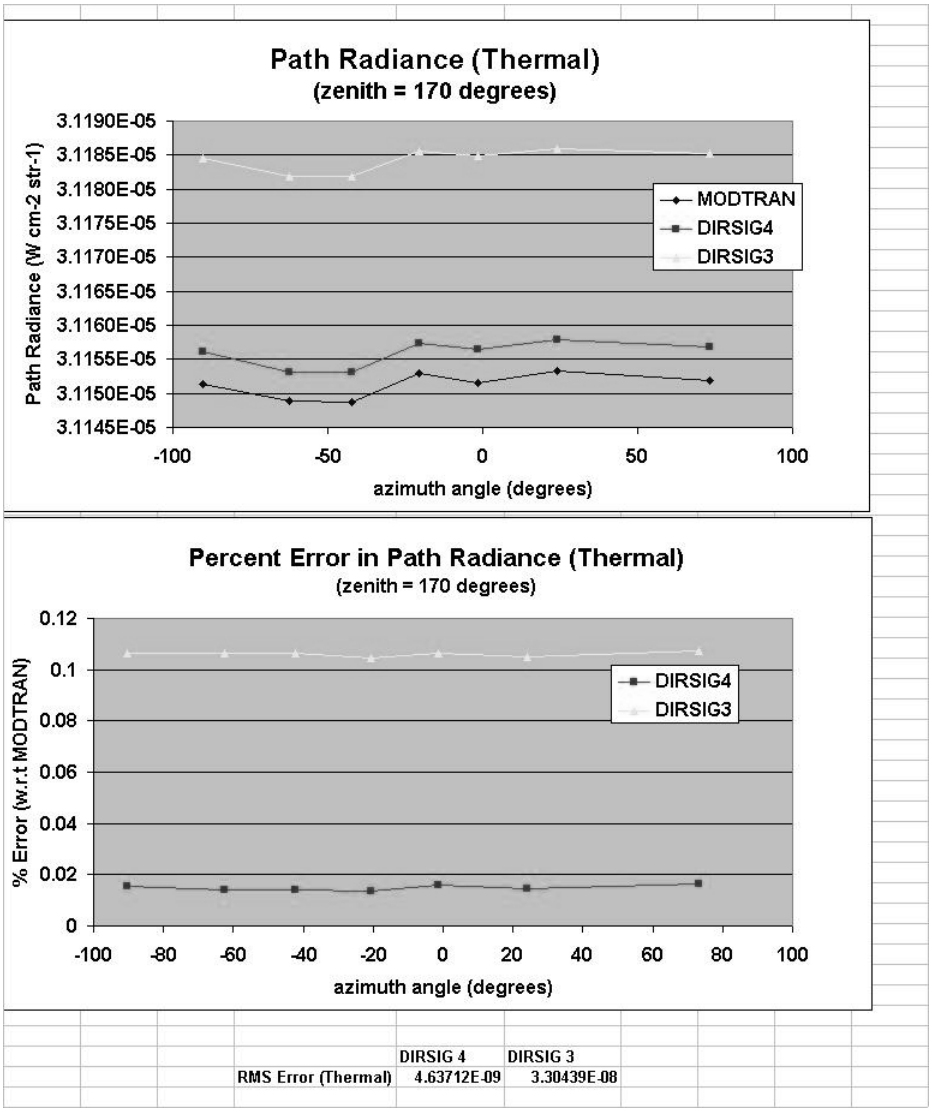

Figure B.48: Test Scene 1a_urban (azimuth variation): The upper graph shows the thermal path radiance obtained by MODTRAN, DIRSIG 4 and DIRSIG 3. The lower graph shows the percent error of DIRSIG 4 and DIRSIG 3 relative to MODTRAN. The RMS errors for the points shown on the graph are listed below the graphs.

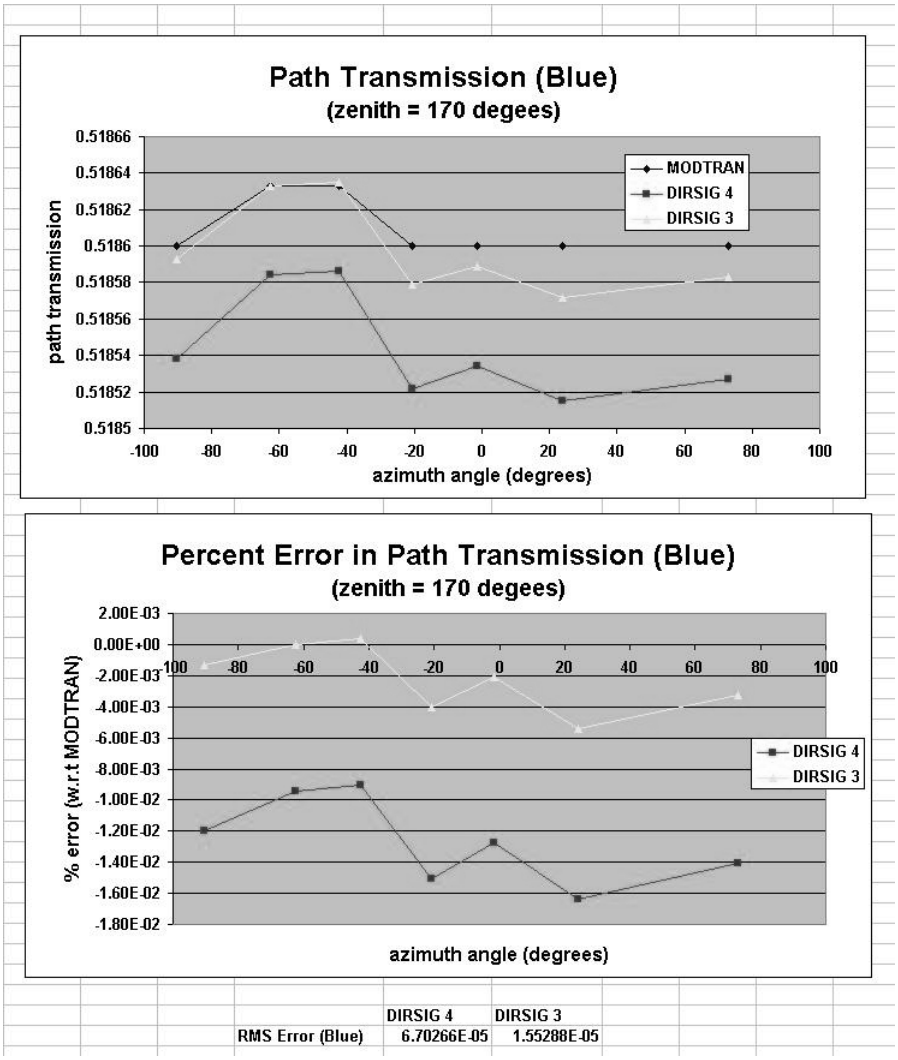

Figure B.49: Test Scene 1a_urban (azimuth variation): The upper graph shows the blue path transmission obtained by MODTRAN, DIRSIG 4 and DIRSIG 3. The lower graph shows the percent error of DIRSIG 4 and DIRSIG 3 relative to MODTRAN. The RMS errors for the points shown on the graph are listed below the graphs.

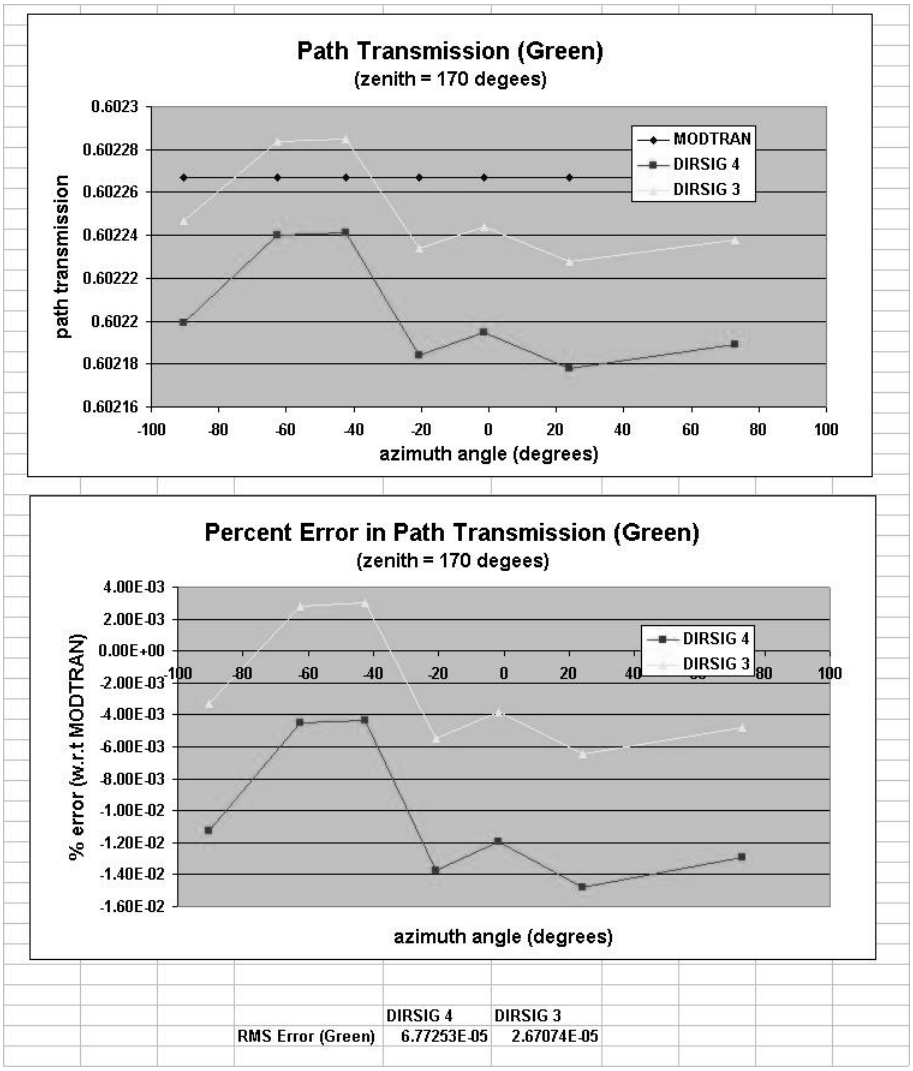

Figure B.50: Test Scene 1a_urban (azimuth variation): The upper graph shows the green path transmission obtained by MODTRAN, DIRSIG 4 and DIRSIG 3. The lower graph shows the percent error of DIRSIG 4 and DIRSIG 3 relative to MODTRAN. The RMS errors for the points shown on the graph are listed below the graphs.

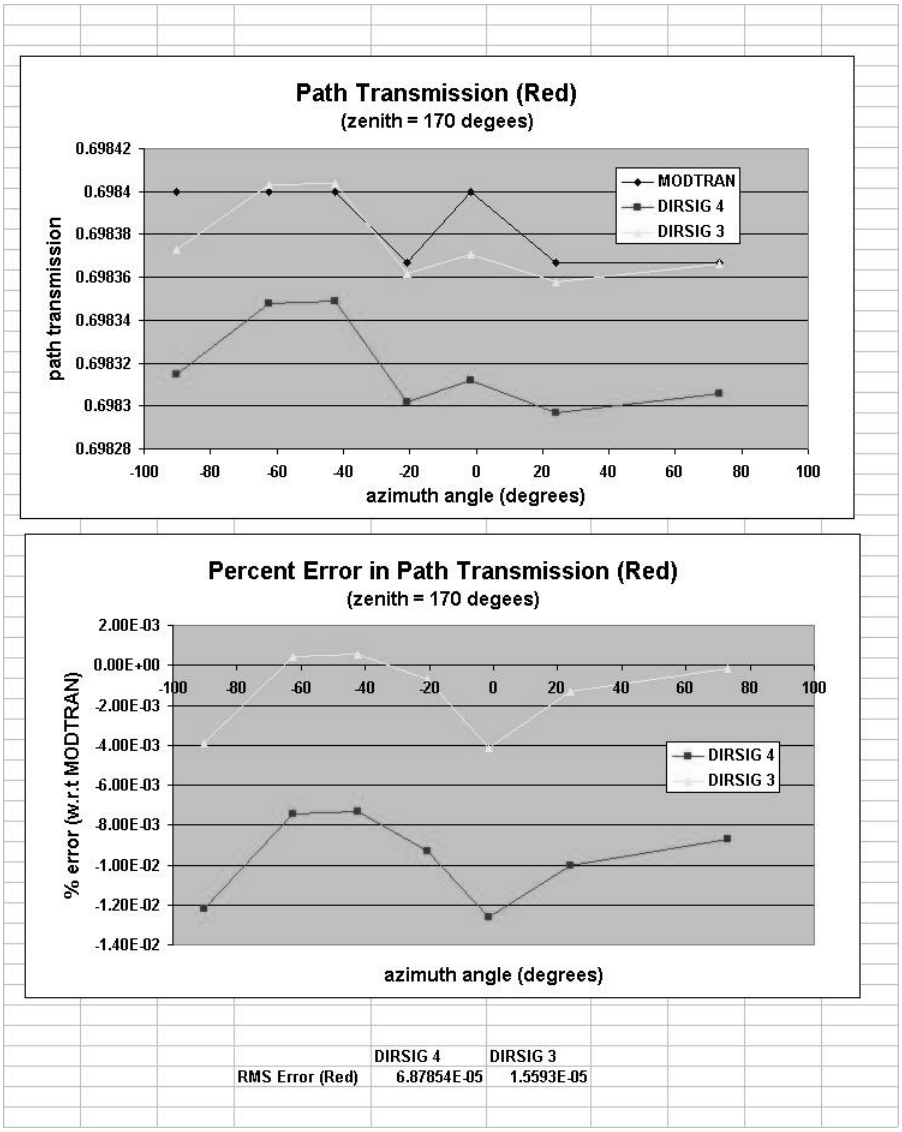

Figure B.51: Test Scene 1a_urban (azimuth variation): The upper graph shows the red path transmission obtained by MODTRAN, DIRSIG 4 and DIRSIG 3. The lower graph shows the percent error of DIRSIG 4 and DIRSIG 3 relative to MODTRAN. The RMS errors for the points shown on the graph are listed below the graphs.

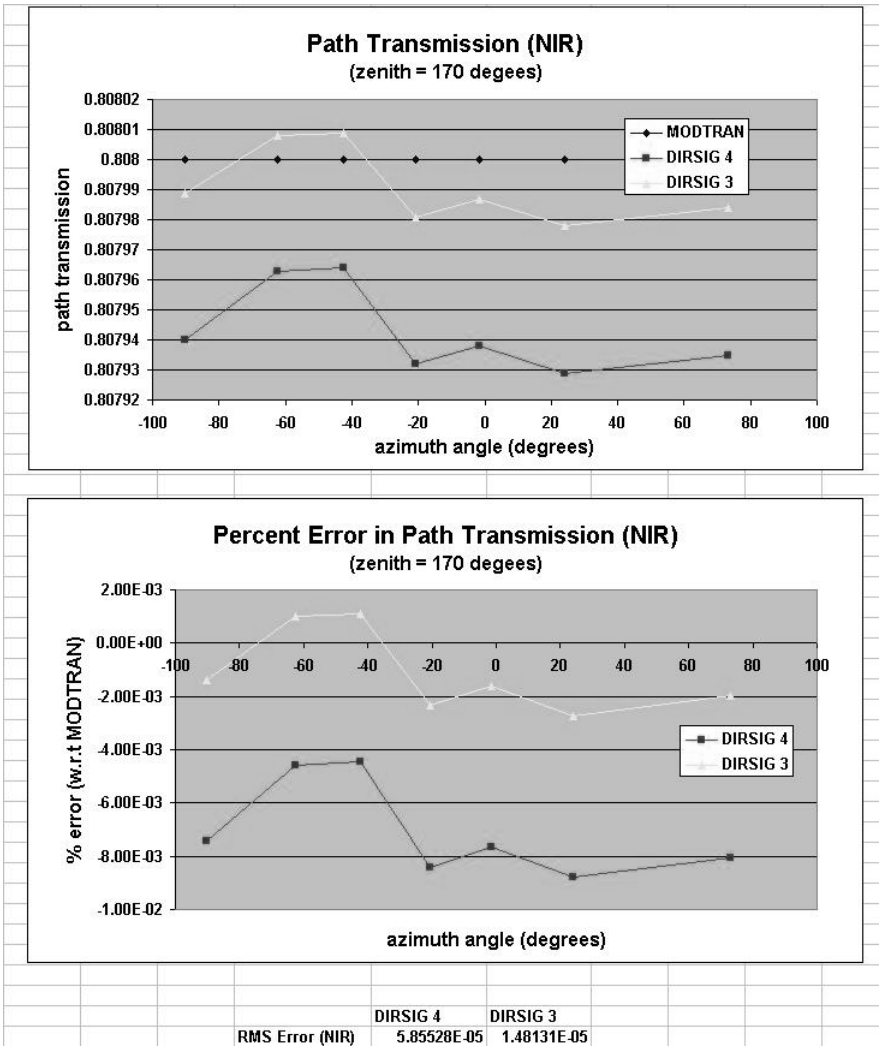

Figure B.52: Test Scene 1a_urban (azimuth variation): The upper graph shows the NIR path transmission obtained by MODTRAN, DIRSIG 4 and DIRSIG 3. The lower graph shows the percent error of DIRSIG 4 and DIRSIG 3 relative to MODTRAN. The RMS errors for the points shown on the graph are listed below the graphs.

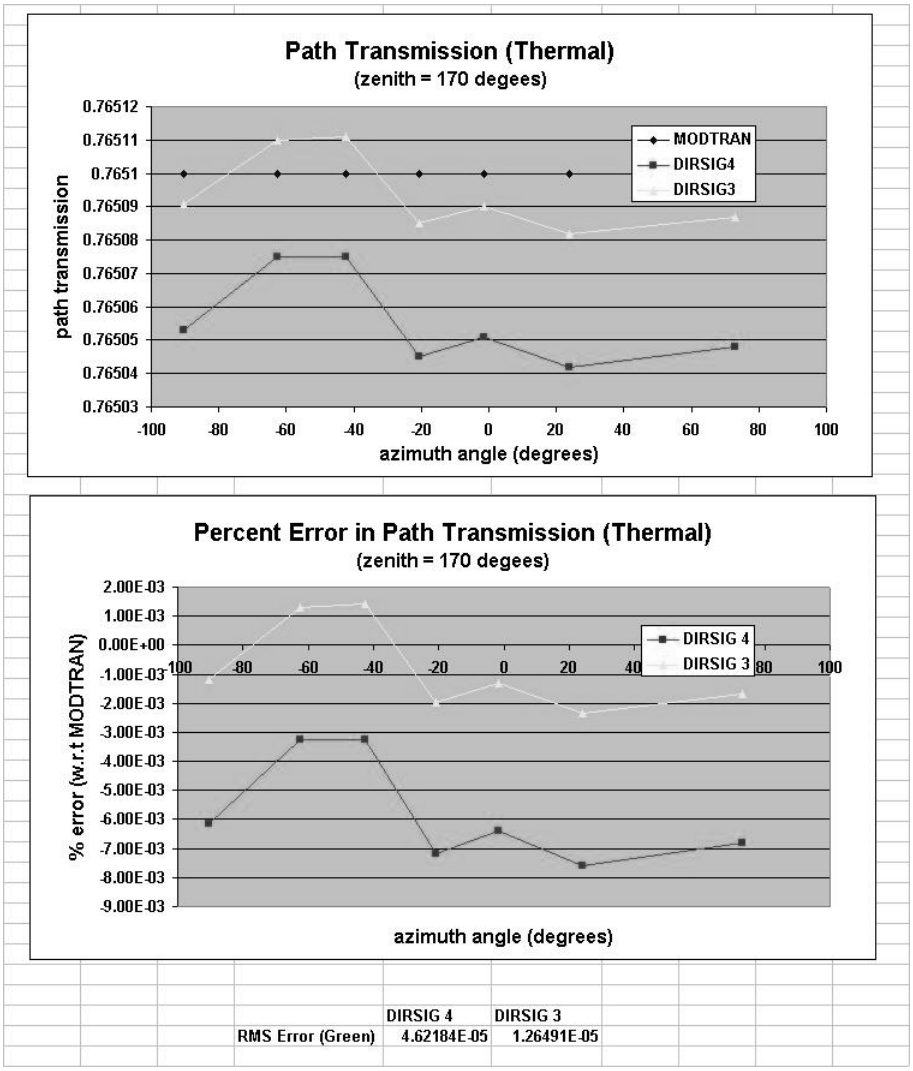

Figure B.53: Test Scene 1a_urban (azimuth variation): The upper graph shows the thermal path transmission obtained by MODTRAN, DIRSIG 4 and DIRSIG 3. The lower graph shows the percent error of DIRSIG 4 and DIRSIG 3 relative to MODTRAN. The RMS errors for the points shown on the graph are listed below the graphs.

B.4.1 Test Image 1a_urban Grid Results.

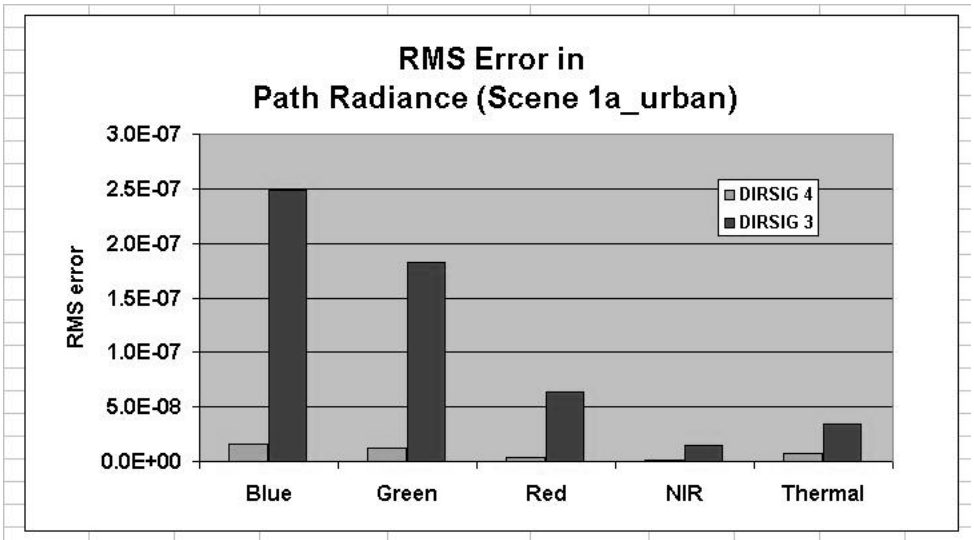

band	DIRSIG 4	DIRSIG 3
Blue	1.618388E-08	2.480506E-07
Green	1.178428E-08	1.830066E-07
Red	4.028965E-09	6.312646E-08
NIR	1.093790E-09	1.525163E-08
Thermal	7.732399E-09	3.377584E-08

Figure B.54: The RMS error in radiance for each band in image 1a_urban.

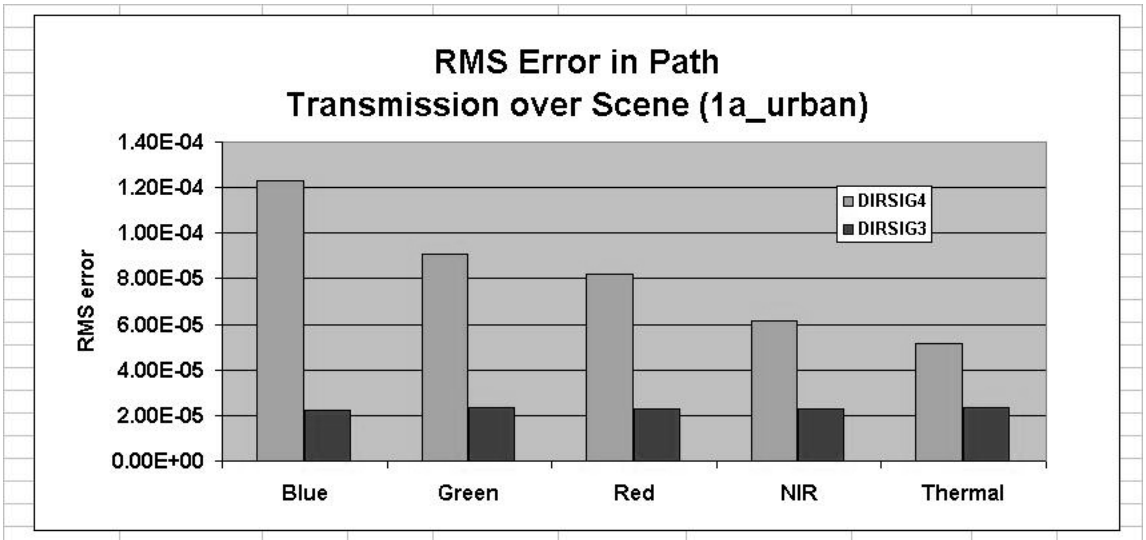

band	DIRSIG4	DIRSIG3
Blue	1.228785E-04	2.229798E-05
Green	9.075704E-05	2.342733E-05
Red	8.228682E-05	2.260000E-05
NIR	6.172455E-05	2.311277E-05
Thermal	5.131121E-05	2.357456E-05

Figure B.55: The RMS error in transmission for each band in image 1a_urban.

B.5 Test Image 2a.

This test case was intended to highlight how the two interpolators perform at non-zero altitudes. The scene consists of a simple pyramid of zero reflectance. (A graphical representation of the scene, as well as the points at which they were sampled can be seen in chapter 4.)

The atmosphere for test scene 2a was rendered under sunset conditions.

B.5.1 Test Image 2a Altitude Variation.

Nearly the identical study was performed on this test case. The only difference being that the altitude dimension was examined, and not the zenith or azimuth angles. A visible radiance image of the results of DIRSIG 3 and DIRSIG 4, as well as a set of points which were sampled can be found in figure B.56.

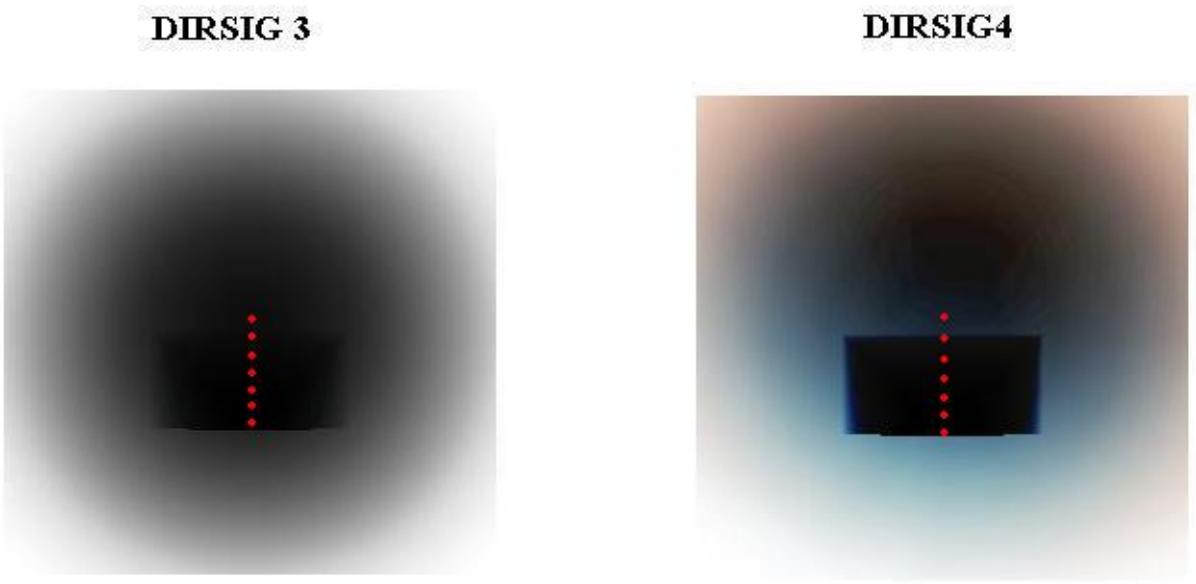

Figure B.56: The dots represent points analyzed in the image.

The following set of graphs show the path radiance and relative error for each band, and the RMS (root-mean-squared) error for all of the points. These are found in figure B.57 through B.66.

The next set of figures (B.62 through B.66) shows the path transmission results of the same study.

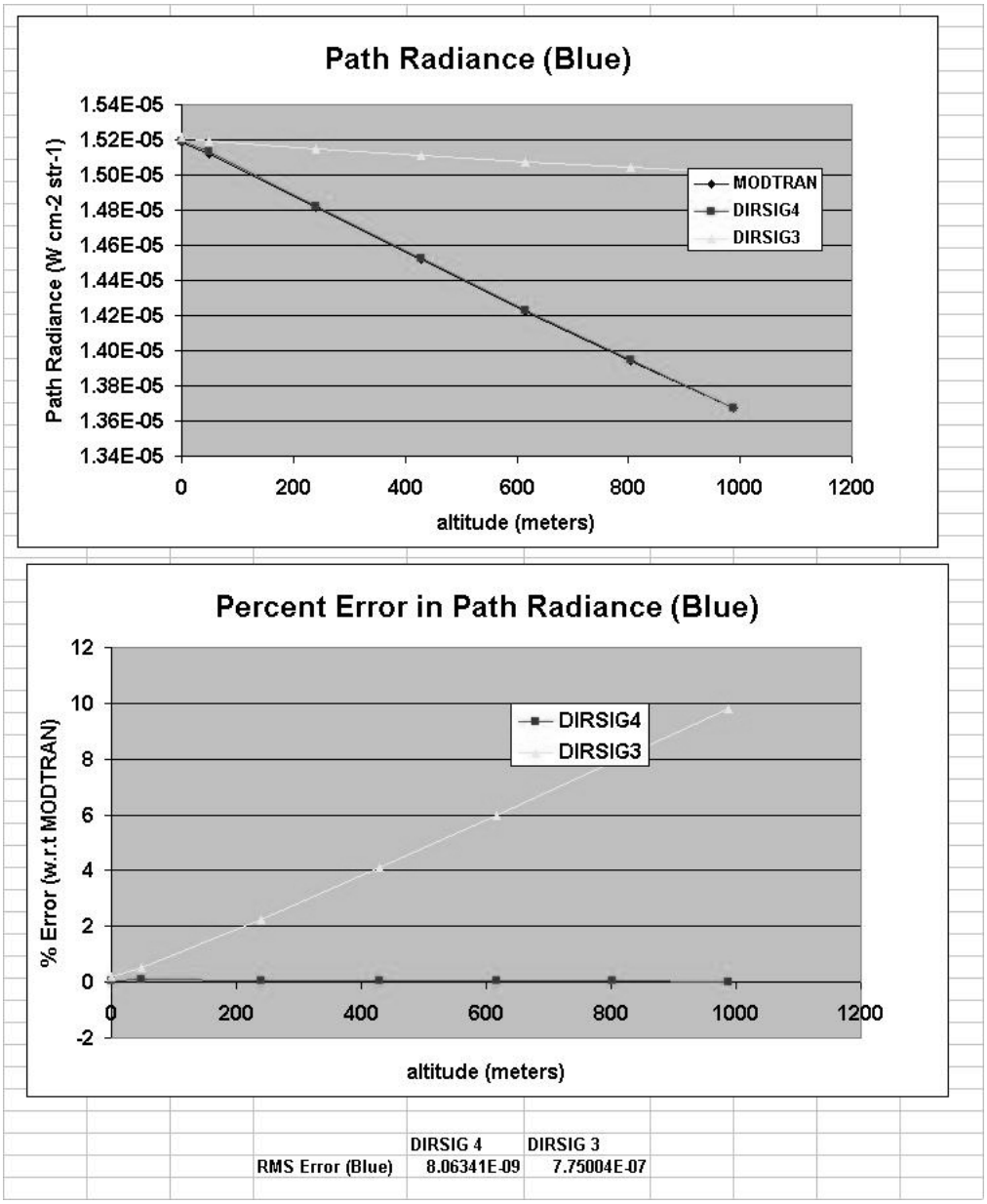

Figure B.57: Test Scene 2a (altitude variation): The upper graph shows the blue path radiance obtained by MODTRAN, DIRSIG 4 and DIRSIG 3. The lower graph shows the percent error of DIRSIG 4 and DIRSIG 3 relative to MODTRAN. The RMS errors for the points shown on the graph are listed below the graphs.

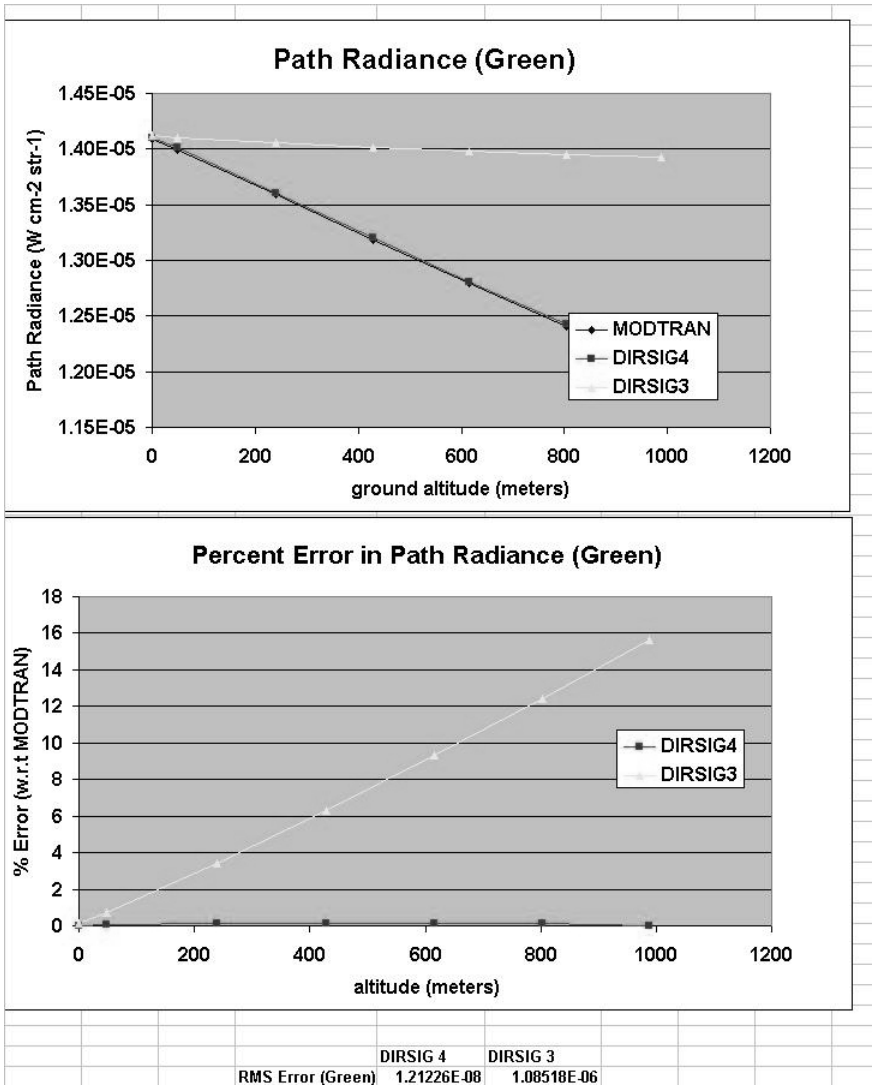

Figure B.58: Test Scene 2a (altitude variation): The upper graph shows the green path radiance obtained by MODTRAN, DIRSIG 4 and DIRSIG 3. The lower graph shows the percent error of DIRSIG 4 and DIRSIG 3 relative to MODTRAN. The RMS errors for the points shown on the graph are listed below the graphs.

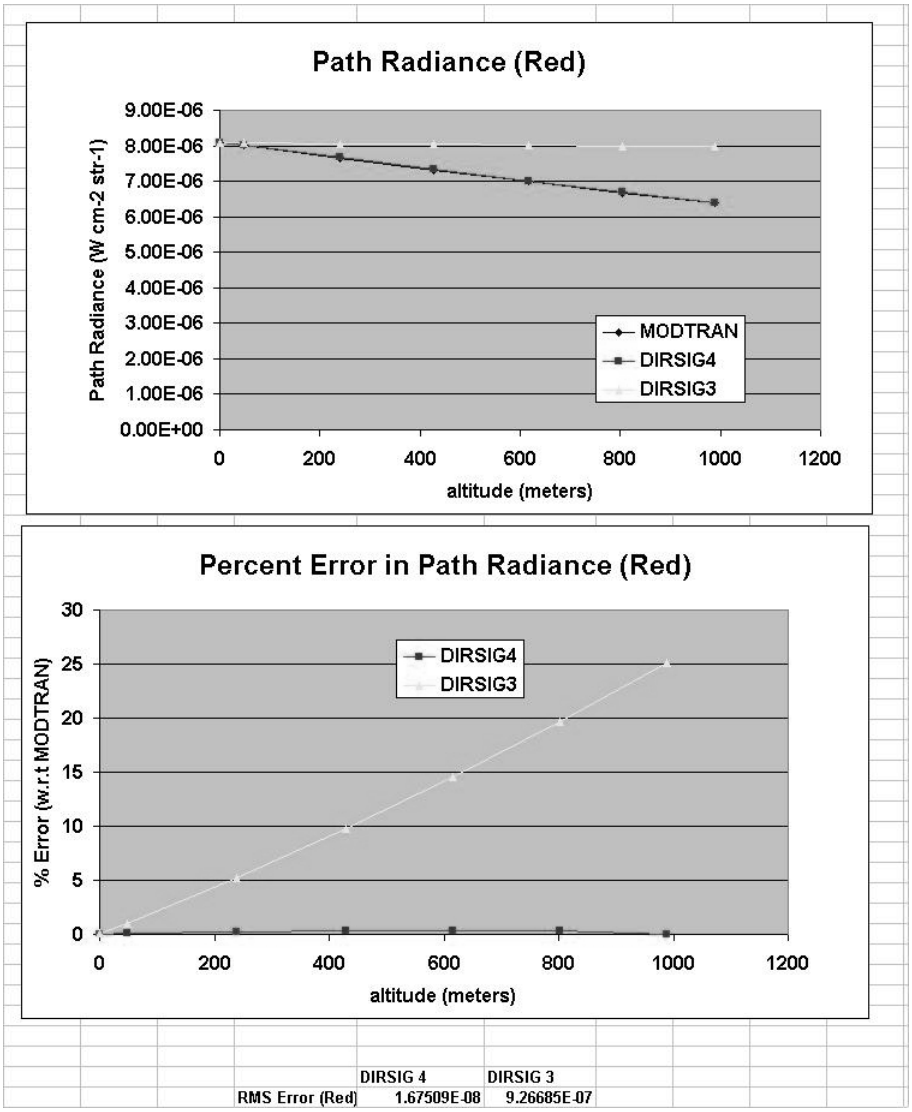

Figure B.59: Test Scene 2a (altitude variation): The upper graph shows the red path radiance obtained by MODTRAN, DIRSIG 4 and DIRSIG 3. The lower graph shows the percent error of DIRSIG 4 and DIRSIG 3 relative to MODTRAN. The RMS errors for the points shown on the graph are listed below the graphs.

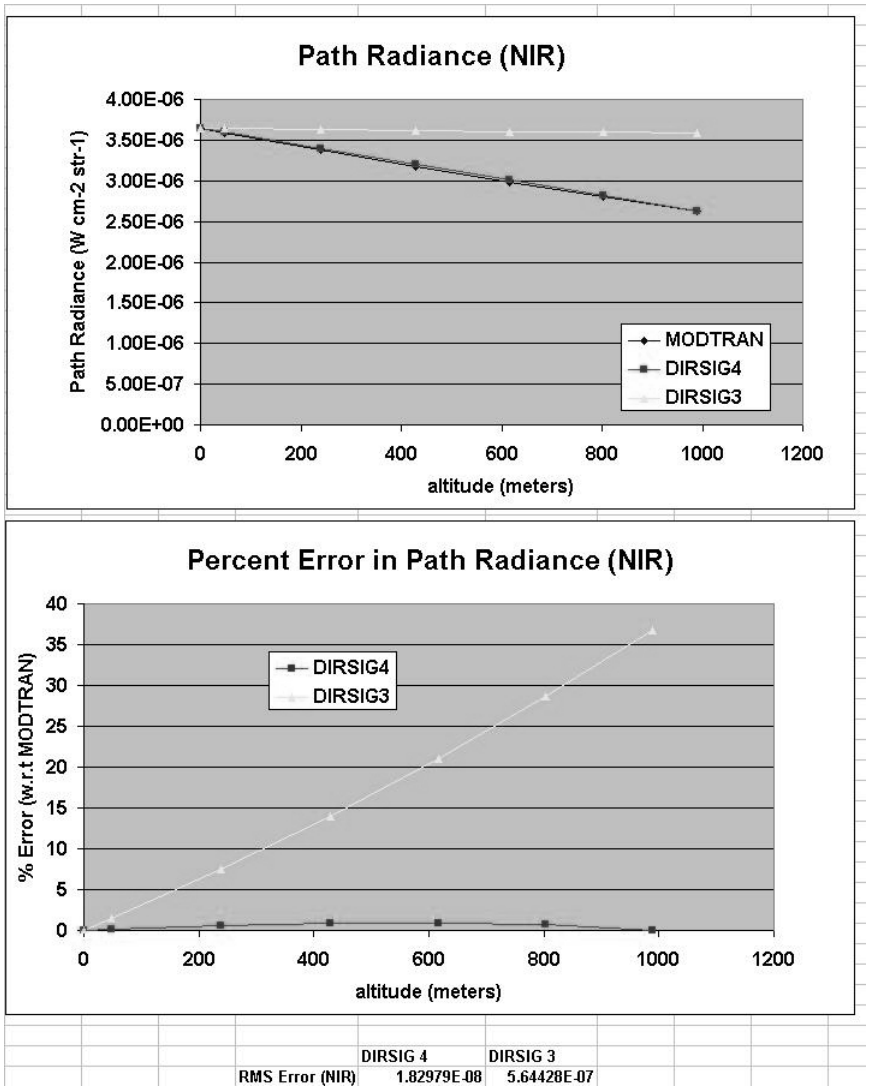

Figure B.60: Test Scene 2a (altitude variation): The upper graph shows the NIR path radiance obtained by MODTRAN, DIRSIG 4 and DIRSIG 3. The lower graph shows the percent error of DIRSIG 4 and DIRSIG 3 relative to MODTRAN. The RMS errors for the points shown on the graph are listed below the graphs.

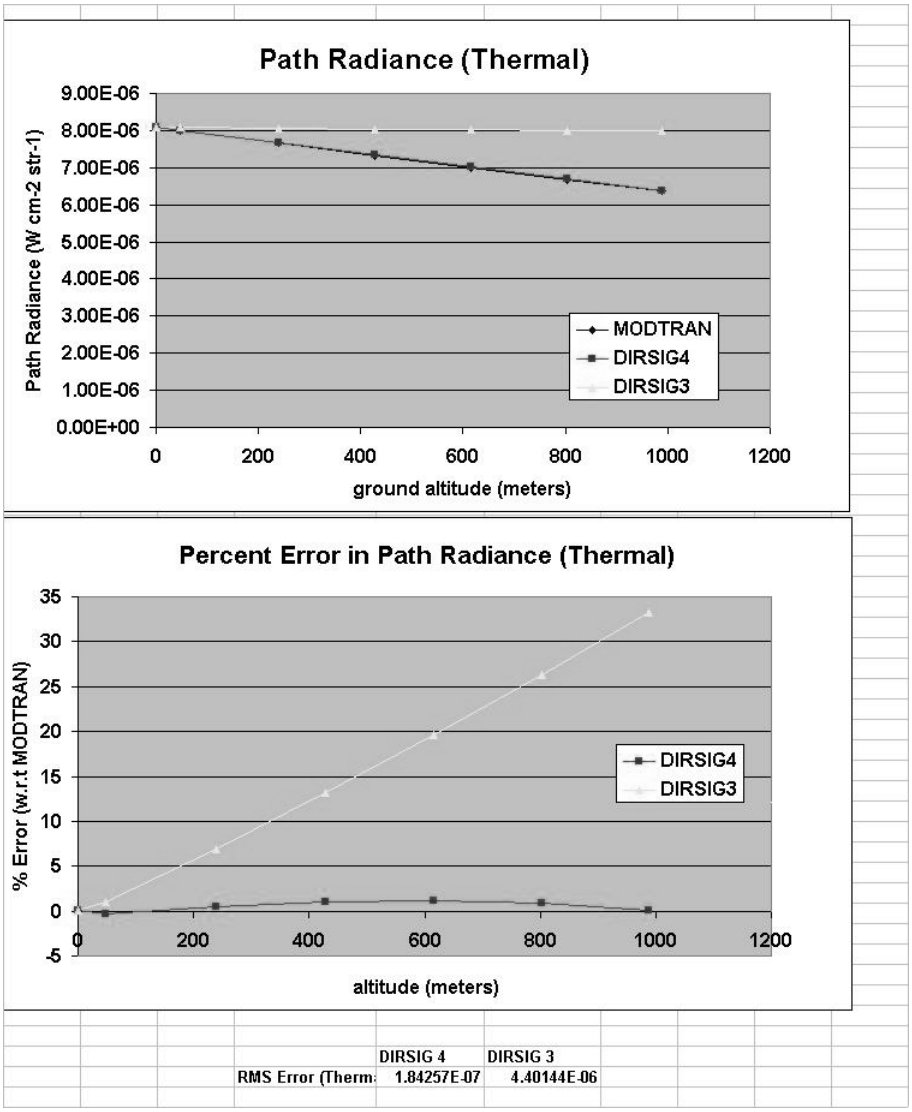

Figure B.61: Test Scene 2a (altitude variation): The upper graph shows the thermal path radiance obtained by MODTRAN, DIRSIG 4 and DIRSIG 3. The lower graph shows the percent error of DIRSIG 4 and DIRSIG 3 relative to MODTRAN. The RMS errors for the points shown on the graph are listed below the graphs.

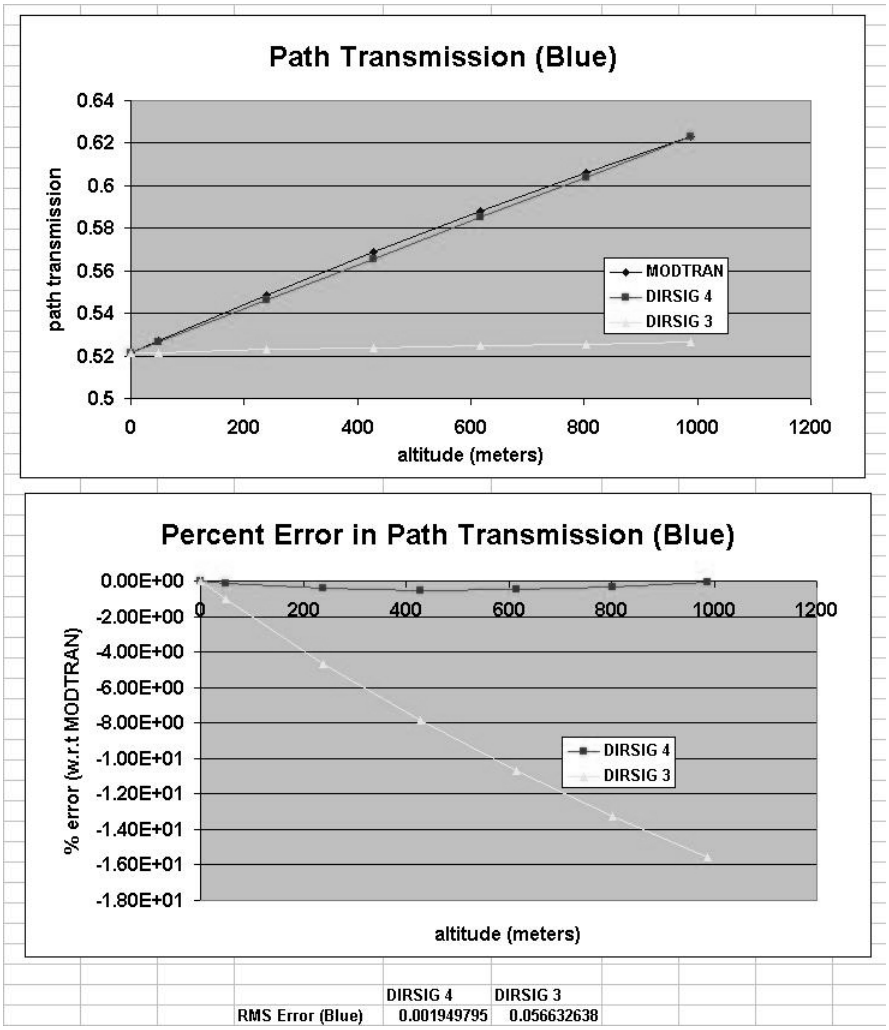

Figure B.62: Test Scene 2a (altitude variation): The upper graph shows the blue path transmission obtained by MODTRAN, DIRSIG 4 and DIRSIG 3. The lower graph shows the percent error of DIRSIG 4 and DIRSIG 3 relative to MODTRAN. The RMS errors for the points shown on the graph are listed below the graphs.

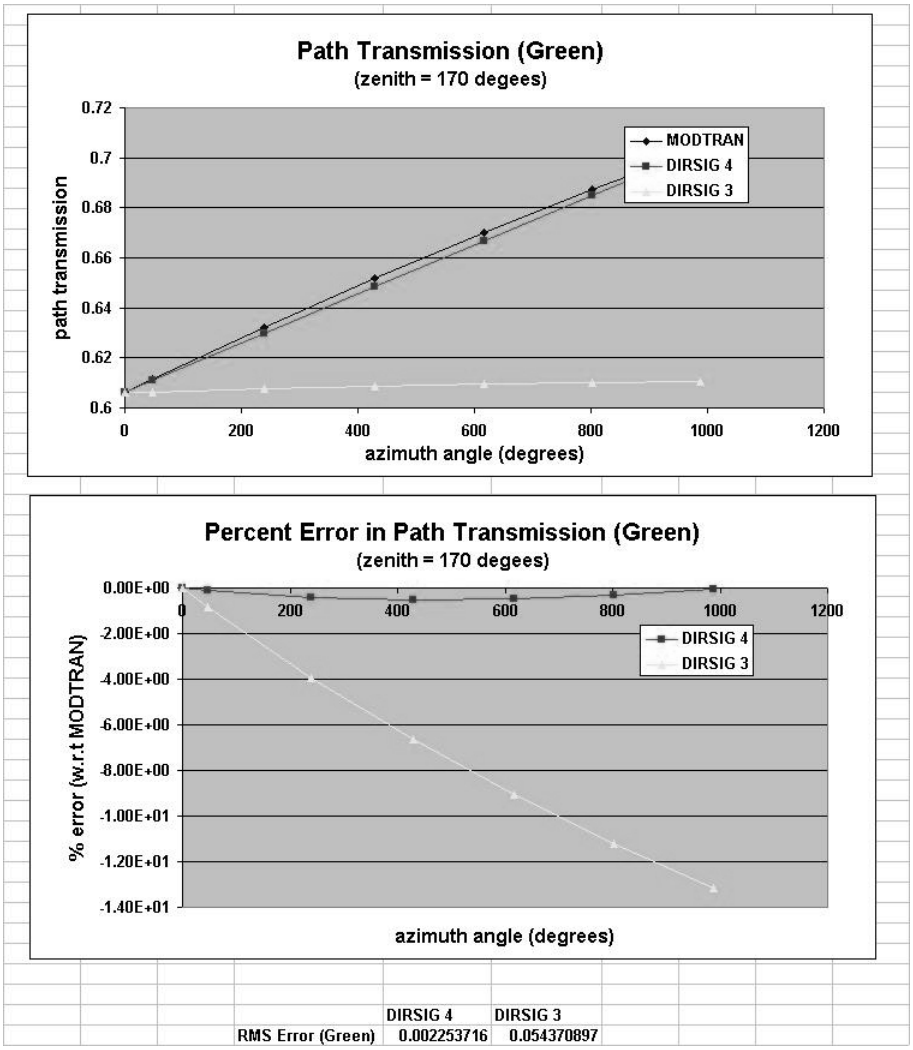

Figure B.63: Test Scene 2a (altitude variation): The upper graph shows the green path transmission obtained by MODTRAN, DIRSIG 4 and DIRSIG 3. The lower graph shows the percent error of DIRSIG 4 and DIRSIG 3 relative to MODTRAN. The RMS errors for the points shown on the graph are listed below the graphs.

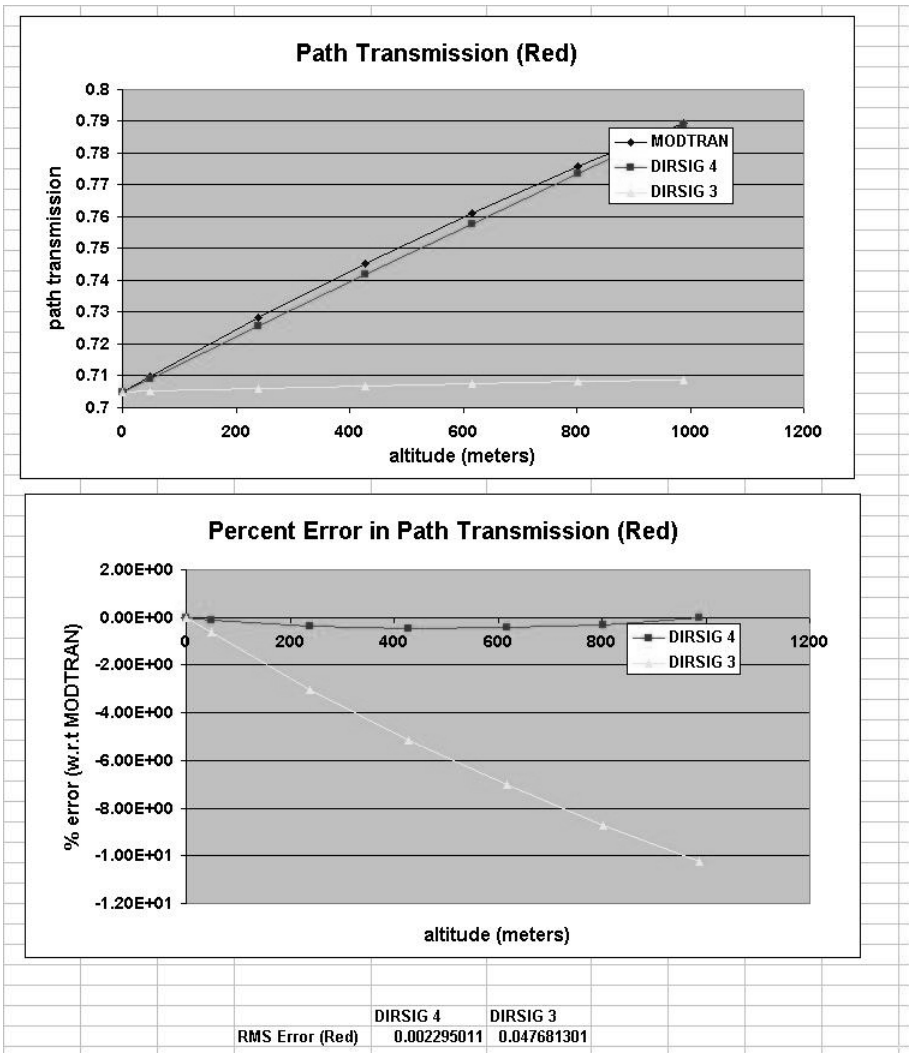

Figure B.64: Test Scene 2a (altitude variation): The upper graph shows the red path transmission obtained by MODTRAN, DIRSIG 4 and DIRSIG 3. The lower graph shows the percent error of DIRSIG 4 and DIRSIG 3 relative to MODTRAN. The RMS errors for the points shown on the graph are listed below the graphs.

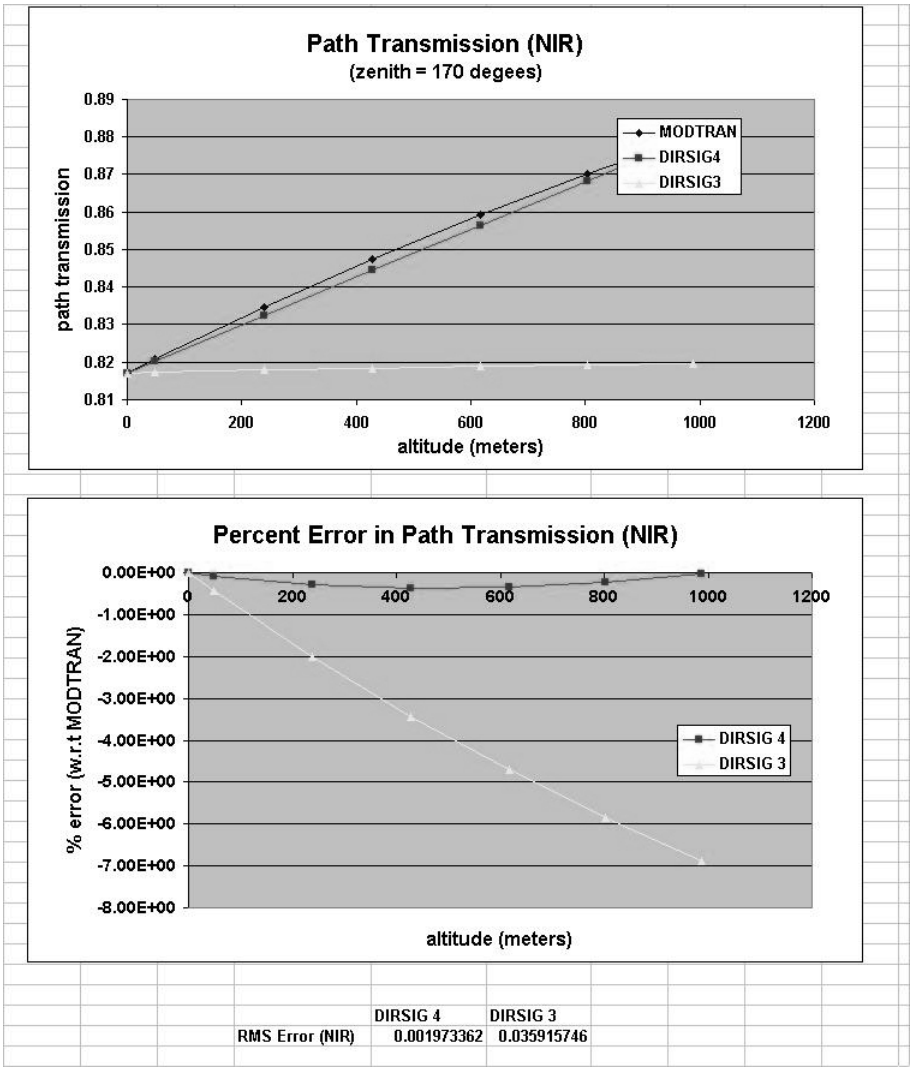

Figure B.65: Test Scene 2a (altitude variation): The upper graph shows the NIR path transmission obtained by MODTRAN, DIRSIG 4 and DIRSIG 3. The lower graph shows the percent error of DIRSIG 4 and DIRSIG 3 relative to MODTRAN. The RMS errors for the points shown on the graph are listed below the graphs.

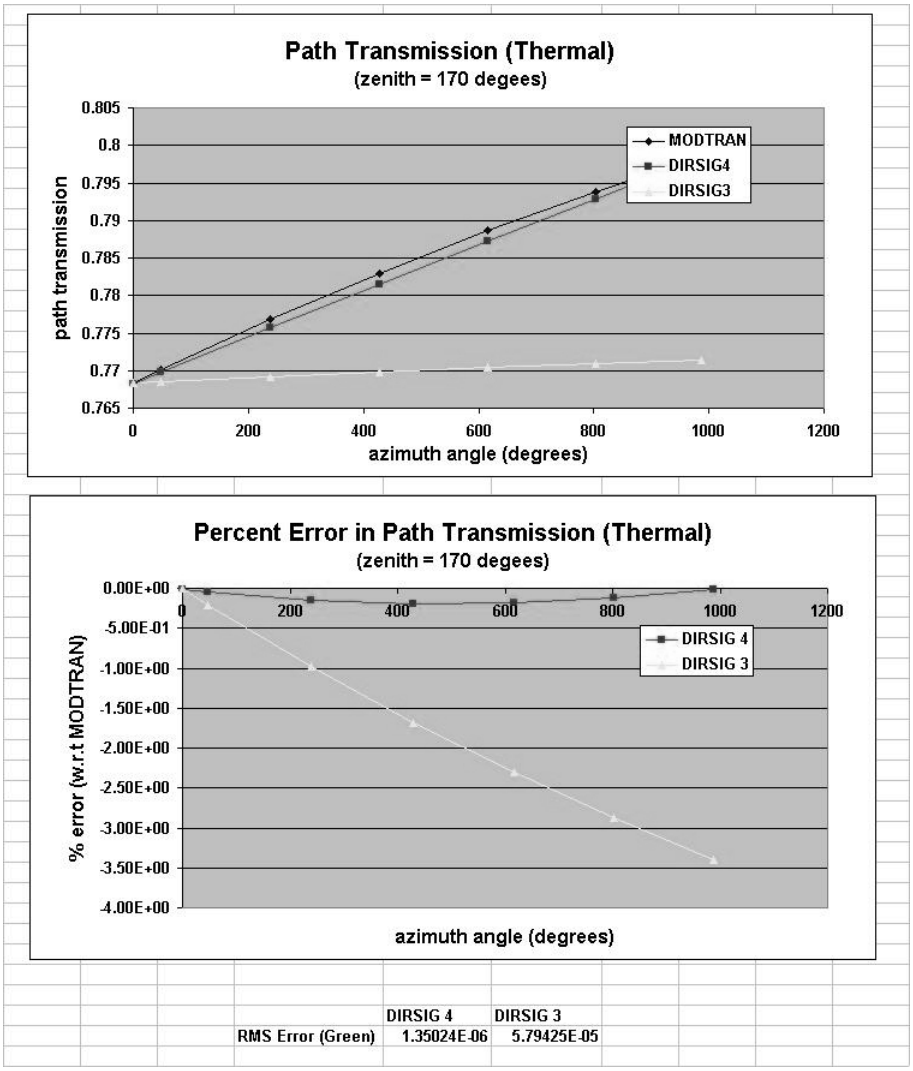

Figure B.66: Test Scene 2a (altitude variation): The upper graph shows the thermal path transmission obtained by MODTRAN, DIRSIG 4 and DIRSIG 3. The lower graph shows the percent error of DIRSIG 4 and DIRSIG 3 relative to MODTRAN. The RMS errors for the points shown on the graph are listed below the graphs.

B.5.2 Test Image 2a Grid Results

To assess the performance of both interpolators over the entire image, the images were analyzed at nearly regular spatial intervals (see figure 4.24). The RMS error for each band was calculated for all of the points. The RMS error (by band) is shown in figure B.67 for the path radiance and in figure B.68 for the transmission.

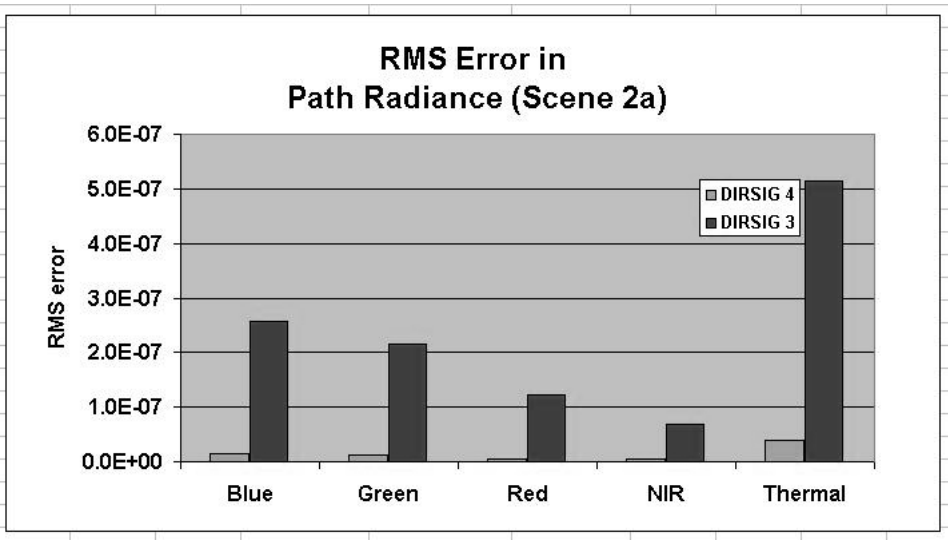

band	DIRSIG 4	DIRSIG 3
Blue	1.554921E-08	2.566496E-07
Green	1.148758E-08	2.150688E-07
Red	5.953634E-09	1.214150E-07
NIR	5.660207E-09	6.756662E-08
Thermal	3.842272E-08	5.142521E-07

Figure B.67: The RMS error in radiance for each band in image 2a.

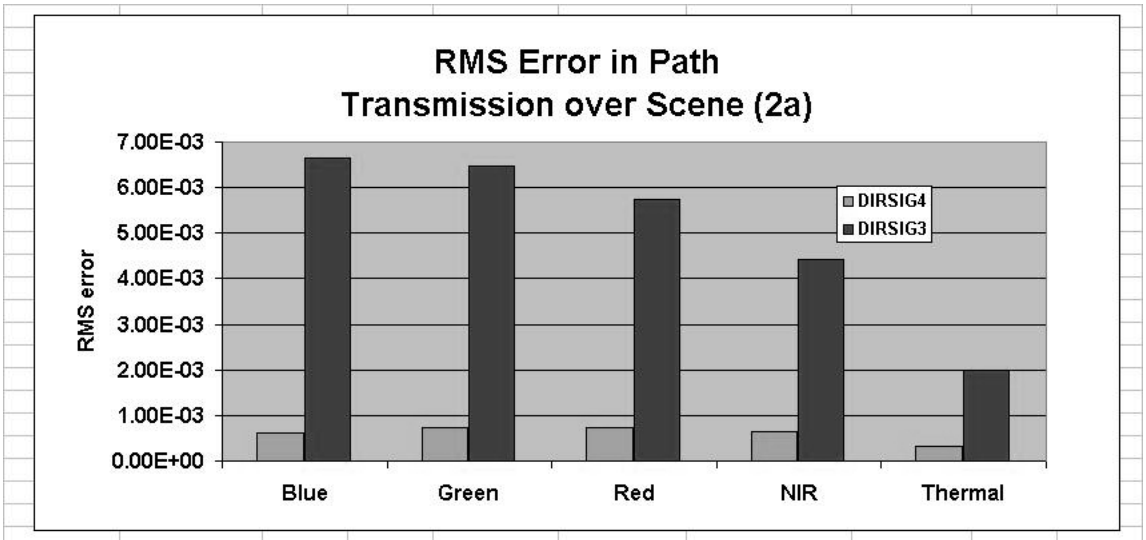

band	DIRSIG4	DIRSIG3
Blue	6.248552E-04	6.654635E-03
Green	7.247670E-04	6.476439E-03
Red	7.298150E-04	5.749041E-03
NIR	6.394742E-04	4.410101E-03
Thermal	3.307902E-04	2.002049E-03

Figure B.68: The RMS error in transmission for each band in image 2a.

B.6 Test Image 2b

This test image is identical to image 2a, the only difference is that it was rendered at noon. The same analysis was done on this image as well. However, because the transmission values will not change with the sun's position, the results for image 2b will be identical to those in 2a. Those transmission analysis results are omitted.

B.6.1 Test Image 2b Altitude Variation.

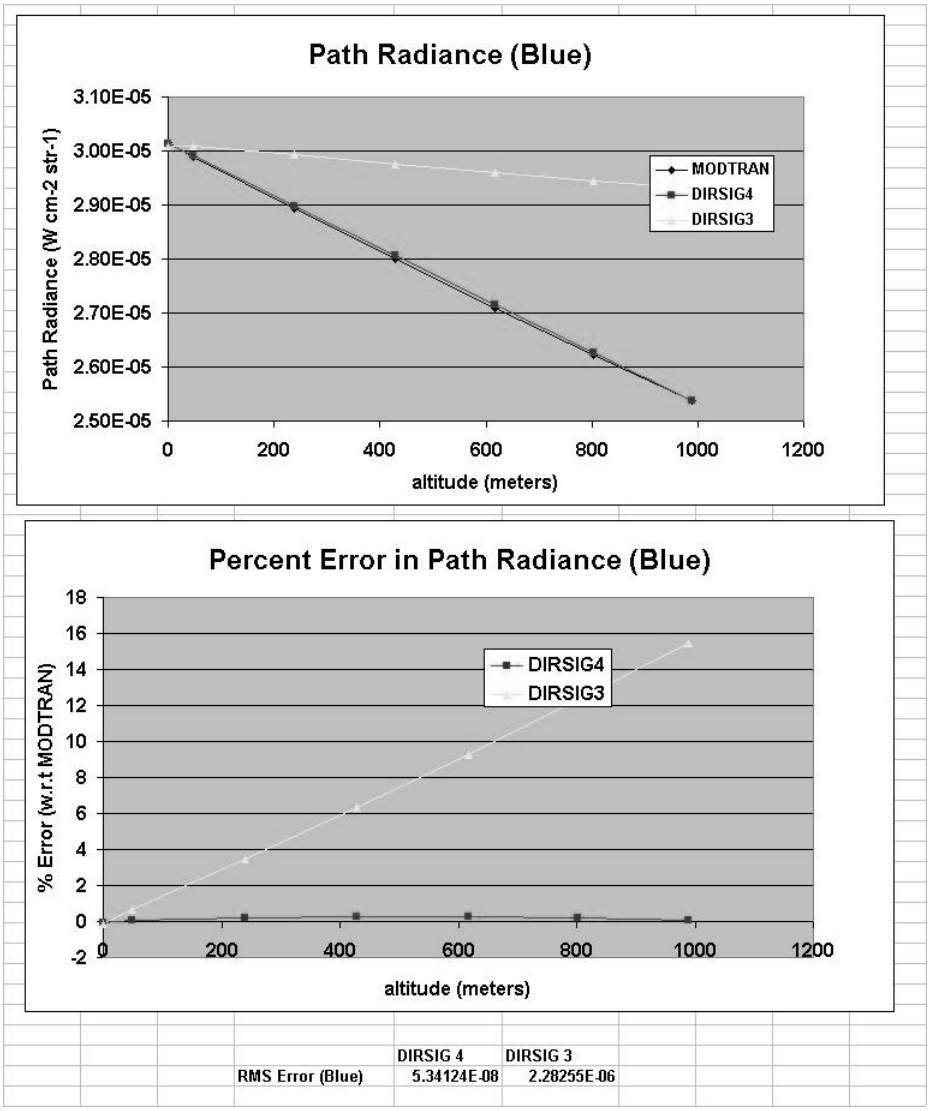

Figure B.69: Test Scene 2b (altitude variation): The upper graph shows the blue path radiance obtained by MODTRAN, DIRSIG 4 and DIRSIG 3. The lower graph shows the percent error of DIRSIG 4 and DIRSIG 3 relative to MODTRAN. The RMS errors for the points shown on the graph are listed below the graphs.

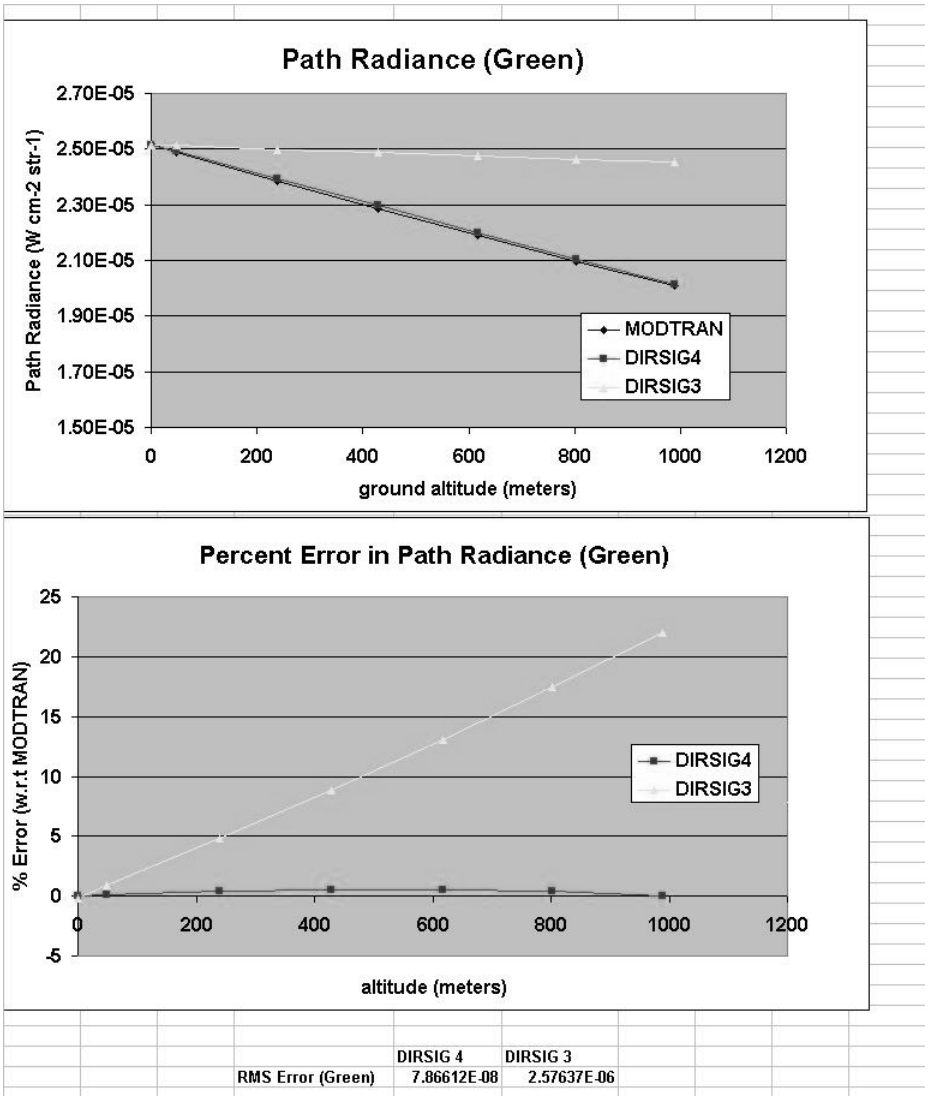

Figure B.70: Test Scene 2b (altitude variation): The upper graph shows the green path radiance obtained by MODTRAN, DIRSIG 4 and DIRSIG 3. The lower graph shows the percent error of DIRSIG 4 and DIRSIG 3 relative to MODTRAN. The RMS errors for the points shown on the graph are listed below the graphs.

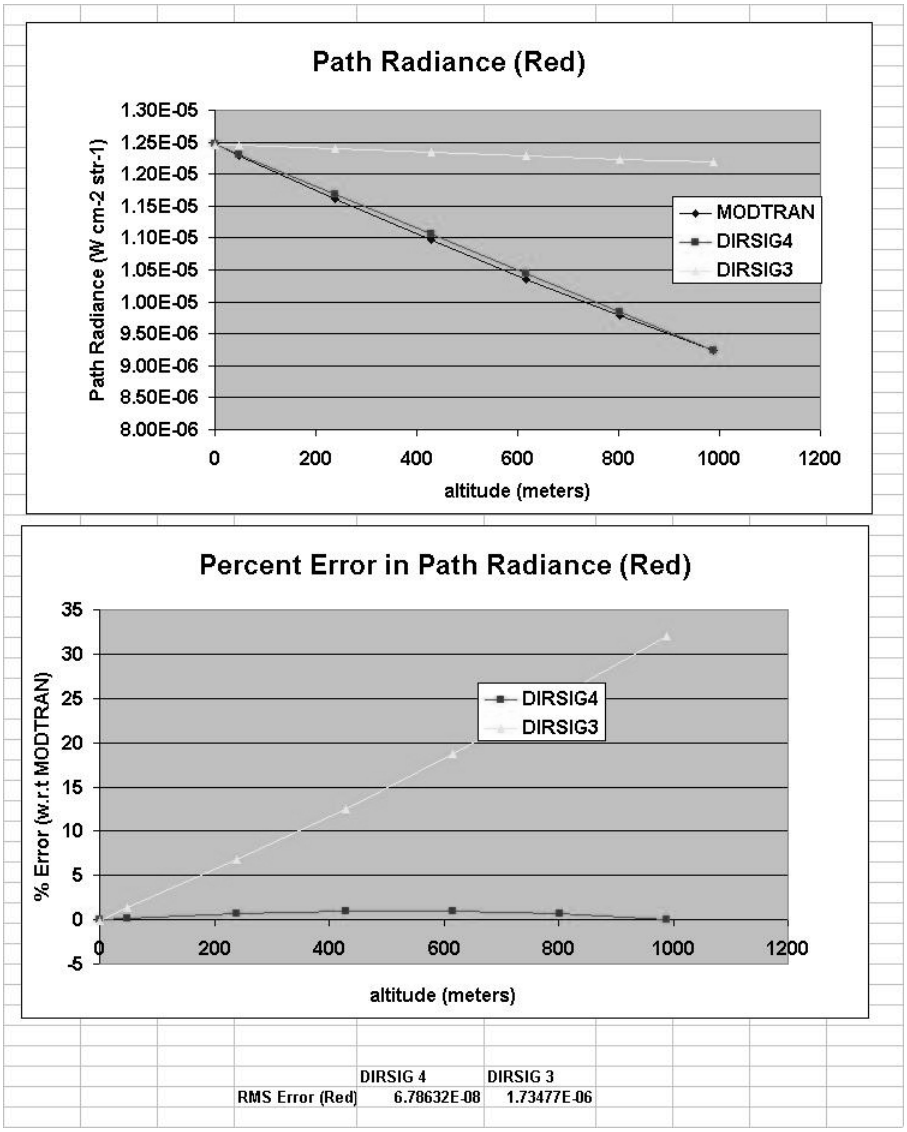

Figure B.71: Test Scene 2b (altitude variation): The upper graph shows the red path radiance obtained by MODTRAN, DIRSIG 4 and DIRSIG 3. The lower graph shows the percent error of DIRSIG 4 and DIRSIG 3 relative to MODTRAN. The RMS errors for the points shown on the graph are listed below the graphs.

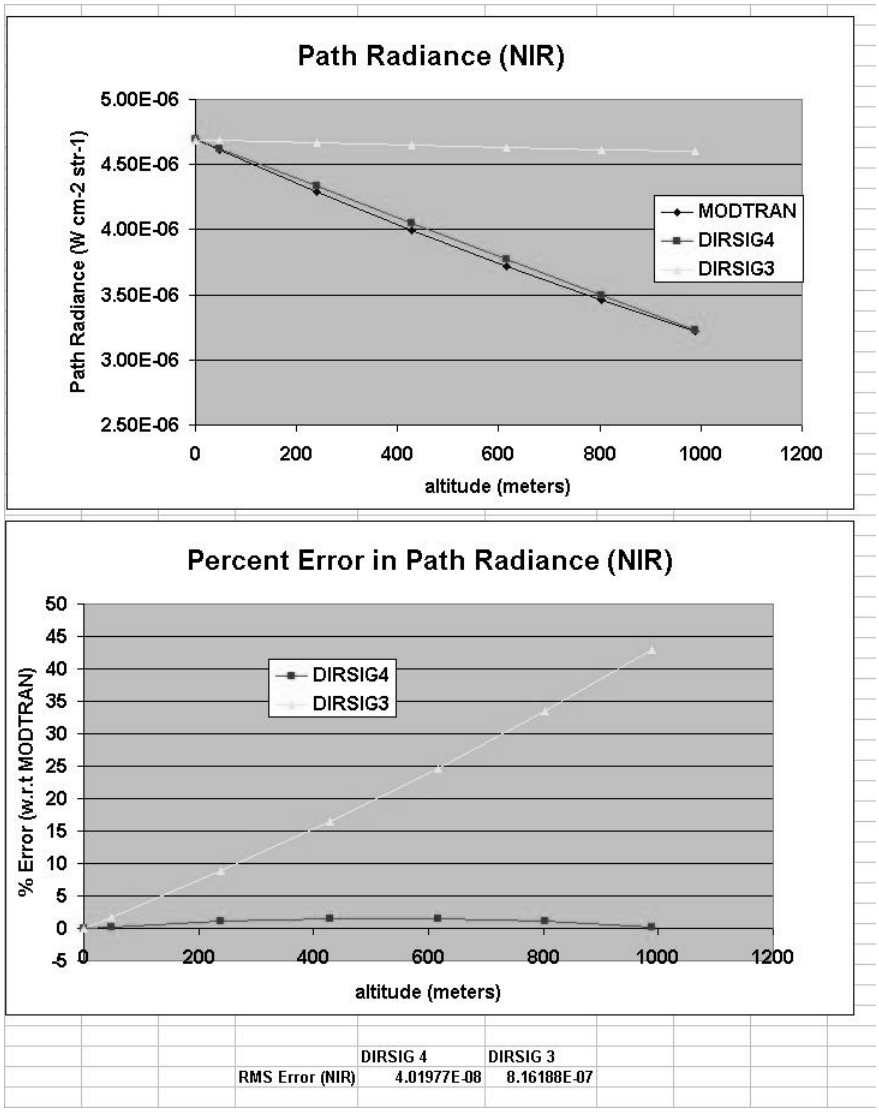

Figure B.72: Test Scene 2b (altitude variation): The upper graph shows the NIR path radiance obtained by MODTRAN, DIRSIG 4 and DIRSIG 3. The lower graph shows the percent error of DIRSIG 4 and DIRSIG 3 relative to MODTRAN. The RMS errors for the points shown on the graph are listed below the graphs.

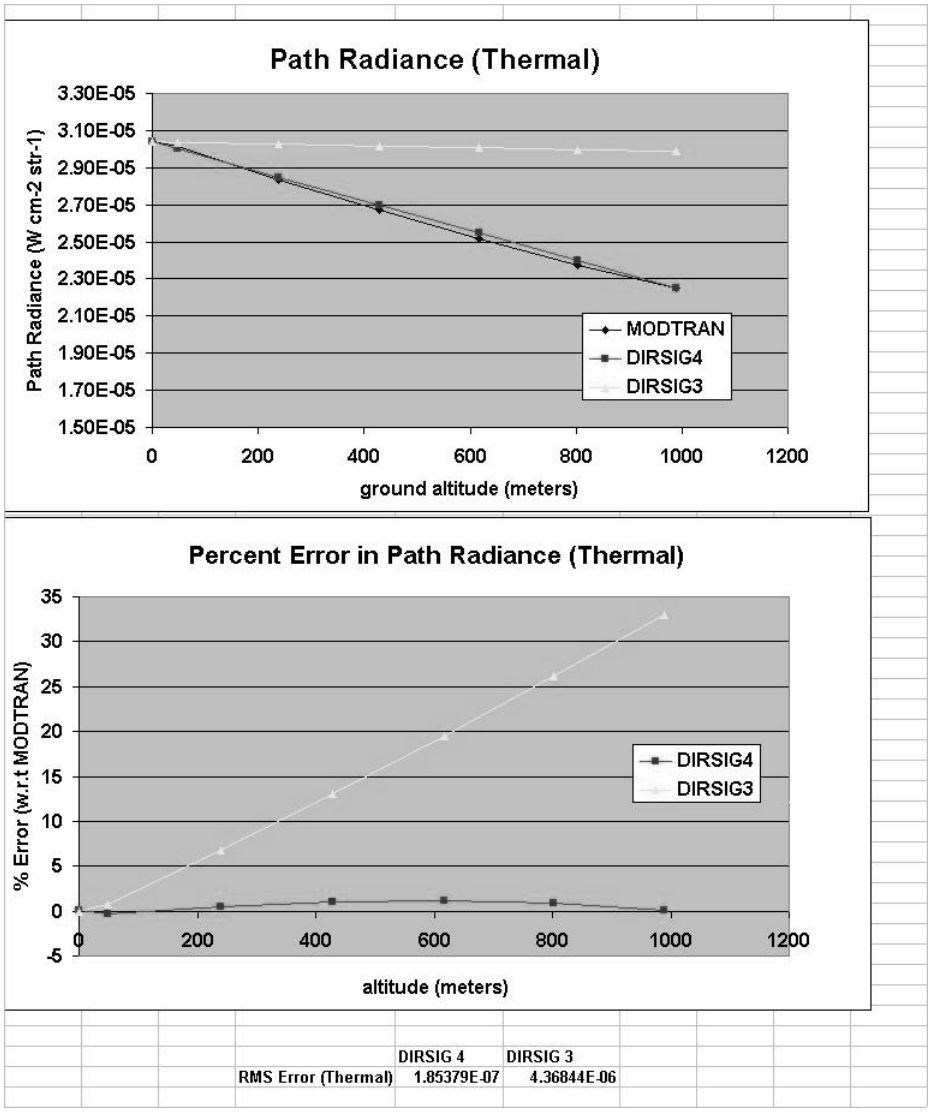

Figure B.73: Test Scene 2b (altitude variation): The upper graph shows the thermal path radiance obtained by MODTRAN, DIRSIG 4 and DIRSIG 3. The lower graph shows the percent error of DIRSIG 4 and DIRSIG 3 relative to MODTRAN. The RMS errors for the points shown on the graph are listed below the graphs.

B.6.2 Test Image 2b Grid Results.

To assess the performance of both interpolators over the entire image, analysis was performed at nearly regular spatial intervals (see figure B.56). The RMS error for each band was calculated for all of the points, as in image 2a. The RMS error (by band) in path radiance is shown in figure B.74.

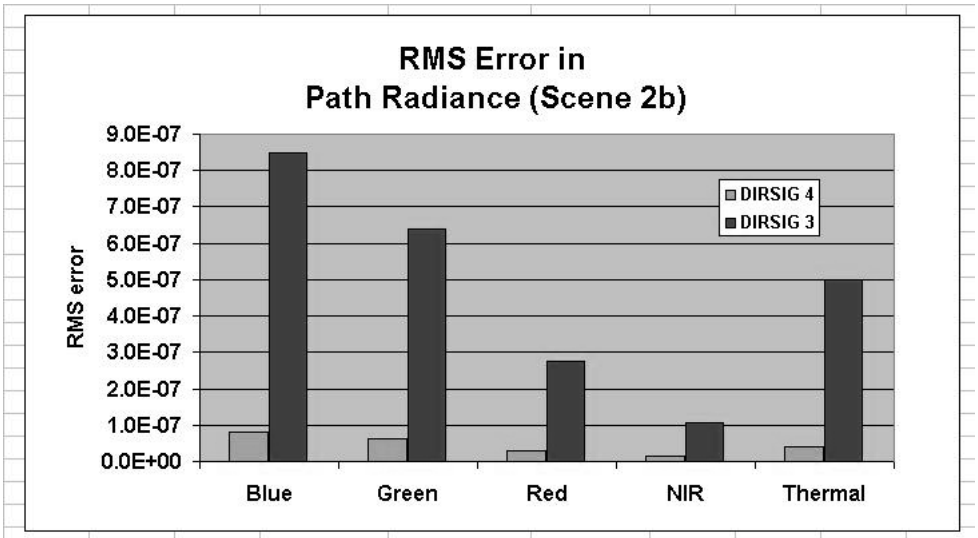

band	DIRSIG 4	DIRSIG 3
Blue	8.170116E-08	8.489303E-07
Green	6.063222E-08	6.375236E-07
Red	2.795390E-08	2.771802E-07
NIR	1.338654E-08	1.071137E-07
Thermal	3.882464E-08	5.006475E-07

Figure B.74: The RMS error in radiance for each band in image 2b.

B.7 Test Image 2c

This test image is identical to image 2a, the only difference is that it was rendered at sunrise. The same analysis was done on this image as well. However, because the transmission values will not change with the sun's position, the results for image 2c will be identical to those in 2a. Those transmission analysis results are omitted.

B.7.1 Test Image 2c Altitude Variation.

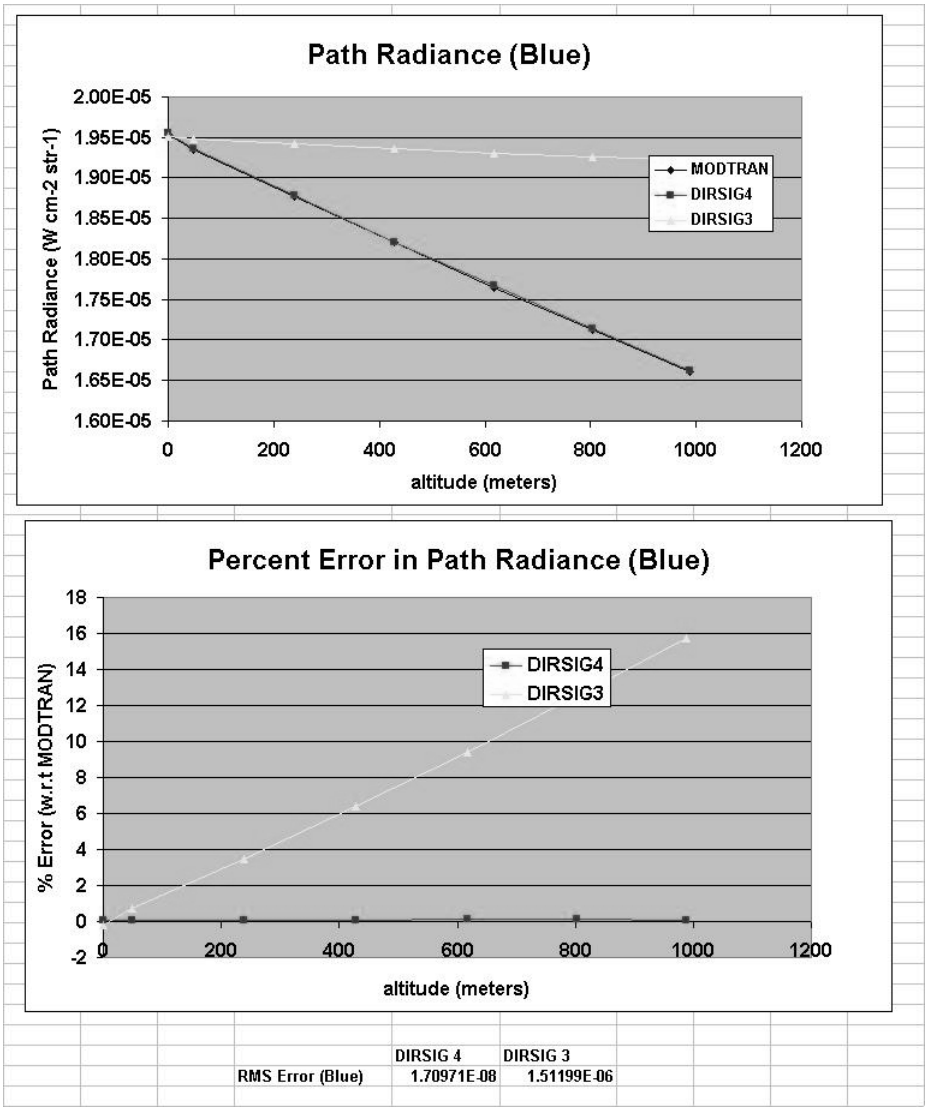

	DIRSIG 4	DIRSIG 3
RMS Error (Blue)	1.70971E-08	1.51199E-06

Figure B.75: Test Scene 2c (altitude variation): The upper graph shows the blue path radiance obtained by MODTRAN, DIRSIG 4 and DIRSIG 3. The lower graph shows the percent error of DIRSIG 4 and DIRSIG 3 relative to MODTRAN. The RMS errors for the points shown on the graph are listed below the graphs.

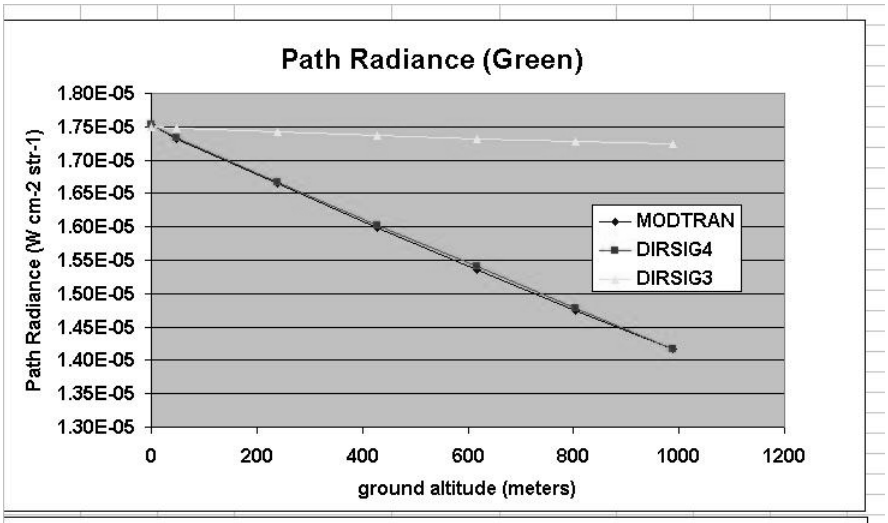

	DIRSIG 4	DIRSIG 3
RMS Error (Green)	2.98228E-08	1.78179E-06

Figure B.76: Test Scene 2c (altitude variation): The upper graph shows the green path radiance obtained by MODTRAN, DIRSIG 4 and DIRSIG 3. The lower graph shows the percent error of DIRSIG 4 and DIRSIG 3 relative to MODTRAN. The RMS errors for the points shown on the graph are listed below the graphs.

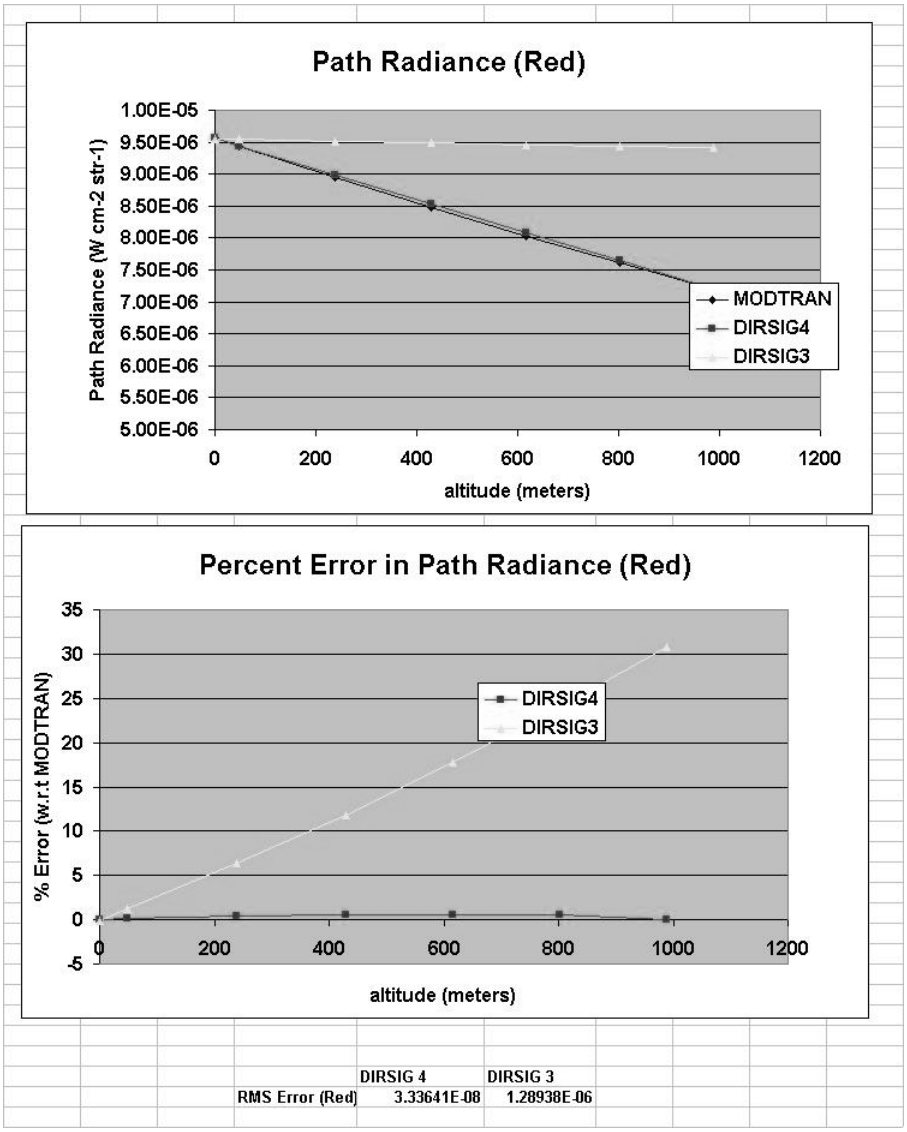

Figure B.77: Test Scene 2c (altitude variation): The upper graph shows the red path radiance obtained by MODTRAN, DIRSIG 4 and DIRSIG 3. The lower graph shows the percent error of DIRSIG 4 and DIRSIG 3 relative to MODTRAN. The RMS errors for the points shown on the graph are listed below the graphs.

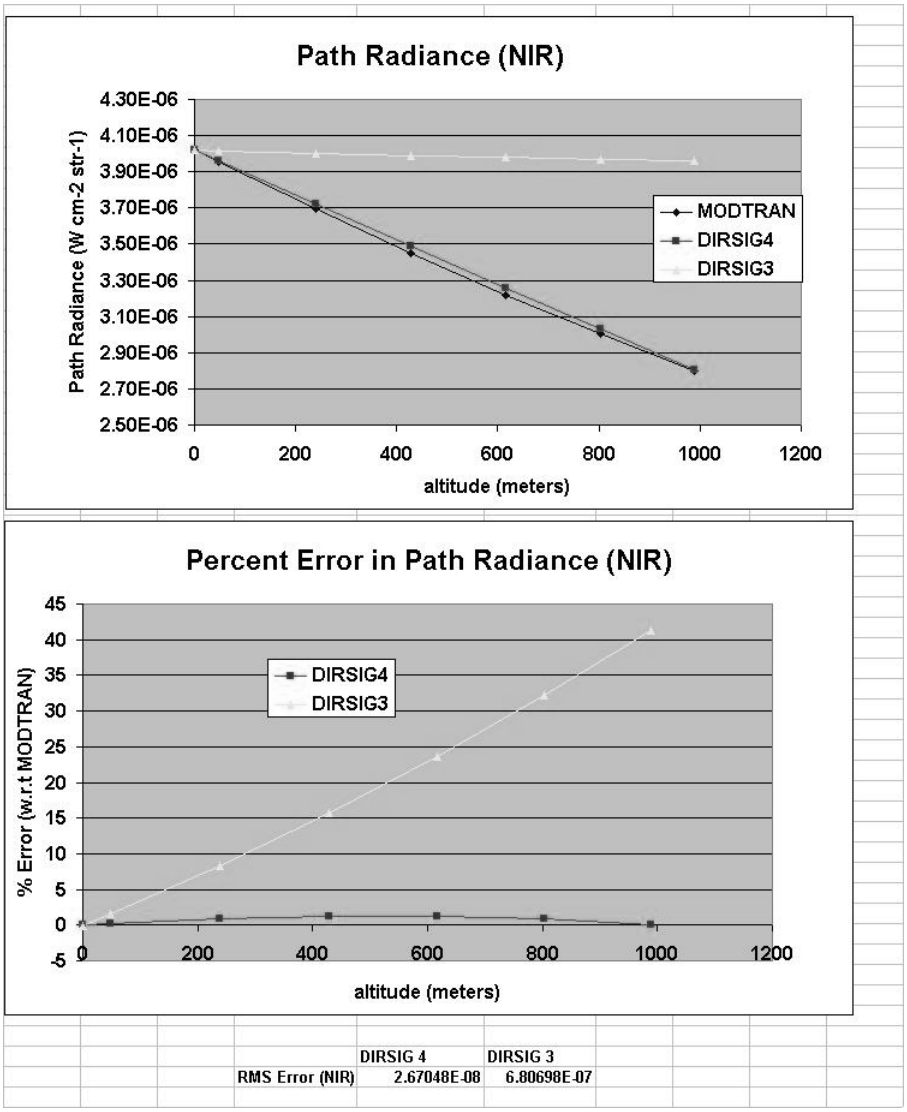

Figure B.78: Test Scene 2c (altitude variation): The upper graph shows the NIR path radiance obtained by MODTRAN, DIRSIG 4 and DIRSIG 3. The lower graph shows the percent error of DIRSIG 4 and DIRSIG 3 relative to MODTRAN. The RMS errors for the points shown on the graph are listed below the graphs.

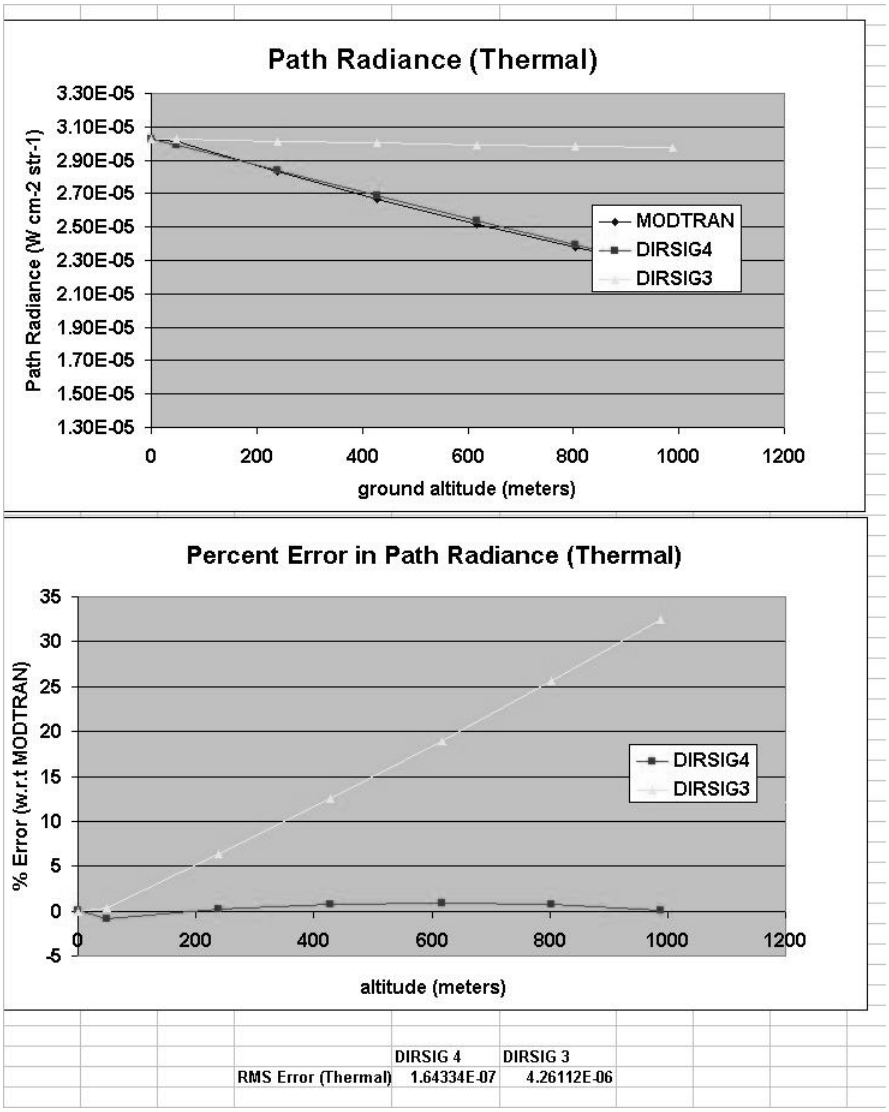

Figure B.79: Test Scene 2c (altitude variation): The upper graph shows the thermal path radiance obtained by MODTRAN, DIRSIG 4 and DIRSIG 3. The lower graph shows the percent error of DIRSIG 4 and DIRSIG 3 relative to MODTRAN. The RMS errors for the points shown on the graph are listed below the graphs.

B.7.2 Test Image 2c Grid Results.

To assess the performance of both interpolators over the entire image, analysis was performed at nearly regular spatial intervals (see figure B.56). The RMS error for each band was calculated for all of the points, as in image 2a. The RMS error (by band) in path radiance is shown in figure B.80.

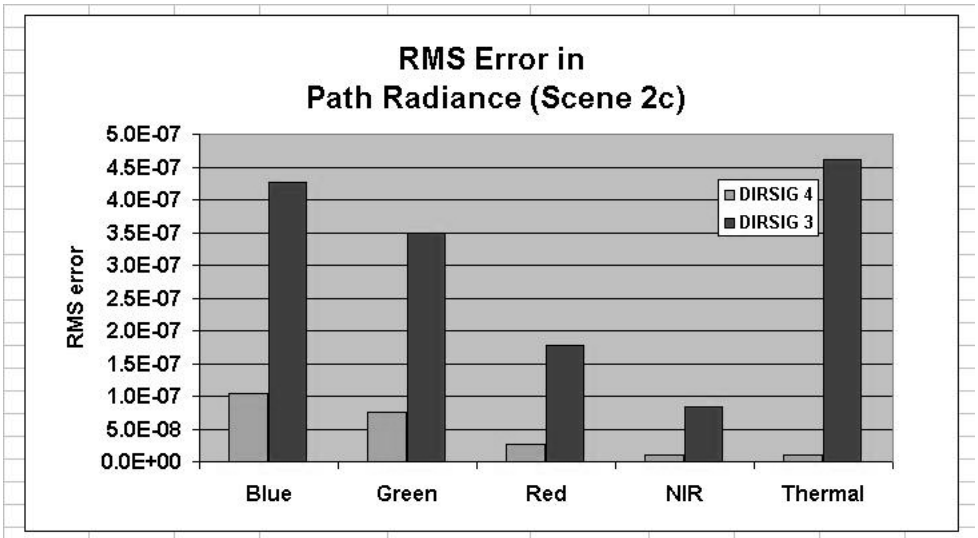

band	DIRSIG 4	DIRSIG 3
Blue	1.048826E-07	4.270471E-07
Green	7.529243E-08	3.481686E-07
Red	2.642797E-08	1.776157E-07
NIR	9.616555E-09	8.391835E-08
Thermal	1.042466E-08	4.617851E-07

Figure B.80: The RMS error in radiance for each band in image 2c.

B.8 Test Image 3

Up to this point, the point of test images were to focus on the improvement of the geometric aspects of the new interpolator. This is the first test image which directly examines a horizontally varying atmosphere. Test image 3 is identical to test image 1a, except that there is horizontally varying water vapor map in the scene. This map has a column water vapor value of 1 g/cm2, at the upper (Western) edge of the image. The water vapor value increases linearly to the East until it reaches a maximum of 2.5 g/cm2 at the lower (Eastern) edge.

A visualization of this map found in chapter 4.

Figure B.81 shows the path radiance in the 'water2' band (940 nm) of image 3 rendered with the DIRSIG 4 interpolator.

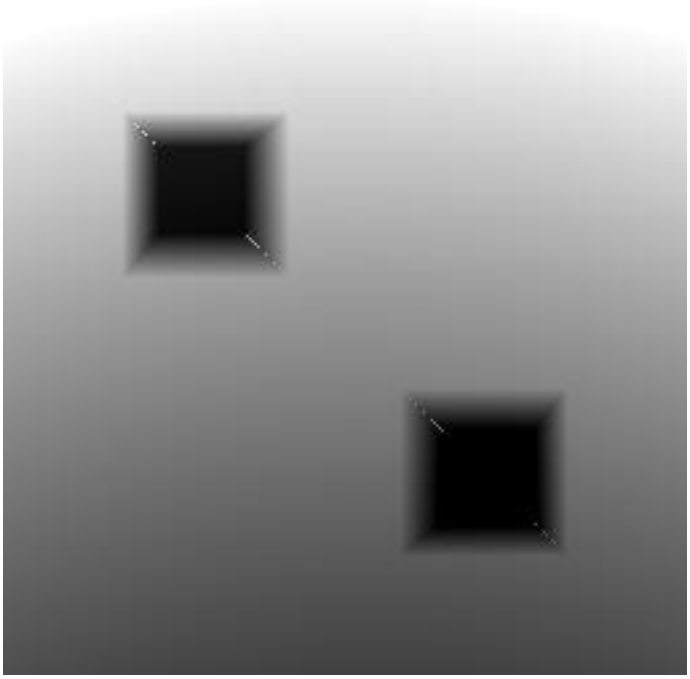

Figure B.81: The path radiance of image 3 in the 'water2' band (940 nm), rendered by DIRSIG 4.

B.8.1 Test Image 3 Water Variation

To observe the effect of the water vapor wedge, a line of points were analyzed. These points are shown in figure B.82, and mark a linear increase in the amount of water vapor present in the atmosphere. It should be noted that all of the other dimensions (zenith, azimuth, and altitude) except for visibility will be varying as well.

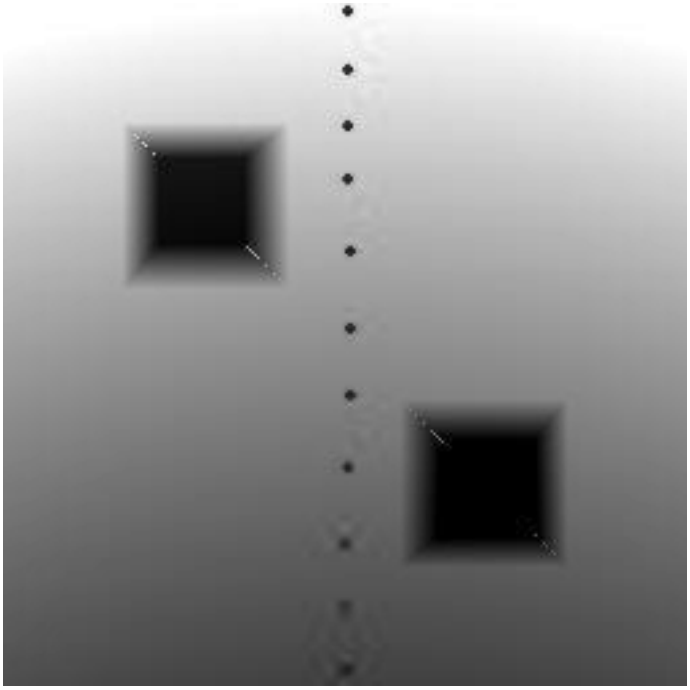

Figure B.82: The path radiance of image 3 in the 'water2' band (940 nm), rendered by DIRSIG 4.

The radiance results for all of the bands are shown in the following figures (Figures B.83 through B.88.)

The transmission results for all of the bands are shown in the following figures (Figures B.89 through B.94.)

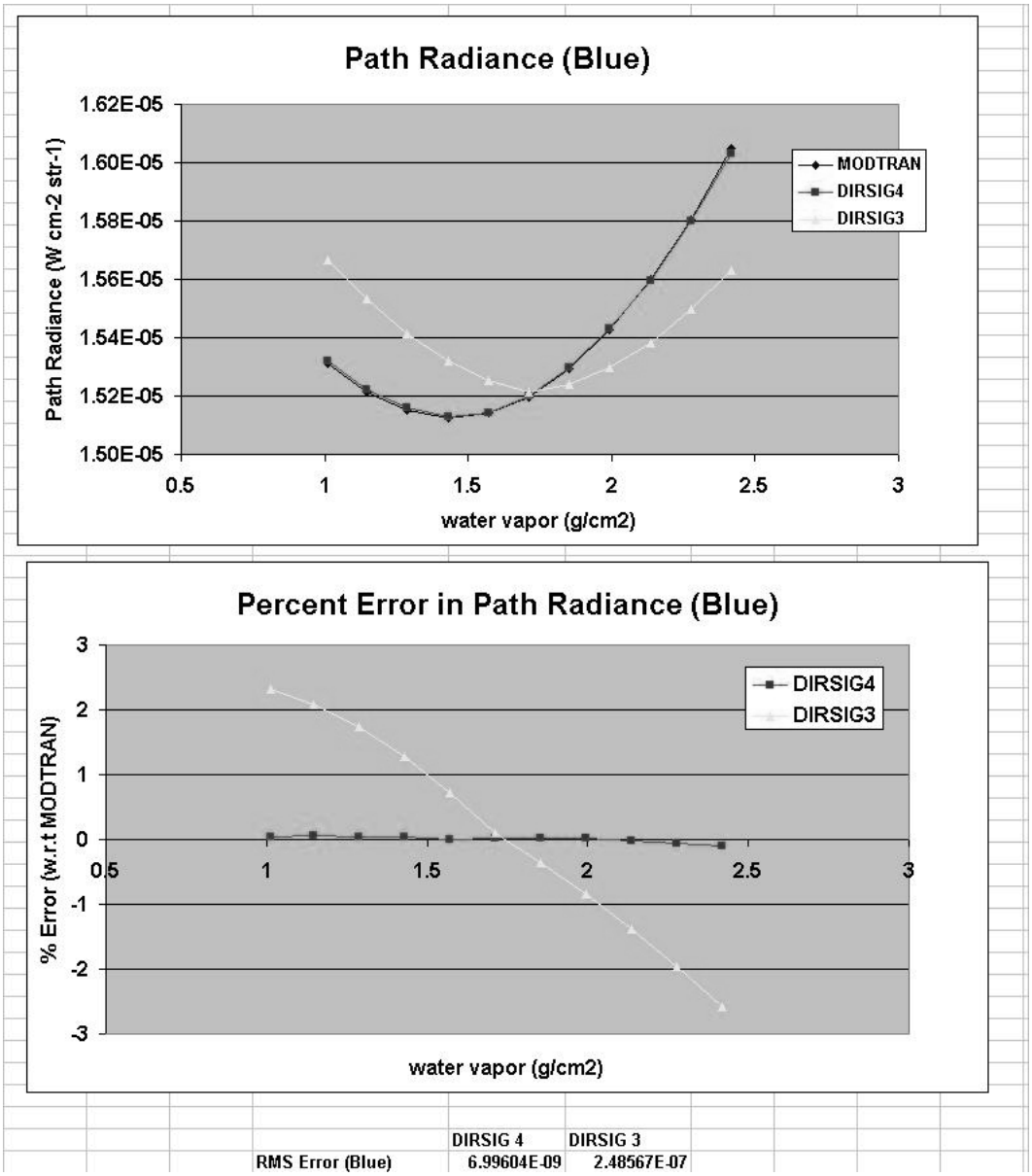

Figure B.83: Test Scene 3 (water variation): The upper graph shows the blue path radiance obtained by MODTRAN, DIRSIG 4 and DIRSIG 3. The lower graph shows the percent error of DIRSIG 4 and DIRSIG 3 relative to MODTRAN. The RMS errors for the points shown on the graph are listed below the graphs.

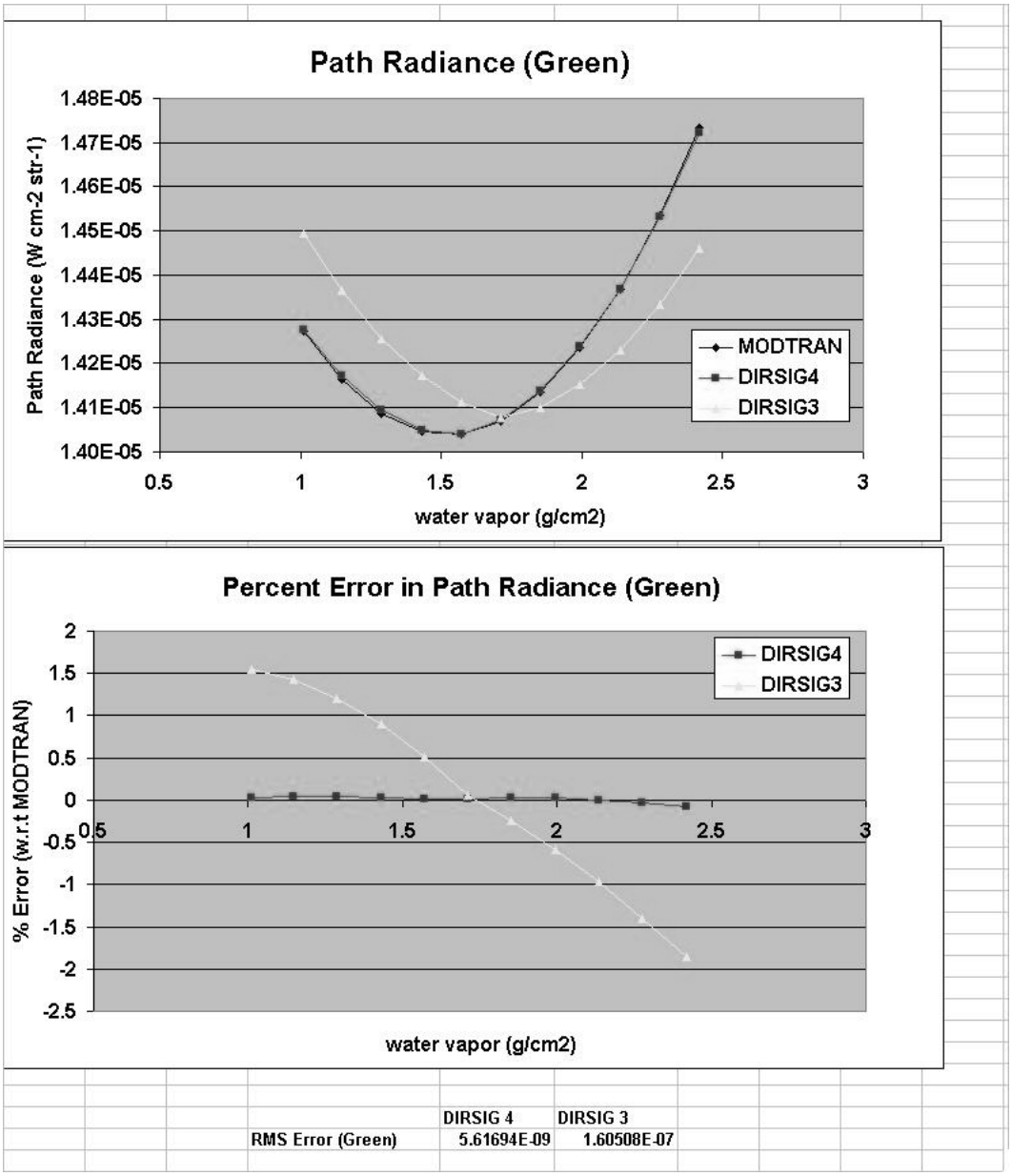

Figure B.84: Test Scene 3 (water variation): The upper graph shows the green path radiance obtained by MODTRAN, DIRSIG 4 and DIRSIG 3. The lower graph shows the percent error of DIRSIG 4 and DIRSIG 3 relative to MODTRAN. The RMS errors for the points shown on the graph are listed below the graphs.

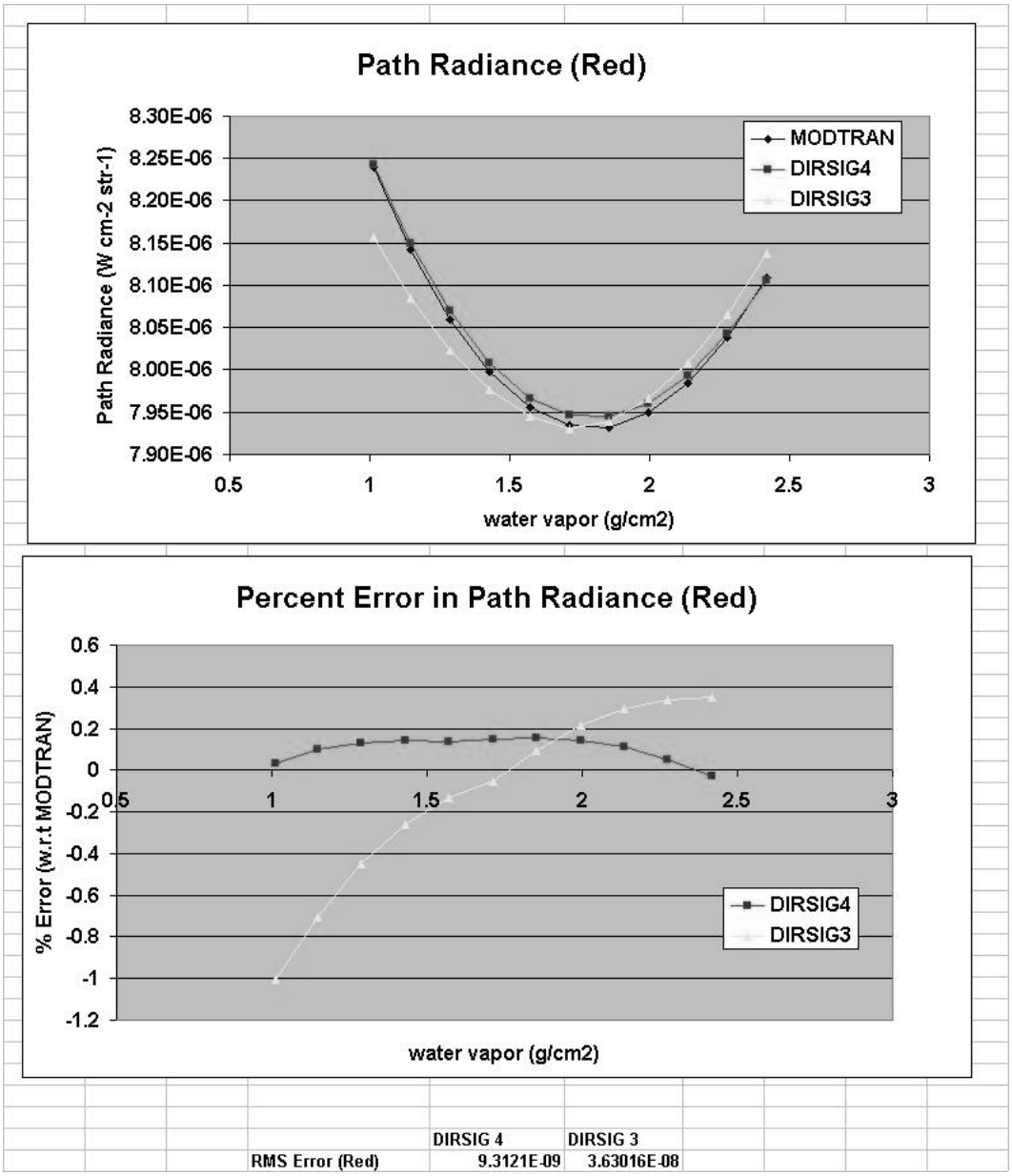

Figure B.85: Test Scene 3 (water variation): The upper graph shows the red path radiance obtained by MODTRAN, DIRSIG 4 and DIRSIG 3. The lower graph shows the percent error of DIRSIG 4 and DIRSIG 3 relative to MODTRAN. The RMS errors for the points shown on the graph are listed below the graphs.

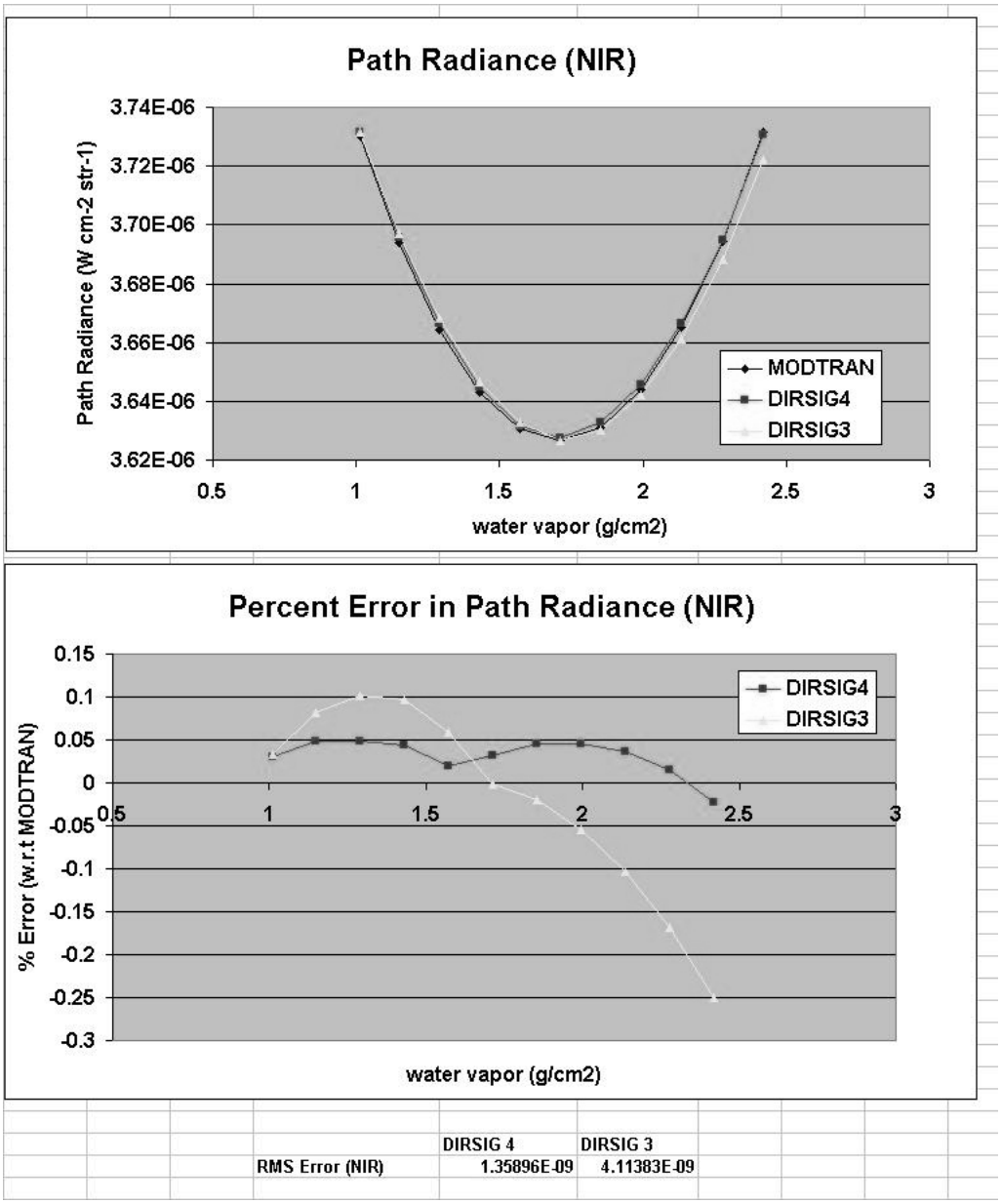

Figure B.86: Test Scene 3 (water variation): The upper graph shows the NIR path radiance obtained by MODTRAN, DIRSIG 4 and DIRSIG 3. The lower graph shows the percent error of DIRSIG 4 and DIRSIG 3 relative to MODTRAN. The RMS errors for the points shown on the graph are listed below the graphs.

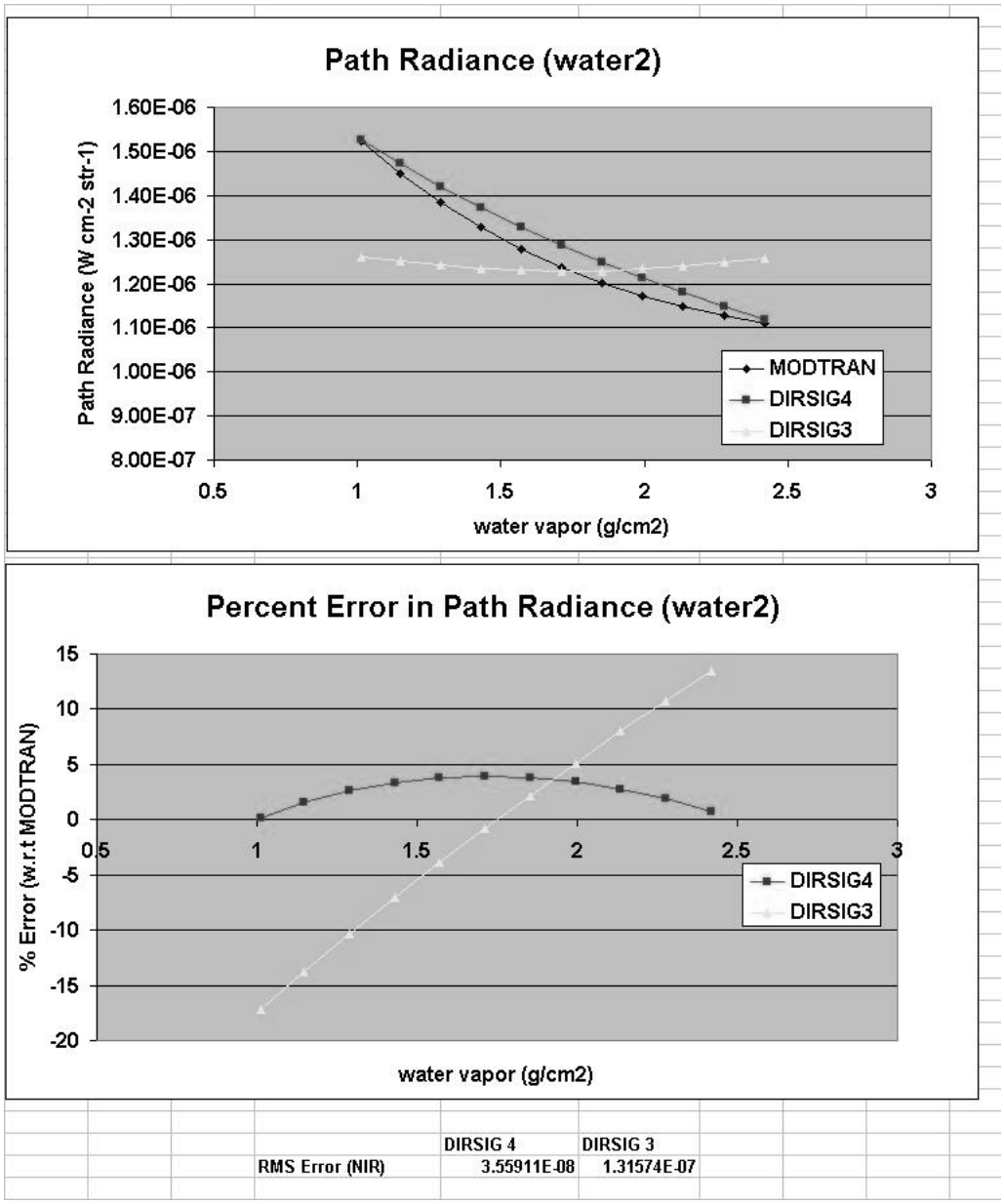

Figure B.87: Test Scene 3 (water variation): The upper graph shows the water2 path radiance obtained by MODTRAN, DIRSIG 4 and DIRSIG 3. The lower graph shows the percent error of DIRSIG 4 and DIRSIG 3 relative to MODTRAN. The RMS errors for the points shown on the graph are listed below the graphs.

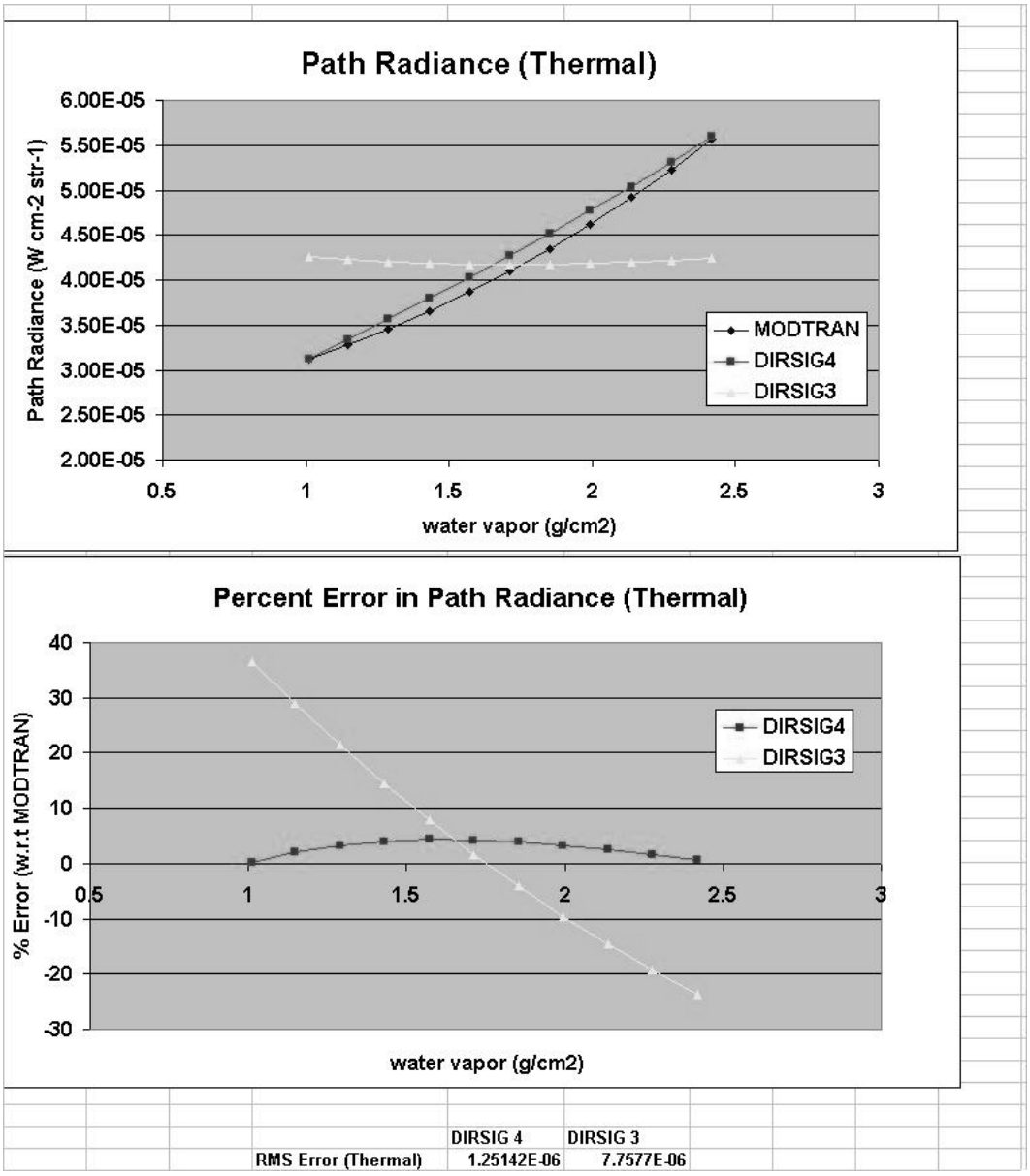

Figure B.88: Test Scene 3 (water variation): The upper graph shows the Thermal path radiance obtained by MODTRAN, DIRSIG 4 and DIRSIG 3. The lower graph shows the percent error of DIRSIG 4 and DIRSIG 3 relative to MODTRAN. The RMS errors for the points shown on the graph are listed below the graphs.

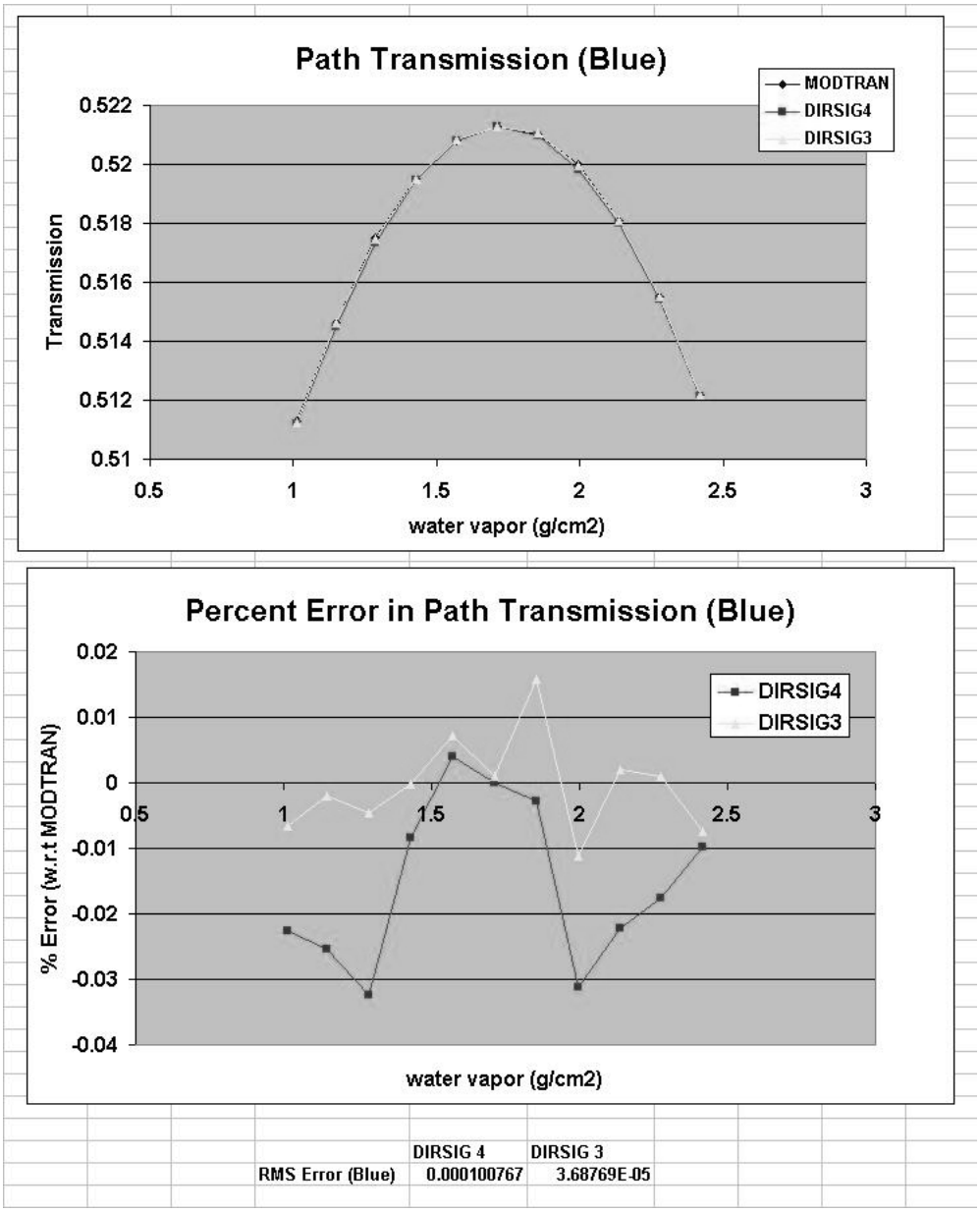

	DIRSIG 4	DIRSIG 3
RMS Error (Blue)	0.000100767	3.68769E-05

Figure B.89: Test Scene 3 (water variation): The upper graph shows the blue path transmission obtained by MODTRAN, DIRSIG 4 and DIRSIG 3. The lower graph shows the percent error of DIRSIG 4 and DIRSIG 3 relative to MODTRAN. The RMS errors for the points shown on the graph are listed below the graphs.

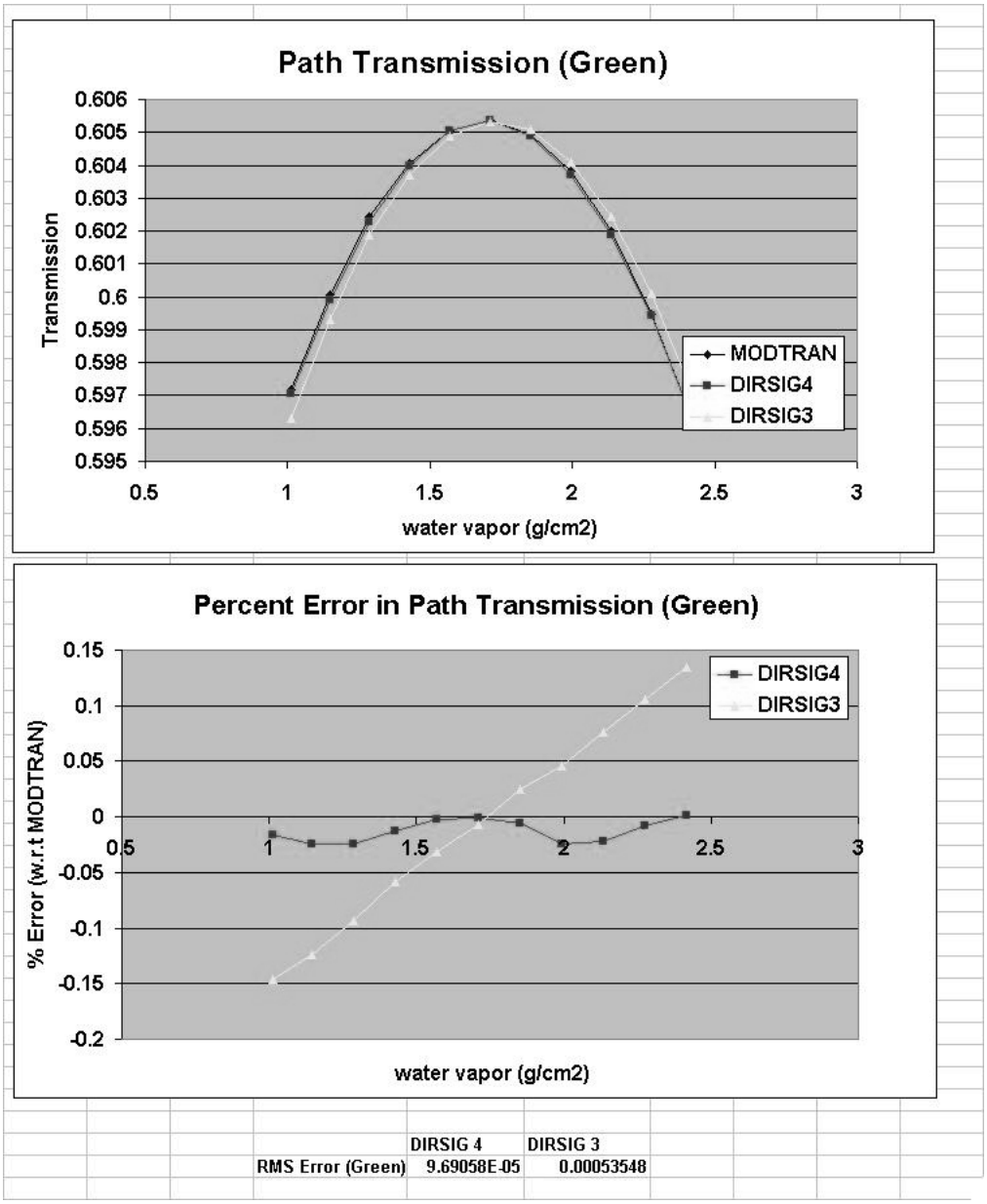

Figure B.90: Test Scene 3 (water variation): The upper graph shows the green path transmission obtained by MODTRAN, DIRSIG 4 and DIRSIG 3. The lower graph shows the percent error of DIRSIG 4 and DIRSIG 3 relative to MODTRAN. The RMS errors for the points shown on the graph are listed below the graphs.

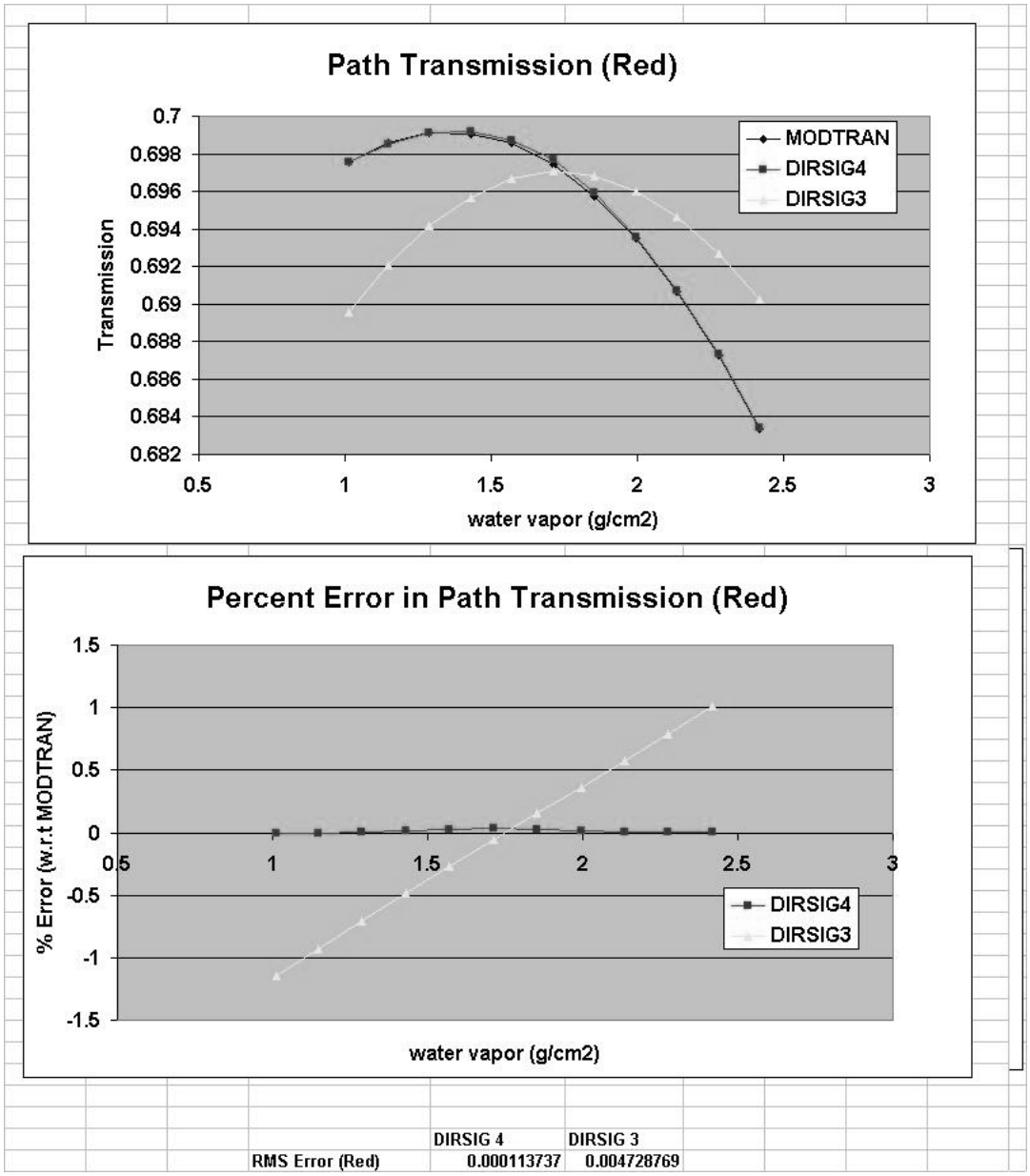

Figure B.91: Test Scene 3 (water variation): The upper graph shows the red path transmission obtained by MODTRAN, DIRSIG 4 and DIRSIG 3. The lower graph shows the percent error of DIRSIG 4 and DIRSIG 3 relative to MODTRAN. The RMS errors for the points shown on the graph are listed below the graphs.

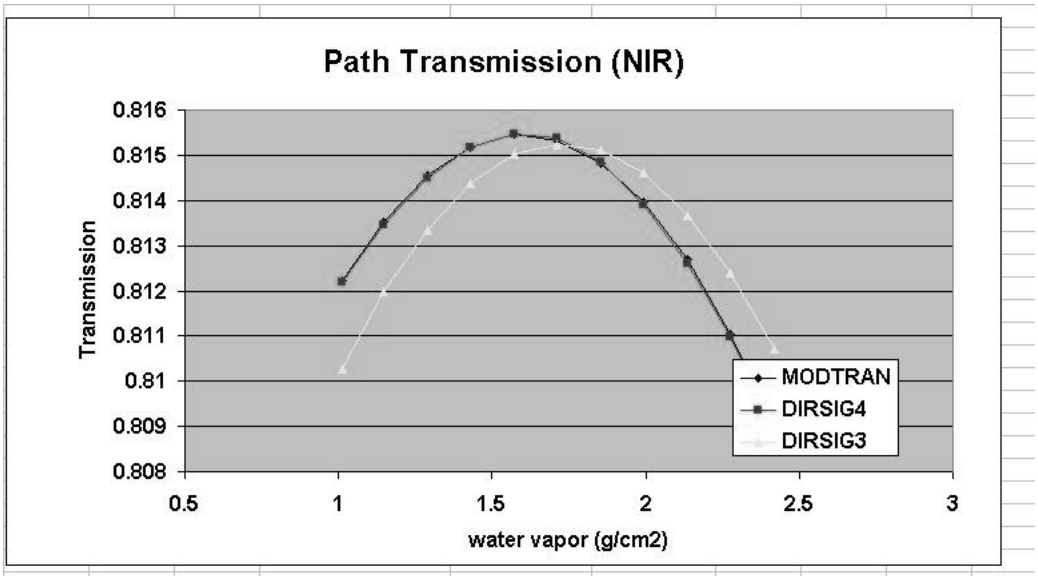

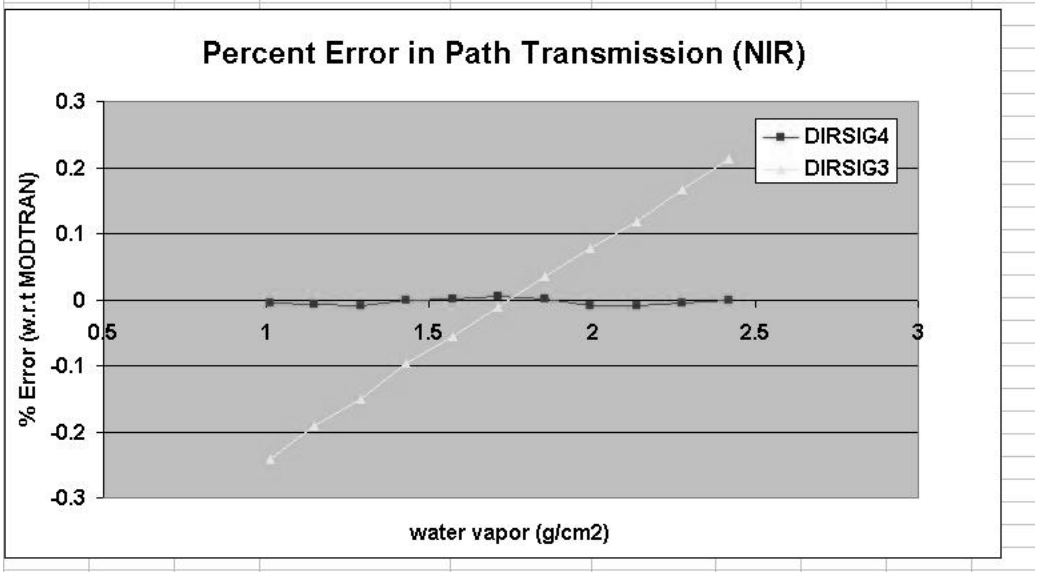

	DIRSIG 4	DIRSIG 3
RMS Error (NIR)	4.95617E-05	0.001162929

Figure B.92: Test Scene 3 (water variation): The upper graph shows the NIR path transmission obtained by MODTRAN, DIRSIG 4 and DIRSIG 3. The lower graph shows the percent error of DIRSIG 4 and DIRSIG 3 relative to MODTRAN. The RMS errors for the points shown on the graph are listed below the graphs.

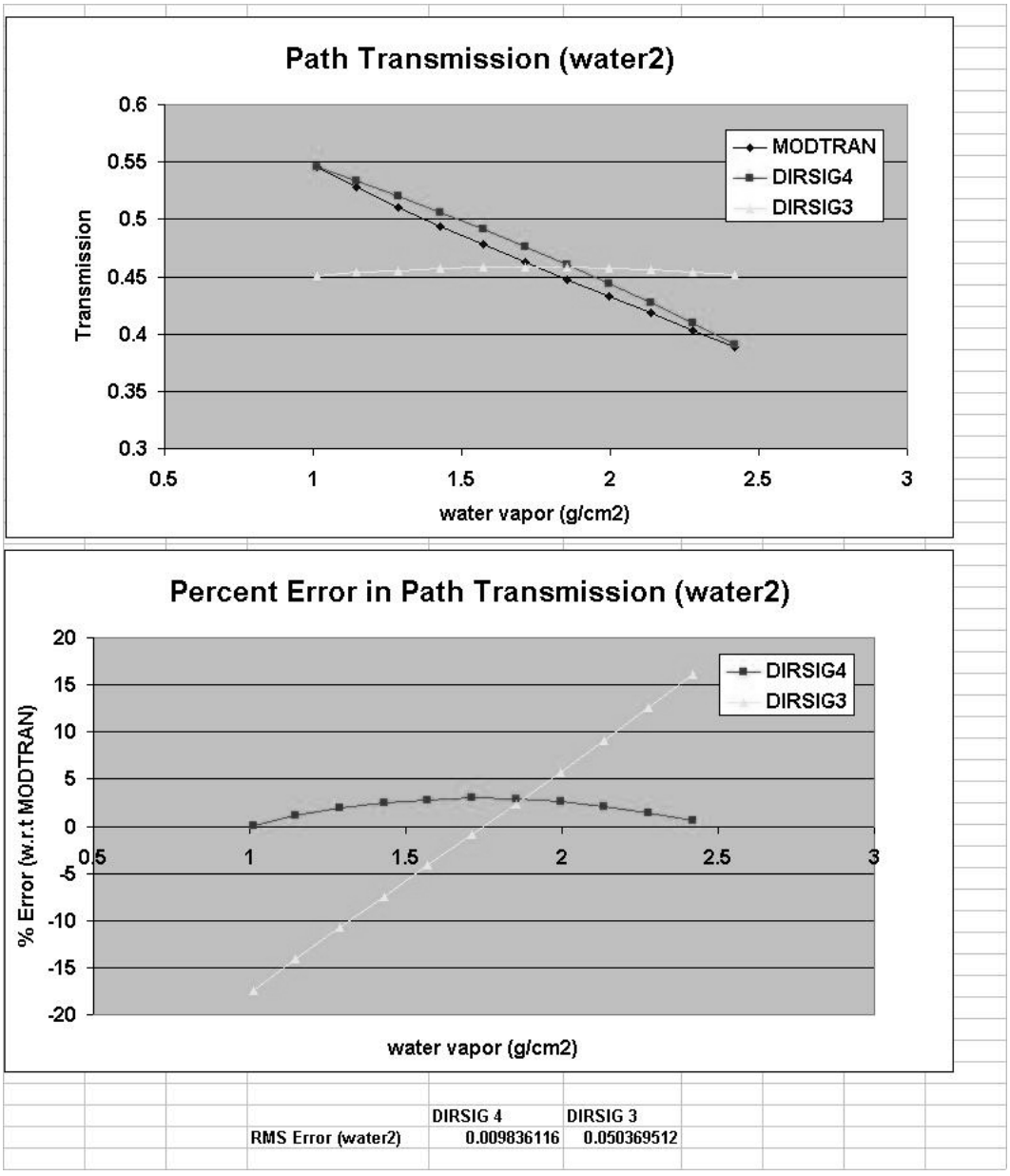

	DIRSIG 4	DIRSIG 3
RMS Error (water2)	0.009836116	0.050369512

Figure B.93: Test Scene 3 (water variation): The upper graph shows the water2 path transmission obtained by MODTRAN, DIRSIG 4 and DIRSIG 3. The lower graph shows the percent error of DIRSIG 4 and DIRSIG 3 relative to MODTRAN. The RMS errors for the points shown on the graph are listed below the graphs.

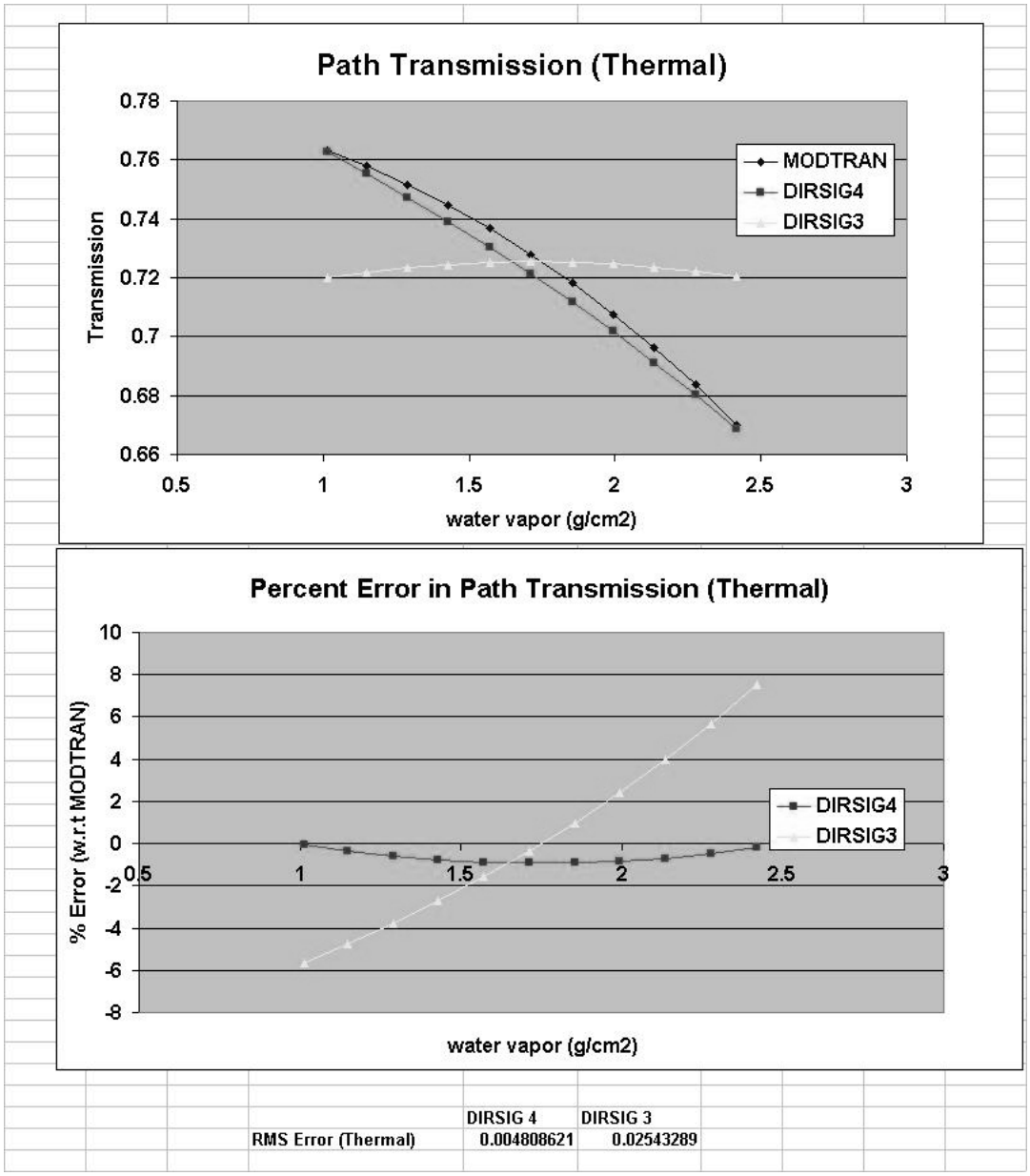

	DIRSIG 4	DIRSIG 3
RMS Error (Thermal)	0.004808621	0.02543289

Figure B.94: Test Scene 3 (water variation): The upper graph shows the Thermal path transmission obtained by MODTRAN, DIRSIG 4 and DIRSIG 3. The lower graph shows the percent error of DIRSIG 4 and DIRSIG 3 relative to MODTRAN. The RMS errors for the points shown on the graph are listed below the graphs.

B.8.2 Test Image 3 Grid Results

To assess the performance of both interpolators, the images were analyzed at nearly regular spatial intervals (see figure B.19). As well, two additional points at the top of each of the truncated pyramids were included, to bring non-zero altitudes into the analysis. The RMS error for each band was calculated for all of the points.

These errors for path radiances are shown in figure B.95 , and for transmission in figure B.96.

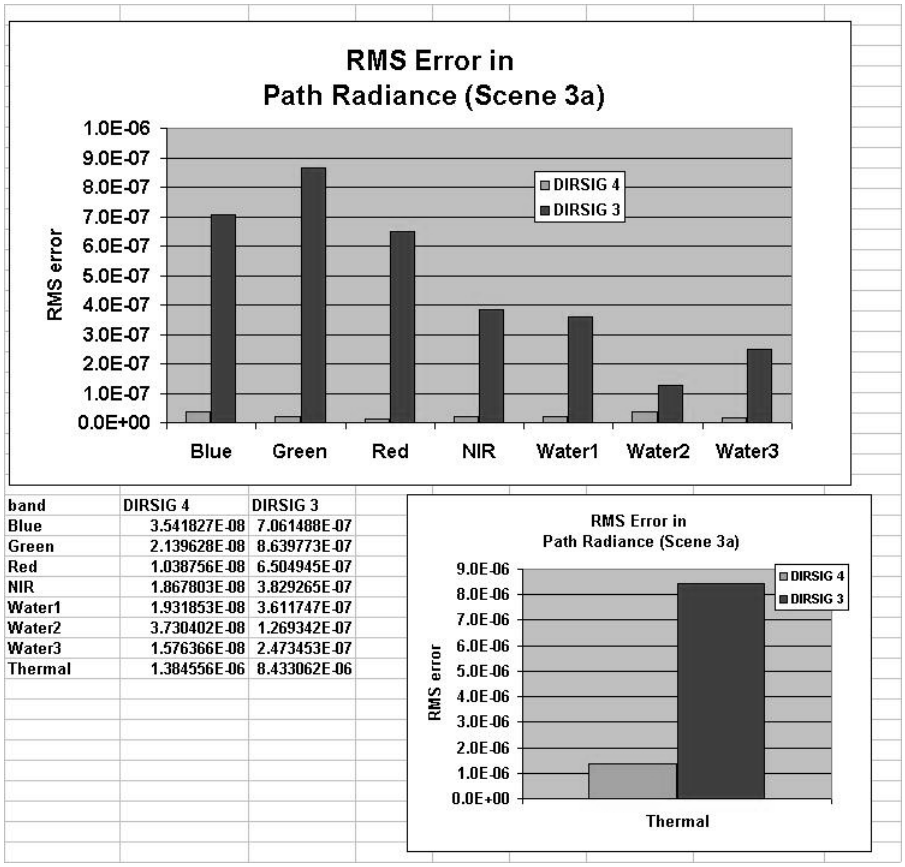

band	DIRSIG 4	DIRSIG 3
Blue	3.541827E-08	7.061488E-07
Green	2.139628E-08	8.639773E-07
Red	1.038756E-08	6.504945E-07
NIR	1.867803E-08	3.829265E-07
Water1	1.931853E-08	3.611747E-07
Water2	3.730402E-08	1.269342E-07
Water3	1.576366E-08	2.473453E-07
Thermal	1.384556E-06	8.433062E-06

Figure B.95: The RMS error in radiance for each band in image 3.

The bands labeled "Water1", "Water2", and "Water3" correspond to spectral values about and centered on the water vapor absorption feature at 940 nm. The three bands correspond to 880 nm, 940 nm, and 1,000 nm.

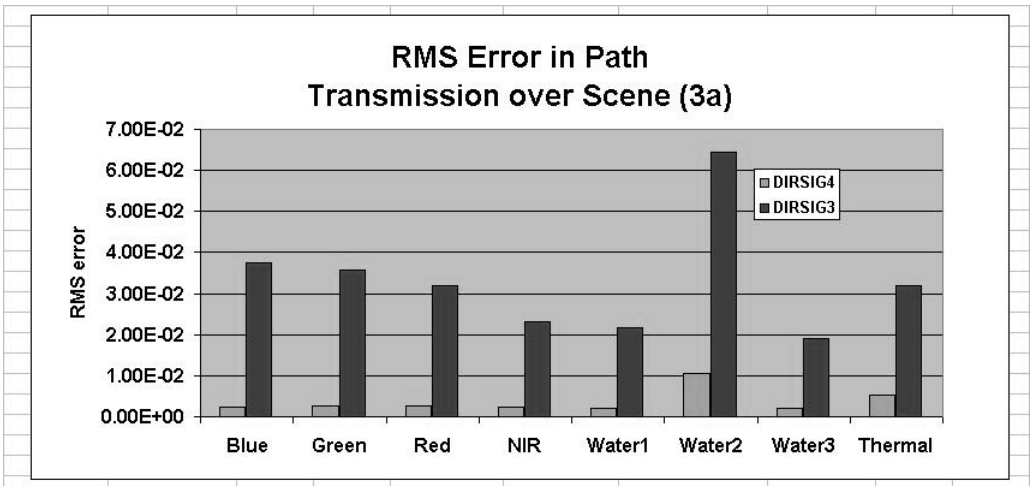

band	DIRSIG4	DIRSIG3
Blue	2.377344E-03	3.759451E-02
Green	2.674025E-03	3.567550E-02
Red	2.691113E-03	3.191789E-02
NIR	2.271498E-03	2.307631E-02
Water1	2.182873E-03	2.175919E-02
Water2	1.046241E-02	6.430360E-02
Water3	1.965138E-03	1.912360E-02
Thermal	5.131777E-03	3.183733E-02

Figure B.96: The RMS error in transmission for each band in image 3.

B.9 Test Image 4a

This test image directly examines an atmosphere with horizontally varying visibility. Test image 4a is identical to test image 1a, except that there is horizontally varying visibility map in the scene. This map has a visibility value of 1 km at the upper (Western) edge of the image, and the visibility value increases linearly to the East until it reaches a maximum of 23 km at the lower (Eastern) edge.

Figure B.97 shows the path radiance (RGB) from test image 4a rendered with the DIRSIG 4 interpolator.

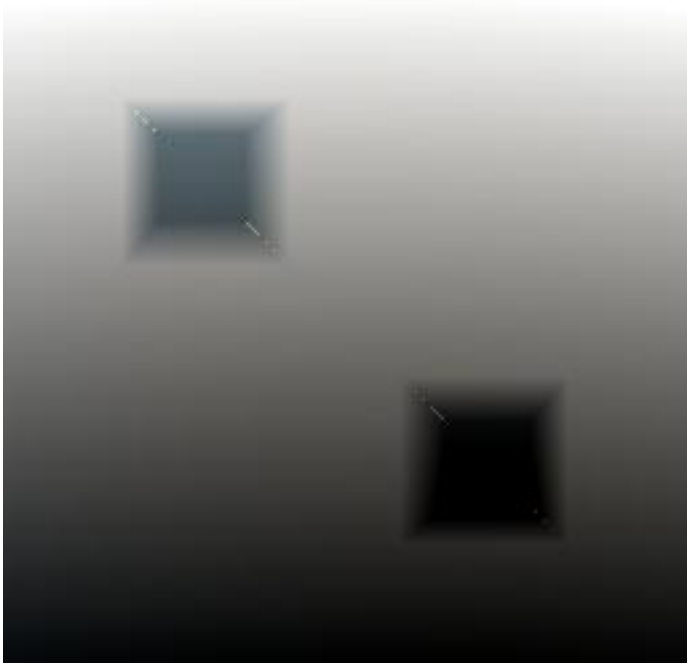

Figure B.97: The RGB path radiance of test image 4a rendered by DIRSIG 4.

B.9.1 Test Image 4a Visibility Variation

To observe the effect of the visibility wedge, a line of points were analyzed. These points are shown in figure B.82, and mark roughly a linear increase in the visibility of the aerosols in the atmosphere. It should be noted that all of the other dimensions (zenith, azimuth, and altitude) except for water vapor will be varying as well.

The radiance results for all of the bands are shown in the following figures (Figures B.98 through B.103.)

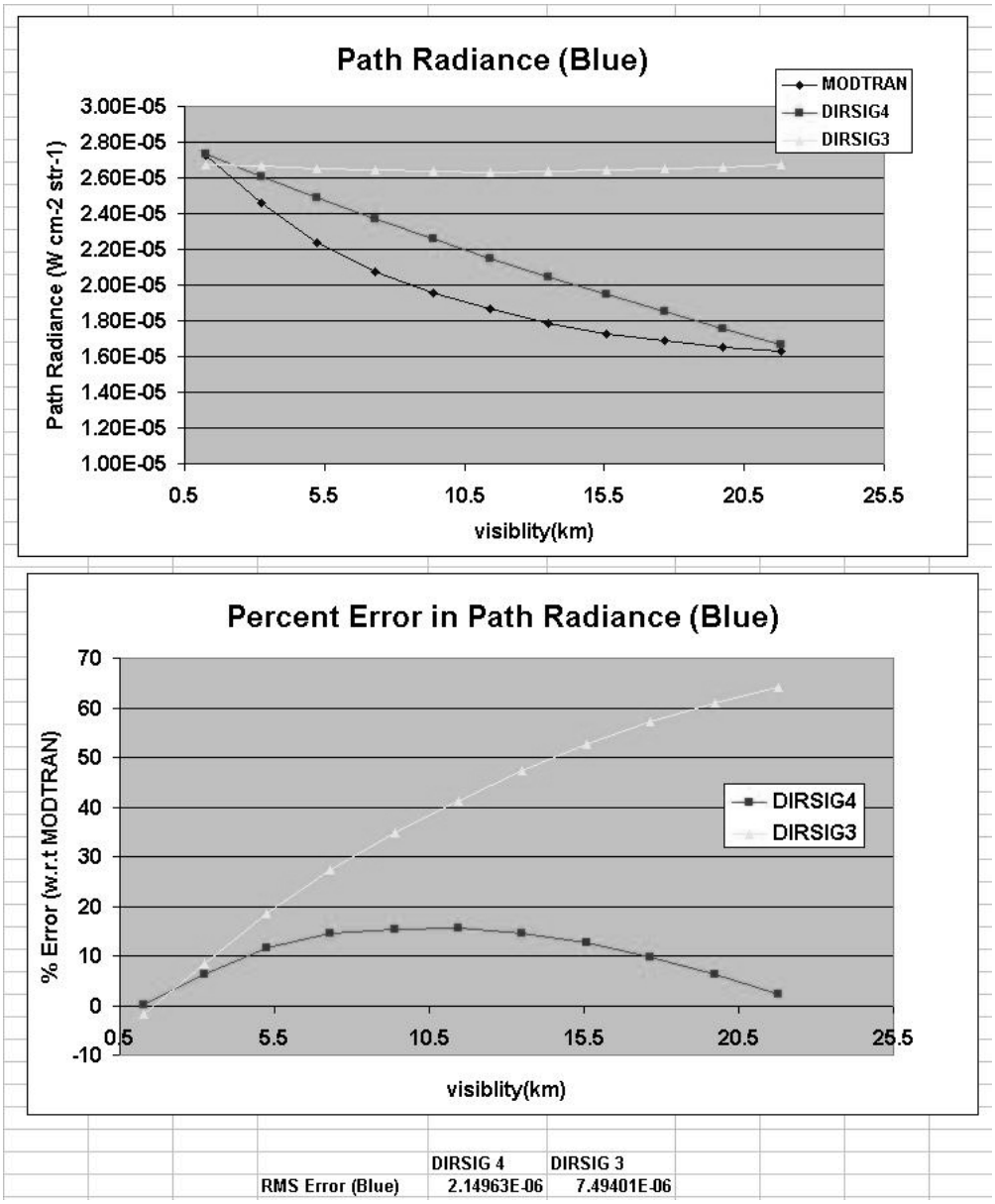

Figure B.98: Test Scene 4a (visibility variation): The upper graph shows the blue path radiance obtained by MODTRAN, DIRSIG 4 and DIRSIG 3. The lower graph shows the percent error of DIRSIG 4 and DIRSIG 3 relative to MODTRAN. The RMS errors for the points shown on the graph are listed below the graphs.

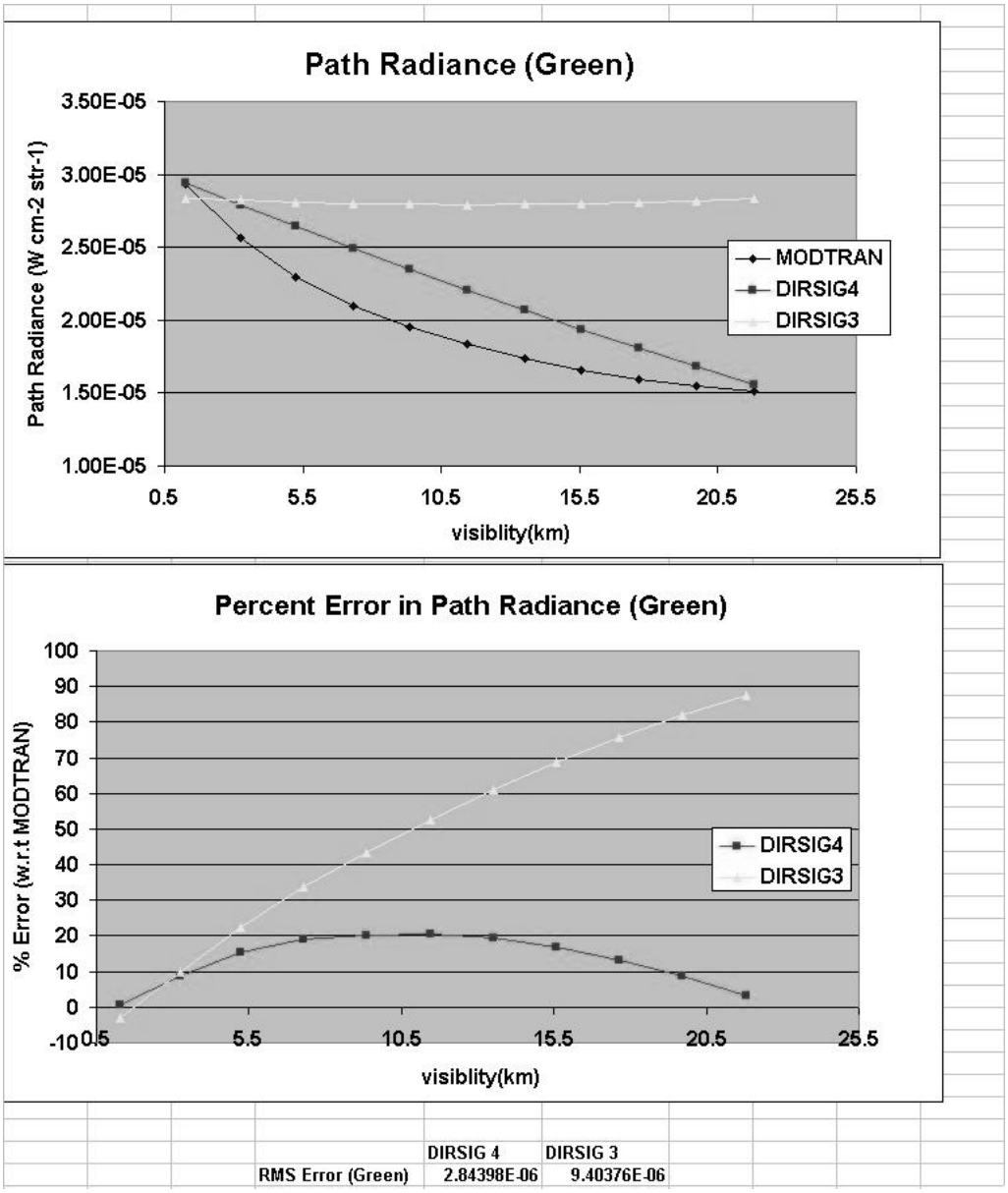

Figure B.99: Test Scene 4a (visibility variation): The upper graph shows the green path radiance obtained by MODTRAN, DIRSIG 4 and DIRSIG 3. The lower graph shows the percent error of DIRSIG 4 and DIRSIG 3 relative to MODTRAN. The RMS errors for the points shown on the graph are listed below the graphs.

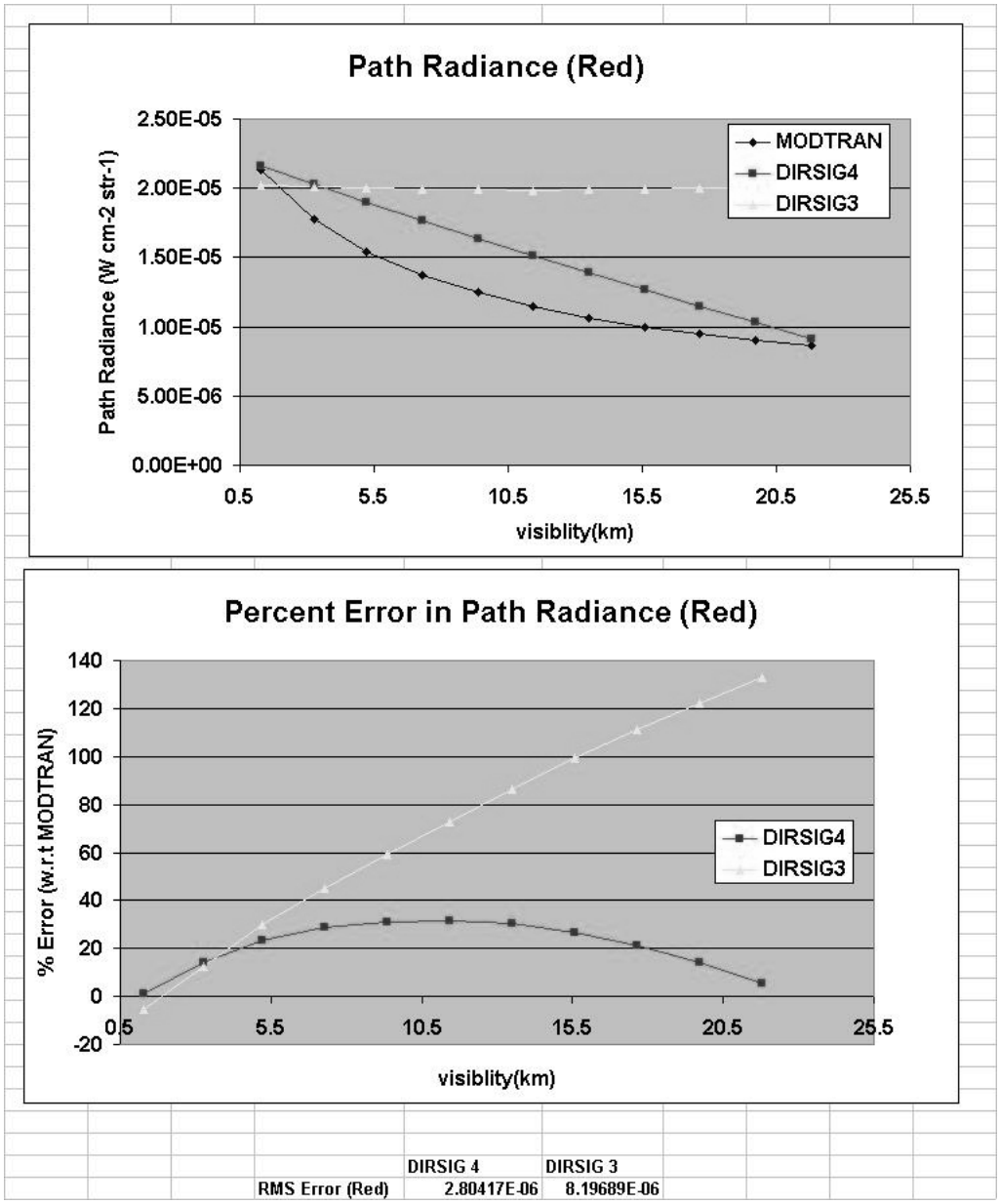

Figure B.100: Test Scene 4a (visibility variation): The upper graph shows the red path radiance obtained by MODTRAN, DIRSIG 4 and DIRSIG 3. The lower graph shows the percent error of DIRSIG 4 and DIRSIG 3 relative to MODTRAN. The RMS errors for the points shown on the graph are listed below the graphs.

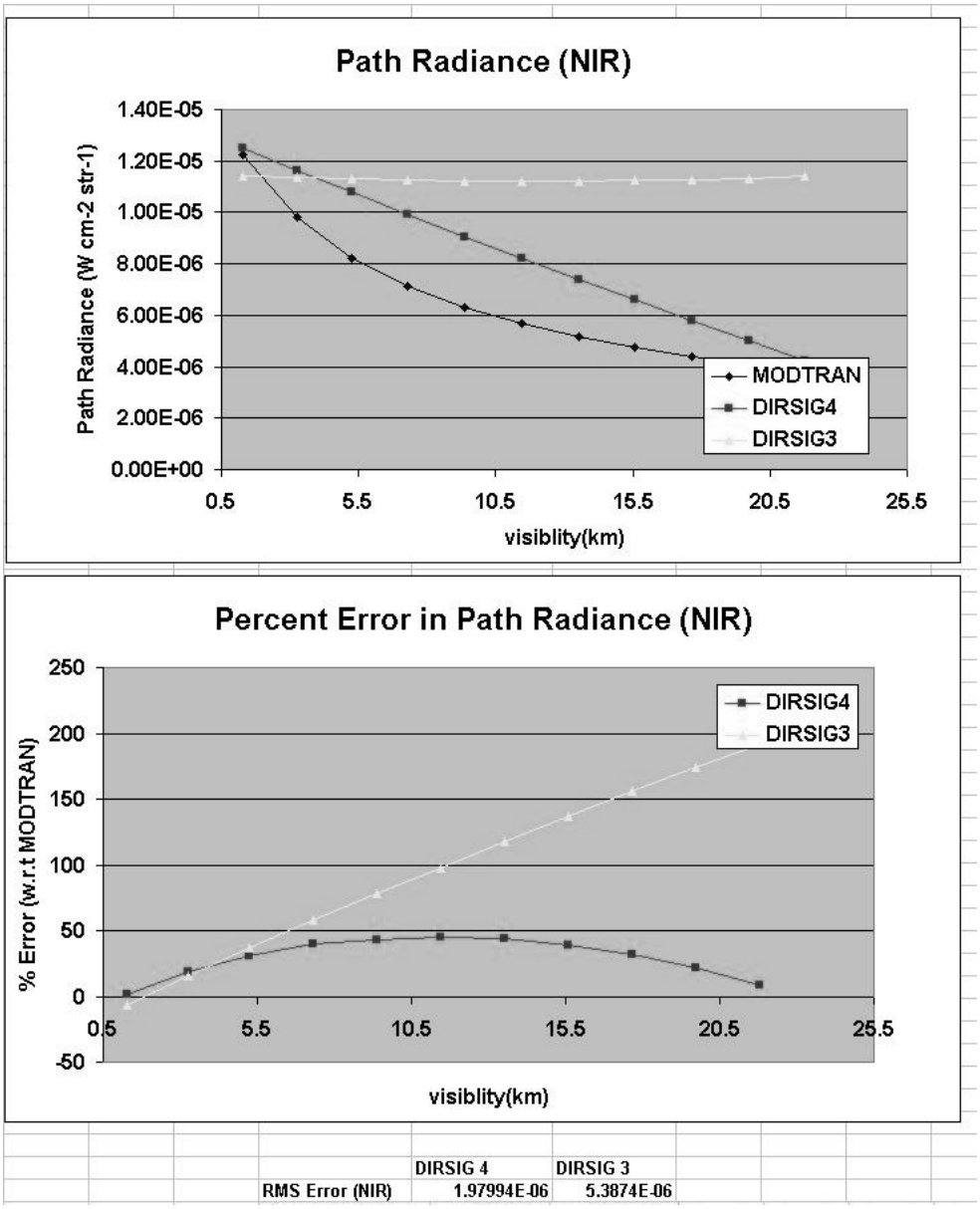

Figure B.101: Test Scene 4a (visibility variation): The upper graph shows the NIR path radiance obtained by MODTRAN, DIRSIG 4 and DIRSIG 3. The lower graph shows the percent error of DIRSIG 4 and DIRSIG 3 relative to MODTRAN. The RMS errors for the points shown on the graph are listed below the graphs.

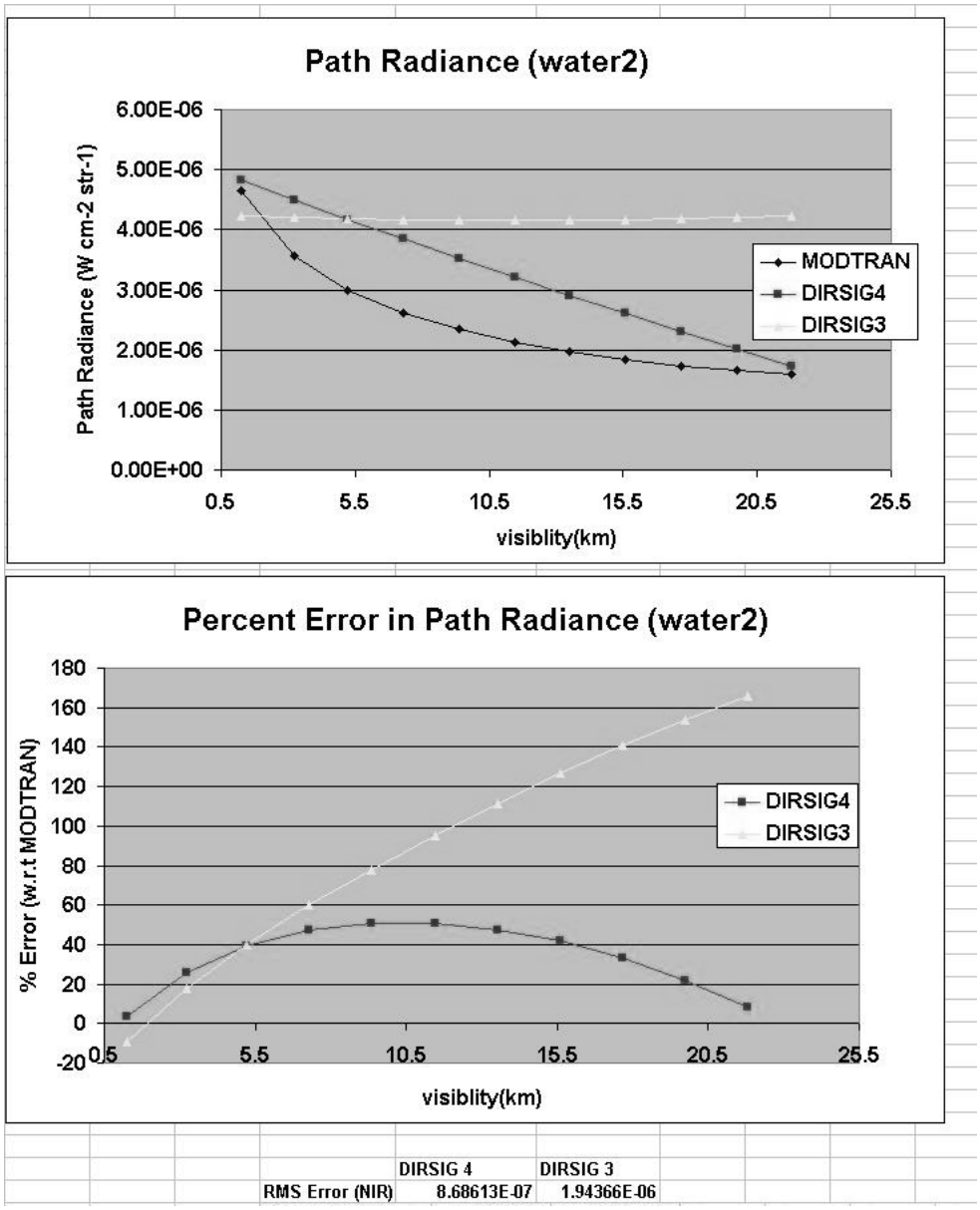

Figure B.102: Test Scene 4a (visibility variation): The upper graph shows the water2 path radiance obtained by MODTRAN, DIRSIG 4 and DIRSIG 3. The lower graph shows the percent error of DIRSIG 4 and DIRSIG 3 relative to MODTRAN. The RMS errors for the points shown on the graph are listed below the graphs.

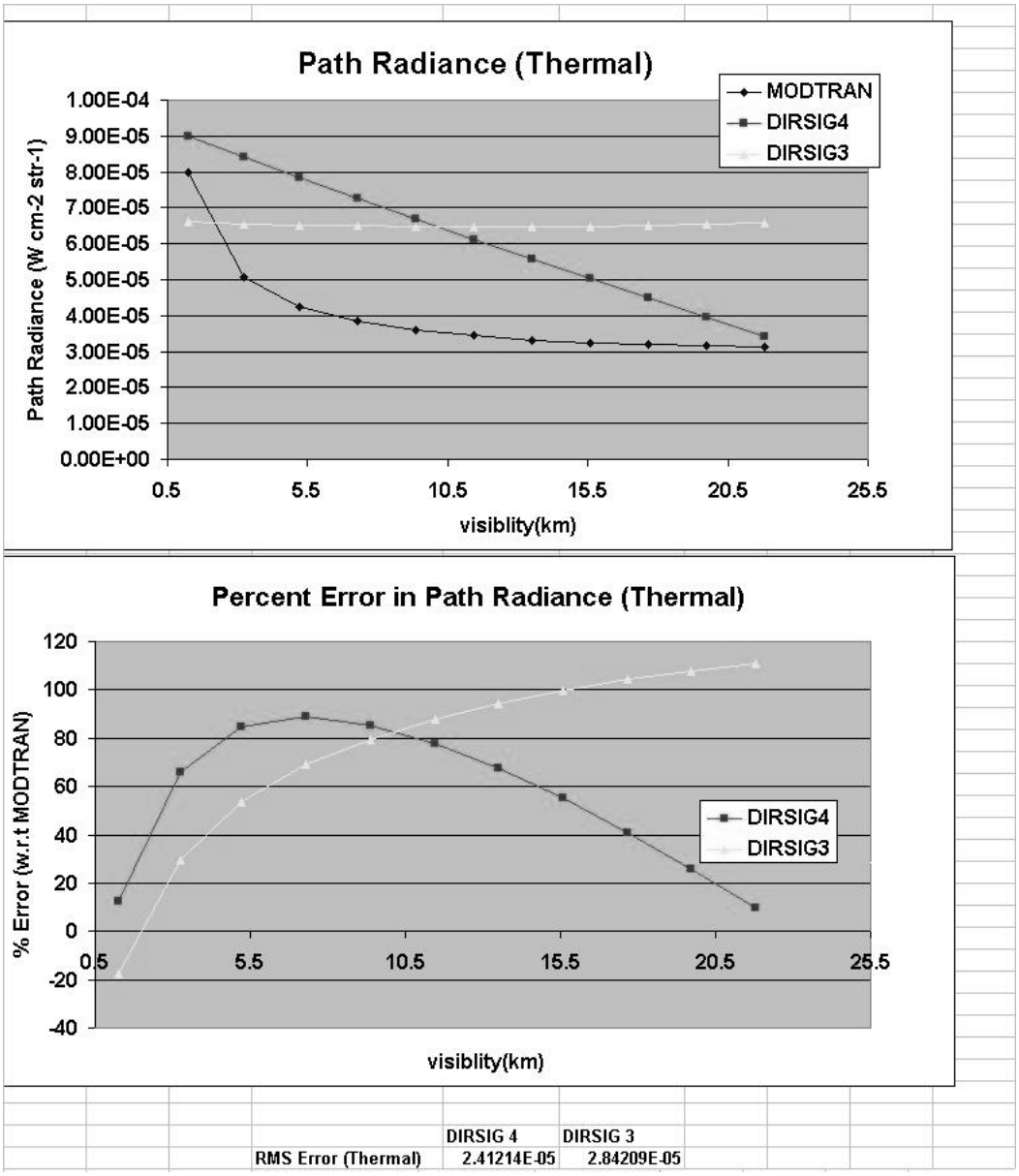

Figure B.103: Test Scene 4a (visibility variation): The upper graph shows the Thermal path radiance obtained by MODTRAN, DIRSIG 4 and DIRSIG 3. The lower graph shows the percent error of DIRSIG 4 and DIRSIG 3 relative to MODTRAN. The RMS errors for the points shown on the graph are listed below the graphs.

The transmission results for all of the bands are shown in the following figures (Figures B.104 through B.109.)

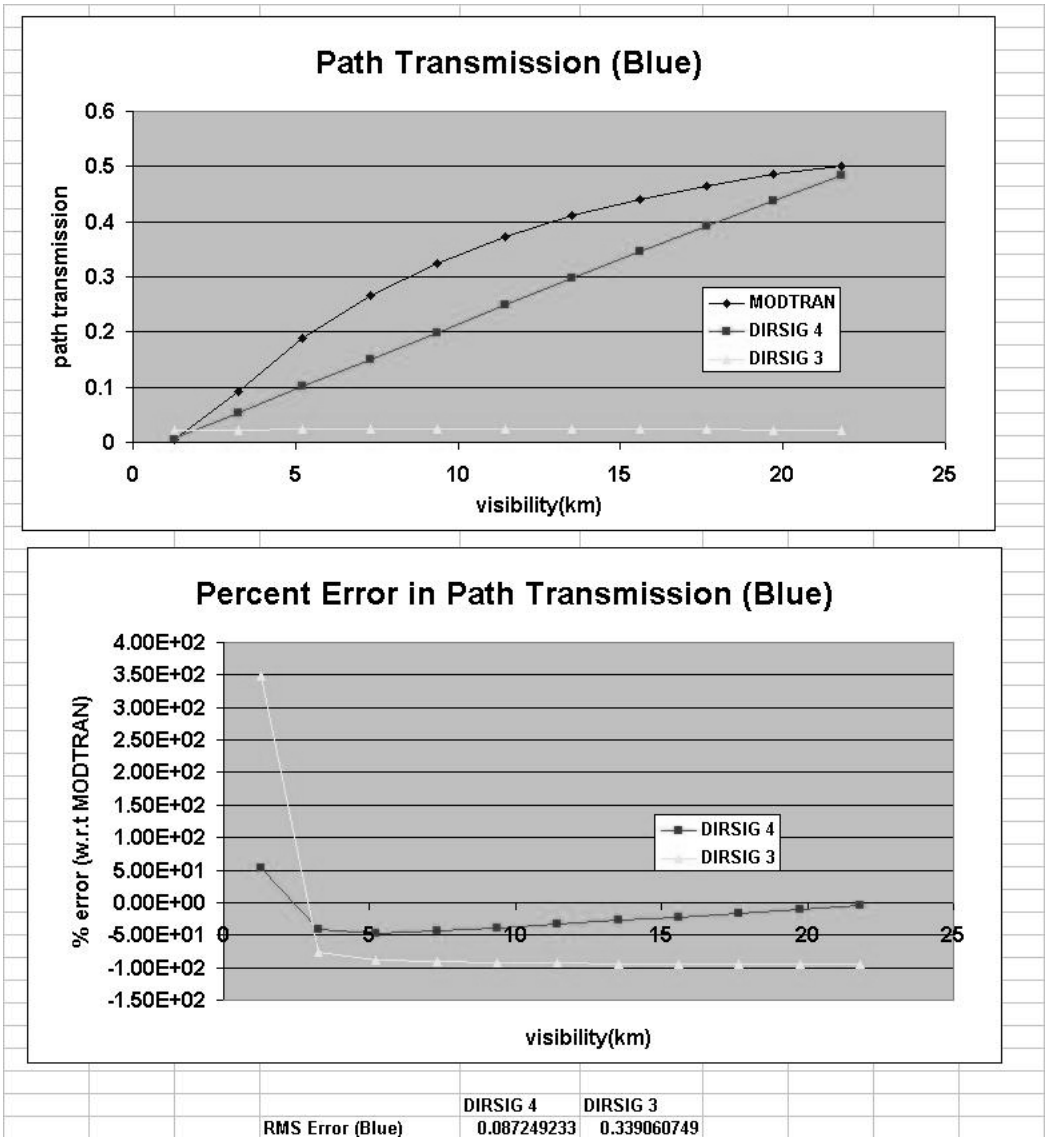

Figure B.104: Test Scene 4a (visibility variation): The upper graph shows the blue path transmission obtained by MODTRAN, DIRSIG 4 and DIRSIG 3. The lower graph shows the percent error of DIRSIG 4 and DIRSIG 3 relative to MODTRAN. The RMS errors for the points shown on the graph are listed below the graphs.

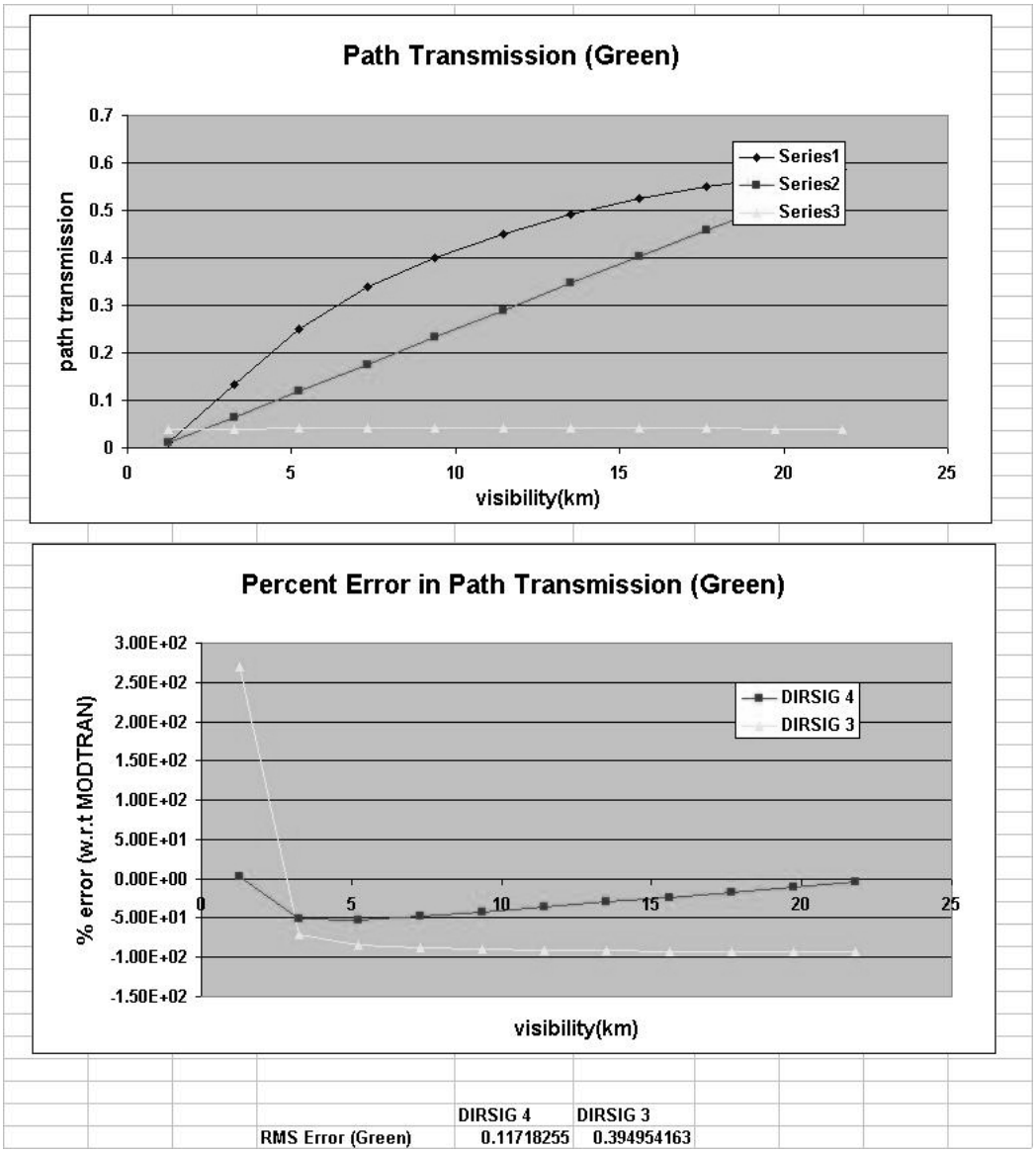

Figure B.105: Test Scene 4a (visibility variation): The upper graph shows the green path transmission obtained by MODTRAN, DIRSIG 4 and DIRSIG 3. The lower graph shows the percent error of DIRSIG 4 and DIRSIG 3 relative to MODTRAN. The RMS errors for the points shown on the graph are listed below the graphs.

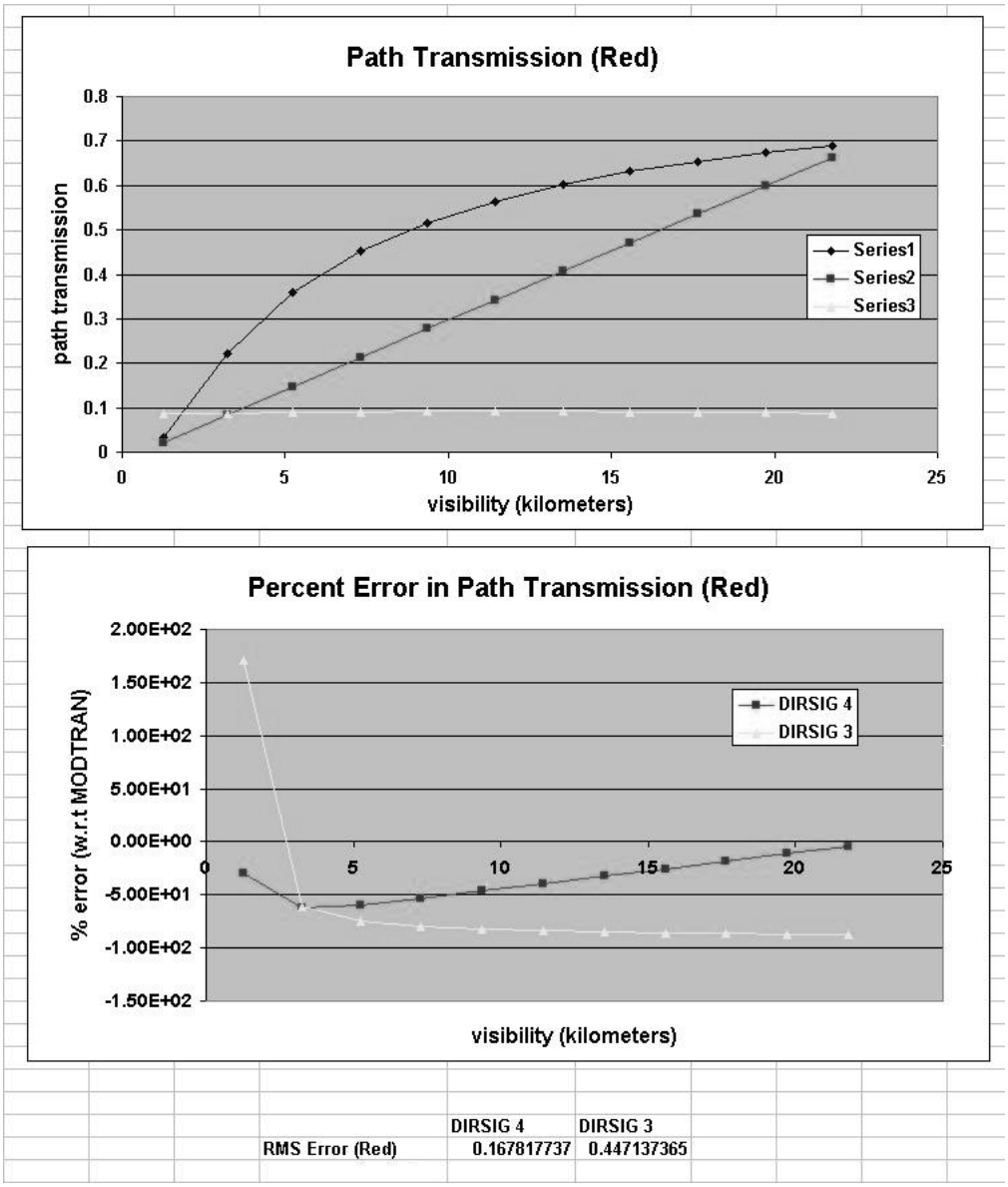

	DIRSIG 4	DIRSIG 3
RMS Error (Red)	0.167817737	0.447137365

Figure B.106: Test Scene 4a (visibility variation): The upper graph shows the red path transmission obtained by MODTRAN, DIRSIG 4 and DIRSIG 3. The lower graph shows the percent error of DIRSIG 4 and DIRSIG 3 relative to MODTRAN. The RMS errors for the points shown on the graph are listed below the graphs.

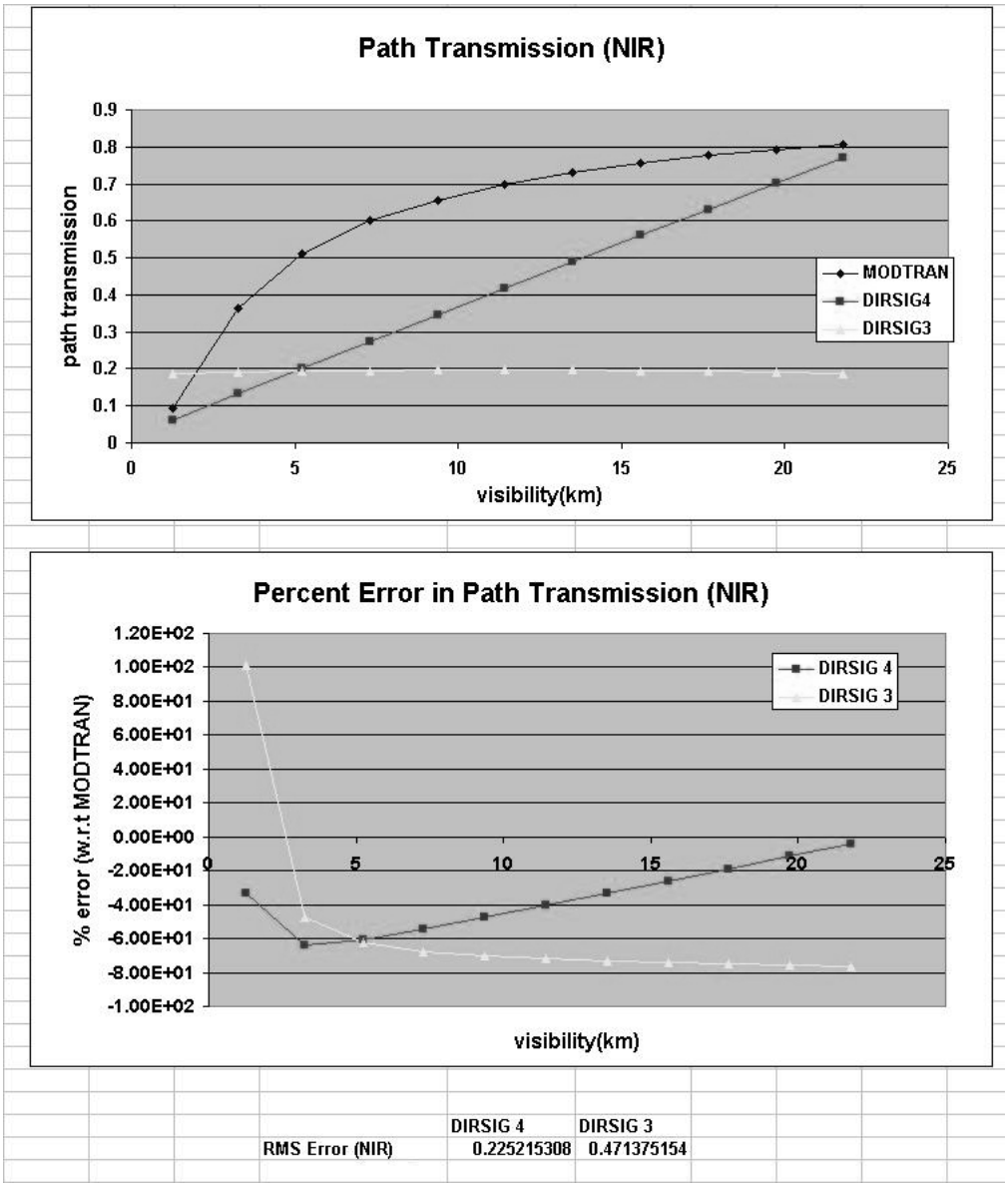

	DIRSIG 4	DIRSIG 3
RMS Error (NIR)	0.225215308	0.471375154

Figure B.107: Test Scene 4a (visibility variation): The upper graph shows the NIR path transmission obtained by MODTRAN, DIRSIG 4 and DIRSIG 3. The lower graph shows the percent error of DIRSIG 4 and DIRSIG 3 relative to MODTRAN. The RMS errors for the points shown on the graph are listed below the graphs.

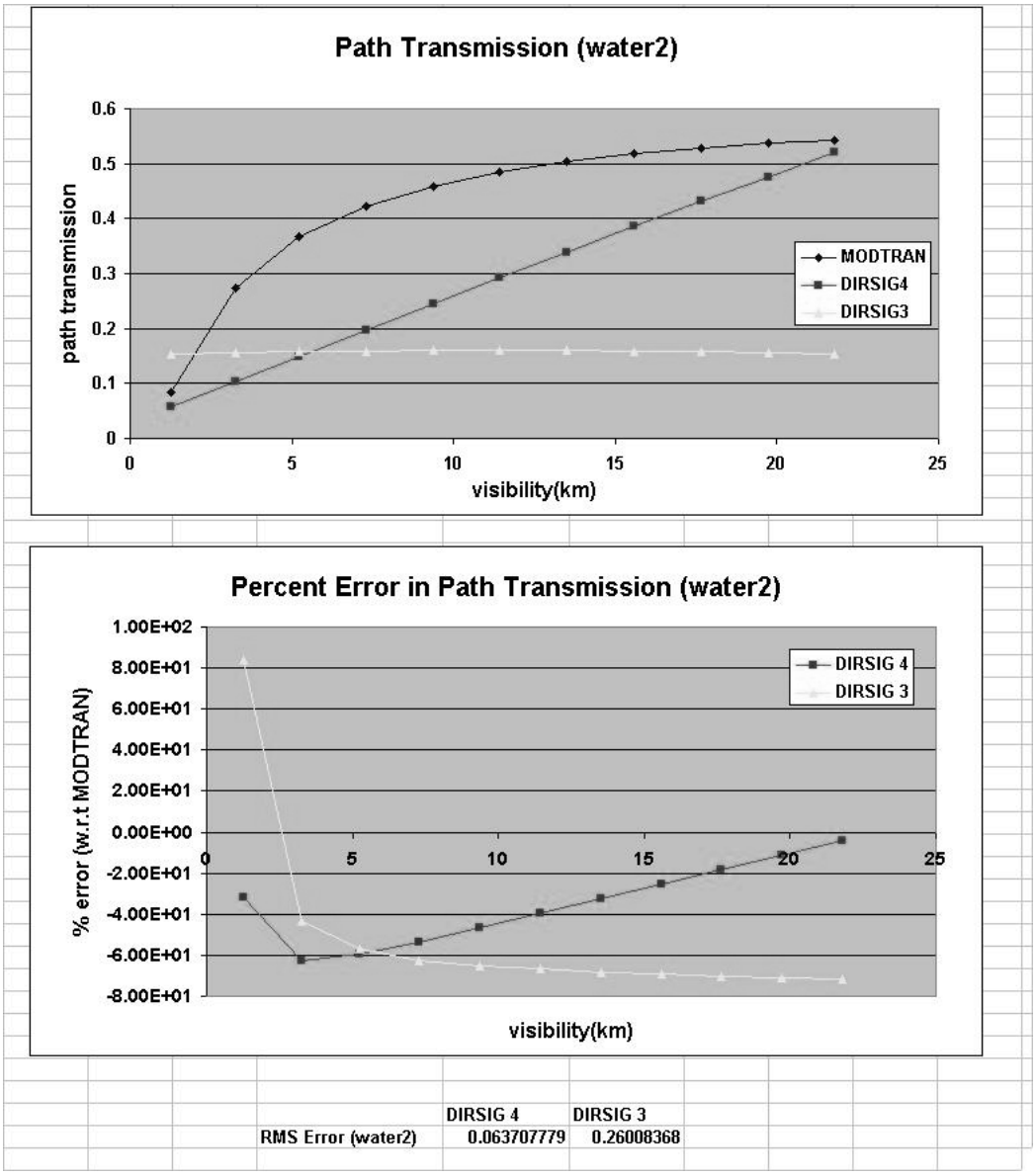

Figure B.108: Test Scene 4a (visibility variation): The upper graph shows the water2 path transmission obtained by MODTRAN, DIRSIG 4 and DIRSIG 3. The lower graph shows the percent error of DIRSIG 4 and DIRSIG 3 relative to MODTRAN. The RMS errors for the points shown on the graph are listed below the graphs.

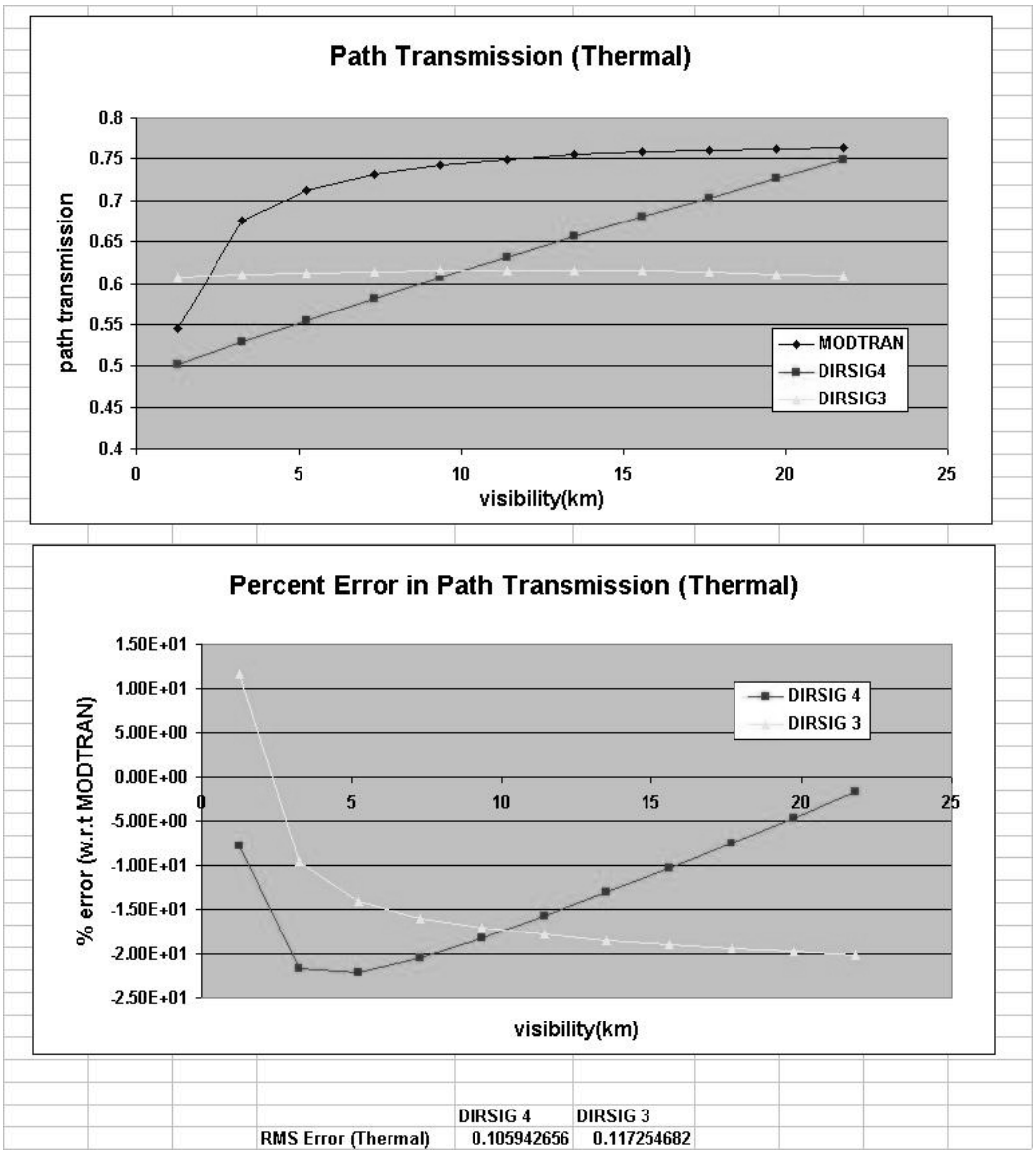

	DIRSIG 4	DIRSIG 3
RMS Error (Thermal)	0.105942656	0.117254682

Figure B.109: Test Scene 4a (visibility variation): The upper graph shows the Thermal path transmission obtained by MODTRAN, DIRSIG 4 and DIRSIG 3. The lower graph shows the percent error of DIRSIG 4 and DIRSIG 3 relative to MODTRAN. The RMS errors for the points shown on the graph are listed below the graphs.

B.9.2 Test Image 4a Grid Results

To assess the performance of both interpolators, the images were analyzed at nearly regular spatial intervals (see figure B.19). As well, two additional points at the top of each of the truncated pyramids were included, to bring non-zero altitudes into the analysis. The RMS error for each band was calculated for all of the points.

These errors for path radiances are shown in figure B.110 , and for transmission in figure B.111.

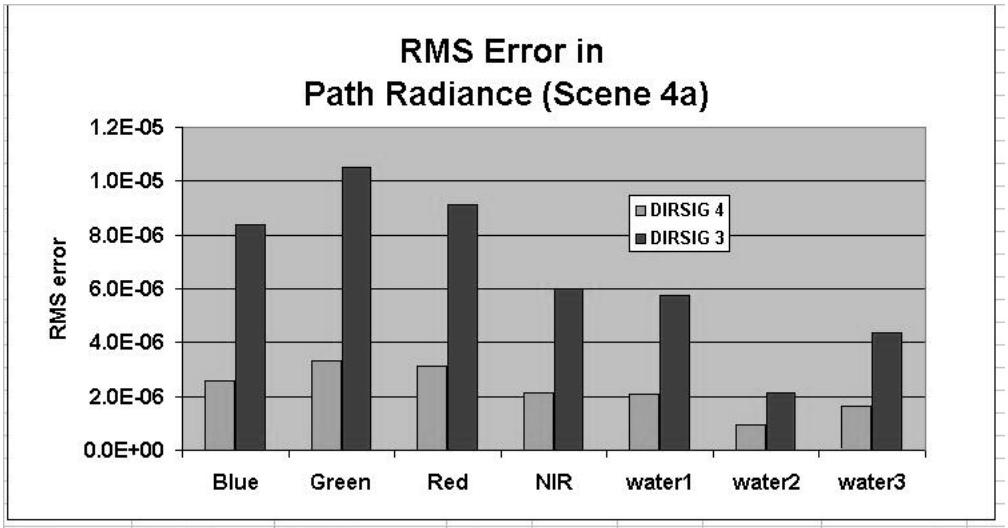

band	DIRSIG 4	DIRSIG 3
Blue	2.573181E-06	8.367654E-06
Green	3.333684E-06	1.050941E-05
Red	3.129291E-06	9.131512E-06
NIR	2.129757E-06	5.984098E-06
water1	2.058766E-06	5.737088E-06
water2	9.241937E-07	2.140534E-06
water3	1.649444E-06	4.374523E-06
Thermal	2.421366E-05	3.121015E-05

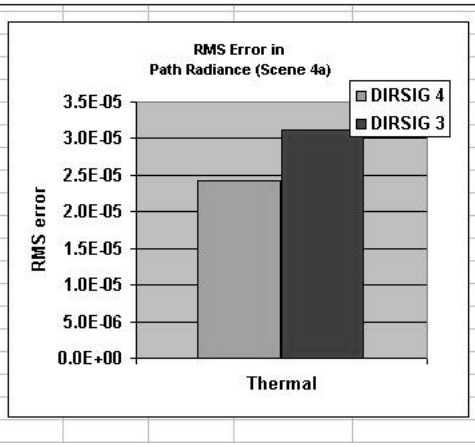

Figure B.110: The RMS error in radiance for each band in image 4a.

;The bands labeled "Water1", "Water2", and "Water3" correspond ;to spectral values about and centered on the water vapor absorption ;feature at 940 nm. The three bands correspond to 880 nm, 940 nm, and ;1,000 nm.

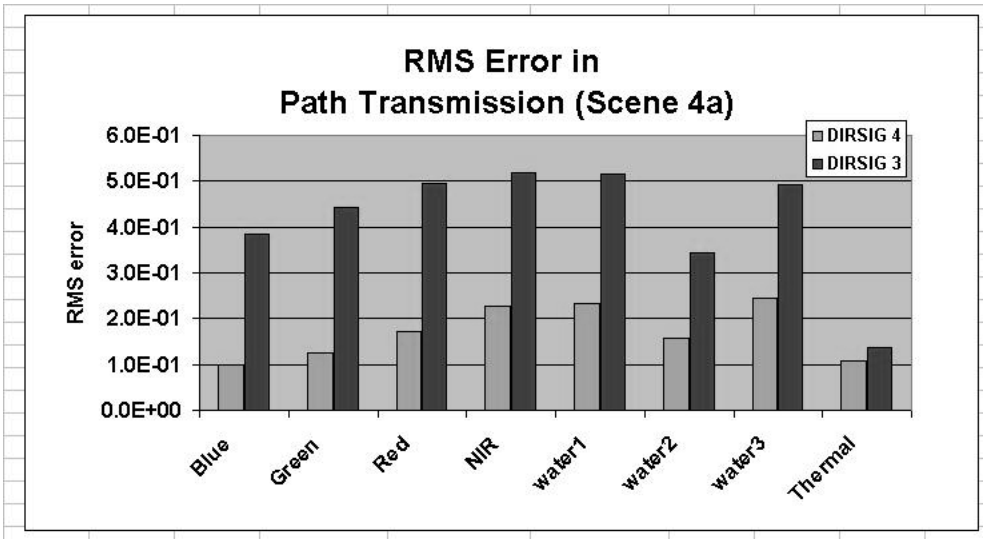

band	DIRSIG 4	DIRSIG 3
Blue	9.882552E-02	3.844451E-01
Green	1.253754E-01	4.431449E-01
Red	1.718385E-01	4.958410E-01
NIR	2.274717E-01	5.171230E-01
water1	2.328728E-01	5.148695E-01
water2	1.575418E-01	3.428576E-01
water3	2.452037E-01	4.932932E-01
Thermal	1.064599E-01	1.379924E-01

Figure B.111: The RMS error in transmission for each band in image 4a.

B.10 Test Image 5

This test image directly examine a horizontally varying atmosphere. Test image 5 is identical to test image 1a, except that there are two atmospheric maps present. This test case includes the atmospheric maps found in test image 3 as well as the one found in test image 4a. (The water vapor map from test image 3 is rotated 90 degrees.)

B.10.1 Test Image 5 Grid Results

To assess the performance of both interpolators, the images were analyzed at nearly regular spatial intervals (see figure B.19). As well, two additional points at the top of each of the truncated pyramids were included, to bring non-zero altitudes into the analysis. The RMS error for each band was calculated for all of the points.

These errors for path radiances are shown in figure B.112 , and for transmission in figure B.113.

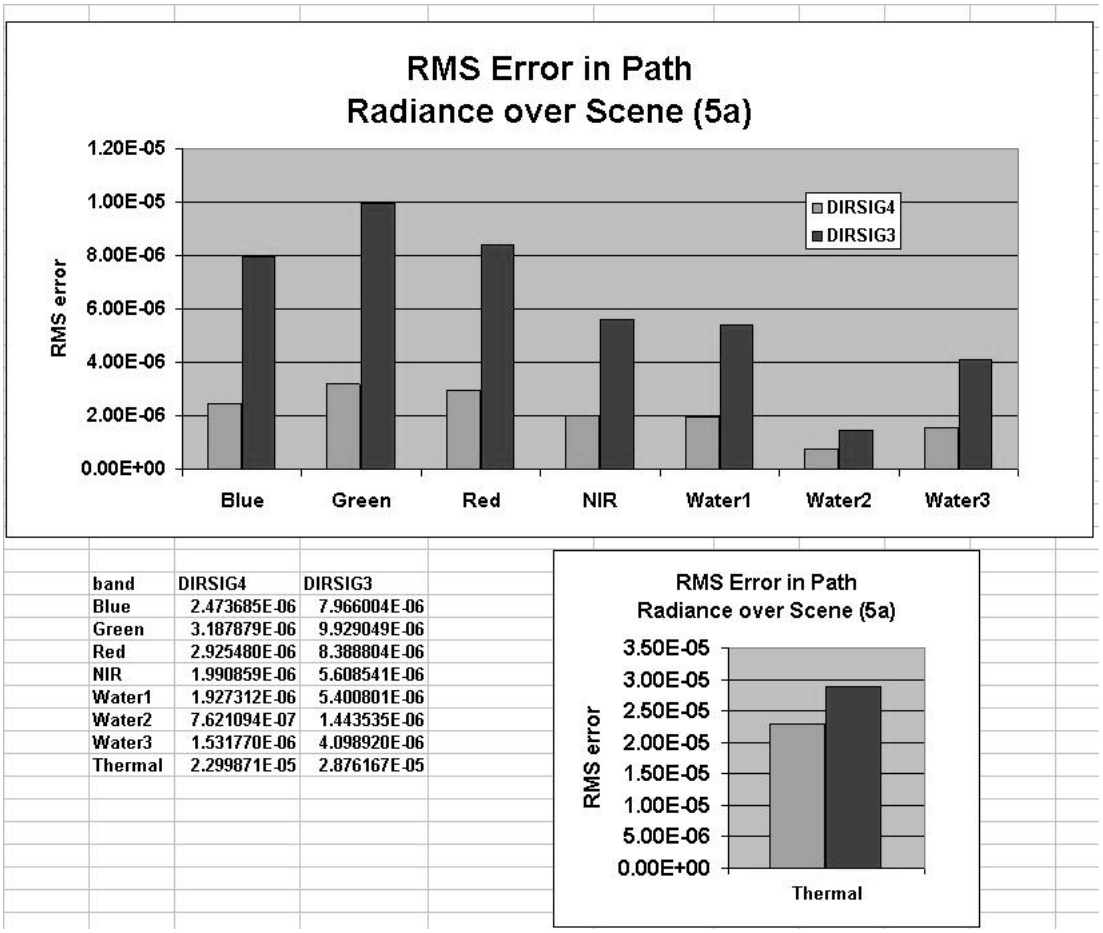

band	DIRSIG4	DIRSIG3
Blue	2.473685E-06	7.966004E-06
Green	3.187879E-06	9.929049E-06
Red	2.925480E-06	8.388804E-06
NIR	1.990859E-06	5.608541E-06
Water1	1.927312E-06	5.400801E-06
Water2	7.621094E-07	1.443535E-06
Water3	1.531770E-06	4.098920E-06
Thermal	2.299871E-05	2.876167E-05

Figure B.112: The RMS error in radiance for each band in image 5a.

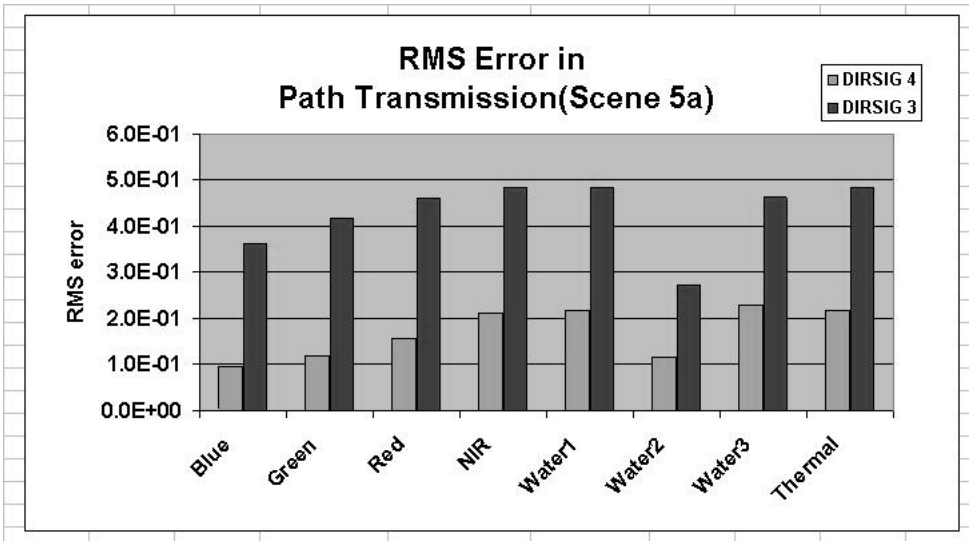

band	DIRSIG 4	DIRSIG 3
Blue	9.460178E-02	3.636671E-01
Green	1.174828E-01	4.179188E-01
Red	1.569164E-01	4.619888E-01
NIR	2.103372E-01	4.850049E-01
Water1	2.159697E-01	4.836337E-01
Water2	1.166384E-01	2.739077E-01
Water3	2.280516E-01	4.624263E-01
Thermal	2.159697E-01	4.836337E-01

Figure B.113: The RMS error in transmission for each band in image 5a.

Appendix C

Horizon Calculator

Contents

C.1 Determine the MODTRAN horizon 317
C.2 The Function getModtran 318

This chapter will describe a tool programmed in IDL which finds the horizon in MODTRAN.

Because the direct calculation of the true horizon is often a difficult and complicated task, a more empirical method is used. This consists of using the tape5 file and running MODTRAN at a number of zenith angles. The method is based on the fact that MODTRAN, when running with parameter $ITYPE$ set to 2 ("slant path between two altitudes" mode), will crash if the sensor is aimed above the horizon. Using this, the process is one of narrowing down the zenith angle which is the lowest possible without causing a MODTRAN failure.

The algorithm is described below. It should be noted that this method is designed to return a single horizon value for a given sensor altitude and tape5 file. This code is not actually incorporated into the make_adb described in section 3.1. There is no assurance that the horizon derived will work in all cases. There is the possibility that different atmospheric conditions may lead to different scattering behavior which may or may not effect the effective location of the horizon.

C.1 Determine the MODTRAN horizon

Algorithm A. *(Determination of the MODTRAN horizon).* This algorithm uses a MODTRAN tape5 file, and an input altitude to determine the angle at while the MODTRAN horizon exists.

Required variables

- *alt* The altitude of the sensor. [km]
- *high_zen* An initial zenith look angle of the sensor. [degrees]
- *low_zen* An initial zenith look angle of the sensor. [degrees]
- *mod_fname* The path and file name of the template MODTRAN input file. (Should be the same used in the generation of the ADB.)

It is important that these zenith angles are selected so that the *low_zen* angle is above the horizon, and would cause MODTRAN to fail if ran at that angle. As well, the variable *high_zen* variable should be below the horizon so that MODTRAN runs normally. [1]

[1] The naming convention here may be confusing. In MODTRAN, the zenith angle is 0 degrees when looking perpendicular

A1. [Define the variable *prev_ave_zen*] Declare variable *num* as a float equal to 9999.9.

A2. [Define the variable *ave_zen* as the average of the initial zenith angles.] Declare variable *num* as a float equal to $(high_zen + low_zen)/2$.

A3. [Loop until the difference between the current average zenith and the previous zenith angle is less than or equal to 0.0001] Perform step A4 through A7 while $abs((ave_zen + prev_ave_zen)/2)$ is greater than 0.0001.

A4. [Set the value of the previous average zenith angle equal to the current average zenith angle.] Set the value of *pre_ave_zenequal* to *ave_zen*.

A5. [Determine if the current average zenith value runs successfully in MODTRAN (ie the angle is below the horizon).] Pass *fname*, *ave_zen*, and *alt* to the function getModtran. (Described in section C.2.) This returns a boolean (*is_good*); 1 if the angle is below the horizon, 0 if not.

A6. [Examine *is_good*] If *is_good* is true, set $high_zen = ave_zen$; otherwise, set $low_zen = ave_zen$;

A7. [Define *ave_zen* as the average of the high and low zenith angles] Set $ave_zen = (high_zen + low_zen)/2$.

A8. [Display the current value *ave_zen* as the horizon angle (after the while loop.)] Print *ave_zen*.

C.2 The Function getModtran

This function's purpose is to take in a zenith angle, a tape5 file, and an altitude and determine if the angle is greater than or less than the horizon. It then returns a boolean; 1 if the input zenith angle is below the horizon, 0 if it is above.

Algorithm B. *(Testing of a specific MODTRAN angle).* This algorithm determines if a given zenith angle can be run with the MODTRAN tape5 input file.

Required input variables

- *alt* The altitude of the sensor. [km]
- *zen* The specific zenith angle. [degrees]
- *fname* The path and file name of the template MODTRAN input file.

B1. [Copy first three lines of the MODTRAN template file into a temporary file] Using the IDL spawn command, and the UNIX head command: spawn, "head -3 "+fname+" > head1"

B2. [Copy last eighteen lines of the MODTRAN template file into a temporary file] Using the IDL spawn command, and the UNIX tail command: spawn, "tail -18 "+fname+" > tail1"

B3. [Define variables to hold values to be output into the modified tape5 file.] Declare variables B, C, D, E, F, G as integers equal to 0.

B4. [Print out a line of data which will become the Card 3 line of a modified tape5.] Print variables *alt*, B, *zen*, D, E, F, G in the proper MODTRAN format for Card 3. (see [1]).

B5. [Create a modified tape5 file using the two temporary files created, and the Card 3 line.] Using the IDL spawn command, and the UNIX cat command: spawn, "cat head1 line tail1 > modrun.tp5".

B6. [Execute MODTRAN using this modified tape5 file "modrun.tp5".] Using the IDL spawn command, and the MODTRAN script /dirs/common/bin/modtran4.bat command: spawn, "/dirs/common/bin/modtran4.bat modrun.tp5"

B7. [Retrieve the number of lines in the resulting tape7.scn file] Using the IDL file_lines function, set the variable *out_lines* equal to the result of the file_lines function when operating on the "tape7.scn" file.

to the surface of the earth (straight up), and 180 degrees when looking straight down at the ground. Therefore, a zenith angle lower than the horizon sees space (and, therefore, is *above* the horizon), and zenith angles higher than the horizon sees the ground (and are *below* the horizon.)

B8. [Examine the variable *out_lines*] If *out_lines* is equal to 8, then set the variable *r_val* equal to 0; otherwise, set it equal to 1.

B9. [Return the value of *r_val*.]

Appendix D

Sample DIRSIG configuration (CFG) file

This file contains or references everything DIRSIG needs to create a synthetic image. The first section contains the locations (absolute or local paths) for the the GDB (Geometric DataBase) file, which contains the facets which make up all of the objects in DIRSIG. As well, it has the paths to find the files containing all other kinds of information on the material used in the scene, from emissivity to sensor response.

The "SCENE" section has the specific names of the GDB file and the material file,, as well as the location of the target, and the local time and GMT offset.

The "ENVIRONMENT" section contains the specific tape 5 (MODTRAN's input file), ADB file name, and weather filename.

The "PLATFORM" section includes all of the information concerning the sensor such as the type (in this case, framing array), spectral and spatial resolution. Within this section is the "POSITION", which contains two sets of three dimensional coordinates. This simply defines the sensor-target relationship. The sensor will always look directly at the target. In this example, the sensor (0, 0, 5000) is directly above the target (0,0,0), looking straight down.

The next sections give the user an array of options, such as activating the thermal models or the generation of ground truth maps. On a side note, this ability to generate truth maps is one of the most valuable aspects of DIRSIG. Its possible to analyze the atmosphere, image processing algorithms, material classification algorithms, target detection schemes and a whole variety of remote sensing applications with great confidence because the ground truth is known absolutely.

```
DIRSIG_CFG

PATHS {
    GDB_PATH = /dirs/home/bmd1603/downwelled
    EMISSIVITY_PATH = /dirs/home/bmd1603/downwelled
    EXTINCTION_PATH = $DIRSIG_HOME/lib/data/extinction
    ABSORPTION_PATH = $DIRSIG_HOME/lib/data/absorption
    MATERIAL_PATH = /dirs/home/bmd1603/downwelled
    WEATHER_PATH = /dirs/lib/data/weather
    TAPE5_PATH = /dirs/home/bmd1603/dobbs
    MAPS_PATH = $DIRSIG_HOME/lib/data/maps
    SOURCES_PATH = $DIRSIG_HOME/lib/data/sources
    RESPONSE_PATH = $DIRSIG_HOME/lib/data/responses
    PROFILE_PATH = $DIRSIG_HOME/lib/data/profiles
}
```

```
SCENE {
    GDB_FILENAME = wall.gdb
    GDB_UNITS = METERS
    MATERIAL_FILENAME = BBground.mat
    GROUND_ALTITUDE = 0.000
    DATE = 6 25 2001
    GMT_TIME = 12.000
    GMT_OFFSET = 5.000
    LOCAL_TIME = 7.000
    LATITUDE = 44.000
    LONGITUDE = 76.000
}

ENVIRONMENT {
    TAPE5_FILENAME = base.tp5
    ADB_FILENAME = tran1.adb
    WEATHER_FILENAME = mls.wth
}

PLATFORM {
    NAME =
    INSTRUMENT {
        NAME = Framing Array
        TYPE = FRAMING_ARRAY
        FOCAL_LENGTH = 50.000000
        BAND_LIST {
            BAND {
                NAME = visible
                MINIMUM_WAVELENGTH = 0.3000
                MAXIMUM_WAVELENGTH = 0.8000
                DELTA_WAVELENGTH = 0.1000
                X_PIXELS = 256
                Y_PIXELS = 256
                X_PIXEL_SIZE = 96.000000
                Y_PIXEL_SIZE = 96.000000
                RESPONSE_FILENAME = IDEAL
                IMAGE_FILENAME = vis.img
            }
        }
    }
    POSITION {
        TARGET_LOCATION = 0.0000, 0.0000, 0.0000
        PLATFORM_LOCATION = 0.0000, 0.0000, 50000.0000
    }

}

OPTIONS {
    ENABLE_TRUTH_IMAGES = TRUE
    ENABLE_THERMAL_MODEL = FALSE
    ENABLE_BRDF = TRUE
    ENABLE_MAPS = TRUE
    ENABLE_SOURCES = FALSE
```

```
    ENABLE_PLUME = FALSE
    REMOVE_SENSOR_PATH = FALSE
    ENABLE_LINE_SKEW = FALSE
    ENABLE_EARTH_ROTATION = FALSE
    REGISTER_BANDS = FALSE
    REGISTER_DETECTORS = FALSE
    GENERATE_IMAGE_PER_SCAN = FALSE
    GENERATE_TRUTH_PER_SCAN = FALSE
    USE_SCENE_PLATFORM_ANGLES_TAG = FALSE
    ENABLE_APODIZATION = FALSE
    ENABLE_OFF_AXIS_ERROR = FALSE
    ENABLE_OPD_ERROR = FALSE
    USE_STEPWISE_PLUME = FALSE
}

TRUTH_IMAGES {
    IMAGE_FILENAME = truth.img
    MATERIAL_MAPS = TRUE
    SHADOW_MAPS = FALSE
    SHAPE_FACTOR_MAP = TRUE
    HIT_MAPS = TRUE
    PATH_ANGLE_MAPS = FALSE
    TEMPERATURE_MAPS = FALSE
    EMISSIVITY_MAPS = FALSE
    UPWELLED_RADIANCE_MAPS = TRUE
    DOWNWELLED_RADIANCE_MAPS = TRUE
    SOLAR_RADIANCE_MAPS = TRUE
    PATH_TRANSMISSION_MAP = TRUE
    PLUME_MAPS = FALSE
}
```

Appendix E

Sample Atmospheric Database (ADB) file

This file is used by DIRSIG to calculate path radiances and transmissions through the atmosphere for a number of different geometries. The atmospheric values for any geometries *not* shown here are interpolated by DIRSIG. For space reasons only, this ADB has a very low spectral resolution (0.1 micron). In practice, spectral resolutions are generally much smaller, yielding much larger ADB files.

Starting off, the ADB file reiterates some of the information contained in the CFG file (see appendix D) that is pertinent to the atmospheric realm. As well, the header has information about the field of view (in the form of the zenith angle) and the angular resolution of the sampling. This determines how often (angularly) the upwelled radiance of the scene will be sampled.

The first of the 3 main sections of the ADB are the "SOURCE PATHS" section. This has the exoatmospheric irradiances of both the sun and the moon, as well as the atmospheric transmissions for each. These 3 main sections contain one or more spectral blocks (a set of spectral data). The "SOURCE PATHS" section contains one of these spectral blocks, with four pieces of data for each of the spectral points specified in the spectral resolution of the cfg file.

The next section is the "SENSOR PATHS" section, which contains all of the upwelling radiance and transmission data. The spectral block here will contain the thermal and solar upwelled radiance values, along with the transmission from the ground to the sensor (tau 2). Because the geometry in this section changes, there will be more than one spectral block. DIRSIG will sweep through a series of zenith angles, making a MODTRAN run for each angle, and storing the data here. As stated above, if a given geometry is needed and not here, DIRSIG will interpolate between these values. Some of the spectral blocks were deleted for space purposes only. For this configuration file, there will be 21 spectral block, starting at -23.0 degrees, and moving up in increments of 2.3 degrees, up to (+)23.0 degrees.

The second to last section is the "DOWNWELLED PATHS". This is similar to the "SENSOR PATHS" section in that it contains both the thermal and solar radiance at each spectral point. It does *not* include the transmission term. Another, significant difference here is that these are values from downwelled radiance. You can imagine this as the sensor looking "up". This section has the radiance that was scattered (or emitted) from the atmosphere and struck the target. Because DIRSIG is trying to get a full sampling of the sky dome, the position of the sensor and target in MODTRAN will change, and therefore we will have multiple spectral blocks. The sampling scheme is an evenly spaced number of zenith and azimuth angles. There are 7 zenith and 12 azimuth angles, which makes a total of 72 distinct spectral blocks. Again, most of these spectral blocks are omitted for display reasons.

The final portion of the downwelled section is the "TOTAL" section. This contains the total integrated downwelled radiance for all of the angles sampled.

```
DIRSIG_ADB
SCENE {
    GROUND_ALTITUDE = 0.0000
    DATE = 6 25 2001
    LOCAL_TIME = 7.00
    GMT_TIME = 12.00
    GMT_OFFSET = 5.00
    LATITUDE = 44.0000
    LONGITUDE = 76.0000
}

PLATFORM {
    INSTRUMENT {
        BAND_LIST {

            BAND {
                MINIMUM_WAVELENGTH = 0.4000
                MAXIMUM_WAVELENGTH = 0.6000
                DELTA_WAVELENGTH = 0.1000
            }
        }

        FIELD_OF_VIEW {
            MINIMUM_ZENITH = -23.00
            MAXIMUM_ZENITH = 23.00
            DELTA_ZENITH = 2.30
        }
    }
}


#
# SECTION:  SOURCE_PATHS
# CONTENTS: Exoatmospheric Solar and Lunar
#           irradiances and atmospheric
#           transmission to ground (tau #1)
# FORMAT:   spectral center, E_sun, T_sun, E_moon, T_moon
#
SOURCE_PATHS {
    SPECTRAL_DATA {
        0.4000 1.3800e-01 4.1600e-01 0.0000e+00 0.0000e+00
        0.5000 1.8500e-01 6.7680e-01 0.0000e+00 0.0000e+00
        0.6000 1.6900e-01 7.7400e-01 0.0000e+00 0.0000e+00
    }
}

#
# SECTION:  SENSOR_PATHS
# CONTENTS: Atmospheric radiances (thermal and
#           solar) and transmission along the path
#           from the sensor to the target.
# FORMAT:   spectral center, thermal, solar, tau2
#
SENSOR_PATHS {
```

```
    PATH {
        ZENITH = -23.0000
        AZIMUTH = 0.0000
        GROUND_RANGE = 54.3180
        SPECTRAL_DATA {
            0.4000 0.0000e+00 3.0377e-03 6.4900e-01
            0.5000 0.0000e+00 1.9562e-03 8.3190e-01
            0.6000 2.6933e-31 8.2179e-04 8.8590e-01
        }
    }

    PATH {
        ZENITH = -20.7000
        AZIMUTH = 0.0000
        GROUND_RANGE = 53.4506
        SPECTRAL_DATA {
            0.4000 0.0000e+00 3.0060e-03 6.5330e-01
            0.5000 0.0000e+00 1.9343e-03 8.3440e-01
            0.6000 2.6672e-31 8.1261e-04 8.8770e-01
        }
    }
.
.
.
[ Lines omitted for display purposes. ]
.
.
.

}


#
# SECTION:  DOWNWELLED_PATHS
# CONTENTS: Downwelled thermal and solar
#           radiances
# FORMAT:   spectral center, thermal, solar
#
DOWNWELLED_PATHS {

    PATH {
        ZENITH = 7.5000
        AZIMUTH = 0.0000
        SPECTRAL_DATA {
            0.4000 0.0000e+00 2.8034e-03
            0.5000 0.0000e+00 1.8777e-03
            0.6000 3.4100e-30 8.0891e-04
        }
    }

    PATH {
        ZENITH = 7.5000
        AZIMUTH = 30.0000
```

```
        SPECTRAL_DATA {
            0.4000 0.0000e+00 2.8821e-03
            0.5000 0.0000e+00 1.9435e-03
            0.6000 3.4100e-30 8.4013e-04
        }
    }
.
.
.
[Lines omitted for display purposes.}
.
.
.


    PATH {
        ZENITH = 82.5000
        AZIMUTH = 330.0000
        SPECTRAL_DATA {
            0.4000 0.0000e+00 7.0765e-03
            0.5000 0.0000e+00 7.5360e-03
            0.6000 1.9285e-29 4.0354e-03
        }
    }
    TOTAL {
        SPECTRAL_DATA {
            0.4000 0.0000e+00 4.2974e-03
            0.5000 0.0000e+00 3.3699e-03
            0.6000 6.0386e-30 1.5706e-03
        }
    }
}
```

Appendix F

Sample MODTRAN input file (tape5)

This is the tape5 file, which is the input to MODTRAN. DIRSIG uses this to create a LUT (know as the Atmospheric DataBase [see appendix E for more details]) which it references during the image rendering process. In creating the ADB, DIRSIG will read in this tape5 file, make some modifications (see chapter 1 for more details.), and run MODTRAN a number of times, storing the outputs. This provides a file that DIRSIG can quickly reference when it needs information about the atmosphere.

```
TS  2    2    2   -1    2    2    2    2    2    2    1    0    0   0.000   0.00
F   0F   0   0.00000         0         0 F F F         0.000
    0    0    0    3    0    0     0.000     0.000     0.000     0.000     0.000
   100.000     0.000   180.000     0.000     0.000     0.000    0          0.000
    0    0    0    0
    43.000    77.000    18.968     0.955     0.000   180.000     0.000     0.000
     0.300     0.800     0.001     0.001TMtesting MT A
    0
```

Appendix G

Interpolator Inputs

This chapter contains the ".h" file which is used by the atmospheric interpolator. It has many of the required initial values, as well as the the structure which holds all of the atmospheric spectral data. The use of this structure is described in chapter 3.

```
<<CDModtranTent.h>>=
#ifndef _CDMODTRANP_H_
#define _CDMODTRANP_H_
#include "CDAtmosphere.h"
#include "CDAtmosphereProps.h"
#include "CDEphemeris.h"
/////////////////  #include "adbtent.h" ////////////////////////////
//////////////////////////////////////////////////////////////////
#include <string>
#include <vector>
#define n_points 3 //defines number of spectral points per band
#define number_of_bands 8
#define n_elements n_points*number_of_bands
//This is the total number of spectral points in each spectral block.

#define real_number_of_zeniths 8
#define real_number_of_azimuths 8
#define number_of_altitudes 2
#define d_alt 1 //This is the value of the interval in the altitude.
#define zenith_offset 0.0 //This is the value of the interval in the altitude.
//These show the structure of the new Sensor Paths section.

#define number_of_zeniths real_number_of_zeniths * real_number_of_azimuths * number_of_altitudes
/**This is actually the number of zenith angles, times the number
*of azimuth angles, times the number of altitudes in the Sensor
*Path's section.  It was left as this constant name because the
*old ADB's sensor path was defined only by the number of zenith's
*/

#define number_of_down_zeniths 6
#define number_of_down_azimuths 12
#define number_of_down_altitudes 2
#define delta_down_zenith 15
#define delta_down_azimuth 30
```

```
#define number_of_zeniths_times_azimuths number_of_down_zeniths*number_of_down_azimuths*number_of_down_a

#define sensor_height 50.0
//#define horizon 97.026825
#define OUTPUT_LENGTH 255
#define MAX_POINTS 1000
#define MAX_POINTS_UP 10000
#define MAX_POINTS_DOWN 10000

#define DEFAULT_AERO_TYPE 1
#define DEFAULT_VIS 23.0
//#define SIMPLEUP 0
//#define DOWNCHUNK 0
//#define DEBUG3 1

//This is the same old structure of the downwelled section, but
//multiplied by the number of altitudes in the downwelled section.


//After the downwelled section is changed.
#define n_water  2
#define n_aerosols  2
#define n_vis  2

#define POLARIZED_OFF 1

//DEBUGGERS:
//#define UPCHUNK 1

//Structures to hold the ADB
//**********************SOURCE SECTION**********************//
struct spectral_data_source{

float spectral_center[ n_elements ];
float E_sun[ n_elements ];
float T_sun[ n_elements ];
float E_moon[ n_elements ];
float T_moon[ n_elements ];
};

struct source_path {

float altitude;
spectral_data_source spectral_data;
};

//**********************SENSOR SECTION**********************//
struct spectral_data_sensor{

float spectral_center[ n_elements ];
float thermal[ n_elements ];
float solar[ n_elements ];
float tau2[ n_elements ];
float depth[ n_elements ];
```

```
float polang[ n_elements ];
float trad2[ n_elements ];
float trad3[ n_elements ];
float trad4[ n_elements ];
};


struct sensor_path {
float zenith;
float azimuth;
float altitude;
spectral_data_sensor spectral_data;
};

//**********************DOWNWELLED SECTION*****************//

struct spectral_data_downwelled{

float spectral_center[ n_elements ];
float thermal[ n_elements ];
float solar[ n_elements ];
float depth[ n_elements ];
float polang[ n_elements ];
float trad2[ n_elements ];
float trad3[ n_elements ];
float trad4[ n_elements ];
};

struct downwelled_path {
float zenith;
float azimuth;
float altitude;
spectral_data_downwelled spectral_data;
};

//**********************TOTAL SECTION**********************//

struct spectral_data_total{

float spectral_center[ n_elements ];
float thermal[ n_elements ];
float solar[ n_elements ];
};

struct total {
spectral_data_total spectral_data[ number_of_down_altitudes ];
};

//*********************************************************//
//Putting all of the sections together into one ADB.
//*********************************************************//

struct adb {
```

```
float vis_value;
int IHAZE_value;
float water_value;
source_path section_1[ number_of_altitudes ];
sensor_path section_2[number_of_zeniths];
downwelled_path section_3[number_of_zeniths_times_azimuths * number_of_down_altitudes];
total section_4;

};


//*********************************************************//
//Putting all of the ADB's together into one variable.
//All of the atmospheric structure must be included.
//*********************************************************//

struct vis {

adb visibility[ n_vis ];
};

struct aero_type {


vis aerosol_type[ n_aerosols ];
};

struct water_struct {

//add in ephemeris data for solar angle calculation
        int month;
        int day;
        int year;
//        float sensor_altitude;
        float local_time;
        float gmt_time;
        float gmt_offset;
        float latitude;
        float longitude;
aero_type water[ n_water ];
};
```